CURRENT TOPICS IN MARINE ORGANIC BIOGEOCHEMICAL RESEARCH

EDITED BY: Carol Arnosti, Thorsten Dittmar, Kai-Uwe Hinrichs, Cindy Lee and Stuart Wakeham

PUBLISHED IN: Frontiers in Marine Science

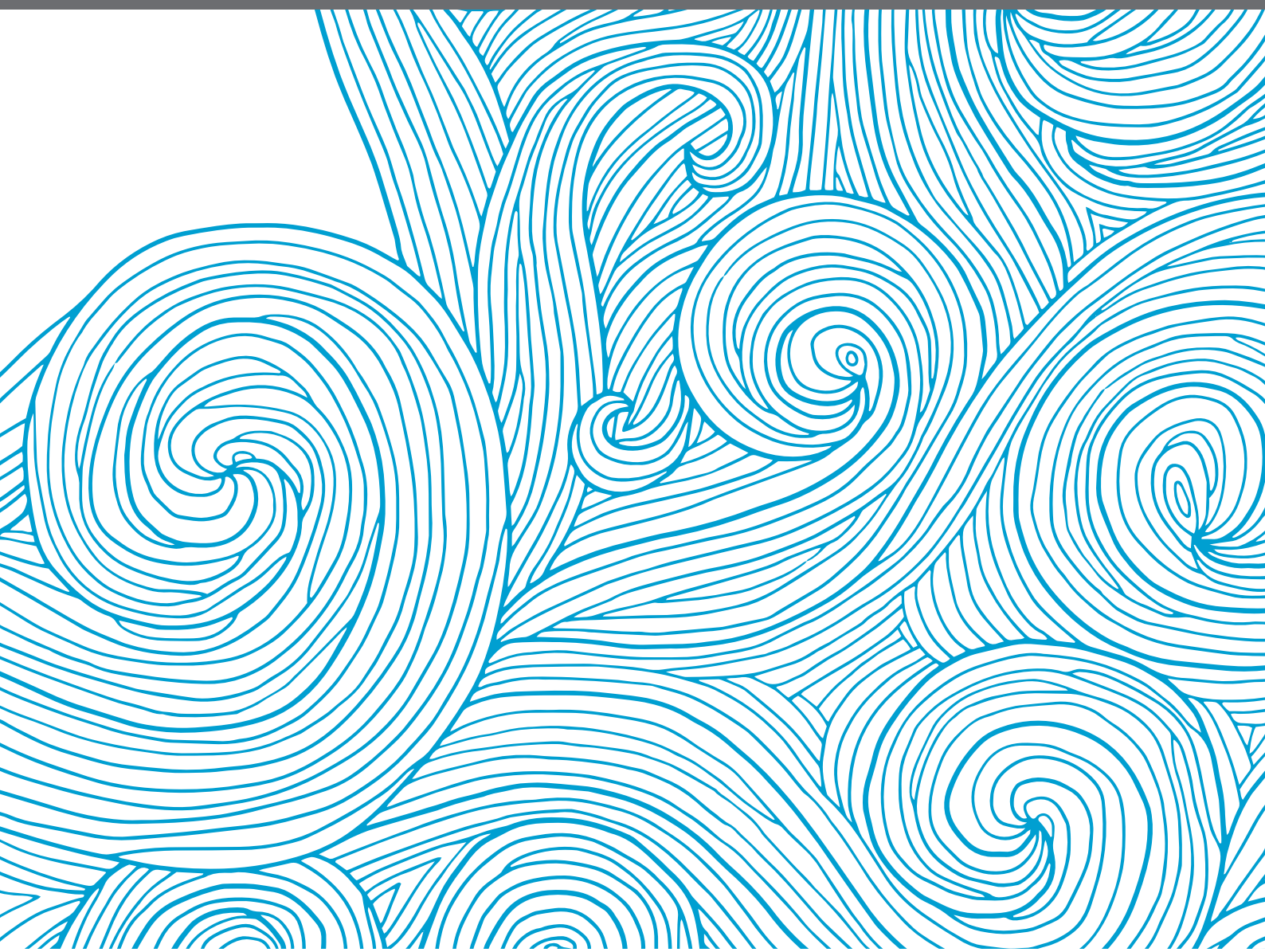

frontiers Research Topics

frontiers

ISSN 1664-8714
ISBN 978-2-88966-464-1
DOI 10.3389/978-2-88966-464-1

About Frontiers

Frontiers is more than just an open-access publisher of scholarly articles: it is a pioneering approach to the world of academia, radically improving the way scholarly research is managed. The grand vision of Frontiers is a world where all people have an equal opportunity to seek, share and generate knowledge. Frontiers provides immediate and permanent online open access to all its publications, but this alone is not enough to realize our grand goals.

Frontiers Journal Series

The Frontiers Journal Series is a multi-tier and interdisciplinary set of open-access, online journals, promising a paradigm shift from the current review, selection and dissemination processes in academic publishing. All Frontiers journals are driven by researchers for researchers; therefore, they constitute a service to the scholarly community. At the same time, the Frontiers Journal Series operates on a revolutionary invention, the tiered publishing system, initially addressing specific communities of scholars, and gradually climbing up to broader public understanding, thus serving the interests of the lay society, too.

Dedication to Quality

Each Frontiers article is a landmark of the highest quality, thanks to genuinely collaborative interactions between authors and review editors, who include some of the world's best academicians. Research must be certified by peers before entering a stream of knowledge that may eventually reach the public - and shape society; therefore, Frontiers only applies the most rigorous and unbiased reviews.
Frontiers revolutionizes research publishing by freely delivering the most outstanding research, evaluated with no bias from both the academic and social point of view. By applying the most advanced information technologies, Frontiers is catapulting scholarly publishing into a new generation.

What are Frontiers Research Topics?

Frontiers Research Topics are very popular trademarks of the Frontiers Journals Series: they are collections of at least ten articles, all centered on a particular subject. With their unique mix of varied contributions from Original Research to Review Articles, Frontiers Research Topics unify the most influential researchers, the latest key findings and historical advances in a hot research area! Find out more on how to host your own Frontiers Research Topic or contribute to one as an author by contacting the Frontiers Editorial Office: frontiersin.org/about/contact

CURRENT TOPICS IN MARINE ORGANIC BIOGEOCHEMICAL RESEARCH

Topic Editors:
Carol Arnosti, University of North Carolina at Chapel Hill, United States
Thorsten Dittmar, University of Oldenburg, Germany
Kai-Uwe Hinrichs, University of Bremen, Germany
Cindy Lee, Stony Brook University, United States
Stuart Wakeham, University of Georgia, United States

Citation: Arnosti, C., Dittmar, T., Hinrichs, K.-U., Lee, C., Wakeham, S., eds. (2021). Current Topics in Marine Organic Biogeochemical Research. Lausanne: Frontiers Media SA. doi: 10.3389/978-2-88966-464-1

Table of Contents

frontiers in Marine Science

EDITORIAL
published: 23 December 2020
doi: 10.3389/fmars.2020.628071

Editorial: Current Topics in Marine Organic Biogeochemical Research

Stuart G. Wakeham[1]*, *Cindy Lee*[2], *Carol Arnosti*[3], *Thorsten Dittmar*[4], *Kai-Uwe Hinrichs*[5] *and Ann Pearson*[6]

[1] Skidaway Institute of Oceanography, University of Georgia, Savannah, GA, United States, [2] School of Marine and Atmospheric Sciences, Stony Brook University, Stony Brook, NY, United States, [3] Department of Marine Sciences, University of North Carolina-Chapel Hill, Chapel Hill, NC, United States, [4] Institute for Chemistry and Biology of the Marine Environment (ICBM) and Helmholtz Institute for Functional Marine Biodiversity (HIFMB), Carl von Ossietzky University of Oldenburg, Oldenburg, Germany, [5] MARUM – Center for Marine Environmental Sciences, University of Bremen, Bremen, Germany, [6] Department of Earth and Planetary Sciences, Harvard University, Cambridge, MA, United States

Keywords: marine organic biogeochemistry, dissolved organic matter, particulate organic matter, sedimentary organic matter, analytical challenges

Editorial on the Research Topic

Current Topics in Marine Organic Biogeochemical Research

Complex and incompletely understood chemical, biological and physical processes affect the delivery, transport, and storage of organic matter (OM) in the ocean. Atmospheric and climate-relevant gases, primarily carbon dioxide, are closely linked to the production and flux of organic matter within the ocean via the biological pump. Marine and continental OM is transformed in the water column, some is transported to the sediments where a fraction is stored over geological time, and some marine OM is released to the atmosphere. These functions are intimately linked to global nutrient cycles and ecosystem processes. Perhaps indicative of how the field has matured, the multidisciplinary nature of ocean carbon studies and the importance of biological processes in organic carbon cycling has resulted in a morphing of "marine organic geochemistry" into "marine organic biogeochemistry." Marine organic biogeochemistry now provides a molecular-level window onto the functioning and scale of processes that control the behavior of OM in the ocean. New sampling tools, analytical methods, and data handling capabilities have been applied to marine chemistry since the 1970s; and in tandem with coordinated, international and interdisciplinary research programs, this has led to explosive growth of marine organic biogeochemistry.

More than four decades have passed since the first community-wide marine organic geochemistry workshop was held in 1976 to assess progress, identify continuing challenges, and recommend future research needs (Andersen, 1977). Major topics at that workshop were: (i) global biogeochemical cycles; (ii) macromolecular material; (iii) transformations in the water column; (iv) diagenesis in sediments; (v) molecular paleontology; and (vi) physical organic chemistry. Follow-on symposia in 1990 (Farrington, 1992), 1999 (Hedges et al., 2000), and 2003 (Benner et al., 2004) provided updates via cross-disciplinary exchange of ideas and new concepts to address analytical, methodological and conceptual questions pivotal to the field of marine organic biogeochemistry. Several recent reviews (summarized by Wakeham and Lee, 2019) have placed marine organic geochemistry within the context of the oceanic carbon cycle and biogeochemistry as it is understood today.

This special issue highlights a workshop that was held at the Hanse Wissenschaftskolleg (HWK Institute for Advanced Studies, Delmenhorst, Germany) in April 2019 and that was designed to stimulate discussion about current topics in molecular marine organic biogeochemical research

Edited and reviewed by:
Eric 'Pieter Achterberg, GEOMAR Helmholtz Center for Ocean Research Kiel, Germany

***Correspondence:**
Stuart G. Wakeham
stuart.g.wakeham@gmail.com

Specialty section:
This article was submitted to Marine Biogeochemistry, a section of the journal Frontiers in Marine Science

Received: *10 November 2020*
Accepted: *03 December 2020*
Published: *23 December 2020*

Citation:
Wakeham SG, Lee C, Arnosti C, Dittmar T, Hinrichs K-U and Pearson A (2020) Editorial: Current Topics in Marine Organic Biogeochemical Research. Front. Mar. Sci. 7:628071. doi: 10.3389/fmars.2020.628071

among scientists working on multiple aspects of biogeochemistry. Marine OM covers a wide size continuum that includes particulate (POM), colloidal (COM), and dissolved (DOM) phases that are largely operationally defined. There is considerable overlap in their analyses and biogeochemical processes. Of particular interest to the workshop were the links between production and fluxes of OM in the ocean and the roles these processes play in ocean biogeochemical cycles. The goals of the workshop were to develop (i) a better understanding of organic biogeochemical processes in the ocean; (ii) a clear picture of the most important gaps in knowledge; and (iii) a path forward toward addressing these deficiencies. Discussion groups were constituted for three broad themes (POM, DOM, and analytical methods) and the three working group reports included here assess the state-of-the-art for each theme and highlight needs and challenges for future research. Additionally, 17 articles were contributed within these broad themes and center on other aspects of organic biogeochemistry, biological processing of organic materials, isotope biogeochemistry, and analytical advances.

The working group on POM (Kharbush et al.) uses an overview of autochthonous, allochthonous, and anthropogenic components of oceanic particulate organic carbon (POC) to assess recent progress in understanding its distribution in the ocean, its composition and its cycling. This report suggests various research directions needed to bridge diverse databases that can link the identity and structural diversity of POC to its sources and transformation processes. The DOM working group report (Wagner et al.) synthesizes fluxes of oceanic dissolved organic carbon (DOC), considers what is meant by DOC "recalcitrance," spotlights new isotopic approaches for probing the distribution of DOC in the ocean, and postulates changes to DOC quantity and composition that may occur in response to climate change. The analytical working group (Steen et al.) compiles examples of recent developments in analytical methods that have made possible transformative advances in marine organic biogeochemistry over the past decade and projects some challenges and opportunities for the future to insure continued evolution in understanding the cycling of organic carbon in the ocean. Collectively, these summaries set the stage for in-depth exploration of the three focus areas and provide contextual framework for the discipline-focused articles.

Recent progress in understanding the composition and biogeochemical behavior of DOM is described in two articles. Srain et al. investigate pathways of organic carbon degradation in the oxygen minimum zone within the Humboldt Current off the coast of Chile. Over a 15-month period, concentrations of volatile fatty acids, ethanol, and CO_2, typical products of fermentation reactions, were measured at different depths in the upper water column. Incubation experiments with added amino acids, glucose, and acetate, were also carried out to link water column concentrations in the seasonally changing environment with potential transformation pathways of organic matter. Ziervogel and Arnosti measured the activities and substrate specificities of microbial extracellular enzymes in waters of the Guaymas Basin (Gulf of California), where hot hydrothermal fluids "cook" the thick layers of phytoplankton-derived organic matter in surficial sediments, yielding high concentrations of DOC that permeate into bottom waters. Enzyme activities in the deepest part of the water column are similar to or higher than in the upper water column, and are measurable for a broader spectrum of substrates, suggesting that sediment-derived DOC enhances microbial activities in bottom water.

Seven articles focus on various aspects of POM. van der Jagt et al. provide direct evidence that filter-feeding copepods are responsible for much of the attenuation in aggregate POC flux in the Arctic Ocean near Svalbard by directly ingesting and fragmenting settling marine snow. Optical systems that can obtain vertical profiles of particle size-distribution and abundance are often used to estimate POC fluxes and distributions in the water column. By combining different optical systems to detect a range of organic and inorganic particle types, Markussen et al. show that better estimates of fluxes of both small and large particles can be obtained. Using cell membrane derived intact polar lipids (IPLs) as biomarkers, Cantarero et al. find major differences between the oxygen minimum zone off Chile and other similar areas. These IPLs indicate contrasting distributions of free-living and particle-attached microbes and also suggest that microbial production in low oxygen environments may be more important than previously thought. Close and Henderson have compiled published reports of stable carbon isotope compositions ($\delta^{13}C$ values) of POC in the upper water column that show a widespread isotopic pattern in oceanic POC. They further discuss the implications of this pattern in terms of vertical differences in algal photosynthetic growth rates or algal community composition, effects of degradation on the composition of POM, isotopic disequilibrium within the dissolved inorganic carbon pool, particle dynamics, and vertical mixing processes. The stable carbon isotope signature of POC and particulate amino acids in the hypoxic water column of the northern South China Sea were investigated by Yang et al. to better understand the sources and cycling of OM in the coastal environment. These authors found no apparent differences in the carbon isotopic distributions of particulate amino acids between hypoxic and oxic waters. Engel et al. review the widespread abundance of two major types of microgels throughout the ocean in terms of their importance to DOC. They discuss how microgel distributions provide information about productivity and particle dynamics in the ocean. Le Moigne assembles published studies that quantify sinking fluxes of fecal pellets, phytoplankton cells, and aggregates, as well as the redistribution of organic matter via physical mixing processes and via migration. He points out knowledge gaps that affect estimates of the biological pump, and potential means to address them.

Organic biogeochemistry of sedimentary environments and sedimentary organic matter is discussed in four articles. In a study of bottom waters and sediment porewaters at sites spanning the eastern to western Fram Strait, Rossel et al. report DOC concentrations and molecular composition, finding that regional and interannual differences in sediment DOC concentration can be linked to surface productivity differences in this variably ice-covered region. Bao and Blattmann discuss insights gained from and challenges remaining to using natural abundance radiocarbon (^{14}C) of sinking POM and sedimentary

OM to better characterize source-to-sink dynamics in the contemporary ocean, using the East Asian Seas as model systems. Bacteriohopanepolyols (BHPs), which are important biomarkers for bacterial cell membranes, are investigated by Kusch, Sepulveda et al.; Kusch, Benthien et al. in density-fractionated sediments from the highly dynamic Mississippi River Delta and adjacent coastal Gulf of Mexico to assess the provenance and hydrodynamic sorting of particulate matter as it is transported across the continental shelf. Arnosti et al. discuss unsolved questions related to sedimentary microbial communities and uncharacterized sedimentary organic matter, and suggest several specific research focal points that would help answer these questions.

Recent progress in application of new analytical methodologies to marine organic biogeochemistry is reported in the final four articles. Rattray and Smittenberg describe an improved high-pressure liquid chromatography approach for measuring the analytically challenging diversity of structural and stereoisomers of glycerol dialkyl glycerol tetraethers. These compounds have gained wide usage as biomarkers in marine and terrestrial research. The remaining three articles address natural abundance radiocarbon (^{14}C) measurements, particularly at the compound-specific level. Blattmann and Ishikawa discuss how compound-specific radiocarbon analysis can shed light on the turnover, age, and sources of a range of biomarkers in various environmental matrices. They particularly address the research potential of amino acid-specific radiocarbon analysis to investigate the biogeochemistry of food webs and sedimentary organic carbon. Although a key requirement for accurate determination of carbon transfer during manipulative experiments using compound-specific radiocarbon analysis is the availability of authentic biomarker standards of known natural abundance ^{14}C compositions, Kusch et al. point out the challenges to obtaining such standards in light of pervasive ^{14}C contamination of blanks arising from preparative isolation of target biomarkers obtained from algal culturing experiments. Lastly, Blattmann et al. describe a new liquid chromatographic method for isolating individual amino acids from sedimentary material for radiocarbon dating to better understand the sources, cycling, and preservation of these important compounds in marine sediments.

This volume provides a brief indication of the current state of the art and suggestions for pathways forward for some of the pressing issues and questions related to production, transformation, and fate of organic matter in the ocean. We, the workshop organizers, hope that this special issue will form the basis of further discussion and will foster future cross-disciplinary research in marine organic biogeochemistry.

AUTHOR CONTRIBUTIONS

All authors listed have made a substantial, direct and intellectual contribution to the work, and approved it for publication.

ACKNOWLEDGMENTS

The Hanse-Wissenschaftskolleg, Delmenhorst, Germany, sponsored and provided funding for the Frontiers in Marine Organic Biogeochemistry workshop in April 2019, from which the articles in this special issue were derived. We especially thank Doris Meyerdierks and staff at the HWK who contributed substantially to the success of this workshop. The workshop was also funded by the Deutsche Forschungsgemeinschaft (DFG, German Research Foundation)—project number: 422798570. The Geochemical Society provided additional funding for the conference.

REFERENCES

Andersen, N. R. (ed). (1977). Concepts in marine organic chemistry. *Mar. Chem.* 5, 303–638. doi: 10.1016/0304-4203(77)90025-1

Benner, R. H., Lee, C., and Wakeham, S. G. (eds.). (2004). New approaches in marine organic biogeochemistry: a tribute to the life and science of John I. Hedges. *Mar. Chem.* 92, 1–374. Available online at: https://www.sciencedirect.com/journal/marine-chemistry/vol/92/issue/1

Farrington, J. W. (1992). Overview and key recommendations. Marine organic geochemistry workshop, January 1990. *Mar. Chem.* 39, 5–9. doi: 10.1016/0304-4203(92)90089-S

Hedges, J. I., Eglinton, G., Hatcher, P. G., Kirchman, D. L., Arnosti, C., Derenne, S., et al. (2000). The molecularly-uncharacterized component of nonliving organic matter in natural environments. *Org. Geochem.* 31, 945–958. doi: 10.1016/S0146-6380(00)00096-6

Wakeham, S. G., and Lee, C. (2019). Limits of our knowledge, Part 2: selected frontiers in marine organic biogeochemistry. *Mar. Chem.* 212, 16–46. doi: 10.1016/j.marchem.2019.02.005

Conflict of Interest: The authors declare that the research was conducted in the absence of any commercial or financial relationships that could be construed as a potential conflict of interest.

frontiers in Marine Science

MINI REVIEW
published: 09 October 2019
doi: 10.3389/fmars.2019.00634

Pathways of Organic Carbon Downward Transport by the Oceanic Biological Carbon Pump

*Frédéric A. C. Le Moigne**

Mediterranean Institute of Oceanography, UM 110, Aix-Marseille Université, CNRS, IRD, Marseille, France

The oceanic biological carbon pump (BCP) regulates the Earth carbon cycle by transporting part of the photosynthetically fixed CO_2 into the deep ocean. Suppressing this mechanism would result in an important increase of atmospheric CO_2 level. The BCP occurs mainly in the form of (1) organic carbon (OC) particles sinking out the surface ocean, of (2) neutrally buoyant OC (dissolved or particulate) entrained by downward water masses movements and/or mixing, and of (3) active transport of OC by migrating animals such as zooplankton and fishes. These various pools of OC differ in size since their sinking, production and decomposition rates vary spatially and temporally. Moreover, the OC transported to depths via these various export pathways as well as their decomposition pathways all have different ecological origins and therefore may response differently to climate changes. Currently, most ocean biogeochemical models do not resolve these various of OC pathways explicitly; rather, they imply that OC is therein created and destroyed equally. In addition, the organic composition of these various pools is largely unknown, especially at depths below 500 m. Here, known processes of OC export from the surface ocean to the mesopelagic zone (100–1000 m) are briefly reviewed. Three OC export pathways and some of their sub-categories are considered. I refer to published studies of OC fluxes associated with the specific downward export pathways and identify gaps that need to be addressed to better understand the OC fluxes associated with the BCP.

Keywords: plankton, biogeochemical processes, carbon cycle, ecological process, biological carbon pump

OPEN ACCESS

Edited by:
Stuart Wakeham,
University of Georgia, United States

Reviewed by:
Emma Louise Cavan,
University of Tasmania, Australia
Adrian Benedict Burd,
University of Georgia, United States

***Correspondence:**
Frédéric A. C. Le Moigne
frederic.lemoigne@mio.osupytheas.fr

Specialty section:
This article was submitted to Marine Biogeochemistry, a section of the journal Frontiers in Marine Science

Received: *02 July 2019*
Accepted: *27 September 2019*
Published: *09 October 2019*

Citation:
Le Moigne FAC (2019) Pathways of Organic Carbon Downward Transport by the Oceanic Biological Carbon Pump. Front. Mar. Sci. 6:634. doi: 10.3389/fmars.2019.00634

INTRODUCTION

The oceanic biological carbon pump (BCP) is a complex mechanism regulating the Earth carbon (C) cycle by sequestrating part of the photosynthetically fixed CO_2 into the deep ocean and the seafloor. Suppressing this mechanism would increase the current levels of atmospheric CO_2 level by about 50% (Sarmiento et al., 2004; Parekh et al., 2006). Currently, the variability in the proportion of surface primary production (PP) leaving the euphotic zone and the amount of organic carbon (OC) exported to a certain depth via the BCP are challenging to explain. This prevents robust predictions of how C cycle, and hence climate, will change in the future.

Three major forms of the BCP are distinguished: (i) gravitational, (ii) mixing and (iii) migration. The gravitational pump (i) involves downward sinking of the OC contained in various particles

(POC) of planktonic origin from the surface ocean to depth due to their large size and/or high density (Siegel et al., 2016). This sinking POC is termed "marine snow" and can be made of single phytoplankton cells (DiTullio et al., 2000; Rembauville et al., 2016; Leblanc et al., 2018), various types of aggregates resulting from coagulation processes (Alldredge and Jackson, 1995; Riley et al., 2012; Laurenceau-Cornec et al., 2015) and zooplankton fecal pellets (FP) (Turner, 2002; Cavan et al., 2015). The mixing pump (ii) occurs when neutrally buoyant OC is transported to depth by downward-moving water masses and/or mixing. This OC is either dissolved (DOC) or entrained in particles which are too small in size or positively buoyant relative to seawater to sink on their own (Hansell et al., 2009; Le Moigne et al., 2016). The physical mechanisms that transport the OC downward can be either diapycnal with DOC diffusing out of the surface waters, or isopycnal, when water mass movements eddies and/or mixed layer bring DOC and/or suspended particles to depth (Hansell et al., 2009; Omand et al., 2015; Dall'Olmo et al., 2016). (iii) Diurnal vertical migration (DVM) of zooplankton and fish is a common feature in oceanic ecosystems (Longhurst, 1991; Steinberg, 2000; Landry and Calbet, 2004). In order to avoid predation, swimmers feed at night in surface waters and defecate deeper in the mesopelagic during the day. Doing so, they actively transport OC into the ocean's interior.

The presence, absence, and dominance of each of these different export pathways are controlled by biological (Piontek et al., 2014; Agusti et al., 2015; Le Moigne et al., 2016), chemical (Edwards et al., 2015), ecological (Cavan et al., 2015; Guidi et al., 2016), and physical (Levy et al., 2013; Taucher et al., 2014; Dall'Olmo et al., 2016) processes. They all vary in time and space and at depth. Most of these processes, however, are still poorly understood which hinders mechanistic predictions of the magnitude of the downward OC fluxes. At the base of the euphotic zone, the sinking of particles (termed gravitational flux) dominate the amount of OC (Giering et al., 2014). However, in the end of winter, the OC flux is induced by the so-called mixed layer pump which is driven by the seasonal entrainment of surface waters in deeper layers (Gardner et al., 1995) and can supply a substantial amount of OC to the deep ocean. Also, while globally the proportion of OC transported by migrating zooplankton and larger organisms relative to total OC flux is $<$20%, this active flux can occasionally dominate the total OC flux [(Aumont et al., 2018) and references therein].

These examples demonstrate the need for more systematic and simultaneous knowledge (ecological, biological, and geochemical) of the various pathways of OC export and at a given location and time. As such, the various individual export pathways (Siegel et al., 2016) for POC sinking from the euphotic zone to the mesopelagic and below have to be quantified. This would, for example, improve our understanding of the imbalance between supply and metabolic demand of OC (Steinberg et al., 2008; Burd et al., 2010; Collins et al., 2015) and the discrepancy between observed and modeled O_2 concentration in the mesopelagic zone (Gutknecht and Perruche, 2016). Currently our knowledge of the processes occurring in of the mesopelagic zone is incomplete despite its importance for the air sea carbon balance (Kwon et al., 2009). In this mini-review, I list the OC fluxes associated to the specific downward export pathways published in literature. Missing knowledge in estimates of specific export pathways that need to be addressed to better understand the OC fluxes associated with the BCP are identified.

THE GRAVITATIONAL PUMP FLUX

As stated above, the gravitational flux of OC occurs in the form of various particles of planktonic origin sinking from the surface ocean due to their large size and/or high density. The gravitational pump includes particles that are single phytoplankton cells, various types of aggregates, and zooplankton dejections termed fecal pellets.

Fecal Pellets Flux

Specific OC flux associated with zooplankton fecal pellets is relatively easy to measure. Fecal pellets are compact and have distinctive shapes and thus can easily identified and picked out from samples collected using different types of sediment traps (Refaeli et al., 2008; Turner, 2015). However, some pellets can experience degradation in moored sediment traps cups and are not being counted as such (Wilson et al., 2008). This may result in underestimation of the flux of fecal pellets. The OC flux associated with fecal pellets in the global ocean from 0 to 3500 m depth (n = 374) are shown in **Figure 1** and also compiled in **Supplementary Table S2**. The fluxes classified by depth are presented in **Figures 1A–C**. Note that **Figure 1** only presents the values that were readily available in the literature. I consider that the factors used by the authors to convert fecal pellets count into OC are correct. Counts of fecal pellets observed in various sediment traps if they were not converted to OC fluxes are not reported.

Figure 1A shows the OC flux from 0 to 100 m depth. The OC flux varies from 0–218 mg C m^{-2} d^{-1} with the large OC fecal pellets fluxes recorded in high latitudes [e.g., Kerguelen Island in the Southern Ocean (Ebersbach and Trull, 2008; Laurenceau-Cornec et al., 2015)] and upwelling zones (Le Moigne et al., 2018). Yet, some studies also report absence of fecal pellets in high latitudes regions [e.g., (Cavan et al., 2015)]. Fecal pellets fluxes are significantly lower in mesotrophic and oligotrophic regions (Carroll et al., 1998; Shatova et al., 2012). In the upper mesopelagic zone (100–500 m; **Figure 1B**), the OC flux of fecal pellets ranges from 0 to 71 mg C m^{-2} d^{-1} and on regional scale broadly follows the pattern observed in the upper ocean. At depths below 500 m (**Figure 1C**), fecal pellet fluxes are generally low (0 to 1.5 mg C m^{-2} d^{-1}). No reports of the OC flux below 500 m exist for the high latitude ocean. Fecal pellets sink fast and resist degradation well even under high hydrostatic pressure (Turley and Mackie, 1994; Tamburini et al., 2006; Riou et al., 2017) and thus their flux is expected to be high below 500 m. Coprorhexy (fragmentation of pellets by copepods) and/or coprophagy (ingestion of fecal pellets by copepods) could, however, lower the abundance of fecal pellets and hence the associated OC flux in the lower mesopelagic (Iversen and Poulsen, 2007). Additionally, such a trend could

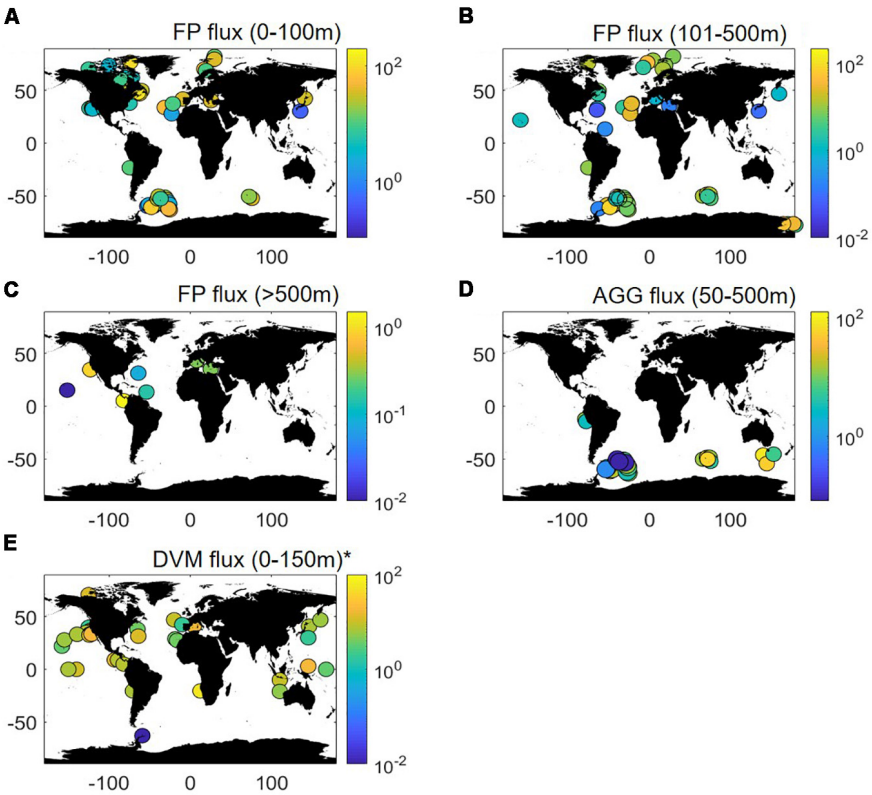

FIGURE 1 | Global distribution of downward flux of organic carbon (OC; units are mg of OC m^{-2} d^{-1}) associated to various export pathways (see main text). Panel **(A)** represents the flux associated to fecal pellets (FP) collected between 0–100 m; **(B)** 101–500 m and **(C)** below 500 m. Panel **(D)** represents the flux of aggregates collected between 50–500 m. Panel **(E)** represents the flux associated to vertically migrating organisms. *Replotted after Aumont et al. (2018). All references/sources are provided in the main text and in **Supplementary Tables S1–S3**.

also result from fish and large zooplankton species (such as siphonophores) feeding on the pellet flux (Proud et al., 2019).

Phytoplankton Cells Flux

Turbulent mixing and buoyancy regulation tend to retain single phytoplankton single cells tend in the surface ocean. However, despite of their small Reynolds number [describes the nature of the surrounding flow and its fall velocity (Stokes, 1851)], some intact cells (not grazed or aggregated) are found in sediment traps. This can happen to single live or dead phytoplankton cells, resting spores or cysts, and colonies.

Phytoplankton cells sink into the ocean's interior as single cells which are live, senescent and/or dead. DiTullio et al. (2000) observed single cells of *Phaeocystis antarctica* in the lower mesopelagic zone (500–600 m) in the Ross sea and concluded that they were exported rapidly and alive following a large *Phaeocystis antarctica* bloom. However, the mechanism delivering these cells down to the mesopelagic zone is unclear. Although physical processes could entrain surface cells to depth (see following sections), the cells observed at 500 m were still photosynthesizing, which suggests that their export to depth was likely too rapid to be induced by a physical process. Phytoplankton cells also sink dead. For example (Salter et al., 2007), observed dead cells of large diatoms *Eucampia antarctica* being selectively exported relative to the surface phytoplankton community in the Southern Ocean. These diatoms were exported rapidly owing to their heavily silicified, and thus dense, frustule (Salter et al., 2007). Phytoplankton resting spores and/or cysts are also exported from the surface ocean down to bathypelagic/abyssal depths (>1000 m). They are formed strategically by some phytoplankton in response to nutrient limitation and contain significant amounts of OC. In sediment traps located within an iron-fertilized bloom in the Southern Ocean near the Kerguelen Islands, Rembauville et al. (2016) measured OC fluxes associated with resting spores of diatoms *Chaetoceros Hyalochaete* or *Thalassiosira Antarctica*. The resting spores of a single species can account for up to 90% of the total gravitational OC flux (Rembauville et al., 2016). Acantharian cysts (unicellular organisms related to Radiolaria producing celestite, the densest biomineral in the ocean) were abundant in deep sediment trap material in the Iceland Basin (Martin et al., 2010) and the Southern Ocean (Belcher et al., 2018). High cyst flux was restricted to only 2 weeks but contributed up to half of the total gravitational OC flux during this period (Martin et al., 2010; Decelle et al., 2013). The Acantarian cysts are made of dense celestite which ensures their fast sedimentation to the bathypelagic depths. Phytoplankton cell colonies and chains are also observed in sediment traps samples. Laurenceau-Cornec

et al. (2015) found chains of the pennate diatoms *Fragilariopsis* sp. in the Southern Ocean, while Pabortsava et al. (2017) collected intact colonies of nitrogen-fixing *Trichodesmium* species in the deep traps (3000 m) collecting in the North Atlantic gyre.

However, all published sediment trap studies do not necessarily report the OC flux associated with phytoplankton cell export. This is because phytoplankton enumeration methods require a substantial amount of cells to be identified in order to provide robust estimates. This is not always possible, and counting is often performed only on a small area imaged under microscopes (Leblanc et al., 2018). Quantification of the cell size (or biovolume) to OC content for a given species is also not straightforward (Gosselain et al., 2000) and varies substantially depending on upper ocean nutrients regime (Davidson and Marchant, 1992). Grouping phytoplankton cell flux in an ecologically meaningful way might be especially advantageous for numerical models as providing the OC flux associated with sinking cells of individual phytoplankton species is computationally inefficient. Future effort may require grouping phytoplankton cell flux functionally based on size, nutrients affinity, and ecological/physiological traits. Therefore, no global maps of the OC flux associated to sinking phytoplankton cells are provided here.

Aggregate Flux

Evaluating OC flux associated with aggregates is challenging as their structure is often fragile and erratic (Alldredge, 1998). In moored sediment traps, marine aggregates lose their shapes. Unlike fecal pellets (see section above), aggregates in the bulk sediment trap material are clumped and thus difficult to pick out individually. The use of polyacrylamide gels as preservative in the sediment traps collection tubes/cups has, however, enabled significant improvements of estimating the aggregates flux (Lundsgaard, 1995; Waite et al., 2000). These highly viscous gels preserve the morphological characteristics of marine particles as they sink through the water column and into collection cups. Gels provide a slow deceleration of sinking particles and isolate particles allowing for quantitative image analysis (Ebersbach and Trull, 2008).

Only few studies quantified aggregate-associated OC flux to date. Most estimates are from the Southern Ocean (Ebersbach and Trull, 2008; Cavan et al., 2015; Laurenceau-Cornec et al., 2015) and upwellings (Le Moigne et al., 2018). Largest OC fluxes (110 mg m^{-2} d^{-1}) were recorded in the Sub-Antarctic zone south of Tasmania (Ebersbach et al., 2011). Large fluxes were also observed in the vicinity of the Kerguelen islands (Laurenceau-Cornec et al., 2015) and in the South Georgia bloom (Cavan et al., 2015) (**Supplementary Table S1**). Vertically, the flux of aggregates rarely shows a clear decrease with depth indicating significant changes in aggregates dynamics with depth. This highlights the importance of disaggregation and aggregation processes. Although overall disaggregation vastly dominates particles dynamics below the surface ocean (Stemmann et al., 2004; Lam and Marchal, 2015), aggregation by differential settling (Lam and Marchal, 2015) does occur in the mesopelagic zone. In addition, while the ratio of disaggregation to aggregation increases with depth, it tends to decrease with increasing PP (Lam and Marchal, 2015). This may partly explain why the vertical fluxes of aggregates presented here show limited decrease with depth.

Quantification of the aggregate-associated OC flux requires the knowledge of the relationship between aggregates biovolume to OC content, which is not straightforward (Alldredge and Crocker, 1995; Alldredge and Jackson, 1995). Laurenceau-Cornec et al. (2015) report particle-specific relationships compiled in the literature from which the OC content of aggregates can be estimated (Alldredge, 1998; Ebersbach and Trull, 2008). However, the database on the aggregates biovolume to OC content has to be significantly expanded to improve the statistical confidence of this relationship and also considering more diverse aggregates types. For example, tools like the Marine Snow Catcher (Riley et al., 2012; Cavan et al., 2015) could be used to collect particles and quantify their size, geochemical content and biological characteristics. The amount of particles collected per deployment can be small with the amount of OC entrained being too low to measure analytically (McDonnell et al., 2015). This device also likely misses the largest particles but pulling particles from multiple deployments or using devices of a larger volume (Cavan et al., 2017) could, however, resolve this issue.

THE MIXING FLUX

Several ocean physical processes transport slow-sinking, neutrally buoyant or dissolved OC (DOC) from the surface where they are produced to the mesopelagic zone. Recently, "mixing fluxes" gained more importance (see following references). This is mainly due the development of semi-automated platforms and devices which enabled high frequency sizing of particles (Picheral et al., 2010; Claustre et al., 2011). Large-scale ocean circulation is also one of the processes transporting particles produced in the surface to ocean's interior. For instance, regions of deep water formation are hotspots for such transport (Levy et al., 2013).

The mixed layer pump is another process that redistributes dissolved OC, neutrally buoyant or slow-sinking organic matter down the water column (Dall'Olmo et al., 2016). This process occurs during transient stratifications at the start of the productive season when suspended POC first accumulates in surface, and then redistributed throughout the water column by deep mixing. Globally, the mixed layer pump is responsible for a flux of 0.5 Gt C yr^{-1}. This process supplies POC mainly to locations with deep winter mixing such as the North Atlantic Ocean or the Southern Ocean (Dall'Olmo et al., 2016).

The water mass subduction induced by eddies also pumps POC into the mesopelagic zone. Omand et al. (2015) quantified the amount of suspended POC sinking following eddy driven subduction in the North Atlantic. In essence, suspended POC produced in surface sink along tilted isopycnals. Globally, eddy-driven subduction of POC is responsible for an export flux of ~1 Gt C yr^{-1} (Omand et al., 2015). Altogether, these processes may export up to 2 Gt of POC yr^{-1}, nearly a third of the gravitational flux (Boyd et al., 2019).

Large-scale circulation, mixing and eddies subduction also transport DOC beneath the surface ocean. Examining large

scale variability of DOC concentrations, Hansell et al. (2009) estimated that DOC export represents 20% that of gravitational POC export flux in the global ocean. However, the amount of DOC transported by processes such as eddy driven subduction and mixed layer pump (see references above) have poor spatial coverage both on local and global scales. Using an artificial neural network, Roshan and DeVries (2017) reconstructed global DOC concentrations distribution. Here, DOC production and export fluxes were estimated by coupling reconstructed DOC concentrations to a global ocean circulation model (DeVries and Primeau, 2011). Large annual DOC export rates were shown in the tropics (50–80 mg of OC m^{-2} d^{-1}) and low in high latitudes (0–40 mg of OC m^{-2} d^{-1}), contrary to findings by Dall'Olmo et al. (2016) and Omand et al. (2015). Their model, however, extrapolated DOC concentrations measured during summer to a global scale. This may have limited the effect of the aforementioned physical processes. More work is required to estimate the annual flux of DOC from the surface ocean.

The global maps of the OC flux associated to the various mixing fluxes are not shown here but are available in the literature cited above.

THE ACTIVE MIGRATION FLUX

The concept of active flux by migrating organisms (also known as "swimmers") in the mesopelagic is based on widespread observations of DVM of zooplankton and fish caught in nets (Longhurst, 1991; Steinberg, 2000; Landry and Calbet, 2004). In essence, to avoid predation swimmers feed at night in surface waters and defecate deeper in the mesopelagic during the day (Steinberg and Landry, 2017). Inverted DVM and desynchronized vertical migration do exist (Neill, 1990; Cohen and Forward, 2016), however, typical DVM as described above are more common in marine systems. This actively supplies OC to depth with minimizing decomposition. To date, estimates of DVM have mostly been focused on mesozooplankton because they are readily caught in multiple opening/closing towed nets (Tarling et al., 2002). DVM is a difficult process to model (Hansen and Visser, 2016), however, this field has made significant progresses recently (Aumont et al., 2018; Archibald et al., 2019; Gorgues et al., 2019).

The active transport of OC by migrating mesozooplankton can contribute up to 40% of the gravitational flux (Stukel et al., 2013) with global estimates ranging from 0.2 to 71 mg m^{-2} d^{-1} (Aumont et al., 2018; **Figure 1E** and **Supplementary Table S3**). Most studies of mesozooplankton associated OC flux were conducted in coastal and upwelling regions, while data from high latitudes and polar waters are scarce (**Figure 1E**). The largest flux is recorded in the Benguela upwelling system while the smallest are observed near the Antarctic peninsula. Large DVM fluxes in upwelling system is counterintuitive given that these waters are productive but often poorly oxygenated below surface. However, some migrating organisms can survive with little oxygen concentrations by adopting adaptive metabolic strategies (Bianchi et al., 2013, 2014; Kiko et al., 2015). Excluding the extreme values of 0.2 and 71 mg m^{-2} d^{-1}, the OC fluxes associated with migratory organisms appear to be relatively homogeneous and in the order of 9.8 ± 7.3 mg C m^{-2} d^{-1}.

The OC flux associated to DVM of both macrozooplankton and fishes are, however, more challenging to estimate. These organisms are not always quantitatively represented in net catchments (Sameoto et al., 2007). Acoustics techniques are promising for estimating these (Lebourges-Dhaussy and Josse, 2008; Lebourges-Dhaussy et al., 2014) and dedicated surveys performed on large scales are starting to emerge (Bianchi et al., 2013; Irigoien et al., 2014). Most of the available observations involve mesozooplankton and/or micronekton. The whole community is, however, represented only by a limited number of datapoints (Aumont et al., 2018). Moreover, these fluxes mostly represent the active flux between the surface and the upper mesopelagic zone. DVM OC fluxes between surface and the lower mesopelagic zone are more rarely estimated. This is despite the presence of migrating species deeper down in the mesopelagic zone (Sutton, 2013; D'Elia et al., 2016).

CONCLUSION AND PERSPECTIVES

In the last decade, numerous studies highlighted the importance and the complexity of the BCP. As our understanding of the BCP advances, new research directions into the functioning of the BCP also emerged building on knowledge about the chemical composition of the bulk export fluxes. For instance, the importance of the types, transport pathways, particles associated communities, and fates of sinking particles have become apparent thanks to technological breakthroughs, and thus need further research. Known processes of OC export from the surface ocean to the mesopelagic zone (100–1000 m) were reviewed. I provided a list of the published OC fluxes associated to the specific downward export pathways involving zooplankton fecal pellets, aggregates, and by vertical migrating organisms. However, while data on phytoplankton cell flux exist, estimates of the OC flux associated to sinking single cells are challenging. Moreover, processes responsible for the sinking of phytoplankton single cells are unclear. I report global estimates of the physically driven processes that supply slow sinking and/or neutrally buoyant and dissolved OC to the dark ocean. However, locally, their contribution relative to the total gravitational flux is often missing, especially in high latitude regions. In addition, most estimates of vertical migration concern only part of the community and organisms migrating deeper are overlooked.

AUTHOR CONTRIBUTIONS

The author confirms being the sole contributor of this work and has approved it for publication.

FUNDING

This work was funded by the Deutsche Forschungsgemeinschaft (DFG, German Research Foundation) – Project Number: 422798570 and by the Hanse-Wissenschaftskolleg, Delmenhorst.

ACKNOWLEDGMENTS

I would like to thank the Cindy Lee, Stuart Wakeham, Kai-Uwe Hinrichs, Carol Arnosti, Anne Pearson, and Thorsten Dittmar for organizing the Marine Organic Biogeochemistry workshop held at the Hanse-Wissenschaftskolleg, Delmenhorst, Germany, April 27 to 30th 2019. I thank Emmanuel Laurenceau-Cornec (University of Tasmania, Institute for Marine and Antarctic Studies, Hobart, Australia), Katsiaryna Pabortsava (NOC, Southampton, United-Kingdom), and Morten Iversen (MARUM, AWI, Bremerhaven, Germany) for advices on aggregates fluxes, Olivier Aumont (IRD, LOCEAN, Paris, France) for sharing data on migration fluxes and the two reviewers for their constructive comments.

SUPPLEMENTARY MATERIAL

The Supplementary Material for this article can be found online at: https://www.frontiersin.org/articles/10.3389/fmars.2019.00634/full#supplementary-material

REFERENCES

Agusti, S., González-Gordillo, J. I., Vaqué, D., Estrada, M., Cerezo, M. I., Salazar, J., et al. (2015). Ubiquitous healthy diatoms in the deep sea confirm deep carbon injection by the biological pump. *Nat. Commun.* 6:7608. doi: 10.1038/ncomms8608

Alldredge, A. (1998). The carbon, nitrogen and mass content of marine snow as a function of aggregate size. *Deep. Res. I* 45, 529–541. doi: 10.1016/s0967-0637(97)00048-4

Alldredge, A. L., and Crocker, K. M. (1995). Why do sinking mucilage aggregates accumulate in the water column. *Sci. Total Environ.* 165, 15–22. doi: 10.1016/0048-9697(95)04539-d

Alldredge, A. L., and Jackson, G. A. (1995). Aggregation in marine systems - preface. *Deep. Res. Part II Top. Stud. Oceanogr.* 42, 1–7.

Archibald, K. M., Siegel, D. A., and Doney, S. C. (2019). Modeling the impact of zooplankton diel vertical migration on the carbon export flux of the biological pump. *Global Biogeochem. Cycles* 33, 181–199. doi: 10.1029/2018gb005983

Aumont, O., Maury, O., Lefort, S., and Bopp, L. (2018). Evaluating the potential impacts of the diurnal vertical migration by marine organisms on marine biogeochemistry. *Global Biogeochem. Cycles* 32, 1622–1643. doi: 10.1029/2018GB005886

Belcher, A., Manno, C., Thorpe, S., and Tarling, G. (2018). Acantharian cysts: high flux occurrence in the bathypelagic zone of the Scotia Sea. *Southern Ocean. Mar. Biol.* 165:117. doi: 10.1007/s00227-018-3376-1

Bianchi, D., Babbin, A. R., and Galbraith, E. D. (2014). Enhancement of anammox by the excretion of diel vertical migrators. *Proc. Natl. Acad. Sci. U.S.A.* 111, 15653–15658. doi: 10.1073/pnas.1410790111

Bianchi, D., Galbraith, E. D., Carozza, D. A., Mislan, K. A. S., and Stock, C. A. (2013). Intensification of open-ocean oxygen depletion by vertically migrating animals. *Nat. Geosci.* 6, 545–548. doi: 10.1038/ngeo1837

Boyd, P. W., Claustre, H., Levy, M., Siegel, D. A., and Weber, T. (2019). Multi-faceted particle pumps drive carbon sequestration in the ocean. *Nature* 568, 327–335. doi: 10.1038/s41586-019-1098-2

Burd, A., Hansell, D. A., Steinberg, D. K., Anderson, T. R., Aristegui, J., Baltar, F., et al. (2010). Assessing the apparent imbalance between geochemical and biochemical indicators of meso- and bathypelagic biological activity: what the @$# is wrong with present calculations of carbon budgets? *Deep sea Res. II* 57, 1557–1571. doi: 10.1016/j.dsr2.2010.02.022

Carroll, M. L., Miquel, J. C., and Fowler, S. W. (1998). Seasonal patterns and depth-specific trends of zooplankton fecal pellet fluxes in the northwestern Mediterranean Sea. *Deep. Res. Part I Oceanogr. Res. Pap.* 45, 1303–1318. doi: 10.1016/S0967-0637(98)00013-2

Cavan, E., Le Moigne, F. A. C., Poulton, A. J., Daniels, C. J., Fragoso, G., and Sanders, R. J. (2015). Zooplankton fecal pellets control the attenuation of particulate organic carbon flux in the Scotia Sea, Southern Ocean. *Geophys. Res. Lett.* 42, 821–830. doi: 10.1002/2014GL062744

Cavan, E., Trimmer, M., Shelley, F., and Sanders, R. (2017). Remineralization of particulate organic carbon in an ocean oxygen minimum zone. *Nat. Commun.* 8:14847. doi: 10.1038/ncomms14847

Claustre, H., Antoine, D., Boehme, L., Boss, E., D'Ortenzio, F., Fanton, D., et al. (2011). "Guidelines towards an integrated ocean observation system for ecosystems and biogeochemical cycles," in *Proceedings of the OceanObs'09: Sustained Ocean Observations and Information for Society*, Vol. 1, (Venice: ESA Publication), 21–25.

Cohen, J. H., and Forward, R. B. (2016). Zooplankton diel vertical migration - a review of proximate control. *Oceanogr. Mar. Biol.* 47, 77–109. doi: 10.1201/9781420094220.ch2

Collins, J. R., Edwards, B. R., Thamatrakoln, K., Ossonlinski, J. E., DiTullio, G. R., Bidle, K. D., et al. (2015). The multiple fates of sinking particles in the North Atlantic Ocean. *Global Biogeochem. Cycles* 29, 1471–1494. doi: 10.1002/2014gb005037

Dall'Olmo, G., Dingle, J., Polimene, L., Brewin, R. J. W., and Claustre, H. (2016). Substantial energy input to the mesopelagic ecosystem from the seasonal mixed-layer pump. *Nat. Geosci.* 9, 820–823. doi: 10.1038/NGEO2818

Davidson, A. T., and Marchant, H. J. (1992). Protist abundance and carbon concentration during a phaeocystis-dominated bloom at an antarctic coastal site. *Polar Biol.* 12, 387–395.

Decelle, J., Martin, P., Pabortsava, K., Pond, D. W., Tarling, G., Mahe, F., et al. (2013). Diversity, ecology and biogeochemistry of cyst-forming acantharia (Radiolaria) in the oceans. *PLoS One* 8:e53598. doi: 10.1371/journal.pone.0053598

D'Elia, M., Warren, J. D., Rodriguez-Pinto, I., Sutton, T. T., Cook, A., and Boswell, K. M. (2016). Diel variation in the vertical distribution of deep-water scattering layers in the Gulf of Mexico. *Deep. Res. Part I Oceanogr. Res. Pap.* 115, 91–102. doi: 10.1016/j.dsr.2016.05.014

DeVries, T., and Primeau, F. (2011). Dynamically and observationally constrained estimates of water-mass distributions and ages in the global ocean. *J. Phys. Oceanogr.* 41, 2381–2401. doi: 10.1175/jpo-d-10-05011.1

DiTullio, G. R., Grebmeier, J. M., Arrigo, K. R., Lizotte, M. P., Robinson, D. H., Leventer, A., et al. (2000). Rapid and early export of Phaeocystis antarctica blooms in the Ross Sea, Antarctica. *Nature* 404, 595–598. doi: 10.1038/35007061

Ebersbach, F., and Trull, T. W. (2008). Sinking particle properties from polyacrylamide gels during the kerguelen ocean and plateau compared study (KEOPS): zooplankton control of carbon export in an area of persistent natural iron inputs in the Southern Ocean. *Limnol. Oceanogr.* 53, 212–224. doi: 10.4319/lo.2008.53.1.0212

Ebersbach, F., Trull, T. W., Davies, D. M., and Bray, S. G. (2011). Controls on mesopelagic particle fluxes in the Sub-Antarctic and Polar Frontal Zones in the Southern Ocean south of Australia in summer – Perspectives from free-drifting sediment traps. *Deep Sea Res. II* 58, 2260–2276. doi: 10.1016/j.dsr2.2011.05.025

Edwards, B. R., Bidle, K. D., and Van Mooy, B. A. S. (2015). Dose dependent regulation of microbial activity on sinking particles by polyunsaturated aldehydes: implications for the carbon cycle. *PNAS* 112, 5909–5914. doi: 10.1073/pnas.1422664112

Gardner, W. D., Chung, S. P., Richardson, M. J., and Walsh, I. D. (1995). The oceanic mixed-layer pump. *Deep Sea Res. Part II Top. Stud. Oceanogr.* 42, 757–765.

Giering, S. L. C., Sanders, R. J., Lampitt, R. S., Anderson, T. R., Tamburini, C., Boutrif, M., et al. (2014). Reconciliation of the carbon budget in the ocean's twilight zone. *Nature* 507, 480–483. doi: 10.1038/nature13123

Gorgues, T., Aumont, O., and Memery, L. (2019). Simulated changes in the particulate carbon export efficiency due to diel vertical migration of zooplankton in the North Atlantic. *Geophys. Res. Lett.* 46, 5387–5395. doi: 10.1029/2018GL081748

Gosselain, V., Hamilton, P. B., and Descy, J. P. (2000). Estimating phytoplankton carbon from microscopic counts: an application for riverine systems. *Hydrobiologia*. 438, 75–90. doi: 10.1023/A:1004161928957

Guidi, L., Chaffron, S., Bittner, L., Eveillard, D., Larhlimi, A., Roux, S., et al. (2016). Plankton networks driving carbon export in the oligotrophic ocean. *Nature* 532, 465–470. doi: 10.1038/nature16942

Gutknecht, E., and Perruche, C. (2016). "Evaluation de la configuration globale Mercator Océan à partir des données Bio-Argo," in *Paper presented at the Annuel Meeting of the NAOS 21-22/09/2016*, Belgium.

Hansell, D. A., Carlson, C. A., Repeta, D. J., and Schlitzer, R. (2009). Dissolved organic matter in the ocean: a controversy stimulates New Insights. *Oceanography* 22, 202–211. doi: 10.5670/oceanog.2009.109

Hansen, A. N., and Visser, A. W. (2016). Carbon export by vertically migrating zooplankton: an optimal behavior model. *Limnol. Oceanogr.* 61, 701–710. doi: 10.1002/lno.10249

Irigoien, X., Klevjer, T. A., Røstad, A., Martinez, U., Boyra, G., Acuña, J. L., et al. (2014). Large mesopelagic fishes biomass and trophic efficiency in the open ocean. *Nat. Commun.* 5:3271. doi: 10.1038/ncomms4271

Iversen, M. H., and Poulsen, L. K. (2007). Coprorhexy, coprophagy, and coprochaly in the copepods Calanus helgolandicus, Pseudocalanus elongatus, and Oithona similis. *Mar. Ecol. Prog. Ser.* 350, 79–89. doi: 10.3354/meps07095

Kiko, R., Hauss, H., Dengler, M., Sommer, S., and Melzner, F. (2015). The squat lobster *Pleuroncodes monodon* tolerates anoxic "dead zone" conditions off Peru. *Mar. Biol.* 162, 1913–1921. doi: 10.1007/s00227-015-2709-6

Kwon, E. Y., Primeau, F., and Sarmiento, J. L. (2009). The impact of remineralization depth on the air-sea carbon balance. *Nat. Geosci.* 2, 630–635. doi: 10.1038/ngeo612

Lam, P. J., and Marchal, O. (2015). Insights into particle cycling from thorium and particle data. *Ann. Rev. Mar. Sci.* 7, 159–184. doi: 10.1146/annurev-marine-010814-015623

Landry, M. R., and Calbet, A. (2004). Microzooplankton production in the oceans. *ICES J. Mar. Sci.* 61, 501–507. doi: 10.1016/j.icesjms.2004.03.011

Laurenceau-Cornec, E. C., Trull, T. W., Davies, D. M., Bray, S. G., Doran, J., Planchon, F., et al. (2015). The relative importance of phytoplankton aggregates and zooplankton fecal pellets to carbon export: insights from free-drifting sediment trap deployments in naturally iron-fertilised waters near the Kerguelen Plateau. *Biogeosciences* 12, 1007–1027. doi: 10.5194/bg-12-1007-2015

Leblanc, K., Quéguiner, B., Diaz, F., Cornet, V., Michel-Rodriguez, M., Durrieu De Madron, X., et al. (2018). Nanoplanktonic diatoms are globally overlooked but play a role in spring blooms and carbon export. *Nat. Commun.* 9: 953. doi: 10.1038/s41467-018-03376-9

Lebourges-Dhaussy, A., Huggett, J., Ockhuis, S., Roudaut, G., Josse, E., and Verheye, H. (2014). Zooplankton size and distribution within mesoscale structures in the Mozambique Channel: a comparative approach using the TAPS acoustic profiler, a multiple net sampler and ZooScan image analysis. *Deep. Res. Part II Top. Stud. Oceanogr.* 100, 136–152. doi: 10.1016/j.dsr2.2013.10.022

Lebourges-Dhaussy, A., and Josse, E. (2008). Acoustical methods that provide an integrated view of the marine ecosystem. *J. Acoust. Soc. Am.* 123:2992. doi: 10.1121/1.2932534

Le Moigne, F. A. C., Cisternas-Novoa, C., Laurenceau-Cornec, E. C., and Engel, A. (2018). "Pathways of gravitational particle export in the peruvian OMZ," in *Proceedings of the Ocean Deoxygenation Conference*, (Kiel: Kiel University).

Le Moigne, F. A. C., Henson, S. A., Cavan, E., Georges, C., Pabortsava, K., Achterberg, E. P., et al. (2016). What causes the inverse relationships between primary production and export efficiency in the southern ocean? *Geophys. Res. Lett.* 43, 4457–4466. doi: 10.1002/2016GL068480

Levy, M., Bopp, L., Karleskind, P., Resplandy, L., Ethe, C., and Pinsard, F. (2013). Physical pathways for carbon transfers between the surface mixed layer and the ocean interior. *Global Biogeochem. Cycles.* 27, 1001–1012. doi: 10.1002/gbc.20092

Longhurst, A. R. (1991). Large marine ecosystems - patterns, processes and yields. *Mar. Policy* 15, 377–378.

Lundsgaard, C. (1995). "Use of a high viscosity medium in studies of aggregates," in *Sediment trap studies in the Nordic countries 3. Proceedings of the Symposium on Seasonal Dynamics of Planktonic Ecosystems and Sedimentation in Coastal Nordic Waters*, eds S. Floderus, A. S. Heisakanen, M. Oleson, and P. Wassman, (Helsinki: Finnish Environment Agency), 141–152.

Martin, P., Allen, J. T., Cooper, M. J., Johns, D. G., Lampitt, R. S., Sanders, R., et al. (2010). Sedimentation of acantharian cysts in the Iceland Basin: strontium as a ballast for deep ocean particle flux, and implications for acantharian reproductive strategies. *Limnol. Oceanogr.* 55, 604–614. doi: 10.4319/lo.2009.55.2.0604

McDonnell, A. M. P., Lam, P. J., Lamborg, C. H., Buesseler, K. O., Sanders, R., and Riley, J. S. (2015). The oceanographic toolbox for the collection of sinking and suspended marine particles. *Prog. Oceanogr.* 133, 17–31. doi: 10.1016/j.pocean.2015.01.007

Neill, W. E. (1990). Induced vertical migration in copepods as a defence against invertebrate predation. *Nature* 345, 524–526. doi: 10.1038/345524a0

Omand, M. M., D'asaro, E., Lee, C., Perry, M. J., Briggs, N., Cetini, I., et al. (2015). Eddy-driven subduction exports particulate organic carbon from the spring bloom. *Science* 348, 222–225. doi: 10.1126/science.1260062

Pabortsava, K., Lampitt, R. S., Benson, J., Crowe, C., McLachlan, R., Le Moigne, F. A. C., et al. (2017). Carbon sequestration in the deep Atlantic enhanced by Saharan dust. *Nat. Geosci.* 10, 189–194. doi: 10.1038/ngeo2899

Parekh, P., Dutkiewicz, S., Follows, M. J., and Ito, T. (2006). Atmospheric carbon dioxide in a less dusty world. *Geophys. Res. Lett.* 33:L03610. doi: 10.1029/2005GL025098

Picheral, M., Guidi, L., Stemmann, L., Karl, D. M., Iddaoud, G., and Gorsky, G. (2010). The underwater vision profiler 5: an advanced instrument for high spatial resolution studies of particle size spectra and zooplankton. *Limnol. Oceanogr. Methods* 8, 462–473. doi: 10.4319/lom.2010.8.462

Piontek, J., Sperling, M., Nothig, E. M., and Engel, A. (2014). Regulation of bacterioplankton activity in Fram Strait (Arctic Ocean) during early summer: the role of organic matter supply and temperature. *J. Mar. Syst.* 132, 83–94. doi: 10.1016/j.jmarsys.2014.01.003

Proud, R., Handegard, N. O., Kloser, R. J., Cox, M. J., and Brierley, A. S. (2019). From siphonophores to deep scattering layers: uncertainty ranges for the estimation of global mesopelagic fish biomass. *ICES J. Mar. Sci.* 76, 718–733. doi: 10.1093/icesjms/fsy037

Refaeli, Y., Young, R. M., Turner, B. C., Duda, J., Field, K. A., and Bishop, J. M. (2008). The B cell antigen receptor and overexpression of MYC can cooperate in the genesis of B cell lymphomas. *PLoS Biol.* 6:e152. doi: 10.1371/journal.pbio.0060152

Rembauville, M., Manno, C., Tarling, G. A., Blain, S., and Salter, I. (2016). Strong contribution of diatom resting spores to deep-sea carbon transfer in naturally iron-fertilized waters downstream of South Georgia. *Deep Sea Res. I* 115, 22–35. doi: 10.1016/j.dsr.2016.05.002

Riley, J., Sanders, R., Marsay, C., Le Moigne, F. A. C., Achterberg, E., and Poulton, A. (2012). The relative contribution of fast and slow sinking particles to ocean carbon export. *Global Biogeochem. Cycles* 26:GB1026. doi: 10.1029/2011GB004085

Riou, V., Para, J., Garel, M., Guigue, C., Al Ali, B., Santinelli, C., et al. (2017). Biodegradation of *Emiliania huxleyi* aggregates by natural prokaryotic communities under increasing hydrostatic pressure. *Prog. Oceanogr.* 163, 271–281. doi: 10.1016/j.pocean.2017.01.005

Roshan, S., and DeVries, T. (2017). Efficient dissolved organic carbon production and export in the oligotrophic ocean. *Nat. Commun.* 8:2036. doi: 10.1038/s41467-017-02227-3

Salter, I., Lampitt, R. S., Sanders, R., Poulton, A., Kemp, A. E. S., Boorman, B., et al. (2007). Estimating carbon, silica and diatom export from a naturally fertilised phytoplankton bloom in the Southern Ocean using PELAGRA: a novel drifting sediment trap. *Deep. Res. Part Ii-Topical Stud. Oceanogr.* 54, 2233–2259. doi: 10.1016/j.dsr2.2007.06.008

Sameoto, D., Wiebe, P., Runge, J., Postel, L., Dunn, J., Miller, C., et al. (2007). "Collecting zooplankton," in *ICES Zooplankton Methodology Manual*, eds R. Harris, P. Wiebe, J. Lenz, H. R. Skjoldal, and M. Huntley, (San Diego, CA: Academic Press).

Sarmiento, J. L., Slater, R., Barber, R., Bopp, L., Doney, S. C., Hirst, A. C., et al. (2004). Response of ocean ecosystems to climate warming. *Global Biogeochem. Cycles* 18:GB3003. doi: 10.1029/2003GB002134

Shatova, O., Koweek, D., Conte, M. H., and Weber, J. C. (2012). Contribution of zooplankton fecal pellets to deep ocean particle flux in the Sargasso Sea

assessed using quantitative image analysis. *J. Plankton Res.* 34, 905–921. doi: 10.1093/plankt/fbs053

Siegel, D. A., Buesseler, K. O., Behrenfeld, M. J., Benitez-Nelson, C. R., Boss, E., Brzezinski, M. A., et al. (2016). Prediction of the export and fate of global ocean net primary production: the EXPORTS science plan. *Front. Mar. Sci.* 3:22. doi: 10.3389/fmars.2016.00022

Steinberg, D. K. (2000). Zooplankton vertical migration and the active transport of dissolved organic and inorganic carbon in the Sargasso Sea. *Deep Sea Res. Part I Oceanogr. Res. Pap.* 47, 137–158. doi: 10.1016/s0967-0637(99)00052-7

Steinberg, D. K., and Landry, M. R. (2017). Zooplankton and the ocean carbon cycle. *Ann. Rev. Mar. Sci.* 9, 413–444. doi: 10.1146/annurev-marine-010814-015924

Steinberg, D. K., Van Mooy, B. A. S., Buesseler, K. O., Boyd, P. W., Kobari, T., and Karl, D. M. (2008). Bacterial vs. zooplankton control of sinking particle flux in the ocean's twilight zone. *Limnol. Oceanogr.* 53, 1327–1338. doi: 10.4319/lo.2008.53.4.1327

Stemmann, L., Jackson, G. A., and Ianson, D. (2004). A vertical model of particle size distributions and fluxes in the midwater column that includes biological and physical processes - Part I: model formulation. *Deep. Res. Part I Oceanogr. Res. Pap.* 51, 885–908. doi: 10.1016/j.dsr.2004.03.001

Stokes, G. G. (1851). On the effect of the internal friction of fluids on the motion of pendulums. *Trans. Cambridge Philos. Soc.* 9, 8–106. doi: 10.1017/cbo9780511702266.002

Stukel, M. R., Ohman, M. D., Benitez-Nelson, C. R., and Landry, M. R. (2013). Contributions of mesozooplankton to vertical carbon export in a coastal upwelling system. *Mar. Ecol. Prog. Ser.* 491, 47–65. doi: 10.3354/meps10453

Sutton, T. (2013). Vertical ecology of the pelagic ocean: classical patterns and new perspectives. *J. Fish Biol.* 83, 1508–1527. doi: 10.1111/jfb.12263

Tamburini, C., Garcin, J., Gregori, G., Leblanc, K., Rimmelin, P., and Kirchman, D. L. (2006). Pressure effects on surface mediterranean prokaryotes and biogenic silica dissolution during a diatom sinking experiment. *Aquat. Microb. Ecol.* 43, 267–276. doi: 10.3354/ame043267

Tarling, G. A., Jarvis, T., Emsley, S. M., and Matthews, J. B. L. (2002). Midnight sinking behaviour in *Calanus finmarchicus*: a response to satiation or krill predation? *Mar. Ecol. Prog. Ser.* 240, 183–194. doi: 10.3354/meps240183

Taucher, J., Bach, L., Riebesell, U., and Oschlies, A. (2014). The viscosity effect on marine particle flux: a climate relevant feedback mechanism. *Global Biogeochem. Cycles* 28, 415–422. doi: 10.1002/2013GB004728

Turley, C. M., and Mackie, P. J. (1994). Biogeochemical significance of attached and free-living bacteria and the flux of particles in the NE Atlantic Ocean. *Mar. Ecol. Prog. Ser.* 115, 191–203. doi: 10.3354/meps115191

Turner, J. T. (2002). Zooplankton fecal pellets, marine snow and sinking phytoplankton blooms. *Aquat. Microb. Ecol.* 27, 57–102. doi: 10.3354/ame027057

Turner, J. T. (2015). Zooplankton fecal pellets, marine snow, phytodetritus and the ocean's biological pump. *Prog. Oceanogr.* 130, 205–248. doi: 10.1016/j.pocean.2014.08.005

Waite, A. M., Safi, K. A., Hall, J. A., and Nodder, S. D. (2000). Mass sedimentation of picoplankton embedded in organic aggregates. *Limnol. Oceanogr.* 45, 87–97. doi: 10.4319/lo.2000.45.1.0087

Wilson, S. E., Steinberg, D. K., and BUesseler, K. O. (2008). Changes in fecal pellet characteristics with depth as indicators of zooplankton repackaging of particles in the mesopelagic zone of the subtropical and subarctic North Pacific Ocean. *Deep Sea Res. II* 55, 1636–1647. doi: 10.1016/j.dsr2.2008.04.019

Conflict of Interest: The author declares that the research was conducted in the absence of any commercial or financial relationships that could be construed as a potential conflict of interest.

frontiers in Marine Science

OPINION
published: 11 October 2019
doi: 10.3389/fmars.2019.00629

The Enduring Questions: What's for Dinner? Where's My Knife? …and Can I Use My Fingers? (Unanswered) Questions Related to Organic Matter and Microbes in Marine Sediments

Carol Arnosti[1]*, *Kai-Uwe Hinrichs*[2], *Sarah Coffinet*[2], *Heinz Wilkes*[3] and *Silvio Pantoja*[4]

[1] Department of Marine Sciences, University of North Carolina-Chapel Hill, Chapel Hill, NC, United States, [2] MARUM Center for Marine Environmental Sciences, University of Bremen, Bremen, Germany, [3] Institute for Chemistry and Biology of the Marine Environment, Carl von Ossietzky University, Oldenburg, Germany, [4] Department of Oceanography and COPAS Sur-Austral, University of Concepción, Concepción, Chile

Keywords: marine sediments, degradation, organic matter characterization, heterotrophic prokaryotes, deep biosphere, fungi

OPEN ACCESS

Edited by:
Jiasong Fang,
Hawaii Pacific University,
United States

Reviewed by:
Dennis A. Bazylinski,
University of Nevada, Las Vegas,
United States

***Correspondence:**
Carol Arnosti
arnosti@email.unc.edu

Specialty section:
This article was submitted to Marine Biogeochemistry, a section of the journal Frontiers in Marine Science

Received: *26 August 2019*
Accepted: *24 September 2019*
Published: *11 October 2019*

Citation:
Arnosti C, Hinrichs K-U, Coffinet S, Wilkes H and Pantoja S (2019) The Enduring Questions: What's for Dinner? Where's My Knife? …and Can I Use My Fingers? (Unanswered) Questions Related to Organic Matter and Microbes in Marine Sediments. Front. Mar. Sci. 6:629. doi: 10.3389/fmars.2019.00629

Heterotrophic microbial communities play key roles in processing and remineralizing organic matter in marine sediments: they are the "final gatekeepers" that determine the types and quantity of organic matter that is ultimately buried in sediments—processes important to our understanding of past global environments, as well as to the production of petroleum products that still fuel much of modern society. These communities' capabilities also help us understand the energetic and metabolic boundaries of life. Work over the past decades has revealed much information about sedimentary microbial communities: their overall composition (Bacteria and Archaea), the sequence of terminal respiration processes occurring with progressive burial depth in sediments, and the depth to which they can be detected; research on the members and metabolism in the "deep biosphere" has assumed a central position in organic geochemistry, environmental microbiology, and molecular ecology (Orcutt et al., 2013; D'Hondt et al., 2019).

Despite this gain in knowledge, we are left with important questions about heterotrophic microbial communities in sediments, some of which can be summarized simply: What do they eat? How do they gain access to their substrates? How do they sense that specific substrates are out there? Our understanding is particularly incomplete with regard to the types of complex organic matter accessed by these communities. At a recent workshop[1], we discussed a number of key questions with respect to these issues, and here we focus on some of the questions raised in our discussion, in the hope that they will spur further thought and research.

[1] "Future directions in marine organic biogeochemistry," held at the Hanse Institute for Advanced Study, Delmenhorst, Germany; April 27-30 2019.

SEDIMENTARY ORGANIC MATTER

What does sedimentary organic matter look like, how do organisms see It? What are key characteristics of organic matter at different geographic locations and of different ages that sustain microbial life? How could we measure the impact of microbial processing on the structure of organic matter? How can we constrain the selectivity of microbial utilization of organic matter in sedimentary contexts?

From an analytical perspective, the fraction of "uncharacterized" organic matter is already high in surficial sediments (e.g., Hedges et al., 2000), although in such sediments, microbial consumption of this uncharacterized material can be rapid (Arnosti and Holmer, 2003). Deeper in sediments, with fewer cells and lower activities, much of the organic matter is also uncharacterized. How does this uncharacterized material change with depth, such that a fraction is bioavailable in surficial sediments, but much of the rest apparently is unavailable at deeper depths? Our measurements are not yet capturing what is important for microbial communities in terms of their activity and the reactivity of organic matter.

Bulk measurements of organic matter are often not particularly enlightening in this respect; we do not understand the constraints on the microbial populations found in sediments with high dissolved organic carbon (DOC) or high sedimentary organic matter concentrations, where activity apparently is low. For example, in Mediterranean sediments, differences in cell abundances between organic-rich sapropels and the adjacent non-sapropels are not proportional to the vast differences in organic matter concentration (Coolen et al., 2002). Marine-derived organic matter with unusually high C/N ratios in Mediterranean sediments (e.g., Calvert and Fontugne, 2001) and in Cretaceous Black Shales (e.g., Meyers et al., 2006) suggests particularly efficient degradation of the N-rich organic matter fraction in these settings. Is N removal occurring at burial, rather than at depth? How could we measure these processes, how could we determine what is a suitable structural feature for a microbe to metabolize?

The focus on characterizing bulk structures or specific components of larger macromolecules might miss important features if microbial communities are "nibbling around the edges" of macromolecules—selectively utilizing certain structural moieties (such as methoxy groups, for example). The number and types of reactive sites present in sedimentary organic matter must decrease in deeper sediments, but we don't capture this feature with our current measurements, nor do we know the types of reactive sites/functional groups that are important.

In terms of overall controlling factors on organic matter processing in sediments, to what extent do abiotic reactions also affect organic matter availability? Are physical factors that we do not capture with adequate resolution important in determining organic matter availability? What role does upward migration of smaller organic molecules from geothermally heated sediments play in feeding heterotrophic metabolism? Do small molecules in such systems trigger microbial activities, and lead to degradation of other types of organic matter?

ORGANISMS OF THE DEEP

How are communities of organisms organized in the deep? What are the characteristics of these organisms? Are there important properties of sedimentary microbial communities that we don't know about, such as metabolic networks?

How important is cell-cell communication in the deep biosphere? At cell densities of ca. 10^2 to 10^6 cm^{-3} at burial depth in excess of 1 km (Parkes et al., 2014; Inagaki et al., 2015), perhaps there is no communication among cells, as from a microbial perspective, cells are separated by astronomically long distances. But perhaps these organisms are clustered together in small communities ("frontier towns," so to speak), and the longest distances are between communities, rather than individual organisms.

Especially in this respect, are fungi important? Marine fungi with the capabilities for extracellular hydrolysis of model macromolecules are being detected more frequently in the marine environment (Gutiérrez et al., 2011). Fungi have been detected in sediments deep in the ocean (Le Calvez et al., 2009) as well as in the deep biosphere (Edgcomb et al., 2011; Liu et al., 2017; Ivarsson et al., 2018), which brings the possibility of exploring metabolic networks of bacteria and fungi in the marine sedimentary environment, as previously found above sea level. An alternative to overcome astronomically long distances, from a microbial perspective, is the possibility of bacterial mobilization through fungal hyphae (a "fungal highway"), as documented in soil (Kohlmeier et al., 2005), and food chemistry (Zhang et al., 2018) literature. There is already evidence for potential consortia of fungi and sulfate-reducing bacteria in deep granite fractures (Drake et al., 2017). Something is going on. Deeper insight into metabolic networks of bacteria, archaea, and fungi may shed light on microbial organization in the deep biosphere.

In this respect, better knowledge of the means by which electrons are transferred between partners would be helpful. For example, are quinones important? These compounds engage in facile and reversible redox reactions and are known moieties of complex natural organic matter. In soil and river sediments, they can catalyze redox reactions by an electron shuttling mechanism (Uchimiya and Stone, 2009). To date, little is known about such mechanisms in marine sediments. Perhaps this is an area in which work with pure cultures, as well as experiments with defined members, would be useful in order to better understand interactions in the environment. Isolating bacteria in the lab tears apart degradative networks, so we have a very incomplete picture of microbial interactions, but such isolates provide the opportunity for detailed physiological investigations that cannot be carried out in the environment.

SOME THOUGHTS, MOVING FORWARD

- *A renewed focus on process-based studies* would be helpful, given that in surficial sediments (where organic matter transformations are sufficiently rapid), we can currently measure the "bookends" of organic matter transformations: initial enzymatic hydrolysis of macromolecules, and terminal respiration rates (e.g., Arnosti and Jørgensen, 2006). The

sequential transformations of complex macromolecules that occur between these steps are largely unknown, however.

- *Better identification of proteins produced by sedimentary communities* would provide much-needed insight into their metabolism. Since current protein databases overwhelmingly do not represent organisms from marine sediments (much less the deep biosphere), and organisms in these environments probably have metabolic solutions to physiological/geochemical "problems" that are not found in more-typically investigated environments, we end up with a substantial fraction of unclassified proteins. Focused culture work might provide some of the missing answers.
- *Alternative methods to determine microbial activity and growth* are needed. Measurement of protein production (leucine incorporation) seems problematic, given the very slow growth in the deep biosphere, where most carbon may go to respiration rather than to an increase in cellular biomass. Although high concentrations of isotopically-labeled substrates have been used in the lab to demonstrate viability of cells from the deep biosphere (e.g., Morono et al., 2011), what other approaches could be used to get at growth rates under quasi-*in-situ* conditions? Optimization of the lipid-based dual stable isotope approach introduced by Wegener et al. (2012) could be a good start, as exemplified by increased sensitivity recently achieved using radioisotopic labeling (Evans et al., 2019).
- *New methods to analyze macromolecular organic matter* will be required. Some techniques (such as thermochemical analyses of organic matter) may be informative in cases where there is a thermal gradient in deeply buried sediments. Significant progress has been made in characterizing lipids in sediments (e.g., Wörmer et al., 2015), but lipids do not constitute the bulk of sedimentary organic matter. Other techniques that might provide information about bioavailable functional groups, or provide better characterization of complex macromolecules under conditions more reminiscent of sedimentary matrices, would be extremely helpful.

Considering the initial question—what's for dinner?—we are left with the image of hungry cells in the dark, sensing their environment, trying to determine whether a knife or fingers would be more helpful in acquiring food. Filling in this picture with a more realistic view of key unknowns—how organisms sense their substrates, what characteristics make these substrates suitable, and how organismal requirements and substrate characteristics change with depth and location in marine sediments—will doubtless keep the research community occupied for the next decades.

AUTHOR CONTRIBUTIONS

The manuscript was written by CA, based on notes taken during the workshop breakout group discussion, with input by all co-authors.

FUNDING

We are grateful for the funding by the Hanse Institute for Advanced Studies (HWK) and the Deutsche Forschungsgemeinschaft grant HI 616/19-1, which made the workshop possible. CA was also funded by NSF (OCE-1736772), and SP by COPAS Sur-Austral CONICYT PIA AFB170006.

ACKNOWLEDGMENTS

We thank the staff of the HWK for their excellent logistics and organizational skills which contributed greatly to the success of the workshop.

REFERENCES

Arnosti, C., and Holmer, M. (2003). Carbon cycling in a continental margin sediment: contrasts between organic matter characteristics and remineralization pathways. *Estuar. Coast. Shelf Sci.* 58, 197–208. doi: 10.1016/S0272-7714(03)00077-5

Arnosti, C., and Jørgensen, B. B. (2006). Organic carbon degradation in Arctic marine sediments, Svalbard: a comparison of initial and terminal steps. *Geomicrobiol. J.* 23, 551–563. doi: 10.1080/01490450600897336

Calvert, S. E., and Fontugne, M. R. (2001). On the late Pleistocene-Holocene sapropel record of climatic and oceanographic variability in the eastern Mediterranean. *Paleoceanography* 16, 78–94. doi: 10.1029/1999PA000488

Coolen, M. J. L., Cyprionka, H., Sass, A. M., and Overmann, J. (2002). Ongoing modification of Mediterranean Pleistocene sapropels mediated by prokaryotes. *Science* 296, 2407–2410. doi: 10.1126/science.1071893

D'Hondt, S., Inagaki, F., Orcutt, B. N., and Hinrichs, K.-U. (2019). IODP advances in the understanding of subseafloor life. *Oceanography* 32, 198–207. doi: 10.5670/oceanog.2019.146

Drake, H., Ivarsson, M., Bengtson, S., Heim, C., Siljeström, S., Whitehouse, M. J., et al. (2017). Anaerobic consortia of fungi and sulfate reducing bacteria in deep granite fractures. *Nat. Commun.* 8:55. doi: 10.1038/s41467-017-00094-6

Edgcomb, V. P., Beaudoin, D., Gast, R., Biddle, J. F., and Teske, A. (2011). Marine subsurface eukaryotes: the fungal majority. *Environ. Microb.* 13, 172–183. doi: 10.1111/j.1462-2920.2010.02318.x

Evans, T. W., Coffinet, S., Könneke, M., Lipp, J. S., Becker, K. W., Elvert, M., et al. (2019). Assessing the carbon assimilation and production of benthic archaeal lipid biomarkers using lipid-RIP. *Geochim. Cosmochim. Acta.* 265, 431–442. doi: 10.1016/j.gca.2019.08.030

Gutiérrez, M. H., Pantoja, S., Tejos, E., and Quiñones, R. A. (2011). Extracellular enzymatic hydrolysis in the upwelling ecosystem off Chile: the role of fungi processing marine organic matter. *Mar. Biol.* 158, 205–219. doi: 10.1007/s00227-010-1552-z

Hedges, J. I., Eglinton, G., Hatcher, P. G., Kirchman, D. L., Arnosti, C., Derenne, S., et al. (2000). The molecularly-uncharacterized component of nonliving organic matter in natural environments. *Org. Geochem.* 31, 945–958. doi: 10.1016/S0146-6380(00)00096-6

Inagaki, F., Hinrichs, K.-U., Kubo, Y., Bowles, M. W., Heuer, V. B., Hong, W.-L., Hoshino, T., et al. (2015). Exploring deep microbial life in coal-bearing sediment down to ∼ 2.5 km below the ocean floor. *Science* 349, 420–424. doi: 10.1126/science.aaa6882

Ivarsson, M., Bengtson, S., Drake, H., and Warren, F. (2018). Fungi in deep subsurface environments. *Adv. Appl. Microbiol.* 102, 83–116. doi: 10.1016/bs.aambs.2017.11.001

Kohlmeier, S., Smits, T. H. M., Ford, R. M., Keel, C., Harms, H., and Wick, L. Y. (2005). Taking the fungal highway: mobilization of pollutant-degrading bacteria by fungi. *Environ. Sci. Technol.* 39, 4640–4646. doi: 10.1021/es047979z

Le Calvez,T., Burgaud, G., Mahé, S., and Barbier, G., Vandenkoornhuyse, P. (2009). Fungal diversity in deep-sea hydrothermal ecosystems. *Appl. Environ. Microbiol*. 75, 6415–6421. doi: 10.1128/AEM.00653-09

Liu, C.-H., Huang, X., Xie, T.-N., Duan, N., Xue, Y.-R., Zhao, T.-X., et al. (2017). Exploration of cultivable fungal communities in deep coal-bearing sediments from∼ 1.3 to 2.5 km below the ocean floor. *Environ. Microbiol*. 19, 803–819. doi: 10.1111/1462-2920.13653

Meyers, P. A., Benasconi, S. M., and Forster, A. (2006). Origins and accumulation of organic matter in expanded Albian to Santonian black shale sequences on the Demerara Rise, South American margin. *Org. Geochem*. 37, 1816–1830. doi: 10.1016/j.orggeochem.2006.08.009

Morono, Y., Terada, T., Nishizawa, M., Ito, M., Hillion, F., Takahata, N., et al. (2011). Carbon and nitrogen assimilation in deep subseafloor microbial cells. *Proc. Natl. Acad. Sci. U.S.A*. 108, 18295–18300. doi: 10.1073/pnas.1107763108

Orcutt, B. N., LaRowe, D. E., Biddle, J. F., Colwell, F. S., Glazer, B. T., Reese, B. K., et al. (2013). Microbial activity in the marine deep biosphere: progress and prospects. *Front. Microbiol*. 4:189. doi: 10.3389/fmicb.2013.00189

Parkes, R. J., Cragg, B. A., Roussel, E., Webster, G., Weightman, A., and Sass, H. (2014). A review of prokaryotic populations and processes in sub-seafloor sediments, including biosphere:geosphere interactions. *Mar. Geol*. 352, 409–425. doi: 10.1016/j.margeo.2014.02.009

Uchimiya, M., and Stone, A. T. (2009). Reversible redox chemistry of quinones: Impact on biogeochemical cycles. *Chemosphere* 77, 451–458. doi: 10.1016/j.chemosphere.2009.07.025

Wegener, G., Bausch, M., Holler, T., Thankg, N. M., Prieto, M. X., Kellermann, M. Y., et al. (2012). Assessing sub-seafloor microbial activity by combined stable isotope probing with deuterated water and ^{13}C-bicarbonate. *Environ. Microbiol*. 14, 1517–1527. doi: 10.1111/j.1462-2920.2012.02739.x

Wörmer, L., Lipp, J. S., and Hinrichs, K.-U. (2015). "Comprehensive analysis of microbial lipids in environmental samples through HPLC-MS protocols," in *Hydrocarbon and Lipid Microbiology Protocols,* eds T. J. McGenity, K. N. Timmis, and F. B. Nogales (Berlin; Heidelburg: Springer), 289–317. doi: 10.1007/8623_2015_183

Zhang, Y., Kastman, E. K., Guasto, J. S., and Wolfe, B. E. (2018). Fungal networks shape dynamics of bacterial dispersal and community assembly in cheese rind microbiomes. *Nat. Commun*. 9:336. doi: 10.1038/s41467-017-02522-z

Conflict of Interest: The authors declare that the research was conducted in the absence of any commercial or financial relationships that could be construed as a potential conflict of interest.

frontiers in Marine Science

ORIGINAL RESEARCH
published: 27 November 2019
doi: 10.3389/fmars.2019.00729

Origin of Sedimentary BHPs Along a Mississippi River–Gulf of Mexico Export Transect: Insights From Spatial and Density Distributions

Stephanie Kusch[1], Julio Sepúlveda[2] and Stuart G. Wakeham[3]*

[1] University of Cologne-Centre for Accelerator Mass Spectrometry, University of Cologne, Cologne, Germany, [2] Organic Geochemistry Laboratory, Department of Geological Sciences, Institute of Arctic and Alpine Research, University of Colorado Boulder, Boulder, CO, United States, [3] Skidaway Institute of Oceanography, University of Georgia, Savannah, GA, United States

We investigated the origin of sedimentary bacteriohopanepolyols (BHPs) in low-density ($<$1.6 g cm^{-3}), mesodensity (1.6–2.0 and 2.0–2.5 g cm^{-3}) and high-density fractions ($>$2.5 g cm^{-3}) as well as unfractionated bulk samples in a highly dynamic coastal setting along a transect spanning from the Mississippi Delta into the Gulf of Mexico (GOM). We observe selective partitioning of BHPs among density fractions both in total abundance and structural diversity. BHPs primarily accumulate in the low-density fraction at all sites. Good correlation with other particle properties [surface area-normalized organic carbon loadings (OC/SA), C/N ratios, Δ^{14}C values, and lignin phenol abundances] and the spatial distribution of absolute and relative BHP abundances suggests that a significant fraction of BHPs are terrestrially sourced and entrained in the OC pool that is stabilized on clay particles or associated with plant fragments. Only a small subset of BHPs seems to have a significant autochthonous origin at the station furthest offshore and they are associated with the low and mesodensity fractions. While provenance and hydrodynamic sorting of particles across the shelf seem to primarily determine BHP inventories along the transect, the samples also harbor an unusual diversity of amino-functionalized BHPs. A subset of these BHPs appears to derive from aerobic methane oxidizing bacteria and are likely exported with particles from the coastal swamps in the Mississippi Delta. Other amino-functionalized BHPs seem to derive from aerobic ammonia oxidizing bacteria thriving in the nutrient-rich Mississippi River plume. We find no evidence for anaerobic ammonium oxidizing bacteria related to recurring seasonal hypoxia on the Louisiana Shelf.

Keywords: bacteriohopanepolyols, BHPs, density fraction, Gulf of Mexico, Mississippi River, methanotrophy

OPEN ACCESS

Edited by:
Selvaraj Kandasamy, Xiamen University, China

Reviewed by:
Yuan-Pin Chang, National Sun Yat-sen University, Taiwan
Thomas S. Bianchi, University of Florida, United States

****Correspondence:***
Stephanie Kusch
stephanie.kusch@uni-koeln.de

Specialty section:
This article was submitted to Marine Biogeochemistry, a section of the journal Frontiers in Marine Science

Received: *30 September 2019*
Accepted: *08 November 2019*
Published: *27 November 2019*

Citation:
Kusch S, Sepúlveda J and Wakeham SG (2019) Origin of Sedimentary BHPs Along a Mississippi River–Gulf of Mexico Export Transect: Insights From Spatial and Density Distributions. Front. Mar. Sci. 6:729. doi: 10.3389/fmars.2019.00729

INTRODUCTION

Bacteriohopanepolyols (BHPs) are pentacyclic triterpenoids mainly synthesized by bacteria. Their physiological role in cell membranes has so far been linked to lipid raft formation (Sáenz, 2010; Sáenz et al., 2012), pH homeostasis (Welander et al., 2009; Schmerk et al., 2011), antibiotic resistance (Schmerk et al., 2011), temperature stress (Doughty et al., 2011), intracytoplasmic

membrane formation and cell survival in late stationary phase (Welander and Summons, 2012), and potentially cell curvature generation (Doughty et al., 2014). In addition to improving membrane resistance in the free-living state, BHPs also appear to aid in plant-microbe symbiosis (Silipo et al., 2014; Kulkarni et al., 2015).

Although there is growing evidence that BHPs may be useful biomarkers to trace cell physiological processes, their environmental and taxonomic origin remains largely elusive, particularly in the marine environment. Studies investigating the distribution of BHPs in the marine water column and sediments are still relatively sparse and the global ocean metagenome shows that most BHP-producing bacteria are yet to be characterized taxonomically (Pearson and Rusch, 2009). However, the capability of marine bacteria to produce BHPs, as determined based on squalene-hopene-cyclase (*sqhC*) gene abundances, seems to be phylogenetically diverse, yet the BHP diversity does not seem to mirror the genetic diversity (Pearson and Rusch, 2009; Kharbush et al., 2013). Generally, BHP diversity seems to be higher under suboxic or anoxic marine conditions in comparison to oxic marine environments (Wakeham et al., 2007; Sáenz et al., 2011b; Kharbush et al., 2013), but both *sqhC* abundances and BHPs are much more varied in terrestrial settings in comparison to fully marine settings (Pearson et al., 2007, 2009; Sáenz et al., 2011a). While some BHPs have been assigned a primarily terrestrial origin, namely the soil-marker BHPs (Cooke et al., 2008; Zhu et al., 2011), we still lack a comprehensive understanding of the extent to which the diversity of BHPs in marine sediments derives from the continent, whether they are exported with the gross terrestrial organic carbon (OC) pool or by distinct OC sub-pools, and the mechanisms by which they are transported and/or exported within the ocean. Density fractionation of marine sediments may provide a valuable tool to understand these processes (Arnarson and Keil, 2001; Sampere et al., 2008; Wakeham et al., 2009; Wakeham and Canuel, 2016).

Here, we investigate the BHP molecular compositions of bulk sediment and sedimentary density fractions along an export transect from the Mississippi River to the northern Gulf of Mexico (GOM) for which previous studies have revealed selective partitioning of bulk OC and lignin phenols in density fractions (Sampere et al., 2008; Wakeham et al., 2009). In this highly dynamic shelf system, the OC distribution seems to be primarily determined by OC provenance and density-driven hydrodynamic sorting, which includes re-distribution and aging during cross-shelf transport in the benthic boundary layer (Sampere et al., 2008; Wakeham et al., 2009). Terrestrial OC is particularly enriched in the <1.6 g cm^{-3} density fraction as indicated by high lignin phenol abundances, high C/N ratios, and pronounced δ^{13}C- and Δ^{14}C-depletion. In contrast, the mesodensity fractions (1.6–2.0 and 2.0–2.5 g cm^{-3}) have much lower lignin concentrations, lower C/N ratios, and enriched δ^{13}C and Δ^{14}C values indicative of a significant marine component (Wakeham et al., 2009). In conjunction with these previous data, we aim at deciphering the origin of BHPs (both provenance and biogeochemical sources), the importance of hydrodynamic sorting on sedimentary BHP inventories, and diagenetic effects that might occur during cross-shelf transport or seasonal hypoxia.

MATERIALS AND METHODS

Three surface sediment samples (0–5 cm) were taken along a transect from the Mississippi River into the GOM during an *R*/*V* Pelican cruise in 2003 (**Figure 1**). Station Miss R (29°15.73′N, 89°20.15′W; 26 m water depth) was sampled within the Mississippi Delta, station GOM 50 (28°55.80′N, 89°30.39′W; 50 m water depth) in the marine prodelta close to the river mouth, and station GOM 540 (28°31.63′N, 89°47.98′W; 540 m water depth) at the head of the Mississippi Canyon. Samples were retrieved using a box corer (50 × 50 × 50 cm), the upper 5 cm of the box core were subsampled and homogenized on board, and samples were stored frozen at −20°C until analysis. Environmental conditions [water depth, salinity, oxygen content, and fluorescence (chlorophyll *a*)] were collected from each site during the cruise using a CTD (conductivity–temperature–depth) sensor (Waterson and Canuel, 2008).

Samples were extracted in bulk or following partitioning into four density fractions using sodium metatungstate solutions corresponding to <1.6, 1.6–2.0, 2.0–2.5 and >2.5 g cm^{-3}; a detailed description of the density fractionation procedure is provided by Wakeham et al. (2009). Lipids were extracted from freeze-dried bulk sediments (25–40 g dry weight; gdw) and density-fractionated sediments (0.1–12 gdw) using an accelerated solvent extractor (ASE) and dichloromethane:methanol (2:1). Extracts were archived at −20°C until aliquots were taken for this investigation. The TLE aliquots were spiked with 5α-pregnane-3β,20β-diol as internal standard and acetylated using pyridine: acetic acid 1:1 (v:v) at 50°C for 1 h and then left reacting overnight. Afterwards, the samples were filtered over 0.45 μm PTFE filters using 3:2 methanol: propan-2-ol (v:v). BHPs were analyzed using a Thermo Ultimate 3000 HPLC connected to a Q Exactive Focus Orbitrap MS equipped with an APCI ion source in the Organic Geochemistry Laboratory at the University of Colorado Boulder. Chromatographic separation was achieved on an ACE® C_{18} column (2.1 × 150 mm, 3 μm; Advanced Chromatography Technologies Ltd.) maintained at 25°C. BHPs were chromatographically separated using the solvent gradient described in Talbot et al. (2007) and a flow rate of 0.2 ml/min. APCI settings were optimized for bacteriohopanetetrol (BHT), 2-methyl-BHT (2Me-BHT), aminotriol, adenosylhopane, BHT cyclitol ether, BHT glucosamine, BHT pentose, and BHhexol cyclitol ether (**Figure 2**) using an in-house standard sample and were as follows: vaporizer temperature 325°C, capillary temperature 155°C, corona discharge current 8, sheath gas flow 40 arbitrary units (AU), aux gas flow 10 AU, S lens RF level 50 AU. BHP concentrations are reported semi-quantitatively. In the absence of commercially available authentic BHP standards, accurate MS response factors between 5α-pregnane-3β,20β-diacetate and BHPs with different functionalities cannot be determined. However, all samples were analyzed with the same Orbitrap MS system, thus, differences in the respective BHP inventories are directly comparable between samples.

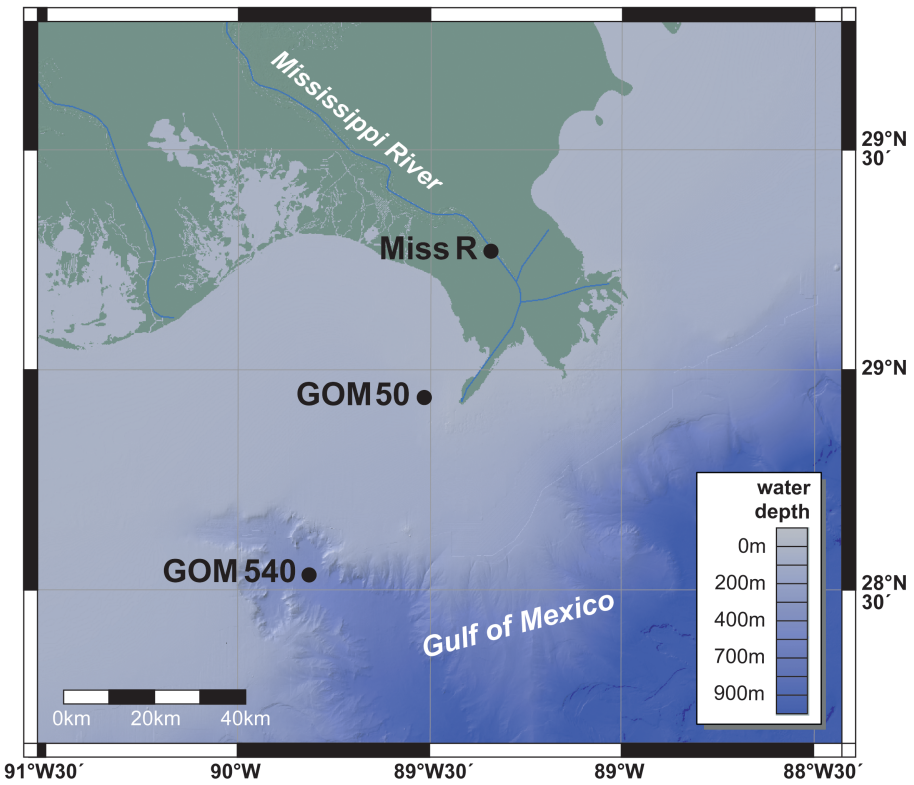

FIGURE 1 | Sampling locations.

RESULTS

Bacteriohopanepolyol diversity (**Figure 3**) is high in the Mississippi River and GOM samples (7–24 BHPs). Besides various composite and soil-marker BHPs (listed in **Figure 3**), which have more complex sugar or amino sugar side chain structures, we observe an unusual diversity of amino-functionalized BHPs including N-acylated aminotriol with C_{16} or C_{19} moieties, isomers of aminotriol and methylated aminotriol, and aminopentol and aminotetrol alongside some more ubiquitous (other) BHPs. The structural BHP diversity is relatively similar in the bulk sediments and the <1.6, 1.6–2.0, and 2.0–2.5 g cm^{-3} density fractions, but lower in the high density (>2.5 g cm^{-3}) fractions. Total mass-normalized BHP concentrations (**Figure 4**) range from 0.6 ng g^{-1} (GOM 50) to 15.4 ng g^{-1} (Miss R) in the bulk samples and 0.1 ng g^{-1} (Miss R > 2.5 g cm^{-3}) to 279.5 ng g^{-1} (GOM 540 < 1.6 g cm^{-3}) in the density fractions. Total BHP concentrations are highest in the <1.6 g cm^{-3} fraction at each station and also significantly enriched in the 1.6–2.0 g cm^{-3} fraction at station GOM 540 (**Figure 4**). Along the transect, BHP concentrations are highest at station Miss R and lowest at station GOM 50. This pattern is also evident for most individual BHPs except for BHT-CE, BHT glucosamine, 3Me-BHT, BHT, BHT II, and anhydroBHT, which show highest concentrations at station GOM 540 (**Figure 5**). We observe good correlation between total BHP concentrations (**Figure 4**) and individual BHP concentrations (**Figure 5**) (Pearson correlation coefficient $r > 0.57$) for all BHPs except for those that were detected in a few samples only (e.g., 2Me-BHT pentose, BHT pentose, aminotriol II, 2Me-adenosylhopane-type 3).

Bacteriohopanetetrol is the most abundant BHP (40.3–76.8% of total BHPs) in all samples irrespective of density fraction (**Figures 3**, **5**), thus, primarily determining total BHP concentrations ($r = 0.967$). However, at all stations, relative BHT abundances are consistently lower (by 8.0–36.5%) in the <1.6 g cm^{-3} fraction compared to in the other density fractions, all of which agree within a standard deviation (SD) of 5%. C_{16}-acyl-aminotriol is the second most abundant BHP (3.8–30.2%) in the majority of samples and is particularly abundant in the <1.6 and 1.6–2.0 g cm^{-3} density fractions. Adenosylhopane, 2Me-BHT, 3Me-BHT, and BHT II also occur in high relative abundance in all samples as well as anhydroBHT, which is particularly abundant in the <1.6 g cm^{-3} fraction at station GOM 540.

Overall, soil-marker BHP relative abundances are low compared to BHT abundances, resulting in low R_{soil} indices [soil-marker BHPs/(soil-marker BHPs + BHT) (Zhu et al., 2011)], which are <0.1 in all samples. R_{soil} indices are highest in the <1.6 and >2.5 g cm^{-3} fractions at each station (**Figure 6**). Moreover, relative abundances among soil-marker BHPs differ between density fractions and bulk samples. While adenosylhopane is the most abundant soil-marker BHP (42.1–93.7% of that subset) in all density fractions except the 2.0–2.5 g cm^{-3} fraction at station GOM 540, it only represents 2.5–8.8% of the soil-marker

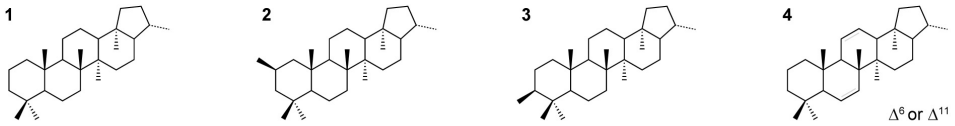

A

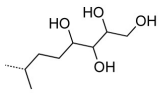

1a) bacteriohopane-32,33,34,35-tetrol (BHT & BHT II)
2a) 2β-methyl-bacteriohopane-32,33,34,35-tetrol (2Me-BHT)
3a) 3β-methyl-bacteriohopane-32,33,34,35-tetrol (3Me-BHT)

B

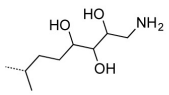

1b) 35-aminobacteriohopane-32,33,34-triol (aminotriol & aminotriol II)
2b) 2β-methyl-35-aminobacteriohopane-32,33,34-triol (2Me-aminotriol)
3b) 3β-methyl-35-aminobacteriohopane-32,33,34-triol (3Me-aminotriol)

C

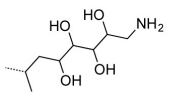

1c) 35-aminobacteriohopane-31,32,33,34-tetrol (aminotetrol)

D

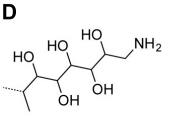

1d) 35-aminobacteriohopane-30,31,32,33,34-pentol (aminopentol)

E

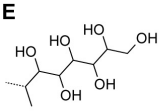

1e) bacteriohopane-30,31,32,33,34,35-hexol (BHhexol)

F

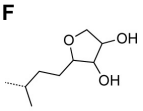

1f) 32,35-anhydrobacteriohopanetetrol (anhydro-BHT)
4f) 32,35-anhydro-Δ^X-bacteriohopanetetrol (unsat. anhydro-BHT)

G

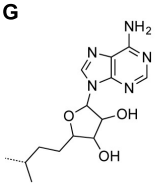

1g) 30-(5'-adenosyl)hopane (adenosylhopane)
2g) 2β-methyl-adenosylhopane (2Me-adenosylhopane)

H

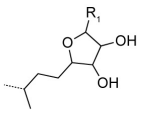

1h) adenosylhopane-type-2 (R_1: unknown structure)
2h) 2Me-adenosylhopane-type-2 (R_1: unknown structure)

I

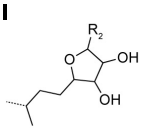

1i) adenosylhopane-type-3 (R_2: unknown structure)
2i) 2Me-adenosylhopane-type-3 (R_2: unknown structure)

J

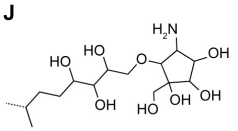

1j) bacteriohopanetetrol cyclitol ether (BHT-CE)

K

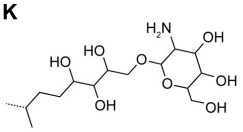

1k) bacteriohopanetetrol glucosamine (BHT glucosamine)

L

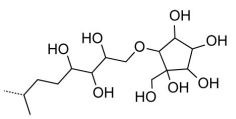

1l) bacteriohopanetetrol pentose (BHT pentose)
2l) 2β-methyl-bacteriohopanetetrol pentose (2Me-BHT pentose)
4l) Δ^X-bacteriohopanetetrol pentose (BHT pentose)

M

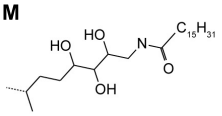

1m) C_{16} acyl-35-aminobacteriohopanetriol (C_{16} acylaminotriol)
4m) C_{16} acyl-35-amino-Δ^X-bacteriohopanetriol (unsat. C_{16} acylaminotriol)

N

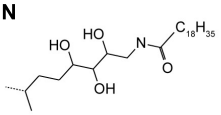

1n) C_{19} acyl-35-amino-bacteriohopanetriol (C_{19} acylaminotriol)

FIGURE 2 | BHP structures identified in this study.

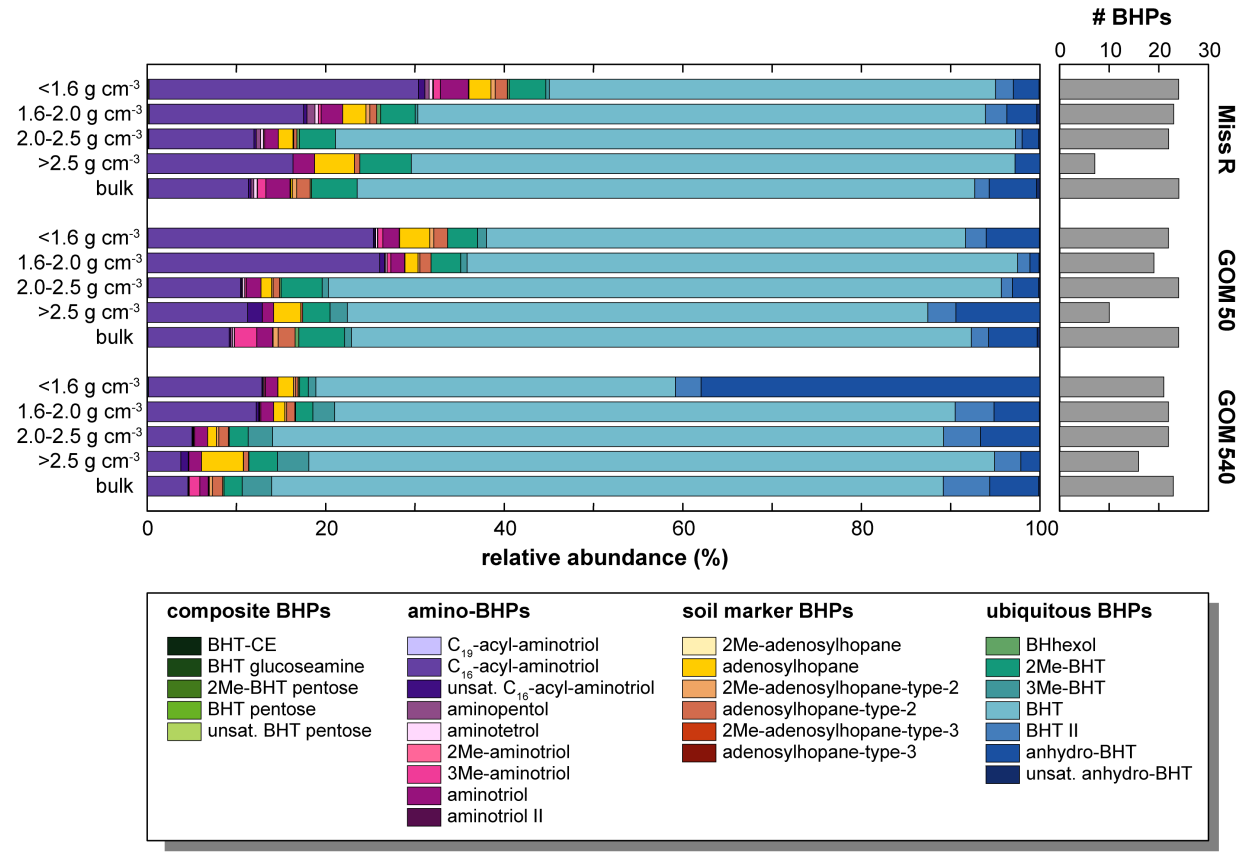

FIGURE 3 | Relative abundance and structural diversity of BHPs in density fractions and bulk sediment samples along the Miss R – GOM transect. Note that relative abundances <1% are not well resolved graphically, we refer to **Supplementary Table S1** for details.

BHPs in the bulk samples (**Figure 6**). Among soil-marker BHPs, bulk sediment samples are characterized by high abundances of adenosylhopane-type-2 (69.3–74.8%).

DISCUSSION

Density Partitioning of BHPs

Organic carbon is partitioned among the different density fractions of the three sediments at stations Miss R, GOM 50, and GOM 540 (Wakeham et al., 2009). OC is particularly enriched in the <1.6 g cm^{-3} density fraction, which has the highest OC/SA loadings, while the >2.5 g cm^{-3} fraction is OC-poor, primarily consists of unaggregated mineral grains, and has low OC/SA loadings (**Figure 7**). Moreover, C/N ratios decrease with increasing density and the <1.6 g cm^{-3} density fractions are significantly enriched in lignin phenols (**Figure 7**). Carbon isotope data reveal that the <1.6 g cm^{-3} fraction is also more $\delta^{13}C$- and $\Delta^{14}C$-depleted while the mesodensity fractions (1.6–2.5 g cm^{-3}) are generally most isotopically enriched (**Figure 7**). These observations were primarily attributed to selective transport (hydrodynamic sorting), selective preservation (clay mineral association), and/or provenance of the OC (Hedges et al., 1997; Baldock and Skjemstad, 2000; Arnarson and Keil, 2001).

Overall, our BHP data agree well with these previous results (**Figure 7**). BHPs generally are enriched in the <1.6 g cm^{-3} density fractions and total BHP concentrations correlate particularly well with OC/SA ratios (r = 0.760). These features could simply reflect a preference of aquatic heterotrophic bacteria (both in the water column and in the sediment) for those particles with high OC/SA loadings (i.e., high substrate availability) irrespective of particle origin. However, total BHP concentrations also correlate with C/N ratios (r = 0.697) and, to a lesser extent, with $\Delta^{14}C$ values (r = −0.369), and soil-marker BHP concentrations correlate positively with lignin phenol concentrations (r = 0.447). This rather suggests that significant amounts of BHPs are indeed terrestrially sourced and entrained in the OC pool that is stabilized on clay particles or associated with plant fragments (Arnarson and Keil, 2001; Wakeham et al., 2009; Wakeham and Canuel, 2016). Accordingly, the processes governing general OC properties likely also influence BHP abundances, including selective transport and preservation and/or OC provenance.

The relative abundances of BHPs in the different density fractions (**Figure 3**), as well as the bulk samples, also vary. The relative abundance of composite, soil-marker, and amino-BHPs is highest in the <1.6 and 1.6–2.0 g cm^{-3} fractions and shows a decreasing trend with distance from

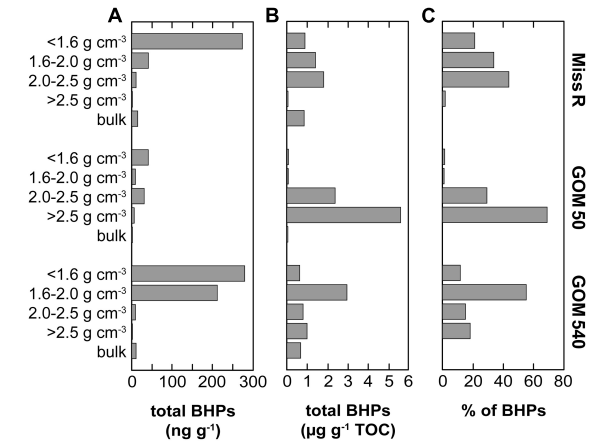

FIGURE 4 | Abundance of BHPs in density fractions and bulk sediment samples along the Miss R – GOM transect. **(A)** Mass-normalized absolute BHP abundance and **(B)** TOC-normalized absolute BHP abundance calculated based on the data of Wakeham et al. (2009). **(C)** Relative abundance of BHPs among density fractions.

the Mississippi River consistent with changing provenance of BHPs across the shelf. However, soil-marker BHP relative abundances reveal a substantial difference between bulk sediment samples and density fractions (**Figure 6**). While adenosylhopane is the dominant soil-marker BHP in the density fractions (42.1–93.7% of soil marker BHPs), its relative abundance is significantly lower in the bulk samples (2.5–8.8%), which have distinctly higher adenosylhopane-type-2 (69.3–74.8%) and 2Me-adenosylhopane-type-2 (21.6–22.6%) abundances. Accordingly, the bulk sample relative BHP distribution cannot mathematically be explained (as per mass balance) by any admixture of the different density fractions. Unfortunately, we cannot determine whether the different distributions represent true environmental heterogeneity of soil-marker BHPs or whether they are due to analytical effects stemming from the density fractionation procedure. Nevertheless, differences between relative BHP abundances in bulk samples and density fractions appear to be less pronounced for composite, amino, and "other" (rather ubiquitous) BHPs, although bulk samples show much higher 3Me-aminotriol abundances than the respective density fractions (**Figures 3**, **5**).

Soil-marker BHP concentrations agree well with total BHP concentrations (r = 0.933) and are highest in the <1.6 g cm^{-3} fractions of stations Miss R and GOM 540, while they are notably lower at station GOM 50. Other individual BHP concentrations follow this trend except BHT-CE, BHT glucosamine, 3Me-BHT, BHT, BHT II, and anhydroBHT, which have highest concentrations in the <1.6 g cm^{-3} and/or 1.6–2.0 g cm^{-3} fractions at station GOM 540 (**Figure 5**). This pattern is not evident for lignin phenols, thus, unlikely results from solely hydrodynamic sorting of terrestrial particles across the shelf. Instead it suggests additional input of BHPs at station GOM 540, implying that both sources and provenance determine BHP abundances spatially and among density fractions.

BHP Sources and Provenance

Autochthonous vs. Allochthonous Input

The Mississippi Delta and adjacent shelf represents a highly dynamic environment that receives input from various autochthonous and allochthonous OC sources (Goñi et al., 1997; Waterson and Canuel, 2008; Wakeham et al., 2009). Previous analyses of our samples revealed that C/N ratios decrease along the transect and bulk samples as well as long-chain fatty acids and the <1.6 g cm^{-3} density fraction are characterized by increasing δ^{13}C and decreasing Δ^{14}C values along the transect (**Figure 7**; Wakeham et al., 2009). These trends indicate an increasing proportion of marine OC with distance offshore and aging of terrestrial OC during cross-shelf transport. This general pattern is also mirrored in the relative abundances of autochthonous and allochthonous fatty acids as well as sterols in the same (bulk) samples (Waterson and Canuel, 2008), while lignin phenols only display this trend in the <1.6 g cm^{-3} density fractions (Sampere et al., 2008; Wakeham et al., 2009).

Data relevant to transport of BHPs from continent to ocean in other regions show high BHP diversity in terrestrial settings in comparison to low diversity in marine settings (Pearson et al., 2009; Sáenz et al., 2011a; Zhu et al., 2011). Accordingly, the consistently high BHP diversity in our samples suggests a substantial terrestrial BHP component in all of our samples. Soil-marker BHPs and the associated R_{soil} index are the primary tool to trace the input of terrestrial BHPs into marine systems (Handley et al., 2010; Zhu et al., 2011; Doğrul Selver et al., 2015; De Jonge et al., 2016), although adenosylhopane has also been shown to be an intermediate in BHP side chain synthesis (Bradley et al., 2010). The good correlation of soil-marker BHP concentrations with C/N ratios (r = 0.715) and lignin phenol concentrations (r = 0.447) in our samples suggests that the majority of soil-marker BHPs is indeed sourced from the continent. These results agree well with the dataset of Waterson and Canuel (2008), which shows clustering of bacterial branched fatty acids with terrestrial C_{29} sterols and long-chain fatty acids. R_{soil} indices also anticorrelate (r = −0.412) with Δ^{14}C values (Wakeham et al., 2009), suggesting that the majority of soil-marker BHPs is exported as part of a stabilized pre-aged sediment fraction that experiences further aging during cross-shelf transport. However, R_{soil} indices are low and do not show a pronounced decreasing trend along the transect irrespective of density fraction (**Figure 6**) as could be expected due to increasing contribution of marine OC with distance offshore. This trend likely results from a high relative contribution of riverine and/or marine BHT at all locations, subduing the soil-marker BHP contribution and consequently lowering R_{soil} index values. Accordingly, R_{soil} does not seem to be a good proxy to quantitatively trace terrestrial input into the GOM. However, the R_{soil}-derived spatial pattern of terrestrial OC input differs from the spatial pattern evident from absolute soil-marker BHP abundances. R_{soil} shows similar values for station Miss R and GOM 50 and slightly lower values at station GOM 540, whereas absolute soil-marker BHP abundances are highest at stations Miss R and GOM 540 and significantly lower at station

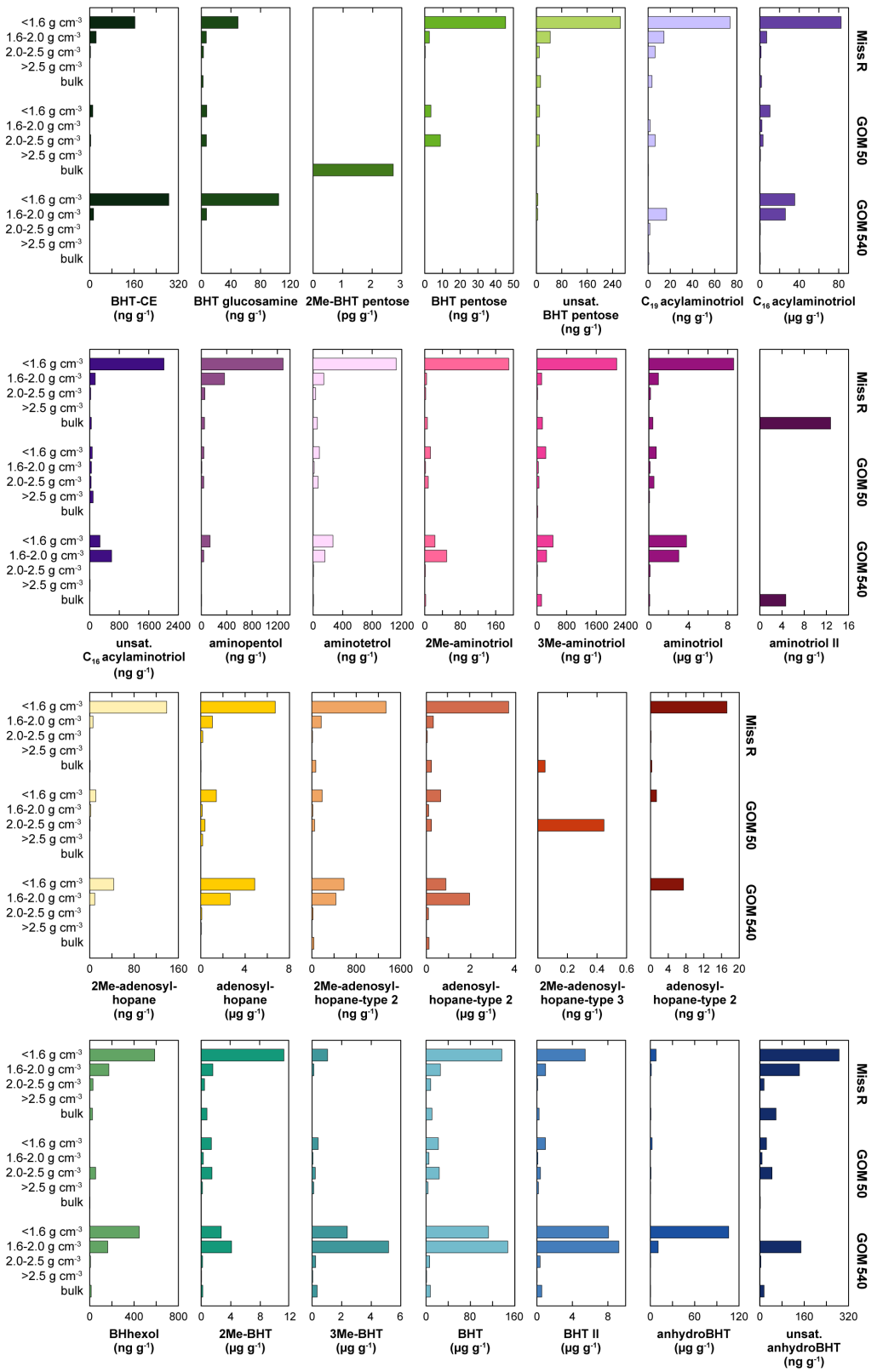

FIGURE 5 | Absolute abundance of individual BHPs in density fractions and bulk sediment samples along the Miss R – GOM transect. Individual BHP abundances are mass-normalized to better reflect the physical partitioning of particles during cross shelf transport. Low abundances are not well resolved graphically, we refer to **Supplementary Table S1** for details. Also note different scales.

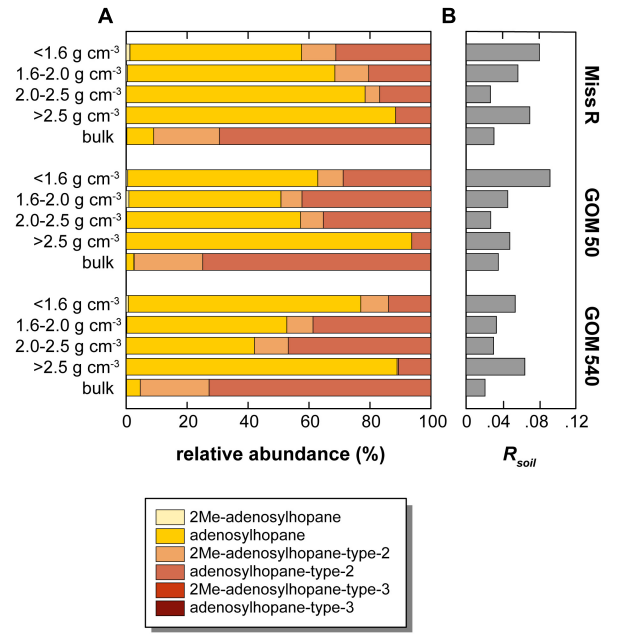

FIGURE 6 | Relative abundance of soil-marker BHPs in density fractions and bulk sediment samples along the Miss R – GOM transect. **(A)** Relative abundance of soil-marker BHPs, **(B)** R_{soil} values. Note that relative abundances <1% are not well resolved graphically, we refer to **Supplementary Table S1** for details.

GOM 50. As stated above, with a few exceptions most BHPs show this same pattern (**Figure 5**), including C-2 methylated BHPs such as 2Me-BHT, which could be sourced, among others, from plant-associated bacteria (Ricci et al., 2014; Silipo et al., 2014; Kulkarni et al., 2015). The low BHP abundance at station GOM 50 results from low BHP contribution to total OC in the <1.6 and 1.6–2.0 g cm^{-3} density fractions (**Figure 4**). This likely results from dilution with other compounds such as sterols and pigments that are particularly enriched at station GOM 50 in comparison to stations Miss R and GOM 540 (Sampere et al., 2008; Waterson and Canuel, 2008).

Although TOC-normalized BHP concentrations are very high in the 2.0–2.5 and >2.5 g cm^{-3} fractions (**Figure 4B**), their low %TOC (Wakeham et al., 2009) results in low mass-normalized BHP abundances (**Figure 4A**) at station GOM 50. Accordingly, we attribute the low BHP abundances at station GOM 50 to dilution with another molecular OC pool rather than a significant inversion of relative BHP sources (allochthonous vs. autochthonous), in agreement with the spatial R_{soil} index pattern. As stated above, along the transect individual BHT-CE, BHT glucosamine, 3Me-BHT, BHT, BHT II, and anhydroBHT concentrations are higher in the <1.6 g cm^{-3} and/or 1.6–2.0 g cm^{-3} fractions at station GOM 540 than at station Miss R (**Figure 5**). Particularly high abundances of these BHPs in the 1.6–2.0 g cm^{-3} fraction suggest that they may have an additional marine source (in the water column or sediment) accumulating in the $\Delta^{14}C$-enriched mesodensity fraction. In contrast, the exported terrestrial BHP component seems to be primarily associated with the <1.6 g cm^{-3} density fraction as expected due to hydrodynamic sorting. Whereas BHT-CE, BHT glucosamine, and BHT are rather ubiquitous and have been identified in a range of environments and bacterial cultures (Talbot et al., 2008, 2016; Pearson et al., 2009; Sáenz et al., 2011a,b; Eickhoff et al., 2014; Höfle et al., 2015; Spencer-Jones et al., 2015), other BHPs such as anhydroBHT, 3Me-BHT, and BHT II potentially carry additional information about source organisms and/or redox conditions or diagenesis (see below).

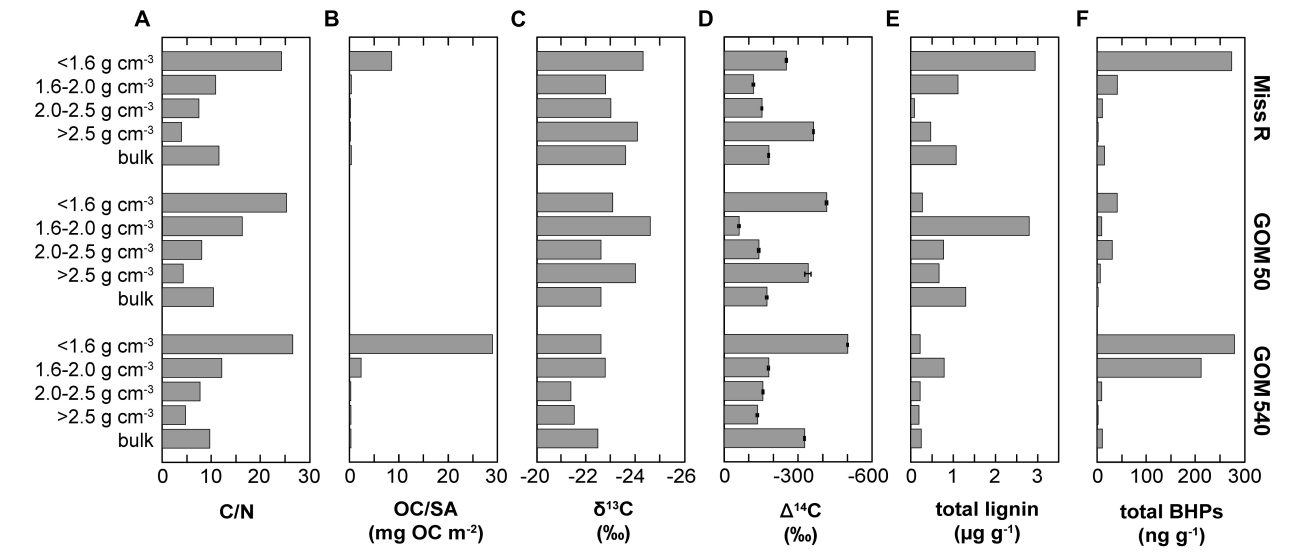

FIGURE 7 | Relationship between sedimentary parameters and BHP abundances in density fractions and bulk sediment samples along the Miss R – GOM transect. **(A)** C/N ratios, **(B)** surface area-normalized organic carbon loadings (OC/SA), **(C)** $\delta^{13}C$ of OC, **(D)** $\Delta^{14}C$ of OC, **(E)** total lignin phenol concentrations, and **(F)** mass-normalized absolute BHP abundances. Data displayed in panels **(A)** through **(E)** were previously published by Wakeham et al. (2009).

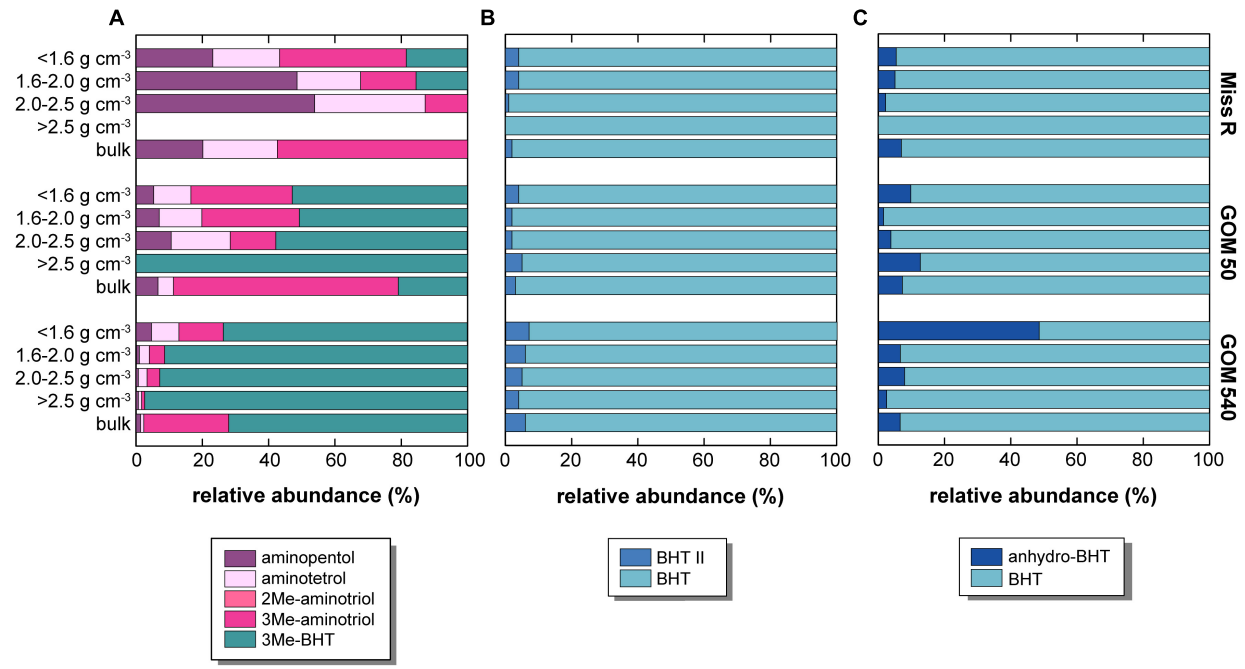

FIGURE 8 | Relative abundance of selected BHP sub-pools in density fractions and bulk sediment samples along the Miss R – GOM transect. **(A)** Relative abundance of putative methanotrophic BHPs, **(B)** relative abundance of BHT II and BHT (BHT II ratio), and **(C)** relative abundances of anhydro-BHT and BHT.

Aminopolyol Sources

Our samples show an unusually high diversity of aminopolyols. Aminopentol and aminotetrol have been primarily detected in proteobacterial Type I and Type II methanotrophs, respectively (Rohmer et al., 1984; Talbot et al., 2001; van Winden et al., 2012) and their presence in near-shore marine sediments has been attributed to the supply of continental wetland-derived OC off, for example, the Amazon and Congo rivers (Talbot et al., 2014; Wagner et al., 2014). Although aminopentol has thus far been regarded as the most taxonomically specific BHP methanotrophy proxy, Rush et al. (2016) recently challenged its proficiency as proxy for Type I aerobic methanotrophy except in the case of terrestrial wetland methanotrophy (Rush et al., 2016). We observe a general decrease of both aminopentol and aminotetrol abundances from station Miss R to station GOM 540 (**Figure 8**). Both aminotetrol and aminopentol have been identified in cultures of several sulfate reducing bacteria belonging to the genus *Desulfovibrio* and this source seems to be discernible by characteristically low ratios of aminopentol: aminotriol (∼1:1350) and aminotetrol: aminotriol (1:20–1:100) (Rush et al., 2016 and references therein). Accordingly, high aminopentol: aminotriol ratios (1:3–1:133) and aminotetrol: aminotriol ratios (1:5–1:45) suggest overall negligible contributions from *Desulfovibrio* except in the 2.0–2.5 g cm^{-3} (aminotetrol:aminotriol 1:21) and >2.5 g cm^{-3} density fraction (aminotetrol:aminotriol 1:45) at station GOM 540. In our investigation, aminopentol and aminotetrol abundances are highest in the <1.6 g cm^{-3} fraction at station Miss R and correlate strongly with soil-marker BHPs ($r = 0.889$) suggesting that aminopentol and aminotetrol primarily derive from continental sources, possibly the anaerobic sediments found in coastal swamps in the Mississippi Delta (DeLaune et al., 1986). This result is consistent with the observations of Bianchi et al. (2011), who demonstrated that coastal swamps/marshes are a significant and previously under-estimated contributor to the sedimentary OC on the Louisiana shelf. Using a three-component endmember model based on sedimentary $\delta^{13}C$ values, lignin concentrations, and C/N ratios, these authors calculated that coastal marshes supply up to ∼34% of the OC deposited during springtime. Similarly, Goñi et al. (1997) showed that C_3 plant-derived lignin from coastal forests and swamps primarily accumulates in sediments off the Mississippi river mouth, while C_4 plant-derived lignin from grassland soils of the Mississippi catchment is transported much further offshore. Interestingly, aminopentol: aminotriol and aminotetrol: aminotriol ratios decrease with distance offshore, which may indicate the increasing presence of *Desulfovibrio*. Alternatively, the lower ratios could also result from aminotriol production by some other marine source since aminotriol also shows a relative enrichment in the 1.6–2.0 g cm^{-3} fraction (in comparison to station Miss R) that is likely associated with *in situ* production.

Our samples contain additional BHPs that may have a methanotrophic source. C-3 methylation of amino-BHPs as well as BHT (Neunlist and Rohmer, 1985; Zundel and Rohmer, 1985; Rush et al., 2016) has been detected in various Type I methanotrophic bacteria, although 3Me-BHT has also been identified in acetic acid bacteria (Zundel and Rohmer, 1985). The hopanoid C-3 methylase (*hpnR*) is phylogenetically diverse among bacteria (Welander and Summons, 2012). More recently, 3Me-aminotriol was identified in haloalkaliphilic (Type I)

Methylomicrobium alcaliphilum (Banta et al., 2015; Rush et al., 2016) and was also detected in a *Sphagnum* peat (Talbot et al., 2016). In the latter, 3Me-aminotriol abundances mirrored the depth profile of aminopentol, providing circumstantial evidence that 3Me-aminotriol could be produced by other Type I methanotrophs. In our samples, aminopentol and aminotetrol absolute abundances (**Figure 5**) correlate well with 3Me-aminotriol (r = 0.981) but do not correlate with 3Me-BHT abundances (r = 0.164). The contribution of 3Me-BHT increases with distance offshore, particularly in the 1.6–2.0 g cm^{-3} fraction (**Figure 8**), suggesting 3Me-BHT may also have a marine origin in the GOM which may or may not include methanotrophic bacteria. *Methylomirabilis oxyfera* (Kool et al., 2014) is currently the only known non-thermophilic source organism for BHhexol (the only other confirmed source being *Alicyclobacillus acidoterrestris;* Řezanka et al., 2011), but its origin is less well constrained. BHhexol was also identified in a marine sponge (likely representing bacterial symbionts; Shatz et al., 2000), however, De Jonge et al. (2016) suggested a terrestrial origin due to its near-shore presence in the Kara Sea as well as other shelf systems and soils. Analogous to 3Me-aminotriol, absolute BHhexol abundances correlate well (r = 0.858) with aminopentol and aminotetrol, indicating that BHhexol seems to be associated with the terrestrial BHP pool, but a methanotrophic source cannot be elucidated based on our data.

In addition to the isomers of aminotriol [which seems to correspond to the isomer identified at a nearby station FCC-1 (29.16°N, 89.20°; 27 m water depth) by Kusch et al., 2018] and methylated aminotriol, we detected three N-acylaminotriols. N-acylaminotriols have so far been detected in purple non-sulfur bacteria as well as *Nitrosomonas europaea* (Seemann et al., 1999; Talbot et al., 2007). *N. europaea* is a chemolithoautotrophic aerobic ammonium oxidizing bacterium (AOB) that is widespread in nitrogen-rich terrestrial ecosystems. N-acylaminotriol abundances correlate well with soil-marker BHPs (r = 0.991) and aminopentol and aminotetrol (r = 0.934) abundances suggesting a primarily terrestrial source. Nonetheless, these BHPs have so far not been reported from soils. *N. europaea* has also been shown to oxidize a range of hydrocarbons (Keener and Arp, 1994). Thus, high N supply in the Mississippi River plume (Pakulski et al., 2000), natural seepage of hydrocarbons in the northern GOM, and anthropogenic inputs from the Mississippi River itself (MacDonald et al., 2015) could provide conditions under which *N. europaea* may thrive in the water column or sediments. To our knowledge, *N. europaea* has not been directly detected off the Mississippi River. However, it is normally abundant in coastal environments and under high ammonia concentrations, and AOB related to *N. europaea* were identified in NW GOM sediments off the Texas coast in conjunction with aerobic ammonium oxidizing archaea (Flood et al., 2014). Archaeal ammonia monooxygenase (*amoA*) genes, typically much more abundant than bacterial *amoA* genes (Wuchter et al., 2006), are also frequently identified in high abundance in the water column in or near the mouth of the Mississippi River and are associated with low salinity as well as seasonal hypoxia (Gillies et al., 2015; Mason et al., 2016).

Diagenetic and Redox Influence on BHP Distributions

Since the 1950s, the inner shelf areas of the northern GOM experience recurring summer bottom water hypoxia. Hypoxia is driven by the high freshwater input and nutrient loads from the Mississippi and Atchafalaya Rivers causing strong thermohaline stratification, eutrophication, and intense microbial respiration and oxygen consumption (Dagg et al., 2007; Bianchi et al., 2010; Rabalais et al., 2010). This hypoxia influences the microbial community structures (Gillies et al., 2015; Gillies Campbell et al., 2019) and BHP assemblages have been shown to vary with redox conditions elsewhere (Wakeham et al., 2007; Sáenz et al., 2011b; Kharbush et al., 2013; Ricci et al., 2014; Rush et al., 2014; Höfle et al., 2015; Matys et al., 2017). BHT II accumulates under suboxic and anoxic conditions (Sáenz et al., 2011b; Matys et al., 2017) and, more recently, it has been used as a proxy for anammox bacteria when present in high abundance relative to BHT [BHT II ratios; BHT II/(BHT + BHT II)] (Rush et al., 2014, 2019; Matys et al., 2017). Support for an anammox origin of BHT II comes from its significantly $\delta^{13}C$-depleted values (–50.6%) in a Mediterranean Sea sediment (Hemingway et al., 2018). Hypoxia usually extends along the continental shelf to the west of our study area (e.g., in 2002)[1] although it is generally less well documented directly off the Mississippi River mouth. At times, bottom waters in the northern GOM can become anoxic (Rabalais et al., 2010); thus, anammox may occur in bottom waters, at the sediment-water interface, or in sediments. Thus far, however, conclusive evidence for anammox in the area of our study is missing. McCarthy et al. (2015) used ^{15}N isotope labeling and nitrite reductase (*nirS*) gene microarrays (from *K. stuttgartiensis*) in sediments from the northern GOM including our study area. While isotope labeling did not permit differentiating $^{29}N_2$ production from denitrification or anammox, the authors concluded that the detection of *nirS* from *K. stuttgartiensis* confirmed the presence of anammox and estimated that it may be a significant N sink (potentially as high as 29%) in the northern GOM. However, "*Candidatus* Scalindua" spp. is the typical marine anammox clade (Oshiki et al., 2016) rather than the freshwater *K. stuttgartiensis,* and *C.* Scalindua has been shown to produce significant amounts of BHT II (Rush et al., 2014). Accordingly, BHT II ratios may aid at identifying whether anammox is present at our stations and whether BHT II is linked to specific density fractions. The latter would support observations that larger aggregates may hold oxygen-depleted micro-niches, which could harbor anammox bacteria under otherwise inhibitive external O_2 concentrations (Woebken et al., 2007). BHT II ratios in our samples are consistently low, ranging from 0 to 0.07 in the Miss R, GOM 50, and GOM 540 samples irrespective of density fraction (**Figure 8**), which is consistent with surface sediment data from the nearby station FCC-1 (Kusch et al., 2018). We observe a slight increase of BHT II ratio offshore, however, ratios are still well below those observed in a "*Candidatus* Scalindua profunda" enrichment culture or in upwelling-induced oxygen minimum zones (>0.5) (Rush et al., 2014; Matys et al., 2017). We also do

[1] https://service.ncddc.noaa.gov/website/Hypoxia/viewer.htm

not observe association of BHT II with a specific density fraction at any site as the observed difference of BHT II ratios between density fractions is well within analytical reproducibility (±0.02 SD; repeated analyses of an in-house standard sample). Either anammox abundances are too low to result in significant BHT II concentrations in our samples or, more likely, O_2 concentrations during seasonal hypoxia still exceed the tolerance levels of anammox (Kalvelage et al., 2011; Bristow et al., 2016). Bianchi et al. (2010) highlighted that stratification and hypoxia show strong spatial and temporal variability not only on a seasonal basis but even on a daily basis. Thus, depending on the timing of O_2 measurements during a monitoring campaign, waters may be classified hypoxic, but this "snapshot" hypoxia may not persist locally and consequently such locations would in general not support anoxic metabolisms such as anammox.

If the water column and surface sediments at our stations are primarily oxic for most of the year, BHPs may likely be affected by *in situ* degradation during cross-shelf transport and after deposition in sediments. Lignin phenols in our samples show an increase of vanillyl acid to aldehyde ratios with density fraction, indicating increased oxidation of those phenols associated with the high density, primarily mineral-rich fractions (Sampere et al., 2008; Wakeham et al., 2009). AnhydroBHT is interpreted to represent a degradation product of BHPs (Handley et al., 2010; Eickhoff et al., 2014). Its high abundance in the <1.6 g cm^{-3} density fraction at station GOM 540 suggests enhanced diagenetic alteration of BHPs in this sample, which agrees well with its strongly $\Delta^{14}C$-depleted values (**Figure 7**) assuming OC degradation primarily depends on oxygen exposure time (Hartnett et al., 1998). Indeed, anhydroBHT has a significantly lower abundance in the <1.6 g cm^{-3} fraction at station Miss R (more than one order of magnitude; **Figure 5**). BHT-normalized anhydroBHT abundances [anhydroBHT/(BHT + anhydroBHT)] increase in the <1.6 g cm^{-3} fractions along the transect (**Figure 8**), from 0.05 (Miss R) to 0.10 (GOM 50) and 0.49 (GOM 540), supporting a diagenetic origin of anhydroBHT during cross-shelf transport. Interestingly, unsat. anhydroBHT (**Figure 5**) shows a very different pattern both spatially and among density fractions; it correlates very well with soil-marker BHPs (r = 0.785) and aminopentol and aminotetrol (r = 0.867) abundances indicating that unsat. anhydroBHT derives from the continent. If unsat. anhydroBHT is a diagenetic product of unsaturated BHPs, unsat. BHT pentose and unsat. C_{16}-acylaminotriol represent possible precursor compounds. Strong correlation of unsat. anhydroBHT with unsat. BHT pentose (r = 0.856) and unsat. C_{16}-acylaminotriol (r = 0.883) may support this argument, although it could also simply mirror provenance rather than source. Overall, the provenance of BHPs seems to have a much stronger imprint on BHP inventories in our samples than water column and sediment redox conditions.

SUMMARY AND CONCLUSION

Surface sediments along a transect spanning from the Mississippi Delta into the GOM were fractionated into four density fractions and BHPs were analyzed to investigate their origin. For comparison, BHPs were also analyzed in bulk samples. Our results show that BHP abundances are highest in the <1.6 g cm^{-3} fraction and correlate well with high OC/SA ratios, C/N ratios, and lignin phenol abundances as well as low $\Delta^{14}C$ values in this fraction. This combined evidence suggests that the majority of BHPs in these sediments have a terrestrial origin and are subjected to hydrodynamic sorting during cross-shelf transport. This trend is not quantitatively reflected by the R_{soil} proxy, which does not seem to be a good proxy for terrestrial input in this setting. A small sub-set of BHPs including BHT-CE, BHT glucosamine, 3Me-BHT, BHT, BHT II, and anhydroBHT seem to have an additional source offshore and are abundant in both the <1.6 and 1.6–2.0 g cm^{-3} fractions. These BHPs likely derive from autochthonous *in situ* production in the water column and/or degradation of BHPs during transport across the shelf. Moreover, we observe an unusually high diversity of amino-functionalized BHPs that are likely synthesized by aerobic methane oxidizing bacteria and exported from the Mississippi Delta swamps as well as by aerobic ammonia oxidizing bacteria in the Mississippi River plume. In contrast, anaerobic ammonium oxidizing bacteria do not seem to be present during recurring seasonal hypoxia on the shelf.

Our data helps deconvolute the origin of BHPs in a highly dynamic shelf system exposed to a large gradient of organic matter sources. Our results also highlight the need for additional culture-based constraints on the diversity of BHPs produced by different bacteria under different environmental conditions. This is particularly obvious for BHPs such as N-acylaminotriols, for which known source organisms cannot be matched to published metagenomic data off the Mississippi River. In addition, the marked difference between soil-marker BHP relative abundances in bulk samples and density fractions warrants further investigation to determine whether this is an analytical artifact or a "real" signal and, in case of the latter, which mechanisms explain this observation.

DATA AVAILABILITY STATEMENT

All datasets generated for this study are included in the manuscript/**Supplementary Files**.

AUTHOR CONTRIBUTIONS

SK, JS, and SW designed the study. SK and SW performed the analyses and all authors contributed to the data interpretation. SK wrote the manuscript with input from all co-authors.

FUNDING

SK was supported by the University of Cologne via a "Network Exchange – NetEx" grant. JS thanks the University of Colorado Boulder for funding. SW acknowledges support by NSF grants OCE-0223226 and DEB-0454741. The Gulf of Mexico project was a collaboration with Thomas S. Bianchi and Elizabeth

A. Canuel whose participation was supported by NSF grants OCE-0223334 (TSB) and OCE-0223295 (EAC). The authors would like to thank the Hanse-Wissenschaftskolleg Delmenhorst, Germany, for sponsoring the "Marine Organic Biogeochemistry" workshop in April 2019. The workshop was funded by the Deutsche Forschungsgemeinschaft (DFG, German Research Foundation) – project number: 422798570.

ACKNOWLEDGMENTS

The authors thank Nadia Dildar for laboratory assistance in the Organic Geochemistry Laboratory at the University of Colorado Boulder. The authors also thank the captain and crew of R/V Pelican for aid in sample collection, and colleagues Troy Sampere, Elizabeth Lerberg (née Waterson), Brent McKee, Meade Allison, and Reide Corbett for their participation in this program. This is a contribution to the Frontiers in Marine Science Marine Biogeochemistry Research Topic emanating the "Marine Organic Biogeochemistry" workshop.

SUPPLEMENTARY MATERIAL

The Supplementary Material for this article can be found online at: https://www.frontiersin.org/articles/10.3389/fmars.2019.00729/full#supplementary-material

REFERENCES

Arnarson, T. S., and Keil, R. G. (2001). Organic-mineral interactions in marine sediments studied using density fractionation and X-ray photoelectron spectroscopy. *Org. Geochem.* 32, 1401–1415. doi: 10.1016/s0146-6380(01)00114-0

Baldock, J. A., and Skjemstad, J. O. (2000). Role of the soil matrix and minerals in protecting natural organic materials against biological attack. *Org. Geochem.* 31, 697–710. doi: 10.1016/s0146-6380(00)00049-8

Banta, A. B., Wei, J. H., and Welander, P. V. (2015). A distinct pathway for tetrahymanol synthesis in bacteria. *Proc. Natl. Acad. Sci. U.S.A.* 112, 13478–13483. doi: 10.1073/pnas.1511482112

Bianchi, T. S., DiMarco, S. F., Cowan, J. H. Jr., Hetland, R. D., Chapman, P., Day, J. W., et al. (2010). The science of hypoxia in the Northern Gulf of Mexico: a review. *Sci Total Environ.* 408, 1471–1484. doi: 10.1016/j.scitotenv.2009.11.047

Bianchi, T. S., Wysocki, L. A., Schreiner, K. M., Filley, T. R., Corbett, D. R., and Kolker, A. S. (2011). Sources of terrestrial organic carbon in the Mississippi Plume region: evidence for the importance of coastal marsh inputs. *Aquat. Geochem.* 17, 431–456. doi: 10.1007/s10498-010-9110-3

Bradley, A. S., Pearson, A., Sáenz, J. P., and Marx, C. J. (2010). Adenosylhopane: the first intermediate in hopanoid side chain biosynthesis. *Org. Geochem.* 41, 1075–1081. doi: 10.1016/j.orggeochem.2010.07.003

Bristow, L. A., Dalsgaard, T., Tiano, L., Mills, D. B., Bertagnolli, A. D., Wright, J. J., et al. (2016). Ammonium and nitrite oxidation at nanomolar oxygen concentrations in oxygen minimum zone waters. *Proc. Natl. Acad. Sci. U.S.A.* 113, 10601–10606. doi: 10.1073/pnas.1600359113

Cooke, M. P., Talbot, H. M., and Farrimond, P. (2008). Bacterial populations recorded in bacteriohopanepolyol distributions in soils from Northern England. *Org. Geochem.* 39, 1347–1358. doi: 10.1016/j.orggeochem.2008.05.003

Dagg, M. J., Ammerman, J. W., Amon, R. M. W., Gardner, W. S., Green, R. E., and Lohrenz, S. E. (2007). A review of water column processes influencing hypoxia in the northern Gulf of Mexico. *Estuaries Coast.* 30, 735–752. doi: 10.1007/bf02841331

De Jonge, C., Talbot, H. M., Bischoff, J., Stadnitskaia, A., Cherkashov, G., and Sinninghe Damsté, J. S. (2016). Bacteriohopanepolyol distribution in Yenisei River and Kara Sea suspended particulate matter and sediments traces terrigenous organic matter input. *Geochim. Cosmochim. Acta* 174, 85–101. doi: 10.1016/j.gca.2015.11.008

DeLaune, R. D., Smith, C. J., and Patrick, W. H. (1986). Methane production in Mississippi river deltaic plain peat. *Org. Geochem.* 9, 193–197. doi: 10.1016/0146-6380(86)90069-0

Doğrul Selver, A., Sparkes, R. B., Bischoff, J., Talbot, H. M., Gustafsson, Ö., Semiletov, I. P., et al. (2015). Distributions of bacterial and archaeal membrane lipids in surface sediments reflect differences in input and loss of terrestrial organic carbon along a cross-shelf Arctic transect. *Org. Geochem.* 83-84, 16–26. doi: 10.1016/j.orggeochem.2015.01.005

Doughty, D. M., Coleman, M. L., Hunter, R. C., Sessions, A. L., Summons, R. E., and Newman, D. K. (2011). The RND-family transporter, HpnN, is required for hopanoid localization to the outer membrane of Rhodopseudomonas palustris TIE-1. *Proc. Natl. Acad. Sci. U.S.A.* 108, E1045–E1051. doi: 10.1073/pnas.1104209108

Doughty, D. M., Dieterle, M., Sessions, A. L., Fischer, W. W., and Newman, D. K. (2014). Probing the subcellular localization of hopanoid lipids in bacteria using NanoSIMS. *PLoS One* 9:e84455. doi: 10.1371/journal.pone.0084455

Eickhoff, M., Birgel, D., Talbot, H. M., Peckmann, J., and Kappler, A. (2014). Diagenetic degradation products of bacteriohopanepolyols produced by Rhodopseudomonas palustris strain TIE-1. *Org. Geochem.* 68, 31–38. doi: 10.1016/j.orggeochem.2014.01.002

Flood, M., Frabutt, D., Floyd, D., Powers, A., Ezegwe, U., Devol, A., et al. (2014). Ammonia-oxidizing bacteria and archaea in sediments of the Gulf of Mexico. *Environ. Technol.* 36, 124–135. doi: 10.1080/09593330.2014.942385

Gillies, L. E., Thrash, J. C., deRada, S., Rabalais, N. N., and Mason, O. U. (2015). Archaeal enrichment in the hypoxic zone in the northern Gulf of Mexico. *Environ. Microbiol.* 17, 3847–3856. doi: 10.1111/1462-2920.12853

Gillies Campbell, L., Thrash, J. C., Rabalais, N. N., and Mason, O. U. (2019). Extent of the annual Gulf of Mexico hypoxic zone influences microbial community structure. *PLoS One* 14:e209055. doi: 10.1371/journal.pone.0209055

Goñi, M. A., Ruttenberg, K. C., and Eglinton, T. I. (1997). Source and contribution of terrigenous organic carbon to surface sediments in the Gulf of Mexico. *Nature* 389, 275–278. doi: 10.1038/38477

Handley, L., Talbot, H. M., Cooke, M. P., Anderson, K. E., and Wagner, T. (2010). Bacteriohopanepolyols as tracers for continental and marine organic matter supply and phases of enhanced nitrogen cycling on the late Quaternary Congo deep sea fan. *Org. Geochem.* 41, 910–914. doi: 10.1016/j.orggeochem.2010.04.016

Hartnett, H. E., Keil, R. G., Hedges, J. I., and Devol, A. H. (1998). Influence of oxygen exposure time on organic carbon preservation in continental margin sediments. *Nature* 391, 572–574.

Hedges, J. I., Keil, R. G., and Benner, R. (1997). What happens to terrestrial organic matter in the ocean? *Org. Geochem.* 27, 195–212. doi: 10.1016/s0146-6380(97)00066-1

Hemingway, J. D., Kusch, S., Walter, S. R. S., Polik, C. A., Elling, F. J., and Pearson, A. (2018). A novel method to measure the ^{13}C composition of intact bacteriohopanepolyols. *Org. Geochem.* 123, 144–147. doi: 10.1016/j.orggeochem.2018.07.002

Höfle, S. T., Kusch, S., Talbot, H. M., Mollenhauer, G., Zubrzycki, S., Burghardt, S., et al. (2015). Characterisation of bacterial populations in Arctic permafrost soils using bacteriohopanepolyols. *Org. Geochem.* 88, 1–16. doi: 10.1016/j.orggeochem.2015.08.002

Kalvelage, T., Jensen, M. M., Contreras, S., Revsbech, N. P., Lam, P., Günter, M., et al. (2011). Oxygen sensitivity of anammox and coupled N-Cycle processes in oxygen minimum zones. *PLoS One* 6:e29299. doi: 10.1371/journal.pone.0029299

Keener, W. K., and Arp, D. J. (1994). Transformations of aromatic compounds by *Nitrosomonas europaea*. *Appl. Environ. Microbiol.* 60, 1914–1920.

Kharbush, J. J., Ugalde, J. A., Hogle, S. L., Allen, E. E., and Aluwihare, L. I. (2013). Composite bacterial hopanoids and their microbial producers across

oxygen gradients in the water column of the California Current. *Appl. Environ. Microbiol.* 79, 7491–7501. doi: 10.1128/AEM.02367-13

Kool, D. M., Talbot, H. M., Rush, D., Ettwig, K., and Sinninghe Damsté, J. S. (2014). Rare bacteriohopanepolyols as markers for an autotrophic, intra-aerobic methanotroph. *Geochim. Cosmochim. Acta* 136, 114–125. doi: 10.1016/j.gca.2014.04.002

Kulkarni, G., Busset, N., Molinaro, A., Gargani, D., Chaintreuil, C., Silipo, A., et al. (2015). Specific hopanoid classes differentially affect free-living and symbiotic states of bradyrhizobium diazoefficiens. *mBio* 6:e1251-15. doi: 10.1128/mBio.01251-15

Kusch, S., Walter, S. R. S., Hemingway, J. D., and Pearson, A. (2018). Improved chromatography reveals multiple new bacteriohopanepolyol isomers in marine sediments. *Org. Geochem.* 124, 12–21. doi: 10.1016/j.orggeochem.2018.07.010

MacDonald, I. R., Garcia-Pineda, O., Beet, A., Daneshgar Asl, S., Feng, L., Graettinger, G., et al. (2015). Natural and unnatural oil slicks in the Gulf of Mexico. *J. Geophys. Res.* 120, 8364–8380.

Mason, O. U., Canter, E. J., Gillies, L. E., Paisie, T. K., and Roberts, B. J. (2016). Mississippi river plume enriches microbial diversity in the Northern Gulf of Mexico. *Front. Microbiol.* 7:1048. doi: 10.3389/fmicb.2016.01048

Matys, E. D., Sepúlveda, J., Pantoja, S., Lange, C. B., Caniupán, M., Lamy, F., et al. (2017). Bacteriohopanepolyols along redox gradients in the humboldt current system off northern Chile. *Geobiology* 15, 844–857. doi: 10.1111/gbi.12250

McCarthy, M. J., Newell, S. E., Carini, S. A., and Gardner, W. S. (2015). Denitrification dominates sediment nitrogen removal and is enhanced by bottom-water hypoxia in the Northern Gulf of Mexico. *Estuaries Coast.* 38, 2279–2294. doi: 10.1007/s12237-015-9964-0

Neunlist, S., and Rohmer, M. (1985). Novel hopanoids from the methylotrophic bacteria *Methylococcus capsulatus* and *Methylomonas methanica* - (22S)-35-aminobacteriohopane-30,31,32,33,34-pentol and (22S)-35-amino-3-beta-methylbacteriohopane-30,31,32,33,34-pentol. *Biochem. J.* 231, 635–639. doi: 10.1042/bj2310635

Oshiki, M., Satoh, H., and Okabe, S. (2016). Ecology and physiology of anaerobic ammonium oxidizing bacteria. *Environ. Microbiol.* 18, 2784–2796. doi: 10.1111/1462-2920.13134

Pakulski, J. D., Benner, R., Whitledge, T., Amon, R., Eadie, B., Cifuentes, L., et al. (2000). Microbial metabolism and nutrient cycling in the mississippi and atchafalaya river plumes. *Estuarine Coast. Shelf Sci.* 50, 173–184. doi: 10.1006/ecss.1999.0561

Pearson, A., Flood Page, S. R., Jorgenson, T. L., Fischer, W. W., and Higgins, M. B. (2007). Novel hopanoid cyclases from the environment. *Environ. Microbiol.* 9, 2175–2188. doi: 10.1111/j.1462-2920.2007.01331.x

Pearson, A., Leavitt, W. D., Sáenz, J. P., Summons, R. E., Tam, M. C. M., and Close, H. G. (2009). Diversity of hopanoids and squalene-hopene cyclases across a tropical land-sea gradient. *Environ. Microbiol.* 11, 1208–1223. doi: 10.1111/j.1462-2920.2008.01817.x

Pearson, A., and Rusch, D. B. (2009). Distribution of microbial terpenoid lipid cyclases in the global ocean metagenome. *ISME J.* 3, 352–363. doi: 10.1038/ismej.2008.116

Rabalais, N. N., Diaz, R. J., Levin, L. A., Turner, R. E., Gilbert, D., and Zhang, J. (2010). Dynamics and distribution of natural and human-caused hypoxia. *Biogeosciences* 7, 585–619. doi: 10.5194/bg-7-585-2010

Řezanka, T., Siristova, L., Melzoch, K., and Sigler, K. (2011). N-acylated bacteriohopanehexol-mannosamides from the thermophilic bacterium *Alicyclobacillus acidoterrestris*. *Lipids* 46, 249–261. doi: 10.1007/s11745-010-3482-4

Ricci, J. N., Coleman, M. L., Welander, P. V., Sessions, A. L., Summons, R. E., Spear, J. R., et al. (2014). Diverse capacity for 2-methylhopanoid production correlates with a specific ecological niche. *ISME J.* 8, 675–684. doi: 10.1038/ismej.2013.191

Rohmer, M., Bouvier-Nave, P., and Ourisson, G. (1984). Distribution of hopanoid triterpenes in prokaryotes. *Microbiology* 130, 1137–1150. doi: 10.1099/00221287-130-5-1137

Rush, D., Osborne, K. A., Birgel, D., Kappler, A., Hirayama, H., Peckmann, J., et al. (2016). The bacteriohopanepolyol inventory of novel aerobic methane oxidising bacteria reveals new biomarker signatures of aerobic methanotrophy in marine systems. *PLoS One* 11:e165635. doi: 10.1371/journal.pone.0165635

Rush, D., Sinninghe Damsté, J. S., Poulton, S. W., Thamdrup, B., Garside, A. L., González, J. A., et al. (2014). Anaerobic ammonium-oxidising bacteria: a biological source of the bacteriohopanetetrol stereoisomer in marine sediments. *Geochim. Cosmochim. Acta* 140, 50–64. doi: 10.1016/j.gca.2014.05.014

Rush, D., Talbot, H. M., van der Meer, M., Hopmans, E. C., Douglas, B., and Sinninghe Damsté, J. S. (2019). Biomarker evidence for the occurrence of anaerobic ammonium oxidation in the eastern mediterranean sea during quaternary and pliocene sapropel formation. *Biogeosciences* 16, 2467–2479. doi: 10.5194/bg-16-2467-2019

Sáenz, J. P. (2010). Hopanoid enrichment in a detergent resistant membrane fraction of *Crocosphaera watsonii*: implications for bacterial lipid raft formation. *Org. Geochem.* 41, 853–856. doi: 10.1016/j.orggeochem.2010.05.005

Sáenz, J. P., Eglinton, T. I., and Summons, R. E. (2011a). Abundance and structural diversity of bacteriohopanepolyols in suspended particulate matter along a river to ocean transect. *Org. Geochem.* 42, 774–780. doi: 10.1016/j.orggeochem.2011.05.006

Sáenz, J. P., Wakeham, S. G., Eglinton, T. I., and Summons, R. E. (2011b). New constraints on the provenance of hopanoids in the marine geologic record: bacteriohopanepolyols in marine suboxic and anoxic environments. *Org. Geochem.* 42, 1351–1362. doi: 10.1016/j.orggeochem.2011.08.016

Sáenz, J. P., Sezgin, E., Schwille, P., and Simons, K. (2012). Functional convergence of hopanoids and sterols in membrane ordering. *Proc. Natl. Acad. Sci. U.S.A.* 109, 14236–14240. doi: 10.1073/pnas.1212141109

Sampere, T. P., Bianchi, T. S., Wakeham, S. G., and Allison, M. A. (2008). Sources of organic matter in surface sediments of the louisiana continental margin: effects of major depositional/transport pathways and Hurricane Ivan. *Cont. Shelf Res.* 28, 2472–2487. doi: 10.1016/j.csr.2008.06.009

Schmerk, C. L., Bernards, M. A., and Valvano, M. A. (2011). Hopanoid production is required for Low-pH tolerance, antimicrobial resistance, and motility in *Burkholderia cenocepacia*. *J. Bacteriol.* 193, 6712–6723. doi: 10.1128/JB.05979-11

Seemann, M., Bisseret, P., Tritz, J.-P., Hooper, A. B., and Rohmer, M. (1999). Novel bacterial triterpenoids of the hopane series from *Nitrosomonas europaea* and their significance for the formation of the C35 bacteriohopane skeleton. *Tetrahedron Lett.* 40, 1681–1684. doi: 10.1016/s0040-4039(99)00064-7

Shatz, M., Yosief, T., and Kashman, Y. (2000). Bacteriohopanehexol, a new triterpene from the marine sponge *Petrosia* species. *J. Nat. Prod.* 63, 1554–1556. doi: 10.1021/np000190r

Silipo, A., Vitiello, G., Gully, D., Sturiale, L., Chaintreuil, C. E. M., Fardoux, J., et al. (2014). Covalently linked hopanoid-lipid A improves outer-membrane resistance of a Bradyrhizobium symbiont of legumes. *Nat. Comms.* 5, 1–11. doi: 10.1038/ncomms6106

Spencer-Jones, C. L., Wagner, T., Dinga, B. J., Schefuß, E., Mann, P. J., Poulsen, J. R., et al. (2015). Bacteriohopanepolyols in tropical soils and sediments from the Congo River catchment area. *Org. Geochem.* 89-90, 1–13. doi: 10.1016/j.orggeochem.2015.09.003

Talbot, H. M., Handley, L., Spencer-Jones, C. L., Dinga, B. J., Schefuß, E., Mann, P. J., et al. (2014). Variability in aerobic methane oxidation over the past 1.2 Myrs recorded in microbial biomarker signatures from Congo fan sediments. *Geochim. Cosmochim. Acta* 133, 387–401. doi: 10.1016/j.gca.2014.02.035

Talbot, H. M., McClymont, E. L., Inglis, G. N., Evershed, R. P., and Pancost, R. D. (2016). Origin and preservation of bacteriohopanepolyol signatures in Sphagnum peat from Bissendorfer Moor (Germany). *Org. Geochem.* 97, 95–110. doi: 10.1016/j.orggeochem.2016.04.011

Talbot, H. M., Rohmer, M., and Farrimond, P. (2007). Rapid structural elucidation of composite bacterial hopanoids by atmospheric pressure chemical ionisation liquid chromatography/ion trap mass spectrometry. *Rapid Commun. Mass Spectrom.* 21, 880–892. doi: 10.1002/rcm.2911

Talbot, H. M., Summons, R. E., Jahnke, L. L., Cockell, C. S., Rohmer, M., and Farrimond, P. (2008). Cyanobacterial bacteriohopanepolyol signatures from cultures and natural environmental settings. *Org. Geochem.* 39, 232–263. doi: 10.1016/j.orggeochem.2007.08.006

Talbot, H. M., Watson, D. F., Murrell, J. C., Carter, J. F., and Farrimond, P. (2001). Analysis of intact bacteriohopanepolyols from methanotrophic bacteria by reversed-phase high-performance liquid chromatography-atmospheric pressure chemical ionisation mass spectrometry. *J. Chromatogr. A* 921, 175–185. doi: 10.1016/s0021-9673(01)00871-8

van Winden, J. F., Talbot, H. M., Kip, N., Reichart, G.-J., Pol, A., McNamara, N. P., et al. (2012). Bacteriohopanepolyol signatures as markers for methanotrophic

bacteria in peat moss. *Geochim. Cosmochim. Acta* 77, 52–61. doi: 10.1016/j.gca.2011.10.026

Wagner, T., Kallweit, W., Talbot, H. M., Mollenhauer, G., Boom, A., and Zabel, M. (2014). Microbial biomarkers support organic carbon transport from methane-rich Amazon wetlands to the shelf and deep sea fan during recent and glacial climate conditions. *Org. Geochem.* 67, 85–98. doi: 10.1016/j.orggeochem.2013.12.003

Wakeham, S. G., Amann, R., Freeman, K. H., Hopmans, E. C., Jørgensen, B. B., Putnam, I. F., et al. (2007). Microbial ecology of the stratified water column of the Black Sea as revealed by a comprehensive biomarker study. *Org. Geochem.* 38, 2070–2097. doi: 10.1016/j.orggeochem.2007.08.003

Wakeham, S. G., and Canuel, E. A. (2016). The nature of organic carbon in density-fractionated sediments in the Sacramento-San Joaquin River Delta (California). *Biogeosciences* 13, 567–582. doi: 10.5194/bg-13-567-2016

Wakeham, S. G., Canuel, E. A., Lerberg, E. J., Mason, P., Sampere, T. P., and Bianchi, T. S. (2009). Partitioning of organic matter in continental margin sediments among density fractions. *Mar. Chem.* 115, 211–225. doi: 10.1016/j.marchem.2009.08.005

Waterson, E. J., and Canuel, E. A. (2008). Sources of sedimentary organic matter in the Mississippi River and adjacent Gulf of Mexico as revealed by lipid biomarker and δ^{13}CTOC analyses. *Org. Geochem.* 39, 422–439. doi: 10.1016/j.orggeochem.2008.01.011

Welander, P. V., Hunter, R. C., Zhang, L., Sessions, A. L., Summons, R. E., and Newman, D. K. (2009). Hopanoids play a role in membrane integrity and pH homeostasis in *Rhodopseudomonas palustris* TIE-1. *J. Bacteriol.* 191, 6145–6156. doi: 10.1128/JB.00460-09

Welander, P. V., and Summons, R. E. (2012). Discovery, taxonomic distribution, and phenotypic characterization of a gene required for 3-methylhopanoid production. *Proc. Natl. Acad. Sci. U.S.A.* 109, 12905–12910. doi: 10.1073/pnas.1208255109

Woebken, D., Fuchs, B. M., Kuypers, M. M. M., and Amann, R. (2007). Potential interactions of particle-associated anammox bacteria with bacterial and archaeal partners in the namibian upwelling system. *Appl. Environ. Microbiol.* 73, 4648–4657. doi: 10.1128/aem.02774-06

Wuchter, C., Abbas, B., Coolen, M. J. L., Herfort, L., van Bleijswijk, J., Timmers, P., et al. (2006). Archaeal nitrification in the ocean. *Proc. Natl. Acad. Sci. U.S.A.* 103, 12317–12322. doi: 10.1073/pnas.0600756103

Zhu, C., Talbot, H. M., Wagner, T., Pan, J.-M., and Pancost, R. D. (2011). Distribution of hopanoids along a land to sea transect: implications for microbial ecology and the use of hopanoids in environmental studies. *Limnol. Oceangr.* 56, 1850–1865. doi: 10.4319/lo.2011.56.5.1850

Zundel, M., and Rohmer, M. (1985). Prokaryotic triterpenoids. 1. 3 beta-methylhopanoids from Acetobacter species and *Methylococcus capsulatus*. *Eur. J. Biochem.* 150, 23–27. doi: 10.1111/j.1432-1033.1985.tb08980.x

Conflict of Interest: The authors declare that the research was conducted in the absence of any commercial or financial relationships that could be construed as a potential conflict of interest.

frontiers in Marine Science

BRIEF RESEARCH REPORT
published: 20 December 2019
doi: 10.3389/fmars.2019.00780

Dead in the Water: The Vicious Cycle of Blanks During Natural Level ^{14}C Manipulation of Marine Algal Cultures

Stephanie Kusch[1,2†], Albert Benthien[1], Klaus-Uwe Richter[1], Björn Rost[1,3] and Gesine Mollenhauer[1,2]*

[1] Alfred Wegener Institute for Polar and Marine Research, Bremerhaven, Germany, [2] Department of Geosciences, University of Bremen, Bremen, Germany, [3] Faculty of Biology/Chemistry, University of Bremen, Bremen, Germany

OPEN ACCESS

Edited by:
Cindy Lee,
Stony Brook University, United States

Reviewed by:
Tiantian Tang,
Harvard University, United States
Thomas Michael Blattmann,
Japan Agency for Marine-Earth Science and Technology, Japan
Elizabeth Minor,
University of Minnesota Duluth, United States

***Correspondence:**
Stephanie Kusch
stephanie.kusch@uni-koeln.de

†Present address:
Stephanie Kusch,
CologneAMS, University of Cologne, Cologne, Germany

Specialty section:
This article was submitted to Marine Biogeochemistry, a section of the journal Frontiers in Marine Science

Received: 11 September 2019
Accepted: 03 December 2019
Published: 20 December 2019

Citation:
Kusch S, Benthien A, Richter K-U, Rost B and Mollenhauer G (2019) Dead in the Water: The Vicious Cycle of Blanks During Natural Level ^{14}C Manipulation of Marine Algal Cultures. Front. Mar. Sci. 6:780. doi: 10.3389/fmars.2019.00780

Authentic biomarker standards were obtained from algal cultures in an attempt to accurately determine blank C added during sample processing for compound-specific radiocarbon analysis. *Emiliania huxleyi* and *Thalassiosira pseudonana* were grown under manipulated $\Delta^{14}C$ dissolved inorganic carbon (DIC) levels and chlorophyll *a* and either alkenones (*E. huxleyi*) or low molecular weight (LMW) alkanoic acids (*T. pseudonana*) were isolated from the respective biomass using preparative liquid chromatography (LC), wet chemical techniques or preparative gas chromatography, respectively. DI^{14}C in the seawater medium was determined pre- and post-growth. Biomarker $\Delta^{14}C$ values mostly agree within 1σ or 2σ analytical uncertainties. In those cases where biomarker $\Delta^{14}C$ values differ significantly, chlorophyll *a* is up to 104‰ more ^{14}C-depleted than alkenones or LMW alkanoic acids, consistent with a larger LC blank compared to the other purification methods. However, in the majority of experimental setups pre- and post-growth DIC $\Delta^{14}C$ values seem to be compromised by an unknown and variable blank C contribution. DIC $\Delta^{14}C$ values deviate strongly from the anticipated $\Delta^{14}C$ values (by up to ca. 560‰), pre- and post-growth $\Delta^{14}C$ values differ significantly (by up to ca. 460‰), and changes are not unidirectional. Accordingly, since the substrate $\Delta^{14}C$ value cannot unequivocally be constrained, blank C contributions for the different biomarker purification methods cannot be accurately calculated. This study illustrates the challenges and problems of producing authentic standards that are not readily commercially available and exemplifies how a laborious and time-consuming culturing approach may enter a vicious cycle of blank C contamination hampering accurate blank C determination.

Keywords: compound-specific radiocarbon analysis, authentic standards, blank, chlorophyll *a*, alkenones, alkanoic acids, algal cultures, natural level ^{14}C manipulation

INTRODUCTION

Compound-specific radiocarbon analysis (CSRA) has revolutionized our understanding of carbon cycling in the ocean including both sedimentary and metabolic processes in the water column and sediments (e.g., Pearson et al., 2005; Ingalls et al., 2006; Mollenhauer and Eglinton, 2007; Mollenhauer et al., 2007), as well as land to ocean carbon transfer (e.g., Drenzek et al., 2009;

Kusch et al., 2010b; Feng et al., 2013). Accordingly, there are efforts to extend CSRA to an ever-increasing number of compounds and compound classes. Nonetheless, CSRA is quite laborious and compound isolation requires various wet-chemical techniques as well as analytically more advanced steps such as preparative gas chromatography (GC) or preparative liquid chromatography (LC). In order to achieve meaningful results, it is a pivotal necessity to accurately determine the blank carbon contribution associated with compound isolation (sample processing), i.e., both the amount as well as ^{14}C isotopic composition of this blank C (e.g., Shah and Pearson, 2007). Two approaches can be taken for this purpose (i) obtaining "true" blank runs void of any sample, e.g., collection of the LC effluent volume, or (ii) processing authentic standards with known Δ^{14}C values. "True" blank runs require the pooling of many consecutive runs in order to retrieve sufficient C amounts for ^{14}C analysis, which may not always be successful (Shah and Pearson, 2007), and yield the combined blank C isotopic composition. In contrast, processing of authentic standards is likely quicker and allows the characterization of blank C contributions from both fossil ("^{14}C-dead") and modern (atmospheric ^{14}C) sources if these standards have modern and fossil Δ^{14}C values, respectively.

However, for a range of compounds or even compound classes typically found in marine particulate organic matter, authentic standards are not readily available. Either, they are not produced commercially or are manufactured solely from either plant biomass or petroleum sources limiting our ability to characterize either the fossil or modern blank sources, respectively. Under these circumstances, scientists are required to use surrogate standards (e.g., Shah and Pearson, 2007; Birkholz et al., 2013) or to obtain their own authentic standards for example via culturing approaches (Mollenhauer et al., 2005). Surrogate standards only provide the best approximation of the actual blank C, since they do not have chemical properties identical to the target compounds, e.g., they will show different chromatographic behavior and, thus, entrain slightly different column "bleed" from stationary phases during chromatography. Authentic standards can be obtained when culturing marine algae in the laboratory under controlled dissolved inorganic carbon (DIC) Δ^{14}C levels (Mollenhauer et al., 2005). While this approach is laborious and time-consuming, it allows for the determination of blank C contribution associated with the isolation of target compounds from different compound classes and with various Δ^{14}C endmembers. However, it is crucial that the Δ^{14}C isotopic composition of C sources during culturing remains constrained and the culturing experiments themselves are not associated with significant blank C contributions.

Here, we illustrate the challenging nature of natural level ^{14}C manipulation in batch cultures of *Emiliania huxleyi* and *Thalassiosira pseudonana* grown under three different Δ^{14}C DIC levels (40‰, –480‰, and –1000‰). We show that blank C of unknown origin contributed significantly to the DIC Δ^{14}C isotopic composition during the experiments, impairing a valuable assessment of blank C associated with the purification of chlorophyll *a* as well as alkenones (*E. huxleyi*) and low molecular weight (LMW) alkanoic acids (*T. pseudonana*).

MATERIALS AND METHODS

Algal Culture Conditions

North Sea seawater was enriched with nutrients including nitrate, phosphate, silicate (for *T. pseudonana*), metals, and vitamins at concentrations equaling f/2 medium (Guillard and Ryther, 1962). The seawater was filtered through sterile 0.2 µm PTFE filters and collected in sterile 2.4 l borosilicate glass bottles. The seawater was percolated with CO_2-free air for 36 h at 25°C to expel DIC species (**Figure 1**). A similar setup is routinely used to achieve DIC-free medium, which has been verified by direct measurements using Membrane-Inlet MS (Rost et al., 2007). Subsequently, CO_2 of known ^{14}C isotopic composition was percolated through the seawater at 380 ppm for 48 h at 25°C each. CO_2 endmembers represent "Modern" (40‰; ambient air in AD2010/AD2011; Levin et al., 2013) and "Fossil" (–1000‰; Air Liquide N45) Δ^{14}C values as well as a 1:1 "Intermediate" mixture (–480‰; gas volume v:v using a custom-made gas flow controller). The seawater was cooled to 15°C and the *E. huxleyi* strain RCC 1238 (Roscoff Culture Collection) or the *T. pseudonana* strain CCMP 1335 (Provasoli-Guillard National Center for Culture of Marine Phytoplankton) were inoculated at a cell density of approximately 200 cells ml^{-1}. Both strains were checked for their vitality under a light microscope prior to inoculation. Culture bottles were topped with seawater to reduce headspace volume and closed with sterile PTFE-lined caps (to limit diffusion of atmospheric ^{14}C). Bottles were stored in a RUMED 1200 light-thermostat at 15°C with a photon flux density of 100 µmol photons m^{-2} s^{-1} to stimulate pigment production (Nielsen, 1997). Starter cultures were grown in 16 h: 8 h light: dark cycles until they reached stationary phase (based on cell densities determined from 1 ml aliquots). Cell densities were determined using a Beckman Multisizer 3 Coulter Counter (*E. huxleyi*) or visual counting under a microscope (*T. pseudonana*). Afterward

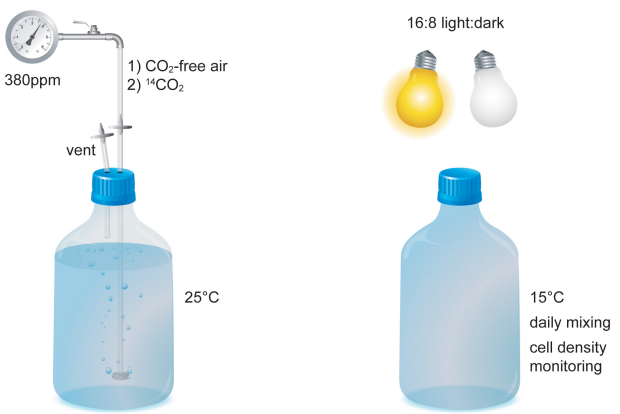

FIGURE 1 | Schematic of the experimental setup during **(A)** DIC ^{14}C manipulation and **(B)** batch culture growth of the *E. huxleyi* and *T. pseudonana* cultures.

an aliquot of the starter cultures was taken and approximately 200 cells ml^{-1} of the isotopically equilibrated starter culture were then inoculated into triplicates of new medium (sterile 2.4 l borosilicate glass bottles) and main cultures were grown in 16 h: 8 h light: dark cycles. After reaching stationary phase (9–13 days), an aliquot of the main culture was taken for final cell density determination and cultures were harvested (mid-day) by filtration onto pre-combusted GF/F filters (–200 m bar; triplicates of each batch were combined) and stored frozen at –20°C in the dark until analysis.

Pigment and Lipid Extraction and Purification

For pigment extraction, GF/F filters were transferred into pre-combusted glass vials and 20 ml dehydrated acetone was added, samples were extracted for 15 min in an ultrasonic ice bath, centrifuged at 1200 rpm for 3 min, and the acetone was recovered. This extraction step was repeated twice. Subsequently, the combined acetone extracts were concentrated under N_2 and transferred into a 1:3 hexane: Seralpure® mixture for liquid-liquid extraction. Liquid-liquid extraction was performed using hexane (pigments) and dichloromethane (residual lipids), each extraction was repeated until the solvent layer was colorless. The hexane fraction was concentrated under N_2, rinsed through pre-combusted sodium sulfate to remove Seralpure® residues, dehydrated dimethylformamide was added, the sample homogenized, and stored at –20°C overnight. Chlorophyll *a* was purified with an Agilent 1200 Series HPLC/DAD system using the method described in Kusch et al. (2010a). After initial ultrasonic extraction of pigments, the GF/F filters were additionally extracted with 9:1 dichloromethane: methanol using Soxhlet (48 h; cellulose thimbles pre-extracted 24 h) in order to ensure maximum lipid recovery. The total lipid extract (TLE) was combined with the dichloromethane fraction recovered during liquid-liquid extraction of the acetone-Seralpure® mixture. The TLE was saponified in 0.5 M potassium hydroxide in methanol for 3 h at 85°C to separate alkanoic acids and neutral lipids. Alkenones were purified wet-chemically according to Ohkouchi et al. (2005). LMW alkanoic acids were methylated and purified using an Agilent HP6890N GC connected to a Gerstel preparative fraction collector following Kusch et al. (2010b).

Isotope Measurements

For radiocarbon measurements, chlorophyll *a*, alkenones, and LMW alkanoic acids methyl esters (FAMEs) were converted into CO_2. The samples were transferred into pre-combusted quartz tubes (900°C, 4 h), 150 μg pre-combusted copper oxide were added as oxygen source, and samples were evacuated and flame-sealed *in vacuo*. Afterward, the samples were combusted to CO_2 at 900°C for 8 h. The resulting CO_2 gas was stripped of water *in vacuo* and quantified manometrically. AMS measurements of the $\Delta^{14}C$ of chlorophyll *a*, alkenones, and FAME isolates containing >1 μmol CO_2 were performed at the National Ocean Sciences Accelerator Mass Spectrometry Facility (NOSAMS) at Woods Hole Oceanographic Institution, United States following the protocol for small samples (Pearson et al., 1998). Aliquots of the CO_2 were measured on a VG Optima to obtain $\delta^{13}C$ values. ^{14}C analyses of biomarker isolates <1 μmol CO_2 were performed at the Ion Beam Physics Department at ETH, Switzerland using the MICADAS gas ion source system (Ruff et al., 2007). Seawater sampled before and after batch culturing was transferred into 500 ml pre-combusted borosilicate glass bottles, 100 μl saturated mercuric chloride solution was added, and bottles were filled without headspace. Seawater DIC was analyzed at NOSAMS following standard protocols (McNichol et al., 1994).

Radiocarbon data are reported as $\Delta^{14}C$ in ‰ according to Stuiver and Polach (1977), $\delta^{13}C$ data are reported in ‰ relative to Vienna Pee Dee Belemnite (VPDB). FAME $\Delta^{14}C$ and $\delta^{13}C$ values were corrected for the addition of one methyl group during derivatization.

RESULTS

"Modern" Cultures

In the "Modern" *E. huxleyi* culture, pre- and post-growth DIC $\Delta^{14}C$ values are 60.0 ± 3.4‰ and 83.0 ± 3.5‰, respectively (**Figure 2** and **Supplementary Table S1**). The stable carbon isotopic composition ($\delta^{13}C$) of the seawater DIC was –1.0 ± 0.1‰ prior to culture growth and 4.0 ± 0.1‰ after *E. huxleyi* growth. The alkenone $\Delta^{14}C$ value of 77.0 ± 3.9‰ falls within the pre- and post-growth DIC $\Delta^{14}C$ values, while the chlorophyll *a* $\Delta^{14}C$ value (24.5 ± 10.6‰) is significantly (>2σ analytical uncertainty) more depleted. Corresponding $\delta^{13}C$ values are –20.2 ± 0.1‰ for alkenones and –15.4 ± 0.1‰ for chlorophyll *a*.

Pre- and post-growth DIC $\Delta^{14}C$ values for the "Modern" *T. pseudonana* culture show the highest deviation of the entire data set (∼460‰) with a pre-growth $\Delta^{14}C$ value of –43.9 ± 2.9‰ and a post-growth $\Delta^{14}C$ value of –505.2 ± 2.5‰. Analogous to the "Modern" *E. huxleyi* culture, seawater DIC became ^{13}C-enriched during the course of the experiment increasing from a pre-growth $\delta^{13}C$ value of –14.8 ± 0.1‰ to a $\delta^{13}C$ value of –11.0 ± 0.1‰ post-growth. Both, *T. pseudonana* derived $C_{14:0}$ alkanoic acid (–348.8 ± 3.1‰) and chlorophyll *a* (−452.3 ± 1.9‰) $\Delta^{14}C$ values fall within the range of the pre- and post-growth DIC $\Delta^{14}C$ values but deviate significantly (>2σ analytical uncertainty) from one another. The $\delta^{13}C$ values of the $C_{14:0}$ alkanoic acid and chlorophyll *a* are –30.2 ± 0.1‰ and –27.8 ± 0.1‰, respectively.

"Intermediate" Cultures

The seawater DIC $\Delta^{14}C$ value in the "Intermediate" *E. huxleyi* culture was –380.1 ± 2.4‰ before culture growth and −437.1 ± 2.0‰ after growth (**Figure 2** and **Supplementary Table S1**) with corresponding pre- and post-growth $\delta^{13}C$ values of –14.5 ± 1.0‰ and –12.1 ± 0.1‰, respectively. Both, alkenones and chlorophyll *a* from *E. huxleyi* are more ^{14}C-depleted than DIC with $\Delta^{14}C$ values of –451.3 ± 2.1‰ and −463.9 ± 2.0‰, respectively, and $\delta^{13}C$ values of –35.0 ± 0.1‰ and –27.6 ± 0.1‰, respectively.

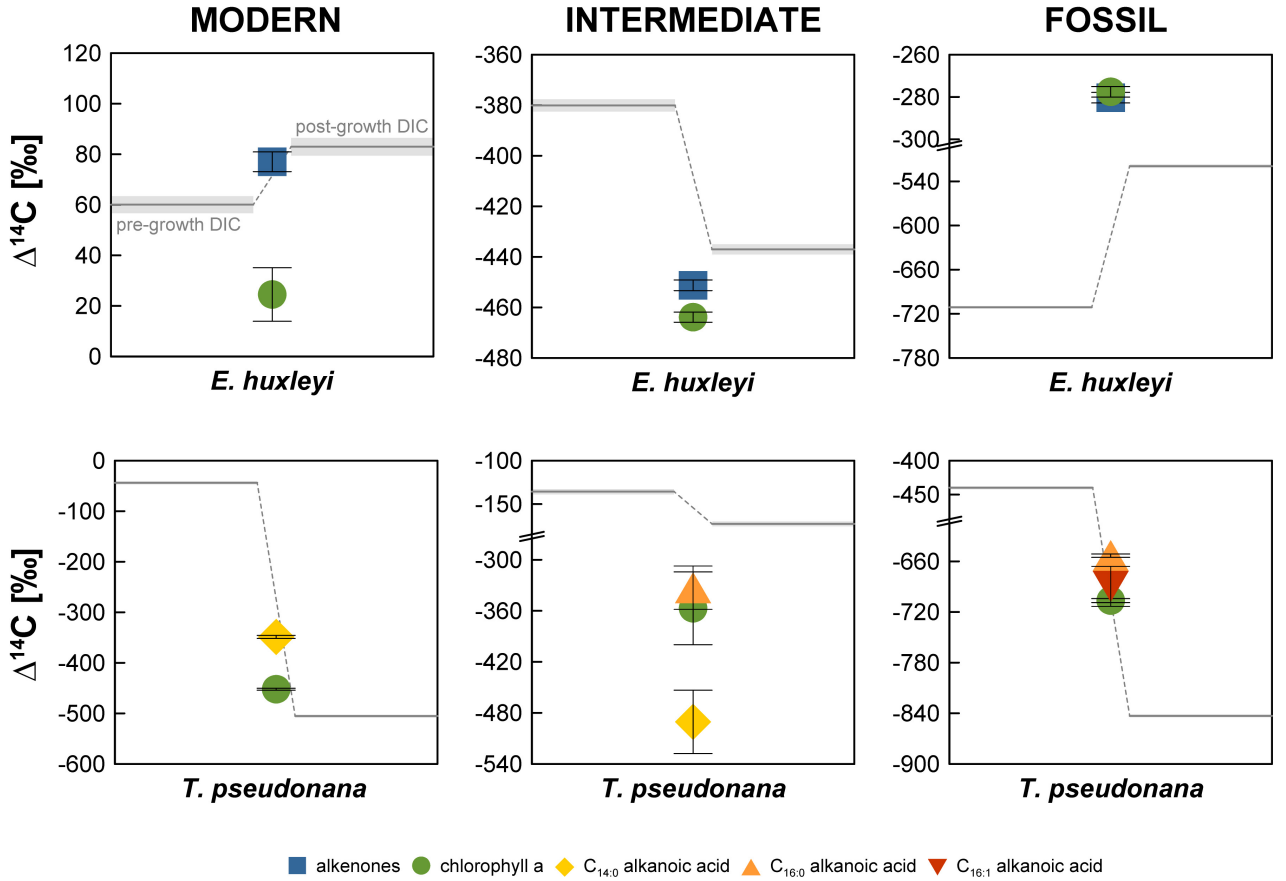

FIGURE 2 | Radiocarbon isotopic composition (Δ^{14}C in ‰) of the *Emiliania huxleyi* and *Thalassiosira pseudonana* cultures. Errors bars (shaded area for DIC) represent 1σ analytical uncertainty.

In the "Intermediate" *T. pseudonana* culture both the pre-growth DIC (–135.7 ± 3.0‰) and the post-growth DIC (–172.8 ± 2.6‰) Δ^{14}C values are considerably ^{14}C-enriched in comparison to the anticipated Δ^{14}C value (ca. –480‰) that should have resulted from a 1:1 CO_2 mixture of ambient air and Air Liquide N45. Pre- and post-growth seawater δ^{13}C values are –8.8 ± 0.1‰ and –2.4 ± 0.1‰, respectively. The biomarker Δ^{14}C values were measured on ultra-small samples sizes (<1 μmol) and are, thus, associated with large errors. While $C_{14:0}$ alkanoic acid (–490.5 ± 37.2‰) and $C_{16:0}$ alkanoic acid (–332.9 ± 25.5‰) deviate significantly, $C_{14:0}$ alkanoic acid and chlorophyll *a* (–357.0 ± 42.8‰) agree within 2σ analytical uncertainty and $C_{16:0}$ alkanoic acid and chlorophyll *a* agree within 1σ analytical uncertainty. Biomarker δ^{13}C values could not be measured independently on splits of the sample CO_2 due to size restrictions.

"Fossil" Cultures

In the "Fossil" *E. huxleyi* culture, pre- and post-growth seawater DIC Δ^{14}C values (–711.1 ± 1.6‰ and –519.4 ± 2.1‰, respectively) differ significantly with a ~200‰ enrichment in ^{14}C during culture growth (**Figure 2** and **Supplementary Table S1**). A concurrent strong isotopic enrichment is also evident for the seawater DIC δ^{13}C. The pre-growth value was –22.1 ± 0.1‰ whereas the post-growth value increased to –13.1 ± 0.1‰. Both alkenones (–280.3 ± 2.5‰) and chlorophyll *a* (–277.6 ± 2.5‰) are even more enriched in ^{14}C than the post-growth DIC but agree within 1σ analytical uncertainty with each other. Alkenones have a δ^{13}C value of –30.2 ± 0.1‰. Chlorophyll *a* has a δ^{13}C value of –22.5 ± 0.1‰.

The pre-growth seawater DIC Δ^{14}C value (–439.8 ± 2.2‰) in the "Fossil" *T. pseudonana* culture is significantly ^{14}C-enriched in comparison to the post-growth Δ^{14}C value (−843.1 ± 1.3‰). The δ^{13}C values of the pre- and post-growth DIC show the exceptional pattern of a ^{13}C-depletion during the culture growth. While the DIC δ^{13}C value equaled –16.5 ± 0.1‰ before growth of *T. pseudonana*, it decreased to –23.6 ± 0.1‰ after culture growth representing the most depleted DIC δ^{13}C value of the entire data set. All biomarker Δ^{14}C values are bracketed by the DIC Δ^{14}C values. The $C_{16:0}$ alkanoic acid (−653.3 ± 2.0‰) and the $C_{16:1}$ alkanoic acid (–689.6 ± 23.7‰) agree within 2σ analytical uncertainty. Chlorophyll *a* is more ^{14}C-depleted (–706.5 ± 2.3‰) than both concurrent alkanoic acids but agrees within 1σ analytical uncertainty with the $C_{16:1}$ alkanoic acid. The δ^{13}C value of the $C_{16:0}$ alkanoic acid (–42.6 ± 1.0‰) is the most ^{13}C-depleted value of the

entire data set. Likewise, chlorophyll *a* is substantially more ^{13}C-depleted (–34.7 ± 1.0‰) than chlorophyll *a* in any of the other cultures.

DISCUSSION

All *E. huxleyi* and *T. pseudonana* main cultures reached stationary phase after 9–13 days. During this time interval, DIC utilization by algae ranged from ∼0.8–1.2 mmol/kg in the *E. huxleyi* cultures (in good agreement with final biomass; r^2 = 0.99) and ∼0.4–0.8 mmol/kg in the *T. pseudonana* cultures (**Supplementary Table S2**). While pre-growth DIC concentrations of 1.8–2.2 mmol/kg were in the range typically observed in the global ocean (Feely et al., 2001), it is obvious that the pre-growth DIC Δ^{14}C values differ from the theoretical values of the CO_2 used to manipulate the original seawater DIC, i.e., 40‰ (ambient air in AD2010/AD2011; Levin et al., 2013), –480‰, and –1000‰ for the "Modern," "Intermediate," and "Fossil" cultures, respectively. Only the pre-growth DIC Δ^{14}C value in the "Modern" *E. huxleyi* culture (60.0 ± 3.4‰) is close to the anticipated Δ^{14}C value. With offsets of approximately –85‰ and –100‰, the pre-growth DIC Δ^{14}C values in the "Modern" *T. pseudonana* culture and the "Intermediate" *E. huxleyi* cultures (**Figure 2** and **Supplementary Table S1**), respectively, are moderately close to the anticipated DIC Δ^{14}C values. In contrast, the pre-growth DIC Δ^{14}C values in the "Intermediate" *T. pseudonana* culture and both "Fossil" cultures are significantly more Δ^{14}C-enriched (∼290–560‰). This ^{14}C-enrichment is significantly higher than the ^{14}C-enrichment observed by Mollenhauer et al. (2005) in their "dead air" *Isochrysis* sp. culture (∼120–170‰). These authors attributed the ^{14}C-enrichment to exchange with the ambient air during the experiment (equaling ca. 10% of the total DIC species). Assuming diffusion of ambient air (Δ^{14}C = 40‰) was the cause in our experiments as well, it would account for 66.2, 27.8, and 53.9% of the DIC species in the "Intermediate" *T. pseudonana* culture, the "Fossil" *E. huxleyi* culture, and the 'Fossil" *T. pseudonana* culture, respectively. However, our post-growth DIC Δ^{14}C values challenge this explanation for our experiments. Relative to pre-growth DIC, the post-growth DIC Δ^{14}C values are only ^{14}C-enriched in the "Modern" and "Fossil" *E. huxleyi* cultures and are in fact more ^{14}C-depleted in the "Intermediate" *E. huxleyi* and all *T. pseudonana* cultures (**Figure 2**), which cannot be explained by diffusion of atmospheric ^{14}C. This observation requires the introduction of a ^{14}C-depleted carbon source to the DIC pool, which, however, is not observed in the post-growth DIC pool of the "Modern" and "Fossil" *E. huxleyi* cultures. The ^{14}C-depletion cannot be explained by kinetic or equilibrium isotope fractionation either. Equilibrium fractionation of carbon isotopes occurs during exchange of gaseous CO_2 and the different seawater DIC species, but equilibrium effects should result in Δ^{14}C-enrichment of bicarbonate and carbonate (the primary DIC species at pH ∼8) relative to $CO_{2(aq)}$/carbonic acid analogous to δ^{13}C values (Mook, 1986; Zhang et al., 1995). For example, an equilibrium effect of ∼8–9‰ in δ^{13}C for total DIC at pH ∼8.2 and 15°C (Mook, 1986; Zhang et al., 1995) would result in an approximately 16–18‰ enrichment in Δ^{14}C. Likewise, algal DIC utilization causes ^{13}C and ^{14}C enrichment of the substrate, as evident for the δ^{13}C values in our data set, which show enrichment ranging from 2.4 to 9.0‰ (**Figure 3** and **Supplementary Table S1**). Accordingly, kinetic effects would account for roughly 5 to 18‰ Δ^{14}C-enrichment irrespective of which DIC species was utilized. However, Δ^{14}C values are corrected for such fractionation effects by normalizing to a δ^{13}C value of –25‰ (Stuiver and Polach, 1977). Accordingly, the ^{14}C-depletion in the "Intermediate" *E. huxleyi* and all *T. pseudonana* cultures have to be explained by other factors.

The mismatch between the anticipated DIC Δ^{14}C values and the measured Δ^{14}C values may indicate problems during initial DIC manipulation. In comparison to Mollenhauer et al. (2005), we did not acidify the seawater to expel DIC, but rather expelled DIC by sparging with CO_2-free air directly. This is a common approach in phytoplankton physiology to achieve DIC-free media, e.g., for testing the DIC-dependence of photosynthesis (Badger et al., 1994; Rost et al., 2003). Even though acidification accelerates the procedure, our setup has been routinely used to achieve DIC-free medium without acidification (typically within 24 h), which has been confirmed by direct measurements using Membrane-Inlet MS (Rost et al., 2007). In general, the measured DIC δ^{13}C and Δ^{14}C values attest to isotopic exchange of the DIC species since they would otherwise mirror natural North Sea surface seawater values, i.e., δ^{13}C values between 0‰ and 1‰ (Burt et al., 2016) and Δ^{14}C values close to atmospheric values in AD2010. We did not obtain Δ^{14}C values for untreated North Sea seawater DIC and (to our knowledge) no direct observational data are available for the most recent decades, but post-bomb surface water Δ^{14}C values until AD1989 inferred from *A. islandica* indicate that Δ^{14}C values should be slightly more enriched than atmospheric Δ^{14}C values (Scourse et al., 2012). Mass balance using pre-growth DIC Δ^{14}C values for the "Fossil" *E. huxleyi* and *T. pseudonana* cultures reveals that 72 and 46% of the total DIC was exchanged, respectively (endmembers –1000‰ and 40‰). We cannot exclude problems during DIC manipulation such as potential contamination with other CO_2 sources in the custom-made gas flow control unit or deviations from 1:1 v:v gas mixtures, which may explain the deviation of the pre-growth DIC Δ^{14}C values from the anticipated values. However, such problems cannot explain the observed isotopic shift to more depleted post-growth DIC Δ^{14}C values in the "Intermediate" *E. huxleyi* and all *T. pseudonana* cultures (**Figure 2**). In the absence of other processes explaining this ^{14}C-depletion, we conclude that contribution of blank carbon is the most likely explanation for the observed isotopic shift between pre- and post-growth DIC Δ^{14}C values.

Final DIC-derived C amounts ranged from 66.7 to 140.6 μmol, i.e., 0.8–1.7 mg C (**Table 1**). Accordingly, we consider combustion and graphitization blanks, combined typically in the range of ∼1 μg C (e.g., Pearson et al., 1998; Shah and Pearson, 2007; Santos et al., 2010), negligible. Hence, it is more likely that the shift in both pre- and post-growth DIC Δ^{14}C values has occurred due to the contribution of some unknown blank source during the experiment or during sample storage until ^{14}C analysis. A significant sample storage effect has been

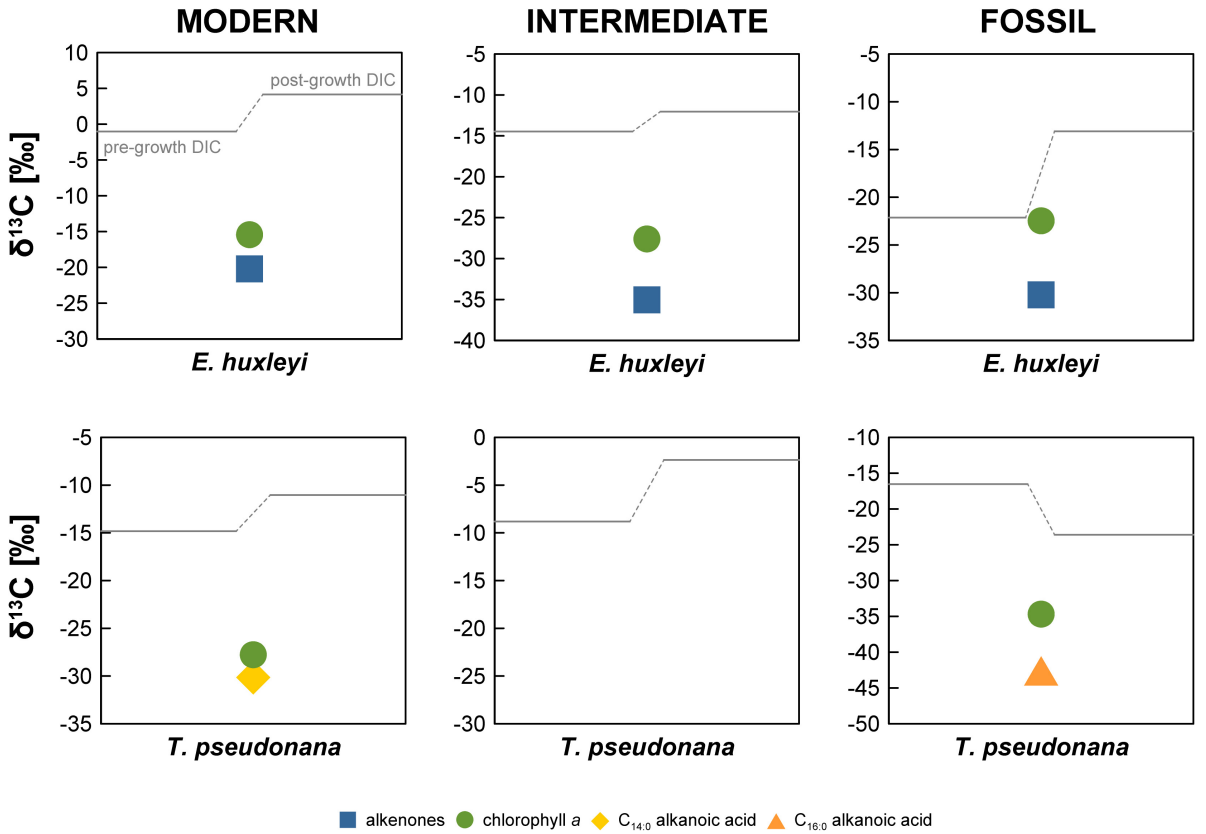

FIGURE 3 | Stable carbon isotopic composition (δ^{13}C in ‰) of the *E. huxleyi* and *T. pseudonana* cultures. Errors bars are ±0.1‰, not shown due to scale.

TABLE 1 | Sample amounts of DIC and purified compounds.

	Modern		Intermediate		Fossil	
Sample	**Graphite (μmol C)**	**GC (μg compound)**	**Graphite (μmol C)**	**GC (μg compound)**	**Graphite (μmol C)**	**GC (μg compound)**
E. huxleyi						
DIC pre-growth	186.2	n.d.	179.3	n.d.	164.0	n.d.
DIC post-growth	66.7	n.d.	115.6	n.d.	73.2	n.d.
chlorophyll *a*	3.9	n.d.	6.7	n.d.	6.1	n.d.
alkenones	75.2	410.0	57.0	147.9	49.2	134.9
T. pseudonana						
DIC pre-growth	209.2	n.d.	217.2	n.d.	232.3	n.d.
DIC post-growth	136.0	n.d.	140.6	n.d.	183.4	n.d.
chlorophyll *a*	6.4	n.d.	n.g.	n.d.	20.0	n.d.
$C_{14:0}$ alkanoic acid	16.5	283.7	n.g.	4.2	–	–
$C_{16:0}$ alkanoic acid	–	–	n.g.	6.4	3.0	23.0
$C_{16:1}$ alkanoic acid	–	–	–	–	n.g.	18.0

n.d., not determine; n.g., not graphitized. Sample analyzed as CO_2.

observed for DIC δ^{13}C values due to gas exchange through the septum even in the absence of an atmospheric headspace (Olack et al., 2018). As discussed above, an atmospheric blank C source cannot explain ^{14}C-depletion of DIC during the "Intermediate" *E. huxleyi* and all *T. pseudonana* experiments or subsequent sample storage, but likely has to derive from material produced from petroleum sources. However, the only such material used during the experiments were the septa, which are made of chemically highly resistant PTFE. It is also puzzling that the observed shifts are not unidirectional in each of the *E. huxleyi* and *T. pseudonana* cultures grown under the same manipulated DIC ^{14}C levels, e.g., ^{14}C-enrichment in the "Fossil" cultures and

^{14}C-depletion in the "Modern" cultures if the actual blank C had some intermediate Δ^{14}C value. The non-unidirectional nature of the shift between pre- and post-growth DIC Δ^{14}C makes it virtually impossible to determine a common blank source in the samples. Moreover, although the pre- and post-growth DIC Δ^{14}C value in the "Modern" *E. huxleyi* culture is close to the anticipated value of 40‰, it is obvious that a ^{14}C-enriched blank C source was added during this particular experiment, resulting in pre- and post-growth DIC Δ^{14}C values of 60.0 ± 3.4‰ and 83.0 ± 3.5‰, respectively. In this particular DIC sample, the δ^{13}C values are ^{13}C-enriched (−1.0 ± 0.1‰ and 4.2 ± 0.1‰, **Figure 3**) in comparison to atmospheric δ^{13}C values, which globally were around −8.3‰ in AD2010/AD2011 (Graven et al., 2017), but in agreement with equilibrium fractionation effects (∼9.0‰ for total DIC at pH ∼8.2 and 15°C; Mook, 1986) in the pre-growth DIC sample. With the exception of the "Fossil" *T. pseudonana* culture, δ^{13}C values in the post-growth DIC are enriched compared to pre-growth DIC as can be expected due to kinetic isotope fractionation during DIC assimilation in algal biomass (Degens et al., 1968). Irrespective of a kinetic effect, however, it is evident that the pre-growth DIC δ^{13}C values differ significantly (5.6–13.8‰) between the *E. huxleyi* and *T. pseudonana* cultures of each ^{14}C manipulation experiment further emphasizing significant blank C contribution of unknown origin during the experiments (based on the ^{14}C-depleted DIC signature of the "Modern" *T. pseudonana culture)*. Overall, the large scatter of DIC Δ^{14}C (and δ^{13}C) values and the non-unidirectionality of the pre- and post-growth DIC Δ^{14}C shifts (**Figure 2**) does not allow us to constrain a common blank C source.

The somewhat random pattern of pre- and post-growth DIC Δ^{14}C values also impairs our ability to accurately quantify the blank C added during biomarker purification. If the DIC Δ^{14}C values were properly constrained (or at least the pre-growth DIC Δ^{14}C value), deviations of biomarker Δ^{14}C values from the DIC Δ^{14}C values could be used to calculate the amount and isotopic composition of the blank C using propagated isotope mass balance (e.g., Shah and Pearson, 2007). In the absence of uncompromised DIC Δ^{14}C values, biomarker Δ^{14}C values can only be compared relative to one another, which may allow blank C calculations. The comparison shows that LC-purified chlorophyll *a* is significantly more ^{14}C-depleted in the "Modern" and "Intermediate" *E. huxleyi* and the "Modern" *T. pseudonana* cultures compared to wet-chemically purified alkenones and the GC-purified $C_{14:0}$ alkanoic acid (**Figure 2**). In contrast, chlorophyll *a* and alkenones as well as chlorophyll *a* and LMW alkanoic acids agree within 2σ analytical uncertainty in the "Fossil" *E. huxleyi* culture and the "Intermediate" and "Fossil" *T. pseudonana* cultures. So far, the wet-chemical alkenone isolation procedure and preparative GC methods have primarily been shown not to add significant blank C to samples, i.e., Δ^{14}C values of pure and processed standards agree within 2σ analytical uncertainty (Mollenhauer et al., 2005; Zencak et al., 2007; Mollenhauer and Rethemeyer, 2009; Wakeham and McNichol, 2014). Theoretically, alkenone and LMW *n*-alkanoic acid Δ^{14}C values should, thus, mirror DIC Δ^{14}C values. In comparison, LC isolation methods have been shown to add blank C with an Δ^{14}C isotopic composition of approximately −400‰ to −600‰, the amount of which depends on the effluent volume (Shah and Pearson, 2007; Birkholz et al., 2013). This would be consistent with a ^{14}C-depletion of chlorophyll *a* in comparison to alkenones and LMW alkanoic acids in the "Modern" cultures. However, closer inspection of the actual Δ^{14}C values of compound pairs in our cultures shows that this is not a consistent pattern. For example, the LMW alkanoic acids in the "Modern" and "Intermediate" *T. pseudonana* cultures agree within 2σ analytical uncertainty, but chlorophyll *a* is significantly more ^{14}C-depleted in the "Modern" culture while it agrees with LMW alkanoic

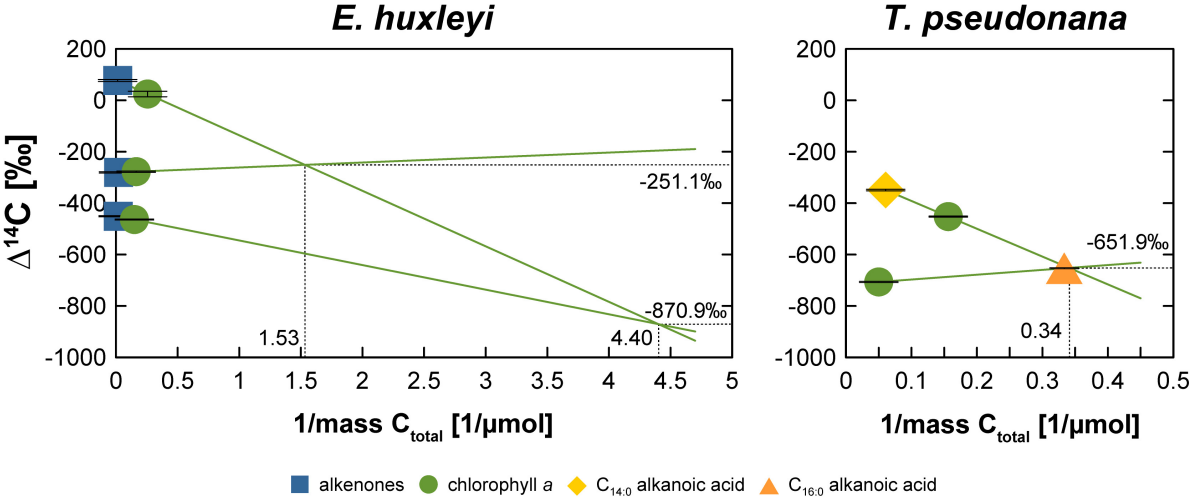

FIGURE 4 | Blank C characterization for the chlorophyll *a* isolation procedure assuming alkenones (*E. huxleyi*) or alkanoic acids (*T. pseudonana*) represent the "true" Δ^{14}C value for the different ^{14}C manipulation experiments of each algal culture. The intercepts of the respective regression lines represent the Δ^{14}C value and mass (1/µmol) of the respective blank C. C_{total} is defined as the C concentration of the sample plus blank.

acids in the "Intermediate" culture (**Figure 2**). Accordingly, if we use the alkenone or alkanoic acid Δ^{14}C values to calculate the blank for the LC-based chlorophyll *a* isolation method (**Figure 4**), a non-unidirectionality of the blank C contribution to the different chlorophyll *a* samples becomes obvious as well as the resulting large range of possible blank amount and isotopic composition. Assuming alkenones or alkanoic acids were unaffected by extraneous carbon (**Supplementary Figures S1–S11**) and represent the Δ^{14}C (DIC) value of each culture, extrapolation of the Δ^{14}C and 1/mass values of the respective compound pairs in each culture reveals that the blank C contribution (based on the intercepts) falls somewhere between 0.23 and 0.65 μmol (2.7 to 7.8 μg) with a Δ^{14}C value of –870.9‰ to –251.1‰, respectively, for the *E. huxleyi* culture and 2.93 μmol (35.3 μg) with a Δ^{14}C value of –651.9‰ in the *T. pseudonana* culture. Further, if 1σ analytical uncertainties are included, the chlorophyll *a* isolation blank in the *E. huxleyi* culture for example ranges from 0.15 μmol with a Δ^{14}C value of –1000.0‰ to 0.89 μmol with a Δ^{14}C value of –223.4‰. Such large ranges are obviously of little help for blank corrections. Whether this simply results from the relative blank C amount in the respective chlorophyll *a* sample or whether alkanoic acids may in fact also be affected by blank C cannot unequivocally be determined in the absence of reliable DIC Δ^{14}C constraints. The respective kinetic ^{13}C fractionation factors also do not aid in distinguishing these effects since they are similar for the alkenones (–19.2‰ and –20.5‰) or chlorophyll *a* (–14.4‰ and –13.1‰) in both the "Modern" and "Intermediate" cultures, respectively (**Figure 3**). Furthermore, in case of the "Fossil" *E. huxleyi* culture, the good agreement of chlorophyll *a* and alkenone Δ^{14}C values and their positive offset to pre-growth DIC Δ^{14}C values would suggest that both purification methods are affected by similar ^{14}C-enriched blank C contributions. However, the δ^{13}C value of chlorophyll *a* in this sample basically mirrors the pre-growth DIC δ^{13}C value, which would imply the absence of any kinetic isotope fractionation during pigment synthesis in this batch. This could result from ^{13}C-enrichment of DIC during batch growth, but DIC uptake was even higher in the "Modern" *E. huxleyi* culture (**Supplementary Table S2**) and chlorophyll *a* is ^{13}C-depleted relative to pre-growth DIC in that culture (and all other cultures). This strongly suggests that the chlorophyll *a* Δ^{14}C value is affected by some modern blank C. Mass balance calculations to obtain blank C amounts and isotopic compositions based on relative biomarker Δ^{14}C differences, thus, need to be corroborated by reliable DIC Δ^{14}C values. Alternatively, bulk biomass Δ^{14}C values could aid at determining blank C contributions, unfortunately, however, sample size restrictions did not permit bulk analyses in our study.

Our study illustrates the difficulties associated with natural level ^{14}C manipulation of algal cultures in an attempt to obtain authentic "isotopically labeled" biomarker standards, which are not commercially available. Our data show that we entered a vicious cycle of blank C contamination hampering our initial goal to accurately determine the blank C associated with different compound purification methods for CSRA. Considering that culturing is a laborious and time-consuming approach to obtain authentic standards, researchers should be certain that natural level ^{14}C manipulation of DIC has yielded the anticipated Δ^{14}C values prior to inoculation of algae and that these Δ^{14}C values can be maintained during the course of the experiment (e.g., via continuous sparging with CO_2). This, however, is only possible if access to AMS facilities and very quick turnaround is assured to avoid blank C addition during sample storage until inoculation. This possibly restricts the ^{14}C-manipulation culturing approach to laboratories housing both culturing and AMS facilities. In any case, potential blank C addition during sample storage should be tested in future studies and we would also recommend obtaining total biomass Δ^{14}C values if samples sizes permit these analyses.

DATA AVAILABILITY STATEMENT

All datasets generated for this study are included in the article/**Supplementary Material**.

AUTHOR CONTRIBUTIONS

SK, GM, and BR designed the study. SK, AB, and K-UR performed the analyses. SK wrote the manuscript with input from all authors.

FUNDING

This study was funded by the Helmholtz Young Investigator Group "Applications of molecular ^{14}C analysis for the study of sedimentation processes and carbon cycling in marine sediments". The workshop was funded by the Deutsche Forschungsgemeinschaft (DFG, German Research Foundation) – project number: 422798570.

ACKNOWLEDGMENTS

The authors thank Ralph Kreutz for help with sample extraction and biomarker purification, and the Hanse-Wissenschaftskolleg Delmenhorst, Germany, for sponsoring the "Marine Organic Biogeochemistry" workshop in April 2019. The authors also thank all reviewers for their constructive feedback which helped to improve this manuscript. This is a contribution to the Frontiers in Marine Science Marine Biogeochemistry Research Topic emanating from this workshop.

SUPPLEMENTARY MATERIAL

The Supplementary Material for this article can be found online at: https://www.frontiersin.org/articles/10.3389/fmars.2019.00780/full#supplementary-material

REFERENCES

Badger, M. R., Palmqvist, K., and Yu, J.-W. (1994). Measurement of CO_2 and HCO_3^- fluxes in cyanobacteria and microalgae during steady-state photosynthesis. *Physiol. Plant.* 90, 529–536. doi: 10.1034/j.1399-3054.1994.900314.x

Birkholz, A., Smittenberg, R. H., Hajdas, I., Wacker, L., and Bernasconi, S. M. (2013). Isolation and compound specific radiocarbon dating of terrigenous branched glycerol dialkyl glycerol tetraethers (brGDGTs). *Organ. Geochem.* 60, 9–19. doi: 10.1016/j.orggeochem.2013.04.008

Burt, W. J., Thomas, H., Hagens, M., Pätsch, J., Clargo, N. M., Salt, L. A., et al. (2016). Carbon sources in the North Sea evaluated by means of radium and stable carbon isotope tracers. *Limnol. Oceangr.* 61, 666–683. doi: 10.1002/lno.10243

Degens, E. T., Guillard, R. R. L., Sackett, W. M., and Hellebust, J. A. (1968). Metabolic fractionation of carbon isotopes in marine plankton—I. Temperature and respiration experiments. *Deep Sea Res. Oceanogr. Abstr.* 15, 1–9. doi: 10.1016/0011-7471(68)90024-7

Drenzek, N. J., Hughen, K. A., Montlucon, D. B., Southon, J. R., Santos dos, G. M., Druffel, E. R. M., et al. (2009). A new look at old carbon in active margin sediments. *Geology* 37, 239–242. doi: 10.1130/g25351a.1

Feely, R. A., Sabine, C. L., Takahashi, T., and Wanninkhof, R. (2001). Uptake and storage of carbon dioxide in the ocean: the global CO_2 survey. *Oceanography* 14, 18–32. doi: 10.5670/oceanog.2001.03

Feng, X., Vonk, J., van Dongen, B., Gustafsson, Ö, Semiletov, I. P., Dudarev, O. V., et al. (2013). Differential mobilization of terrestrial carbon pools in Eurasian Arctic river basins. *Proc. Natl. Acad. Sci. U.S.A.* 110, 14168–14173. doi: 10.1073/pnas.1307031110

Graven, H., Allison, C. E., Etheridge, D. M., Hammer, S., Keeling, R. F., Levin, I., et al. (2017). Compiled records of carbon isotopes in atmospheric CO_2 for historical simulations in CMIP6. *Geosci. Model Dev.* 10, 4405–4417. doi: 10.5194/gmd-10-4405-2017

Guillard, R. R. L., and Ryther, J. H. (1962). Studies of marine planktonic diatoms: I. *Cyctotella nana* Hustedt, and *Detonula confervacea* (Cleve) gran. *Can. J. Microbiol.* 8, 229–239. doi: 10.1139/m62-029

Ingalls, A. E., Shah, S. R., Hansman, R. L., Aluwihare, L. I., Santos, G., Druffel, E. R. M., et al. (2006). Quantifying archaeal community autotrophy in the mesopelagic ocean using natural radiocarbon. *Proc. Natl. Acad. Sci. U.S.A.* 103, 6442–6447. doi: 10.1073/pnas.0510157103

Kusch, S., Kashiyama, Y., Ogawa, N. O., Altabet, M., Butzin, M., Friedrich, J., et al. (2010a). Implications for chloro-and pheopigment synthesis and preservation from combined compound-specific $\delta^{13}C$, $\delta^{15}N$, and $\Delta^{14}C$ analysis. *Biogeosciences* 7, 4105–4118. doi: 10.5194/bg-7-4105-2010

Kusch, S., Rethemeyer, J., Schefuß, E., and Mollenhauer, G. (2010b). Controls on the age of vascular plant biomarkers in Black Sea sediments. *Geochim. Cosmochim. Acta* 74, 7031–7047. doi: 10.1016/j.gca.2010.09.005

Levin, I., Kromer, B., and Hammer, S. (2013). Atmospheric $\Delta^{14}CO_2$ trend in Western European background air from 2000 to 2012. *Tellus B* 65, 57–57.

McNichol, A. P., Osborne, E. A., Gagnon, A. R., Fry, B., and Jones, G. A. (1994). TIC, TOC, DIC, DOC, PIC, POC—unique aspects in the preparation of oceanographic samples for ^{14}C-AMS. *Nuclear Instr. Methods Phys. Res. B* 92, 162–165. doi: 10.1016/0168-583x(94)95998-6

Mollenhauer, G., and Eglinton, T. I. (2007). Diagenetic and sedimentological controls on the composition of organic matter preserved in California Borderland Basin sediments. *Limnol. Oceangr.* 52, 558–576. doi: 10.4319/lo.2007.52.2.0558

Mollenhauer, G., Inthorn, M., Vogt, T., Zabel, M., Sinninghe Damsté, J. S., and Eglinton, T. I. (2007). Aging of marine organic matter during cross-shelf lateral transport in the Benguela upwelling system revealed by compound-specific radiocarbon dating. *Geochem. Geophys. Geosyst.* 8:Q09004. doi: 10.1029/2007GC001603

Mollenhauer, G., Montlucon, D. B., and Eglinton, T. I. (2005). Radiocarbon dating of alkenones from marine sediments: II. Assessment of carbon process blanks. *Radiocarbon* 47, 413–424. doi: 10.1017/s0033822200035190

Mollenhauer, G., and Rethemeyer, J. (2009). Compound-specific radiocarbon analysis – Analytical challenges and applications. *IOP Confer. Ser. Earth Environ. Sci.* 5, 1–9.

Mook, W. G. (1986). ^{13}C in atmospheric CO_2. *Netherlands J. Sea Res.* 20, 211–223. doi: 10.1016/0077-7579(86)90043-8

Nielsen, M. V. (1997). Growth, dark respiration and photosynthetic parameters of the coccolithophorid *Emiliania huxleyi* (prymnesiophyceae) acclimated to different day length-irradiance combinations. *J. Phycol.* 33, 818–822. doi: 10.1111/j.0022-3646.1997.00818.x

Ohkouchi, N., Xu, L., Reddy, C. M., Montlucon, D., and Eglinton, T. I. (2005). Radiocarbon dating of alkenones from marine sediments: I. Isolation protocol. *Radiocarbon* 47, 401–412. doi: 10.1017/s0033822200035189

Olack, G. A., Colman, A. S., Pfister, C. A., and Wootton, J. T. (2018). Seawater DIC analysis: the effects of blanks and long-term storage on measurements of concentration and stable isotope composition. *Limnol. Oceanogr. Methods* 16, 160–179. doi: 10.1002/lom3.10235

Pearson, A., McNichol, A. P., Schneider, R. J., von, R. F., and Zheng, Y. (1998). Microscale AMS ^{14}C measurement at NOSAMS. *Radiocarbon* 40, 61–75. doi: 10.1017/s0033822200017902

Pearson, A., Seewald, J. S., and Eglinton, T. I. (2005). Bacterial incorporation of relict carbon in the hydrothermal environment of Guaymas Basin. *Geochim. Cosmochim. Acta* 69, 5477–5486. doi: 10.1016/j.gca.2005.07.007

Rost, B., Kranz, S. A., Richter, K.-U., and Tortell, P. D. (2007). Isotope disequilibrium and mass spectrometric studies of inorganic carbon acquisition by phytoplankton. *Limnol. Oceanogr. Meth.* 5, 328–337. doi: 10.4319/lom.2007.5.328

Rost, B., Riebesell, U., Burkhardt, S., and Sültemeyer, D. (2003). Carbon acquisition of bloom-forming marine phytoplankton. *Limnol. Oceanogr.* 48, 55–67. doi: 10.4319/lo.2003.48.1.0055

Ruff, M., Wacker, L., Gäggeler, H. W., Suter, M., Synal, H.-A., and Szidat, S. (2007). A gas ion source for radiocarbon measurements at 200kV. *Radiocarbon* 49, 307–314. doi: 10.1017/s0033822200042235

Santos, G. M., Southon, J. R., Drenzek, N. J., Ziolkowski, L. A., Druffel, E., Xu, X., et al. (2010). Blank assessment for ultra-small radiocarbon samples: chemical extraction and separation versus AMS. *Radiocarbon* 52, 1322–1335. doi: 10.1017/s0033822200046415

Scourse, J. D., Wanamaker, A. D., Weidman, C., Heinemeier, J., Reimer, P. J., Butler, P. G., et al. (2012). The marine radiocarbon bomb pulse across the temperate North Atlantic: a compilation of Δ^{14}C time histories from *Arctica islandica* growth increments. *Radiocarbon* 54, 165–186. doi: 10.2458/azu_js_rc.v54i2.16026

Shah, S. R., and Pearson, A. (2007). Ultra-microscale (5–25 μg C) analysis of individual lipids by ^{14}C AMS: assessment and correction for sample processing blanks. *Radiocarbon* 49, 69–82. doi: 10.1017/s0033822200041904

Stuiver, M., and Polach, H. A. (1977). Discussion: reporting of ^{14}C Data. *Radiocarbon* 19, 355–363. doi: 10.1017/s0033822200003672

Wakeham, S. G., and McNichol, A. P. (2014). Transfer of organic carbon through marine water columns to sediments - insights from stable and radiocarbon isotopes of lipid biomarkers. *Biogeosciences* 11, 6895–6914. doi: 10.5194/bg-11-6895-2014

Zencak, Z., Reddy, C. M., Teuten, E. L., Xu, L., McNichol, A. P., and Gustafsson, Ö (2007). Evaluation of gas chromatographic isotope fractionation and process contamination by carbon in compound-specific radiocarbon analysis. *Anal. Chem.* 79, 2042–2049. doi: 10.1021/ac061821a

Zhang, J., Quay, P. D., and Wilbur, D. O. (1995). Carbon-isotope fractionation during gas-water exchange and dissolution of CO_2. *Geochim. Cosmochim. Acta* 59, 107–114. doi: 10.1016/0016-7037(95)91550-d

Conflict of Interest: The authors declare that the research was conducted in the absence of any commercial or financial relationships that could be construed as a potential conflict of interest.

frontiers in Marine Science

BRIEF RESEARCH REPORT
published: 15 January 2020
doi: 10.3389/fmars.2019.00815

Substantial Carbohydrate Hydrolase Activities in the Water Column of the Guaymas Basin (Gulf of California)

Kai Ziervogel[1]* *and Carol Arnosti*[2]

[1] Institute for the Study of Earth, Oceans and Space, University of New Hampshire, Durham, NH, United States,
[2] Department of Marine Sciences, The University of North Carolina at Chapel Hill, Chapel Hill, NC, United States

The Guaymas Basin spreading center situated in the Gulf of California is characterized by a thick layer of organic-rich sediments that are thermally altered by hydrothermal fluids, thereby providing a bottom water source of dissolved organic carbon (DOC) to the water column. The potential for heterotrophic microbial communities in the water column to metabolize this organic matter source has not yet been investigated, however. In order to assess heterotrophic potential in the water column of the Guaymas Basin, we measured the activities of carbohydrate-hydrolyzing extracellular enzymes at the chlorophyll maximum, the oxygen minimum, the deep-water turbidity plume, and bottom waters. These measurements were carried out using water obtained from repeat CTD casts over the course of a week, and from bottom water collected by HOV *Alvin* at hydrothermally active areas with extensive chemosynthetic microbial mats. Repeat measurements at subsurface depths were very comparable across sampling dates and CTD casts. Exo-acting (terminal-unit-cleaving) monosaccharide hydrolase activities were typically higher in deeper waters than in surface waters, despite colder temperatures. In bottom water, the spectrum of endo-acting (mid-chain-cleaving) polysaccharide hydrolase activities was broader than at shallower depths. The high enzyme activities in Guaymas Basin bottom waters indicate an unusually active heterotrophic community that is responding to influx of DOC and nutrients into bottom waters from the hydrothermally affected sediments, or to the availability of chemosynthetically produced biomass.

Keywords: heterotrophic activity, extracellular enzymes, polysaccharides, dissolved organic carbon, hydrothermal vent, water column, Gulf of California, Guaymas Basin

OPEN ACCESS

Edited by:
Gordon T. Taylor,
Stony Brook University, United States

Reviewed by:
Maria Montserrat Sala,
Institute of Marine Sciences (CSIC), Spain
Brian Gaas,
Government of Yukon, Canada

***Correspondence:**
Kai Ziervogel
kai.ziervogel@unh.edu

Specialty section:
This article was submitted to Marine Biogeochemistry, a section of the journal Frontiers in Marine Science

Received: *08 September 2019*
Accepted: *17 December 2019*
Published: *15 January 2020*

Citation:
Ziervogel K and Arnosti C (2020) Substantial Carbohydrate Hydrolase Activities in the Water Column of the Guaymas Basin (Gulf of California). Front. Mar. Sci. 6:815. doi: 10.3389/fmars.2019.00815

INTRODUCTION

The Guaymas Basin is part of a spreading center that underlies highly productive surface waters in the Gulf of California (Kahru et al., 2004). The flux of organic matter from the surface has accumulated to a sediment layer several hundred meters in thickness (Einsele et al., 1980; Schrader et al., 1980) that is substantially modified by the passage of hydrothermal fluids (Simoneit et al., 1979; Von Damm et al., 1985). This organic matter fuels a diverse community of benthic microbes carrying out autotrophic and heterotrophic processes based on the flux of reduced elements into the water column as well as the availability of hydrothermally-produced petroleum products (Teske et al., 2002, 2014; Dombrowski et al., 2018).

The water column of the Guaymas Basin is also greatly affected by hydrothermal activity, with plumes of vent fluids influencing the chemistry of the water column below the basin

sill depth of 1560 m (Campbell and Gieskes, 1984). Previous research has demonstrated the presence of autotrophic microbes and autotrophic production fueled by reduced metals, sulfur and hydrogen metabolism (e.g., Anantharaman et al., 2013). Active seeping of fluids from the organic-rich sediments carries high concentrations of dissolved organic carbon (DOC) into the water column (Lin et al., 2017). This DOC could potentially stimulate activities of heterotrophic microbes, providing a source of organic substrates at depth that could supplement the sinking flux of particulate organic carbon from the surface ocean. This possibility has not yet been investigated, however.

Here we report results of a survey of heterotrophic microbial activities in the water column of the Guaymas Basin. We focused on measurement of the activities of extracellular enzymes that catalyze the initial step in microbial degradation of high molecular weight (HMW) substrates. These enzymes are selective for specific structural features and hydrolyze HMW substrates to sizes sufficiently small for cellular uptake (Arnosti, 2011). The focus here is on carbohydrate-hydrolyzing enzymes, which are responsible for hydrolysis of a major class of marine organic matter. Two general modes of hydrolysis characterize extracellular enzymes: exo-acting extracellular enzymes cleave subunits from ends of a chain, while endo-acting enzymes cleave HMW substrates mid-chain. We used an array of different substrate proxies and HMW polysaccharides to measure both categories of enzyme activities. Measurements of carbohydrate-hydrolyzing enzyme activities in surface waters are quite common; there are far fewer measurements of exo-acting (Baltar et al., 2009, 2010) and endo-acting (Hoarfrost and Arnosti, 2017; Balmonte et al., 2018) carbohydrate hydrolase activities in the deep ocean. Sampling in the Guaymas Basin provides the opportunity to assess microbial heterotrophic activities in an environment that is potentially fueled with substrates from the bottom as well as from the surface ocean. Repeat CTD casts and water samples collected from HOV *Alvin* over the course of the cruise provided the opportunity to assess the range and variability of heterotrophic enzyme activities in this hydrothermally affected location.

MATERIALS AND METHODS

Sampling and Site Description

Water column samples were collected in the southern trough of the Guaymas Basin aboard RV *Atlantis* (AT15–56). Water column samples were taken from the depth of the deep chlorophyll maximum (DCM), the lower part of the oxygen minimum zone (OMZ), deep water turbidity plumes (Plume; ∼200 m above seafloor), and bottom waters (Bottom; ∼50 m above seafloor) with Niskin bottles mounted on a CTD rosette (CTD profiles are published on figshare). Samples from these four depths were taken during five CTD deployments (hereafter referred to as CTD1-CTD5) between November 22 and December 01, 2009, within an area of approximately 5000 m^2. Near bottom water samples (∼2 m above seafloor) were retrieved by a Niskin bottle mounted on the Human Occupied Vehicle (HOV) *Alvin* during four dives in the same area as the CTD deployments. The sediments ranged from hydrothermally active to bare sediments (see **Table 1** for a detailed description of sampling sites). Previously reported DOC concentrations in waters above the sediment were highly variable, ranging between 300 μM (Dive 4563) to over 2000 μM (Dive 4565) (Lin et al., 2017).

TABLE 1 | Sampling sites and water column parameters.

Sample ID	Lat/Long	Sampling depth, description	Temp (°C)	DOC (μM)	Bacterial cells (L^{-1})
CTD 1	27° 00.45N 111° 24.51W	50 m, DCM	24.5	234 ± 2.2	1.2E + 08
		900 m, OMZ	4.9	131 ± 2.3	5.1E + 07
		1950 m, Bottom	2.9	1292 ± 13.4	5.8E + 07
CTD 2	27° 00.47N 111° 24.41W	50 m, DCM	23.7	241 ± 5.6	n.a.
		1950 m, Bottom	2.9	160 ± 3.5	n.a.
CTD 3	27° 00.47N 111° 24.39W	50 m, DCM	24.1	192 ± 1.2	1.3E + 08
		920 m, OMZ	4.9	329 ± 5.7	7.9E + 07
		1800 m, Plume	2.9	148 ± 1.5	6.4E + 07
		1950 m, Bottom	2.9	785 ± 5.4	1.3E + 08
CTD 4	27° 00.46N 111° 24.44W	50 m, DCM	23.9	464 ± 3.2	1.5E + 08
		890 m, OMZ	4.9	847 ± 2.6	1.1E + 08
		1800 m, Plume	2.9	636 ± 7.4	6.5E + 07
		1950 m, Bottom	2.9	121 ± 2.0	8.5E + 07
CTD 5	27° 00.43N 111° 24.45W	50 m, DCM	22.5	157 ± 2.6	n.a.
		845 m, OMZ	5.3	1647 ± 2.8	n.a.
		1815 m, Plume	2.9	237 ± 2.9	n.a.
		1950 m, Bottom	2.9	141 ± 1.7	n.a.
Dive 4563	27° 00.47N 111° 24.43W	2009 m, Above patch of white, yellow and orange mat	2.9	303 ± 2.5*	4.1E + 07
Dive 4565	27° 00.70N 111° 24.27W	2010 m, Cathedral Hill: yellow and white sediment near massive structure of hydrothermal deposits	2.9	2112 ± 13.6*	5.1E + 07
Dive 4567	27° 00.54N 111° 24.49W	2011 m, Reference site, non-hydrothermal brown sediment	2.9	698 ± 6.9*	7.8E + 07
Dive 4570	27° 00.47N 111° 24.43W	2010 m, Large orange and white *Beggiatoa* mat	2.9	111 ± 2.4*	8.7E + 07

*Temp, water temperature; DOC, dissolved organic carbon; n.a., means not available; *means data were previously published in Lin et al. (2017).*

Measurements of Hydrolytic Enzyme Activities

Enzyme activities were measured using two experimental approaches that provide different information about the activities of specific types of enzymes. The first approach

used MUF-α-D-glucopyranoside (a-glu), MUF-ß-D-glucopyranoside (b-glu), MUF-β-D-fucoside (b-fu), and MUF-β-D-xylopyranoside (b-xyl) (all Sigma-Aldrich) as small substrate proxies to measure activities of exo-acting enzymes, which cleave terminal units from carbohydrates (Hoppe, 1983). These activities can be measured with short-term (several hour) incubations, reflecting enzymatic responses of the microbial community present in the sample at the time the substrate is added. Enzyme assays with the four substrate proxies were conducted in all of the samples in **Table 1** except for b-glu in CTD 4 (OMZ) and CTD 5 (all depths) due to a shortage of substrate. Incubations were conducted in replicate 4 mL acrylic cuvettes ($n = 3$) containing single substrates at enzyme-saturating levels (15 μM final concentration; determined at the beginning of the expedition) and 1.5 mL of seawater. The cuvettes were incubated in the dark for up to 12 h. Incubation temperatures were close to *in situ* temperatures (DCM: 20°C; OMZ: 5°C; Plume: 5°C; Bottom and near bottom: 3°C). Fluorescence was measured at the beginning and the end point using a Turner Biosystems TBS-380 fluorometer, with excitation/emission channels set to "UV" (365 nm excitation, 440–470 nm emission). Control cuvettes were prepared with artificial seawater (Sea salts, 38 g L^{-1}; Sigma) and MUF-substrates and incubated under the same conditions as the live cuvettes to control for abiotic substrate degradation, which was always minor. Fluorescence changes over time were calibrated using MUF standard and used to calculate potential hydrolysis rates.

The second experimental approach measured the activities of specific endo-acting enzymes that cleave target polysaccharides mid-chain. These experiments require comparatively long incubation times and therefore integrate microbial enzymatic induction and growth responses (including possible changes in community composition) to substrate addition. Longer incubation times are necessary because the time that is required for a polysaccharide pool to be hydrolyzed to lower molecular weights is not known *a priori* (Arnosti, 2003). Endo-acting enzyme activities were measured at three depths (DCM, OMZ, Bottom) in CTD 1, and in *Alvin*-collected water (Dive 4567, 4565) using fluorescently-labeled (FLA) pullulan, laminarin, xylan, and fucoidan (polysaccharides from Fluka or Sigma). The four polysaccharides differ in monomer composition and linkage position; they are components of marine algae (Painter, 1983) and are therefore present in considerable quantities in the ocean (Alderkamp et al., 2007). Moreover, activities of enzymes that specifically hydrolyze these substrates have been measured in a variety of marine environments (Arnosti et al., 2011), and genes corresponding to these enzymes have been identified in the genomes of marine bacterial isolates (Weiner et al., 2008; Wegner et al., 2013; Kabisch et al., 2014).

The substrates were labeled with fluoresceinamine and used to measure extracellular enzyme activities as described in Arnosti (1996, 2003). In brief, single substrates were added to 15 ml of samples water at a final concentration of 3.5 μM monomer equivalent. Two replicate vials per substrate and sample were prepared and incubated in the dark for 21 days at close to *in situ* temperature (see above). Throughout the incubation, 1 mL subsamples were taken after 0, 1.5, 4, 7, 11, and 21 days (CTD cast) and after 0, 1, 3, 7, and 14 days (*Alvin* water). Subsamples were immediately filtered through 0.2-μm surfactant free cellulose acetate (SFCA) syringe filters and the filtrate was stored at −20°C until analysis on a gel-permeation chromatography system with fluorescence detection, as described in detail in Arnosti (2003). The maximum hydrolysis rate among all time points in a sample was used as a measure of the maximum potential rate at which the microbial community could access a specific polysaccharide. Control incubations with artificial seawater did not reveal abiotic substrate degradation.

All rates reported here represent potential hydrolysis rates, as added substrate competes with naturally occurring substrates for active enzyme sites. Given the level of substrate addition, however, hydrolysis rates are likely zero order with respect to substrate and represent maximum potential rates.

Bacterial Cell Counts

Bacterial cells were fixed with formalin (2% final conc.) and stained with 4′, 6-diamidino-2-phenylindole (DAPI; Porter and Feig, 1980) on a 0.2-μm polycarbonate filter. Either 40 frames of view or 200 cells were counted per slide using epifluorescence microscopy (Olympus, magnification ×1000).

Dissolved Organic Carbon (DOC)

Water was filtered through 0.2-μm SFCA syringe filters and stored at −20°C in precombusted scintillation vials until analysis. Thawed samples were acidified with phosphoric acid (50% v/v) and analyzed by high temperature catalytic oxidation using a Shimadzu TOC-5000. Replicate measurements of a single sample ($n = 6$) were used to calculate average DOC centration ± standard deviations. Note that DOC concentrations in waters collected during *Alvin* dives 4563, 4565, 4567, 4570 were previously reported in Lin et al. (2017).

Statistical Analysis

Differences in hydrolysis rates (averages of $n = 3$) were tested with one-way ANOVAs and Student's *t*-test at the 5% significance level. Results from ANOVAs were compared with Tukey's *post hoc* test. Statistical analysis was conducting using JMP Pro 14 software.

RESULTS

Water column CTD profiles were very similar to the composite profile of Guaymas Basin from Campbell and Gieskes (1984). Water temperature was 24°C at the DCM, 4.9°C at the OMZ, and 2.9°C at the bottom (**Table 1**). Beam transmissometry data suggest presence of significant quantities of particles in lower portion of water column, including the 1800 and 1950 m sampling depths; these are likely due to abundant Mn oxides in the water column (Lesniewski et al., 2012).

DOC concentrations were generally higher at depths below the DCM than at the DCM, except for CTD 2 (**Table 1**). Highest DOC levels at 2112 ± 13.6 μM were found in *Alvin* water near a massive structure of hydrothermal deposits (Dive 4565). Bacterial

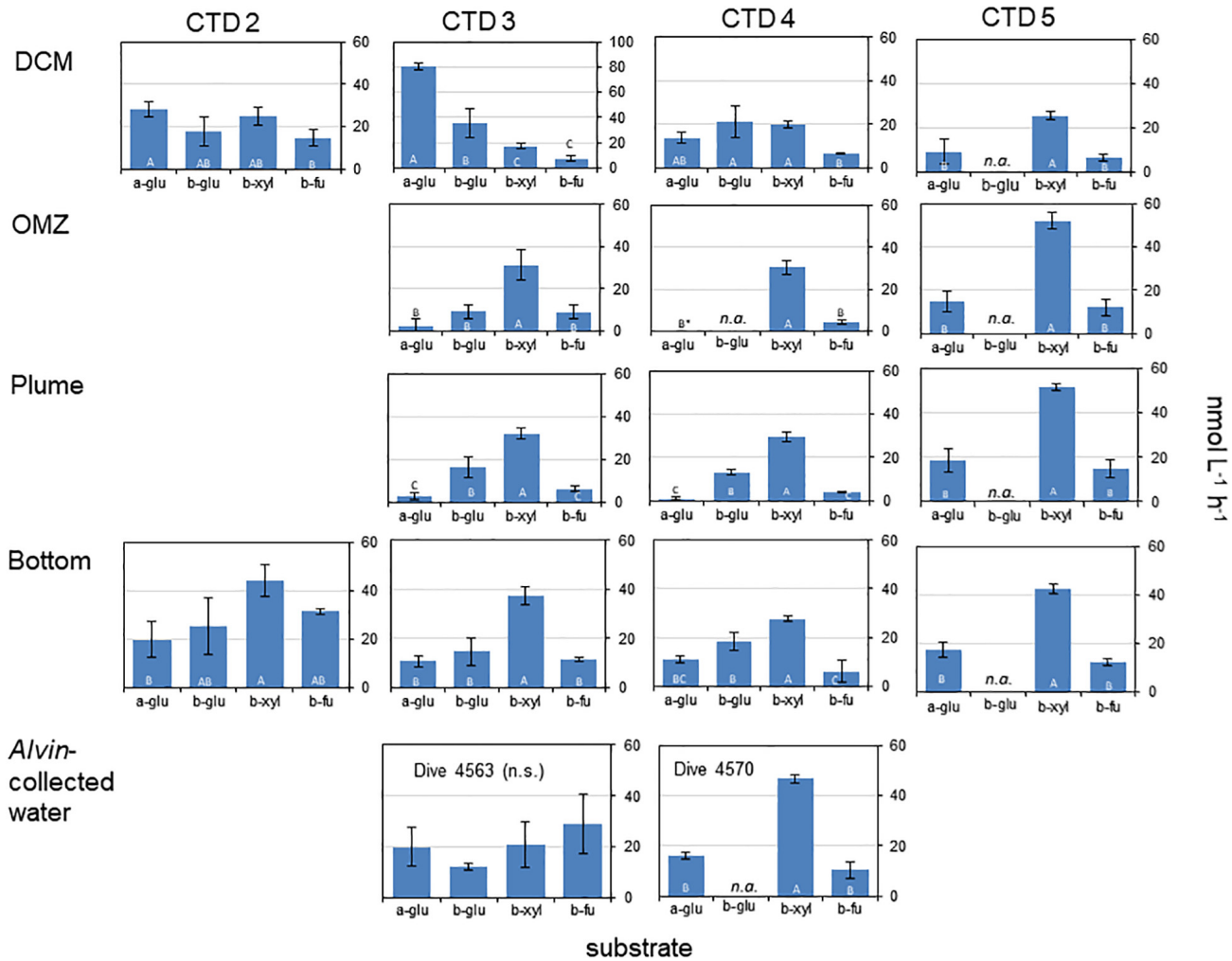

FIGURE 1 | Activities of exo-acting enzymes in water taken from CTD casts 2 – 5 and in water taken with HOV *Alvin*. a-glu - 4-MUF α-D-glucopyranoside; b-glu - 4-MUF β-D-glucopyranoside; b-xyl - 4-MUF ß-D-xylopyranoside; b- fu - 4-MUF ß-D-fucoside. DCM, Deep chlorophyll maximum; OMZ, Oxygen minimum zone; Bottom, Bottom water; Plume, Turbidity plume near the bottom (see **Table 1** for water depths and temperatures). Hydrolysis rates are average rates of $n = 3 \pm$ standard deviation. Letters indicate results of the *post hoc* analysis of treatment-specific differences in rates (one-way ANOVAs, $p < 0.05$); rates with the same letters are indistinguishable from one another. n.a. means not available; * means that a-glu activity was 0.

cell numbers at 50 m were somewhat higher (CTD 1 and CTD 4) or at the same level (CTD 3) than those at the bottom.

Activities of exo-acting enzymes (a-glu, b-glu, b-xyl, b-fu) were measurable at all depths for all CTD casts, with the exception of a-glu at OMZ for CTD4 where no activity was measurable (**Figure 1**).

Two particularly notable features stand out: despite a strong water column temperature gradient between the DCM and the depths below 50 m, rates of exo-acting enzyme activities did not decrease systematically with depth. This pattern was most pronounced for b-xyl activities that were always more rapid at the depths below 50 m than at 50 m. For CTD 2, activities of b-fu were also higher at the bottom compared to the DCM (**Table 2**). In addition, the patterns of enzyme activities – a high level of b-xyl activity, which was approximately twice as high as the other activities – was similar for all subsurface depths of all CTD casts (**Figure 1**). At the DCM, patterns of enzyme activities varied more among casts. At this depth, a-glu activities varied by a factor of ca. 8 among casts, and b-glu and b-fu activities varied by a factor of approximately 2 among casts; b-xyl activities were similar among casts, with average activities ranging from ∼17 to 25 nmol L^{-1} h^{-1}. The range of exo-acting activities (approximately 12–46 nmol L^{-1} h^{-1}) in *Alvin*-collected water was similar to the range of activities measured in water collected at depths of 1800 and 1950 m; b-xyl activities were notably higher than the other activities in Dive 5470 water, however.

Only 2 of the 4 polysaccharide hydrolase activities (laminarinase and pullulanase) were measurable at the DCM and OMZ; hydrolysis of laminarin and pullulan were a factor of 2–4 times highest at the DCM compared with the OMZ and Bottom. Xylanase activity was also measurable at the bottom

TABLE 2 | Results from *post hoc* comparison of depth-specific differences in exo-acting enzyme activities following a one-way ANOVA or a *T*-Test (CTD 2 only) with $p < 0.05$.

Substrate, sample	CTD 2	CTD 3	CTD 4	CTD 5
a-glu, DCM	n.s.	A	A	n.s.
a-glu, OMZ		C	B	
a-glu, Plume		C	B	
a-glu, Bottom		B	A	
b-glu, DCM	n.s.	A	n.s.	
b-glu, OMZ		B		
b-glu, Plume		B		
b-glu, Bottom		B		
b-xyl, DCM	B	B	B	C
b-xyl, OMZ	n.a.	A	A	A
b-xyl, Plume	n.a.	A	A	A
b-xyl, Bottom	A	A	A	B
b-fu, DCM	B	n.s.	n.s.	n.s.
b-fu, OMZ	n.a.			
b-fu, Plume	n.a.			
b-fu, Bottom	A			

Letter A indicates highest activity, letter B indicates intermediate activity, and letter C indicates lowest activity. n.s. means not significant; n.a. means not available.

at a rate that was faster than for laminarinase or pullulanase activities. Fucoidan hydrolysis was not detected in any depths of CTD 1. All 4 polysaccharides tested here, including Fucoidan, were hydrolyzed in *Alvin*-collected water, however. Considerable fucosidase activity (2.5–3.3 nmol monomer L^{-1} h^{-1}) was measurable in water collected above a microbial mat (Dive 4565) and in water collected over bare sediment (Dive 4567) (**Figure 2**). Xylan hydrolysis was also measurable (in one of two replicates for Dive 4567; at trace levels in water from Dive 4565), and hydrolysis of laminarin and pullulan was comparable to rates measured in bottom water.

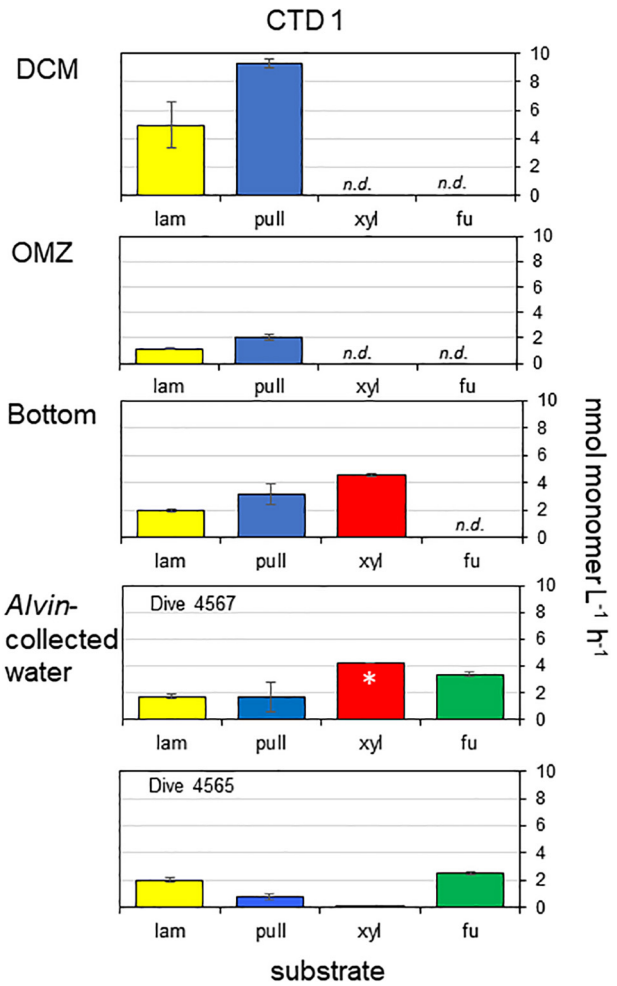

FIGURE 2 | Activities of endo-acting enzymes in water taken from CTD cast 1 and in water taken with HOV *Alvin*. Lam, laminarin; pull, pullulan; xyl, xylan; fu, fucoidan. Hydrolysis rates are average rates of $n = 2 \pm$ their range. n.d. means not detectable. * means that hydrolysis was detected in only one of the replicates.

DISCUSSION

The Guaymas Basin has considerable hydrothermal input that is retained to some extent at depths below its sill at 1560 m (Campbell and Gieskes, 1984), resulting in deep water that is hydrothermally affected and has a longer residence time than comparable depths in the open ocean. Focused investigations of microbial communities in the water column of the Guaymas Basin have centered primarily on comparisons between the sedimentary and water column communities (e.g., Dick and Tebo, 2010; Dick et al., 2013), and on autotrophic organisms that may thrive on the hydrothermal input of sulfur and reduced metals (Lesniewski et al., 2012; Anantharaman et al., 2013; Dick, 2019). The thick layer of organic matter blanketing the system (Simoneit et al., 1979; Schrader et al., 1980), however, is the source of a substantial flux of DOC from the sediments to the deep waters of the basin (**Table 1**; Lin et al., 2017), in addition to input of sinking POC from the productive surface waters.

The high activities of exo-acting enzymes, and the observation that these rates do not generally decrease with depth in the Guaymas Basin (**Figure 1**), indicate the presence of highly active heterotrophic microbial communities throughout the water column. Rates of b-glu, for example, ranged from 9 to 25 nmol L^{-1} h^{-1} over the depth range of 845–1950 m (**Figure 1**); at comparable depths in the central Atlantic Ocean, for example, rates of 0.05–0.25 nmol L^{-1} h^{-1} have been reported (Baltar et al., 2010), and in the subtropical Atlantic, rates at comparable depths ranged from ca. 0.02–0.04 nmol L^{-1} h^{-1} (Baltar et al., 2009). Activities of a-glu were similar or lower than b-glu activities in the Atlantic (Baltar et al., 2009, 2010); in the Guaymas Basin, they were also in general similar to or lower than b-glu activities, but were substantially higher than at similar depths in the Atlantic Ocean, ranging from ca. 1–19 nmol L^{-1} h^{-1} (**Figure 1**). Activities of a-glu at the DCM were similar to or higher than rates reported for the southwest Atlantic (Hoarfrost and Arnosti, 2017) and higher than rates reported in the surface waters of the Adriatic Sea (Karner et al., 1992).

Although b-xyl activities are frequently measured in terrestrial systems, there are few data on b-xyl activities from marine waters (Alonso-Sáez et al., 2008), and somewhat more data from rivers (e.g., Kirchman et al., 2004). Activities measured in the Guaymas Basin (17 to 52 nmol L^{-1} h^{-1}) considerably exceed activities measured in the Hudson River (range of 3–10 pmol L^{-1} h^{-1}; Kirchman et al., 2004) and were on average somewhat higher than a site in the northwest Mediterranean Sea, where rates ranged from 1 to 46 nmol L^{-1} h^{-1} (Alonso-Sáez et al., 2008). Activities of b-fu have not, to the best of our knowledge, been previously reported for the marine water column; hydrolysis rates were generally comparable to those of the other substrates measured here.

Endo-acting polysaccharide hydrolase activities in the Guaymas Basin present a different pattern than the exo-acting activities: polysaccharide hydrolase activities decreased somewhat with depth, and only a subset of the polysaccharides were hydrolyzed at depths above the bottom water. The overall pattern of polysaccharide hydrolase activities was quite unusual, since a broader spectrum of polysaccharides were hydrolyzed in bottom waters than at shallower depths (**Figure 2**). A more typical pattern is a narrowing spectrum of polysaccharide hydrolase activities with depth (Steen et al., 2012; D'Ambrosio et al., 2014; Hoarfrost and Arnosti, 2017; Balmonte et al., 2018). Hydrolysis rates at depth in the Guaymas Basin were considerably more rapid than rates measured at comparable depths in the South Atlantic (Hoarfrost and Arnosti, 2017), but were comparable to rates measured in the deep Pacific Ocean (Balmonte and Arnosti, unpublished data). Fucoidan hydrolysis deep in the water column is quite remarkable, however, given the lack of this activity in many locations in the surface ocean (Arnosti et al., 2011) and in most of the other deep ocean locations that have been investigated, including in the Arctic (Balmonte et al., 2018), the South Atlantic (Hoarfrost and Arnosti, 2017), the Pacific (Balmonte et al., unpublished data), and the Gulf of Mexico (Steen et al., 2012). Fucoidan hydrolysis at a depth of ca 190 m has, however, also been measured in water collected above the sediments on the continental shelf of the northwest Atlantic Ocean (Balmonte et al., 2019).

The observation that all four polysaccharides were hydrolyzed in waters immediately above the sediments suggests a direct influence of the sediments on activities in the overlying water column, since the spectrum of polysaccharide hydrolase activities in sediments is typically much broader than in the overlying water column (e.g., Arnosti, 2000, 2008). The high influx of sediment-derived DOC into the water column (Lin et al., 2017), and elevated levels of polysaccharide-rich, transparent exopolymeric particles (TEP) in bottom waters immediately above the sediments (Prieto and Cowen, 2007) are also evidence of such a connection between the sediments and the water column. TEP are often enriched in deoxy sugar-containing sulfated polysaccharides such as fucoidan, possibly explaining substantial fucoidanase activities in *Alvin*-collected waters (**Figure 2**).

The contrast in patterns of exo- and endo-acting activities may provide a clue as to the types of carbohydrates that are enzymatically hydrolyzed in the waters of the Guaymas Basin. In particular, the high rates of exo-acting b-xyl activities and considerable rates of exo-acting b-fu activities at the DCM and OMZ contrast sharply with the lack of measurable endo-acting xylanase and fucoidanase activities at the same depths in the water column. Exo-acting enzymes hydrolyze individual monosaccharides either from the terminal end of a chain, or as branches off a complex structure. We suggest that the exo-acting enzymes are therefore targeting specific branches of complex polysaccharides in the water column; deeper in the water column, particularly directly over the sediments, where both endo- and exo-acting enzymes are active, fucoidan-like and xylan-like polysaccharides (potentially sourced from the sediments) are more likely being hydrolyzed.

The generally high rates of exo-acting enzyme activities reported here are likely characteristic of the Guaymas Basin deep water column, given the overall similarity of hydrolysis rates and patterns among CTD casts collected within an area of ca. 5000 m^2 over the course of a week (**Figure 1**). These high rates of activity likely reflect the dual sources of potential substrates in the basin: (i) an influx of hydrothermally affected dissolved organic matter (DOM) from the sediments (Lin et al., 2017), and (ii) input of sinking POM that generally reaches highest levels from November through March during winter diatom blooms (Lyons et al., 2011). In the event of a sinking diatom bloom, microbial degradation of sinking POM alters its composition toward more degradable compounds, which could also explain the depth-related shifts in exo-acting enzyme activities (i.e., glucosidase-dominated activities at the DCM; xylose-dominated activities in deeper waters) and endo-acting enzyme activities (i.e., broader spectrum of polysaccharide hydrolases at depth). Both sources of organic matter (sediment and surface waters) account for the rapid enzymatic activities at depth in the basin, with the potential to support a considerable population of heterotrophic bacteria, explaining elevated cell numbers throughout the water column (**Table 1**).

Investigations of microbial communities in the water column of the Guaymas Basin have demonstrated that the hydrothermal plume and non-plume (background seawater) communities are very similar in composition (Dick and Tebo, 2010; Dick, 2019). To date, heterotrophic metabolism has been little studied in Guaymas Basin; autotrophic metabolism, including oxidation of methane, and chemolithoautotrophy, has been a focus (e.g., Lesniewski et al., 2012; Anantharaman et al., 2013; Dick et al., 2013). Since gene transcripts for specific aspects of heterotrophic metabolism are not as easily assigned as for other types of metabolism, the importance of heterotrophy to microbial community metabolism cannot easily be assessed via metatranscriptomic approaches. Much remains to be discovered about the microbial communities of the Guaymas Basin: metagenomic investigation of water column communities determined that approximately 35% of 16S sequences could not be identified at domain level (Lesniewski et al., 2012) and much of metatranscriptomic data could also not be assigned at a functional level function, although many of these unclassified genes were highly transcribed (Lesniewski et al., 2012).

Although the microbial communities of the Guaymas Basin water were predominantly studied for their chemosynthetic and autotrophic capabilities (e.g., Lesniewski et al., 2012; Anantharaman et al., 2013), our results indicate that hydrothermal influence in the water column promotes active heterotrophic microbial communities as well. Rapid hydrolysis of a broad spectrum of carbohydrates at depth suggests the presence of a highly active heterotrophic microbial community deep in the Guaymas Basin fueled by DOC (Lin et al., 2017) and supplied with nutrients (Von Damm et al., 1985) produced through hydrothermal alteration of the thick layer of surface-ocean derived organic matter (Schrader et al., 1980). Further characterization of microbial heterotrophic activities and the organisms carrying it out should be a next step in investigation of this unique environment.

DATA AVAILABILITY STATEMENT

The data from this study are available on figshare at https://figshare.com/articles/Hydrolytic_enzyme_activities_and_CTD_data/11120501.

AUTHOR CONTRIBUTIONS

Both authors planned the research and wrote the manuscript. KZ carried out all shipboard measurements and analyzed samples post-cruise.

FUNDING

Funding for this work came from NSF OCE-0848793 and OCE-1736772 to CA and UNC Office of Postdoctoral affairs to KZ. Funding for the research expedition came from NSF OCE-0647633 to Andreas Teske (chief scientist).

ACKNOWLEDGMENTS

We thank Andreas Teske for the invitation to join the cruise, and the captain, crew, and scientific party of R/V *Atlantis* (AT 15-56) for their assistance at sea. We also thank the Martens lab at UNC for assistance with the DOC analysis. This study was supported by NSF.

REFERENCES

Alderkamp, A.-C., van Rijssel, M., and Bolhuis, H. (2007). Characterization of marine bacteria and the activity of their enzyme systems involved in degradation of the algal storage glucan laminarin. *FEMS Microbiol. Ecol.* 59, 108–117. doi: 10.1111/j.1574-6941.2006.00219.x

Alonso-Sáez, L., Vazquez-Dominguez, E., Cardelus, C., Pinhassi, J., Sala, M. M., Lekunberri, I., et al. (2008). Factors controlling the year-round variability in carbon flux through bacteria in a coastal marine system. *Ecosystems* 11, 397–409. doi: 10.1007/s10021-008-9129-0

Anantharaman, K., Breier, J. A., Sheik, C. S., and Dick, G. J. (2013). Evidence for hydrogen oxidation and metabolic plasticity in widespread deep-sea sulfur-oxidizing bacteria. *Porc. Natl. Acad. Sci. U.S.A.* 110, 330–335. doi: 10.1073/pnas.1215340110

Arnosti, C. (1996). A new method for measuring polysaccharide hydrolysis rates in marine environments. *Org. Geochem.* 25, 105–115. doi: 10.1016/s0146-6380(96)00112-x

Arnosti, C. (2000). Substrate specificity in polysaccharide hydrolysis: contrasts between bottom water and sediments. *Limnol. Oceanogr.* 45, 1112–1119. doi: 10.4319/lo.2000.45.5.1112

Arnosti, C. (2003). Fluorescent derivatization of polysaccharides and carbohydrate-containing biopolymers for measurement of enzyme activities in complex media. *J. Chromatogr. B* 793, 181–191. doi: 10.1016/s1570-0232(03)00375-1

Arnosti, C. (2008). Functional differences between Arctic sedimentary and seawater microbial communities: contrasts in microbial hydrolysis of complex substrates. *FEMS Microb. Ecol.* 66, 343–351. doi: 10.1111/j.1574-6941.2008.00587.x

Arnosti, C. (2011). Microbial extracellular enzymes and the marine carbon cycle. *Ann. Rev. Mar. Sci.* 3, 401–425,.

Arnosti, C., Steen, A. D., Ziervogel, K., Ghobrial, S., and Jeffrey, W. H. (2011). Latitudinal gradients in degradation of marine dissolved organic carbon. *PLoS One* 6:e28900. doi: 10.1371/journal.pone.0028900

Balmonte, J. P., Buckley, A., Hoarfrost, A., Ghobrial, S., Ziervogel, K., Teske, A., et al. (2019). Community structural differences shape microbial responses to high molecular weight organic matter. *Environ. Microb.* 21, 557–571. doi: 10.1111/1462-2920.14485

Balmonte, J. P., Teske, A., and Arnosti, C. (2018). Structure and function of high Arctic pelagic, particle-associated, and benthic bacterial communities. *Environ. Microb.* 20, 2941–2954. doi: 10.1111/1462-2920.14304

Baltar, F., Aristegui, J., Gasol, J. M., Sintes, E., van Aken, H. M., and Herndl, G. J. (2010). High dissolved extracellular enzyme activity in the deep central Atlantic Ocean. *Aquat. Microb. Ecol.* 58, 287–302. doi: 10.3354/ame01377

Baltar, F., Aristegui, J., Sintes, E., van Aken, H. M., Gasol, J. M., and Herndl, G. J. (2009). Prokaryotic extracellular enzymatic activity in relation to biomass production and respiration in the meso- and bathypelagic waters of the (sub)tropical Atlantic. *Environ. Microbiol.* 11, 1998–2014. doi: 10.1111/j.1462-2920.2009.01922.x

Campbell, A. C., and Gieskes, J. M. (1984). Water column anomalies associated with hydrothermal activity in the Guaymas Basin, Gulf of California. *Earth Planet. Sci. Lett.* 6, 57–72. doi: 10.1016/0012-821x(84)90140-7

D'Ambrosio, L., Ziervogel, K., MacGregor, B., Teske, A., and Arnosti, C. (2014). Composition and enzymatic function of particle-associated and free-living bacteria: a coastal/offshore comparison. *ISME J.* 8, 2167–2179. doi: 10.1038/ismej.2014.67

Dick, G. J. (2019). The microbiomes of deep-sea hydrothermal vents: distributed globally, shaped locally. *Nat. Revi. Microbiol.* 17, 271–283. doi: 10.1038/s41579-019-0160-2

Dick, G. J., Anantharaman, K., Baker, B. J., Li, M., Reed, D. C., and Sheik, C. S. (2013). The microbiology of deep-sea hydrothermal vent plumes: ecological and biogeographic linkages to seafloor and water column habitats. *Front. Microbiol.* 4:124. doi: 10.3389/fmicb.2013.00124

Dick, G. J., and Tebo, B. M. (2010). Microbial diversity and biogeochemistry of the Guaymas Basin deep-sea hydrothermal plume. *Environ. Microbiol.* 12, 1334–1347. doi: 10.1111/j.1462-2920.2010.02177.x

Dombrowski, N., Teske, A. P., and Baker, B. J. (2018). Expansive microbial metabolic versatility and biodiversity in dynamic Guaymas Basin hydrothermal sediments. *Nat. Comm.* 9:4999. doi: 10.1038/s41467-018-07418-0

Einsele, G., Gieskes, J. M., Curray, J., Moore, D. M., Aguayo, E., Aubry, M.-P., et al. (1980). Intrusion of basaltic sills into highly porous sediments, and resulting hydrothermal activity in the Guaymas Basin, Gulf of California. *Nature* 283, 441–445. doi: 10.1038/283441a0

Hoarfrost, A., and Arnosti, C. (2017). Heterotrophic extracellular enzymatic activities in the Atlantic Ocean follow patterns across spatial and depth regimes. *Front. Mar. Sci.* 4:200. doi: 10.3389/fmars.2017.00200

Hoppe, H.-G. (1983). Significance of exoenzymatic activities in the ecology of brackish water: measurements by means of methylumbelliferyl-substrates. *Mar. Ecol. Prog. Ser.* 11, 299–308. doi: 10.3354/meps011299

Kabisch, A., Otto, A., Konig, S., Becher, D., Albrecht, D., Schuler, M., et al. (2014). Functional characterization of polysaccharide utilization loci in the marine

Bacteroidetes '*Gramella forsetti*' KT 0803. *ISME J.* 8, 1492–1502. doi: 10.1038/ismej.2014.4

Kahru, M., Marinone, S. G., Lluch-Cota, S. E., Pares-Sierra, A., and Mitchell, B. G. (2004). Ocean-color variability in the Gulf of California: scales from days to ENSO. *Deep Sea Res. II Top. Stud. Oceanogr.* 51, 139–146. doi: 10.1016/j.dsr2.2003.04.001

Karner, M., Fuks, D., and Herndl, G. J. (1992). Bacterial activity along a trophic gradient. *Microb. Ecol.* 24, 243–257. doi: 10.1007/BF00167784

Kirchman, D. L., Dittel, A. K., Findlay, S. E. G., and Fischer, D. (2004). Changes in bacterial activity and community structure in response to dissolved organic matter in the Hudson River, New York. *Aquat. Microb. Ecol.* 35, 243–257. doi: 10.3354/ame035243

Lesniewski, R. A., Jain, S., Anantharaman, K., Schloss, P. D., and Dick, G. J. (2012). The metatranscriptome of a deep-sea hydrothermal plume is dominated by water column methanotrophs and lithotrophs. *ISME J.* 6, 2257–2268. doi: 10.1038/ismej.2012.63

Lin, Y.-S., Koch, B. P., Feseker, T., Ziervogel, K., Goldhammer, T., Schmidt, F., et al. (2017). Near-surface heating of young rift sediment causes mass production and discharge of reactive dissolved organic matter. *Sci. Rep.* 7:44864. doi: 10.1038/srep44864

Lyons, G., Benitez-Nelson, C. R., and Thunell, R. C. (2011). Phosphorus composition of sinking particles in the Guaymas Basin, Gulf of California. *Limnol. Oceanogr.* 56, 1093–1105. doi: 10.4319/lo.2011.56.3.1093

Painter, T. J. (1983). "Algal polysaccharides," in *The Polysaccharides*, ed. G. O. Aspinall (New York, NY: Academic Press), 195–285.

Porter, K. G., and Feig, Y. S. (1980). The use of DAPI for identifying and counting aquatic microflora. *Limnol. Oceanogr.* 25, 943–948. doi: 10.4319/lo.1980.25.5.0943

Prieto, L., and Cowen, J. P. (2007). Transparent exopolymer particles in a deep-sea hydrothermal system: Guaymas Basin, Gulf of California. *Mar. Biol.* 150, 1093–1101. doi: 10.1007/s00227-006-0430-1

Schrader, H., Kelts, K., Curray, J., Moore, D., Aguayo, E., Aubry, M. P., et al. (1980). Laminated diatomaceous sediments from the guaymas basin slope (central gulf of california): 250,000-year old climate record. *Science* 207, 1207–1209. doi: 10.1126/science.207.4436.1207

Simoneit, B. R., Mazurek, M. A., Brenner, S., Crisp, P. T., and Kaplan, I. R. (1979). Organic geochemistry of recent sediments from Guaymas Basin, Gulf of California. *Deep Sea Res. A Oceanogr. Res. Pap.* 26A, 879–891. doi: 10.1016/0198-0149(79)90102-x

Steen, A. D., Ziervogel, K., Ghobrial, S., and Arnosti, C. (2012). Functional variation among polysaccharide-hydrolyzing microbial communities in the Gulf of Mexico. *Mar. Chem.* 138, 13–20. doi: 10.1016/j.marchem.2012.06.001

Teske, A., Callaghan, A. V., and LaRowe, D. E. (2014). Biosphere frontiers of subsurface life in the sedimented hydrothermal system of Guaymas Basin. *Front. Microbiol.* 5:362. doi: 10.3389/fmicb.2014.00362

Teske, A., Hinrichs, K.-U., Edgcomb, V., de Vera Gomez, A., Kysela, D., Sylva, S. P., et al. (2002). Microbial diversity in hydrothermal sediments in the Guaymas Basin: evidence for anaerobic methanotrophic communities. *Appl.Environ. Microbiol.* 68, 1994–2007. doi: 10.1128/aem.68.4.1994-2007.2002

Von Damm, K. L., Edmond, J. M., Measures, C. I., and Grant, B. (1985). Chemistry of submarine hydrothermal solutions at Guaymas Basin, Gulf of California. *Geochim. Cosmochim. Acta* 49, 2221–2237. doi: 10.1016/0016-7037(85)90223-6

Wegner, C.-E., Richter-Heitmann, T., Klindworth, A., Klockow, C., Richter, M., and Achstetter, T. (2013). Expression of sulfatases in *Rhodopirellula baltica* and the diversity of sulfatases in the genus *Rhodopirellula*. *Mar. Genom.* 9, 51–61. doi: 10.1016/j.margen.2012.12.001

Weiner, R. M., Taylor, L. E. I. I., Henrissat, B., Hauser, L., Land, M., and Coutinho, P. M. (2008). Complete genome sequence of the complex carbohydrate-degrading marine bacterium, *Saccharophagus degradans* strain 2-40T. *PLoS Genet.* 5:e1000087. doi: 10.1371/journal.pgen.1000087

Conflict of Interest: The authors declare that the research was conducted in the absence of any commercial or financial relationships that could be construed as a potential conflict of interest.

frontiers in Marine Science

METHODS
published: 20 March 2020
doi: 10.3389/fmars.2020.00174

Liquid Chromatographic Isolation of Individual Amino Acids Extracted From Sediments for Radiocarbon Analysis

Thomas M. Blattmann[1,2], Daniel B. Montluçon[2], Negar Haghipour[2,3], Naoto F. Ishikawa[1,2] and Timothy I. Eglinton[2]*

[1] Biogeochemistry Program, Research Institute for Marine Resources Utilization, Japan Agency for Marine-Earth Science and Technology, Yokosuka, Japan, [2] Geological Institute, Department of Earth Sciences, ETH Zurich, Zurich, Switzerland, [3] Laboratory of Beam Physics, Department of Physics, ETH Zurich, Zurich, Switzerland

The "building blocks of life" are found nearly ubiquitously in the environment in the form of proteins, peptides, and single amino acids. To shed light on amino acid sources, cycling, and preservation in sedimentary environments, we present a method using high-pressure liquid chromatography to separate and isolate underivatized amino acids extracted from sediments to conduct compound-specific radiocarbon analysis. This method consists of three main steps including (1) amino acid extraction by hydrofluoric and hydrochloric acids followed by desalting, (2) liquid chromatographic isolation and purification using two complementary column chemistries, and (3) post-purification and measurement by accelerator mass spectrometry. The resulting blank of this procedure is estimated to contain 2.2 ± 1.3 μgC with 0.25 ± 0.09 Fm.

Keywords: ^{14}C, compound-specific radiocarbon analysis, demineralization, hydrolysis, desalting, protein, peptide, purification

OPEN ACCESS

Edited by:
Cindy Lee,
Stony Brook University, United States

Reviewed by:
Zhanfei Liu,
University of Texas at Austin, United States
Rienk H. Smittenberg,
Stockholm University, Sweden

****Correspondence:***
Thomas M. Blattmann
blattmannt@jamstec.go.jp

Specialty section:
This article was submitted to Marine Biogeochemistry, a section of the journal Frontiers in Marine Science

Received: *29 October 2019*
Accepted: *05 March 2020*
Published: *20 March 2020*

Citation:
Blattmann TM, Montluçon DB, Haghipour N, Ishikawa NF and Eglinton TI (2020) Liquid Chromatographic Isolation of Individual Amino Acids Extracted From Sediments for Radiocarbon Analysis. Front. Mar. Sci. 7:174. doi: 10.3389/fmars.2020.00174

INTRODUCTION

Compound-specific radiocarbon in environmental samples has seen an explosion in interest for various biomolecules including steroids (Eglinton et al., 1996, 1997; Griffith et al., 2012), lipids (Eglinton et al., 1996, 1997; Smittenberg et al., 2004; Shah et al., 2008; Druffel et al., 2010; Birkholz et al., 2013; Wakeham and McNichol, 2014), lignin (Feng et al., 2013, 2017), pollutants (Giger et al., 1984; Griffith et al., 2012), pigments (Kusch et al., 2010), biomineral occluded compounds (Ingalls et al., 2004), and pyrogenic carbon (Coppola et al., 2018). Amino acids are among the most abundant and ubiquitous organic molecules in the environment and, to date, their stable carbon and nitrogen isotopic information has been investigated for both ecological (Ohkouchi et al., 2017) and sedimentary studies (Keil and Fogel, 2001). Previous investigations in distal deep-sea sediments on the radiocarbon content of the amino acid compound class reflects its primary productivity source (Wang et al., 1996, 1998; Hwang et al., 2005). However, the information contained in their amino acid-specific radiocarbon content has hitherto remained sparingly investigated. For amino acids, procedures for analyzing their compound-specific radiocarbon content have been developed for dissolved organic matter (Quan, 2005), collagen (Tripp et al., 2006), and for animal tissue (Ishikawa et al., 2018). Motivated by the prospect of exploring new research frontiers in

biogeochemistry including food webs and organic matter-mineral interactions (Blattmann and Ishikawa, Unpublished), we report a method to conduct compound-specific radiocarbon on amino acids extracted from sediments.

MATERIALS AND METHODS

The methodology for sedimentary amino acid-specific radiocarbon isotope analysis introduced here is subdivided into three main steps: (1) amino acid extraction, (2) amino acid isolation, and (3) final amino acid purification and radiocarbon analysis. An overview of the procedure is provided in **Figure 1**. This section also contains discussion and rationale concerning method choice, which is specific to and modifiable for other studies as a function of their specific scientific objectives and sample matrix.

Blanks, Standard Amino Acid Mixture, and Test Samples

The five samples discussed here include a (I) procedural blank without added compounds (hitherto sample "I") covering the entire procedure (see **Figure 1**), (II) a standard amino acid mixture with known concentrations and amino acid-specific radiocarbon isotopic compositions which was (a) subject to acid hydrolysis (Sample "IIa"; Steps 1a–2a), and (b) a second set which was only processed by liquid chromatographic separation and isolation (Sample "IIb"; from step 2a onward), and (III) two natural sediments (Sample "III"; Steps 1a–2a). This study reports chromatograms from samples listed under I, II, and III and the radiocarbon concentrations recovered from samples listed under I and IIb.

During protein hydrolysis by HCl, which frees amino acids by cleaving peptide bonds, tryptophan, cysteine, and methionine are partially degraded (Otter, 2012) and asparagine and glutamine are deaminated to aspartic acid and glutamic acid, respectively (Hunt, 1985). For these reasons, asparagine, cysteine, and glutamine were not included in the standard amino acid mixture. The standard amino acid mixture consisted of alanine, arginine, aspartic acid, glutamic acid, glycine, histidine, hydroxyproline, isoleucine, leucine, lysine, methionine, phenylalanine, proline, serine, threonine, tryptophan, tyrosine, and valine. The concentrations and consensus radiocarbon concentrations of the amino acids ultimately investigated in this study are reported in **Table 1**.

The two riverbed sediments test samples (Sample "III") were from the termini of large southeast Asian rivers collected in 2016 with one sample from the mouth of the Pearl River in southern China, hitherto referred to as sample "PO3," and one from the mouth of the Cagayan River from the Philippines, hitherto referred to as sample "LZ31TB." Upon sampling, samples were kept cool and frozen as soon as possible until they were freeze-dried. The sediments were dry sieved to < 200 μm, which was chosen over wet sieving to not risk sorptive exchanges. From each sample, approximately 30 g of dry sample material was then weighed in for analysis.

Amino Acid Extraction

Rationale

In geosciences, hydrolysis of proteins in dissolved organic matter, particulate organic matter, and sediments is usually carried out using HCl of different concentrations (6–12 M HCl), temperature (100–150°C), and time (70 min–24 h) (c.f. Keil et al., 1998; McCarthy et al., 2004; Lang et al., 2013; Priotto and Lara, 2013). Additional variants of amino acid extraction include vapor phase HCl treatment of seawater dissolved organic matter (Keil and Kirchman, 1991) and combinations of HF and HCl treatments and non-hydrolytic amino acid recovery techniques from marine sediments (Nunn and Keil, 2005, 2006). However, yields of amino acids extracted from mineral matrices are increased (variable but in some cases by >300%) by treatment of sample material with HF prior to HCl hydrolysis (Stevenson and Cheng, 1970; Cheng, 1975; Cheng et al., 1975), as some amino acids are strongly associated with silicate minerals, precluding their extraction with HCl hydrolysis alone (Cheng, 1975; Stevenson and Cheng, 1970; c.f. Blattmann and Ishikawa, Unpublished). Therefore, following the primary research objectives to investigate organic matter-mineral interactions set forth by Blattmann (2018), sequential HF and HCl extraction/hydrolysis was pursued here.

Procedure Description

Extraction

Samples were introduced in 300 ml Teflon beakers (Savillex) and were spiked with 700 μl norleucine standard (841 μg/ml) as internal reference. Slowly, ≈280 ml 38–40% HF (Merck 1.000329.1000) was added to each beaker to allow controlled release of carbonate-bound CO_2. Beakers were heated on hotplates with heat conducting racks (Analab) at 40°C for 2 days under acid reflux conditions. After 2 days, samples were agitated, and pelleted sample material was crushed with a metallic spatula to promote further demineralization and the temperature was increased to 50°C to begin drying. Samples were dried over the course of 35 days. Upon reaching complete dryness, which was assessed visually, the demineralized sample mass was transferred to 60 ml Savillex Teflon hydrolysis vessels. 30 ml of 6 M HCl (prepared from 37% AnalaR NORMAPUR Reag. Ph. Eur. 20252.290), was added to vessel and the headspace was purged with nitrogen gas and then sealed. After 16 h buried in a sand bath at 110°C (± 5°C), the samples were cooled and transferred to glass centrifuge tubes where the hydrolysates were washed three times with MilliQ water to separate them from the solid residue. The supernatants were collected and dried on a solvent evaporator system (Büchi Multi-vapor P12 unit coupled to Büchi V-700 vacuum pump and Büchi F-105 recirculating chiller) with NaOH pellets in the solvent trap of the vertical condenser to reduce HCl vapor exposure to the membrane pump. Dried hydrolysates were then dissolved in MilliQ water and passed through a 47 mm diameter 0.2 μm pore size polyethersulfone membrane filter (Sterlitech) and then dried again on the solvent evaporator system.

Desalting

Using cation exchange resin, inorganic salt was removed following modified methods (Degens and Bajor, 1960;

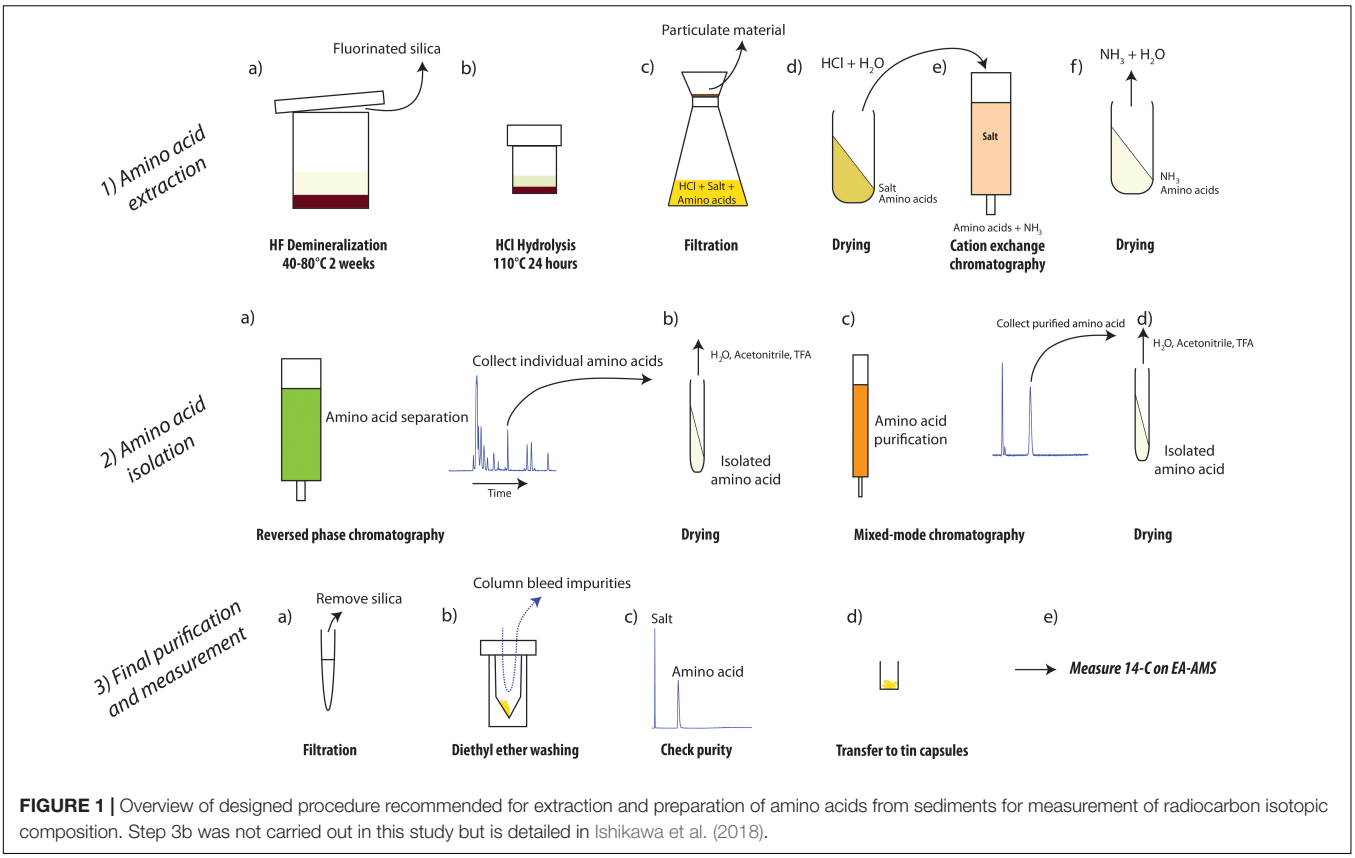

FIGURE 1 | Overview of designed procedure recommended for extraction and preparation of amino acids from sediments for measurement of radiocarbon isotopic composition. Step 3b was not carried out in this study but is detailed in Ishikawa et al. (2018).

TABLE 1 | Analyzed amino acids with consensus radiocarbon values from unprocessed reference materials and their respective constant contamination-corrected radiocarbon concentrations measured on processed standards (IIb) based on 23 injections of 80 µl of standard mixture.

Amino acid	Standard mixture				Radiocarbon measurement				
	ETH nr.	Concentration (µg compound/ml)	Fm	Uncertainty (± abs.)	ETH nr.	Percent recovery	µgC measured	Fm	Propagated uncertainty (± abs.)
Arginine	59052.1.1	67	1.03	0.01	90850.1.1	16	20	1.02	0.06
Isoleucine	59062.1.1	47	1.04	0.01	90853.1.1	24	21	1.04	0.06
Leucine	59063.1.1	68	1.06	0.01	90856.1.1	30	38	1.07	0.03
Phenylalanine	59066.1.1	34	1.03	0.01	90859.1.1	12	8	1.21	0.23
Valine	59072.1.1	37	1.06	0.01	90861.1.1	56	38	1.04	0.03

Cheng, 1975; Takano et al., 2010; Rubino et al., 2014). A column was packed with a bedload volume of 60 ml of 200–400 mesh Dowex 50W X8 cation exchange resin (Fluka 44519-100g). Both ends were capped with glass wool (11 µm diameter) and mobile phases were passed through the resin with a Teflon-tape wrapped stopper and tubing introducing nitrogen gas at 2–4 ml/s. The NH_3 solution was prepared from a 25% stock solution (VWR AnalaR NORMAPUR 1133.1000), the NaOH solution was prepared from pellets (Reg. Ph. Eur. VWR 28244.295), the HCl was prepared from a 37% stock solution (37% AnalaR NORMAPUR Reag. Ph. Eur. 20252.290), and H_2SO_4 solution was prepared from a 95.0–98.0% stock solution (Sigma-Aldrich 258105-500ML). The resin was conditioned for desalting following Takano et al. (2010): (1) 180 ml of 1M HCl, (2) 180 ml of water, (3) 180 ml of 1M NaOH, (4) 180 ml of water, (5) 180 ml of HCl, and (6) 180 ml of water. Once conditioned, 10 ml of sample solution (redissolved in 80 ml of 0.1 M HCl) was transferred to the column. The column was washed with MilliQ water until eluent approached near neutral (pH ≈ 6) as monitored using pH strips (typically required 500–1500 ml for sediment samples). Amino acids were then eluted with 240 ml 10% NH_3. The desalted amino acid fraction was then dried on the solvent evaporator system. Following sediment samples, pronounced darkening of the cation exchange resin was observed. These strongly retained substances could only be eluted with 0.5 M oxalic acid solution modified after the recommendation by Rubino et al. (2014). Approximately 3–6 bed loads sufficed in removing these retained impurities by acting as a complexing agent and eluting these unknown cations in a flocculent brine. The column was then regenerated using

the sequence recommended by Takano et al. (2010). Despite this, some discoloration became apparent after several runs, which appeared not to affect column performance. However, in between samples, enhanced column regeneration was carried out by rinsing with 0.5 M H_2SO_4 (Small et al., 1975) and allowing the cation exchange beads to rest for a few hours in this mobile phase. During this treatment, the resin filled itself with gaseous voids and returned to its factory-original golden hue. The gas that evolves from the reaction indicates oxidation of organic substances retained on the cation exchange resin.

Chromatographic Separation

Rationale

This section describes the chromatographic separation of underivatized amino acids. In the case of adding a derivative to an amino acid, the carbon isotopic influence of the added carbon needs to be subtracted from the indigenous amino acid carbon to calculate the true radiocarbon isotopic composition. In the case of derivatization (e.g., ethyl ester) the resulting propagated error would quickly balloon to unacceptably large values for radiocarbon isotopic composition apparent from calculations analogous to stable carbon isotopic composition corrections (Chikaraishi and Ohkouchi, 2010). Therefore, only underivatized amino acid preparation with offline carbon isotopic determination was considered during the design of this method (c.f. Hare et al., 1991; Broek et al., 2013; Takano et al., 2015).

The two liquid chromatographic isolation steps following the desalting procedure are necessary given the presence of other compounds in fractions isolated by the first separation. The same conclusion was reached previously in complex environmental matrices (high molecular weight dissolved organic matter), which contained impurities including, among others, monosaccharides and deoxy sugars (Quan, 2005). In contrast to Quan (2005), who used a cation exchange resin after reversed phase chromatography, a mixed mode cation exchange-reversed phase column chemistry was used here.

Procedure Description

For all separations and detection runs, an Agilent 1260 high-performance liquid chromatograph (HPLC) coupled to a charged aerosol detector (CAD) (ESA Corona CAD and Thermo Fisher Scientific Corona CAD Veo) was used. For the liquid chromatographic separation of amino acids, two columns were used using MilliQ water, acetonitrile (Fisher Chemical Optima LC/MS grade A955-212), and trifluoroacetic acid (for HPLC $\geq$ 99.0% Sigma-Aldrich 302031-100ML) in the mobile phases. In a first step, a reversed-phase CAPCELL PAK C18 MG column (preparative scale, 20 mm $\times$ 250 mm, particle size 5 μm, Shiseido, Tokyo, Japan) performed the separations shown in **Figure 2**. This column achieved baseline separation of phenylalanine, isoleucine, leucine, valine, proline, and arginine from the remaining amino acids. In a second step, phenylalanine, isoleucine, leucine, valine, and arginine were purified using a mixed mode ion-exchange reversed-phase Primesep A column (analytical scale, 4.6 mm $\times$ 50 mm, particle size 5 μm, SIELC Technologies, IL, United States). The sample material was dissolved in solvent matching the chemistry of the mobile phase at the time of sample injection of the next respective chromatographic run. For collection of chromatographic isolates in both steps, an Agilent fraction collector cooled to approximately 15°C with 40 round-bottom glass vials (20 ml each) was employed. Following the steps outlined in **Figure 1**, the chromatographic isolates from both steps were dried on the solvent evaporator system described previously. Following Ishikawa et al. (2018), the mobile phases used for the preparative scale CAPCELL C18 column were MilliQ water with 0.1% (v/v) TFA (solvent A), and acetonitrile with 0.1% (v/v) TFA (solvent B). To protect the column, a Supelco ColumnSaver (0.5 μm filter; 55214-U) and C18 phase guard column (Phenomenex Kinetex C18 5 μm) were used. Each sample injection was set at 80 μl, the column compartment was set at a constant 30°C, and the solvent gradient for each run was linearly programmed as follows: 0 min (A: 100%, B: 0%) to 30 min (A: 90%, B: 10%), to 80 min (A: 80%, B: 20%), to 100 min (A: 80%, B: 20%). The column is then flushed with 100% B for 20 min followed by equilibration with 100% A for 60 min for the next injection at a constant flow rate of 2 ml/min. See **Figure 2** for chromatograms and see **Supplementary Table 1** for sample collection time windows.

The mobile phases used for the analytical scale Primesep A column were MilliQ water with 0.05% (v/v) TFA (solvent A), and acetonitrile with 0.05% (v/v) TFA (solvent B). Here, amino acids were purified with a constant flow rate of 1.5 ml/min under isocratic conditions (A: 95%, B: 5%) for phenylalanine, isoleucine, leucine, and valine, After each injection, the column was flushed with 100% B for 5 min (linearly increasing the flow from 1.5 to 2 ml/min) followed by equilibration (A: 95%, B: 5%) for the next injection for 15 min at 1.5 ml/min. The column compartment was set at a constant 20°C. For arginine, a different isocratic mixture was used (A: 65%, B: 35%) and the flow rate was set at a constant 2 ml/min with a flushing time of 5 min with 100% B followed by equilibration for 15 min (A: 65%, B: 35%). See **Supplementary Table 1** for sample collection time windows.

Throughout the isolation and purification steps, the CAD was removed from the column outflow and the eluent was directed to the fraction collector while a diode array detector (carefully monitoring the 200–214 nm wavelength region) was used to monitor elution times of amino acids to quality control the separation performance.

Purification and Measurement

Purified amino acid isolates were dried on the solvent evaporator system and dissolved in ≈500 μl of 0.1 M HCl. Following procedures recommended in Ishikawa et al. (2018), these were then introduced into Eppendorf tubes with internal filters (NANOSEP MF GHP.45 μm hydrophilic polypropylene membrane) to remove any precipitates. Prior to use, the Eppendorf nanosep tubes were leached and centrifuged (Eppendorf Centrifuge 5418) with 0.1 M HCl twice. Sample material was then transferred and dried in V-bottom combusted (450°C) glass vials (BGB 080400-XL-ML 0.9 ml) under a gentle stream of N_2 with a heating block set at 40°C. Upon dryness, 1 ml of MilliQ water was added, and the amino acids were dissolved

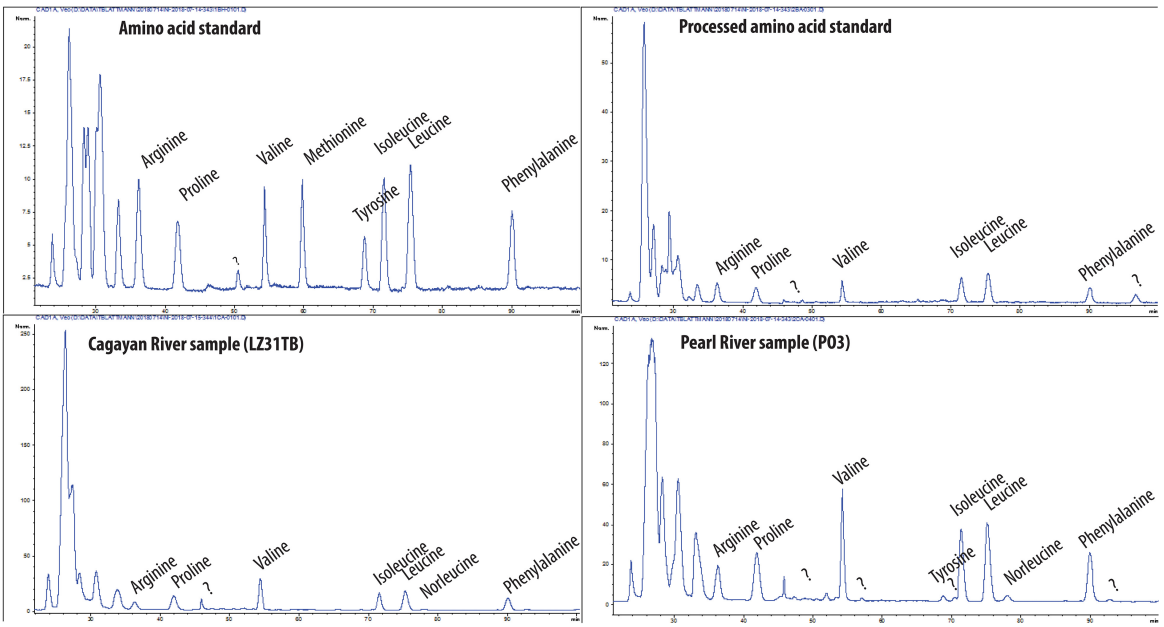

FIGURE 2 | Chromatograms showing CAD traces using the preparative scale CAPCELL C18 column. Top left: unprocessed 18 amino acid standard; top right: 18 amino acid standard which has been subject to the acid hydrolysis and desalting procedure; bottom left: Cagayan River sample LZ31TB; bottom right: Pearl River sample PO3.

over several hours at 40°C. To check the purity of the amino acids, a small aliquot (1–2 μl) was injected on an analytical-scale reversed-phase column, either Phenomenex Kinetex core shell C18 (4.6 mm × 100 mm, particle size 5 μm) or Shiseido C18 CAPCELL PAK C18 MG column (4.6 mm × 250 mm, particle size 5 μm), monitoring eluent with CAD. Samples that showed a single peak after the initial injection peak were deemed pure and were prepared for radiocarbon analysis (see **Supplementary Table 1**).

Isolated amino acids and blanks, denoted IIb and I, respectively, were introduced into tin capsules (Elementar 2.88 × 6 × 0.1 mm; product number 03 951 620). Prior to use, tin capsules were rinsed with dichloromethane three times over a glass fiber filter (Whatman GF/F) held on a combusted all-glass vacuum filtration unit, reducing extraneous carbon from the capsules surfaces (Ogawa et al., 2010; Ruff et al., 2010). Dried capsules were then set on a hotplate at 95°C and sample solution was added by syringe in the desired amounts. Tin capsules were wrapped and radiocarbon isotopic composition was measured on an elemental analyzer coupled to a MICADAS accelerator mass spectrometer (EA-AMS) in a setup described elsewhere (Synal et al., 2007; McIntyre et al., 2017).

DISCUSSION

The procedural blank revealed no CAD-detectable extraneous compounds during the liquid chromatographic retention times relevant for the collection of amino acids. However, non-volatile contaminants were introduced during the prior procedure (HF demineralization, HCl hydrolysis, filtering, and desalting). The retention time of non-volatile contaminants (presumably from solvent residues) are consistent with the presence of inorganic salts (see **Supplementary Figure 1**; Ishikawa et al., 2018). Additionally, the elution of a substance at 33–36 min (only detected by ultraviolet absorption) is possibly attributable to column bleed from the cation exchange resin (divinylbenzene and styrene). In the second liquid chromatographic separation by HPLC using the PrimesepA column, the blank for collected CAPCELL fractions corresponding to the amino acid retention times of valine, isoleucine, leucine, and phenylalanine (I) reveal the absence of co-eluting substances in the relevant time windows. In the case of the CAPCELL blank corresponding to the amino acid retention times of arginine, the CAD detector revealed the presence of non-volatile eluents on the PrimesepA column (I), which however elute approximately 2 min prior to the elution of arginine, thereby eliminating this unknown substance from the final product during fraction collection in the defined time window.

The chromatograms of procedural blank I (see **Supplementary Figures 1–6**) demonstrate that extraneous amino acids were not a contamination issue, which is a concern owing to their ubiquity (skin flakes, dust, etc.) and possible amino acid contaminants in acids used for hydrolysis (Wolman and Miller, 1971). Each step adds and removes different forms of contamination (Ishikawa et al., 2018) and assuming here that the history of sample processing prior to step 2a (**Figure 1**) is irrelevant due to removal of contaminants inherited from previous steps, the blank correction applied here is represented by the blank observed by EA-AMS from procedural blank I. In the case of amino acids collected under isocratic 95-5-0.05 water-acetonitrile-TFA conditions (v/v) for the purification of isoleucine, leucine,

phenylalanine, and valine, the blanks (n = 4), which were determined by direct measurement of their mass and radiocarbon isotopic composition using EA-AMS, averaged 0.23 ± 0.08 Fm and 2.3 ± 1.5 μgC (see **Supplementary Table 2**). In the case of arginine collected under isocratic 65-35-0.05 water-acetonitrile-TFA conditions, a larger blank may be expected due to increased column bleed under mobile phase conditions with a higher proportion of organic solvent (Bour et al., 2016; Ishikawa et al., 2018). However, for the arginine equivalent time window, a blank of 1.7 μgC with 0.32 ± 0.01 Fm was quantified by direct EA-AMS measurement (see **Supplementary Table 2**), appearing slightly smaller than the average blank size mentioned previously, but within uncertainty of the previous blank. For correcting the processed standards, a constant contamination of 2.2 ± 1.3 μgC with 0.25 ± 0.09 Fm (average of all five direct blank measurements) was applied which bins together the blanks isolated under elution time windows corresponding to those of the reported amino acids and purified with the PrimesepA column under isocratic 95-5-0.05 and 65-35-0.05 water-acetonitrile-TFA conditions. This simplified assignment of constant contamination has large uncertainty compared to more rigorously constrained contamination case studies (Haghipour et al., 2019), yet, using Equations 1 and 2 [following Wacker and Christl (2012); see **Supplementary Material**], corrects all standards (IIb) within error of their respective consensus radiocarbon isotopic compositions (**Table 1**). Nonetheless, this blank size is consistent with observations made by Ishikawa et al. (2018) who quantify the total blank as approximately 2.4 μgC for samples without "post-purification" (filtration and rinsing with diethyl ether; see procedure 3b in **Figure 1**). Ishikawa et al. (2018) argue that extraneous carbon in the form of column bleed is effectively removed with the diethyl ether rinsing approach, which based on the experiences gained here, is a position which is further recommended here. Overall, these results, together with the chromatographic baseline separation and purity of amino acids (arginine, valine, leucine, isoleucine, and phenylalanine) recovered after demineralization, hydrolysis, and desalting from standard (IIa) and sample material (III) (see **Figure 2** and **Supplementary Figures 7–20**), demonstrate the suitability of this approach for conducting amino acid-specific radiocarbon measurements on complex environmental matrices.

SUMMARY AND OUTLOOK

Here, we demonstrate the successful extraction and liquid chromatographic separation of underivatized amino acids from sediments. Isolated amino acids from a standard reference mixture were measured for their radiocarbon isotopic composition by EA-AMS. Blanks and procedural amino acid standards provide preliminary constraints on contamination input, which brings processed amino acid standards within error of their consensus values. In order to improve the quality of the measurements, diethyl ether rinsing of amino acids should be carried out to remove impurities derived from column bleed as recommended by Ishikawa et al. (2018). The results of the measurements of sedimentary amino acids together with refined blank assessments will be reported in forthcoming publications.

DATA AVAILABILITY STATEMENT

All datasets generated for this study are included in the article/**Supplementary Material**.

AUTHOR CONTRIBUTIONS

TB, DM, NH, and NI conducted and supported the laboratory work and measurements. TB, DM, and TE designed the study. All authors contributed to the discussion and writing.

FUNDING

This work was supported by the ETH Zurich (ETH Research Grant 41 14-1) and JAMSTEC.

ACKNOWLEDGMENTS

Fernando Siringan and Erin Tinacba (Marine Science Institute, University of the Philippines), Meixun Zhao and Pengfei Hou (Ocean University of China, Qingdao), and Andrea Winter (ETH Zurich) are thanked for their fieldwork and logistical support. Cameron McIntyre and Lukas Wacker (Laboratory of Ion Beam Physics, ETH Zurich) are thanked for radiocarbon measurements and support. This work benefited from discussions with Yoshinori Takano (JAMSTEC). We thank the reviewers RS and ZL for their careful reviews of this work. We are indebted to the Hanse-Wissenschaftskolleg and the Geochemical Society for providing funding for the conference in which this work was presented and the Deutsche Forschungsgemeinschaft (DFG, German Research Foundation) project number 422798570.

SUPPLEMENTARY MATERIAL

The Supplementary Material for this article can be found online at: https://www.frontiersin.org/articles/10.3389/fmars.2020.00174/full#supplementary-material

REFERENCES

Birkholz, A., Smittenberg, R. H., Hajdas, I., Wacker, L., and Bernasconi, S. M. (2013). Isolation and compound specific radiocarbon dating of terrigenous branched glycerol dialkyl glycerol tetraethers (brGDGTs). *Organ. Geochem.* 60, 9–19. doi: 10.1016/j.orggeochem.2013.04.008

Blattmann, T. M. (2018). *Topics on Radiocarbon Geochemistry and Organic Matter-Mineral Interactions*. Ph.D. thesis, ETH Zürich, Zürich. doi: 10.3929/ethz-b-000313397

Bour, A. L., Walker, B. D., Broek, T. A. B., and McCarthy, M. D. (2016). Radiocarbon analysis of individual amino acids: carbon blank quantification for a small-sample high-pressure liquid chromatography purification

method. *Analy. Chem.* 88, 3521–3528. doi: 10.1021/acs.analchem.5b03619

Broek, T. A. B., Walker, B. D., Andreasen, D. H., and McCarthy, M. D. (2013). High-precision measurement of phenylalanine δ15N values for environmental samples: a new approach coupling high-pressure liquid chromatography purification and elemental analyzer isotope ratio mass spectrometry. *Rapid Commun. Mass Spectr.* 27, 2327–2337. doi: 10.1002/rcm.6695

Cheng, C. N. (1975). Extracting and desalting amino acids from soils and sediments: evaluation of methods. *Soil Biol. Biochem.* 7, 319–322. doi: 10.1016/0038-0717(75)90074-7

Cheng, C. N., Shufeldt, R. C., and Stevenson, F. J. (1975). Amino acid analysis of soils and sediments: extraction and desalting. *Soil Biol. Biochem.* 7, 143–151. doi: 10.1016/0038-0717(75)90012-7

Chikaraishi, Y., and Ohkouchi, N. (2010). "An improved method for precise determination of carbon isotopic composition of amino acids," in *Earth, Life, and Isotopes*, eds N. Ohkouchi, I. Tayasu, and K. Koba (Kyoto: Kyoto University Press), 355–366.

Coppola, A. I., Wiedemeier, D. B., Galy, V., Haghipour, N., Hanke, U. M., Nascimento, G. S., et al. (2018). Global-scale evidence for the refractory nature of riverine black carbon. *Nat. Geosci.* 11, 584–588. doi: 10.1038/s41561-018-0159-8

Degens, E. T., and Bajor, M. (1960). Die Verteilung von Aminosäuren in bituminösen Sedimenten und ihre Bedeutung für die Kohlen- und Erdölgeologie. *Glückauf* 96, 1525–1534.

Druffel, E. R. M., Zhang, D., Xu, X., Ziolkowski, L. A., Southon, J. R., dos Santos, G. M., et al. (2010). Compound-specific radiocarbon analyses of phospholipid fatty acids and n-alkanes in ocean sediments. *Radiocarbon* 52, 1215–1223. doi: 10.1017/s0033822200046294

Eglinton, T. I., Aluwihare, L. I., Bauer, J. E., Druffel, E. R. M., and McNichol, A. P. (1996). Gas chromatographic isolation of individual compounds from complex matrices for radiocarbon dating. *Anal. Chem.* 68, 904–912. doi: 10.1021/ac9508513

Eglinton, T. I., Benitez-Nelson, B. C., Pearson, A., McNichol, A. P., Bauer, J. E., and Druffel, E. R. M. (1997). Variability in radiocarbon ages of individual organic compounds from marine sediments. *Science* 277, 796–799. doi: 10.1126/science.277.5327.796

Feng, X., Benitez-Nelson, B. C., Montluçon, D. B., Prahl, F. G., McNichol, A. P., Xu, L., et al. (2013). 14C and 13C characteristics of higher plant biomarkers in Washington margin surface sediments. *Geochim. Cosmochim. Acta* 105, 14–30. doi: 10.1016/j.gca.2012.11.034

Feng, X., Vonk, J. E., Griffin, C., Zimov, N., Montluçon, D. B., Wacker, L., et al. (2017). 14C variation of dissolved lignin in arctic river systems. *ACS Earth Space Chem.* 1, 334–344. doi: 10.1021/acsearthspacechem.7b00055

Giger, W., Sturm, M., Sturm, H., Schaffner, C., Bonani, G., Balzer, R., et al. (1984). 14C/12C-ratios in organic matter and hydrocarbons extracted from dated lake sediments: nuclear instruments and methods in physics research section B. *Beam Interact. Mater. Atoms* 5, 394–397. doi: 10.1016/0168-583x(84)90548-2

Griffith, D. R., Wacker, L., Gschwend, P. M., and Eglinton, T. I. (2012). Carbon isotopic (13C and 14C) composition of synthetic estrogens and progestogens. *Rapid Commun. Mass Spectr.* 26, 2619–2626. doi: 10.1002/rcm.6385

Haghipour, N., Ausin, B., Usman, M. O., Ishikawa, N., Wacker, L., Welte, C., et al. (2019). Compound-specific radiocarbon analysis by elemental analyzer–accelerator mass spectrometry: precision and limitations. *Anal. Chem.* 91, 2042–2049. doi: 10.1021/acs.analchem.8b04491

Hare, P. E., Fogel, M. L., Stafford, T. W. Jr., Mitchell, A. D., and Hoering, T. C. (1991). The isotopic composition of carbon and nitrogen in individual amino acids isolated from modern and fossil proteins. *J. Archaeol. Sci.* 18, 277–292. doi: 10.1016/0305-4403(91)90066-x

Hunt, S. (1985). "Degradation of amino acids accompanying in vitro protein hydrolysis," in *Chemistry and Biochemistry of the Amino Acids*, ed. G. C. Barrett (Dordrecht: Springer), 376–398. doi: 10.1007/978-94-009-4832-7_12

Hwang, J., Druffel, E. R. M., and Komada, T. (2005). Transport of organic carbon from the California coast to the slope region: a study of Δ14C and δ13C signatures of organic compound classes. *Glob. Biogeochem. Cycles* 19, 1–9. doi: 10.1029/2004GB002422

Ingalls, A. E., Anderson, R. F., and Pearson, A. (2004). Radiocarbon dating of diatom-bound organic compounds. *Mar. Chem.* 92, 91–105. doi: 10.1016/j.marchem.2004.06.019

Ishikawa, N. F., Itahashi, Y., Blattmann, T. M., Takano, Y., Ogawa, N. O., Yamane, M., et al. (2018). Improved method for isolation and purification of underivatized amino acids for radiocarbon analysis. *Anal. Chem.* 90, 12035–12041. doi: 10.1021/acs.analchem.8b02693

Keil, R. G., and Fogel, M. L. (2001). Reworking of amino acid in marine sediments: stable carbon isotopic composition of amino acids in sediments along the Washington coast. *Limnol. Oceanogr.* 46, 14–23. doi: 10.4319/lo.2001.46.1.0014

Keil, R. G., and Kirchman, D. L. (1991). Dissolved combined amino acids in marine waters as determined by a vapor-phase hydrolysis method. *Mar. Chem.* 33, 243–259. doi: 10.1016/0304-4203(91)90070-d

Keil, R. G., Tsamakis, E., Giddings, J. C., and Hedges, J. I. (1998). Biochemical distributions (amino acids, neutral sugars, and lignin phenols) among size-classes of modern marine sediments from the Washington coast. *Geochim. Cosmochim. Acta* 62, 1347–1364. doi: 10.1016/s0016-7037(98)00080-5

Kusch, S., Kashiyama, Y., Ogawa, N. O., Altabet, M., Butzin, M., Friedrich, J., et al. (2010). Implications for chloro- and pheopigment synthesis and preservation from combined compound-specific δ13C, δ15N, and Δ14C analysis. *Biogeosciences* 7, 4105–4118. doi: 10.5194/bg-7-4105-2010

Lang, S. Q., Früh-Green, G. L., Bernasconi, S. M., and Butterfield, D. A. (2013). Sources of organic nitrogen at the serpentinite-hosted Lost City hydrothermal field. *Geobiology* 11, 154–169. doi: 10.1111/gbi.12026

McCarthy, M. D., Benner, R., Lee, C., Hedges, J. I., and Fogel, M. L. (2004). Amino acid carbon isotopic fractionation patterns in oceanic dissolved organic matter: an unaltered photoautotrophic source for dissolved organic nitrogen in the ocean? *Mar. Chem.* 92, 123–134. doi: 10.1016/j.marchem.2004.06.021

McIntyre, C. P., Wacker, L., Haghipour, N., Blattmann, T. M., Fahrni, S., Usman, M., et al. (2017). Online 13C and 14C gas measurements by EA-IRMS–AMS at ETH Zürich. *Radiocarbon* 59, 893–903. doi: 10.1017/rdc.2016.68

Nunn, B. L., and Keil, R. G. (2005). Size distribution and amino acid chemistry of base-extractable proteins from Washington coast sediments. *Biogeochemistry* 75, 177–200. doi: 10.1007/s10533-004-6546-9

Nunn, B. L., and Keil, R. G. (2006). A comparison of non-hydrolytic methods for extracting amino acids and proteins from coastal marine sediments. *Mar. Chem.* 98, 31–42. doi: 10.1016/j.marchem.2005.06.005

Ogawa, N. O., Nagata, T., Kitazato, H., and Ohkouchi, N. (2010). "Ultra-sensitive elemental analyzer/isotope ratio mass spectrometer for stable nitrogen and carbon isotope analyses," in *Earth, Life, and Isotopes*, eds N. Ohkouchi, I. Tayasu, and K. Koba (Kyoto: Kyoto University Press), 339–353.

Ohkouchi, N., Chikaraishi, Y., Close, H. G., Fry, B., Larsen, T., Madigan, D. J., et al. (2017). Advances in the application of amino acid nitrogen isotopic analysis in ecological and biogeochemical studies. *Organ. Geochem.* 113, 150–174. doi: 10.1016/j.orggeochem.2017.07.009

Otter, D. E. (2012). Standardised methods for amino acid analysis of food. *Br. J. Nutr.* 108, S230–S237. doi: 10.1017/S0007114512002486

Priotto, S., and Lara, R. J. (2013). On the optimization of hydrolysis conditions for simultaneous determination of amino acids and amino sugars in marine sediments. *J. Mar. Biol. Oceanogr.* 2, 1–5.

Quan, T. M. (2005). *Chemical Characterization of Dissolved Organic Matter (DOM) in Seawater: Structure, Cycling, and the Role of Biology*. Ph.D. thesis, Massachusetts Institute of Technology, Woods Hole Oceanographic Institution. doi: 10.1575/1912/1569

Rubino, M., Milin, S., D'Onofrio, A., Signoret, P., Hatté, C., and Balesdent, J. (2014). Measurement of δ13C values of soil amino acids by GC–C–IRMS using trimethylsilylation: a critical assessment. *Isotopes Environ. Health Stud.* 50, 516–530. doi: 10.1080/10256016.2014.959444

Ruff, M., Fahrni, S., Gäggeler, H. W., Hajdas, I., Suter, M., Synal, H. A., et al. (2010). On-line radiocarbon measurements of small samples using elemental analyzer and MICADAS gas ion source. *Radiocarbon* 52, 1645–1656. doi: 10.1017/s003382220005637x

Shah, S. R., Mollenhauer, G., Ohkouchi, N., Eglinton, T. I., and Pearson, A. (2008). Origins of archaeal tetraether lipids in sediments: insights from radiocarbon analysis. *Geochim. Cosmochim. Acta* 72, 4577–4594. doi: 10.1016/j.gca.2008.06.021

Small, H., Stevens, T. S., and Bauman, W. C. (1975). Novel ion exchange chromatographic method using conductimetric detection. *Anal. Chem.* 47, 1801–1809. doi: 10.1021/ac60361a017

Smittenberg, R. H., Hopmans, E. C., Schouten, S., Hayes, J. M., Eglinton, T. I., and Sinninghe Damsté, J. S. (2004). Compound-specific radiocarbon dating of the varved holocene sedimentary record of saanich Inlet, Canada. *Paleoceanography* 19, 1–16. doi: 10.1029/2003PA000927

Stevenson, F. J., and Cheng, C. N. (1970). Amino acids in sediments: recovery by acid hydrolysis and quantitative estimation by a colorimetric procedure. *Geochim. Cosmochim. Acta* 34, 77–88. doi: 10.1016/0016-7037(70)90152-3

Synal, H.-A., Stocker, M., and Suter, M. (2007). MICADAS: a new compact radiocarbon AMS system: nuclear instruments and methods in physics research section B. *Beam Interact. Mater. Atoms* 259, 7–13. doi: 10.1016/j.nimb.2007.01.138

Takano, Y., Chikaraishi, Y., and Ohkouchi, N. (2015). Isolation of underivatized amino acids by ion-pair high performance liquid chromatography for precise measurement of nitrogen isotopic composition of amino acids: development of comprehensive LC×GC/C/IRMS method. *Intern. J. Mass Spectr.* 379, 16–25. doi: 10.1016/j.ijms.2014.11.012

Takano, Y., Kashiyama, Y., Ogawa, N. O., Chikaraishi, Y., and Ohkouchi, N. (2010). Isolation and desalting with cation-exchange chromatography for compound-specific nitrogen isotope analysis of amino acids: application to biogeochemical samples. *Rapid Commun. Mass Spectr.* 24, 2317–2323. doi: 10.1002/rcm.4651

Tripp, J. A., McCullagh, J. S. O., and Hedges, R. E. M. (2006). Preparative separation of underivatized amino acids for compound-specific stable isotope analysis and radiocarbon dating of hydrolyzed bone collagen. *J. Separat. Sci.* 29, 41–48. doi: 10.1002/jssc.200500247

Wacker, L., and Christl, M. (2012). Data reduction for small radiocarbon samples: error propagation using the model of constant contamination. *Lab. Ion Beam Phys. Ann. Rep.* 2011:36.

Wakeham, S. G., and McNichol, A. P. (2014). Transfer of organic carbon through marine water columns to sediments - insights from stable and radiocarbon isotopes of lipid biomarkers. *Biogeosciences* 11, 6895–6914. doi: 10.5194/bg-11-6895-2014

Wang, X.-C., Druffel, E. R. M., Griffin, S., Lee, C., and Kashgarian, M. (1998). Radiocarbon studies of organic compound classes in plankton and sediment of the northeastern Pacific Ocean. *Geochim. Cosmochim. Acta* 62, 1365–1378. doi: 10.1016/s0016-7037(98)00074-x

Wang, X.-C., Druffel, E. R. M., and Lee, C. (1996). Radiocarbon in organic compound classes in particulate organic matter and sediment in the deep northeast Pacific Ocean. *Geophys. Res. Lett.* 23, 3583–3586. doi: 10.1029/96gl03423

Wolman, Y., and Miller, S. L. (1971). Amino-acid contamination of aqueous hydrochloric acid. *Nature* 234, 548–549. doi: 10.1038/234548a0

Conflict of Interest: The authors declare that the research was conducted in the absence of any commercial or financial relationships that could be construed as a potential conflict of interest.

frontiers in Marine Science

HYPOTHESIS AND THEORY
published: 05 May 2020
doi: 10.3389/fmars.2020.00302

Theoretical Amino Acid-Specific Radiocarbon Content in the Environment: Hypotheses to Be Tested and Opportunities to Be Taken

Thomas M. Blattmann[1,2]* *and Naoto F. Ishikawa*[1,2]*

[1] *Biogeochemistry Program, Research Institute for Marine Resources Utilization, Japan Agency for Marine-Earth Science and Technology, Yokosuka, Japan,* [2] *Geological Institute, Department of Earth Sciences, ETH Zürich, Zurich, Switzerland*

OPEN ACCESS

Edited by:
Stuart Wakeham, University of Georgia, United States

Reviewed by:
Ann P. McNichol, Woods Hole Oceanographic Institution, United States
Stephanie Kusch, University of Cologne, Germany

***Correspondence:**
Thomas M. Blattmann
blattmannt@jamstec.go.jp
Naoto F. Ishikawa
ishikawan@jamstec.go.jp

Specialty section:
This article was submitted to Marine Biogeochemistry, a section of the journal Frontiers in Marine Science

Received: *29 October 2019*
Accepted: *15 April 2020*
Published: *05 May 2020*

Citation:
Blattmann TM and Ishikawa NF (2020) Theoretical Amino Acid-Specific Radiocarbon Content in the Environment: Hypotheses to Be Tested and Opportunities to Be Taken. Front. Mar. Sci. 7:302. doi: 10.3389/fmars.2020.00302

Tracing of biogeochemical pathways using molecular approaches has advanced our basic understanding of the carbon cycle and life's legacy in the sedimentary record. To this end, compound-specific radiocarbon analysis has been instrumental in shedding light on the turnover, age, and sources of a range of biomarkers embedded within complex environmental matrices. However, despite their foundational importance for life and their omnipresence throughout geologic space and time, the biogeochemical cycling of amino acids remains largely unexplored. Here, we discuss the potential of using amino acid-specific radiocarbon to deepen our knowledge of the biogeochemistry of food webs and sedimentary organic carbon.

Keywords: amino acid, radiocarbon, ecology, food web, organic matter-mineral interactions, peptide, compound specific isotope analysis, protein

INTRODUCTION

The "building blocks of life" constitute a common foundation which all life on Earth shares and depends on (Miller and Urey, 1959; Kitadai and Maruyama, 2018) and amino acids are one of the largest pools of characterizable organic matter found in sedimentary environments (Trask, 1936; Degens, 1970; Lee et al., 1983; Wakeham et al., 1997; Hedges et al., 2001). In contrast to other biomarkers where source specificity is a key attribute for understanding sedimentary and biogeochemical cycling pathways [e.g., lignin from the terrestrial biosphere (Hedges and Parker, 1976), lipids from the marine biosphere (Volkman et al., 1980)], amino acids are arguably among the least specific "biomarkers" as the molecules themselves are omnipresent in all life forms and occur across most of geologic space and time (Abelson, 1954; Erdman et al., 1956; Degens and Bajor, 1960; Hare, 1969). Embracing this property of environmental omnipresence, previous workers, as summarized by Kvenvolden (1975), have provided insights on the utility of amino acids (and their degradation products) as molecular clocks, (paleo)thermometers, and diagenesis proxies. Since then, appreciable progress on compound-specific isotope measurements has been made. Here, we share our perspectives on how amino acid-specific radiocarbon

content can theoretically provide insights into a variety of biogeochemical studies.

BIOGEOCHEMISTRY OF AMINO ACIDS IN FOOD WEBS

Although amino acids are part of the living fabric of all organisms, not all amino acids can be synthesized by all organisms leading to facultative or mandatory dietary acquisition of certain amino acids. This circumstance leads to different pathways of carbon and nitrogen propagating through the food web up to higher trophic positions. $\Delta^{14}C$ is successfully used to trace carbon pathways in bulk biomass (Williams et al., 1987; Ishikawa et al., 2013), a point we will get back to later. Analytical developments first opened stable carbon and nitrogen isotopic compositions of amino acids ($\delta^{13}C$ and $\delta^{15}N$, respectively) to exploration and our current state of knowledge rests on what these isotopes have revealed. The isotopic composition of amino acids within organisms reflect the isotopic composition of carbon and nitrogen sources in the food web with superimposed effects of metabolic processes (Hare et al., 1991; Carstens et al., 2013). "Trophic" amino acids fractionate heavily against ^{15}N due to preferential deamination or transamination during metabolism, enriching the ^{15}N in the remaining trophic amino acids (Macko et al., 1986; Goto et al., 2018). In contrast, "source" amino acids show no or a lesser extent of ^{15}N fractionation, because their amino group is preserved during metabolism (Chikaraishi et al., 2009). This allows amino acid nitrogen isotopic compositions to be used as excellent proxies for determination of trophic position of organisms in recent and paleo studies (Ohkouchi et al., 2017) and provides useful information for identifying ecological niches of organisms in food webs (Ishikawa, 2018). The "trophic" and "source" categories are controlled by catabolism of amino acids, such as deamination (Chikaraishi et al., 2015), whereas the "essential" and "non-essential" categories are controlled by anabolism such as biosynthesis (McMahon et al., 2010). Metabolic energy is produced in the former and consumed in the latter (Bender, 2012). In autotrophs, the $\delta^{13}C$ profile of "essential" amino acids are influenced by biosynthetic processes specific to phylogeny because diverse precursors, intermediates, and reactions produce a different pattern of ^{13}C fractionation among amino acids (Larsen et al., 2009). Using normalized $\delta^{13}C$ of several essential amino acids, Larsen et al. (2009) found that plants, fungi, and bacteria can be discriminated from each other in multivariate space. Higher organisms such as vertebrates are unable to biosynthesize essential amino acids, which are exclusively derived from their diets. This is reflected in the findings of McMahon et al. (2010) which show that $\delta^{13}C$ of essential amino acids in fish are consistent with those of their diet, whereas $\delta^{13}C$ of non-essential amino acids deviate, suggesting that non-essential amino acids are at least partly biosynthesized by higher organisms using different compound and carbon skeleton precursors, which can be exploited to trace dietary sources at higher trophic positions such as for zooplankton and fish (Larsen et al., 2013; McMahon et al., 2016). Therefore, the stable carbon isotopic compositions of amino acids, especially of essential amino acids, are used as a fingerprint of primary producers. Stable carbon and nitrogen isotopic investigations of amino acids in organisms have currently led literature to two contrasting dichotomies, i.e., "trophic" vs. "source" and "essential" vs. "non-essential" (**Figure 1**). While there are wide overlaps between the source and essential categories and for trophic and non-essential categories, a few amino acids behave out of line. Additionally, the carbon pools from which the carbon atoms of the amino acids stem remain loosely constrained. Catalyzed by recent advances in accelerator mass spectrometry enabling the routine analysis of small-scale radiocarbon measurements (McIntyre et al., 2017), methods have been developed to investigate amino acid-specific radiocarbon in soft tissue of organisms opening a new frontier in research possibilities (Ishikawa et al., 2018).

In this context, natural abundance $\Delta^{14}C$ appears a promising tool to help disentangle complex amino acid metabolic pathways and offer new leads in resolving the differences between these competing dichotomies (**Figure 1**). Unlike $\delta^{15}N$ and $\delta^{13}C$, isotopic fractionation for $\Delta^{14}C$ is internally canceled out by definition (Stuiver and Polach, 1977). Therefore, metabolic effects should be canceled out with $\Delta^{14}C$ and its value should reflect that of their carbon origin(s), such as dissolved inorganic carbon (Broecker and Walton, 1959; Guillemette et al., 2017) or organic materials (Petsch et al., 2001). Most amino acids in the biosphere can be expected to bear a "modern" signature (Wang et al., 1996, 1998; Hwang et al., 2005). However, carbon originating from the atmosphere, dissolved inorganic and organic carbon, surface sediments, methane, and kerogen (often) show contrasting radiocarbon fingerprints. If an ecosystem intersects two or more of these domains, the radiocarbon gradient should be exploitable. To date, efforts have focused on radiocarbon dating of amino acids (particularly hydroxyproline) found in bone collagen for archeological applications (McCullagh et al., 2010). For the "building blocks of life," there is nearly no data on amino acid radiocarbon in flora and fauna and there is

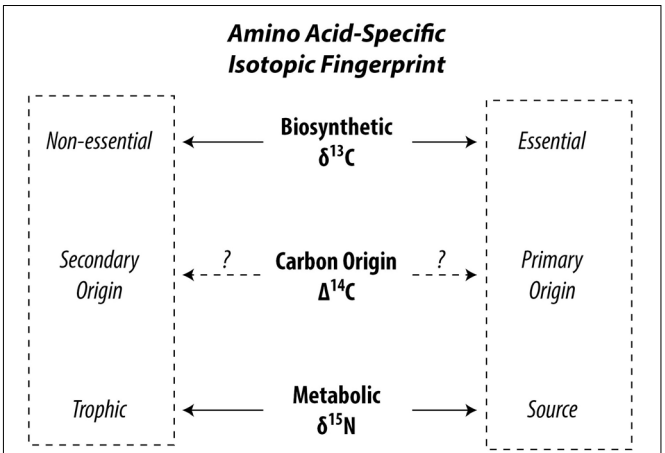

FIGURE 1 | Conceptual division for categorizing amino acids in the context of food web studies. The $\Delta^{14}C$ signature of amino acids has potential to integrate $\delta^{13}C$ and $\delta^{15}N$.

clearly incentive to shed light on this area of basic research (c.f. Bour et al., 2016).

BIOGEOCHEMISTRY OF SEDIMENTARY AMINO ACIDS

The importance of organic matter-mineral interactions in soils began to emerge in the mid-20th Century (Beutelspacher, 1955) and their importance for the stabilization of organic matter in marine sediments became recognized in the 1990s (Keil et al., 1994b; Mayer, 1994; Kennedy et al., 2002). These processes influence contrasting degrees of loss-and-replacement of terrestrial with marine organic matter along land-ocean transitions (Keil et al., 1997; Blattmann et al., 2018, 2019).

Nitrogenous compounds are classically considered biogeochemically labile and therefore are efficiently remineralized (Vernadsky, 1930). In the case of amino acids, their sustained existence is unlikely due to their intrinsic lability (Kirchman, 1990; Pantoja and Lee, 2003) leaving stabilization by mineral surfaces as the likeliest explanation (Keil et al., 1994a; Hedges et al., 2001). The modes of interactions between organic matter and minerals include ligand exchange, ion exchange, cation bridging, van der Waals forces, hydrogen bonding, hydrophobic interactions, and combinations thereof (Beutelspacher, 1955; Keil and Mayer, 2014). The stabilization of amino acids and their polymers have been hypothesized and identified as important in the formation of recalcitrant organic nitrogen (e.g. Müller, 1977; Henrichs and Sugai, 1993; Keil et al., 1994a; Hedges et al., 2001; Estes et al., 2019). Different amino acids and structurally related compounds exhibit very different sorption affinities for phyllosilicate mineral surfaces (Hedges, 1978; Hedges and Hare, 1987). Sorption experiments have demonstrated the strong participation of basic amino acids by way of electrostatic interactions in forming phyllosilicate-amino acid/protein complexes (Ensminger and Gieseking, 1941; Hedges, 1978; Hedges and Hare, 1987; Cowie and Hedges, 1992). This effect appears mirrored in nature with the high abundance of basic amino acids found in continental margin sediments (Keil et al., 1998). Amino acids and proteins associated with phyllosilicates and natural sediments have revealed sometimes erratic and irreversible desorption behavior (Henrichs and Sugai, 1993; Wang and Lee, 1993; Montluçon and Lee, 2001; Ding and Henrichs, 2002), which may ultimately influence their bioavailability (Pinck and Allison, 1951). Amino acids are likely more representative of bulk sedimentary organic matter than most other compounds, yet their ubiquity limits their value in quantitatively assessing contributions from sedimentary organic matter sources. On a molecular level, sedimentary amino acids are subject to differential microbial processing and loss-and-replacement of terrestrial with marine amino acids as revealed by stable carbon isotopes (Keil and Fogel, 2001) and therefore source apportionments recorded by individual amino acids are overlain by a variety of effects.

Amino acids stabilized by mineral surfaces are expected to exhibit very slow turnover rates and or would resist loss-and-replacement during land-ocean transit, giving rise to depleted radiocarbon fingerprints borne by mineral-stabilized amino acids. It is thus hypothesized, that radiocarbon isotopic compositions of individual amino acids can provide a biomarker tool to measure the effect of organic matter-mineral interactions in natural sedimentary environments (**Figure 2**; see also ideas by Keil et al., 1998). One of the greatest uncertainties in studying the stabilization effects of minerals on organic matter in nature is the longstanding and ongoing discussion whether organic matter is stabilized by minerals or if organic matter is intrinsically stable due to its structural characteristics or by other factors (compare Hedges et al., 2001; Eusterhues et al., 2005; Schmidt et al., 2011; Keil and Mayer, 2014; Kleber et al., 2015). To this end, amino acid-specific radiocarbon can offer new perspectives in this ongoing debate. Method developments have also opened up this frontier of amino acid-specific radiocarbon in sediments to exploration (Blattmann et al., 2020).

IS ENANTIOMER-SPECIFIC RADIOCARBON THE NEXT FRONTIER?

With methods for amino acid-specific radiocarbon now developed for biological (Ishikawa et al., 2018) and earthen (Blattmann et al., 2020) samples, we share our thoughts on the merits of what we see as a promising next analytical frontier. Radiocarbon isotopic composition of individual compounds reflects a combination of influences stemming from aging, mixing, reservoir effects, etc. By isolating the effect of radioactive decay, constraints on the time since synthesis are attainable (Libby et al., 1949). In addition to this radioactive clock common to all organic compounds, amino acids distinguish themselves by having enantiomers (i.e., mirror image molecular structure like our left and right hands). In the biosphere, the L-form dominates, with certain organisms containing D-amino acids including bacteria (Corrigan, 1969; Lam et al., 2009), plants (Neuberger, 1948), freshwater and marine algae (Yokoyama et al., 2003), and higher organisms including insects and mammals (Neuberger, 1948; Corrigan, 1969). In a process called racemization, L-amino acids switch into D-configuration and vice versa. Racemization is a time and temperature dependent process and is also influenced by humidity, pH, and a host of matrix effects (see review by Bada, 1985). Over time, increasing

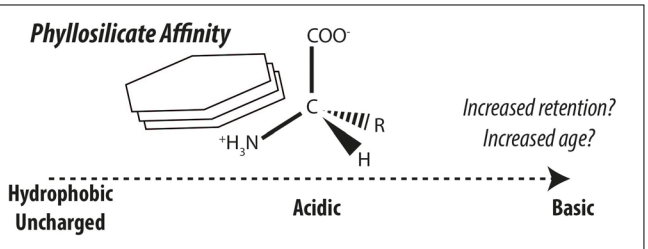

FIGURE 2 | Generalized affinity of amino acids for kaolinite simplified after the findings of Hedges and Hare (1987). Increased affinity is hypothesized to enhance retention and protection of different amino acid classes, thereby leading to greater discrepancies in their radiocarbon ages.

amounts of D-amino acids are present in living tissue with slow turnover (e.g., dentin and eye lenses) such as for whales (Olsen and Sunde, 2002) and humans (Masters et al., 1977). This trend continues in organic remains such as in wood (Lee et al., 1976), bones (Bada et al., 1973, 1989), and in biospheric remains in the form of dissolved organic matter (Yamaguchi and McCarthy, 2018), subfossil foraminifera (Harada and Handa, 1995), and sedimentary organic matter (Bada et al., 1970; Kvenvolden et al., 1970; Bada and Schroeder, 1975; Bada and Man, 1980). Over time (within 15 million years), a steady state is approached where all amino acid enantiomers are present in a racemic mixture (i.e., D/L ratios equal to 1), which is mostly the case in kerogen (Kvenvolden, 1975) and extraterrestrial amino acids (Engel and Nagy, 1982). In addition to racemization producing D-amino acids, D-amino acids are actively removed from soils by way of enzymatic activity (racemase) by microbes (Zhang and Sun, 2014), further construing environmental amino acid enantiomeric ratios. However, despite these compications, with constraints on temperature history (e.g., organism and sediment temperature), amino acid enantiomers harbor rich information on age constraints (or vice versa), with less precision than radiocarbon, but extending back further in time (see also reviews by Kvenvolden, 1975 and Kaufman and Miller, 1992).

Going a step beyond amino acid-specific radiocarbon, development of a method for enantiomer-specific radiocarbon could be pursued. The technical feasibility of such an approach was recently made plausible, where underivatized individual amino acids, which were previously isolated from sediments, were chromatographically separated into their L and D forms (Blattmann, 2018). If collected, such isolates can provide insight into the radiocarbon population distributions of a single compound on a coarsest of levels. Other efforts to constrain the complex age distributions of organic matter using compound-specific radiocarbon (using fatty acids) have recently come to fruition using time series inversion approaches deconvolving pools of organic matter with different turnovers (French et al., 2018; Vonk et al., 2019). However, even without performing inversions, enantiomer-specific radiocarbon can provide direct insight into the radiocarbon population distributions of individual amino acids. In a simplest end member of cases involving conservative mixing, contributions of biospheric L-amino acids can be teased apart from petrogenic sources, which exhibit D/L ratios equal to 1. In such a case, the age of biospheric L-amino acids can be assessed by mass balance as petrogenic amino acids would equally contribute to the radiocarbon fingerprint of L- and D-amino acids, while biospheric sources would exclusively contribute to the L-amino acid pool (c.f. Silfer et al., 1994). In open systems involving dynamic changes such as contributions of D-amino acids stemming from peptidoglycan from bacteria (c.f. Pelz et al., 1998; Glaser and Amelung, 2002; Veuger et al., 2005), an enantiomer-specific approach can provide insight into microbial pathways of carbon flow embedded in the tapestry of radiocarbon ages contained within dissolved and sedimentary organic matter (e.g., incorporation of carbon derived from young, labile organic matter into bacterial biomass). Additionally, for calibrations of archeological and geochronological time using amino acid enantiomer ratios (e.g., Bada et al., 1984; Kosnik et al., 2013; Simonson et al., 2013), the integrity of purportedly closed systems such as within biominerals can be tested with enantiomer-specific radiocarbon, which can provide insight into radiocarbon disequilibria between enantiomers thereby unveiling open system behavior. The possibility of performing

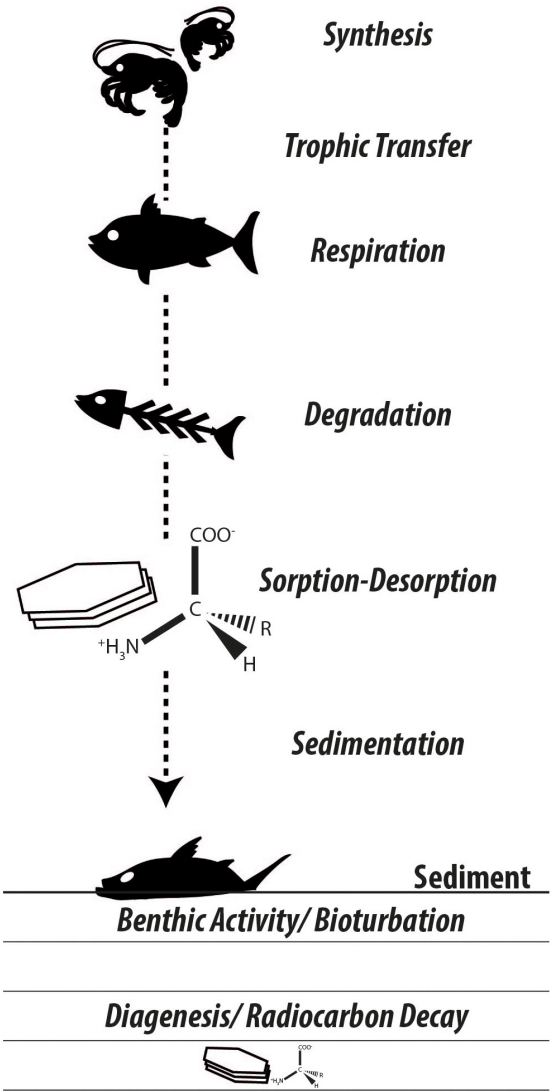

FIGURE 3 | Synthesizing the many unknowns in amino acid biogeochemistry. As carbon is incorporated in biomass and propagates through the food chain, radiocarbon isotopic signatures in individual amino acids should reflect primary (e.g., dissolved inorganic carbon) and secondary (e.g., benthic-derived organic matter) carbon sources. Biomass subject to decay releases amino acids that undergo differential degradation and interact with available mineral substrates, thereby influencing their bioavailability and sealing their fate in the geosphere.

enantiomer-specific radiocarbon for amino acids is unique among most other compounds and the hypothesized benefits for understanding biogeochemical cycles for ecological as well as environmental applications look promising.

SYNTHESIS AND OUTLOOK

Following the biospheric pathways along which amino acids are synthesized, propagate through food webs, and decay with a very small fraction finding its way into the geosphere, many questions arise regarding the origin and fate of carbon in these biosphere internal and biosphere-geosphere exchanges (**Figure 3**). Following their purposes in the biosphere, amino acids face extensive degradation and diagenetic changes, yet remain among the largest characterizable fractions of organic matter preserved in the geologic record (Trask, 1936; Erdman et al., 1956; Wakeham et al., 1997). Amino acid-specific radiocarbon appears a promising tool to confront a range of ecological, sedimentological, and biogeochemical challenges. The authors will report on their progress in future contributions.

AUTHOR CONTRIBUTIONS

Both authors equally contributed and wrote this manuscript.

FUNDING

The authors acknowledge financial support from ETH Research Grant ETH-41 14-1 and JAMSTEC.

ACKNOWLEDGMENTS

We thank colleagues at JAMSTEC and ETH for stimulating discussions and are grateful for the reviews provided by A. McNichol and S. Kusch. We acknowledge the Hanse-Wissenschaftskolleg Delmenhorst, Germany, for sponsoring the "Marine Organic Biogeochemistry" workshop in April 2019. The workshop was funded by the Deutsche Forschungsgemeinschaft (DFG, German Research Foundation) – project number: 422798570.

REFERENCES

Abelson, H. (1954). *Organic Constituents of Fossils: Carnegie Institute of Washington Year Book*, Vol. 53. Washington, DC: Carnegie Institution of Washington, 97–101.

Bada, J. L., Luyendyk, B. P., and Maynard, J. B. (1970). Marine sediments: dating by the racemization of amino acids. *Science* 170, 730–732. doi: 10.1126/science.170.3959.730

Bada, J. L., Kvenvolden, K. A., and Peterson, E. (1973). Racemization of amino acids in bones. *Nature* 245, 308–310. doi: 10.1038/245308a0

Bada, J. L., and Schroeder, R. A. (1975). Amino acid racemization reactions and their geochemical implications. *Naturwissenschaften* 62, 71–79. doi: 10.1007/BF00592179

Bada, J. L., and Man, E. H. (1980). Amino acid diagenesis in deep sea drilling project cores: kinetics and mechanisms of some reactions and their applications in geochronology and in paleotemperature and heat flow determinations. *Earth Sci. Rev.* 16, 21–55. doi: 10.1016/0012-8252(80)90003-3

Bada, J. L., Gillespie, R., Gowlett, J. A. J., and Hedges, R. E. M. (1984). Accelerator mass spectrometry radiocarbon ages of amino acid extracts from Californian palaeoindian skeletons. *Nature* 312, 442–444. doi: 10.1038/312442a0

Bada, J. L. (1985). "Racemization of amino acids," in *Chemistry and Biochemistry of the Amino Acids*, ed. G. C. Barrett (Dordrecht: Springer), 376–398. doi: 10.1007/978-94-009-4832-7_12

Bada, J. L., Herrmann, B., Payan, I. L., and Man, E. H. (1989). Amino acid racemization in bone and the boiling of the German Emperor Lothar I. *Appl. Geochem.* 4, 325–327. doi: 10.1016/0883-2927(89)90036-X

Bender, D. A. (2012). *Amino Acid Metabolism*, 3rd Edn. Oxford: Wiley-Blackwell. doi: 10.1002/9781118357514

Beutelspacher, H. (1955). Wechselwirkung zwischen anorganischen und organischen Kolloiden des Bodens. *Zeitschrift Pflanzenernährung Düngung Bodenkunde* 69, 108–115. doi: 10.1002/jpln.19550690118

Blattmann, T. M. (2018). *Topics on Radiocarbon Geochemistry and Organic Matter-Mineral Interactions*. Ph.D. thesis, ETH Zürich, Zurich. doi: 10.3929/ethz-b-000313397

Blattmann, T. M., Zhang, Y., Zhao, Y., Wen, K., Lin, S., Li, J., et al. (2018). Contrasting fates of petrogenic and biospheric carbon in the South China Sea. *Geophys. Res. Lett.* 45, 9077–9086. doi: 10.1029/2018GL079222

Blattmann, T. M., Liu, Z., Zhang, Y., Zhao, Y., Haghipour, N., Montluçon, D. B., et al. (2019). Mineralogical control on the fate of continentally derived organic matter in the ocean. *Science* 366:eaax5345. doi: 10.1126/science.aax5345

Blattmann, T. M., Montlucon, D. B., Haghipour, N., Ishikawa, N. F., and Eglinton, T. I. (2020). Liquid chromatographic isolation of individual amino acids extracted from sediments for radiocarbon analysis. *Front. Mar. Sci.* 7:174. doi: 10.3389/fmars.2020.00174

Bour, A. L., Walker, B. D., Broek, T. A. B., and McCarthy, M. D. (2016). Radiocarbon analysis of individual amino acids: carbon blank quantification for a small-sample high-pressure liquid chromatography purification method. *Anal. Chem.* 88, 3521–3528. doi: 10.1021/acs.analchem.5b03619

Broecker, W. S., and Walton, A. (1959). The geochemistry of C14 in fresh-water systems. *Geochim. Cosmochim. Acta* 16, 15–38. doi: 10.1016/0016-7037(59)90044-4

Carstens, D., Lehmann, M. F., Hofstetter, T. B., and Schubert, C. J. (2013). Amino acid nitrogen isotopic composition patterns in lacustrine sedimenting matter. *Geochim. Cosmochim. Acta* 121, 328–338. doi: 10.1016/j.gca.2013.07.020

Chikaraishi, Y., Ogawa, N. O., Kashiyama, Y., Takano, Y., Suga, H., Tomitani, A., et al. (2009). Determination of aquatic food-web structure based on compound-specific nitrogen isotopic composition of amino acids. *Limnol. Oceanogr. Methods* 7, 740–750. doi: 10.1016/j.jchromb.2016.09.004

Chikaraishi, Y., Steffan, S. A., Takano, Y., and Ohkouchi, N. (2015). Diet quality influences isotopic discrimination among amino acids in an aquatic vertebrate. *Ecol. Evol.* 5, 2048–2059. doi: 10.1002/ece3.1491

Corrigan, J. J. (1969). D-Amino acids in animals. *Science* 164, 142–149. doi: 10.1126/science.164.3876.142

Cowie, G. L., and Hedges, J. I. (1992). Improved amino acid quantification in environmental samples: charge-matched recovery standards and reduced analysis time. *Mar. Chem.* 37, 223–238. doi: 10.1016/0304-4203(92)90079-P

Degens, E. T., and Bajor, M. (1960). Die Verteilung von Aminosäuren in bituminösen Sedimenten und ihre Bedeutung für die Kohlen- und Erdölgeologie. *Glückauf* 96, 1525–1534.

Degens, E. T. (1970). "Molecular nature of nitrogenous compounds in sea water and recent marine sediments," in *Proceedings of the Symposium on Organic Matter in Natural Waters*, ed. D. H. Hood (Alaska: Institute of Marine Science University), 77–106.

Ding, X., and Henrichs, S. M. (2002). Adsorption and desorption of proteins and polyamino acids by clay minerals and marine sediments. *Mar. Chem.* 77, 225–237. doi: 10.1016/S0304-4203(01)00085-8

Engel, M. H., and Nagy, B. (1982). Distribution and enantiomeric composition of amino acids in the Murchison meteorite. *Nature* 296, 837–840. doi: 10.1038/296837a0

Ensminger, L. E., and Gieseking, J. E. (1941). The adsorption of proteins by montmorillonitic clays and its effect on base-exchange capacity. *Soil Sci.* 51, 125–132.

Erdman, J. G., Marlett, E. M., and Hanson, W. E. (1956). Survival of amino acids in marine sediments. *Science* 124, 1026–1026. doi: 10.1126/science.124.3230.1026

Estes, E. R., Pockalny, R., D'Hondt, S., Inagaki, F., Morono, Y., Murray, R. W., et al. (2019). Persistent organic matter in oxic subseafloor sediment. *Nat. Geosci.* 12, 126–131. doi: 10.1038/s41561-018-0291-5

Eusterhues, K., Rumpel, C., and Kögel-Knabner, I. (2005). Stabilization of soil organic matter isolated via oxidative degradation. *Organ. Geochem.* 36, 1567–1575. doi: 10.1016/j.orggeochem.2005.06.010

French, K. L., Hein, C. J., Haghipour, N., Wacker, L., Kudrass, H. R., Eglinton, T. I., et al. (2018). Millennial soil retention of terrestrial organic matter deposited in the Bengal Fan. *Sci. Rep.* 8:11997. doi: 10.1038/s41598-018-30091-8

Glaser, B., and Amelung, W. (2002). Determination of 13C natural abundance of amino acid enantiomers in soil: methodological considerations and first results. *Rapid Commun. Mass Spectrom.* 16, 891–898. doi: 10.1002/rcm.650

Goto, A. S., Miura, K., Korenaga, T., Hasegawa, T., Ohkouchi, N., and Chikaraishi, Y. (2018). Fractionation of stable nitrogen isotopes (15N/14N) during enzymatic deamination of glutamic acid: implications for mass and energy transfers in the biosphere. *Geochem. J.* 52, 273–280. doi: 10.2343/geochemj.2.0513

Guillemette, F., Bianchi, T. S., and Spencer, R. G. M. (2017). Old before your time: ancient carbon incorporation in contemporary aquatic foodwebs. *Limnol. Oceanogr.* 62, 1682–1700. doi: 10.1002/lno.10525

Harada, N., and Handa, N. (1995). Amino acid chronology in the fossil planktonic foraminifera, Pulleniatina obliquiloculata from Pacific Ocean. *Geophys. Res. Lett.* 22, 2353–2356. doi: 10.1029/95GL02112

Hare, E. (1969). "Geochemistry of proteins, peptides, and amino acids," in *Organic Geochemistry: Methods and Results*, eds G. Eglinton and M. T. J. Murphy (Berlin: Springer), 438–462. doi: 10.1007/978-3-642-87734-6_22

Hare, E., Fogel, M. L., Stafford, T. W. Jr., Mitchell, A. D., and Hoering, T. C. (1991). The isotopic composition of carbon and nitrogen in individual amino acids isolated from modern and fossil proteins. *J. Arch. Sci.* 18, 277–292. doi: 10.1016/0305-4403(91)90066-X

Hedges, J. I, and Parker, L. (1976). Land-derived organic matter in surface sediments from the Gulf of Mexico. *Geochim. Cosmochim. Acta* 40, 1019–1029. doi: 10.1016/j.marpolbul.2017.04.042

Hedges, J. I. (1978). The formation and clay mineral reactions of melanoidins. *Geochim. Cosmochim. Acta* 42, 69–76. doi: 10.1016/0016-7037(78)90218-1

Hedges, I., and Hare, E. (1987). Amino acid adsorption by clay minerals in distilled water. *Geochim. Cosmochim. Acta* 51, 255–259. doi: 10.1016/0016-7037(87)90237-7

Hedges, I., Baldock, J. A., Gélinas, Y., Lee, C., Peterson, M., and Wakeham, S. G. (2001). Evidence for non-selective preservation of organic matter in sinking marine particles. *Nature* 409, 801–804. doi: 10.1038/35057247

Henrichs, S. M., and Sugai, S. F. (1993). Adsorption of amino acids and glucose by sediments of Resurrection Bay, Alaska, USA: functional group effects. *Geochim. Cosmochim. Acta* 57, 823–835. doi: 10.1016/0016-7037(93)90171-R

Hwang, J., Druffel, E. R. M., and Komada, T. (2005). Transport of organic carbon from the California coast to the slope region: a study of Δ14C and δ13C signatures of organic compound classes. *Glob. Biogeochem. Cycles* 19:GB2018. doi: 10.1029/2004GB002422

Ishikawa, N. F., Hyodo, F., and Tayasu, I. (2013). Use of carbon-13 and carbon-14 natural abundances for stream food web studies. *Ecol. Res.* 28, 759–769. doi: 10.1007/s11284-012-1003-z

Ishikawa, N. F., Itahashi, Y., Blattmann, T. M., Takano, Y., Ogawa, N. O., Yamane, M., et al. (2018). Improved method for isolation and purification of underivatized amino acids for radiocarbon analysis. *Anal. Chem.* 90, 12035–12041. doi: 10.1021/acs.analchem.8b02693

Ishikawa, N. F. (2018). Use of compound-specific nitrogen isotope analysis of amino acids in trophic ecology: assumptions, applications, and implications. *Ecol. Res.* 33, 825–837. doi: 10.1007/s11284-018-1616-y

Kaufman, D. S., and Miller, G. H. (1992). Overview of amino acid geochronology: comparative biochemistry and physiology Part B. *Comp. Biochem.* 102, 199–204. doi: 10.1016/0305-0491(92)90110-D

Keil, R. G., Montluçon, D. B., Prahl, F. G., and Hedges, J. I. (1994a). Sorptive preservation of labile organic matter in marine sediments. *Nature* 370, 549–552. doi: 10.1038/370549a0

Keil, R. G., Tsamakis, E., Fuh, C. B., Giddings, J. C., and Hedges, J. I. (1994b). Mineralogical and textural controls on the organic composition of coastal marine sediments: hydrodynamic separation using SPLITT-fractionation. *Geochim. Cosmochim. Acta* 58, 879–893. doi: 10.1016/0016-7037(94)90512-6

Keil, R. G., Mayer, L. M., Quay, D., Richey, J. E., and Hedges, J. I. (1997). Loss of organic matter from riverine particles in deltas. *Geochim. Cosmochim. Acta* 61, 1507–1511. doi: 10.1016/S0016-7037(97)00044-6

Keil, R. G., Tsamakis, E., Giddings, J. C., and Hedges, J. I. (1998). Biochemical distributions (amino acids, neutral sugars, and lignin phenols) among size-classes of modern marine sediments from the Washington coast. *Geochim. Cosmochim. Acta* 62, 1347–1364. doi: 10.1016/S0016-7037(98)00080-5

Keil, R. G., and Fogel, M. L. (2001). Reworking of amino acid in marine sediments: stable carbon isotopic composition of amino acids in sediments along the Washington coast. *Limnol. Oceanogr.* 46, 14–23. doi: 10.4319/lo.2001.46.1.0014

Keil, R. G., and Mayer, L. M. (2014). "Mineral matrices and organic matter," in *Treatise on Geochemistry*, eds H. D. Holland and K. K. Turekian (Oxford: Elsevier), 337–359. doi: 10.1016/B978-0-08-095975-7.01024-X

Kennedy, M. J., Pevear, D. R., and Hill, R. J. (2002). Mineral surface control of organic carbon in black shale. *Science* 295, 657–660. doi: 10.1126/science.1066611

Kirchman, D. L. (1990). Limitation of bacterial growth by dissolved organic matter in the subarctic Pacific. *Mar. Ecol. Prog. Ser.* 62, 47–54. doi: 10.3354/meps062047

Kitadai, N., and Maruyama, S. (2018). Origins of building blocks of life: a review. *Geosci. Front.* 9, 1117–1153. doi: 10.1016/j.gsf.2017.07.007

Kleber, M., Eusterhues, K., Keiluweit, M., Mikutta, C., Mikutta, R., and Nico, S. (2015). "Mineral–organic associations: formation, properties, and relevance in soil environments," in *Advances in Agronomy*, Vol. 130, ed. D. L. Sparks (Cambridge, MA: Academic Press), 1–140. doi: 10.1016/bs.agron.2014.10.005

Kosnik, M. A., Kaufman, D. S., and Hua, Q. (2013). Radiocarbon-calibrated multiple amino acid geochronology of Holocene molluscs from Bramble and Rib Reefs (Great Barrier Reef, Australia). *Quat. Geochronol.* 16, 73–86. doi: 10.1016/j.quageo.2012.04.024

Kvenvolden, K. A., Peterson, E., and Brown, F. S. (1970). Racemization of amino acids in sediments from Saanich Inlet, British Columbia. *Science* 169, 1079–1082. doi: 10.1126/science.169.3950.1079

Kvenvolden, K. A. (1975). Advances in the geochemistry of amino acids. *Annu. Rev. Earth Planet. Sci.* 3, 183–212. doi: 10.1146/annurev.ea.03.050175.001151

Lam, H., Oh, D.-C., Cava, F., Takacs, C. N., Clardy, J., de Pedro, M. A., et al. (2009). D-Amino acids govern stationary phase cell wall remodeling in bacteria. *Science* 325, 1552–1555. doi: 10.1126/science.1178123

Larsen, T., Taylor, D. L., Leigh, M. B., and O'Brien, D. M. (2009). Stable isotope fingerprinting: a novel method for identifying plant, fungal, or bacterial origins of amino acids. *Ecology* 90, 3526–3535. doi: 10.1890/08-1695.1

Larsen, T., Ventura, M., Andersen, N., O'Brien, D. M., Piatkowski, U., and McCarthy, M. D. (2013). Tracing carbon sources through aquatic and terrestrial food webs using amino acid stable isotope fingerprinting. *PLoS One* 8:e73441. doi: 10.1371/journal.pone.0073441

Lee, C., Bada, J. L., and Peterson, E. (1976). Amino acids in modern and fossil woods. *Nature* 259, 183–186. doi: 10.1038/259183a0

Lee, C., Wakeham, S. G., and Farrington, J. W. (1983). Variations in the composition of particulate organic matter in a time-series sediment trap. *Mar. Chem.* 13, 181–194. doi: 10.1016/0304-4203(83)90013-0

Libby, W. F., Anderson, E. C., and Arnold, J. R. (1949). Age determination by radiocarbon content – World-wide assay of natural radiocarbon. *Science* 109, 227–228. doi: 10.1126/science.109.2827.227

Macko, S. A., Estep, M. L. F., Engel, M. H., and Hare, E. (1986). Kinetic fractionation of stable nitrogen isotopes during amino acid transamination. *Geochim. Cosmochim. Acta* 50, 2143–2146. doi: 10.1016/0016-7037(86)90068-2

Masters, M., Bada, J. L., and Samuel Zigler, J. (1977). Aspartic acid racemisation in the human lens during ageing and in cataract formation. *Nature* 268, 71–73. doi: 10.1038/268071a0

Mayer, L. M. (1994). Surface area control of organic carbon accumulation in continental shelf sediments. *Geochim. Cosmochim. Acta* 58, 1271–1284. doi: 10.1016/0016-7037(94)90381-6

McCullagh, J. S. O., Marom, A., and Hedges, R. E. M. (2010). Radiocarbon dating of individual amino acids from archaeological bone collagen. *Radiocarbon* 52, 620–634. doi: 10.1017/S0033822200045653

McIntyre, C. P., Wacker, L., Haghipour, N., Blattmann, T. M., Fahrni, S., Usman, M., et al. (2017). Online 13C and 14C gas measurements by EA-IRMS–AMS at ETH Zürich. *Radiocarbon* 59, 893–903.

McMahon, K. W., Fogel, M. L., Elsdon, T. S., and Thorrold, S. R. (2010). Carbon isotope fractionation of amino acids in fish muscle reflects biosynthesis and isotopic routing from dietary protein. *J. Anim. Ecol.* 79, 1132–1141. doi: 10.1111/j.1365-2656.2010.01722.x

McMahon, K. W., Thorrold, S. R., Houghton, L. A., and Berumen, M. L. (2016). Tracing carbon flow through coral reef food webs using a compound-specific stable isotope approach. *Oecologia* 180, 809–821. doi: 10.1007/s00442-015-3475-3

Miller, S. L., and Urey, H. C. (1959). Organic compound synthesis on the primitive Earth. *Science* 130, 245–251. doi: 10.1126/science.130.3370.245

Montluçon, D. B., and Lee, C. (2001). Factors affecting lysine sorption in a coastal sediment. *Organ. Geochem.* 32, 933–942. doi: 10.1016/S0146-6380(01)00050-X

Müller, J. (1977). C/N ratios in Pacific deep-sea sediments: effect of inorganic ammonium and organic nitrogen compounds sorbed by clays. *Geochim. Cosmochim. Acta* 41, 765–776. doi: 10.1016/0016-7037(77)90047-3

Neuberger, A. (1948). "Stereochemistry of amino acids," in *Advances in Protein Chemistry*, eds M. L. Anson and J. T. Edsall (Cambridge, MA: Academic Press), 297–383. doi: 10.1016/S0065-3233(08)60009-1

Ohkouchi, N., Chikaraishi, Y., Close, H. G., Fry, B., Larsen, T., Madigan, D. J., et al. (2017). Advances in the application of amino acid nitrogen isotopic analysis in ecological and biogeochemical studies. *Organ. Geochem.* 113, 150–174. doi: 10.1016/j.orggeochem.2017.07.009

Olsen, E., and Sunde, J. (2002). Age determination of minke whales (*Balaenoptera acutorostrata*) using the aspartic acid racemization technique. *Sarsia* 87, 1–8. doi: 10.1080/003648202753631686

Pantoja, S., and Lee, C. (2003). Amino acid remineralization and organic matter lability in Chilean coastal sediments. *Organ. Geochem.* 34, 1047–1056. doi: 10.1016/S0146-6380(03)00085-8

Pelz, O., Cifuentes, L. A., Hammer, B. T., Kelley, C. A., and Coffin, R. B. (1998). Tracing the assimilation of organic compounds using δ13C analysis of unique amino acids in the bacterial peptidoglycan cell wall. *FEMS Microbiol. Ecol.* 25, 229–240. doi: 10.1111/j.1574-6941.1998.tb00475.x

Petsch, S. T., Eglinton, T. I., and Edwards, K. J. (2001). 14C-dead living biomass: evidence for microbial assimilation of ancient organic carbon during shale weathering. *Science* 292, 1127–1131. doi: 10.1126/science.1058332

Pinck, L. A., and Allison, F. E. (1951). Resistance of a protein-montmorillonite complex to decomposition by soil microorganisms. *Science* 114, 130–131. doi: 10.1126/science.114.2953.130

Schmidt, M. W. I., Torn, M. S., Abiven, S., Dittmar, T., Guggenberger, G., Janssens, I. A., et al. (2011). Persistence of soil organic matter as an ecosystem property. *Nature* 478, 49–56. doi: 10.1038/nature10386

Silfer, J. A., Qian, Y., Macko, S. A., and Engel, M. H. (1994). Stable carbon isotope compositions of individual amino acid enantiomers in mollusc shell by GC/C/IRMS. *Organ. Geochem.* 21, 603–609. doi: 10.1016/0146-6380(94)90006-X

Simonson, A. E., Lockwood, R., and Wehmiller, J. F. (2013). Three approaches to radiocarbon calibration of amino acid racemization in *Mulinia lateralis* from the Holocene of the Chesapeake Bay, USA. *Quat. Geochronol.* 16, 62–72. doi: 10.1016/j.quageo.2012.06.005

Stuiver, M., and Polach, H. A. (1977). Discussion: reporting of 14C data. *Radiocarbon* 19, 355–363. doi: 10.1017/S0033822200003672

Trask, D. (1936). Inferences about the origin of oil as indicated by the composition of the organic constituents of sediments. *Paper Presented at the Washington: United States Government Printing Office, Professional Paper / United States Department of the Interior, Geological Survey*, Washington, DC.

Vernadsky, W. J. (1930). *Geochemie in Ausgewählten Kapiteln*. Leipzig: Akademische Verlagsgesellschaft, 370.

Veuger, B., Middelburg, J. J., Boschker, H. T. S., and Houtekamer, M. (2005). Analysis of 15N incorporation into D-alanine: a new method for tracing nitrogen uptake by bacteria. *Limnol. Oceanogr. Methods* 3, 230–240. doi: 10.4319/lom.2005.3.230

Volkman, J. K., Eglinton, G., Corner, E. D. S., and Forsberg, T. E. (1980). Long-chain alkenes and alkenones in the marine coccolithophorid *Emiliania huxleyi*. *Phytochemistry* 19, 2619–2622. doi: 10.1016/s0031-9422(00)00120-5

Vonk, J. E., Drenzek, N. J., Hughen, K. A., Stanley, R. H. R., McIntyre, C., Montluçon, D. B., et al. (2019). Temporal deconvolution of vascular plant-derived fatty acids exported from terrestrial watersheds. *Geochim. Cosmochim. Acta* 244, 502–521. doi: 10.1016/j.gca.2018.09.034

Wakeham, S. G., Lee, C., Hedges, J. I., Hernes, J., and Peterson, M. J. (1997). Molecular indicators of diagenetic status in marine organic matter. *Geochim. Cosmochim. Acta* 61, 5363–5369. doi: 10.1016/S0016-7037(97)00312-8

Wang, X.-C., and Lee, C. (1993). Adsorption and desorption of aliphatic amines, amino acids and acetate by clay minerals and marine sediments. *Mar. Chem.* 44, 1–23. doi: 10.1016/0304-4203(93)90002-6

Wang, X.-C., Druffel, E. R. M., and Lee, C. (1996). Radiocarbon in organic compound classes in particulate organic matter and sediment in the deep northeast Pacific ocean. *Geophys. Res. Lett.* 23, 3583–3586. doi: 10.1029/96GL03423

Wang, X.-C., Druffel, E. R. M., Griffin, S., Lee, C., and Kashgarian, M. (1998). Radiocarbon studies of organic compound classes in plankton and sediment of the northeastern Pacific ocean. *Geochim. Cosmochim. Acta* 62, 1365–1378. doi: 10.1016/S0016-7037(98)00074-X

Williams, M., Druffel, E. R. M., and Smith, K. L. (1987). Dietary carbon sources for deep-sea organisms as inferred from their organic radiocarbon activities: deep sea research part A. *Oceanogr. Res. Pap.* 34, 253–266. doi: 10.1016/0198-0149(87)90085-9

Yamaguchi, Y. T., and McCarthy, M. D. (2018). Sources and transformation of dissolved and particulate organic nitrogen in the North Pacific Subtropical Gyre indicated by compound-specific δ15N analysis of amino acids. *Geochim. Cosmochim. Acta* 220, 329–347. doi: 10.1016/j.gca.2017.07.036

Yokoyama, T., Kan-No, N., Ogata, T., Kotaki, Y., Sato, M., and Nagahisa, E. (2003). Presence of free D-amino acids in microalgae: bioscience. *Biotechnol. Biochem.* 67, 388–392. doi: 10.1271/bbb.67.388

Zhang, G., and Sun, H. J. (2014). Racemization in reverse: evidence that D-amino acid toxicity on earth is controlled by bacteria with racemases. *PLoS One* 9:e92101. doi: 10.1371/journal.pone.0092101

Conflict of Interest: The authors declare that the research was conducted in the absence of any commercial or financial relationships that could be construed as a potential conflict of interest.

frontiers in Marine Science

REVIEW
published: 25 May 2020
doi: 10.3389/fmars.2020.00341

Soothsaying DOM: A Current Perspective on the Future of Oceanic Dissolved Organic Carbon

Sasha Wagner[1], Florence Schubotz[2], Karl Kaiser[3,4], Christian Hallmann[2,5], Hannelore Waska[6], Pamela E. Rossel[6], Roberta Hansman[7†], Marcus Elvert[2], Jack J. Middelburg[8], Anja Engel[9], Thomas M. Blattmann[10], Teresa S. Catalá[6], Sinikka T. Lennartz[6], Gonzalo V. Gomez-Saez[6,11], Silvio Pantoja-Gutiérrez[12], Rui Bao[13] and Valier Galy[14]*

[1] Department of Earth and Environmental Sciences, Rensselaer Polytechnic Institute, Troy, NY, United States, [2] MARUM - Center for Marine Environmental Sciences, University of Bremen, Bremen, Germany, [3] Department of Marine and Coastal Environmental Science, Texas A&M Galveston Campus, Galveston, TX, United States, [4] Department of Oceanography, Texas A&M University, College Station, TX, United States, [5] Max Planck Institute for Biogeochemistry, Jena, Germany, [6] ICBM-MPI Bridging Group for Marine Geochemistry, Institute for Chemistry and Biology of the Marine Environment, University of Oldenburg, Oldenburg, Germany, [7] International Atomic Energy Agency (IAEA) - Environment Laboratories, Monaco, Monaco, [8] Department of Earth Sciences, Utrecht University, Utrecht, Netherlands, [9] GEOMAR Helmholtz Centre for Ocean Research Kiel, Kiel, Germany, [10] Biogeochemistry Program, Japan Agency for Marine-Earth Science and Technology, Yokosuka, Japan, [11] Alfred Wegener Institute, Alfred Wegener Institute for Polar and Marine Research, Bremerhaven, Germany, [12] Department of Oceanography, Center for Oceanographic Research COPAS Sur-Austral, University of Concepción, Concepción, Chile, [13] Frontiers Science Center for Deep Ocean Multispheres and Earth System, and Key Laboratory of Marine Chemistry Theory and Technology, Ministry of Education, Ocean University of China, Qingdao, China, [14] Woods Hole Oceanographic Institution, Woods Hole, MA, United States

OPEN ACCESS

Edited by:
Stuart Wakeham, University of Georgia, United States

Reviewed by:
Dennis Arthur Hansell, University of Miami, United States
Ronald Benner, University of South Carolina, United States

***Correspondence:**
Sasha Wagner
wagnes3@rpi.edu

†Present address:
Roberta Hansman, Woods Hole Oceanographic Institution, Woods Hole, MA, United States

Specialty section:
This article was submitted to Marine Biogeochemistry, a section of the journal Frontiers in Marine Science

Received: *28 February 2020*
Accepted: *23 April 2020*
Published: *25 May 2020*

Citation:
Wagner S, Schubotz F, Kaiser K, Hallmann C, Waska H, Rossel PE, Hansman R, Elvert M, Middelburg JJ, Engel A, Blattmann TM, Catalá TS, Lennartz ST, Gomez-Saez GV, Pantoja-Gutiérrez S, Bao R and Galy V (2020) Soothsaying DOM: A Current Perspective on the Future of Oceanic Dissolved Organic Carbon. Front. Mar. Sci. 7:341. doi: 10.3389/fmars.2020.00341

The vast majority of freshly produced oceanic dissolved organic carbon (DOC) is derived from marine phytoplankton, then rapidly recycled by heterotrophic microbes. A small fraction of this DOC survives long enough to be routed to the interior ocean, which houses the largest and oldest DOC reservoir. DOC reactivity depends upon its intrinsic chemical composition and extrinsic environmental conditions. Therefore, recalcitrance is an emergent property of DOC that is analytically difficult to constrain. New isotopic techniques that track the flow of carbon through individual organic molecules show promise in unveiling specific biosynthetic or degradation pathways that control the metabolic turnover of DOC and its accumulation in the deep ocean. However, a multivariate approach is required to constrain current carbon fluxes so that we may better predict how the cycling of oceanic DOC will be altered with continued climate change. Ocean warming, acidification, and oxygen depletion may upset the balance between the primary production and heterotrophic reworking of DOC, thus modifying the amount and/or composition of recalcitrant DOC. Climate change and anthropogenic activities may enhance mobilization of terrestrial DOC and/or stimulate DOC production in coastal waters, but it is unclear how this would affect the flux of DOC to the open ocean. Here, we assess current knowledge on the oceanic DOC cycle and identify research gaps that must be addressed to successfully implement its use in global scale carbon models.

Keywords: dissolved organic carbon, global carbon cycle, recalcitrance, isotopic probing, climate change

INTRODUCTION

Containing roughly the same amount of carbon as terrestrial biomass, or CO_2 in the atmosphere, the oceanic dissolved organic matter (DOM) pool represents one of Earth's large organic carbon reservoirs (660 Pg-C; Hansell et al., 2009; Houghton, 2014). Global carbon cycling models generally consider the total ocean split into three "boxes" – the surface ocean (<200 m), the twilight or mesopelagic zone (200–1,000 m) and the interior ocean (>1,000 m). This compartmentalization of oceanic water masses is driven by our current understanding of how carbon is produced, cycled, and stored with depth. Oceanic DOM derives mainly from autochthonous production by phytoplankton in surface waters where it is rapidly recycled and serves as an energy source for heterotrophic microbes. A small portion of DOM produced in surface waters is eventually routed to the ocean's interior, which houses the bulk of the oceanic dissolved organic carbon (DOC) pool and cycles on much longer timescales. However, mechanisms controlling the accumulation of DOM in the interior ocean remain poorly understood. The oceanic DOC cycle is an essential component of the global carbon cycle, thus imbalances among oceanic DOC pools would impact future climate scenarios. However, global scale carbon models lack a coherent implementation of DOC at present.

Surface, mesopelagic, and interior ocean DOM each exhibit distinct latitudinal trends (Carlson et al., 2010). The distribution of DOM among these ocean boxes is largely mediated by biological activity. The "biological carbon pump" is a conceptual framework that describes the cumulative processes involved in the transport of biogenic material from the surface to the deeper ocean, including the formation and settling of particulate organic matter (POM), the active migration of zooplankton and other mobile organisms and the physical overturning of ocean water, including its organic constituents (Sarmiento and Gruber, 2006; Lutz et al., 2007; Jiao et al., 2010). Taken together, these mechanisms result in the total export of ca. 0.2 Pg-C yr^{-1} as DOC from the surface and mesopelagic ocean (<1,000 m; 180 Pg-C) to the interior ocean (>1,000 m), contributing to the large, slowly cycling DOC pool that resides there (480 Pg-C; Hansell et al., 2009). However, balancing oceanic DOC budgets is challenging, particularly in the transitional mesopelagic zone where isopycnal gradients and microbial activity results in a DOM pool with a wide spectrum of reactivity (Carlson and Hansell, 2015). Labile DOM is taken up by heterotrophic organisms within hours to days in shallow ocean depths. Refractory DOM is largely resistant to microbial degradation and therefore cycles on millennial timescales. It is proposed that the continous and/or repeated reworking of freshly produced DOM in surface waters results in the accumulation of recalcitrant DOM (Jiao et al., 2010), which is comprised of molecular components that fall along a reactivity continuum (Carlson and Hansell, 2015). Radiocarbon and stoichiometric analyses provide evidence for the accumulation of apparently old (~6,000 ^{14}C-years; Williams and Druffel, 1987) and carbon-enriched (Hopkinson and Vallino, 2005) DOM in the deep ocean. However, the distribution of labile and refractory DOM can also be explained by the "dilution hypothesis," which argues that the degradation of DOM is controlled by its concentration rather than its intrinsic chemical reactivity (Jannasch, 1967; Arrieta et al., 2015). If the formation of the recalcitrant DOM pool is not strictly dependent upon microbial lability, then a holistic approach, one that considers environmental redox conditions, concentration, time, etc. is needed to further refine current and predict future oceanic carbon cycles (see section "DOM Recalcitrance Is an Emergent Property").

Although contemporary carbon flux estimates have benefited from a two-component model approach involving labile and refractory fractions (Williams and Druffel, 1987; Druffel et al., 1992; Bauer et al., 1998), spatial mapping of DOM throughout the global oceans reveals a more dynamic system at play (Hansell et al., 2009). Oceanic DOC concentrations range from 40 to 80 μM-C where observed gradients are driven by vertical stratification and mixing, biological degradation, and terrigenous inputs (Hansell et al., 2009). Although the formation and degradation of recalcitrant DOM occurs on relatively long timescales, the spatial and temporal variability of this accumulated fraction of DOM has a major impact on the long-term storage of carbon in the ocean's interior, thus affecting global carbon cycles and associated climate change. As our analytical capabilities continue to advance, so should our understanding of the fine-scale processes that govern the global distribution of oceanic DOC. In turn, a clearer view of fine-scale biogeochemistry will allow for improved oceanic representation in global carbon cycling and Earth system models. This review of oceanic fluxes focuses upon DOC only (see section "Current Understanding of Marine DOM"). While some information on the cycling of organic heteroatoms exist (Pohlabeln and Dittmar, 2015; Gomez-Saez et al., 2016; Ksionzek et al., 2016; Pohlabeln et al., 2017; Broek et al., 2019), data available for dissolved organic nitrogen, sulfur, and phosphorous are extremely limited compared to DOC measurements. Here, we synthesize both well and poorly characterized fluxes of oceanic DOC, consider what is meant by DOM "recalcitrance," spotlight new isotopic approaches for probing the oceanic distribution of DOC, and discuss changes to DOM quantity and composition that are expected to occur in response to our changing climate.

CURRENT UNDERSTANDING OF MARINE DOM

Implementing oceanic DOC in the global carbon cycle and associated climate models requires an improved quantitative understanding of marine DOC. Here, we provide an overview of DOC sources and sinks as currently estimated for the surface and interior ocean. These fluxes are summarized in **Figure 1**. The apparent imbalance between sources and sinks can be ascribed to unconstrained loss estimates within the water column by either DOC remineralization or sorption to particles. In this section, we also highlight research gaps that must be addressed for a more accurate view of marine DOC cycling and how it may be altered with future climatic and oceanic change.

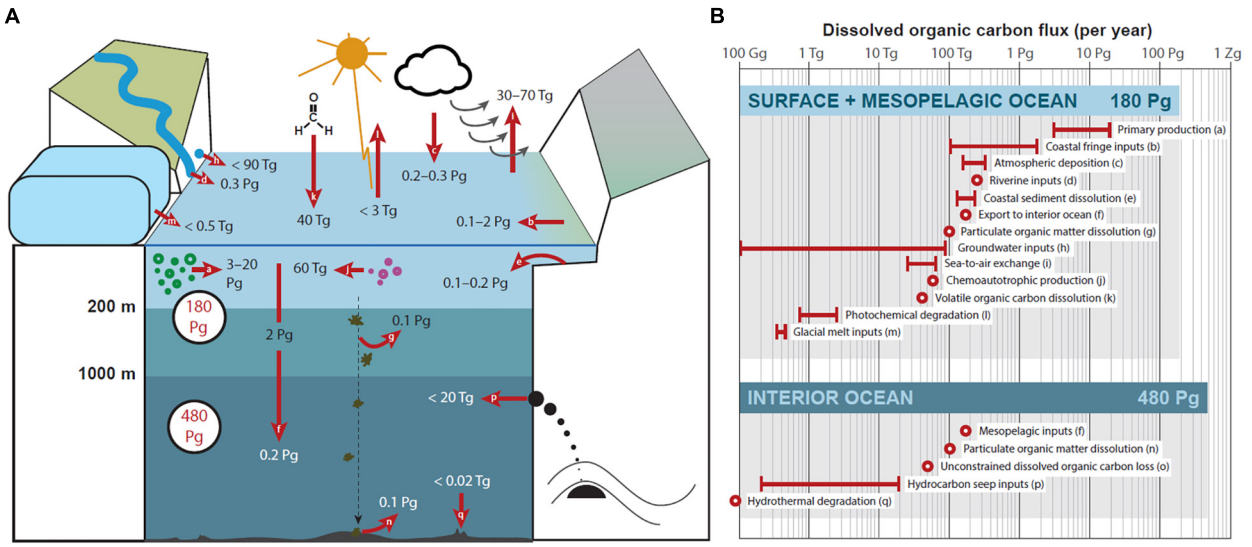

FIGURE 1 | The current understanding of dissolved organic carbon (DOC) fluxes in the surface, mesopelagic, and interior ocean. In panel **(A)** oceanic DOC stocks are shown in black circles with red font and units are Pg-C. DOC fluxes are shown in black and white font and units are either Tg-C yr^{-1} or Pg-C yr^{-1}. Letters in arrows and associated flux values correspond to descriptions displayed in **(B)**, which lists sources and sinks of oceanic DOC described in the text (see section "Current Understanding of Marine DOM").

Surface Ocean

Biotic Processes

Primary production (about 50 Pg-C yr^{-1}) is the main source of DOC in oceanic surface waters (3–20 Pg-C yr^{-1}) with significantly smaller contributions deriving from chemoautotrophic production (0.06 Pg-C yr^{-1}) (Middelburg, 2011; Carlson and Hansell, 2015). Intracellular organic matter accumulates when cell division is limited. This excess material is subsequently discharged via extracellular release (Fogg, 1966; Engel et al., 2004). Specific mechanisms of release are yet not fully understood, but low molecular weight DOC can leak through the cell membrane directly (Fogg, 1966) and high molecular weight DOC is actively exudated via exocytosis or similar processes (Leppard, 1995). Extracellular release is a cellular overflow mechanism shedding excess carbon, where compounds released are depleted in biolimiting elements (Wood and Van Valen, 1990; Engel et al., 2002; Schartau et al., 2007). Thus, the extracellular release of carbon-enriched DOM represents a significant source for DOC in the upper ocean (Aluwihare et al., 1997) and partly explains seasonal variations observed for Redfield ratios (Williams, 1995; Søndergaard et al., 2000). DOC is also released when zooplankton feed on phytoplankton in surface waters. The production of DOC from "sloppy feeding" ranges from 3 to 70% of the total mass of phytoplankton carbon ingested and is generally a function of predator-to-prey size (Copping and Lorenzen, 1980; Bjornsen, 1988; Moller, 2005, 2007; Saba et al., 2011). The amount of DOC released during zooplankton grazing ranges from 2 to 10% of the total zooplankton carbon mass (Steinberg et al., 2000, 2002). Similarly, microzooplankton have been shown to ingest 20–50% of algal biomass carbon during grazing, the majority of which is subsequently released as DOC (Nagata et al., 2000). However, given the high degree of spatiotemporal variability of zooplankton feeding, global DOC flux values for grazing and sloppy feeding have not been adequately constrained (Steinberg and Landry, 2017).

Viral infections are a major cause of marine microbial mortality (Wilhelm and Suttle, 1999; Suttle, 2007) and result in cell lysis and release of DOM during cell death. An estimated 6–26% of annual marine primary production flows through the viral shunt producing 3–13 Pg-C as DOC per year (Wilhelm and Suttle, 1999; Carlson and Hansell, 2015). Compositionally, viral lysates are rich in dissolved amino acids, carbohydrates, and nucleic acids (Weinbauer and Peduzzi, 1995; Middelboe and Jorgensen, 2006; Holmfeldt et al., 2010). Most of the DOC produced in the surface ocean is then routed through microorganisms and remineralized to CO_2 within an annual cycle (Azam et al., 1983). Only a small fraction of autotrophic DOC is converted to recalcitrant forms of DOC and survives long enough to be exported to the interior ocean (Gruber et al., 2006; Brophy and Carlson, 1989). Microbes utilize the diverse pool of organic compounds through direct uptake of small molecules or extracellular enzymatic hydrolysis to initiate decomposition (Weiss et al., 1991; Arnosti, 2004). The degradation of macromolecular structures is thereby linked enzymatic capabilities of the heterotrophic microbes.

Air-Sea Exchange

The transfer of organic matter from the atmosphere to the ocean occurs by dry deposition (settling of organic gases or particles) or by wet deposition (organic molecules dissolved in rainwater). Atmospheric deposition (wet plus dry) delivers 0.25 Pg-C yr^{-1} to the global surface ocean (Jurado et al., 2008; Kanakidou et al., 2012). However, atmospheric contributions to oceanic DOC depend largely upon the solubility of the deposited organic

matter. Most wet deposition organics are presumed to be water soluble DOC (>90%; Kanakidou et al., 2012). Therefore, a lower limit for atmospheric DOC fluxes can be derived considering only wet deposition, which equates to 0.17 Pg-C yr^{-1}, while an upper limit of 0.25 Pg-C yr^{-1} implies that all atmospherically deposited organic carbon dissolves within oceanic surface waters. Volatile organic molecules can also be transferred between the surface skin of the ocean and the overlying atmosphere (Liss et al., 2014). The efficiency of this ocean-to-air exchange is dependent upon molecular structure, current regimes, biological productivity, and light availability. Summed across all volatile organic compound classes, the ocean constitutes a net sink of short-lived gases [41 Tg-C yr^{-1}; (Heikes et al., 2002; Marandino et al., 2005; Shim et al., 2007; Millet et al., 2008; Liss et al., 2014)]. Marine aerosols are produced from both primary (bursting bubbles and breaking waves) and secondary processes (nucleation and oxidative reactions) and are highly enriched in organic matter compared to seawater (Keene et al., 2007; O'Dowd and de Leeuw, 2007; Quinn et al., 2014). Model estimates suggest the ocean-air flux of organic matter from primary marine aerosol production (8–50 Tg-C yr^{-1}) (Roelofs, 2008; Spracklen et al., 2008) can exceed that of organic matter transferred during secondary marine aerosol production (18 Tg-C yr^{-1}) (Andreae and Rosenfeld, 2008). Primary marine organic aerosols are also comprised of roughly one third refractory carbon (Kieber et al., 2016; Beaupre et al., 2019). Thus, the atmospheric release of marine aerosols is a significant loss mechanism for recalcitrant DOM in the surface ocean.

Terrestrial Inputs

Globally, the export of riverine DOC to the coast is estimated to be 0.25 Pg-C yr^{-1} (Hedges et al., 1997; Raymond and Spencer, 2015). Within the last decade, efforts have been aimed to refine flux estimates from individual rivers. For example, due to increased temporal sampling resolution that now includes periods of high DOC export (spring freshet), estimated DOC fluxes for major Arctic Rivers have increased by ∼10 Tg-C yr^{-1} (Holmes et al., 2012). Rivers with high DOC yields export more carbon per unit area (e.g., the Amazon and Congo; Raymond and Spencer, 2015), and thus represent key targets for research seeking to constrain fluxes of terrestrial carbon to the ocean. Mountain glaciers export 0.58 Tg-C as DOC annually (Hood et al., 2015), but the majority of this glacial melt-derived DOC feeds primarily into fluvial systems and is thus captured by riverine DOC flux estimates and/or is highly bioavailable and degrades before reaching the ocean (Hemingway et al., 2019). At present, glacial melt represents a small source of terrestrial DOC to the coastal ocean (0.32–0.46 Tg-C yr^{-1}; Priscu and Christner, 2004; Bamber et al., 2012; Hood et al., 2015). However, continued climate warming could unlock and mobilize a significant portion of the organic carbon currently stored in glacial ice (5.9 Pg-C) (Hood et al., 2015). Although glacial DOC is generally old, it is highly labile (Hood et al., 2009), which suggests the majority of glacier-derived DOC would be rapidly remineralized post-melt. However, more research is needed to estimate this potential loss of terrestrial DOC. In addition, it is unlikely that most riverine DOC would reach the open ocean due to efficient removal in estuaries and on the shelf (Fichot and Benner, 2014; Kaiser et al., 2017; Sharples et al., 2017).

Submarine groundwater flows from land to sea by gravity and is comprised of both a terrestrial component (meteoric groundwater) and a seawater component that circulates through the coastal aquifer through wave and tidal pumping (Burnett et al., 2003). Terrestrial DOM, which is transported directly by groundwater from inland watersheds, has global average DOC concentrations of 2.7 mg-C L^{-1} (McDonough et al., 2020). Thus, assuming fresh groundwater discharge equates to 0.3–10% of surface runoff, then terrestrial groundwater DOC inputs would account for 0.1–90 Tg-C yr^{-1} (Burnett et al., 2003; McDonough et al., 2020). However, coastal peatlands and marsh areas have been shown to spike local groundwater and recirculating seawater with DOC to increase concentrations up to 20-fold higher than the global average (Goñi and Gardner, 2003; Seidel et al., 2014). Therefore, subterranean inputs of terrestrial DOM may be much larger than currently assumed.

Coastal Fringe

Coastal fringe ecosystems are among the highest in productivity on Earth and include mangroves, salt marshes, and seagrass beds (Jennerjahn and Ittekkot, 2002). Intertidal sediments that house these highly productive coastal plant communities and their detritus are permanently flooded, which contributes to consistently high DOC yields. Combined, coastal fringe ecosystems are thought to export an estimated 0.1–1.9 Pg-C per year as DOC (Duarte, 2017). Since coastal fringe-derived DOC has been suggested to subsidize respiration in the open ocean (Barrón and Duarte, 2015), much of the DOC exported by these ecosystems may be rapidly remineralized by microbes. However, it is reported that as much as one third of the total DOC flux derived from coastal fringe ecosystems survives degradation and is eventually mobilized to the interior ocean (Krause-Jensen and Duarte, 2016). Further offshore, terrestrial and marine organic matter that is temporarily stored in coastal and continental margin sediments is laterally transported to deliver an additional 0.12–0.23 Pg-C yr^{-1} as DOC to open oceanic surface waters (Burdige et al., 1999; Burdige and Komada, 2015).

Photodegradation

The photomineralization of DOC in sunlit surface waters is an important, yet poorly understood, mechanism for the degradation of oceanic organic matter. Estimates currently suggest 0.7–2.7 Tg-C DOC is lost annually via photomineralization (Mopper and Kieber, 2002; Stubbins et al., 2006). The photomineralization of DOC depends upon several factors, including DOM composition, prior irradiation history, irradiation conditions, and the model used to fit the photobleaching kinetics (Mopper et al., 2014). DOM compounds exist along a continuum of varying photolability (Stubbins et al., 2010). For example, sulfur-containing compounds from sulfidic sediments are more photosensitive than bulk DOC (Gomez-Saez et al., 2017). Aromatic, refractory DOM is comprised of organic compounds that are most susceptible to photodegradation and have an estimated removal rate of up to 0.5 Tg-C yr^{-1} (Anderson and Williams, 1999; Stubbins et al., 2012). Partially

degraded DOM compounds may be more bioavailable than organic molecules shielded from sunlight, thus coupled photo- and bio- degradation can remineralize more refractory DOC than photodegradation alone (Fichot and Benner, 2014; Shen and Benner, 2018). Degradation of recalcitrant DOC is likely also controlled by physical ocean circulation, specifically the rate at which deep water upwelling returns deep ocean DOC to the photic zone.

Interior Ocean

Net Losses

Of all the DOC that enters or is produced within surface waters each year, only 1.9 Pg-C yr^{-1} is exported to mesopelagic depths and a mere 0.18 Pg-C yr^{-1} survives long enough to reach the ocean's interior (Carlson and Hansell, 2015). The exponential decrease in DOC export from the surface to deep ocean indicates the majority of exported DOC (∼99%) is respired in the water column, is incorporated into microbial biomass, or forms aggregates to sink and ultimately become stored in sediments as particulate organic carbon (POC). Respiration is the primary mode of DOC removal in surface waters, yet the complex cascade of processes that encompass a variety of biotic and abiotic mechanisms that control the formation of the recalcitrant DOM pool remains poorly understood. Upon entering the ocean's interior, there is a net loss of refractory DOC (50 Tg-C yr^{-1}), which cycles on millennial timescales (Hansell et al., 2009). The removal of refractory DOC from the deep ocean is ascribed to heterotrophic remineralization and/or sorption onto sinking particles, however, the relative contributions of these biogeochemical processes are largely unknown (Hansell et al., 2009).

Sorption and Dissolution

Organic matter-mineral interactions can lead to the ballasting and/or removal of DOC throughout the water column (Keil et al., 1994, 1997; Blattmann et al., 2018). The export of sediment from land to the ocean releases terrestrial organic matter, including labile compounds (Keil et al., 1994; Blattmann et al., 2018). The surfaces of terrestrial minerals are then repopulated with marine organic matter (Keil et al., 1997; Kennedy et al., 2002; Blattmann et al., 2018), an exchange process that depends upon sediment mineralogy (Blattmann et al., 2019). Since the degree of sorption is a function of surface area and DOC concentration (Henrichs, 1995; Kennedy et al., 2002), the removal of DOC from the water column likely scales with its concentration as well as availability of reactive sorption sites for organic compounds that persist in the interior ocean. While the loss and replacement of terrestrial and marine organic matter from mineral surfaces might pose no net sink or source of DOC, it may alter the composition and lability of the oceanic DOC pool. However, the abiotic exchange of organic matter between the operational POM and DOM fractions is a process that is not well understood (Carlson, 2002) and is in need of further research.

The imbalance of POM fluxes from the surface to depth and from depth to the seafloor (7.3 Pg-C yr^{-1}) points to a likely source of DOC within the oceanic water column (Carlson and Hansell, 2015). POM loss processes are not well understood, but it is estimated that half is remineralized (3.6 Pg-C yr^{-1}) and half is taken up by heterotrophic bacteria (3.6 Pg-C yr^{-1}) (Carlson and Hansell, 2015). Sinking particles are enriched in organic and inorganic nutrients, thus representing energy hotspots in the open ocean. Microbes colonize the sinking particles and break down the POM into soluble components, releasing a trail of DOM that serves as a substrate to free floating microbes (Cho and Azam, 1988; Kiørboe, 2011). A small portion of this POM-derived DOC accumulates in the surface ocean at an estimated rate of 0.1 Pg-C yr^{-1} (Hansell, 2013; Carlson and Hansell, 2015). As particle flux decreases with depth, it is therefore unlikely that the flux of POM-derived DOC to the interior ocean is substantial. However, the dissolution of POM accumulated in ocean sediments contributes 0.1 Pg-C yr^{-1} (Dunne et al., 2007; Burdige and Komada, 2015), representing an important carbon and nutrient source to benthic microorganisms (Jones et al., 2014). A fraction of this sediment-derived DOC may also escape degradation and diffuse into deep waters overlying the seafloor, consistent with higher DOC concentrations observed in sediment porewaters compared to bottom waters (Burdige et al., 1992; Schmidt et al., 2011; Rossel et al., 2016). Consequently, sediment-derived DOC may subsidize benthic microbial communities and thus be an important source of the recalcitrant carbon observed in bottom waters (Burdige and Komada, 2015).

Seeps and Vents

Located along continental margins, hydrocarbon seeps represent an external source of DOC to the deep ocean. Current flux estimates (0.2–20 Tg-C yr^{-1}) are based only upon data collected from known mud volcano seeps (Pohlman et al., 2010). These values likely underrepresent true DOC fluxes since current estimates omit inputs from other seep types, including seeps that have not yet been discovered. Depending upon the study, seep-derived DOC has been shown to either not accumulate or comprise up to 30% of DOC in the overlying water (Wang et al., 2001; Walker et al., 2017). Investigations that took place after the *Deepwater Horizon* oil spill (Gulf of Mexico) suggest microbial transformations of seep-derived hydrocarbons may result in the production of refractory DOC years after their release (Bianchi et al., 2014; Walker et al., 2017), thus contributing unknown quantities to the ^{14}C-depleted DOC pool that resides in the deep ocean. Overall, hydrocarbon seeps likely represent a minor contribution to DOC in the ocean interior.

Concentrations of DOC in hydrothermal systems vary by an order of magnitude and are generally higher at low temperature diffusive systems compared to high temperature vents (Lang et al., 2006, 2010; Yamanaka et al., 2013; Hawkes et al., 2015). Hydrothermal circulation that exposes fluids to high temperatures (>400°C; Fontaine et al., 2009) is generally considered a sink of deep ocean DOC (Lang et al., 2006; Lin et al., 2012; Hawkes et al., 2015; Rossel et al., 2017), but these fluxes may be somewhat offset by cooler diffuse vent systems which are suggested to be a minor source of deep ocean DOC (Lang et al., 2006). Based upon data collected from DOC isolated by solid phase extraction, which is presumed to represent the less biologically labile fraction of marine DOC, high temperature

fluids remove an estimated 0.02 Tg-C of refractory DOC per year (Hawkes et al., 2015). However, this flux estimate only considers the extractable portion of DOC, which becomes smaller with increased temperature (Hawkes et al., 2015, 2016) and largely excludes low molecular weight compounds (Klevenz et al., 2010; Lang et al., 2010; Fuchida et al., 2014; Reeves et al., 2014; McDermott et al., 2015; Longnecker et al., 2018). Hydrothermal vent-derived DOC may be a source of carbon for the deep ocean microbial communities (Winkel et al., 2014; Rossel et al., 2015), but fluxes have not yet been determined.

DOM RECALCITRANCE IS AN EMERGENT PROPERTY

Dissolved organic matter is a heterogeneous pool of thousands, likely millions, of organic compounds. These compounds differ not only in composition and concentration (from pM to μM), but also originate from various organisms (phytoplankton, zooplankton, and bacteria) and environments (terrestrial vegetation and soils, coastal fringe ecosystems) and may have been produced recently or thousands of years ago. Moreover, even organic compounds deriving from the same source and of the same age may have been subjected to different processing histories prior to accumulating within the same pool of DOM.

Interior ocean DOM is a highly modified fraction that remains after years of exposure to sunlight, utilization by heterotrophs, flocculation and coagulation, and interaction with particles. Many of these processes within the DOM pool are compound- or class-specific. For example, condensed aromatic compounds are highly photosensitive (Stubbins et al., 2012), whereas proteins, carbohydrates, and their monomers are readily taken up by bacteria (Hodson et al., 1981; Hollibaugh and Azam, 1983; Ferguson and Sunda, 1984). Microbes and other consumers are selective in the type of DOM they utilize and typically prefer certain organic compounds over others. Consequently, DOM becomes less reactive as it is continually reworked. Said another way, the DOM pool becomes less labile and more refractory with degradation. As it is reworked, organic compounds are continually being added to the bulk DOM pool by physical mixing, exchange with particles, and/or production of organic molecules by the consumer community (Ogawa et al., 2001; Kaiser and Benner, 2008; Jiao et al., 2010; Shen and Benner, 2018). As such, the compositional changes that occur during degradation are more complex than the simple removal of more labile components and resultant accumulation of remaining, less labile compounds. The combined effect of the physicochemical and biological reworking of individual molecules on the overall molecular diversity and apparent recalcitrance of bulk interior ocean DOM is illustrated in **Figure 2**.

Dissolved organic matter recalcitrance (i.e., its overall reactivity toward degradation and/or utilization) is therefore an emergent property. Thus, the perception of DOM recalcitrance changes during organic matter degradation and in conjunction with any other process that removes or adds organic compounds to the DOM pool under consideration. While it is possible

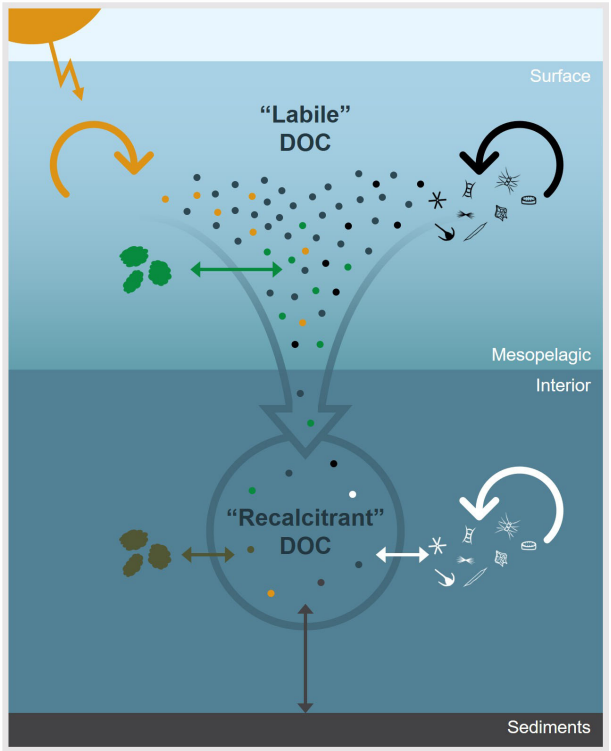

FIGURE 2 | A conceptual diagram of some of the major environmental processes which control the apparent recalcitrance of oceanic DOC. The dots represent DOC molecules and arrows represent physicochemical and biological processes that impact DOC concentration and molecular composition. In the surface ocean, DOC derived from primary production is rapidly remineralized or transformed through microbial degradation (black arrow), photochemical degradation (yellow arrow), or particle exchange (green arrow). Labile components are removed down the water column and DOC becomes diluted by processes, such as particle exchange (brown arrow), sediment dissolution (gray arrow), and microbial reworking (white arrow), which continue to alter, add, and/or remove molecules from the bulk DOC pool. Thus, the apparent recalcitrance of DOC in the ocean's interior is an emergent property that is largely controlled by environmental context.

to experimentally quantify the lability of very reactive, non-recalcitrant material on short time scales (Hodson et al., 1981; Hollibaugh and Azam, 1983; Ferguson and Sunda, 1984), we must infer DOM reactivities from chemical proxies, such as molecular composition, size distribution, and/or radiocarbon ages, for longer experimental temporal domains (i.e., more than 1 year). For example, older (^{14}C-depleted) DOC is considered more refractory than young (^{14}C-enriched) DOC and components with higher molecular mass are more reactive than components with lower molecular mass (Amon and Benner, 1994, 1996; Benner and Amon, 2015; Walker et al., 2016).

The reactivity of DOM is not only dependent upon intrinsic chemical characteristics of the organic compounds, but also depends upon the consumer community composition (e.g., microbes versus metazoans) (de Goeij et al., 2013). The availability of nutrients and biolimiting elements also comes into play, potentially limiting or promoting primary production

and/or microbial consumption of DOM. Consumers must invest in structural or enzymatic machinery for harvesting certain compound classes. If target compound classes persist at very low concentration levels, the energetic gain from taking up these compounds may not be balanced by the cost of constructing the machinery required to utilize them. Consequently, even intrinsically labile DOM may not be readily degraded due to limited availability or access to such molecules (Jannasch, 1967; Arrieta et al., 2015). Thus, the apparent recalcitrance of DOM described by the dilution hypothesis is a property of the consumer or environmental context rather than the intrinsic chemical lability of substrate (Middelburg, 2015), yet provides a coherent explanation for the size and apparent age observed for the marine DOC pool (Mentges et al., 2019).

NEW ISOTOPIC APPROACHES FOR PROBING THE ORIGIN AND FATE OF OCEANIC DOC

The marine DOC pool is molecularly complex, where compounds produced contemporaneously from the same source may have different degradation pathways and compounds that appear to be molecularly identical (i.e., have the same molecular formula or bulk isotopic composition) may have diverse sources and biogeochemical histories. Thus, in addition to analytical challenges, the flow of carbon through different organic molecules is highly convoluted, preventing a clear view of biotic drivers that control the production of recalcitrant DOC and its accumulation in the interior ocean. Natural abundance radiocarbon (^{14}C) measurements are a powerful tool for assessing the age of oceanic DOC that cycles on centennial to millennial timescales (McNichol and Aluwihare, 2007), whereas stable carbon isotopic analyses (^{13}C) supply information on carbon origins, degradation pathways, and transfer through marine food webs. At the bulk scale, radiocarbon data suggests oceanic DOC ranges in age from ca. 4,000 to ca. 6,000 ^{14}C-years with older ages in the interior ocean, although spatiotemporal resolution of these measurements is relatively limited (Beaupre, 2015). The World Ocean Circulation Experiment (WOCE) initiated a systematic increase in the resolution of dissolved inorganic carbon (DIC) ^{14}C analyses, which has led to unprecedented insights into the dynamics of the marine carbon reservoir, particularly in the face of increasing atmospheric CO_2 concentrations (McNichol et al., 2000). Thus, more extensive ^{14}C analyses of DOC across our global oceans is needed to refine our understanding of DOC turnover and assess its role in modulating future climate scenarios. Bulk marine DOC is uniformly ^{13}C-enriched and generally consistent with a marine phytoplankton source (Beaupre, 2015). However, compound-specific ^{13}C analysis is an effective approach for discerning the source and fate of different DOM subcomponents, such as black carbon (Wagner et al., 2019). Similarly, ^{14}C measurements on different DOC molecular fractions has revealed that the apparent age and lability is not evenly distributed throughout the marine DOM pool (Follett et al., 2014; Close, 2019; Ishikawa et al., 2019). Thus, targeted isotopic analyses are needed to unveil drivers of DOM accumulation and apparent recalcitrance in the interior ocean.

The enzymatic activity of heterotrophic microbes strongly affects the transformation of labile DOC into semi-labile and refractory DOC, thus altering the reactivity of DOC and modulating carbon fluxes in the ocean (Azam et al., 1983; Azam and Malfatti, 2007; Benner and Herndl, 2011). However, microbial activity is limited by both the accessibility of labile DOC components and nutrient availability. It is debated whether the balance between microbial growth and associated remineralization processes controls DOC cycling and whether this balance enhances or weakens the efficiency of the biological carbon pump (Azam and Malfatti, 2007). Biological carbon turnover is typically tracked by feeding molecular substrates (short-chain fatty acids, sugars, and amino acids) that have been uniformly labeled with stable (^{13}C, ^{15}N) or radiogenic (^{14}C, ^{3}H) isotopes (Ducklow et al., 1986; Jørgensen et al., 1993; Boschker et al., 1998; Keil and Kirchman, 1999; Boschker and Middelburg, 2002; Herndl et al., 2005). Some studies have utilized more complex isotopically labeled substrates, such as bacteria- or algae-derived DOC (Bronk and Glibert, 1993; Veuger et al., 2004; Bronk et al., 2007). However, bulk DOC does not permit distinction between the different carbon pools and uniformly labeled substrates omit the understanding of the fate of single carbon atoms within a molecule that are being differently used during uptake, biosynthesis, molecular transformation, and final release of DIC. Therefore, to specifically trace the microbial conversion of DOC to cellular biomolecules and metabolites or microbial remineralization of DOC to CO_2, novel approaches based on position-specific and dual-isotope stable isotope probing (SIP), lipid radioisotope probing (RIP), and reversed isotope labeling (RIL) have been adapted from routine labeling techniques (**Figure 3**) (Wegener et al., 2012; Dippold and Kuzyakov, 2013; Kellermann et al., 2016; Dong et al., 2017, 2019; Evans et al., 2018, 2019; Aepfler et al., 2019).

Position-specific SIP, where only one carbon position within a particular substrate molecule is labeled with ^{13}C, has been applied extensively for revealing terrestrial carbon pathways (Kuzyakov and Galitsa, 1993; Fischer and Kuzyakov, 2010; Dijkstra et al., 2011; Dippold and Kuzyakov, 2013), but less so in the marine environment. Amino acids are one of the main substrates for heterotrophic bacteria and constitute a large fraction of their carbon demand (Jørgensen et al., 1993). Thus, the amino acids that occur as part of bulk DOC can be isotopically exploited to reveal key biosynthetic and metabolic pathways that link marine carbon and nitrogen cycles. Position-specific SIP has been used to reconstruct metabolic pathways of bacteria, identify substrate specificity of bacterial fatty acid biosynthesis, and quantify the release of metabolic products (e.g., short-chain fatty acids and DIC) (Aepfler et al., 2019). Dual-isotope lipid SIP, which combines D_2O with ^{13}C-labeled DIC, enables the direct quantitative tracking of both autotrophic carbon fixation and heterotrophic lipid production without having to provide an additional energy source in the form of excess carbon substrates (Wegener et al., 2016). This dual-isotopic approach has been utilized to investigate the metabolic activity of microbes in marine sediments, specifically for sulfate

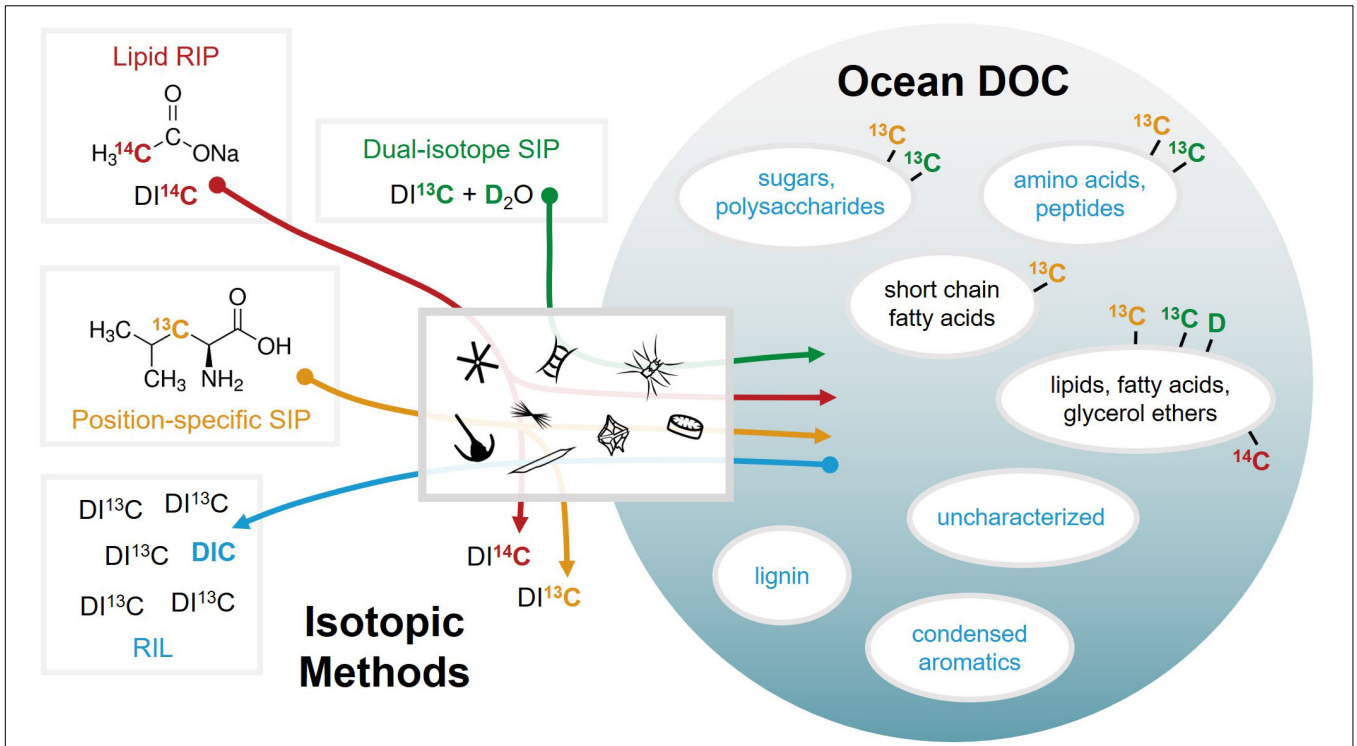

FIGURE 3 | Emerging stable (^{13}C) and radiocarbon (^{14}C) isotopic techniques used to probe metabolic pathways for the biosynthesis and microbial turnover of DOC by planktonic communities in the ocean. These methods include position-specific and dual-isotope stable isotope probing (SIP), lipid radioisotope probing (RIP), and reversed isotope labeling (RIL). The sphere is shaded according to the apparent recalcitrance of DOC compound classes.

reducing bacteria (Wegener et al., 2012), the anaerobic oxidation of methane (Kellermann et al., 2012), and lipid biosynthesis therein (Kellermann et al., 2016). Lipid radioisotope probing has been similarly applied to better understand lipid biosynthetic pathways in marine planktonic archaea (Evans et al., 2018). Natural DOM and environmental organic compounds that are not available in a stable isotope or radiolabeled form are accessible to turnover studies using RIL, in which a pool of ^{13}C-labeled DIC is continuously diluted during microbial degradation of a specific organic substrate or DOM at natural carbon isotope abundance (Dong et al., 2017, 2019). Thus, the change in the isotopic composition of DIC enables quantification of microbial remineralization by mass balance calculations.

DOM FUTURE PROJECTIONS

Concentrations of DOC in marine surface waters are closely linked to biogeochemical cycles and physical forcings. The oligotrophic subtropical gyres typically show higher concentrations (65–80 μM-C) of DOC than subpolar regions and the circumpolar Southern Ocean (40–50 μM-C) (Hansell, 2013). The accumulation and export of DOC in the subtropical gyres contributes to organic carbon flux from surface waters and supports the metabolic demand of heterotrophic microbes in the upper mesopelagic zone (Carlson et al., 2004). Ultimately, the production of DOC in the surface ocean is limited by the magnitude of primary production, which in turn depends on nutrient supply (Carlson and Hansell, 2015; Romera-Castillo et al., 2016). Within these constraints, an intimate feedback between climate systems, nutrient regimes, and community structure can modulate surface DOC inventories on seasonal and decadal time scales. A multiyear net increase of DOC inventories (~300 mmol-C m^2 yr^{-1}) has been reported within the North Pacific Subtropical Gyre, primarily driven by decadal climate variations, along with concurrent shifts in the plankton community and transition from nitrogen- to phosphorus-limitation (Church et al., 2002). The majority of DOC accumulating in the surface ocean is rapidly remineralized in the upper mesopelagic zone (Abell et al., 2000; Kaiser and Benner, 2012). Since a large portion of net primary production is routed through active microbial food webs, the production of recalcitrant DOC should scale proportionally with DOC production (Karl, 1999; Jiao et al., 2010). Heterotrophic microbes transform ~0.02% of primary production carbon into recalcitrant DOC (Benner and Herndl, 2011). Subtropical gyres cover ~60% of the total ocean area (Eppley and Peterson, 1979) and may be expanding in size (Polovina et al., 2008; Sharma et al., 2019). Therefore, small changes to DOC concentrations in these regions can significantly change the size of ocean DOC inventories and funnel a greater fraction to the interior ocean as refractory DOC. Given the multivariate approach required, it is unclear how current oceanic DOC inventories may be altered in response to continued climate change. Here, we

review predictions of how climate change will impact microbial and terrestrial DOC fluxes to the ocean and point out gaps in the current knowledge needed to refine our view of future oceanic DOM cycling.

Ocean Warming and Acidification

As a result of climate change, a concomitant rise in atmospheric temperatures and CO_2 levels have directly contributed to the warming and acidification of global oceans (Doney et al., 2009; Legendre et al., 2015). Controlled experiments have consistently demonstrated enhanced primary production and release of DOC in response to elevated ambient temperatures and CO_2 levels (Egge et al., 2009; Wohlers et al., 2009; Engel et al., 2011, 2013; Kim et al., 2011; Liu et al., 2017; Novak et al., 2018; Sugie et al., 2018). However, enhanced primary productivity may ultimately be balanced or exceeded by respiration rates in a warmer, more acidic ocean (Pomeroy and Wiebe, 2001; Vaquer-Sunyer et al., 2010). Enhanced DOC production under high CO_2 conditions was often accompanied by increased activity of microbial consumers (Engel et al., 2013; Endres et al., 2014), thus counteracting DOC accumulation. Higher DOM degradation rates may be related to extracellular hydrolytic enzymes, which exhibit optimum activity rates under more acidic conditions (Piontek et al., 2010; Endres et al., 2013). However, recent findings suggest that DOC production and quality does not substantially change in the long-term, because either the local phytoplankton communities become nutrient-depleted or the newly produced organic matter is utilized by fast-adapting heterotrophic microbial communities (Zark et al., 2015, 2017; Aparicio et al., 2016; Moran et al., 2016; Kim et al., 2018; Viviani et al., 2018). Regardless of the future balance between production and respiration, modeling of oceanic DOC decay rates suggests that a uniform 1°C warming of the ocean would decrease the global DOC reservoir by ∼7 Pg-C (Lønborg et al., 2018). Given higher activation energies for refractory DOC compared to labile DOC, increased temperatures would also disproportionately impact the degradation of recalcitrant DOC presumed to accumulate in the interior ocean.

Thermohaline circulation in the Atlantic and Pacific Oceans is predicted to decrease within the next century (McPhaden and Zhang, 2002; Stocker et al., 2013). Modeling efforts that seek to couple biogeochemical fluxes to ocean circulation patterns suggest that density stratification will be strengthened as a result of ocean warming (Capotondi et al., 2012). It is unknown whether these combined effects would significantly affect losses of DOM by abiotic processes, such as photodegradation or outgassing (Legendre et al., 2015). However, a reduction in the rate at which deep waters are returned to the surface ocean would significantly impact nutrient availability and primary production and could therefore alter the amount and/or quality of DOM that accumulates at shallower depths or is shunted to the interior ocean. Based upon satellite data, warmer surface ocean temperatures have been shown to diminish the supply of nutrients needed to carry out photosynthesis, and thus reduce oceanic biomass and primary productivity (Behrenfeld et al., 2006; Doney, 2006). These observations are in opposition with results from controlled experiments described previously, which generally show warming and acidification to enhance primary production. This discrepancy spotlights the interdisciplinary and multivariate approach needed to accurately predict DOC production and turnover in the surface ocean.

Oxygen Minimum Zone Expansion

The persistence of organic carbon in the ocean is effectively regulated by O_2 exposure time (Hartnett et al., 1998), which has been linked to the low density of metazoans (Jessen et al., 2017; Middelburg, 2018) and the oxidation reaction energetics of organic matter, which predict the persistence of complex, reduced organic molecules in anoxic settings (LaRowe and Van Cappellen, 2011). As oxygen minimum zones expand in the ocean due to decreased ventilation and increased temperature (Breitburg et al., 2018), the limited catabolic potential under such conditions could render specific molecular structures recalcitrant. Anoxia may have led to larger marine DOC reservoirs in the geological past, as tentatively suggested for the Precambrian and Eocene oceans (Rothman et al., 2003; Sexton et al., 2011; Ridgwell and Arndt, 2015). The deep waters of the Black Sea exhibit DOC concentrations that are 2.5-fold higher than DOC concentrations in the deep ocean (Ducklow et al., 2007; Margolin et al., 2016). It remains unclear whether the DOC accumulation is directly linked to terrestrial DOC inputs to this anoxic basin (Margolin et al., 2016) or is derived from a mixture of terrestrial, marine, and autochthonous DOC (Margolin et al., 2018). The East Japan Sea is a semi-enclosed marginal sea where DOC accumulation is attributed to decreased reactivity resulting from low bottom water temperatures (<1°C) (Kim et al., 2015). Therefore, although these two basins are imperfect modern analogs for future oxygen minimum zone expansion in the global ocean, the Black and East Japan Seas provide contrasting insights as to how the accumulation of marine DOC may increase under reduced O_2 conditions. At present, DOC concentrations in oxygen minimum zones of the Eastern Tropical North Pacific and Eastern Tropical South Pacific Oceans are similar to concentrations observed for the open ocean and are consistent with general water circulation patterns[1]. However, rapid utilization of semi-labile DOM has been observed for the upper oxycline in waters of the Eastern Tropical South Pacific (Loginova et al., 2019), suggesting a high degree of diagenetic DOM alteration at shallow oxygen minimum zone depths compared to the open ocean and to deeper oxic waters. This may be explained by the upwelling of altered DOM and/or extensive heterotrophic DOM utilization. Based upon these observations it is unclear how changing O_2 concentrations in the ocean would affect the size of DOC reservoirs and highlights a need for further research in this area.

Terrestrial Inputs

Riverine DOC fluxes will be closely tied to the effects of climate change within the watershed, particularly via enhanced warming and the increased frequency and severity of hydrological events. Climate change impacts will be enhanced in high latitude

[1] www.clivar.org

regions, where warming occurs at a rate twice that of the global average (Jeffries and Richter-Menge, 2012; Stocker et al., 2013). Glacial melt will not only increase freshwater runoff, but continued warming would also release the ∼6 Pg-C currently stored as DOC in glaciers globally (Hood et al., 2015). Most of the Earth's soil organic carbon is stored in the Arctic, including permafrost (1,300 Pg-C of POC plus DOC) (Hugelius et al., 2014). Increased temperatures will unlock organic matter preserved in these soils, resulting in enhanced DOC export via rivers draining Arctic landscapes (Freeman et al., 2001; de Wit et al., 2016; Wild et al., 2019). In regions where permafrost carbon is a major contributor, riverine DOC may be quickly remineralized to CO_2 before reaching the open ocean (Mann et al., 2015), potentially furthering climate change feedback. In areas of increased runoff, higher DOC concentrations paired with higher discharge will result in concomitantly higher DOC fluxes (Raymond et al., 2016). As such, decreased water residence times during hydrological events will quickly export sediment- and DOC-enriched river water to the coastal ocean. In conjunction with landscape alteration, hydrological events may also result in the enhanced mobilization of aged terrestrial carbon reservoirs (Marwick et al., 2015; Barnes et al., 2018).

The fate of terrestrial DOC also relies upon estuarine behavior and the resilience of coastal fringe ecosystems. These regions are among the highest in productivity on Earth and face increased pressure from anthropogenic and climatic forces (Erwin, 2009; Mitsch and Hernandez, 2013). With continued sea level rise, it is unknown how the migration and/or collapse of these coastal vegetation communities will impact the relative stability of organic matter stored in sediments (Kirwan et al., 2013; Sjøgaard et al., 2017; Ruiz-Fernández et al., 2018; Macreadie et al., 2019). Thus, the net flux of DOC from fringe ecosystems, particularly in tropical regions, is not well constrained. At high latitudes, long-term increases in DOC concentration in coastal surface waters have been observed (Worrall et al., 2004; Filella and Rodríguez-Murillo, 2014). However, when other factors, such as rainfall, land management, and salinity, are also considered, a net decrease in low latitude DOC concentrations is indicated (Regier et al., 2016). Large uncertainties associated with estimating the regional distribution and total land area for sea grasses, salt marshes, and mangrove forests is a major obstacle in constraining global DOC flux values for these coastal ecosystems (Duarte, 2017). These habitats face the fastest loss rates of any ecosystem (1–3% per year), largely as a result of anthropogenic impacts (Duarte, 2017). Therefore, spatial resolution of these ecosystems is critical for enhancing our current and future understanding of their role as an oceanic DOC source.

Anthropogenic Inputs

Poor spatiotemporal resolution of atmospherically deposited organic carbon prevents accurate global ocean flux estimates and highlights a critical area for future research. However, perhaps even more importantly, atmospheric deposition is also a major source of nutrients, such as nitrogen and phosphorus. Ocean stratification driven by a warming climate is expected to further enhance the relative impacts of atmospheric inputs (Kanakidou et al., 2012). Roughly half of all deposited organic nitrogen is derived from human activities (Kanakidou et al., 2012) and primary production has been shown to correlate with anthropogenic aerosol deposition globally (Wang et al., 2015). Paired with riverine export, the deposition of industrial aerosols in northwestern Pacific Ocean has converted surface waters from being nitrogen-limited to phosphorus-limited (Kim et al., 2011). The interplay of atmospheric deposition, ocean warming, and stratification is complex. However, net gains in primary production with continued industrialization and climate change would probably be significant (St-Laurent et al., 2017) and may enhance local DOC export.

Although wildfires are naturally occurring and have punctuated Earth's history since the emergence of land plants (Scott and Glasspool, 2006), anthropogenic climate change, land use change, and fire suppression practices are enhancing the frequency and severity of vegetation fires (Flannigan et al., 2009; Krawchuk et al., 2009). Although the production of refractory charcoal during wildfires may help mitigate the release of CO_2 globally during burn events (Jones et al., 2019), a considerable portion of the charred organic matter is carried by wind to coastal and offshore surface waters (Jurado et al., 2008). Studies investigating the composition of deposited pyrogenic aerosols are limited but appear to be enriched in nitrogen (Bauters et al., 2018), which may fuel primary production or alter local microbial communities. Despite increased occurrence of wildfire in coastal areas, little is known regarding the short- and long-term impacts and fluxes of deposited ash and smoke in oceanic surface waters.

Increased riverine nutrient concentrations resulting from agricultural development and urbanization contribute to coastal eutrophication and hypoxia (Rabalais et al., 2009; Gilbert et al., 2010). Increased primary productivity paired with O_2 depletion in coastal waters may result in favorable conditions for the accumulation of excess organic matter in sediments. However, predicted increases in the frequency and severity of storm events (e.g., hurricanes), which oxygenate surface waters via mixing and freshwater inputs, could temporarily offset sedimentary organic matter storage. Given that coastal sediments are an intermediate reservoir for organic matter, lateral transport of accumulated carbon to the open ocean could increase as a result of nutrient inputs, but research is needed to confirm this. Finally, the input of microplastics to the ocean is estimated to be 1–4 Tg-C yr^{-1} (Jambeck et al., 2015). Exposure to sunlight can degrade microplastics, which undergo photodissolution to produce DOC, although photochemical conversion rates are very low (Zhu et al., 2020). Thus, contributions of plastic-derived DOM to the total oceanic DOC pool are likely negligible.

CONCLUSION

The total DOC flux from external sources is similar to the export of DOC to the mesopelagic and an order of magnitude greater than the export of DOC to the interior ocean. Therefore, even small variations in the amount or composition of external

DOC exported to the ocean could ultimately impact the sum of DOC transferred from the surface to the interior ocean each year. However, at present, the slight imbalance between primary production and respiration in surface waters is the driver of recalcitrant DOC accumulation. Therefore, constraining oceanic DOC fluxes through the microbial food web relies upon both a comprehensive understanding of metabolic pathways and the spatiotemporally refined mapping of plankton and bacterial communities. Broad application of novel stable and radiocarbon isotopic techniques will pave the way for a coherent understanding of marine organic carbon cycling by revealing predominant biosynthetic and degradation pathways that control DOM production and turnover. Isotopic analyses, particularly compound-specific measurements, can be expensive and require large sample sizes in order to obtain robust isotopic signatures. An increased demand for DOC stable and radiocarbon isotopic measurements would continue to fuel ongoing analytical innovations that allow for lower analysis cost and sample size requirements. As we continue to accumulate isotopic measurements, these data should also be paired with less expensive, high throughput analyses (e.g., fluorescence spectroscopy) to allow for the extrapolation of stable and radiocarbon signatures more broadly throughout the global ocean. At present, the limited resolution of surface water plankton and bacterial populations, which vary significantly with latitude and coastal proximity (Fuhrman et al., 2008; Zinger et al., 2011; Sunagawa et al., 2015; Arteaga et al., 2016), prevents a globally relevant view of DOC production. Therefore, research efforts should also focus upon the *in situ* variability and activity of marine microbial communities, particularly in surface waters. A fine-scale approach, both molecularly and spatiotemporally, is necessary to refine the current view of oceanic DOC cycling so that we may accurately gauge the response of this major carbon store to anthropogenic perturbations and global climate change.

AUTHOR CONTRIBUTIONS

SW, FS, KK, CH, HW, PR, RH, ME, JM, AE, TB, TC, SL, GG-S, SP-G, RB, and VG participated in formative discussions as part of the DOM Working Group while attending the Marine Organic Biogeochemistry workshop held at the Hanse-Wissenschaftskolleg Institute for Advanced Study (Delmenhorst, Germany) in April 2019. SW, FS, KK, CH, HW, PR, RH, ME, JM, AE, TB, TC, SL, GG-S, SP-G, RB, and VG wrote and/or provided feedback on sections of the manuscript. SW compiled and organized co-author contributions and wrote the final version of the manuscript. All authors have read and approved the submitted version.

FUNDING

This work was funded by the Deutsche Forschungsgemeinschaft (DFG, German Research Foundation) project number 422798570. The Hanse-Wissenschaftskolleg and the Geochemical Society provided funding for the conference. Additional support was provided by the National Science Foundation OCE #1756812 to SW. TB acknowledges funding from ETH Zürich and JAMSTEC. JM was supported by the Netherlands Earth System Science Centre. SP-G was funded by COPAS Sur-Austral (CONICYT PIA APOYO CCTE AFB170006). GG-S acknowledges funding from DFG, DI 842/6-1.

ACKNOWLEDGMENTS

The authors thank C. Arnosti, T. Dittmar, K.-U. Hinrichs, C. Lee, and S. Wakeham for organizing the Marine Organic Biogeochemistry workshop and leading thought-provoking discussions that resulted in the writing of this manuscript.

REFERENCES

Abell, J., Emerson, S., and Renaud, P. (2000). Distributions of TOP, TON and TOC in the North Pacific subtropical gyre: implications for nutrient supply in the surface ocean and remineralization in the upper thermocline. *J. Mar. Res.* 58, 203–222. doi: 10.1357/002224000321511142

Aepfler, R., Bühring, S. I., and Elvert, M. (2019). Substrate characteristic bacterial fatty acid production based on amino acid assimilation and transformation in marine sediments. *FEMS Microbiol. Ecol.* 95:fiz13. doi: 10.1093/femsec/fiz131

Aluwihare, L. I., Repeta, D. J., and Chen, R. F. (1997). A major biopolymeric component of dissolved organic carbon in surface seawater. *Nature* 387, 166–169. doi: 10.1038/387166a0

Amon, R. M. W., and Benner, R. (1994). Rapid cycling of high molecular weight dissolved organic matter in the ocean. *Nature* 369, 549–552. doi: 10.1038/369549a0

Amon, R. M. W., and Benner, R. (1996). Bacterial utilization of different size classes of dissolved organic matter. *Limnol. Oceanogr.* 41, 41–51. doi: 10.4319/lo.1996.41.1.0041

Anderson, T. R., and Williams, P. J. (1999). A one-dimensional model of dissolved organic carbon cycling in the water column incorporating combined biological-photochemical decomposition. *Glob. Biogeochem. Cycles* 13, 337–349. doi: 10.1029/1999gb900013

Andreae, M. O., and Rosenfeld, D. (2008). Aerosol-cloud-precipitation interactions. Part 1. The nature and sources of cloud-active aerosols. *Earth Sci. Rev.* 89, 13–41. doi: 10.1016/j.earscirev.2008.03.001

Aparicio, F. L., Nieto-Cid, M., Borrull, E., Calvo, E., Pelejero, C., Sala, M. M., et al. (2016). Eutrophication and acidification: Do they induce changes in the dissolved organic matter dynamics in the coastal Mediterranean Sea? *Sci. Total Environ.* 56, 179–189. doi: 10.1016/j.scitotenv.2016.04.108

Arnosti, C. (2004). Speed bumps and barricades in the carbon cycle: substrate structural effects on carbon cycling. *Mar. Chem.* 92, 263–273. doi: 10.1016/j.marchem.2004.06.030

Arrieta, J. M., Mayol, E., Hansman, R. L., Herndl, G. J., Dittmar, T., and Duarte, C. M. (2015). Dilution limits dissolved organic carbon utilization in the deep ocean. *Science* 348, 331–333. doi: 10.1126/science.1258955

Arteaga, L., Pahlow, M., and Oschlies, A. (2016). Modeled Chl:C ratio and derived estimates of phytoplankton carbon biomass and its contribution to total particulate organic carbon in the global surface ocean. *Glob. Biogeochem. Cycles* 30, 1791–1810. doi: 10.1002/2016GB005458

Azam, F., Fenchel, T., Field, J. G., Gray, J. S., Meyer-Reil, L. A., and Thingstad, F. (1983). The ecological role of water-column microbes in the sea. *Mar. Ecol. Prog. Ser.* 10, 257–263. doi: 10.3354/meps010257

Azam, F., and Malfatti, F. (2007). Microbial structuring of marine ecosystems. *Nat. Rev. Microbiol.* 5, 782–791. doi: 10.1038/nrmicro1747

Bamber, J., van den Broeke, M., Ettema, J., Lenaerts, J., and Rignot, E. (2012). Recent large increases in freshwater fluxes from Greenland into the North Atlantic. *Geophys. Res. Lett.* 39:L19501.

Barnes, R. T., Butman, D. E., Wilson, H. F., and Raymone, P. A. (2018). Riverine export of aged carbon driven by flow path depth and residence time. *Environ. Sci. Technol.* 52, 1028–1035. doi: 10.1021/acs.est.7b04717

Barrón, C., and Duarte, C. M. (2015). Dissolved organic carbon pools and export from the coastal ocean. *Glob. Biogeochem. Cycles* 29, 1725–1738. doi: 10.1002/2014GB005056

Bauer, J. E., Druffel, E. R. M., Williams, P. M., Wolgast, D. M., and Griffin, S. (1998). Temporal variability in dissolved organic carbon and radiocarbon in the eastern North Pacific Ocean. *J. Geophys. Res. Oceans* 103, 2867–2881. doi: 10.1029/97JC02545

Bauters, M., Drake, T. W., Verbeeck, H., Bodé, S., Hervé-Fernández, P., Zito, P., et al. (2018). High fire-derived nitrogen deposition on central African forests. *Proc. Nat. Acad. Sci. U.S.A.* 115, 549–554. doi: 10.1073/pnas.1714597115

Beaupre, S. R. (2015). "The carbon and isotopic composition of marine DOC," in *Biogeochemistry of Marine Dissolved Organic Matter*, 2nd Edn, eds D. A. Hansell and C. A. Carlson (Amsterdam: Elsevier Inc), 335–364.

Beaupre, S. R., Kieber, D. J., Keene, W. C., Long, M. S., Maben, J. R., Lu, X., et al. (2019). Oceanic efflux of ancient marine dissolved organic carbon in primary marine aerosol. *Sci. Adv.* 5:eaax6535. doi: 10.1126/sciadv.aax6535

Behrenfeld, M. J., O'Malley, R. T., Siegel, D. A., McClain, C. R., Sarmiento, J. L., Feldman, G. C., et al. (2006). Climate-driven trends in contemporary ocean productivity. *Nat. Lett.* 444, 752–755. doi: 10.1038/nature05317

Benner, R., and Amon, R. M. W. (2015). The size-reactivity continuum of major bioelements in the ocean. *Annu. Rev. Mar. Sci.* 7, 185–205. doi: 10.1146/annurev-marine-010213-135126

Benner, R., and Herndl, G. J. (2011). "Bacterially derived dissolved organic matter in the microbial carbon pump," in *Microbial Carbon Pump in the Ocean*, eds N. Jiao, F. Azam, and S. Sanders (Washington, DC: Science/AAAS), 46–48.

Bianchi, T. S., Osburn, C., Shields, M. R., Yvon-Lewis, S., Young, J., Guo, L., et al. (2014). Deepwater Horizon oil in Gulf of Mexico waters after 2 years: transformation into the dissolved organic matter pool. *Environ. Sci. Technol.* 48, 9288–9297. doi: 10.1021/es501547b

Bjornsen, P. K. (1988). Phytoplankton exudation of organic matter: Why do healthy cells do it? *Limnol. Oceanogr.* 33, 151–154. doi: 10.4319/lo.1988.33.1.0151

Blattmann, T. M., Liu, Z., Zhang, Y., Zhao, Y., Haghipour, N., Montluçon, D. B., et al. (2019). Mineralogical control on the fate of continentally derived organic matter in the ocean. *Science* 366, 742–745. doi: 10.1126/science.aax5345

Blattmann, T. M., Zhang, Y., Zhao, Y., Wen, K., Lin, S., Li, J., et al. (2018). Contrasting fates of petrogenic and biospheric carbon in the South China Sea. *Geophys. Res. Lett.* 45, 9077–9086. doi: 10.1029/2018gl079222

Boschker, H. T. S., and Middelburg, J. J. (2002). Stable isotopes and biomarkers in microbial ecology. *FEMS Microbiol. Ecol.* 40, 85–95. doi: 10.1111/j.1574-6941.2002.tb00940.x

Boschker, H. T. S., Nold, S. C., Wellsbury, P., Bos, D., de Graaf, W., Pel, R., et al. (1998). Direct linking of microbial populations to specific biogeochemical processes by 13C-labeling of biomarkers. *Nature* 392, 801–805. doi: 10.1038/33900

Breitburg, D., Levin, L. A., Oschlies, A., Grégoire, M., Chavez, F. P., Conley, D. J., et al. (2018). Declining oxygen in the global ocean and coastal waters. *Science* 359:eaam7240. doi: 10.1126/science.aam7240

Broek, T. A. B., Bour, A. L., Ianiri, H. L., Guilderson, T. P., and McCarthy, M. D. (2019). Amino acid enantiomers in old and young dissolved organic matter: implications for a microbial nitrogen pump. *Geochim. Cosmochim. Acta* 247, 207–219. doi: 10.1016/j.gca.2018.12.037

Bronk, D. A., and Glibert, P. M. (1993). Application of a 15N tracer method to the study of dissolved organic nitrogen uptake during spring and summer in Chesapeake Bay. *Mar. Biol.* 115, 501–508. doi: 10.1007/bf00349849

Bronk, D. A., See, J. H., Bradley, P., and Killberg, L. (2007). DON as a source of bioavailable nitrogen for phytoplankton. *Biogeosciences* 4, 283–296. doi: 10.1016/j.scitotenv.2020.137837

Brophy, J. E., and Carlson, D. J. (1989). Production of biologically refractory dissolved organic carbon by natural seawater microbial populations. *Deep Sea Res. I* 36, 497–507. doi: 10.1016/0198-0149(89)90002-2

Burdige, D. J., Alperin, M. J., Homstead, J., and Martens, C. S. (1992). The role of benthic fluxes of dissolved organic carbon in oceanic and sedimentary carbon cycling. *Geophys. Res. Lett.* 19, 1851–1854. doi: 10.1029/92GL02159

Burdige, D. J., Berelson, W. M., Coale, K. H., McManus, J., and Johnson, K. S. (1999). Fluxes of dissolved organic carbon from California continental margin sediments. *Geochim. Cosmochim. Acta* 63, 1507–1515. doi: 10.1016/S0016-7037(99)00066-6

Burdige, D. J., and Komada, T. (2015). "Sediment pore waters," in *Biogeochemistry of Marine Dissolved Organic Matter*, 2nd Edn, eds D. A. Hansell and C. A. Carlson (Amsterdam: Elsevier Inc), 535–577. doi: 10.1016/b978-0-12-405940-5.00012-1

Burnett, W. C., Bokuniewicz, H., Huettel, M., Moore, W. S., and Taniguchi, M. (2003). Groundwater and pore water inputs into the coastal zone. *Biogeochemistry* 66, 3–33. doi: 10.1023/b:biog.0000006066.21240.53

Capotondi, A., Alexander, M. A., Bond, N. A., Curchitser, E. N., and Scott, J. (2012). Enhanced upper-ocean stratification with climate change in the CMIP3 models. *J. Geophys. Res.* 117:C04031. doi: 10.1029/2011JC007409

Carlson, C. A. (2002). "Production and removal processes," in *Biogeochemistry of Marine Dissolved Organic Matter*, eds D. A. Hansell and C. A. Carlson (San Diego, CA: Academic Press), 91–151. doi: 10.1016/b978-012323841-2/50006-3

Carlson, C. A., Giovannoni, S. J., Hansell, D. A., Goldberg, S. J., Parsons, R., and Vergin, K. (2004). Interactions among dissolved organic carbon, microbial processes, and community structure in the mesopelagic zone of the northwestern Sargasso Sea. *Limnol. Oceanogr.* 49, 1073–1083. doi: 10.4319/lo.2004.49.4.1073

Carlson, C. A., and Hansell, C. A. (2015). "DOM sources, sinks, reactivity, and budgets," in *Biogeochemistry of Marine Dissolved Organic Matter*, 2nd Edn, eds D. A. Hansell and C. A. Carlson (Amsterdam: Elsevier Inc), 65–126. doi: 10.1016/b978-0-12-405940-5.00003-0

Carlson, C. A., Hansell, D. A., Nelson, N. B., Siegel, D. A., Smethie, W. M., Khatiwala, S., et al. (2010). Dissolved organic carbon export and subsequent remineralization in the mesopelagic and bathypelagic realms of the North Atlantic basin. *Deep Sea Res. II* 57, 1433–1445. doi: 10.1016/j.dsr2.2010.02.013

Cho, B. C., and Azam, F. (1988). Major role of bacteria in biogeochemical fluxes in the ocean's interior. *Nature* 332, 441–443. doi: 10.1038/332441a0

Church, M. J., Ducklow, H. W., and Karl, D. M. (2002). Multi-year increases in dissolved organic matter inventories at station ALOHA in the North Pacific Subtropical Gyre. *Limnol. Oceanogr.* 47, 1–10. doi: 10.4319/lo.2002.47.1.0001

Close, H. G. (2019). Compound-specific isotope geochemistry in the ocean. *Annu. Rev. Mar. Sci.* 11, 27–56. doi: 10.1146/annurev-marine-121916-063634

Copping, A. E., and Lorenzen, C. J. (1980). Carbon budget of marine phytoplankton-herbivore system with carbon-14 as tracer. *Limnol. Oceanogr.* 25, 873–882. doi: 10.4319/lo.1980.25.5.0873

de Goeij, J. M., van Oevelen, D., Vermeij, M. J. A., Osinga, R., Middelburg, J. J., de Goeij, A. F. M. P., et al. (2013). Surviving in a marine desert: The sponge loop retains resources within coral reefs. *Science* 342, 108–110. doi: 10.1126/science.1241981

de Wit, H. A., Valinia, S., Weyhenmeyer, G. A., Futter, M. N., Kortelainen, P., Austnes, K., et al. (2016). Current browning of surface waters will be further promoted by wetter climate. *Environ. Sci. Technol.* 3, 430–435. doi: 10.1021/acs.estlett.6b00396

Dijkstra, P., Dalder, J. J., Selmants, P. C., Hart, S. C., Koch, G. W., Schwartz, E., et al. (2011). Modeling soil metabolic processes using isotopologue pairs of position-specific 13C-labeled glucose and pyruvate. *Soil Biol. Biochem.* 43, 1848–1857. doi: 10.1016/j.soilbio.2011.05.001

Dippold, M. A., and Kuzyakov, Y. (2013). Biogeochemical transformations of amino acids in soil assessed by position-specific labeling. *Plant Soil* 373, 385–401. doi: 10.1007/s11104-013-1764-3

Doney, S. C. (2006). Plankton in a warmer world. *Nature* 444, 695–696. doi: 10.1038/444695a

Doney, S. C., Fabry, V. J., Feely, R. A., and Kleypas, J. A. (2009). Ocean acidification: the other CO_2 problem. *Annu. Rev. Mar. Sci.* 1, 169–192.

Dong, X., Bäcker, L. E., Rahmatullah, M., Schunk, D., Lens, G., and Meckenstock, R. U. (2019). Quantification of microbial degradation activities in biological activated carbon filters by reverse stable isotope labelling. *AMB Express* 9:109. doi: 10.1186/s13568-019-0827-0

Dong, X., Jochmann, M. A., Elsner, M., Meyer, A. H., Backer, L. E., Rahmatullah, M., et al. (2017). Monitoring microbial mineralization using reverse stable isotope labeling analysis by mid-infrared laser spectroscopy. *Environ. Sci. Technol.* 51, 11876–11883. doi: 10.1021/acs.est.7b02909

Druffel, E. R. M., Williams, P. M., Bauer, J. E., and Ertel, J. R. (1992). Cycling of dissolved and particulate organic matter in the open ocean. *J. Geophys. Res.* 97, 15639–15659.

Duarte, C. M. (2017). Reviews and syntheses: hidden forests, the role of vegetated coastal habitats in the ocean carbon budget. *Biogeosciences* 14, 301–310. doi: 10.5194/bg-14-301-2017

Ducklow, H. W., Hansell, D. A., and Morgan, J. A. (2007). Dissolved organic carbon and nitrogen in the Western Black Sea. *Mar. Chem.* 105, 140–150. doi: 10.1016/j.marchem.2007.01.015

Ducklow, H. W., Purdie, D. A., Williams, P. J. L., and Davies, J. M. (1986). Bacterioplankton: a sink for carbon in a coastal marine plankton community. *Science* 232, 865–867. doi: 10.1126/science.232.4752.865

Dunne, J. P., Sarmiento, J. L., and Gnanadesikan, A. (2007). A synthesis of global particle export from the surface ocean and cycling through the ocean interior and on the seafloor. *Glob. Biogeochem. Cycles* 21:GB4006. doi: 10.1029/2006GB002907

Egge, J., Thingstad, T., Larsen, A., Engel, A., Wohlers, J., Bellerby, R. G. J., et al. (2009). Primary production during nutrient-induced blooms at elevated CO_2 concentrations. *Biogeosciences* 6, 877–885. doi: 10.5194/bg-6-877-2009

Endres, S., Galgani, L., Riebesell, U., Schulz, K. G., and Engel, A. (2014). Stimulated bacterial growth under elevated pCO_2: results from an off-shore mesocosm study. *PLoS One* 9:e99228. doi: 10.1371/journal.pone.0099228

Endres, S., Unger, J., Wannicke, N., Nausch, M., Voss, M., and Engel, A. (2013). Response of *Nodularia spumigena* to pCO_2 – Part 2: exudation and extracellular enzyme activities. *Biogeosciences* 10, 567–582. doi: 10.5194/bg-10-567-2013

Engel, A., Borchard, C., Piontek, J., Schulz, K. G., Riebesell, U., and Bellerby, R. (2013). CO_2 increases 14C-primary production in an Arctic plankton community. *Biogeosciences* 10, 1291–1308. doi: 10.5194/bg-10-1291-2013

Engel, A., Delille, B., Jacquet, S., Riebesell, U., Rochelle-Newall, E., Terbrüggen, A., et al. (2004). Transparent exopolymer particles and dissolved organic carbon production by Emiliania huxleyi exposed to different CO_2 concentrations: a mesocosm experiment. *Aquat. Microb. Ecol.* 34, 93–104. doi: 10.3354/ame034093

Engel, A., Goldthwait, S., Passow, U., and Alldredge, A. (2002). Temporal decoupling of carbon and nitrogen dynamics in a mesocosm diatom bloom. *Limnol. Oceanogr.* 47, 753–761. doi: 10.4319/lo.2002.47.3.0753

Engel, A., Händel, N., Wohlers, J., Lunau, M., Grossart, H. P., Sommer, U., et al. (2011). Effects of sea surface warming on the production and composition of dissolved organic matter during phytoplankton blooms: results from a mesocosm study. *J. Plankton Res.* 33, 357–372. doi: 10.1093/plankt/fbq122

Eppley, R. W., and Peterson, B. J. (1979). Particulate organic flux and planktonic new production in the deep ocean. *Nature* 282, 677–680. doi: 10.1038/282677a0

Erwin, K. L. (2009). Wetlands and global climate change: the role of wetland restoration in a changing world. *Wetl. Ecol. Manag.* 17:71. doi: 10.1007/s11273-008-9119-1

Evans, T., Coffinet, S., Könneke, M., Lipp, J. S., Becker, K. W., Elvert, M., et al. (2019). Assessing the carbon assimilation and production of benthic archaeal lipid biomarkers using lipid-RIP. *Geochim. Cosmochim. Acta* 265, 431–442. doi: 10.1016/j.gca.2019.08.030

Evans, T., Könneke, M., Lipp, J. S., Adhikari, R. R., Taubner, H., Elvert, M., et al. (2018). Lipid biosynthesis of *Nitrosopumilus maritimus* dissected by lipid specific radioisotope probing (lipid-RIP) under contrasting ammonium supply. *Geochim. Cosmochim. Acta* 242, 51–63. doi: 10.1016/j.gca.2018.09.001

Ferguson, R. L., and Sunda, W. G. (1984). Utilization of amino acids by planktonic marine bacteria: importance of clean technique and low substrate additions. *Limnol. Oceanogr.* 29, 258–274. doi: 10.4319/lo.1984.29.2.0258

Fichot, C. G., and Benner, R. (2014). The fate of terrigenous dissolved organic carbon in a river-influenced ocean margin. *Glob. Biogeochem. Cycles* 28, 300–318. doi: 10.1002/2013GB004670

Filella, M., and Rodríguez-Murillo, J. C. (2014). Long-term trends of organic carbon concentrations in freshwaters: strengths and weaknesses of existing evidence. *Water* 6, 1360–1418. doi: 10.3390/w6051360

Fischer, H., and Kuzyakov, Y. (2010). Sorption, microbial uptake and decomposition of acetate in soil: transformations revealed by position-specific 14C-labeling. *Soil Biol. Biochem.* 42, 186–192. doi: 10.1016/j.soilbio.2009.10.015

Flannigan, M. D., Krawchuk, M. A., de Groot, W. J., Wotton, B. M., and Gowman, L. M. (2009). Implications of changing climate for global wildland fire. *Int. J. Wildland Fire* 18, 483–507. doi: 10.1080/10962247.2015.1040526

Fogg, G. E. (1966). The extracellular products of algae. *Oceanogr. Mar. Biol. Annu. Rev.* 4, 195–212.

Follett, C. L., Repeta, D. J., Rothman, D. H., Xu, L., and Santinelli, C. (2014). Hidden cycle of dissolved organic carbon in the deep ocean. *Proc. Nat. Acad. Sci. U.S.A.* 111, 16706–16711. doi: 10.1073/pnas.1407445111

Fontaine, F. J., Wilcock, W. S. D., Foustoukos, D. E., and Butterfield, D. A. (2009). A Si-Cl geothermobarometer for the reaction zone of high-temperature, basaltic-hosted mid-ocean ridge hydrothermal systems. *Geochem. Geophys. Geosys.* 10:Q05009. doi: 10.1029/2009GC002407

Freeman, C., Evans, C. D., Monteith, D. T., Reynolds, B., and Fenner, N. (2001). Export of organic carbon from peat soils. *Nature* 412:785. doi: 10.1038/35090628

Fuchida, S., Mizuno, Y., Masuda, H., Toki, T., and Makita, H. (2014). Concentrations and distributions of amino acids in black and white smoker fluids at temperatures over 200°C. *Org. Geochem.* 66, 98–106. doi: 10.1016/j.orggeochem.2013.11.008

Fuhrman, J. A., Steele, J. A., Hewson, I., Schwalbach, M. S., Brown, M. V., Green, J. L., et al. (2008). A latitudinal diversity gradient in planktonic marine bacteria. *Proc. Nat. Acad. Sci. U.S.A.* 105, 7774–7778. doi: 10.1073/pnas.0803070105

Gilbert, D., Rabalais, N. N., Diaz, R. J., and Zhang, J. (2010). Evidence for greater oxygen decline rates in the coastal ocean than in the open ocean. *Biogeosciences* 7, 2283–2296. doi: 10.5194/bg-7-2283-2010

Gomez-Saez, G. V., Niggemann, J., Dittmar, T., Pohlabeln, A. M., Lang, S. Q., Noowong, A., et al. (2016). Molecular evidence for abiotic sulfurization of dissolved organic matter in marine shallow hydrothermal systems. *Geochim. Cosmochim. Acta* 190, 35–52. doi: 10.1016/j.gca.2016.06.027

Gomez-Saez, G. V., Pohlabeln, A., Stubbins, A., Marsay, C. M., and Dittmar, T. (2017). Photochemical alteration of dissolved organic sulfur from sulfidic porewater. *Environ. Sci. Technol.* 51, 14144–14154. doi: 10.1021/acs.est.7b03713

Goñi, M. A., and Gardner, L. R. (2003). Seasonal Dynamics in dissolved organic carbon concentrations in a coastal water-table aquifer at the forest-marsh interface. *Aquat. Geochem.* 9, 209–232. doi: 10.1023/b:aqua.0000022955.82700.ed

Gruber, D. F., Simjouw, J. P., Seitzinger, S. P., and Taghon, G. L. (2006). Dynamics and characterization of refractory dissolved organic matter produced by pure bacterial culture in an experimental predator-prey system. *Appl. Environ. Microbiol.* 72, 4184–4191. doi: 10.1128/aem.02882-05

Hansell, D. A. (2013). "Recalcitrant dissolved organic carbon fractions," in *Annual Review of Marine Science*, Vol. 5, eds C. A. Carlson and S. J. Giovannoni (Palo Alto, CA: Annual Reviews), 421–445. doi: 10.1146/annurev-marine-120710-100757

Hansell, D. A., Carlson, C. A., Repeta, D. J., and Schlitzer, R. (2009). Dissolved organic matter in the ocean: a controversy stimulates new insights. *Oceanography* 22, 202–211. doi: 10.5670/oceanog.2009.109

Hartnett, H. E., Keil, R. G., Hedges, J. I., and Devol, A. H. (1998). Influence of oxygen exposure time on organic carbon preservation in continental margin sediments. *Nature* 391, 572–574.

Hawkes, J. A., Hansen, C. T., Goldhammer, T., Bach, W., and Dittmar, T. (2016). Molecular alteration of marine dissolved organic matter under experimental hydrothermal conditions. *Geochim. Cosmochim. Acta* 175, 68–85. doi: 10.1016/j.gca.2015.11.025

Hawkes, J. A., Rossel, P. E., Stubbins, A., Butterfield, D., Connelly, D. P., Achterberg, E. P., et al. (2015). Efficient removal of recalcitrant deep-ocean dissolved organic matter during hydrothermal circulation. *Nat. Geosci.* 8, 856–860. doi: 10.1038/ngeo2543

Hedges, J. I., Keil, R. G., and Benner, R. (1997). What happens to terrestrial organic matter in the ocean? *Org. Geochem.* 27, 195–212. doi: 10.1016/s0146-6380(97)00066-1

Heikes, B. G., Chang, W., Pilson, M. E. Q., Swift, E., Singh, H. B., Guenther, A., et al. (2002). Atmospheric methanol budget and ocean implication. *Glob. Biogeochem.* 16:1133. doi: 10.1021/es302082p

Hemingway, J. D., Spencer, R. G. M., Podgorski, D. C., Zito, P., Sen, I. S., and Galy, V. (2019). Glacier meltwater and monsoon precipitation drive Upper Ganges Basin dissolved organic matter composition. *Geochim. Cosmochim. Acta* 244, 216–228. doi: 10.1016/j.gca.2018.10.012

Henrichs, S. M. (1995). Sedimentary organic matter preservation: an assessment and speculative synthesis - a comment. *Mar. Chem.* 49, 127–136. doi: 10.1016/0304-4203(95)00012-g

Herndl, G. J., Reinthaler, T., Teira, E., van Aken, H. M., Veth, C., Pernthaler, A., et al. (2005). Contribution of Archaea to total prokaryotic production in the deep Atlantic Ocean. *Appl. Environ. Microbiol.* 71, 2303–2309. doi: 10.1128/aem.71.5.2303-2309.2005

Hodson, R. E., Maccubbin, A. E., and Pomeroy, L. R. (1981). Dissolved adenosine triphosphate utilization by free-living and attached bacterioplankton. *Mar. Biol.* 64, 43–51. doi: 10.1007/bf00394079

Hollibaugh, J. T., and Azam, F. (1983). Microbial degradation of dissolved proteins in seawater. *Limnol. Oceanogr.* 28, 1104–1116. doi: 10.4319/lo.1983.28.6.1104

Holmes, R. M., Coe, M. T., Fiske, G. J., Gurtovaya, T., McClelland, J. W., Shiklomanov, A. I., et al. (2012). "Climate change impacts on the hydrology and biogeochemistry of Arctic Rivers," in *Climatic Change and Global Warming of Inland Waters: Impacts and Mitigation for Ecosystems and Societies*, eds C. R. Goldman, M. Kumagai, and R. D. Robarts (Hoboken, NJ: John Wiley & Sons, Ltd), 1–26. doi: 10.1002/9781118470596.ch1

Holmfeldt, K., Titelman, J., and Riemann, L. (2010). Virus production and lysate recycling in different sub-basins of the Northern Baltic Sea. *Microb. Ecol.* 60, 572–580. doi: 10.1007/s00248-010-9668-8

Hood, E., Battin, T. J., Fellman, J., O'Neel, S., and Spencer, R. G. M. (2015). Storage and release of organic carbon from glaciers and ice sheets. *Nat. Geosci.* 8, 91–96. doi: 10.1038/ngeo2331

Hood, E., Fellman, J., Spencer, R. G. M., Hernes, P. J., Edwards, R., D'Amore, D., et al. (2009). Glaciers as a source of ancient and labile organic matter to the marine environment. *Nature* 462, 1044–1047. doi: 10.1038/nature08580

Hopkinson, C. S., and Vallino, J. J. (2005). Efficient export of carbon to the deep ocean through dissolved organic matter. *Nature* 433, 142–145. doi: 10.1038/nature03191

Houghton, R. A. (2014). "The contemporary carbon cycle," in *Treatise on Geochemistry*, 2nd Edn, eds H. Holland, and K. Turekian (Oxford: Elsevier), 399–435. doi: 10.1016/B978-0-08-095975-7.00810-X

Hugelius, G., Strauss, J., Zubrzycki, S., Harden, J. W., Schuur, E. A. G., Ping, C. L., et al. (2014). Estimated stocks of circumpolar permafrost carbon with quantified uncertainty ranges and identified data gaps. *Biogeosciences* 11, 6573–6593. doi: 10.5194/bg-11-6573-2014

Ishikawa, N. F., Butman, D., and Raymond, P. A. (2019). Radiocarbon age of different photoreactive fractions of freshwater dissolved organic matter. *Org. Geochem.* 135, 11–15. doi: 10.1016/j.orggeochem.2019.06.006

Jambeck, J. R., Geyer, R., Wilcox, C., Siegler, T. R., Perryman, M., Andrady, A., et al. (2015). Plastic waste inputs from land into the ocean. *Science* 347, 768–771. doi: 10.1126/science.1260352

Jannasch, H. W. (1967). Growth of marine bacteria at limiting concentrations of organic carbon in seawater. *Limnol. Oceanogr.* 12, 264–271. doi: 10.4319/lo.1967.12.2.0264

Jeffries, M., and Richter-Menge, J. (2012). The Arctic, in: State of the Climate in 2011, B. *Am. Meteorol. Soc.* 93, 127–147.

Jennerjahn, T. C., and Ittekkot, V. (2002). Relevance of mangroves for the production and deposition of organic matter along tropical continental margins. *Naturwissenschaften* 89, 23–30. doi: 10.1007/s00114-001-0283-x

Jessen, G. L., Lichtschlag, A., Ramette, A., Pantoja, S., Rossel, P. E., Schubert, C. J., et al. (2017). Hypoxia causes preservation of labile organic matter and changes seafloor microbial community composition (Black Sea). *Sci. Adv.* 3:e1601897. doi: 10.1126/sciadv.1601897

Jiao, N., Herndl, G. J., Hansell, D. A., Benner, R., Kattner, G., Wilhelm, S. W., et al. (2010). Microbial production of recalcitrant dissolved organic matter: long-term carbon storage in the global ocean. *Nat. Rev. Microbiol.* 8, 593–599. doi: 10.1038/nrmicro2386

Jones, D. O. B., Yool, A., Wei, C. L., Henson, S. A., Ruhl, H. A., Watson, R. A., et al. (2014). Global reductions in seafloor biomass in response to climate change. *Glob. Change Biol.* 20, 1861–1872. doi: 10.1111/gcb.12480

Jones, M. W., Santin, C., van der Werf, G. R., and Doerr, S. H. (2019). Global fire emissions buffered by the production of pyrogenic carbon. *Nat. Geosci.* 12, 742–747. doi: 10.1038/s41561-019-0403-x

Jørgensen, N. O. G., Kroer, N., Coffin, R. B., Yang, X.-H., and Lee, C. (1993). Dissolved free amino acids, combined amino acids, and DNA as sources of carbon and nitrogen to marine bacteria. *Mar. Ecol. Prog. Ser.* 98, 135–148. doi: 10.3354/meps098135

Jurado, E., Dachs, J., Duarte, C. M., and Simo, R. (2008). Atmospheric deposition of organic and black carbon to the global oceans. *Atmos. Environ.* 42, 7931–7939. doi: 10.1016/j.atmosenv.2008.07.029

Kaiser, K., and Benner, R. (2008). Major bacterial contribution to the ocean reservoir of detrital organic carbon and nitrogen. *Limnol. Oceanogr.* 53, 99–112. doi: 10.4319/lo.2008.53.1.0099

Kaiser, K., and Benner, R. (2012). Organic matter transformations in the upper mesopelagic zone of the North Pacific: Chemical composition and linkages to microbial community structure. *J. Geophys. Res.* 117:C01023. doi: 10.1029/2011JC007141

Kaiser, K., Benner, R., and Amon, R. M. W. (2017). The fate of terrigenous dissolved organic carbon on the Eurasian shelves and export to the North Atlantic. *J. Geophys. Res. Oceans* 122, 4–22. doi: 10.1002/2016jc012380

Kanakidou, M., Duce, R. A., Prospero, J. M., Baker, A. R., Benitez-Nelson, C., Dentener, F. J., et al. (2012). Atmospheric fluxes of organic N and P to the global ocean. *Glob. Biogeochem.* 26:GB3026.

Karl, D. M. (1999). A sea of change: biogeochemical variability in the North Pacific Subtropical Gyre. *Ecosystems* 2, 181–214. doi: 10.1007/s100219900068

Keene, W. C., Maring, H., Maben, J. R., Kieber, D. J., Pszenny, A. A. P., Dahl, E. E., et al. (2007). Chemical and physical characteristics of nascent aerosols produced by bursting bubbles at a model air-sea interface. *J. Geophys. Res.* 112:D21202. doi: 10.1029/2007JD008464

Keil, R. G., and Kirchman, D. L. (1999). Utilization of dissolved protein and amino acids in the Northern Sargasso Sea. *Aquat. Microb. Ecol.* 18, 293–300. doi: 10.3354/ame018293

Keil, R. G., Mayer, L. M., Quay, P. D., Richey, J. E., and Hedges, J. I. (1997). Loss of organic matter from riverine particles in deltas. *Geochim. Cosmochim. Acta* 61, 1507–1511. doi: 10.1016/s0016-7037(97)00044-6

Keil, R. G., Montluçon, D. B., Prahl, F. G., and Hedges, J. I. (1994). Sorptive preservation of labile organic matter in marine sediments. *Nature* 370, 549–552. doi: 10.1038/370549a0

Kellermann, M. Y., Wegener, G., Elvert, M., Yoshinaga, M. Y., Lin, Y. S., Holler, T., et al. (2012). Autotrophy as a predominant mode of carbon fixation in anaerobic methane-oxidizing microbial communities. *Proc. Nat. Acad. Sci. U.S.A.* 109, 19321–19326. doi: 10.1073/pnas.1208795109

Kellermann, M. Y., Yoshinaga, M. Y., Wegener, G., Krukenberg, V., and Hinrichs, K.-U. (2016). Tracing the production and fate of individual archaeal intact polar lipids using stable isotope probing. *Org. Geochem.* 95, 13–20. doi: 10.1016/j.orggeochem.2016.02.004

Kennedy, M. J., Pevear, D. R., and Hill, R. J. (2002). Mineral surface control of organic carbon in black shale. *Science* 295, 657–660. doi: 10.1126/science.1066611

Kieber, D. J., Keene, W. C., Frossard, A. A., Long, M. S., Maben, J. R., Russell, L. M., et al. (2016). Coupled ocean-atmosphere loss of marine refractory dissolved organic carbon. *Geophys. Res. Lett.* 43, 2765–2772. doi: 10.1002/2016gl068273

Kim, E.-H., Kim, G., Lee, S.-A., and Dittmar, T. (2015). Extraordinary slow degradation of dissolved organic carbon (DOC) in a cold marginal sea. *Sci. Rep.* 5:13808. doi: 10.1038/srep13808

Kim, J. M., Lee, K., Suh, Y. S., and Han, I. S. (2018). Phytoplankton do not produce carbon-rich organic matter in high CO_2 oceans. *Geophys. Res. Lett.* 45, 4189–4197. doi: 10.1029/2017gl075865

Kim, T. W., Lee, K., Najjar, R. G., Jeong, H. D., and Jeong, H. J. (2011). Increasing N abundance in the Northwestern Pacific Ocean due to atmospheric nitrogen deposition. *Science* 334, 505–509. doi: 10.1126/science.1206583

Kiørboe, T. (2011). How zooplankton feed: mechanisms, traits and trade-offs. *Biol. Rev.* 86, 311–339. doi: 10.1111/j.1469-185X.2010.00148.x

Kirwan, M. L., Langley, J. A., Guntenspergen, G. R., and Megonigal, J. P. (2013). The impact of sea-level rise on organic matter decay rates in Chesapeake

Bay brackish tidal marshes. *Biogeosciences* 10, 1869–1876. doi: 10.5194/bg-10-1869-2013

Klevenz, V., Sumoondur, A., Ostertag-Henning, C., and Koschinsky, A. (2010). Concentrations and distributions of dissolved amino acids in fluids from Mid-Atlantic ridge hydrothermal vents. *Geochem. J.* 44, 387–397. doi: 10.1111/gbi.12026

Krause-Jensen, D., and Duarte, C. M. (2016). Substantial role of macroalgae in marine carbon sequestration. *Nat. Geosci.* 9, 737–742. doi: 10.1038/NGEO2790

Krawchuk, M. A., Moritz, M. A., Parisien, M. A., Van Dorn, J., and Hayhoe, K. (2009). Global pyrogeography: the current and future distribution of wildfire. *PLoS One* 4:e5102. doi: 10.1371/journal.pone.0005102

Ksionzek, K. B., Lechtenfeld, O. J., McCallister, S. L., Schmitt-Kopplin, P., Geuer, J. K., Geibert, W., et al. (2016). Dissolved organic sulfur in the ocean: biogeochemistry of a petagram inventory. *Science* 354, 456–459. doi: 10.1126/science.aaf7796

Kuzyakov, Y. A., and Galitsa, S. V. (1993). Kinetics of [2-14C] glycine decomposition and its incorporation into humus fractions of sierozem. *Eur. Soil Sci.* 25, 39–53.

Lang, S. Q., Butterfield, D. A., Lilley, M. D., Paul Johnson, H., and Hedges, J. I. (2006). Dissolved organic carbon in ridge-axis and ridge-flank hydrothermal systems. *Geochim. Cosmochim. Acta* 70, 3830–3842. doi: 10.1016/j.gca.2006.04.031

Lang, S. Q., Butterfield, D. A., Schulte, M., Kelley, D. S., and Lilley, M. D. (2010). Elevated concentrations of formate, acetate and dissolved organic carbon found at the Lost City hydrothermal field. *Geochim. Cosmochim. Acta* 74, 941–952. doi: 10.1016/j.gca.2009.10.045

LaRowe, D. E., and Van Cappellen, P. (2011). Degradation of natural organic matter: a thermodynamic analysis. *Geochim. Cosmochim. Acta* 75, 2030–2042. doi: 10.1016/j.gca.2011.01.020

Legendre, L., Rivkin, R. B., Weinbauer, M. G., Guidi, L., and Uitz, J. (2015). The microbial carbon pump concept: potential biogeochemical significance in the globally changing ocean. *Prog. Oceanogr.* 134, 432–450. doi: 10.1016/j.pocean.2015.01.008

Leppard, G. G. (1995). The characterization of algal and microbial mucilages and their aggregates in aquatic ecosystems. *Sci. Total Environ.* 165, 103–131. doi: 10.1016/0048-9697(95)04546-d

Lin, H. T., Cowen, J. P., Olson, E. J., Amend, J. P., and Lilley, M. D. (2012). Inorganic chemistry, gas compositions and dissolved organic carbon in fluids from sedimented young basaltic crust on the Juan de Fuca Ridge flanks. *Geochim. Cosmochim. Acta* 85, 213–227. doi: 10.1016/j.gca.2012.02.017

Liss, P. S., Marandino, C. A., Dahl, E. E., Helmig, D., Hintsa, E. J., Hughes, C., et al. (2014). "Short-lived trace gases in the surface ocean and the atmosphere," in *Ocean-Atmosphere Interactions of Gases and Particles*, eds P. Liss and M. T. Johnson (Berlin: Springer), 1–54. doi: 10.1007/978-3-642-25643-1_1

Liu, X., Li, Y., Wu, Y., Huang, B., Dai, M., Fu, F., et al. (2017). Effects of elevated CO2 on phytoplankton during a mesocosm experiments in the southern eutrophicated coastal waters of China. *Sci. Rep.* 7:6868.

Loginova, A. N., Thomsen, S., Dengler, M., Lüdke, J., and Engel, A. (2019). Diapycnal dissolved organic matter supply into the upper Peruvian oxycline. *Biogeosciences* 16, 2033–2047. doi: 10.5194/bg-16-2033-2019

Lønborg, C., Álvarez-Salgado, X. A., Letscher, R. T., and Hansell, D. A. (2018). Large stimulation of recalcitrant dissolved organic carbon degradation by increasing ocean temperatures. *Front. Mar. Sci.* 4:436. doi: 10.3389/fmars.2017.00436

Longnecker, K., Sievert, S. M., Sylva, S. P., Seewald, J. S., and Kujawinski, E. B. (2018). Dissolved organic carbon compounds in deep-sea hydrothermal vent fluids from the East Pacific Rise at 9°50'N. *Org. Geochem.* 125, 41–49. doi: 10.1016/j.orggeochem.2018.08.004

Lutz, M. J., Caldeira, K., Dunbar, R. B., and Behrenfeld, M. J. (2007). Seasonal rhythms of net primary production and particulate organic carbon flux to depth describe the efficiency of biological pump in the global ocean. *J. Geophys. Res.* 112:C10011. doi: 10.1029/2006JC003706

Macreadie, P. I., Anton, A., Raven, J. A., Beaumont, N., Connolly, R. M., Friess, D. A., et al. (2019). The future of Blue Carbon science. *Nat. Commun.* 10:3998. doi: 10.1038/s41467-019-11693-w

Mann, P. J., Eglinton, T. I., McIntyre, C. P., Zimov, N., Davydova, A., Vonk, J. E., et al. (2015). Utilization of ancient permafrost carbon in headwaters of Arctic fluvial networks. *Nat. Commun.* 6:7856. doi: 10.1038/ncomms8856

Marandino, C. A., de Bruyn, W. J., Miller, S. D., Prather, M. J., and Saltzman, E. S. (2005). Oceanic uptake and the global atmospheric acetone budget. *Geophys. Res. Lett.* 32:L15806.

Margolin, A. R., Gerringa, L. J. A., Hansell, D. A., and Rijkenberg, M. J. A. (2016). Net removal of dissolved organic carbon in the anoxic waters of the Black Sea. *Mar. Chem.* 183, 13–24. doi: 10.1016/j.marchem.2016.05.003

Margolin, A. R., Gonnelli, M., Hansell, D. A., and Santinelli, C. (2018). Black Sea dissolved organic matter dynamics: insights from optical analyses. *Limnol. Oceanogr.* 63, 1425–1443. doi: 10.1002/lno.10791

Marwick, T. R., Tamooh, F., Teodoru, C. R., Borges, A. V., Darchambeau, F., and Boullion, S. (2015). The age of river-transported carbon: a global perspective. *Glob. Biogeochem. Cycles* 29, 122–137. doi: 10.1002/2014GB004911

McDermott, J. M., Seewald, J. S., German, C. R., and Sylva, S. P. (2015). Pathways for abiotic organic synthesis at submarine hydrothermal fields. *Proc. Nat. Acad. Sci. U.S.A.* 112, 7668–7672. doi: 10.1073/pnas.1506295112

McDonough, L. K., Santos, I. R., Andersen, M. S., O'Carroll, D., Rutlidge, H., Meredith, K., et al. (2020). Changes in global groundwater organic carbon driven by climate change and urbanization. *Nat. Commun.* 11:1279. doi: 10.1038/s41467-020-14946-1

McNichol, A. P., and Aluwihare, L. I. (2007). The power of radiocarbon in biogeochemical studies of the marine carbon cycle: insights from studies of dissolved and particulate organic carbon (DOC and POC). *Chem. Rev.* 107, 443–466. doi: 10.1021/cr050374g

McNichol, A. P., Schneider, R. J., von Reden, K. F., Gagnon, A. R., Elder, K. L., Key, R. M., et al. (2000). Ten years after – The WOCE AMS radiocarbon program. *Nucl. Instrum. Methods Phys. Res. Sect. B* 172, 479–484. doi: 10.1016/S0168-583X(00)00093-8

McPhaden, M. J., and Zhang, D. (2002). Slowdown of the meridional overturning circulation in the upper Pacific Ocean. *Nature* 415, 603–608. doi: 10.1038/415603a

Mentges, A., Feenders, C., Deutsch, C., Blasius, B., and Dittmar, T. (2019). Long-term stability of marine dissolved organic carbon emerges from a neutral network of compounds and microbes. *Sci. Rep.* 9:17780. doi: 10.1038/s41598-019-54290-z

Middelboe, M., and Jorgensen, N. O. G. (2006). Viral lysis of bacteria: an important source of dissolved amino acids and cell wall compounds. *J. Mar. Biol. Assoc.* 86, 605–612. doi: 10.1017/s0025315406013518

Middelburg, J. J. (2011). Chemoautotrophy in the ocean. *Geophys. Res. Lett.* 38:L24604.

Middelburg, J. J. (2015). Escape by dilution. *Science* 348:290. doi: 10.1126/science.aaa9852

Middelburg, J. J. (2018). Reviews and syntheses: to the bottom of carbon processing at the seafloor. *Biogeosci.* 15, 413–427. doi: 10.5194/bg-15-413-2018

Millet, D. B., Jacob, D. J., Custer, T. G., de Gouw, J. A., Goldstein, A. H., Karl, T., et al. (2008). New constraints on terrestrial and oceanic sources of atmospheric methanol. *Atmos. Chem. Phys.* 8, 6887–6905. doi: 10.5194/acp-8-6887-2008

Mitsch, W. J., and Hernandez, M. E. (2013). Landscape and climate change threats to wetlands of North and Central America. *Aquat. Sci.* 75, 133–149. doi: 10.1007/s00027-012-0262-7

Moller, E. F. (2005). Sloppy feeding in marine copepods: prey-size-dependent production of dissolved organic carbon. *J. Plankton Res.* 27, 27–35. doi: 10.1093/plankt/fbh147

Moller, E. F. (2007). Production of dissolved organic carbon by sloppy feeding in the copepods *Acartia tonsa*, *Centropages typicus*, and *Temora longicornis*. *Limnol. Oceanogr.* 52, 79–84. doi: 10.4319/lo.2007.52.1.0079

Mopper, K., and Kieber, D. J. (2002). "The photochemistry and cycling of carbon, sulfur, nitrogen and phosphorus," in *Biogeochemistry of Marine Dissolved Organic Matter*, eds D. A. Hansell and C. A. Carlson (San Diego, CA: Academic Press), 455–507. doi: 10.1016/b978-012323841-2/50011-7

Mopper, K., Kieber, D. J., and Stubbins, A. (2014). "Marine photochemistry of organic matter: processes and impacts," in *Biogeochemistry of Marine Dissolved Organic Matter*, eds D. A. Hansell and C. A. Carlson (San Diego, CA: Academic Press), doi: 10.1016/C2012-0-02714-7

Moran, M. A., Kujawinski, E. B., Stubbins, A., Fatland, R., Aluwihare, L. I., Buchan, A., et al. (2016). Deciphering ocean carbon in a changing world. *Proc. Nat. Acad. Sci. U.S.A.* 113, 3143–3151. doi: 10.1073/pnas.1514645113

Nagata, T., Fukuda, H., Fukuda, R., and Koike, I. (2000). Bacterioplankton distribution and production in deep Pacific waters: large-scale geographic variations and possible coupling with sinking particle fluxes. *Limnol. Oceanogr.* 45, 426–435. doi: 10.4319/lo.2000.45.2.0426

Novak, T., Godrijan, J., Pfannkuchen, D. M., Djakovac, T., Mlakar, M., Baricevic, A., et al. (2018). Enhanced dissolved lipid production as a response to the sea surface warming. *J. Mar. Sys.* 180, 289–298. doi: 10.1016/j.jmarsys.2018.01.006

O'Dowd, C. D., and de Leeuw, G. (2007). Marine aerosol production: a review of the current knowledge. *Philos. Trans. R. Soc. Lond. Ser. A.* 365, 1753–1774. doi: 10.1098/rsta.2007.2043

Ogawa, H., Amagai, Y., Kioke, I., Kaiser, K., and Benner, R. (2001). Production of refractory dissolved organic matter by bacteria. *Science* 292, 917–920. doi: 10.1126/science.1057627

Piontek, J., Lunau, M., Händel, N., Borchard, C., Wurst, M., and Engel, A. (2010). Acidification increases microbial polysaccharide degradation in the ocean. *Biogeosciences* 7, 1615–1624. doi: 10.5194/bg-7-1615-2010

Pohlabeln, A. M., and Dittmar, T. (2015). Novel insights into the molecular structure of non-volatile marine dissolved organic sulfur. *Mar. Chem.* 168, 86–94. doi: 10.1016/j.marchem.2014.10.018

Pohlabeln, A. M., Gomez-Saez, G. V., Noriega-Ortega, B. E., and Dittmar, T. (2017). Experimental evidence for abiotic sulfurization of marine dissolved organic matter. *Front. Mar. Sci.* 4:364. doi: 10.3389/fmars.2017.00364

Pohlman, J. W., Bauer, J. E., Waite, W. F., Osburn, C. L., and Chapman, N. R. (2010). Methane hydrate-bearing seeps as a source of aged dissolved organic carbon to the oceans. *Nat. Geosci.* 4, 37–41. doi: 10.1038/ngeo1016

Polovina, J. J., Howell, E. A., and Abecassis, M. (2008). Ocean's least productive waters are expanding. *Geophys. Res. Lett.* 35:L03618.

Pomeroy, L. R., and Wiebe, W. J. (2001). Temperature and substrates as interactive limiting factors for marine heterotrophic bacteria. *Aquat. Microb. Ecol.* 23, 187–204. doi: 10.3354/ame023187

Priscu, J. C., and Christner, B. C. (2004). "Earth's icy biosphere," in *Microbial Diversity and Bioprospecting*, ed. A. T. Bull (Washington, DC: ASM Press), 130–145. doi: 10.1128/9781555817770.ch13

Quinn, P. K., Bates, T. S., Schulz, K. S., Coffman, D. J., Frossard, A. A., Russell, L. M., et al. (2014). Contribution of sea surface carbon pool to organic matter enrichment in sea spray aerosol. *Nat. Geosci.* 7, 228–232. doi: 10.1038/ngeo2092

Rabalais, N. N., Turner, R. E., Diaz, R. J., and Justic, D. (2009). Global change and eutrophication of coastal waters. *ICES J. Mar. Sci.* 66, 1528–1537. doi: 10.1093/icesjms/fsp047

Raymond, P. A., Saiers, J. E., and Sobczak, W. V. (2016). Hydrological and biogeochemical controls on watershed dissolved organic matter transport: pulse-shunt concept. *Ecology* 97, 5–16. doi: 10.1890/14-1684.1

Raymond, P. A., and Spencer, R. G. M. (2015). "Riverine DOM," in *Biogeochemistry of Marine Dissolved Organic Matter*, 2nd Edn, eds D. A. Hansell and C. A. Carlson (Amsterdam: Elsevier Inc), 509–525.

Reeves, E. P., McDermott, J. M., and Seewald, J. S. (2014). The origin of methanethiol in midocean ridge hydrothermal fluids. *Proc. Nat. Acad. Sci. U.S.A.* 111, 5474–5479. doi: 10.1073/pnas.1400643111

Regier, P., Briceno, H., and Jaffe, R. (2016). Long-term environmental drivers of DOC fluxes: Linkages between management, hydrology and climate in a subtropical coastal estuary. *Estuar. Coast. Shelf Sci.* 182, 112–122. doi: 10.1016/j.ecss.2016.09.017

Ridgwell, A., and Arndt, S. (2015). "Why dissolved organics matter: DOC in ancient oceans and past climate change," in *Biogeochemistry of Marine Dissolved Organic Matter*, eds D. A. Hansell and C. A. Carlson (San Diego, CA: Academic Press), 1–20. doi: 10.1016/b978-0-12-405940-5.00001-7

Roelofs, G. J. (2008). A GCM study of organic matter in marine aerosol and its potential contribution to cloud drop activation. *Atmos. Chem. Phys.* 8, 709–719. doi: 10.5194/acp-8-709-2008

Romera-Castillo, C., Letscher, R. T., and Hansell, D. A. (2016). New nutrients exert fundamental control on dissolved organic carbon accumulation in the surface Atlantic Ocean. *Proc. Nat. Acad. Sci. U.S.A.* 113, 10497–10502. doi: 10.1073/pnas.1605344113

Rossel, P. E., Bienhold, C., Boetius, A., and Dittmar, T. (2016). Dissolved organic matter in pore 980 water of Arctic Ocean sediments: environmental influence on molecular composition. *Org. Geochem.* 97, 41–52. doi: 10.1016/j.orggeochem.2016.04.003

Rossel, P. E., Stubbins, A., Hach, P. F., and Dittmar, T. (2015). Bioavailability and molecular composition of dissolved organic matter from a diffuse hydrothermal system. *Mar. Chem.* 177, 257–266. doi: 10.1016/j.marchem.2015.07.002

Rossel, P. E., Stubbins, A., Rebling, T., Koschinsky, A., Hawkes, J. A., and Dittmar, T. (2017). Thermally altered marine dissolved organic matter in hydrothermal fluids. *Org. Geochem.* 110, 73–86. doi: 10.1016/j.orggeochem.2017.05.003

Rothman, D. H., Hayes, J. M., and Summons, R. E. (2003). Dynamics of the Neoproterozoic carbon cycle. *Proc. Nat. Acad. Sci. U.S.A.* 100, 8124–8129. doi: 10.1073/pnas.0832439100

Ruiz-Fernández, A. C., Carnero-Bravo, V., Sanchez-Cabeza, J. A., Pérez-Bernal, L. H., Amaya-Monterrosa, O. A., Bojórquez-Sánchez, S., et al. (2018). Carbon burial and storage in tropical salt marshes under the influence of sea level rise. *Sci. Tot. Environ.* 630, 1628–1640. doi: 10.1016/j.scitotenv.2018.02.246

Saba, G. K., Steinberg, D. K., and Bronk, D. A. (2011). The relative importance of sloppy feeding, excretion and fecal pellet leaching in the release of dissolved organic carbon and nitrogen by *Acartia tonsa* copepods. *J. Exp. Mar. Biol. Ecol.* 404, 47–56. doi: 10.1016/j.jembe.2011.04.013

Sarmiento, J. L., and Gruber, N. (2006). *Ocean Biogeochemical Dynamics*. Princeton, NJ: Princeton University Press.

Schartau, M., Engel, A., Schröter, J., Thoms, S., Völker, C., and Wolf-Gladrow, D. (2007). Modelling carbon overconsumption and the formation of extracellular particulate organic carbon. *Biogeosciences* 4, 433–454. doi: 10.5194/bg-4-433-2007

Schmidt, F., Koch, B. P., Elvert, M., Schmidt, G., Witt, M., and Hinrichs, K. (2011). Diagenetic transformation of dissolved organic nitrogen compounds under contrasting sedimentary redox conditions in the Black Sea. *Environ. Sci. Technol.* 45, 5223–5229. doi: 10.1021/es2003414

Scott, A. C., and Glasspool, I. J. (2006). The diversification of Paleozoic fire systems and fluctuations in atmospheric oxygen concentration. *Proc. Nat. Acad. Sci. U.S.A.* 103, 10861–10865. doi: 10.1073/pnas.0604090103

Seidel, M., Beck, M., Riedel, T., Waska, H., Suryaputra, I. G. N. A., Schnetger, B., et al. (2014). Biogeochemistry of dissolved organic matter in an anoxic intertidal creek bank. *Geochim. Cosmochim. Acta* 140, 418–434. doi: 10.1016/j.gca.2014.05.038

Sexton, P. F., Norris, R. D., Wilson, P. A., Palike, H., Westerhold, T., Rohl, U., et al. (2011). Eocene global warming events driven by ventilation of oceanic dissolved organic carbon. *Nature* 471, 349–352. doi: 10.1038/nature09826

Sharma, P., Marinov, I., Cabre, A., Kostadinov, T., and Singh, A. (2019). Increasing biomass in the warm oceans: unexpected new insights from SeaWiFS. *Geophys. Res. Lett.* 46, 3900–3910. doi: 10.1029/2018gl079684

Sharples, J., Middelburg, J. J., Fennel, K., and Jickells, T. (2017). What proportion of riverine nutrients reaches the open ocean? *Glob. Biogeochem. Cycles* 31, 39–58. doi: 10.1002/2016gb005483

Shen, Y., and Benner, R. (2018). Mixing it up in the ocean carbon cycle and the removal of refractory dissolved organic carbon. *Sci. Rep.* 8:2542. doi: 10.1038/s41598-018-20857-5

Shim, C., Wang, Y., Singh, H. B., Blake, D. R., and Guenther, A. B. (2007). Source characteristics of oxygenated volatile organic compounds and hydrogen cyanide. *J. Geophys. Res.* 112:D10305.

Sjøgaard, K., Treusch, A. H., and Valdemarsen, T. B. (2017). Carbon degradation in agricultural soils flooded with seawater after managed coastal realignment. *Biogeosciences* 14, 4375–4389. doi: 10.5194/bg-14-4375-2017

Søndergaard, M., leB Williams, P. J., Cauwet, G., Riemann, B., Robinson, C., Terzic, S., et al. (2000). Net accumulation and flux of dissolved organic carbon and dissolved organic nitrogen in marine plankton communities. *Limnol. Oceanogr.* 45, 1097–1111. doi: 10.4319/lo.2000.45.5.1097

Spracklen, D. V., Arnold, S. R., Sciare, J., Carslaw, K. S., and Pio, C. (2008). Globally significant oceanic source of organic carbon aerosol. *Geophys. Res. Lett.* 35:L12811. doi: 10.1029/2008GL033359

Steinberg, D. K., Carlson, C. A., Bates, N. R., Goldthwait, S. A., Madin, L. P., and Michaels, A. F. (2000). Zooplankton vertical migration and the active transport of dissolved organic and inorganic carbon in the Sargasso Sea. *Deep Sea Res. I* 47, 137–158. doi: 10.1016/s0967-0637(99)00052-7

Steinberg, D. K., Goldthwait, S. A., and Hansell, D. A. (2002). Zooplankton vertical migration and the active transport of dissolved organic and inorganic nitrogen in the Sargasso Sea. *Deep Sea Res. I* 49, 1445–1461. doi: 10.1016/s0967-0637(02)00037-7

Steinberg, D. K., and Landry, M. R. (2017). Zooplankton and the ocean carbon cycle. *Annu. Rev. Mar. Sci.* 9, 413–444. doi: 10.1146/annurev-marine-010814-015924

St-Laurent, P., Friedrichs, M. A. M., Najjar, R. G., Martins, D. K., Herrmann, M., Miller, S. K., et al. (2017). Impacts of atmospheric nitrogen deposition on surface waters of the Western North Atlantic mitigated by multiple feedbacks. *J. Geophys. Res. Oceans* 122, 8406–8426. doi: 10.1002/2017JC013072

Stocker, T. F., Qin, D., Plattner, G.-K., Tignor, M., Allen, S. K., Boschung, J., et al. (2013). *Climate Change 2013: The Physical Science Basis. Contribution of Working Group I to the Fifth Assessment Report of the Intergovernmental Panel on Climate Change*. Cambridge: Cambridge University Press.

Stubbins, A., Niggemann, J., and Dittmar, T. (2012). Photo-lability of deep ocean dissolved black carbon. *Biogeosciences* 9, 1661–1670. doi: 10.5194/bg-9-1661-2012

Stubbins, A., Spencer, R. G. M., Chen, H., Hatcher, P. G., Mopper, K., Hernes, P. J., et al. (2010). Illuminated dark- ness: molecular signatures of Congo River dissolved organic matter and its photochemical alteration as revealed by ultrahigh precision mass spectrometry. *Limnol. Oceanogr.* 55, 1467–1477. doi: 10.4319/lo.2010.55.4.1467

Stubbins, A., Uher, G., Law, C. S., Mopper, K., Robinson, C., and Upstill-Goddard, R. C. (2006). Open-ocean carbon monoxide photoproduction. *Deep Sea Res. II* 53, 1695–1705. doi: 10.1021/es502057n

Sugie, K., Yoshimura, T., and Wakita, M. (2018). Impact of CO_2 on the elemental composition of the particulate and dissolved organic matter of marine diatoms emerged after nitrate depletion. *Limnol. Oceanogr.* 63, 1924–1943. doi: 10.1002/lno.10816

Sunagawa, S., Coelho, L. P., Chaffron, S., Kultima, J. R., Labadie, K., Salazar, G., et al. (2015). Structure and function of the global ocean microbiome. *Science* 348:1261359. doi: 10.1126/science.1261359

Suttle, C. A. (2007). Marine viruses—major players in the global ecosystem. *Nat. Rev. Microbiol.* 5, 801–812. doi: 10.1038/nrmicro1750

Vaquer-Sunyer, R., Duarte, C. M., Santiago, R., Wassmann, P., and Reigstad, M. (2010). Experimental evaluation of planktonic respiration response to warming in the European Arctic Sector. *Polar Biol.* 33, 1661–1671. doi: 10.1007/s00300-010-0788-x

Veuger, B., Middelburg, J. J., Boschker, H. T. S., Nieuwenhuize, J., van Rijswijk, P., Rochelle-Newall, E. J., et al. (2004). Microbial uptake of dissolved organic and inorganic nitrogen in Randers Fjord. *Estuar. Coast. Shelf Sci.* 61, 507–515. doi: 10.1016/j.ecss.2004.06.014

Viviani, D. A., Böttjer, D., Letelier, R. M., and Church, M. J. (2018). The influence of abrupt increases in seawater pCO_2 on plankton productivity in the subtropical North Pacific Ocean. *PLoS One* 13:e0193405. doi: 10.1371/journal.pone.0193405

Wagner, S., Brandes, J., Spencer, R. G. M., Ma, K., Rosengard, S. Z., Moura, J. M. S., et al. (2019). Isotopic composition of oceanic dissolved black carbon reveals non-riverine source. *Nat. Commun.* 10:5064. doi: 10.1038/s41467-019-13111-7

Walker, B. D., Druffel, E. R. M., Kolasinski, J., Roberts, B. J., Xu, X., and Rosenheim, B. E. (2017). Stable and radiocarbon isotopic composition of dissolved organic matter in the Gulf of Mexico. *Geophys. Res. Lett.* 44, 8424–8434. doi: 10.1002/2017gl074155

Walker, B. D., Primeau, F. W., Beaupré, S. R., Guilderson, T. P., Druffel, E. R. M., and McCarthy, M. D. (2016). Linked changes in marine dissolved organic carbon molecular size and radiocarbon age. *Geophys. Res. Lett.* 43, 10385–10393. doi: 10.1002/2016GL070359

Wang, R., Balkanski, Y., Bopp, L., Aumont, O., Boucher, O., Ciais, P., et al. (2015). Influence of anthropogenic aerosol deposition on the relationship between oceanic productivity and warming. *Geophys. Res. Lett.* 42, 10745–10754. doi: 10.1002/2015GL066753

Wang, X.-C., Chen, R. F., Whelan, J., and Eglinton, L. (2001). Contribution of 'old' carbon from natural marine hydrocarbon seeps to sedimentary and dissolved organic carbon pools in the Gulf of Mexico. *Geophys. Res. Lett.* 28, 3313–3316. doi: 10.1029/2001gl013430

Wegener, G., Bausch, M., Holler, T., Thang, N. M., Prieto-Mollar, X., Kellermann, M. Y., et al. (2012). Assessing sub-seafloor microbial activity by combined stable isotope probing with deuterated water and 13C-bicarbonate. *Environ. Microbiol.* 14, 1517–1527. doi: 10.1111/j.1462-2920.2012.02739.x

Wegener, G., Kellermann, M. Y., and Elvert, M. (2016). Tracking activity and function of microorganisms by stable isotope probing of membrane lipids. *Curr. Opin. Biotechnol.* 41, 43–52. doi: 10.1016/j.copbio.2016.04.022

Weinbauer, M. G., and Peduzzi, P. (1995). Effect of virus-rich high molecular weight concentrates of seawater on the dynamics of dissolved amino acids and carbohydrates. *Mar. Ecol. Prog. Ser.* 127, 245–253. doi: 10.3354/meps127245

Weiss, M. S., Abele, U., Weckesser, J., Welte, W., Schiltz, E., and Schulz, G. E. (1991). Molecular architecture and electrostatic properties of a bacterial porin. *Science* 254, 1627–1630. doi: 10.1126/science.1721242

Wild, B., Andersson, A., Broder, L., Vonk, J., Hugelius, G., McClelland, J. W., et al. (2019). Rivers across the Siberian Arctic unearth the patterns of carbon release from thawing permafrost. *Proc. Nat. Acad. Sci. U.S.A.* 116, 10281–10285. doi: 10.1073/pnas.1811797116

Wilhelm, S. W., and Suttle, C. A. (1999). Viruses and nutrient cycles in the sea - Viruses play critical roles in the structure and function of aquatic food webs. *Bioscience* 49, 781–788. doi: 10.2307/1313569

Williams, P. J. B. (1995). Evidence for the seasonal accumulation of carbon-rich dissolved organic material, its scale in comparison with changes in particulate material and the consequential effect on net C/N assimilation ratios. *Mar. Chem.* 51, 17–29. doi: 10.1016/0304-4203(95)00046-t

Williams, P. M., and Druffel, E. R. M. (1987). Radiocarbon in dissolved organic matter in the central North Pacific Ocean. *Nature* 330, 246–248. doi: 10.1038/330246a0

Winkel, M., Pjevac, P., Kleiner, M., Littman, S., Meyerdierks, A., Rudolf, A., et al. (2014). Identification and activity of acetate-assimilating bacteria in diffusive fluids venting from deep-sea hydrothermal systems. *FEMS Microbiol. Ecol.* 90, 731–746. doi: 10.1111/1574-6941.12429

Wohlers, J., Engel, A., Zöllner, E., Breithaupt, P., Jürgens, K., Hoppe, H. G., et al. (2009). Changes in biogenic carbon flow in response to sea surface warming. *Proc. Nat. Acad. Sci. U.S.A.* 106, 7067–7072. doi: 10.1073/pnas.0812743106

Wood, M. A., and Van Valen, L. M. (1990). Paradox lost? On the release of energy-rich compounds by phytoplankton. *Mar. Microb. Food Webs* 4, 103–116.

Worrall, F., Burt, T., and Admason, J. (2004). Can climate change explain increases in DOC flux from upland peat catchments? *Sci. Total Environ.* 326, 95–112. doi: 10.1016/j.scitotenv.2003.11.022

Yamanaka, T., Maeto, K., Akashi, H., Ishibashi, J. I., Miyoshi, Y., Okamura, K., et al. (2013). Shallow submarine hydrothermal activity with significant contribution of magmatic water producing talc chimneys in the Wakamiko Crater of Kagoshima Bay, southern Kyushu, Japan. *J. Volcanol. Geotherm. Res.* 258, 74–84. doi: 10.1016/j.jvolgeores.2013.04.007

Zark, M., Broda, N. K., Hornick, T., Grossart, H. P., Riebesell, U., and Dittmar, T. (2017). Ocean acidification experiments in large-scale mesocosms reveal similar dynamics of dissolved organic matter production and biotransformation. *Front. Mar. Sci.* 4:271. doi: 10.3389/fmars.2017.00271

Zark, M., Riebesell, U., and Dittmar, T. (2015). Effects of ocean acidification on marine dissolved organic matter are not detectable over the succession of phytoplankton blooms. *Sci. Adv.* 1:e1500531. doi: 10.1126/sciadv.1500531

Zhu, L., Zhao, S., Bittar, T. B., Stubbins, A., and Li, D. (2020). Photochemical dissolution of buoyant microplastics to dissolved organic carbon: rates and microbial impacts. *J. Hazard. Mater.* 383:121065. doi: 10.1016/j.jhazmat.2019.121065

Zinger, L., Amaral-Zettler, L. A., Fuhrman, J. A., Horner-Devine, M. C., Huse, S. M., Welch, D. B. M., et al. (2011). Global patterns of bacterial beta-diversity in seafloor and seawater ecosystems. *PLoS One* 6:e24570. doi: 10.1371/journal.pone.0024570 doi: 10.1371/journal.pone.0024570

Conflict of Interest: The authors declare that the research was conducted in the absence of any commercial or financial relationships that could be construed as a potential conflict of interest.

frontiers in Marine Science

ORIGINAL RESEARCH
published: 05 June 2020
doi: 10.3389/fmars.2020.00405

Marvelous Marine Microgels: On the Distribution and Impact of Gel-Like Particles in the Oceanic Water-Column

Anja Engel[1], Sonja Endres[1,2], Luisa Galgani[3,4] and Markus Schartau[1]*

[1] GEOMAR Helmholtz Centre for Ocean Research Kiel, Kiel, Germany, [2] WTSH Business Development and Technology Transfer Corporation of Schleswig-Holstein, Kiel, Germany, [3] Center for Colloid and Surface Science, Sesto Fiorentino, Italy, [4] Department of Biotechnology, Chemistry and Pharmacy, University of Siena, Siena, Italy

Three-dimensional hydrogels of organic polymers have been suggested to affect a variety of processes in the ocean, including element cycling, microbial ecology, food-web dynamics, and air-sea exchange. However, their abundance and distribution in the ocean are hardly known, strongly limiting an assessment of their global significance. As a consequence, marine gels are often disregarded in biogeochemical or ecosystem models. Here, we demonstrate the widespread abundance of microgels in the ocean, from the surface to the deep sea. We exhibit size spectra of two major classes of marine gels, transparent exopolymer particles (TEP) and Coomassie stainable particles (CSP) for three different ocean regimes: (a) Polar Seas, (b) Eastern Boundary Upwelling Systems, and (c) the oligotrophic open ocean. We show the variations of TEP and CSP over the water-column, and compare them to dissolved organic carbon (DOC). We also discuss how the observed distributional patterns inform about productivity and particle dynamics of these distinct oceanic regimes. Finally, we exploit current research topics, where consideration of microgels may give new insight into the role of organic matter for marine biogeochemical processes.

Keywords: transparent exopolymer particles (TEP), coomassie stainable particles (CSP), DOC (dissolved organic carbon), particle size spectra, water column

OPEN ACCESS

Edited by:
Stuart Wakeham, University of Georgia, United States

Reviewed by:
Roberta L. Hansman, IAEA International Atomic Energy Agency, Monaco
Eva Ortega-Retuerta, UMR 7621 Laboratoire d'Océanographie Microbienne (LOMIC), France

****Correspondence:***
Anja Engel
aengel@geomar.de

Specialty section:
This article was submitted to Marine Biogeochemistry, a section of the journal Frontiers in Marine Science

Received: *11 January 2020*
Accepted: *11 May 2020*
Published: *05 June 2020*

Citation:
Engel A, Endres S, Galgani L and Schartau M (2020) Marvelous Marine Microgels: On the Distribution and Impact of Gel-Like Particles in the Oceanic Water-Column. Front. Mar. Sci. 7:405. doi: 10.3389/fmars.2020.00405

INTRODUCTION

Natural organic gels have gained considerable attention in marine and atmospheric research over the past decades due to their widespread occurrence in the environment and their involvement in biological, chemical, and physical processes. Gels are a fraction of exopolymeric substances (EPS), representing dissolved or particulate polymeric organic substances outside the cell. Marine EPSs typically have a high content of gelling agents, such as mucopolysaccharides and they occur over a large range of sizes in various chemical and structural forms (Verdugo et al., 2004). The large and continuous size spectrum of marine gels is the result of dynamic formation and disintegration processes that yet are not fully understood. A useful concept to describe the structure and properties of gels comes from gelation theory (Chin et al., 1998; Verdugo et al., 2004; Verdugo, 2012; Orellana and Leck, 2015). Here, marine gels are defined as three-dimensional networks of organic polymers with seawater as solvent entrapped in the network pores. Nanogels assemble from individual polymers and are held together by ionic forces, such as divalent cation (Ca^{2+}, Mg^{2+}) bridging

and hydrogen bondings, or by hydrophobic interactions. According to this theory, gel growth is achieved through annealing of small nanogels that can create larger sized gels (~5 μm) (Chin et al., 1998). More stable and larger sized polymer gels result from collisions of two annealing nanogels. In the reverse, processes like fragmentation and dispersions are responsible for gel size reduction.

Gel particles in seawater have been determined through staining with dyes specific for the organic compounds they contain. Alcian Blue, a cationic copper-phthalocyanine dye that reacts with the carboxyl (COO^-) and sulfate half ester (OSO_3^-) functional groups of acid mucopolysaccharides and glycosaminoglycans (Parker and Diboll, 1966; Decho, 1990) and the fluorescein labeled lectin Concanavalin A (ConA) have been used to determine polysaccharide-containing gels, referred to as transparent exopolymer particles (TEP) (Alldredge et al., 1993; Engel et al., 2017). Another dye is Coomassie Brilliant Blue, a disulfonated triphenylmethane dye that binds to proteins and longer peptides (Chial and Splittgerber, 1993). It is used for identifying protein-containing Coomassie stainable particles (CSP) (Long and Azam, 1996). After staining, TEP and CSP can be quantified by spectrophotometric measurements of the total amount of stain absorbed (Passow and Alldredge, 1995; Cisternas-Novoa et al., 2014) or by sizing and counting of individual particles using microscopy (e.g., Engel, 2009). Today, most published information on gels in the marine environment is available for TEP and CSP.

The origin of the polysaccharides contributing to TEP formation is biological production, mainly primary production by plankton in the sunlit surface ocean. Phytoplankton derived hetero-polysaccharides contain neutral sugars like glucose, galactose, arabinose, mannose and xylose, amino sugars like glucosamine and galactosamine, and acidic sugars such as galacturonic and glucuronic acid (Biersmith and Benner, 1998; Borchard and Engel, 2012). Uronic acids are likely involved in the formation process of gel particles as they allow for polymer bridging via divalent cations. Mechanisms involved in the release of polysaccharides from the cell to the extracellular space include exudation, as well as viral lysis of cells and cell breakage, e.g., through sloppy-feeding and bacterial degradation. The "carbon-overflow" hypothesis (Wood and Van Valen, 1990; Engel et al., 2004) predicts that excess photosynthesates are released from the autotrophic (?) cell under conditions of growth limitation by nutrients. As the molecular weight of polysaccharides released from phytoplankton cells is too high for passive, concentration-dependent diffusion through the cell membrane, their release is more likely associated with active exudation processes, including exocytosis and/or transport by specific membrane-bound transport proteins embedded in the plasma membrane (Engel et al., 2004; Borchard and Engel, 2012). Indeed, TEP concentration during phytoplankton blooms typically increases as soon as algal growth has approached nutrient depletion (Logan et al., 1995; Mari and Kiørboe, 1996; Engel et al., 2002; Passow, 2002).

The concentration of dissolved polysaccharides in seawater approximately ranges from 2.6 to 25.8 μM and dominates the upper waters above oxygen minima (Pakulski and Benner, 1994). Supposing homogenous distribution in seawater, the individual polymer chains would likely be too disparate to assemble spontaneously. Accumulation at sites such as boundary layers, air bubbles or the outer cell surface may increase the probability of contact and enable gel formation. For dispersed polymers in seawater, diffusion and shear are the main kinetic processes supporting contact, subsequent adhesion and coagulation (Logan et al., 1995). Modeling studies have shown how observed TEP concentrations can be well-explained by considering nutrient limited phytoplankton growth as a prerequisite for an excessive release of exopolysaccharides and by applying coagulation theory where dissolved exopolysaccharides are treated as polymeric precursors for the formation of TEP (Engel et al., 2004; Schartau et al., 2007; Joassin et al., 2011). Because TEP form from exopolysaccharides, their element content displays a selective enrichment of carbon relative to other major elements like nitrogen and compared to the Redfield ratio of plankton (Redfield, 1958; Mari, 1999; Engel and Passow, 2001). This can be particularly relevant for how measurements of particulate organic carbon (POC) and of particulate organic nitrogen (PON) are interpreted for e.g., model validation and data-model comparisons.

Compared to TEP, information about CSP in marine environments is scarce. Long and Azam (1996) suggested that CSP and TEP are separate particles with CSP exceeding TEP abundance by a factor of up to three. Since CSP contain valuable proteins, it is likely that their polymeric precursors are not actively exuded by the cell but rather originate from cell lysis and breakage by (sloppy) zooplankton grazing. Likewise, the different biochemical composition and carbon to nitrogen ratio of TEP and CSP should differ. TEP and CSP thus have different biochemical and consequently physicochemical properties and satisfy different resource needs of heterotrophic consumers, potentially resulting in different biological degradation patterns. We therefore expect that the environmental control and hence the spatial and temporal patterns of TEP and CSP abundance in the ocean are distinguishable. Indeed, previous studies corroborated distinct properties and dynamics for TEP and CSP. By visual inspection, Cisternas-Novoa et al. (2015) noted different shapes, sizes of TEP and CSP from seawater microcosms, marine algal cultures, and freshwater. Moreover, depth distribution of TEP and CSP was found to diverge in samples from the Sargasso Sea, and Arctic Ocean (Cisternas-Novoa et al., 2015; Busch et al., 2017).

As their organic components originate from microbial production, primarily photosynthesis, marine gels represent a substrate for marine microorganisms to attach and grow upon (Bar-Zeev et al., 2012; Verdugo, 2012). Marine gels therefore often represent hotspots of microbial metabolic activity. Due to a high stickiness, they accelerate particle coagulation and therewith potentially enhance the export of carbon to the deep sea (Engel et al., 2002). Moreover, hydrogel networks accumulate at the air-sea interface, from where they may be emitted to the atmosphere and enter the atmospheric aerosols pool or become nuclei for cloud condensation, depending on their size (Wurl and Holmes, 2008; Cunliffe and Murrell, 2009; Orellana and Leck, 2015).

Despite the presumed importance of microgels, the current knowledge of the quantitative distribution of TEP and CSP in the ocean is still low, severely limiting an assessment of the global significance of marine gels. The size of marine gel particles is an important trait and variations in particle size spectra are particularly useful, as they can inform about formation and loss processes. Thus, changes in the size spectra of biogenic gel particles may be indicative of a variety of ecological and physical processes in the ocean. Here, size spectra of TEP and CSP are depicted and discussed, comparing three different ocean regimes: (a) Polar Seas, (b) Eastern Boundary Upwelling Systems, and (c) the oligotrophic open ocean. We show the vertical distribution of TEP and CSP, and in comparison to dissolved organic carbon (DOC), from the surface to the deep sea. We discuss how these observed distributional patterns relate to the productivity and particle dynamics of these distinct oceanic regimes.

MATERIALS AND METHODS

Sampling Sites

Samples were collected during six cruises to different oceanic regimes, representing 1. open ocean sites: with 1.1 the tropical Indian Ocean and 1.2 the subtropical South West Pacific (SWP), 2. Polar Seas: with 2.1 the Arctic Ocean and 2.2 the Southern Ocean, and 3. Eastern Boundary Upwelling Systems (EBUS): with 3.1 the Eastern Tropical North Atlantic (ETNA), and 3.2 the Eastern Tropical South Pacific (ETSP) (**Figure 1**). During all cruises the depth of the water column at the sampling stations exceeded 1000 m, allowing for attributing data to the epipelagic (0–200 m), mesopelagic (200–1000 m), and bathypelagic ocean (>1000 m). More information about the timing and sampling location is given in **Table 1**. All samples were collected at discrete depths in the water column using Niskin bottles attached to a CTD rosette and processed onboard immediately after sampling. Information on the depth distribution of microgels during ARK29 (Arctic Ocean) and on their bacterial colonization can also be found in Busch et al. (2017).

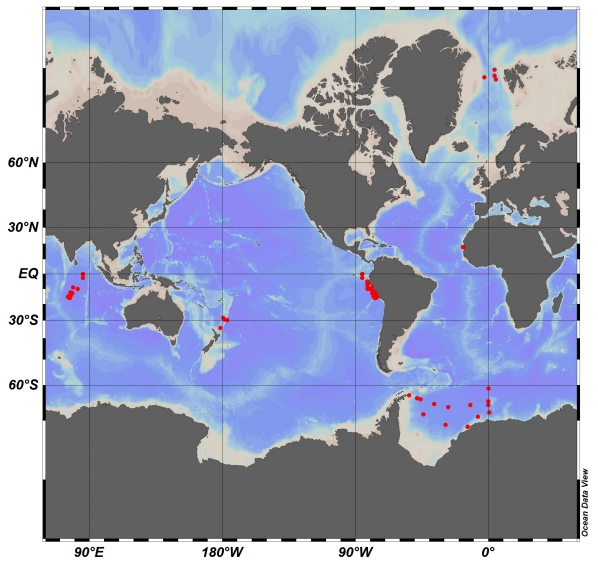

FIGURE 1 | Global map showing the sampling stations at the six different sampling sites.

Analysis of Microgels

Two classes of microgels, i.e., the transparent exopolymer particles (TEP) and the Coomassie stainable particles (CSP), were analyzed by microscopy and semi-automated image analysis following the protocol by Engel (2009). For each sample, 10–250 mL of seawater were filtered onto 0.4 μm Nuclepore membrane filters (Whatman). The volume of samples was selected based on microscopic inspection of the filter directly on board of the research vessel and assuring that the filters contain neither too little nor too high amounts of particles. In particular, a too high particle load should be avoided to allow for later identification of individual particles using automated image analysis. TEP were stained with 1 mL Alcian Blue solution, CSP with 1 mL Coomassie Brilliant Blue G (CBBG) working solution. Filters were mounted onto Cytoclear© slides and stored at −20°C until microscopic analysis in the home laboratory. Abundance, area and size-frequency distribution of TEP and CSP in the size range 1–760 μm were determined after Engel (2009) using a light microscope (Zeiss Axio Scope A.1) connected to a camera (AxioCAM Mrc). Filters were screened at 200× magnification. About 30 pictures were taken randomly from each filter in two perpendicular cross-sections (15 pictures each; resolution 1040 × 1040 pixel, 8-bit color depth). The image analysis software WCIF ImageJ (Version 1.44, Public Domain, developed at the US National Institutes of Health, courtesy of Wayne Rasband, National Institute of Mental Health, Bethesda, MD, United States) was used to semi-automatically analyze particle number and area. Blank filters for TEP and CSP yielded total microgel area values of up to 0.01 cm^2 L^{-1}; we therefore define 0.01 cm^2 L^{-1} as the detection limit of microgels in this study.

The carbon content of TEP (TEP-C) was estimated after Mari (1999) using the size-dependent relationship:

$$TEP - C = a * \sum_i n_i * r_i^D \quad (1)$$

with n_i being the number of TEP in the size class i and r_i being the mean equivalent spherical radius of the size class. The constant $a = 0.25 * 10^{-6}$ (μg C) and the fractal dimension of aggregates $D = 2.55$ were proposed by Mari (1999). To relate to organic carbon concentration in seawater, concentrations of TEP-C are given as μmol L^{-1}, depth-integrated data as mmol m^{-2}.

Continuous size spectra (particle concentration size densities) of CSP and TEP were derived from discrete microscopic counts of particles that were sorted into 19 size intervals between 0.625 and 640 μm equivalent spherical diameter (ESD). Kernel density estimates (KDEs) were computed, based on Gaussian kernels of logarithmic particle size, for resampled subsets of every microscopic sample, mainly to achieve robust size density estimates together with confidence limits. For every subsample the total particle concentration was divided by a factor of three, which implies a maximum precision of 3 particles mL^{-1}.

TABLE 1 | Cruise and sampling information for gel particles.

Region	Latitude range (°N)	Longitude range (°E)	Cruise	Year	Depths	#
Arctic Ocean	78.60/79.82	−2.71/5.07	ARK29	2015	E: 5–200	24
Fram Strait			RV Polarstern		M: 250–1000	13
					B: 1500–2282	12
Southern Ocean	−63.22/−71.36	7.02/−53.70	PS103	2016	E: 2–150	87
Weddell Sea			RV Polarstern		M: 297–999	7
					B: 1001–4821	19
ETNA	18.00/18.19	−16.65/−17.28	M107	2014	E: 10–160	31
Mauretanian			RV Meteor		M: 200–700	14
Upwelling					B: 1001–2100	4
ETSP	−5.00/−15.40	−75.36/−81.83	M91	2012	E: 3–199	82
Peruvian			RV Meteor		M: 200–700	28
Upwelling					B: 1001–1502	12
Indian Ocean	−2.67/−10.50	62.50/72.02	SO235	2014	E: 10–150	19
Open ocean			RV Sonne		M: 200–750	7
					B: 1001–4051	10
SWP	−28.50/−34.23	176.82/179.60	SO255	2017	E: 2–183	21
Open ocean			RV Sonne		M: 202–999	7
					B: 1004–4005	5

Indicated are the minimum and maximum depths where samples were collected in the E, Epipelagic Ocean; M, Mesopelagic Ocean; B, Bathypelagic Ocean. Number of samples: #.

The consideration of only one third of all particles in a subsample reduces computing time for the derivation of KDEs considerably. We note that the so derived size spectra of subsamples were again multiplied by this factor and the integral over all sizes is, in the end, similar to the original total particle concentration. Log-transformed values of ESD were randomly assigned to all subsampled particles, assuming a uniform probability distribution on logarithmic scale, according to the size interval of the particles. Ultimately, mean continuous particle size spectra were calculated from a series of KDEs for specified depth ranges ($z \leq 200$ m, 200 m $< z \leq 1000$ m, and z > 1000 m) for the different sampling regions. The number of samples (=number of KDEs) of every depth range for every region is listed in **Table 1**. We determined respective 95% confidence regions as $\pm 1.96 \times$ standard errors of the corresponding mean particle spectrum (mean of subsample KDEs).

Microgel abundance in the ocean has previously been quantified for specific regions using the microscopical approach, as in this study, or colorimetric methods (Passow and Alldredge, 1995; Cisternas-Novoa et al., 2014). TEP-C data have been derived from both methods and compare generally well, although TEP-C concentrations derived from the colorimetric method seem to be generally higher than those from microscopy (Engel and Passow, 2001). We accounted for this offset, when estimating TEP-C concentration from published colorimetric TEP concentration by using the empirical relationship of Engel and Passow (2001):

$$[TEP - C]_{SFD} = 0.05 * [TEP]_{color} \quad (2)$$

Here $[\text{TEP-C}]_{\text{SFD}}$ is the TEP-C concentration [μmol L^{-1}] corrected for the offset between the methods and $[\text{TEP}]_{\text{color}}$ is the TEP concentration [μg Xeq. L^{-1}] determined by the colorimetric method. Comparing derived TEP-C concentrations is meaningful where data on TEP concentration or abundance are available. However, for some regions included in this study, such as the open Indian Ocean or the SWP, no previous observations on microgels can be found in the literature. Moreover, data on microgel abundance below the surface ocean are largely lacking. Thus, many of our data can only be compared to previous studies on a wider scale, referring to ocean basins or trophic systems rather than to exactly the same sampling region.

Dissolved Organic Carbon (DOC)

Samples for the determination of DOC concentration (20 mL) were collected in combusted glass ampoules after filtration through combusted GF/F filters (8 h, 500°C) or through GHP membrane filters (Pall) after rinsing with 20 mL of MilliQ water and sample. Samples were acidified with 80 μL of 85% phosphoric acid or 20 μL of 30% hydrochloric acid, flame sealed and stored at 4°C in the dark until analysis. DOC samples were analyzed by applying the high-temperature catalytic oxidation method (TOC-VCSH, Shimadzu) modified from Sugimura and Suzuki (1988). Every 8–10 days, the instrument was calibrated with standard solutions of 0, 500, 1000, 1500, 2500, and 5000 μg C L^{-1}, prepared from a potassium hydrogen phthalate standard (Merck 109017). Every measurement day, ultrapure (MilliQ) water was used to determine the instrument blank, which was accepted for values <1 μmol C L^{-1}. Organic carbon analysis was furthermore validated on every measurement day with deep seawater reference (DSR) material provided by the Consensus Reference Materials Project of RSMAS (University of Miami) yielding values within the certified range of 42–45 μmol C L^{-1}. DOC concentration was determined in each sample from 5 to

8 injections. The precision was <4% estimated as the standard deviation of replicate measurements divided by the mean.

Data Analysis

Average values are given by their arithmetic mean value and standard deviation unless otherwise stated. Coefficients of variation were calculated as relative standard deviation (%). Depth-integrated values for the water column were based on average concentration and water column depth. Student's *t*-tests were applied for comparison of averages. Statistical tests in data analysis have been accepted as significant for $p < 0.05$. Calculations, statistical tests and illustration were performed with Microsoft Office Excel 2010, Sigma Plot 12.0 (Systat), and Ocean Data View (Schlitzer, 2015).

RESULTS

Total Microgel Abundance and DOC Concentration at the Study Sites

To compare data between different oceanic sites and to identify overarching patterns in the distribution, we calculated the average abundance of marine microgels in terms of total area per volume for the epi-, meso-, and bathypelagic ocean at each sampling site and compared the spatial variability of microgels to that of DOC concentration (**Figure 2**). DOC distribution is driven by water mass transport and DOC concentration exhibits relatively little variability over time and space, in particular in the deeper water column where the majority of DOC is included in refractory compounds with turn-over times of more than 100 years (Hansell, 2002).

In general, DOC concentration decreased with depth, following previously described patterns. For the epipelagic ocean, observed DOC concentrations ranged from 56 μmol L^{-1} in the Southern Ocean to 73 μmol L^{-1} in the SWP. At mesopelagic depths, DOC concentration was more similar between the ocean regimes and ranged from 47 to 53 μmol L^{-1}. Highest DOC concentration at those depths was observed again in the SWP. In the bathypelagic ocean, variability in DOC concentration was further reduced, approaching concentrations between 43 and 49 μmol L^{-1}.

The abundance of both classes of microgel particles exhibited greater spatial variability than observed for DOC concentration. Overall, we observed variation coefficients to range between 0.5 and 35% for DOC, between 28 and 202% for TEP and between 45 and 292% for CSP. Thereby, microgel abundance did not only vary between oceanic sites but also pronounced over depth. The range of abundance was similar for both gel types, with slightly higher values for CSP than for TEP in particular in the epipelagic ocean where highest microgel abundance was observed. Here, TEP varied from 0.08 cm^2 L^{-1} in the SWP to 2.59 cm^2 L^{-1} in the ETNA, and CSP from 0.03 cm^2 L^{-1} in the Indian Ocean to 2.90 cm^2 L^{-1} in the ETSP. Hence, highest microgel abundance was observed in surface waters of EBUS, while lowest abundance was observed at the two open ocean sites; the tropical Indian Ocean and the subtropical SWP. Microgel abundance in mesopelagic waters was significantly lower than in the epipelagial ($p = 0.01$, $n = 12$). For both TEP and CSP, lowest abundance in the mesopelagial was observed for the Southern Ocean, while highest values were determined in the ETNA. Thereby, TEP abundance in the mesopelagial was rather uniform between the different oceanic sites, apart from high values observed in the ETNA. TEP abundance at even greater depths of the bathypelagial was similar to the mesopelagial with values ranging from 0.03 to 0.08 cm^2 L^{-1} and highest values observed again at the ETNA site with 0.97 cm^2 L^{-1}. For CSP, the regional distribution pattern seen in the mesopelagial also persisted in the bathypelagial, with highest abundance observed at the upwelling sites (ESTP: 0.30 cm^2 L^{-1}, and ETNA: 0.92 cm^2 L^{-1}), and lowest in the Southern Ocean (0.02 cm^2 L^{-1}). No significant relationship was observed between DOC concentration and microgel abundance.

Size Spectra of Microgels

Size spectra for TEP and CSP were calculated for each sample and averaged for the three depth-layers. Abundant particles (>3 mL^{-1}) were determined in the size range 0.7–100 μm for both TEP and CSP, with particle abundance declining with increasing size. Although previously assumed, a single power-law relationship, $y = ax^{-b}$, seems inappropriate for describing the whole size spectra of both types of microgels. On logarithmic scale, this becomes particularly evident for particle sizes smaller than ∼6 μm, where the spectral slope appears to be smaller than for gel particles of larger size. The estimation of two distinct slopes for every TEP or CSP size spectrum would require an exact separation between these two size ranges, which is beyond the scope of this study. Rather than comparing differences between slope estimates, we hereafter focus on predominant differences in size spectra at the different ocean sites.

The two open ocean sites, tropical Indian Ocean and subtropical SWP respectively, had the lowest microgel abundance in the epipelagial and also revealed similar patterns in their size spectra (**Figures 3A,B**). A noticeable difference was the absence of gel particles larger than 50 μm in the SWP samples, while few particles of larger size (up to ∼100 μm) were also measured in the Indian Ocean. At the Indian Ocean stations, size spectra of TEP and CSP at depths below 200 m were alike. This was also true for TEP size spectra in the SWP, while CSP in the size range 3–30 μm showed slightly lower values in the bathypelagial compared to the mesopelagial. Similar patterns between these two sites were also observed for the relative contribution of CSP to total microgel abundance ([CSP]/([CSP] + [TEP])). In general, CSP were more abundant than TEP in all size classes < 60 μm, except for the bathypelagial in the size range 2–∼10 μm, where both gel types either contributed equally (Indian Ocean) or TEP dominated (SWP). The contribution of CSP to total gels increased with size up to ∼30 μm and decreased from surface to depth. However, for the group of very small microgels (<2 μm) highest CSP contributions were observed in the bathypelagial at both sites.

A clear separation of size spectra with depth was observed for the two polar ocean sites (**Figures 3C,D**), with larger microgels being clearly more abundant than at the two tropical/subtropical open ocean sites. While in surface waters of the Arctic Ocean larger gels (>30 μm) were dominated by CSP, larger TEP strongly contributed to the pool of microgels in the Southern Ocean.

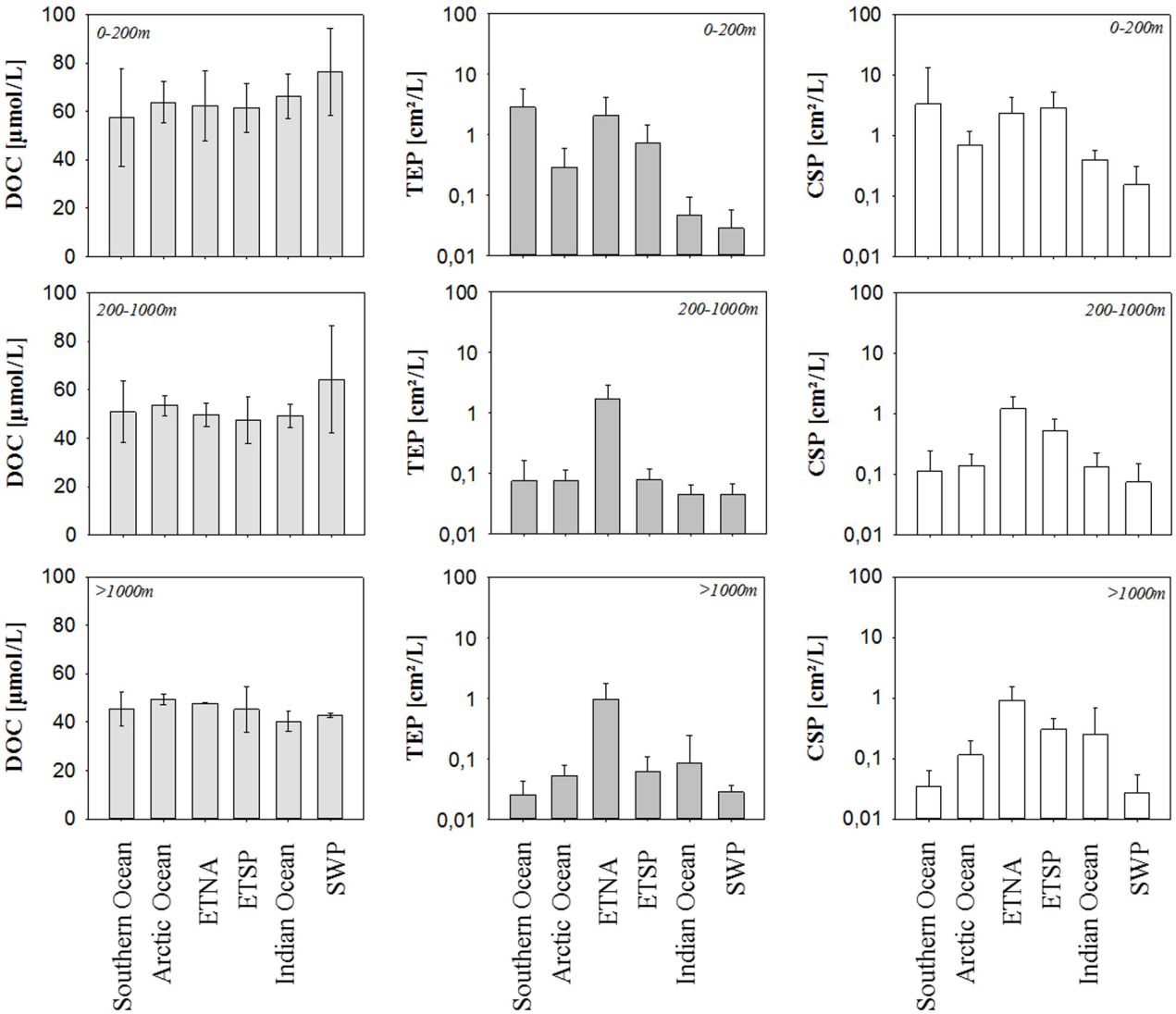

FIGURE 2 | Average concentrations of DOC, TEP, and CSP in the epipelagic, mesopelagic, and bathypelagic ocean of the six study sites. Error bars indicate ± 1 SD. Note log scale for TEP and CSP.

However, surface waters of both polar sites also exhibited a relative increase of CSP in the mid- size range, i.e., between 3 and 30 µm. In general, more than 50% of all microgels >3 µm in the epipelagial of the Arctic Ocean were CSP. Interestingly, CSP in the size range 2–30 µm were underrepresented in the meso- and bathypelagical of both polar ocean sites.

Similarities in size spectra of microgels were also determined for the two EBUS regions, ETNA and ETSP (**Figures 3E,F**). Here, abundance of microgels, and in particular of larger microgels, was highest compared to the polar and open ocean sites. Thereby a high abundance of larger gels was not only observed in the epipelagic but throughout the water column. Differences between size spectra of the depth ranges were less pronounced than at the polar and open ocean sites. In the ETSP, CSP dominated the pool of microgels at all sizes. A peculiarity of microgel size spectra in upwelling regions was the increase of the relative CSP fraction with depth seen for all size classes <60 µm in the ETSP and for all size classes <6 µm in the ETNA. This may point to reduced degradation of CSP in the deeper water column or to enhanced sources of CSP at depth. Highest contribution of CSP to the microgel pool was observed in the bathypelagial, followed by the meso- and the epipelagial. At the ETSP, CSP clearly dominated the pool of microgels <50 µm, contributing >80% to total microgels.

Comparing all sites, a clear indication for higher abundance of microgels >20 µm with higher total microgel abundance was evident, suggesting that the size spectra of both particle types render the process of aggregation (**Figure 4**). We note that the number of particles >20 µm is less than 1% of the total abundance. The abundance of CSP and of TEP were of similar magnitude and their dependencies between particle concentrations with ESD >20 µm and

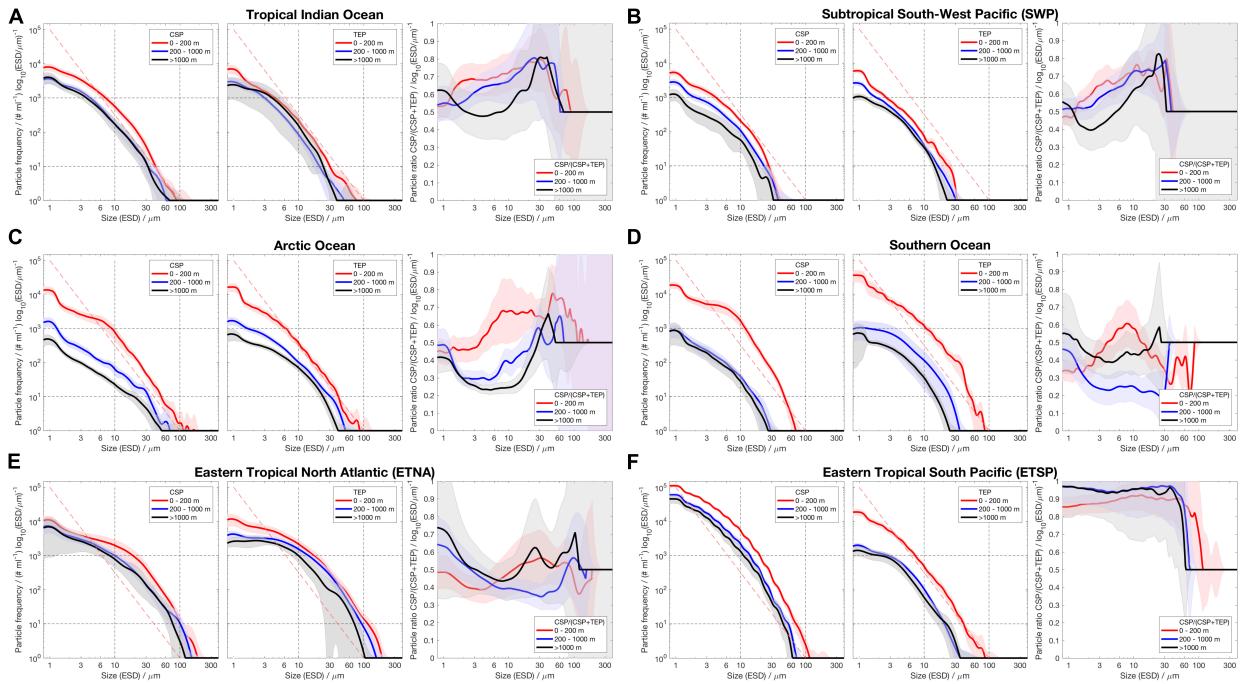

FIGURE 3 | (A–F) Average size frequency distributions of TEP and CSP within the epipelagic (red lines), mesopelagic (blue lines), and bathypelagic (black lines) ocean as well as the respective fractions of CSP over size. Gray shadings indicate the ranges of uncertainty. **(A)** Tropical Indian Ocean, **(B)** Subtropical South-West Pacific (SWP), **(C)** Arctic Ocean, **(D)** Southern Ocean, **(E)** Eastern Tropical North Atlantic (ETNA), **(F)** Eastern Tropical South Pacific (ETSP).

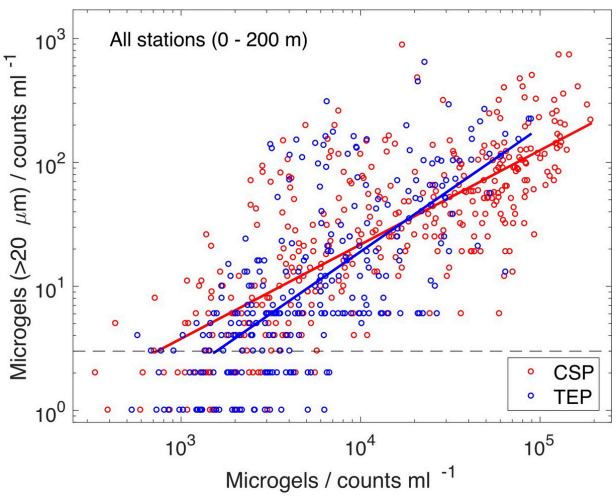

FIGURE 4 | The abundance of microgels with ESD >20 µm increased with the number of total abundance of microgels (Pearson correlation coefficients, ρ_{CSP} = 0.76 and ρ_{TEP} = 0.71). The lines are best estimates (root mean square minimizations on logarithmic scale), assuming a linear relationship between log-transformed values of microgel abundance with ESD >20 µm and total abundance (Σ): $f_{CSP} = 0.76 \cdot [\log_{10}(\Sigma_{CSP}) - 2.24]$ (red line), and $f_{TEP} = 1.0 \cdot [\log_{10}(\Sigma_{TEP}) - 2.72]$ (blue line).

respective total abundance compare well. Variations in total abundance range between 10^3 and 10^5 particles mL^{-1}. The logarithm of the abundance of microgels larger than 20 µm, f(ESD > 20µm), can be approximated with a log-linear relationship, $f_{CSP/TEP} = a \cdot [\log_{10}(\Sigma_{CSP/TEP}) - b]$, where Σ is the total abundance of either CSP or TEP. We combined all respective data of the upper 200 m and minimized root mean square errors of the above described log-linear relationship. Our parameter estimates for TEP (a = 1.0, b = 2.72) turned out to be similar to those for CSP (a = 0.76, b = 2.24). This indicates that the underlying coagulation dynamics (e.g., collision rates and stickiness) of TEP and CSP are likely comparable. In spite of the large variability, we can consolidate a dependency between the number concentrations of particles with ESD >20 µm and total particle abundance. This is possible because of the sufficiently large number of independent datasets available.

Contribution of TEP-C to the Organic Carbon Pool

Concentration of carbon included in TEP (TEP-C) was assessed from abundance and size of particles (Eq. 1) (**Table 2**). The amount of TEP-C relative to the pool of DOC ([TEP-C]:[DOC]), which represents the largest fraction of the total organic carbon pool in surface waters and almost the entire pool in the deep sea (Hansell, 2002), varied strongly between the study sites (**Figure 5**). In the oligotrophic areas of the Indian Ocean and the SWP the depth-integrated pool of TEP-C was largest for the bathypelagial, followed by the mesopelagial and epipelagial. This goes along with the much larger total volume of the deeper ocean compared to the layers above. [TEP-C]:[DOC] was in general less than ∼0.1% throughout the water-column at these sites. In the Arctic and Southern Ocean, a higher amount of TEP-C was observed in the epipelagial, both in terms of

TABLE 2 | Concentrations of carbon contained in TEP (TEP-C) for different stations and depths of the global ocean.

Station	Depth layer	TEP-C (μmol L^{-1})	
		Mean	±SD
Arctic Ocean	E	0.68	0.51
	M	0.14	0.08
	B	0.11	0.09
Southern Ocean	E	3.33	9.71
	M	0.11	0.13
	B	0.03	0.03
ETNA	E	7.10	6.61
	M	4.01	3.53
	B	1.86	1.52
ETSP	E	0.79	1.06
	M	0.13	0.08
	B	0.07	0.07
Indian Ocean	E	0.40	0.18
	M	0.14	0.09
	B	0.25	0.45
SWP	E	0.10	0.04
	M	0.05	0.02
	B	0.03	0.01

total integrated carbon and relative to the DOC pool. At both polar sites, integrated TEP-C values were clearly lower in the meso- than in the epi- and bathypelagial, indicating substantial TEP-C degradation in this layer. Although the depth-integrated amount of TEP-C and the [TEP-C]:[DOC] ratio in the epi- and mesopelagial of the Southern and Arctic Ocean were similar, the bathypelagial of the Southern Ocean showed the least amount of TEP-C of all sites investigated, yielding a total of 0.6 mmol TEP-C m^{-2} and <0.03% DOC.

The highest amounts of total depth-integrated of TEP-C were observed at the two upwelling sites. Interestingly, accumulation of TEP in the bathypelagial leads to a high standing stock of TEP-C, equivalent to >0.1% DOC. In the ETNA the concentration of TEP-C corresponded to ∼10% of DOC concentration in the epipelagial, and to >1% of DOC concentration in the deepest samples. In contrast to the ETSP and to most other sites, the integrated amount of TEP-C continuously increased over depth, suggesting that the export of TEP-C to depth in the ETNA is faster than its degradation.

DISCUSSION

Over the past three decades, organic microgels in the marine environment have gathered attention by scientists from a wide range of disciplines, and with respect to different processes such as element and in particular carbon cycling, microbial ecology, air-sea exchange, transport of pollutants such as oil, toxins and microplastic, as well as seawater desalination. Yet our ability to quantify microgels in the environment, to determine their chemical heterogeneity, as well as their continuous size range is limited by available analytical methods. Extracting three-dimensional, fractal gel particles onto membrane filters, staining, and subsequent measurement of their two dimensional size introduces inevitable inaccuracies. Likewise, estimating their main chemical components by compound-specific stains that may target one but not all components is prone to error. Finally, for quantification of the carbon content of microgels empirical conversion factors are commonly applied that may not be universally applicable and may only be representative for the microgel population sampled at a particular site.

Here, we applied a direct counting and sizing method to quantify microgel distribution in the ocean. In general, we enumerated and sized between 10^2 and 10^4 microgels per sample with replicate samples per depth and several stations per sampling site. In spite of methodological limitations, we found consistent characteristics as well as detailed patterns in our analysis of CSP and TEP, even amongst measurements that were collected at distinct ocean sites. Based on the large number of observations and with analytical restrictions kept in mind, we could derive robust size spectra of microgels that reveal discriminable features in abundance and in size structure along vertical gradients and between different oceanic regimes.

Changes and Differences in Marine Microgel Size Spectra

Variations in microgel size spectra are subject to various processes that can act on similar or overlapping size ranges. For the size range smaller than 5 μm, marine microgels are hypothesized to form by spontaneous assembly of free polymer chains of biogenic origin (Chin et al., 1998; Ding et al., 2009), with the surrounding seawater being the major solvent. Although the mechanism of microgel formation can be identical, the process that generates polymeric precursors of protein enriched CSP and of polysaccharide enriched TEP may differ, if only exopolysaccharides and no proteins are actively exuded by phytoplankton. Whether proteins are actively released by phytoplankton remains unclear (Thornton, 2014), but we may assume that there is no benefit for phytoplankton to expend energy on producing extracellular proteins. A primary source of free protein enriched polymers can rather be attributed to compounds of the cytoplasm released via lysis of starved or infected cells, or by the breaking of prey cells as a result of zooplankton grazing (e.g., Møller, 2007; Saba et al., 2011). Differences in the abundance of small sized CSP and TEP in the productive epipelagial can be interpreted accordingly.

The process of generating microgels larger than ≈5 μm can be well-described by the coagulation theory, where the size of gels increases over time as a consequence of continued aggregation (Mari and Burd, 1998). The aggregation rate depends on the total particle concentration, the collision rate, and the stickiness of the particles (McCave, 1984; Burd and Jackson, 2009). The presence of microgels enhances the total number of particle collisions and can thus effectively promote the formation of larger aggregates that involve other particulate organic matter (POM). We note that the microscopic size measurements of the CSP and TEP are two dimensional projections of fractal structures that can already incorporate smaller phytoplankton cells, detritus and bacteria.

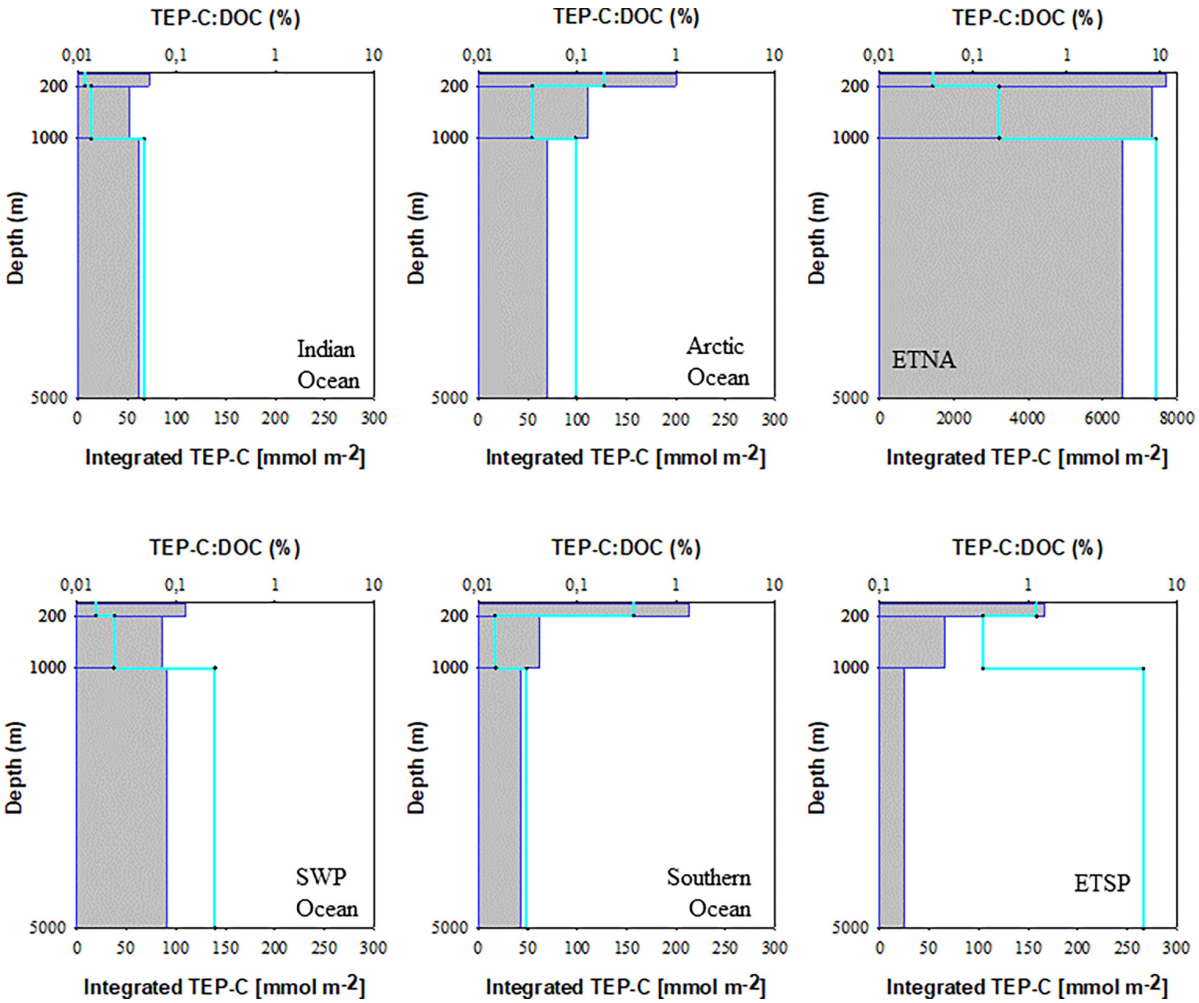

FIGURE 5 | Depth-integrated carbon content of TEP (green line) and TEP-C percentage of DOC (gray bars) for the three studies depth layers of the six study sites.

As TEP and CSP become larger their composition become more heterogeneous (e.g., colonization by bacteria) and their size spectra may eventually coincide with those of typical composite gel-POM aggregates that sink. The number of larger composite aggregates is much lower than of smaller microgels and these particles are hardly captured by the small volumes of our water samples (10–250 mL). Although less abundant, the vertical flux of larger composite gel-POM aggregates and their gradual breakdown (reverse aggregation) likely generate CSP and TEP within the size range <100 μm at depth. Changes in respective size spectra with depth should thus indicate how efficient microgels are exported from the epipelagial, and hydrolyzed and remineralized within the mesopelagial and bathypelagial.

The ingestion of microgels by heterotrophic flagellates and ciliates can introduce variations within specific size ranges. Furthermore, a higher abundance of TEP was shown to incorporate a greater fraction of total bacteria within microgel aggregates (e.g., Mari and Kiørboe, 1996; Mühlenbruch et al., 2018), with implications for the microbial foodweb. Mari and Rassoulzadegan (2004) interpreted the formation and coagulation of microgels and the embedding of bacteria and heterotrophic nanoflagellates in small gel-aggregates as a "trophic elevator" that transfers DOC to higher trophic levels. On the one hand, this mechanism can introduce valuable proteins and carbohydrates as food source for some ciliates whose optimum prey particle size is larger than the size of nanoflagellates and bacteria. Likewise, such trophic elevator has been shown to be active for copepods as well (Ling and Alldredge, 2003). On the other hand, this mechanism can also bypass valuable food as soon as the mixed microgel aggregates become larger than the prey particle size utilizable by some ciliate, e.g., as shown by Mari and Rassoulzadegan (2004) for the ciliate *Strombidium sulcatum*, whose optimum and maximum prey sizes are approximately 3 and 6 μm, respectively. Interestingly, it is this particular size range in our size spectra of CSP and TEP that vastly deviates from a log-linear relationship according to coagulation theory. However, our spectra between 1 and 6 μm are coarse, which limits making inferences on gel-induced microbial dynamics. In order to resolve changes in microgel size spectra due to variations in the microbial

foodweb dynamics in future studies, we suggest deriving KDE size spectra directly from all counted gel particles and their respective individual sizes rather than assigning them to size intervals.

We briefly addressed above the various potential processes that can shape the size spectra of CSP and TEP. Hereafter, we will reconsider some of these aspects in our discussion of the differences between the size spectra at the different ocean regimes.

Global Patterns of Microgel Distribution

Lowest microgel abundance was observed at the two tropical/subtropical open ocean sites of the Indian Ocean and SWP. Both sites are characterized by annually low primary productivity and low surface ocean nutrient concentrations, making them representative sites for the oligotrophic open ocean. As autotrophic production is the major source for biopolymers and microgels, low amounts of microgels observed at these sites throughout the water column likely mirror the low productivity of the system. Low average abundance of TEP (<20 μg Xeq. L^{-1}, equivalent to <1 μmol TEP-C L^{-1}) has previously been observed in the epipelagial of the tropical western Pacific Ocean by Yamada et al. (2017), according with our estimates for the tropical/subtropical open ocean sites (**Table 2**). In the epipelagial of the Indian Ocean, relatively higher amounts of TEP were only seen in the small size fraction (<3 μm), whereas CSP clearly exceeded TEP abundance at all sizes. Like in other tropical systems, picoplankton, including picoeukaryotes, *Prochlorococcus* spp., and in particular *Synecchoccus* spp., had a relatively high contribution to total autotrophic biomass during the Indian Ocean cruise in 2014, as indicated by pigment composition and their share of total chl *a* concentration (Booge et al., 2018). In cultures of *Synecchococcus* spp. a higher production of CSP relative to TEP was observed, with larger microgels also including relatively high amounts of CSP (Cisternas-Novoa et al., 2015). In the absence of larger autotrophs, microgel production may thus be low and driven by picoplankton like *Synecchococcus*. Comparatively low amounts of microgels in the deeper water column of these two study sites suggest little export of microgels in oligotrophic seas. In fact, with ∼0.03 cm^{-2} L^{-1} the bathypelagial of the SWP showed lower amounts of microgels suggesting very low if any input of microgels from overlying waters. This observation is in good accordance with coagulation theory, predicting aggregation rates as a function of total particle abundance (Logan et al., 1995). Hence, aggregation and subsequent sinking of larger particles may be less relevant for microgel loss than heterotrophic degradation in tropical/subtropical systems.

Data from both polar sampling sites showed clear accumulation of microgels in the size range 3–30 μm in the epipelagial compared to the deeper parts of the water column. This accumulation was more pronounced for CSP than for TEP, leading to a relative enrichment of mid-sized CSP in surface waters. Whilst, higher abundance of microgels was observed in the epipelagial of the Southern Ocean, the mesopelagial showed surprisingly similar values for both sites and for both types of microgels. This suggests a substantial loss of microgels in the twilight zone, in particular for protein containing microgels. Microgel degradation is likely driven by microorganisms colonizing the particles and subsiding on their organic content (Grossart et al., 2006; Busch et al., 2017; Zäncker et al., 2019). In polar waters extracellular enzymatic activity has been observed to be higher for proteinaceous material than for sugars, leading to the assumption that polar bacteria degrade proteinaceous organic matter preferentially (Christian and Karl, 1995; Piontek et al., 2014). This view is in accordance with faster decomposition of CSP relative to TEP as suggested previously for the Arctic Ocean by Busch et al. (2017).

High amounts of TEP in surface waters of the Arctic Ocean and specifically inter-annual variability of TEP in the epipelagic Fram Strait have previously been related to the occurrence of the prymnesiophyte *Phaeocystis* spp., specifically to *P. pouchetii* (Engel et al., 2017). *Phaeocystis* spp. is one the main bloom forming phytoplankton species also in the Weddell Sea and was readily abundant during the PS103 cruise (Nöthig, pers. comm.). *Phaeocystis* spp. produce copious amounts of polysaccharides (Alderkamp et al., 2007). Release of polysaccharides occurs from exponentially growing as well as from senescent cells and can induce TEP formation (Passow and Wassmann, 1994; Reigstad and Wassmann, 2007). Deep export of the typically neutrally buoyant gel particles, however, likely relies on the aggregation with heavier particles, acting as ballast material. Export of organic material, including microgels, that was produced during blooms of *Phaeocsystis* spp., may thus be restricted to shallow depths. Observations from the Arctic Ocean showed that carbon export attributed to *P. pouchettii* diminishes quickly over the upper few hundred meters (Reigstad and Wassmann, 2007), supporting relatively high remineralization rates (Le Moigne et al., 2015). Our data for both Polar regions show relatively high concentrations of microgels in the epipelagic zone that decrease rapidly over depth. This is in accordance with previous observations showing high TEP concentrations in the epipelagic Arctic Ocean (range: 5–517 μg Xeq. L^{-1}, equivalent to 0.25–26 μmol TEP-C_{SFD} L^{-1}; Engel et al., 2017) and in the epipelagic Southern Ocean (119 ± 39 μg Xeq. L^{-1}, equivalent to 6.0 ± 2.0 μmol TEP-C_{SFD} L^{-1}, Zamanillo et al., 2019a; <49 μg Xeq. L^{-1}, equivalent to <2.5 μmol TEP-C_{SFD} L^{-1}, Ortega-Retuerta et al., 2009), but relatively low TEP fluxes to depth (Ebersbach et al., 2014). A possible explanation is a high heterotrophic demand for labile organic matter in regions with primary production being temporarily restricted by solar irradiance. Indeed with 0.025 cm^2 L^{-1}, the bathypelagial of the Southern Ocean had lowest TEP concentration observed in this study, only little above the detection limit.

In contrast, high concentrations were observed for TEP and CSP in the ETNA upwelling region off Mauretania. High concentration in surface waters of the ETNA upwelling regions have been reported before. Zamanillo et al. (2019b) found the highest TEP concentration along a transect through the Atlantic Ocean in the coastal upwelling associated to the Canary current system (mean: 446 μg Xeq. L^{-1}, equivalent to 22 μmol TEP-C_{SFD} L^{-1}), even exceeding concentration observed in this study (**Table 2**). In the ETSP upwelling region off Peru, CSP concentrations were one order of magnitude higher than those

of TEP. This was a distinctive feature that clearly differs from our findings within the ETNA region. Yet, at both upwelling sites concentrations of microgels in the mesopelagial were higher than at all other sites, and clearly higher also in the bathypelagial of the ETNA. This suggests that highly productive systems, like EBUS, are deep export sites of microgels and therewith of bioavailable organic matter. Export of organic matter in the coastal upwelling system off North West Africa is driven by rapidly sinking particles, ballasted with biogenic minerals, in particular calcium carbonate, and by dust from the nearby Saharan desert (Fischer et al., 2009). Since microgels coagulate easily with other particles like phytoplankton and minerals, export within fast sinking aggregates could explain the observed high TEP concentration in the deep ETNA. Compared with the ETNA, TEP concentrations decreased much more below the epipelagial in the ETSP, suggesting a lower export efficiency of TEP in this system. The phytoplankton community of Peru is dominated by diatoms, dinoflagellates and coccolithophores, in particular during upwelling times. Those species are likely responsible for the observed high TEP concentration in the epipelagial. Yet, the upwelling regions along South West America are also known for their high trophic efficiency, leading to high grazing rates both by zooplankton and small pelagic fish such as anchovy. Thus, heterotrophic consumption in the epipelagial may diminish particle export to depth, resulting also in lower deep export of TEP. Sloppy feeding may also explain the relatively large amounts of CSP observed off Peru; here >80% of all gel particles <60 μm were CSP.

A remarkable feature of both EBUS sites was the relatively higher abundance of small CSP in the deep water column. Only in EBUS, CSP comprised the highest fraction of microgels in the bathypelagial, followed by the meso- and epipelagial. CSP are assumed to contain nutritionally valuable proteinaceous compounds, thus, the productivity signal of the epipelagial in upwelling systems can be traced down to bathypelagic depths. This was also apparent from our estimates of carbon contained in TEP. At both upwelling sites, the bathypelagial showed the highest depth-integrated concentration of TEP-C. Since no estimate for carbon content of CSP is yet available, we could not estimate the amount of carbon contribution of CSP. However, it can be assumed that CSP contribute substantially to organic C and N in upwelling systems, in particular in the ETSP. Here, those particles may even play an important role in organic matter cycling within the oxygen minimum zone (OMZ). Anaerobic microbial processes such as denitrification are often driven by particle associated bacteria, likewise anaerobic ammonium exudation (anammox) depends on organic nitrogen sources (Wright et al., 2012; Löscher et al., 2016). The role of CSP in suboxic zones like in the OMZ off Peru is yet to be exploited.

Connecting Microgels With Current Topics in Marine Research

Potential Sensitivity of Marine Microgels to Ongoing Environmental Change

Marine microgels play a fundamental role in carbon cycling. Around 10% of the annual oceanic primary productivity (45–55 Pg C yr^{-1}) is potentially channeled into TEP (Mari et al., 2017; Thornton, 2018), and likewise, similar values would be expected for CSP. Between 2005 and 2016, 2.6 ± 0.5 Gt C yr^{-1} of the atmospheric carbon dioxide emitted from human activities was absorbed by the ocean (Le Quéré et al., 2016), inducing higher carbon fixation rates through accelerated phytoplankton growth and release of extracellular substances and marine gels. The biological carbon pump, regarded as the ocean's ability to store fixed carbon plays an essential role in climate regulation (Jiao et al., 2010) and in fact, the absence of this mechanism would increase the atmospheric CO_2 concentration by 50% with respect to present-day values (Le Moigne, 2019). Climate change and related acidification and warming of the surface ocean are supposed to have a variety of consequences for marine carbon and nutrient cycles. Many recent studies highlight strong effects of warming and acidification on microbial metabolic rates and growth dynamics. Acidification and warming will presumably accelerate phytoplankton growth rates, trigger a shift toward pico- and nanophytoplankton (Keller et al., 1999; Sommer and Lengfellner, 2008; Lewandowska and Sommer, 2010; Sommer and Lewandowska, 2011), and increase the rate of extracellular release of organic compounds and the formation of gel particles (e.g., Obernosterer and Herndl, 1995; Engel et al., 2002, 2014; Otero and Vincenzini, 2004; Liu et al., 2010; Borchard and Engel, 2012; Endres et al., 2014). The accumulation of exopolymer substances under elevated CO_2 concentrations may reinforce the importance of gel particles in organic matter fluxes, and potentially increase carbon sequestration to depth in the future ocean (Arrigo, 2007; Engel et al., 2014). On the other hand, accelerated microbial degradation activities on gel particles may counteract the export fluxes to the deep sea preserving more organic matter in the surface ocean (Piontek et al., 2010; Endres et al., 2014). These scenarios are likely to happen in a warmer and more acidic future ocean but not necessarily at the same time and place. Instead, besides the effects on marine microbial communities and metabolic activities, the synergy of both warming and acidification may hinder the ability of seawater dispersed DOM to self-assemble into marine microgels: a moderate temperature increase (of about 2°C) is sufficient to slow this process, whereas acidification lowers the temperature threshold at which the reduction in DOM self-assembly is observed (Chen et al., 2015).

Microscopic plastic fragments and fibers, another recently recognized threat to the environment, are widespread in the oceans and have accumulated in the pelagic zone and sedimentary habitats. Due to their stickiness, gel particles may easily attach on such artificial particles (Michels et al., 2018) and the amount of both TEP and CSP increases in their presence (Galgani et al., 2019). Depending on plastic sizes, material, aging and shape, gel particles act as an accelerator for up- or downward transport of organic matter in the water column, modifying plastic particles buoyancy and bioavailability (Galloway et al., 2017) with potential consequences for global carbon sequestration and turnover.

Implications for Air-Sea Exchange

An increase in atmospheric carbon uptake not only affects the amount and flux of gel particles toward depth, but may also promote a vertical flux of gels toward the surface inducing the production of less dense and swollen structures (Mari, 2008). It is well-known that marine microgels accumulate in the sea-surface microlayer, which has been observed globally (Wurl and Holmes, 2008), and regionally (Leck and Bigg, 2005; Orellana et al., 2011; Engel and Galgani, 2016; Galgani et al., 2016; Dreshchinskii and Engel, 2017; Zäncker et al., 2017). Gels accumulate at the surface through bubble scavenging (Robinson et al., 2019). In EBUS, previous work reports an accumulation of CSP in the sea-surface microlayer independently from wind speed, while TEP dependency on wind speed was evident (Engel and Galgani, 2016). The higher response of TEP to wind speed compared to CSP was also observed during wind channel experiments, where higher wind speed shifted the size distribution of polysaccharidic gels toward smaller particles (Sun et al., 2018). Also, higher temperature can favor the presence of gels in the sea-surface microlayer (Yue et al., 2018). When gel particles are found in higher concentration in the sea-surface microlayer with respect to the underlying water, and confer the surface gelatinous slick-like properties, air-sea CO_2 exchange may be reduced by 15% (Wurl et al., 2016) due to the increased thickness of the diffusion layer; air-sea gas fluxes are particularly reduced at lower wind speeds (Jähne and Haußecker, 1998). Surface tension forces may compress the compounds at the sea-surface, including marine gels, which later can be ejected as sea-spray aerosols (SSA) through bubble bursting and white caps episodes (Frew and Liss, 2005; de Leeuw et al., 2011). During highly productive periods, a great fraction of SSA with r80 <1 μm (the radius of the particle at a relative humidity of 80%) has an organic composition (O'Dowd et al., 2004; de Leeuw et al., 2011). Many of these particles have a gel-like composition, suggesting that the abundance and size of marine gels in the sea surface may influence the organic fraction of SSA (Russell et al., 2010; Orellana et al., 2011). Aerosols are involved in climate radiative effects both directly, through aerosol optical thickness influencing radiative properties, and indirectly through the cloud-forming capabilities in the smallest size fractions (Andreae and Rosenfeld, 2008).

Marine microgels are thus essential elements in the cycling of carbon not only within the ocean's interior, but also across the air-sea interface; by mediating the exchange of gases and particles between the ocean and the atmosphere, marine microgels may thus play a significant role in the oceanic control over climate.

DATA AVAILABILITY STATEMENT

All datasets generated for this study are included in the article/supplementary material.

AUTHOR CONTRIBUTIONS

All authors listed have made a substantial, direct and intellectual contribution to the work, and approved it for publication.

FUNDING

This work was supported by the Helmholtz Association, by the German Research Foundation through the SFB 754 "Climate – Biogeochemistry Interactions in the Tropical Ocean" sub-project B9, and by the BMBF through SOPRAN II and III (Surface Ocean Processes in the Anthropocene, 03F0611C-TP01 and 03F0662A-TP2.2) and SO255 (03G0255A). This study was also a contribution to the BMBF funded project MicroArc (03F0902A). We thank the Hanse-Wissenschaftskolleg Delmenhorst, Germany, for sponsoring the "Marine Organic Biogeochemistry" workshop in April 2019. The workshop was funded by the Deutsche Forschungsgemeinschaft (DFG, German Research Foundation) – project number: 422798570.

ACKNOWLEDGMENTS

We thank the captains, chief scientists, and crews of the cruises SO235, SO255, PS103, ARK29, M91, and M107 for help and technical support. We are also grateful to the many people helping with sampling on board or with sample analysis in the lab in particular Anna Anschütz, Kathrin Busch, Vanessa Lampe, Alexandra Loginova, Jon Roa, Ruth Flerus, and several student workers.

REFERENCES

Alderkamp, A.-C., Buma, A. G. J., and van Rijssel, M. (2007). The carbohydrates of *Phaeocystis* and their degradation in the microbial food web. *Biogeochemistry* 83, 99–118. doi: 10.1007/s10533-007-9078-2

Alldredge, A. L., Passow, U., and Logan, B. E. (1993). The abundance and significance of a class of large, transparent organic particles in the ocean. *Deep Sea Res.* 40, 1131–1140. doi: 10.1016/0967-0637(93)90129-q

Andreae, M. O., and Rosenfeld, D. (2008). Aerosol-cloud-precipitation interactions. Part 1. The nature and sources of cloud-active aerosols. *Earth Sci. Rev.* 89(Pt 1), 13–41. doi: 10.1016/j.earscirev.2008.03.001

Arrigo, K. R. (2007). Carbon cycle: marine manipulations. *Nature* 450, 491–492. doi: 10.1038/450491a

Bar-Zeev, E., Berman-Frank, I., Girshevitz, O., and Berman, T. (2012). Revised paradigm of aquatic biofilm formation facilitated by microgel transparent exopolymer particles. *Proc. Natl. Acad. Sci. U.S.A.* 109, 9119–9124. doi: 10.1073/pnas.1203708109

Biersmith, A., and Benner, R. (1998). Carbohydrates in phytoplankton and freshly produced dissolved organic matter. *Mar. Chem.* 63, 131–144. doi: 10.1016/s0304-4203(98)00057-7

Booge, D., Schlundt, C., Bracher, A., Endres, S., Zäncker, B., and Marandino, C. A. (2018). Marine isoprene production and consumption in the mixed layer of the surface ocean – a field study over two oceanic regions. *Biogeosciences* 15, 649–667. doi: 10.5194/bg-15-649-2018

Borchard, C., and Engel, A. (2012). Organic matter exudation by *Emiliania huxleyi* under simulated future ocean conditions. *Biogeosciences* 9, 3405–3423. doi: 10.5194/bg-9-3405-2012

Burd, A. B., and Jackson, G. A. (2009). Particle aggregation. *Annu. Rev. Mar. Sci.* 1, 65–90. doi: 10.1146/annurev.marine.010908.163904

Busch, K., Endres, S., Iversen, M. H., Michels, J., Nöthig, E.-M., and Engel, A. (2017). Bacterial colonization and vertical distribution of marine gel particles (TEP and CSP) in the arctic fram strait. *Front. Mar. Sci.* 4:166. doi: 10.3389/fmars.2017.00166

Chen, C.-S., Anaya, J. M., Chen, E. Y. T., Farr, E., and Chin, W.-C. (2015). Ocean warming–acidification synergism undermines dissolved organic matter assembly. *PLoS One* 10:e0118300. doi: 10.1371/journal.pone.0118300

Chial, H. J., and Splittgerber, A. G. (1993). A comparison of the binding of Coomassie brilliant blue to proteins at low and neutral pH. *Anal. Biochem.* 213, 362–369. doi: 10.1006/abio.1993.1433

Chin, W.-C., Orellana, M. V., and Verdugo, P. (1998). Spontaneous assembly of marine dissolved organic matter into polymer gels. *Nature* 391, 568–572. doi: 10.1038/35345

Christian, J. R., and Karl, D. M. (1995). Bacterial ectoenzymes in marine waters: activity ratios and temperature responses in three oceanographic provinces. *Limnol. Oceanogr.* 40, 1042–1049. doi: 10.4319/lo.1995.40.6.1042

Cisternas-Novoa, C., Lee, C., and Engel, A. (2014). A semi-quantitative spectrophotometric, dye-binding assay for determination of Coomassie blue stainable particles. *Methods* 12, 604–616. doi: 10.4319/lom.2014.12.604

Cisternas-Novoa, C., Lee, C., and Engel, A. (2015). Transparent exopolymer particles (TEP) and Coomassie stainable particles (CSP): differences between their origin and vertical distributions in the ocean. *Mar. Chem.* 175, 56–71. doi: 10.1016/j.marchem.2015.03.009

Cunliffe, M., and Murrell, J. C. (2009). The sea urface microlayer is a gelatinous biofilm. *ISME J.* 3, 1001–1003. doi: 10.1038/ismej.2009.69

de Leeuw, G., Andreas, E. L., Anguelova, M. D., Fairall, C. W., Lewis, E. R., O'Dowd, C., et al. (2011). Production flux of sea spray aerosol. *Rev. Geophys.* 49:RG2001. doi: 10.1029/2010rg000349

Decho, A. W. (1990). Microbial exopolymer secretions in ocean environments: their role(s) in food webs and marine processes. *Oceanogr. Mar. Biolol. Annu. Rev.* 28, 73–153.

Ding, Y. X., Hung, C. C., Santschi, P. H., Verdugo, P., and Chin, W. C. (2009). Spontaneous assembly of exopolymers from phytoplankton. *Terr. Atmos. Ocean Sci.* 20, 741–747.

Dreshchinskii, A., and Engel, A. (2017). Seasonal variations of the sea surface microlayer at the Boknis Eck times series station (Baltic Sea). *J. Plankton Res.* 39, 943–961. doi: 10.1093/plankt/fbx055

Ebersbach, F., Assmy, P., Martin, P., Schulz, I., Wolzenburg, S., and Nöthig, E.-M. (2014). Particle flux characterisation and sedimentation patterns of protistan plankton during the iron fertilisation experiment LOHAFEX in the Southern Ocean. *Deep Sea Res. Part I Oceanogr. Res. Pap.* 89, 94–103. doi: 10.1016/j.dsr.2014.04.007

Endres, S., Galgani, L., Riebesell, U., Schulz, K. G., and Engel, A. (2014). Stimulated bacterial growth under elevated pCO2: results from an off-shore mesocosm study. *PLoS One* 9:e99228. doi: 10.1371/journal.pone.0099228

Engel, A. (2000). The role of transparent exopolymer particles (TEP) in the increase in apparent particle stickiness (alpha) during the decline of a diatom bloom. *J. Plankton Res.* 22, 485–497. doi: 10.1093/plankt/22.3.485

Engel, A. (2009). "Determination of marine gel particles," in *Practical Guidelines for the Analysis of Seawater*, ed. O. Wurl (Boca Raton, FL: CRC Press), doi: 10.1201/9781420073072.ch710.1201/9781420073072.ch7

Engel, A., and Galgani, L. (2016). The organic sea-surface microlayer in the upwelling region off the coast of Peru and potential implications for air–sea exchange processes. *Biogeosciences* 13, 989–1007. doi: 10.5194/bg-13-989-2016

Engel, A., Goldthwait, S., Passow, U., and Alldredge, A. (2002). Temporal decoupling of carbon and nitrogen dynamics in a mesocosm diatom bloom. *Limnol. Oceanogr.* 47, 753–761. doi: 10.4319/lo.2002.47.3.0753

Engel, A., and Passow, U. (2001). Carbon and nitrogen content of transparent exopolymer particles (TEP) in relation to their Alcian Blue adsorption. *Mar. Ecol. Prog. Ser.* 219, 1–10. doi: 10.3354/meps219001

Engel, A., Piontek, J., Grossart, H. P., Riebesell, U., Schulz, K. G., and Sperling, M. (2014). Impact of CO2 enrichment on organic matter dynamics during nutrient induced coastal phytoplankton blooms. *J. Plankton Res.* 36, 641–657. doi: 10.1093/plankt/fbt125

Engel, A., Piontek, J., Metfies, K., Endres, S., Sprong, P., Peeken, I., et al. (2017). Inter-annual variability of transparent exopolymer particles in the Arctic Ocean reveals high sensitivity to ecosystem changes. *Sci. Rep.* 7:4129. doi: 10.1038/s41598-017-04106-9

Engel, A., Thoms, S., Riebesell, U., Rochelle-Newall, E., and Zondervan, I. (2004). Polysaccharide aggregation as a potential sink of marine dissolved organic carbon. *Nature* 428, 929–932. doi: 10.1038/nature02453

Fischer, G., Karakas, G., Blaas, M., Ratmeyer, V., Nowald, N., Schlitzer, R., et al. (2009). Mineral ballast and particle settling rates in the coastal upwelling system off NW Africa and the South Atlantic. *Int. J. Earth Sci.* 98, 281–298. doi: 10.1007/s00531-007-0234-7

Frew, N. M., and Liss, P. S. (2005). *The Role of Organic Films in Air-Sea Gas Exchange. The Sea Surface and Global Change*. Cambridge: Cambridge University Press.

Galgani, L., Piontek, J., and Engel, A. (2016). Biopolymers form a gelatinous microlayer at the air-sea interface when Arctic sea ice melts. *Sci. Rep.* 6:29465. doi: 10.1038/srep29465

Galgani, L., Tsapakis, M., Pitta, P., Tsiola, A., Tzempelikou, E., Kalantzi, I., et al. (2019). Microplastics increase the marine production of particulate forms of organic matter. *Environ. Res. Lett.* 14:124085. doi: 10.1088/1748-9326/ab59ca

Galloway, T. S., Cole, M., and Lewis, C. (2017). Interactions of microplastic debris throughout the marine ecosystem. *Nat. Ecol. Amp Evol.* 1:0116. doi: 10.1038/s41559-017-0116

Grossart, H.-P., Czub, G., and Simon, M. (2006). Algae–bacteria interactions and their effects on aggregation and organic matter flux in the sea. *Environ. Microbiol.* 8, 1074–1084. doi: 10.1111/j.1462-2920.2006.00999.x

Hansell, D. A. (2002). "Chapter 15 – DOC in the global ocean carbon cycle," in *Biogeochemistry of Marine Dissolved Organic Matter*, eds D. A. Hansell and C. A. Carlson (San Diego, CA: Academic Press), 685–715. doi: 10.1016/B978-012323841-2/50017-8

Jähne, B., and Haußecker, H. (1998). Air-water gas exchange. *Annu. Rev. Fluid Mech.* 30, 443–468.

Jiao, N., Herndl, G. J., Hansell, D. A., Benner, R., Kattner, G., Wilhelm, S. W., et al. (2010). Microbial production of recalcitrant dissolved organic matter: long-term carbon storage in the global ocean. *Nat. Rev. Microbiol.* 8, 593–599. doi: 10.1038/nrmicro2386

Joassin, P., Delille, B., Soetaert, K., Harlay, J., Borges, A. V., Chou, L., et al. (2011). Carbon and nitrogen flows during a bloom of the coccolithophore *Emiliania huxleyi*: modelling a mesocosm experiment. *J. Mar. Syst.* 85, 71–85. doi: 10.1016/j.jmarsys.2010.11.007

Keller, A. A., Oviatt, C. A., Walker, H. A., and Hawk, J. D. (1999). Predicted impacts of elevated temperature on the magnitude of the winter-spring phytoplankton bloom in temperate coastal waters: a mesocosm study. *Limnol. Oceanogr.* 44, 344–356. doi: 10.4319/lo.1999.44.2.0344

Le Moigne, F. A. C. (2019). Pathways of organic carbon downward transport by the oceanic biological carbon pump. *Front. Mar. Sci.* 6:634. doi: 10.3389/fmars.2019.00634

Le Moigne, F. A. C., Poulton, A. J., Henson, S. A., Daniels, C. J., Fragoso, G. M., Mitchell, E., et al. (2015). Carbon export efficiency and phytoplankton community composition in the Atlantic sector of the Arctic Ocean. *JGR Oceans* 120, 3896–3912. doi: 10.1002/2015jc010700

Le Quéré, C., Andrew, R. M., Canadell, J. G., Sitch, S., Korsbakken, J. I., Peters, G. P., et al. (2016). Global carbon budget 2016. *Earth Syst. Sci. Data* 8, 605–649. doi: 10.5194/essd-8-605-2016

Leck, C., and Bigg, E. K. (2005). Biogenic particles in the surface microlayer and overlaying atmosphere in the central Arctic Ocean during summer. *Tellus* 57B, 305–316. doi: 10.1111/j.1600-0889.2005.00148.x

Lewandowska, A., and Sommer, U. (2010). Climate change and the spring bloom: a mesocosm study on the influence of light and temperature on phytoplankton and mesozooplankton. *Mar. Ecol. Prog. Ser.* 405, 101–111. doi: 10.3354/meps08520

Ling, S. C., and Alldredge, A. L. (2003). Does the marine copepod *Calanus pacificus* consume transparent exopolymer particles (TEP)? *J. Plankton Res.* 25, 507–515. doi: 10.1093/plankt/25.5.507

Liu, J., Weinbauer, M. G., Maier, C., Dai, M., and Gattuso, J. P. (2010). Effect of ocean acidification on microbial diversity and on microbe-driven biogeochemistry and ecosystem functioning. *Aquat. Microb. Ecol.* 61, 291–305. doi: 10.3354/ame01446

Logan, B. E., Passow, U., Alldredge, A. L., Grossartt, H.-P., and Simont, M. (1995). Rapid formation and sedimentation of large aggregates is predictable from coagulation rates (half-lives) of transparent exopolymer particles (TEP). *Deep Sea Res. Part II Top. Stud. Oceanogr.* 42, 203–214. doi: 10.1016/0967-0645(95)00012-F

Long, R. A., and Azam, F. (1996). Abundant protein-containing particles in the sea. *Aquat. Microb. Ecol.* 10, 213–221. doi: 10.3354/ame010213

Löscher, C., Bange, H. W., Schmitz, R. A., Callbeck, C. M., Engel, A., Hauss, H., et al. (2016). Water column biogeochemistry of oxygen minimum zones in the eastern tropical North Atlantic and eastern tropical South Pacific Oceans. *Biogeosciences* 13, 3585–3606. doi: 10.5194/bg-13-3585-2016

Mari, X. (1999). Carbon content and C:N ratio of transparent exopolymeric particles (TEP) produced by bubbling exudates of diatoms. *Mar. Ecol. Prog. Ser.* 183, 59–71. doi: 10.3354/meps183059

Mari, X. (2008). Does ocean acidification induce an upward flux of marine aggregates? *Biogeosciences* 5, 1023–1031. doi: 10.5194/bg-5-1023-2008

Mari, X., and Burd, A. (1998). Seasonal size spectra of transparent exopolymeric particles (TEP) in a coastal sea and comparison with those predicted using coagulation theory. *Mar. Ecol. Prog. Ser.* 163, 63–76. doi: 10.3354/meps163063

Mari, X., and Kiørboe, T. (1996). Abundance, size distribution and bacterial colonization of transparent exopolymeric particles (TEP) during spring in the Kattegat. *J. Plankton Res.* 18, 969–986. doi: 10.1093/plankt/18.6.969

Mari, X., Passow, U., Migon, C., Burd, A. B., and Legendre, L. (2017). Transparent exopolymer particles: effects on carbon cycling in the ocean. *Prog. Oceanogr.* 151, 13–37. doi: 10.1016/j.pocean.2016.11.002

Mari, X., and Rassoulzadegan, F. (2004). Role of TEP in the microbial food web structure. I. Grazing behavior of a bacterivorous pelagic ciliate. *Mar. Ecol. Prog. Ser.* 279, 13–22. doi: 10.3354/meps279013

McCave, I. N. (1984). Size spectra and aggregation of suspended particles in the deep ocean. *Deep Sea Res. Part A Oceanogr. Res. Pap.* 31, 329–352. doi: 10.1016/0198-0149(84)90088-8

Michels, J., Stippkugel, A., Lenz, M., Wirtz, K., and Engel, A. (2018). Rapid aggregation of biofilm-covered microplastics with marine biogenic particles. *Proc. Biol. Sci.* 285:20181203. doi: 10.1098/rspb.2018.1203

Møller, E. F. (2007). Production of dissolved organic carbon by sloppy feeding in the copepods *Acartia tonsa*, *Centropages typicus*, and *Temora longicornis*. *Limnol. Oceanogr.* 52, 79–84. doi: 10.4319/lo.2007.52.1.0079

Mühlenbruch, M., Grossart, H.-P., Eigemann, F., and Voss, M. (2018). Mini-review: phytoplankton-derived polysaccharides in the marine environment and their interactions with heterotrophic bacteria. *Environ. Microbiol.* 20, 2671–2685. doi: 10.1111/1462-2920.14302

Obernosterer, I., and Herndl, G. J. (1995). Phytoplankton extracellular release and bacterial growth: dependence on the inorganic N:P ratio. *Mar. Ecol. Prog. Ser.* 116, 247–257. doi: 10.3354/meps116247

O'Dowd, C. D., Facchini, M. C., Cavalli, F., Ceburnis, D., Mircea, M., Decesari, S., et al. (2004). Biogenically driven organic contribution to marine aerosol. *Nature* 431, 676–680. doi: 10.1038/nature02959

Orellana, M. V., and Leck, C. (2015). "Chapter 9 – Marine microgels," in *Biogeochemistry of Marine Dissolved Organic Matter*, 2nd Edn, eds D. A. Hansell and C. A. Carlson (Boston, MA: Academic Press), 451–480. doi: 10.1016/B978-0-12-405940-5.00009-1

Orellana, M. V., Matrai, P. A., Leck, C., Rauschenberg, C. D., Lee, A. M., and Coz, E. (2011). Marine microgels as a source of cloud condensation nuclei in the high Arctic. *Proc. Natl. Acad. Sci. U.S.A.* 108, 13612–13617. doi: 10.1073/pnas.1102457108

Ortega-Retuerta, E., Reche, I., Pulido-Villena, E., Agustí, S., and Duarte, C. M. (2009). Uncoupled distributions of transparent exopolymer particles (TEP) and dissolved carbohydrates in the Southern Ocean. *Mar. Chem.* 115, 59–65. doi: 10.1016/j.marchem.2009.06.004

Otero, A., and Vincenzini, M. (2004). Nostoc (Cyanophyceae) goes nude: extracellular polysaccharides serve as a sink for reducing power under unbalanced C/N metabolism. *J. Phycol.* 40, 74–81. doi: 10.1111/j.0022-3646.2003.03-067.x

Pakulski, J. D., and Benner, R. (1994). Abundance and distribution of carbohydrates in the ocean. *Limnol. Oceanogr.* 39, 930–940. doi: 10.4319/lo.1994.39.4.0930

Parker, B. C., and Diboll, A. G. (1966). Alcian stains for histochemical localization of acid and sulfated polysaccharides in algae. *Phycologia* 6, 37–46. doi: 10.2216/i0031-8884-6-1-37.1

Passow, U. (2002). Transparent exopolymer particles (TEP) in aquatic environments. *Prog. Oceanogr.* 55, 287–333. doi: 10.1016/s0079-6611(02)00138-6

Passow, U., and Alldredge, A. L. (1995). Aggregation of a diatom bloom in a mesocosm: the role of transparent exopolymer particles (TEP). *Deep Sea Res. Part II Top. Stud. Oceanogr.* 42, 99–109. doi: 10.1016/0967-0645(95)00006-c

Passow, U., and Wassmann, P. (1994). On the trophic fate of *Phaeocystis pouchetii* (Hariot): IV. The formation of marine snow by *P. pouchetii*. *Mar. Ecol. Prog. Ser.* 104, 153–161. doi: 10.3354/meps104153

Piontek, J., Lunau, M., Händel, N., Borchard, C., Wurst, M., and Engel, A. (2010). Acidification increases microbial polysaccharide degradation in the ocean. *Biogeosciences* 7, 1615–1624. doi: 10.5194/bg-7-1615-2010

Piontek, J., Sperling, M., Nöthig, E.-M., and Engel, A. (2014). Regulation of bacterioplankton activity in Fram Strait (Arctic Ocean) during early summer: the role of organic matter supply and temperature. *J. Mar. Syst.* 132, 83–94. doi: 10.1016/j.jmarsys.2014.01.003

Redfield, A. C. (1958). The biological control of chemical factors in the environment. *Am. Sci.* 46, 230A–221A.

Reigstad, M., and Wassmann, P. (2007). Does *Phaeocystis* spp. contribute significantly to vertical export of organic carbon? *Biogeochemistry* 83, 217–234. doi: 10.1007/s10533-007-9093-3

Robinson, T.-B., Giebel, H.-A., and Wurl, O. (2019). Riding the plumes: characterizing bubble scavenging conditions for the enrichment of the sea-surface microlayer by transparent exopolymer particles. *Atmosphere* 10:454. doi: 10.3390/atmos10080454

Russell, L. M., Hawkins, L. N., Frossard, A. A., Quinn, P. K., and Bates, T. S. (2010). Carbohydrate-like composition of submicron atmospheric particles and their production from ocean bubble bursting. *Proc. Natl. Acad. Sci. U.S.A.* 107, 6652–6657. doi: 10.1073/pnas.0908905107

Saba, G. K., Steinberg, D. K., and Bronk, D. A. (2011). The relative importance of sloppy feeding, excretion, and fecal pellet leaching in the release of dissolved carbon and nitrogen by *Acartia tonsa* copepods. *J. Exp. Mar. Biol. Ecol.* 404, 47–56. doi: 10.1016/j.jembe.2011.04.013

Schartau, M., Engel, A., Schröter, J., Thoms, S., Völker, C., and Wolf-Gladrow, D. (2007). Modelling carbon overconsumption and the formation of extracellular particulate organic carbon. *Biogeosciences* 4, 433–454. doi: 10.5194/bg-4-433-2007

Schlitzer, R. (2015). *Ocean Data View*. Available online at: http://odv.awi.de (accessed January 30, 2020)

Sommer, U., and Lengfellner, K. (2008). Climate change and the timing, magnitude, and composition of the phytoplankton spring bloom. *Glob. Chang. Biol.* 14, 1199–1208. doi: 10.1111/j.1365-2486.2008.01571.x

Sommer, U., and Lewandowska, A. (2011). Climate change and the phytoplankton spring bloom: warming and overwintering zooplankton have similar effects on phytoplankton. *Glob. Chang. Biol.* 17, 154–162. doi: 10.1111/j.1365-2486.2010.02182.x

Sugimura, Y., and Suzuki, Y. (1988). A high-temperature catalytic oxidation method for the determination of non-volatile dissolved organic carbon in seawater by direct injection of a liquid sample. *Mar. Chem.* 24, 105–131. doi: 10.1016/0304-4203(88)90043-6

Sun, C. C., Sperling, M., and Engel, A. (2018). Effect of wind speed on the size distribution of gel particles in the sea surface microlayer: insights from a wind–wave channel experiment. *Biogeosciences* 15, 3577–3589. doi: 10.5194/bg-15-3577-2018

Thornton, D. C. O. (2014). Dissolved organic matter (DOM) release by phytoplankton in the contemporary and future ocean. *Eur. J. Phycol.* 49, 20–46. doi: 10.1080/09670262.2013.875596

Thornton, D. C. O. (2018). Coomassie stainable particles (CSP): protein containing exopolymer particles in the Ocean. *Front. Mar. Sci.* 5:206. doi: 10.3389/fmars.2018.00206

Verdugo, P. (2012). Marine microgels. *Annu. Rev. Mar. Sci.* 4, 375–400. doi: 10.1146/annurev-marine-120709-142759

Verdugo, P., Alldredge, A. L., Azam, F., Kirchman, D. L., Passow, U., and Santschi, P. H. (2004). The oceanic gel phase: a bridge in the DOM–POM continuum. *Mar. Chem.* 92, 67–85. doi: 10.1016/j.marchem.2004.06.017

Wood, A. M., and Van Valen, L. M. (1990). Paradox Lost? On the release of energy-rich compounds by phytoplankton. *Mar. Microb. Food Webs* 4, 103–116.

Wright, J. J., Konwar, K. M., and Hallam, S. J. (2012). Microbial ecology of expanding oxygen minimum zones. *Nat. Rev. Microbiol.* 10, 381–394. doi: 10.1038/nrmicro2778

Wurl, O., and Holmes, M. (2008). The gelatinous nature of the sea-surface microlayer. *Mar. Chem.* 110, 89–97. doi: 10.1016/j.marchem.2008.02.009

Wurl, O., Stolle, C., Van Thuoc, C., The Thu, P., and Mari, X. (2016). Biofilm-like properties of the sea surface and predicted effects on air–sea CO2 exchange. *Prog. Oceanogr.* 144, 15–24. doi: 10.1016/j.pocean.2016.03.002

Yamada, Y., Yokokawa, T., Uchimiya, M., Nishino, S., Fukuda, H., Ogawa, H. et al. (2017). Transparent exopolymer particles (TEP) in the deep ocean: full-depth distribution patterns and contribution to the organic carbon pool. *Mar. Ecol. Prog. Ser.* 583:81–93. doi: 10.3354/meps12339

Yue, W.-Z., Sun, C.-C., Shi, P., Engel, A., Wang, Y.-S., and He, W.-H. (2018). Effect of temperature on the accumulation of marine biogenic gels in the surface microlayer near the outlet of nuclear power plants and adjacent areas in the Daya Bay, China. *PLoS One* 13:e0198735. doi: 10.1371/journal.pone.0198735

Zamanillo, M., Ortega-Retuerta, E., Nunes, S., Estrada, M., Sala, M. M., Royer, S. J., et al. (2019a). Distribution of transparent exopolymer particles (TEP) in distinct regions of the Southern Ocean. *Sci. Total Environ.* 691, 736–748. doi: 10.1016/j.scitotenv.2019.06.524

Zamanillo, M., Ortega-Retuerta, E., Nunes, S., Rodríguez-Ros, P., Dall'Osto, M., Estrada, M., et al. (2019b). Main drivers of transparent exopolymer particle distribution across the surface Atlantic Ocean. *Biogeosciences* 16, 733–749. doi: 10.5194/bg-16-733-2019

Zäncker, B., Bracher, A., Röttgers, R., and Engel, A. (2017). Variations of the organic matter composition in the sea surface microlayer: a comparison between open ocean, coastal, and upwelling sites off the peruvian coast. *Front. Microbiol.* 8:2369. doi: 10.3389/fmicb.2017.02369

Zäncker, B., Engel, A., and Cunliffe, M. (2019). Bacterial communities associated with individual transparent exopolymer particles (TEP). *J. Plankton Res.* 41, 561–565. doi: 10.1093/plankt/fbz022

Conflict of Interest: The authors declare that the research was conducted in the absence of any commercial or financial relationships that could be construed as a potential conflict of interest.

frontiers in Marine Science

ORIGINAL RESEARCH
published: 17 June 2020
doi: 10.3389/fmars.2020.00428

Molecular Composition of Dissolved Organic Matter in Sediment Porewater of the Arctic Deep-Sea Observatory HAUSGARTEN (Fram Strait)

Pamela E. Rossel[1,2,3], Christina Bienhold[2,3], Laura Hehemann[4], Thorsten Dittmar[1] and Antje Boetius[2,3,5]*

[1] Research Group for Marine Geochemistry (ICBM-MPI Bridging Group), Institute for Chemistry and Biology of the Marine Environment, ICBM, University of Oldenburg, Oldenburg, Germany, [2] HGF-MPG Group for Deep Sea Ecology and Technology, Alfred Wegener Institute, Helmholtz Centre for Polar and Marine Research, Bremerhaven, Germany, [3] HGF-MPG Joint Research Group for Deep Sea Ecology and Technology, Max Planck Institute for Marine Microbiology, Bremen, Germany, [4] Department of Geoscience and Geophysics, Alfred Wegener Institute, Helmholtz Centre for Polar and Marine Research, Bremerhaven, Germany, [5] MARUM Center for Marine Environmental Science, University of Bremen, Bremen, Germany

OPEN ACCESS

Edited by:
Christian Lønborg, Aarhus University, Denmark

Reviewed by:
Krista Longnecker, Woods Hole Oceanographic Institution, United States
Elizabeth Kujawinski, Woods Hole Oceanographic Institution, United States

***Correspondence:**
Pamela E. Rossel
Pamela.rossel.cartes@uni-oldenburg.de

Specialty section:
This article was submitted to Marine Biogeochemistry, a section of the journal Frontiers in Marine Science

Received: *19 February 2020*
Accepted: *15 May 2020*
Published: *17 June 2020*

Citation:
Rossel PE, Bienhold C, Hehemann L, Dittmar T and Boetius A (2020) Molecular Composition of Dissolved Organic Matter in Sediment Porewater of the Arctic Deep-Sea Observatory HAUSGARTEN (Fram Strait). Front. Mar. Sci. 7:428. doi: 10.3389/fmars.2020.00428

Over the last decades, the Arctic Ocean has suffered a substantial decline in sea ice cover due to global warming. The impacts of these variations on primary productivity, fluxes of dissolved and particulate organic matter (OM) and turnover at the seafloor are still poorly understood. Here we focus on the characteristics and dynamics of the pool of marine dissolved OM (DOM) in surface sediments of the Arctic Ocean. To investigate spatial and temporal variations of DOM in relation to particulate OM input and benthic microbial community parameters, sediment porewater and overlying bottom water were collected from the long-term observatory HAUSGARTEN in June 2013 and 2014. The study area in the Fram Strait, which is partially covered by sea ice, was sampled along a bathymetric transect (1050–5500 m water depth), from east to west (7°0.2′ E to 5°17′ W), and from south to north (78°37' to 79°43' N). Molecular data on solid phase extracted DOM obtained via Fourier Transform Ion Cyclotron Resonance Mass Spectrometric analysis and a suite of bulk chemical parameters were related to benthic biogeochemical data. Our results demonstrate a close coupling between the production and input of OM from the surface ocean to the seafloor, and the concentration and composition of DOC/DOM in the deep sea. Surface porewaters collected in 2013 from shallower stations (≤1500 m water depth) in the eastern Fram Strait, had a signal of a larger and more recent input of OM (higher concentrations of phytodetritus). This was associated with higher numbers of molecular formulas, abundances of unsaturated aliphatic and N-containing formulas, in concert with higher enzymatic activity, phospholipids, total organic carbon and protein content. In contrast, porewaters collected in 2014 from deeper stations and from the West, were associated with lower OM input, and showed higher abundances of aromatic and oxygen-poor compounds. Higher OM input was also reflected in higher DOC concentrations and

fluxes from the sediment into the water column. Our study demonstrates that regional and temporal variations in OM input can quickly translate into changes in the quantity and quality of surface porewater DOM, the latter substantially altered by deep-sea sediment bacteria.

Keywords: dissolved organic matter, porewater, Fourier-transform ion cyclotron mass spectrometry, Arctic Ocean, benthic communities

INTRODUCTION

Dissolved organic matter (DOM) is a complex mixture of organic molecules produced as an intermediate during the mineralization of sedimentary OM (Burdige and Komada, 2015). In the Arctic Ocean, which is surrounded by massive shelf zones and margins, a terrestrial signature is found in the DOM from surface sediments of the deep basins (Rossel et al., 2016). DOM plays a crucial role in the global carbon cycle, although its molecular composition, which is expected to influence its susceptibility to biotic and abiotic alteration, is largely unknown (Dittmar and Stubbins, 2014; Zhang et al., 2018 and references therein). At the seafloor, DOM may become a component of sediment porewater or absorbed to the sediment matrix (Burdige and Komada, 2015). Porewater DOM is further reworked during a degradation continuum that begins in surface sediments, with the uptake of monomeric molecules (e.g., amino acids, sugars and fatty acids) by benthic organisms dominated in biomass by bacteria, and continues in deeper sediment layers, with the utilization of more complex substrates by subsurface microbial communities (Burdige and Komada, 2015). Compared to the amount remineralized in the seabed, a significant fraction of this pool escapes diagenesis via diffusion to the water column (Burdige et al., 1992, 1999; Burdige and Komada, 2015; Rossel et al., 2016; Loginova et al., 2020), sorption onto minerals (Arnarson and Keil, 2001; Aufdenkampe et al., 2001), formation of complexes with metals (Seidel et al., 2014, 2015a; Linkhorst et al., 2017) or due to sulfurization, which favors preservation of OM under anoxic conditions (Sinninghe Damste and de Leeuw, 1990; Schmidt et al., 2014; Jessen et al., 2017; Pohlabeln et al., 2017). Although previous studies have evaluated the composition and reactivity of porewater DOM (Burdige and Komada, 2015 and references therein), the complexity of this pool limits our understanding of its role in the preservation and degradation of OM. Also, its influence on the DOM composition of the water column and as a potential carbon source is poorly understood, because the reactivity of the material released into the water column is not well known. Knowledge of these processes is even more restricted in areas of limited access such as the deep-sea floor, which represents 60% of the Earth's surface (Smith et al., 2009).

In the Arctic Ocean, particulate OM (POM) export from the mixed surface layer strongly varies temporally as a result of the pronounced seasonality, and regionally and interannually depending on ocean conditions, such as sea ice cover and extent, and phytoplankton community composition (e.g., Wassmann and Reigstad, 2011; Boetius et al., 2013; Lalande et al., 2013). Sea ice cover and the input of primary produced and terrigenous OM have been shown to modulate the molecular composition and distribution of porewater DOM in central Arctic sediments (Rossel et al., 2016). In addition, the sedimentation of POM is one of the major factors influencing the activity and structure of benthic communities (Boetius and Damm, 1998; Klages et al., 2004; Bienhold et al., 2012; Jacob et al., 2013; Kêdra et al., 2015). Thus, variations in the quality and quantity of OM exported to the seafloor are expected to severely impact benthic communities, as previously reported for other environments (Wohlers et al., 2009; Kortsch et al., 2012; Jones et al., 2014). However, our understanding of the interrelations between DOM composition and benthic communities in deep-sea sediments is still limited. Furthermore, the Arctic Ocean is rapidly changing as a result of ocean warming and the decline and thinning of the sea ice cover (Kwok and Rothrock, 2009; Notz and Stroeve, 2016; Peng and Meier, 2018). The amplified warming trend in the Arctic (Dobricic et al., 2016; Sun et al., 2016) could shift the system from a cold and ice-covered to a warmer and ice-free ocean by the end of the century (Overland and Wang, 2013; Polyakov et al., 2017). This is expected to affect ecosystem structure and function, and OM cycling from the surface to the deep sea (Grebmeier et al., 2006; Leu et al., 2011; Wassmann and Reigstad, 2011; Boetius et al., 2013).

To better understand links between spatial (regional) and temporal (interannual) variations in surface ocean conditions and OM input with benthic communities and the molecular composition of DOM at the Arctic seafloor, we collected porewater and overlying bottom water samples from the well-studied area of the Long-Term Ecological Research (LTER) observatory HAUSGARTEN in Fram Strait (Soltwedel et al., 2016). Surface sediments (0–1 cm) represent the horizon that receives most of the fresh organic material from surface waters, while subsurface sediments, here defined as 1–10 cm due to the low sediment accumulation rates in the Arctic system (Stein, 2008), obtain partly reworked organic matter.

The Fram Strait can be divided into two hydrographic regimes (Bauerfeind et al., 2009). The eastern part is characterized by the inflow of warm and nutrient-rich Atlantic Water to the central Arctic, and the western part is characterized by the outflow of cooler and less saline Polar Water that exits the central Arctic and carries a large part of the Arctic sea ice toward the North Atlantic (Paquette et al., 1985; de Steur et al., 2009; Beszczynska-Moller et al., 2012). The two regions are also characterized by different sea ice conditions. The eastern part is only seasonally ice- covered or permanently ice- free, while the western part is predominantly ice- covered throughout the year (Soltwedel et al., 2016). Previously reported POC fluxes at HAUSGARTEN are around 1.3–1.5 mol C m^{-2} yr^{-1} (45 mg Cm^{-2} d^{-1}, Bauerfeind

et al., 2009; ca. 50 mg C m^{-2} d^{-1}, Lalande et al., 2014), which are in a similar range as fluxes reported for the ice margin (1–3.5 mol C m^{-2} yr^{-1}) of the central Arctic Ocean, and three- to ten-fold higher than those of its permanently ice covered basins (0.1–0.4 mol C m^{-2} yr^{-1}) (Lalande et al., 2014). Observations at HAUSGARTEN have revealed a tight coupling between variations in sea ice cover and hydrography with the development of the seasonal phytoplankton bloom and shifts in species composition on temporal (Nöthig et al., 2015; Soltwedel et al., 2016) and spatial (Fadeev et al., 2018) scales. These changes in the water column also lead to differences in the quantity and quality of POM exported to the deep sea (Lalande et al., 2013; Soltwedel et al., 2016).

Here, we combined DOM molecular characterization using Fourier Transform Ion Cyclotron Resonance Mass Spectrometry (FT-ICR-MS) with the analysis of environmental parameters, including sea ice cover and a range of benthic parameters obtained in the framework of the LTER HAUSGARTEN. We test the hypothesis that the molecular composition of DOM as assessed by FT-ICR-MS, as well as specific derived indicators for OM freshness can resolve spatial and temporal variations across local and ocean-wide scales. Specifically, we tested (i) that regional and interannual differences in the oceanographic regimes of Fram Strait are reflected in the molecular composition of DOM in deep-sea surface sediments, (ii) that these differences are also linked with variations in other benthic parameters, such as OM input, and the abundance, biomass and activity of microbial communities, and (iii) that POM degradation in surface sediments is an important source to DOM in bottom water and subsurface sediments, but that benthic bacteria alter the DOM spectra substantially.

MATERIALS AND METHODS

Sampling Sites and Sample Description

Porewater (0–1, 1–5, and 5–10 cm; n = 124) from oxygenated sediments (Donis et al., 2016; Hoffmann et al., 2018) and overlying bottom water samples (n = 52) were collected at the deep-sea LTER HAUSGARTEN. The LTER HAUSGARTEN is located in the Fram Strait between northern Greenland and the Svalbard archipelago (**Figure 1**), and is the only deep water connection for the exchange of intermediate and deep water masses between the Arctic Ocean and the North Atlantic (Fahrbach et al., 2001). Stations cover a latitudinal and a longitudinal transect, including a bathymetric gradient from around 250 to 5500 m water depth (Soltwedel et al., 2016). Ice conditions vary throughout seasons and years, but there are some general characteristics that define different regimes (Soltwedel et al., 2016): Stations in the eastern Fram Strait (from this study: S1-S3, KH, HGI-HGIX and N4) vary from permanently ice-free in the south to seasonally ice-covered in the center and north. Stations in the west (EGI-EGIV, part of HAUSGARTEN observations since 2014; Soltwedel et al., 2016) are predominantly ice-covered. In summer months, the northern and central stations of the eastern Fram Strait are close to the marginal ice zone, which is rich in nutrients and can cause intense phytoplankton blooms and regionally enhanced fluxes of POM to the seafloor (Schewe and Soltwedel, 2003; Bauerfeind et al., 2009; Soltwedel et al., 2016).

Sampling was performed during two cruises, with RV Maria S. Merian MSM 29 in summer 2013 (23 June-12 July) and with RV Polarstern PS85 in summer 2014 (6 June-3 July). In 2013, sampling mainly took place along the latitudinal gradient in the eastern part of the Strait (between 1270 to 2700 m water depths, **Supplementary Table S1**). During the 2014 expedition, samples were mainly retrieved from the longitudinal East-West transect across Fram Strait (7°0.2′ E to 5°17’ W), including bathymetric transects between 1050 and 5500 m water depth (**Supplementary Table S1**). Three stations were sampled in both years (HGI, HGII, N4). Thus, the combination of both cruises provides a first perception of the spatial (latitudinal and longitudinal trends assessed based on 2013 and 2014 sampling, respectively), and interannual variability of DOM in deep-sea sediments of the Fram Strait.

Sediment cores and bottom water (defined as overlying water collected above the sediment) were collected with a TV-guided multicorer at stations in the eastern and western Fram Strait, between 78–79.5°N and 5°W–7°E (**Figure 1** and **Supplementary Table S1**). After retrieval, the sediment cores were stored in a 0°C cold room, and from these undisturbed cores the bottom water was cautiously collected. Sediment porewater was collected from three sediment depth horizons, i.e., 0–1, 1–5, and 5–10 cm using rhizons (pore size 0.15 μm CSS, Rhizosphere Research Products) connected to 10 ml syringes without rubber on the piston. Porewater was then transferred to 50 ml Sarstedt vials. Two or more pseudoreplicates, prepared with the same porewater mixture collected from the cores at each depth, and replicates from parallel cores were analyzed separately in order to evaluate sampling variability and potential contamination during sample handling (**Supplementary Table S1**). All material had been previously rinsed at least three times with Milli-Q water. Prior to analysis, all samples were stored at −20°C.

Solid Phase Extraction of DOM, and Dissolved Organic Carbon (DOC) and Total Dissolved Nitrogen (TDN) Concentrations

The extraction of DOM from acidified (pH 2) porewater and bottom water samples was performed with 100 mg styrene divinyl benzene polymer columns (Varian PPL, Dittmar et al., 2008), formerly rinsed with MeOH (HPLC grade; Sigma-Aldrich, United States). Before DOM elution, the columns were rinsed several times with ultrapure water acidified at pH 2 with HCl to remove the salt from the cartridges (a prerequisite for MS analysis), and then dried under a stream of ultrapure N_2. Elution of the solid phase extracted (SPE)-DOM from the PPL columns was performed with 1 ml of MeOH. The extracts were stored at −20°C until MS analysis. Analysis of DOC and TDN were performed by hand injection via catalytic oxidation at high temperature with

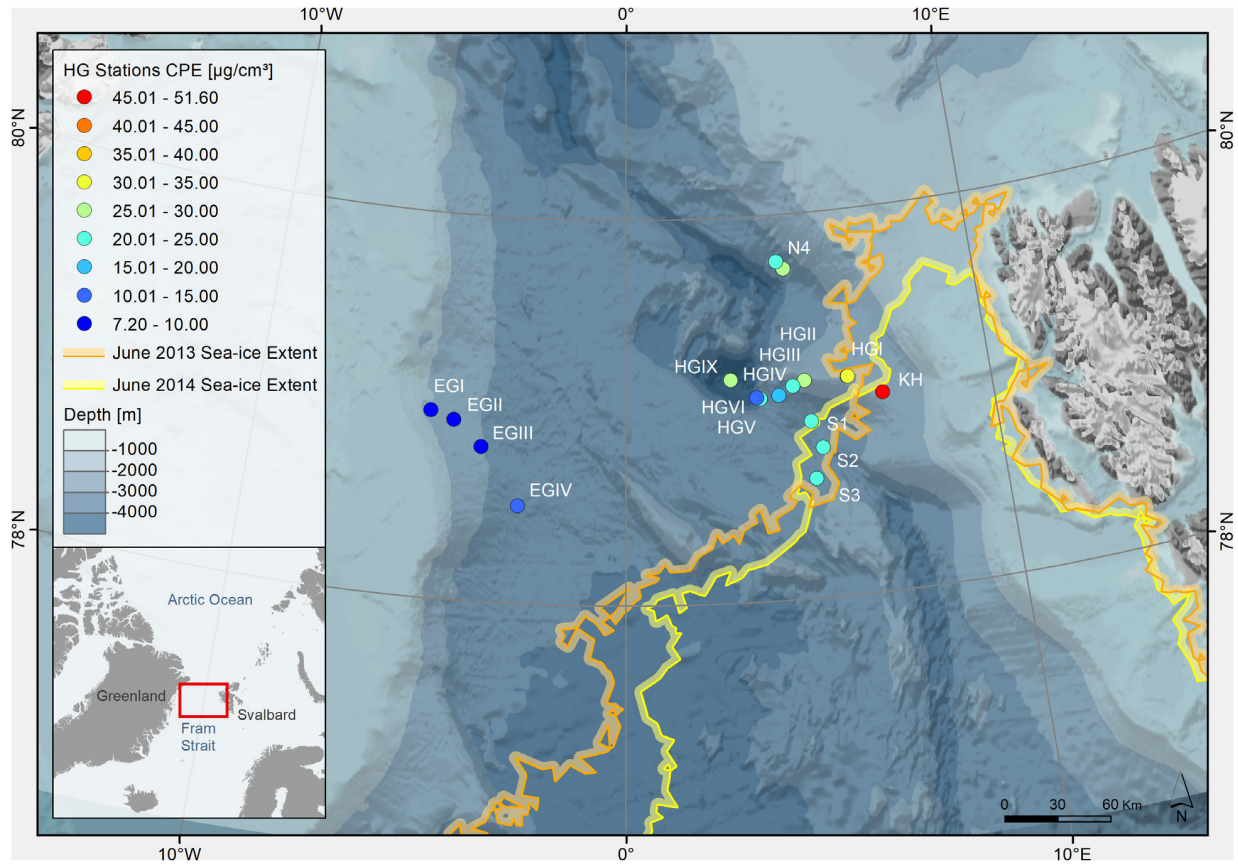

FIGURE 1 | Bathymetric map of the Arctic Ocean indicating sampling stations at the LTER observatory HAUSGARTEN (Fram Strait). The color of the dots indicates concentrations of chloroplastic pigment equivalents (CPE) in surface sediments (0–1 cm, in µg/cm^3 sediment indicated on the color legend on the left). The colors of the lines indicate the location of the sea ice margin during each sampling year, defined as >15% ice coverage (**Supplementary Table S1**).

a TOC-VCPH Shimadzu instrument (Stubbins and Dittmar, 2012) using 1 ml aliquots of each sample, after acidification with HCl (25% Carl Roth, Germany) to pH 2 and purging with synthetic air. The precision of the analysis was better than 6% and was assessed by the analysis of deep-sea water from the Consensus Reference Material Project (University of Miami, United States). DOC and TDN data (**Supplementary Table S1**) were stored in the earth system database PANGAEA (Rossel and Dittmar, 2019a).

DOC Efflux From Porewater Gradients

Dissolved organic matter efflux from the sediment (J_{diff}) was determined according to Fick's first law of diffusion:

$$J_{diff} = -\Phi \times D_{sed} \times dC/dZ$$

where J_{diff}: diffusive flux (mmol/m^2/d), Φ: porosity, D_{sed}: the diffusion coefficient in the sediment (in m^2/s and corrected for temperature) (Iversen and Jorgensen, 1993) and dC/dZ: DOC concentration gradient between bottom water (defined at 0 mm) and 5 mm in the sediment core (**Supplementary Table S1**). Following Burdige et al. (1992), the diffusion coefficient in seawater (D)° was adjusted to the molecular weight of DOM molecules according to the following relationship: Log D° = 1.72–0.39 × log MW_{wa}, where MW_{wa} is the molecular weight intensity-weighted average obtained from the analysis of compounds amenable by electrospray ionization via FT-ICR-MS of each SPE-DOM sample (see section "Molecular Analysis of DOM via FT-ICR-MS"). The diffusion coefficient in the sediment was calculated as Dsed = D°/1-ln(Φ^2) (Boudreau, 1997; Schulz, 2000). To constrain the time (t) for an avg. DOM compound detected by our analysis to diffuse into the sediment, the equation t = L^2/2D was used (Jorgensen, 2006). In this equation, L represents the distance (cm) and D the diffusion coefficient (avg. from all stations). In this calculation, we assume the DOC fluxes in the sediment rather than in the diffusive boundary layer (Rossel et al., 2016), which is a more conservative approach for the resolution of our measurements.

Molecular Analysis of DOM via FT-ICR-MS

Molecular analysis of SPE-DOM from bottom water and porewater samples was performed with a 15 Tesla FT-ICR-MS instrument (Bruker Solarix), equipped with an electrospray ionization source (Bruker Apollo II) in negative ion mode.

Ultrahigh resolution mass spectrometry techniques via FT-ICR-MS have been successfully applied for the analysis of complex DOM molecular mixtures in sediment porewaters from a variety of marine environments (Schmidt et al., 2009, 2014; Seidel et al., 2014, 2015a; Rossel et al., 2016). Prior to analysis, SPE-DOM aliquots were diluted in 1:1 MeOH: ultrapure water to a final DOC concentration of 15–20 mg C/l, assuming extraction efficiency of ca. 50% (due to restricted SPE volumes, SPE-DOM samples were not analyzed for DOC concentration; Schmidt et al., 2009; Schmidt et al., 2017). Samples were infused at 120 µl/h using an ion accumulation of 0.2 s and a capillary voltage of 4 kV. Sample spectrum was obtained after 500 individual scans. External and internal calibrations were performed based on the arginine cluster and based on a list of >30 mass peaks of known formulas in the samples, respectively. Calculation of molecular formulas for all samples was performed using an in-house MATLAB (2010) routine that searches, with an error <0.5 ppm, for all potential combinations of C∞, O∞, H∞, N ≤ 4; S ≤ 2 and P ≤ 1. Formulas were calculated for intensities above the method detection limit (MDL; Riedel and Dittmar, 2014). Molecular masses present in the Milli-Q water blanks were only retained in the dataset if their signal/MDL was <20, since higher intensities in the blanks could indicate these masses are likely present in the samples due to contamination. Furthermore, molecular masses that appeared only once in the whole dataset were eliminated. In order to remove double assignments of formulas to the same mass, CH_2 homologous series extended to lower mass range were considered correct and the combination of >3 N, S or P atoms (NSP, N_2S, N_3S, N_4S, N_2P, N_3P, N_4P, NS_2, N_2S_2, N_3S_2, N_4S_2, S_2P) was not allowed (Rossel et al., 2013, 2017). With this procedure, the whole dataset is represented by 7400 formulas, not considering isotopologues (Rossel and Dittmar, 2019b). To obtain structural information, the aromaticity index (AImod; Koch and Dittmar, 2006; Koch and Dittmar, 2016) and the double bond equivalent (DBE, McLafferty and Turecek, 1994) were used. In addition to the intensity weighted-average values for AImod and DBE, H/C and O/C elemental ratios, as well as the molecular weight, were also calculated (DBE_{wa}, $AImod_{wa}$, H/C_{wa}, O/C_{wa}, MW_{wa}). Additional indices reported to evaluate natural transformation processes in the water column DOM were also calculated for bottom and porewater samples: The SPE-DOM degradation state and lability were evaluated by the I_{Deg} (Flerus et al., 2012) and molecular lability boundary (MLBwl, D'Andrilli et al., 2015), respectively. Furthermore, the recently reported index $I_{bioprod}$, was used to assess the impact of biological production in shaping the DOM present in the samples (Seibt, 2017). The $I_{bioprod}$ index was calculated using the intensity of 10 molecular formulas in each sample according to the following equation:

$$I_{bioprod} = \frac{(C_{13}H_{18}O_5 + C_{13}H_{16}O_6 + C_{13}H_{19}NO_6 + C_{13}H_{17}NO_7 + C_{18}H_{28}O_7)}{(C_{14}H_{16}O_8 + H_{17}H_{24}O_8 + C_{16}H_{22}O_9 + C_{19}H_{28}O_9 + C_{19}H_{28}O_{10})}$$

The formulas in the dividend have been selected as "markers" for bioproduction based on mesocosm experiments (Osterholz et al., 2015), while those in the divisor were not influenced by bioproduction (Seibt, 2017).

In order to provide an overview, molecular formulas were additionally organized into previously defined molecular categories (Seidel et al., 2014; Rossel et al., 2016), even though this categorization is not unambiguous, due to the occurrence of isomers (Zark et al., 2017; Hawkes et al., 2018). However, this categorization has been widely used to represent the regions in the van Krevelen diagram where known molecular groups are located according to their elemental compositions (**Supplementary Table S2** and **Supplementary Figure S1**). Furthermore, carboxyl-rich alicyclic molecules (CRAM-like, **Supplementary Figure S1**), which are considered an important refractory component of DOM, were also calculated based on the ratios DBE/C (0,30–0,68), DBE/H (0,20–0,95), and DBE/O (0,77–1,78) (Hertkorn et al., 2006).

Environmental Parameters

Sea Ice Conditions

Daily sea ice concentration data on a 12.5 × 12.5 km grid were retrieved from the PANGAEA database (Krumpen, 2017). Average sea ice concentrations for June 2013 and June 2014 were calculated for each station to reflect sea ice conditions at the time of sampling. In addition, we calculated average sea ice concentrations over the past 5 years for each station, i.e., from 15 June 2008–15 June 2013 for stations sampled in 2013 and from 15 June 2009–15 June 2014 for stations sampled in 2014, to reflect longer-term trends in sea ice cover at the different stations (**Supplementary Table S1**).

Estimates of Biological Productivity and Particulate Organic Carbon Flux

To estimate biological productivity regimes in surface waters at the time of sampling in 2013 and 2014, we used satellite-based chlorophyll estimates, which were obtained from http://www.globcolour.info (**Supplementary Figure S2**). Particulate organic carbon (POC) flux estimates were obtained from sediment trap moorings (e.g., Lalande et al., 2013, 2016 for description of the moorings) at stations HGIV and N4 in the central and northern parts of the sampling area, respectively (**Supplementary Table S3**).

Environmental Sediment Parameters

Contextual data obtained in the framework of the LTER program at HAUSGARTEN were used to evaluate the DOM molecular composition of porewater and bottom water samples collected in the Fram Strait. Data were retrieved from ICSU World Data Center PANGAEA (see doi links in **Supplementary Table S1**). Briefly, the methods used to generate the reported data were as follows:

Samples from replicate multicorer cores collected at the same stations were used for chlorophyll pigment analyses to evaluate the phytodetritus contribution to the seafloor (Schewe, 2018, Schewe, 2019a-g, 2019a-m in **Supplementary Table S1**). Briefly, pigments were extracted in acetone (90%), using glass beads and grinding of each sample in a cell mill. Concentrations

of chlorophyll *a* (chl *a*) and phaeopigments were determined fluorometrically with a Turner fluorometer (Shuman and Lorenzen, 1975), and the sum of chl *a* and phaeopigments is expressed as chloroplast pigment equivalents (CPE; Thiel, 1982). The ratio of chl *a* to CPE (expressed as a proportion) was used as an indicator of phytodetrital freshness. Benthic community data included phospholipid content (Schewe, 2018, Schewe, 2019a-g; 2019a-m in **Supplementary Table S1**), which were obtained from chloroform-methanol extracts, after lipid-bound phosphates were liberated by persulfate oxidation technique (Findlay et al., 1989; Boetius and Lochte, 1994). Total phospholipids were used as an indicator of total microbial biomass (including bacteria, microbial eukaryotes and meiofauna) (Soltwedel et al., 2016). Particulate proteins (operationally defined as γ-globulin equivalents and from here on referred to as proteins) were analyzed photometrically according to Greiser and Faubel (1989) and represent the bulk of "living" (small organisms) and "dead" biomass (detrital matter) (Schewe, 2018, Schewe, 2019a-g, 2019a-m in **Supplementary Table S1**). The potential activity of hydrolytic exo-enzymes acting as esterases was evaluated according to Köster et al. (1991) using the fluorogenic substrate fluorescein-di-acetate (FDA, from here on referred to as esterase activity) (Schewe, 2018, Schewe, 2019a-m in **Supplementary Table S1**). Bacterial cell counts were performed using acridine orange direct counts (Bienhold, 2019), following the procedure described in Hoffmann et al. (2017). For each sample two replicate filters were counted. Cell volumes were determined using a stage micrometer and converted to biomass using a conversion factor of 3×10^{-13} g C μm^{-3} (Børsheim et al., 1990). Sediment porosity for the stations sampled in 2013 and 2014 (except for N4, for which an avg. value of all stations sampled in 2014 was used) was calculated according to Burdige (2006) and Hoffmann et al. (2018). Additionally, total organic carbon content (TOC) was determined by measuring ash-free dry weight of sediments after combustion at 500°C for 2 h (Schewe, 2018, Schewe, 2019a-g, a-m in **Supplementary Table S1**).

Statistical Analysis

The DOM dataset consisted of 7400 molecular formulas, each one represented by a mass peak whose intensity was normalized to the sum of intensities in the sample. For pseudoreplicates (subsamples from porewater collected from the same sediment core but analyzed separately on the FT-ICR-MS and indicated by sample # in **Supplementary Table S1**), formulas were considered present when they occurred in all pseudoreplicates. For repeated analysis of samples, formulas were considered present when they occurred in all of their respective pseudoreplicates and their average intensity was used for further statistical analysis. This is a conservative approach proposed when no real replicates (i.e., samples from parallel sediment cores) are available (Buttigieg and Ramette, 2014). Thus, each sediment depth in the multivariate statistical analysis is represented by several FT-ICR-MS analysis. In order to give less weight to rare formulas in the multivariate statistical analysis, data were Hellinger transformed (Ramette, 2007).

Contextual data of environmental parameters (ice cover, phytodetrital proxies, benthic community data and sediment properties) were standardized prior to analyses (Ramette, 2007). Geographic distances between stations were calculated using their geographic coordinates. Distances were then represented in a two-dimensional space using a principal coordinate analysis, yielding X (longitude) and Y (latitude) coordinates to be used in further statistical analyses. All of the statistical analyses above were performed in R (v3.1.0; R: A Language and Environment for Statistical Computing, R Core Team R Foundation for Statistical Computing, Vienna, Austria, 2014[1]) using RStudio (v0.99.903; RStudio Team, 2015) and the packages *vegan* (v2.4-1; Oksanen, 2017) and *gmt* (v2.0-1; Magnusson, 2010).

Multivariate statistical analysis was performed by Partial Least Square analysis (PLS; Unscrumbler X v10.5 from Camo Software), which considered the contextual data and the formulas along with their relative abundances in each sample, thereby allowing an identification of formulas that were more strongly associated with the environmental data. PLS has been successfully applied for the statistical analysis of FT-ICR-MS data (Rossel et al., 2016, 2017). The outcome of the PLS analysis is displayed by scores and loadings, the latter for both the environmental (X loadings) and molecular data (Y loadings), which offers a representation of a linear relationship between variables (loadings) and samples (scores). In order to better visualize the results from the PLS analysis, molecular categories, calculated indices and intensity-weighted ratios were also passively displayed in the PLS model, thus they do not influence the model but their location in the PLS indicates their correlation with other variables. Molecular loadings from PLS analysis were also represented in van Krevelen diagrams to better visualize the trends in the relative abundance of the defined molecular categories (see section "Molecular Analysis of DOM via FT-ICR-MS," **Supplementary Figure S1**) in relation to the environmental parameters.

RESULTS

To test our overarching question whether spatial and temporal variations in oceanographic regimes are reflected in the molecular composition of DOM in sediment porewaters, we evaluated data from summer expeditions to Fram Strait in two different years, 2013 and 2014. The sampling campaigns covered longitudinal variations (East-West) between stations of similar water depths (EGI-EGIV vs. HGI-HGIV) sampled during 2014, as well as latitudinal trends (North-South, N4 vs. S1-S3) in 2013. Furthermore, temporal variations (2013 vs. 2014) were determined for eastern stations sampled during both years (HGI-HGII and N4) (for sampling details see section "Sampling Sites and Sample Description"). All data were evaluated with two multivariate statistical analyses (partial least squares, PLS). The first PLS was performed to constrain the role of environmental parameters (longitudinal, latitudinal and temporal variations) for the porewater DOM composition of all sampled sediment

[1]http://www.Rproject.org/

depths. In a second approach, only variations in surface (0–1 cm) porewaters and sediments were assessed. This is where we expect strongest variations due to the input and remineralization of fresh organic material. Benthic environmental parameters were available at a different resolution (i.e. 0–5 cm in 1 cm intervals), but overlapped with DOM measurements for the uppermost horizon of 0–1 cm. Thus, the relationship between DOM and sediment parameters could not be tested for deeper sediment layers.

Environmental Conditions of the Study Area

The ice margin (defined as ≥15% ice cover) in the HAUSGARTEN area was located closest to the southern (S1, S2, and S3) and the shallower eastern stations (KH and HGI), where the latter were sampled in both years (**Figure 1**). Ice cover ranged between 0 and 31% for stations in the eastern part of the Strait, and a maximum ice cover of 57% at the northernmost station in June 2013. In June 2014, ice cover ranged between 10–38% for eastern stations, and 70–91% for western and northern stations (**Supplementary Table S1**). Average sea ice concentrations over the past 5 years reflected similar conditions, with average ice coverage of 0–7% for stations in the eastern and southern part of the Strait, 17–20% at the northern station and 69–84% at western stations. Hydrographical features varied between the three stations that were sampled in both years (i.e., HGI, HGII in the eastern and N4 in the northern part of the sampling area). While at the time of sampling in both years most stations were characterized by Atlantic water and a 30–50 m thick layer of Polar water at the surface, HGI and N4 showed some differences between the years (MSM29, 2013: Wenzhöfer et al., 2013; PS85, 2014: Rabe et al., 2014). During sampling in 2013, HGI was characterized by Atlantic instead of Polar water at the surface, the former of which is usually more nutrient-rich (Randelhoff et al., 2018). At the same time also N4 was characterized by warmer temperatures at the surface in 2013 (≥1°C), suggesting the local absence of ice. In contrast, during sampling in 2014, N4 was characterized by cold surface waters close to the freezing point and with low salinity, indicating the presence of melting ice. Thus, although sampling was performed in the same summer months, ice and hydrographic conditions varied between years and stations.

Satellite-derived chlorophyll concentrations in surface waters of the eastern HAUSGARTEN area, as an indicator of phytoplankton biomass, showed highest values in June 2013 and June 2014, i.e., shortly before or during the time of sampling (**Supplementary Figure S2**). However, the bloom was much stronger (i.e., higher chlorophyll concentrations) in 2013 compared to 2014 (Figure 2 in Engel et al., 2019). Satellite-derived chlorophyll concentrations integrated over the HAUSGARTEN area from April to June were 1.5x higher in 2013 compared to 2014 (4 vs. 2.5 mg Chl *a* m^{-3}) (Engel et al., 2019, Dinter pers. comm.). In 2013 sampling took place about 2–3 weeks after the bloom (6–7 weeks after the first appearance of the bloom), while in 2014 sampling took place in the middle of the bloom, i.e., about 3 weeks after the first chlorophyll peak in the area (see Engel et al., 2019 for indication of blooms based on satellite chlorophyll data for the region).

POC fluxes were measured at the central (HGIV) and northern (N4) HAUSGARTEN stations. Peak POC fluxes from the upper water column (∼200 m water depth) occurred in April and March/April of 2013 and 2014, respectively, and were much higher in 2013 (21 mg POC m^{-2} d^{-1} in 2013; 5 and 8 mg POC m^{-2} d^{-1} in 2014 **Supplementary Table S3**).

Environmental Sediment Parameters, and Porewater DOC and TDN Concentrations

Variations in phytodetritus input as indicated by phytodetritus pigment concentrations in the sediments were related to water depth and were more pronounced in the eastern (HGI-HGIV) than at similar water depths in the western (EGI-IV) Fram Strait (**Figures 1**, **2**). During both sampling years, highest CPE concentrations (see methods for definitions of phytodetritus pigments) were detected in surface sediments (0–1 cm) and decreased in deeper sediment layers (**Supplementary Table S1**). Surface CPE concentrations generally decreased with increasing water depth in the eastern Fram Strait, while in the western part only a slight decrease was observed (**Figure 2** and **Supplementary Table S1**). An exception to the decreasing CPE trend with water depth in the eastern Fram Strait was the deepest station (HGIX), at which also higher values of TOC, phospholipids and protein content were detected in sediments (**Supplementary Table S1**). Surface sediment CPE concentrations in the western Fram Strait were on average much lower than at similar water depths in the East (**Supplementary Table S1**). Nevertheless, based on the proportion of chl *a*, the phytodetrital material at stations in the western and eastern Fram Strait was similarly fresh. In agreement with the differences in surface CPE concentrations between eastern and western Fram Strait, sediment TOC, phospholipid and protein content exhibited generally lower concentrations at western than at eastern stations (**Supplementary Table S1**).

Temporal variations in CPE concentrations and % chl *a* for stations sampled during both cruises (HGI, HGII, N4, **Figure 1**) indicate a larger and more recent (based on the avg. CPE and % chl *a*, respectively), phytodetritus deposition in 2013 compared to 2014, especially at shallower stations (HGI-II; **Figure 2**, **Supplementary Table S1**). Latitudinal variations in CPE in the eastern Fram strait were not as pronounced as the longitudinal trends. Surface CPE concentrations were slightly lower at the southern (S1-S3) than at the northern (N4) stations, although similarly fresh (**Supplementary Table S1**). Furthermore, based on the 2013 data, sediment TOC, enzymatic activity and phospholipid content increased from north to south (**Supplementary Table S1**). Chlorophyll pigment concentrations in the top 5 cm of sediment were significantly correlated ($p \leq 0.05$; **Table 1**) with benthic community activity and biomass (esterase activity, phospholipid and protein concentrations) and TOC content in sediments (**Supplementary Figure S3**). Bacterial abundance and biomass (**Supplementary Table S1**) in

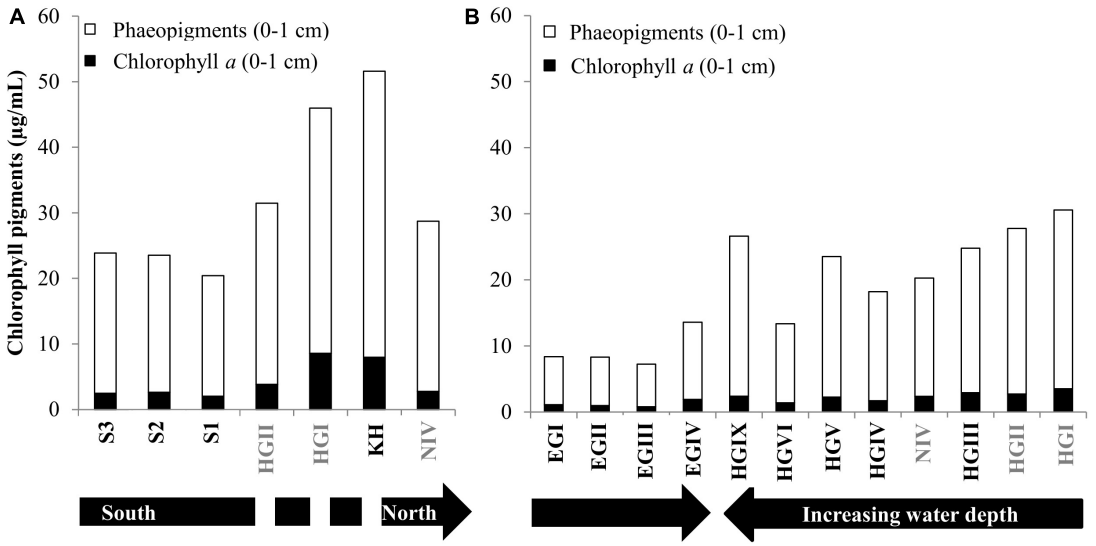

FIGURE 2 | Pigment concentrations. Phaeopigments and Chlorophyll content for surface sediments in 2013 and 2014 (**A,B**, respectively). The discontinuity in the black arrow in panel **(A)**, indicates that HGII, HGI, KH are at a similar latitude. Stations written in gray font were sampled in both years.

surface sediments (0–1 cm), were not significantly correlated with phytodetrital pigments, but followed similar patterns (e.g., higher avg. numbers at eastern compared to western stations, **Supplementary Table S1**).

Dissolved organic matter concentrations in porewater were generally higher in surface sediments and also significantly lower ($p < 0.05$ for paired sample *t*-test) in western Fram Strait compared to similar water depths in the eastern Strait (**Supplementary Table S1** and **Figure 3**). Additionally, on the eastern side (KH, HGI-HGIX), DOC concentrations decreased with increasing water depth (**Supplementary Table S1** and **Figure 3**). Comparing eastern stations sampled in both years, generally higher DOC concentrations were observed in 2013 (HGI and HGII, **Supplementary Table S1** and **Figure 3**). Latitudinal trends indicated that DOC concentrations in the eastern Fram Strait increased from north to south (N4 to S1-S3, **Supplementary Table S1** and **Figure 3**), following the trend of sediment TOC, enzymatic activity and phospholipid content (**Supplementary Table S1**).

Contrary to surface porewater DOC concentrations, TDN concentrations did not decrease with increasing water depth. However, they were lower in the western (EGI-EGIV) than at similar water depths in the eastern Fram Strait (HGI-HGIV) and higher in 2013 compared to 2014 (HGI and HGII, **Supplementary Table S1** and **Figure 3**). Contrary to DOC, latitudinal trends in the eastern Fram Strait showed a decrease in TDN concentrations from north to south (**Supplementary Table S1** and **Figure 3**).

Both DOC and TDN concentrations in porewater were significantly correlated with each other and also with phytodetrital data, enzymatic activity and phospholipid content in the sediments ($p \leq 0.05$; **Table 1**). Additionally, porewater DOC was also significantly correlated with sediment TOC, both also negatively correlated with sea ice cover and distance from the ice margin. The observed differences between eastern and western Fram Strait were also evidenced by a significant correlation between longitude and porewater DOC and TDN, and phytodetrital pigments, phospholipid, protein and TOC content in sediments (**Table 1**), all of which were significantly different between east and west ($p < 0.05$ for paired sample *t*-test), especially at the stations shallower than 2000 m (EGI-III and HGI-III).

Comparison of Bottom Water and Porewater DOM and DOC Efflux

Dissolved organic matter and TDN concentrations in bottom waters (defined as the overlying water collected above the freshly sampled sediment) were two- to four-fold and one- to two-fold lower than in surface sediment porewaters, respectively. Furthermore, DOC and TDN concentrations did not follow variations in water depth, contrary to surface porewater DOC (**Supplementary Table S1** and **Supplementary Figure S4**).

Bottom water DOC concentrations varied spatially and were generally lower and less variable at western stations (EGI-EGIV) compared to similar water depths in the East (HGI-HGIV; **Supplementary Table S1** and **Supplementary Figure S4**). Contrary to DOC, TDN concentrations did not display big differences between stations in the western and eastern Fram Strait.

Comparing both sampling years, DOC and TDN concentrations in bottom waters were higher in 2013 than in 2014 (HGI-HGII, **Supplementary Table S1** and **Supplementary Figure S4**) and also higher at shallower stations located ≤1500 m water depth (KH, HGI and HGII in 2013, **Supplementary Table S1** and **Supplementary Figure S4**).

As a result of the DOC gradients between porewater and bottom waters, which were used to calculate DOC flux, an

TABLE 1 | Pearson correlation matrix between DOC and TDN concentrations, and phytodetrital proxies and benthic community data from the LTER HAUSGARTEN program for the top 5 cm of sediment.

	Water depth	Sediment depth	DOC	TDN	Chl *a*	Phaeop.	CPE	Chl *a*%	Esterase	Phosph.	Protein	TOC	Lat.	Long.	Sea ice monthly avg.	Sea ice 5 yr. avg.	Near distance
Water depth		−0.05	−0.31	−0.36	−0.31	−0.23	−0.24	−0.41*	−0.55***	−0.2	0.17	−0.01	−0.06	0.04	0.38*	−0.1	−0.06
Sediment depth			−0.41*	−0.34	−0.44***	−0.48***	−0.48***	−0.34	−0.42*	−0.2	−0.01	−0.09	−0.06	−0.08	0.07	0.09	0.09
DOC				0.66***	0.89***	0.79***	0.81***	0.71***	0.55***	0.7***	0.42*	0.43***	0.24	0.42*	−0.53***	−0.38*	−0.44***
TDN					0.69***	0.62***	0.64***	0.59***	0.46***	0.46***	0.25	0.22	0.04	0.43*	−0.4*	−0.36	−0.37*
Chl *a*						0.92***	0.94***	0.79***	0.64***	0.75***	0.49***	0.57***	0.16	0.51***	−0.55***	−0.45***	−0.5***
Phaeop.							1***	0.58***	0.68***	0.68***	0.6***	0.71***	0.18	0.65***	−0.62***	−0.59***	−0.63***
CPE								0.62***	0.68***	0.7***	0.59***	0.7***	0.18	0.63***	−0.61***	−0.57***	−0.62***
Chl *a*%									0.49***	0.62***	0.2	0.29	0.06	0.15	−0.26	−0.08	−0.12
Esterase										0.55***	0.25	0.51***	0.25	0.33	−0.52***	−0.33	−0.38*
Phosph.											0.46***	0.63***	0.09	0.41	−0.36	−0.37*	−0.38*
Protein												0.63***	0.34	0.66***	−0.59***	−0.65***	−0.7***
TOC													0.15	0.62***	−0.51***	−0.61***	−0.62***
Latitude														0.16	−0.59***	−0.33	−0.45***
Longitude															−0.73***	−0.97***	−0.93***
Sea ice monthly avg.																0.78***	0.8***
Sea ice 5 yr. avg.																	0.96***
Near distance																	

*ρ values are provided above the diagonal indicating its significance level (*p ≤ 0.05; **p ≤ 0.01; ***p ≤ 0.001). For a graphic representation of this table see* ***Supplementary Figure S3****. Phaeop., phaeopigments. Esterase, esterase activity. Phosph., phospholipid content. Lat., latitude. Long., longitude. Near distance, nearest distance to the ice margin.*

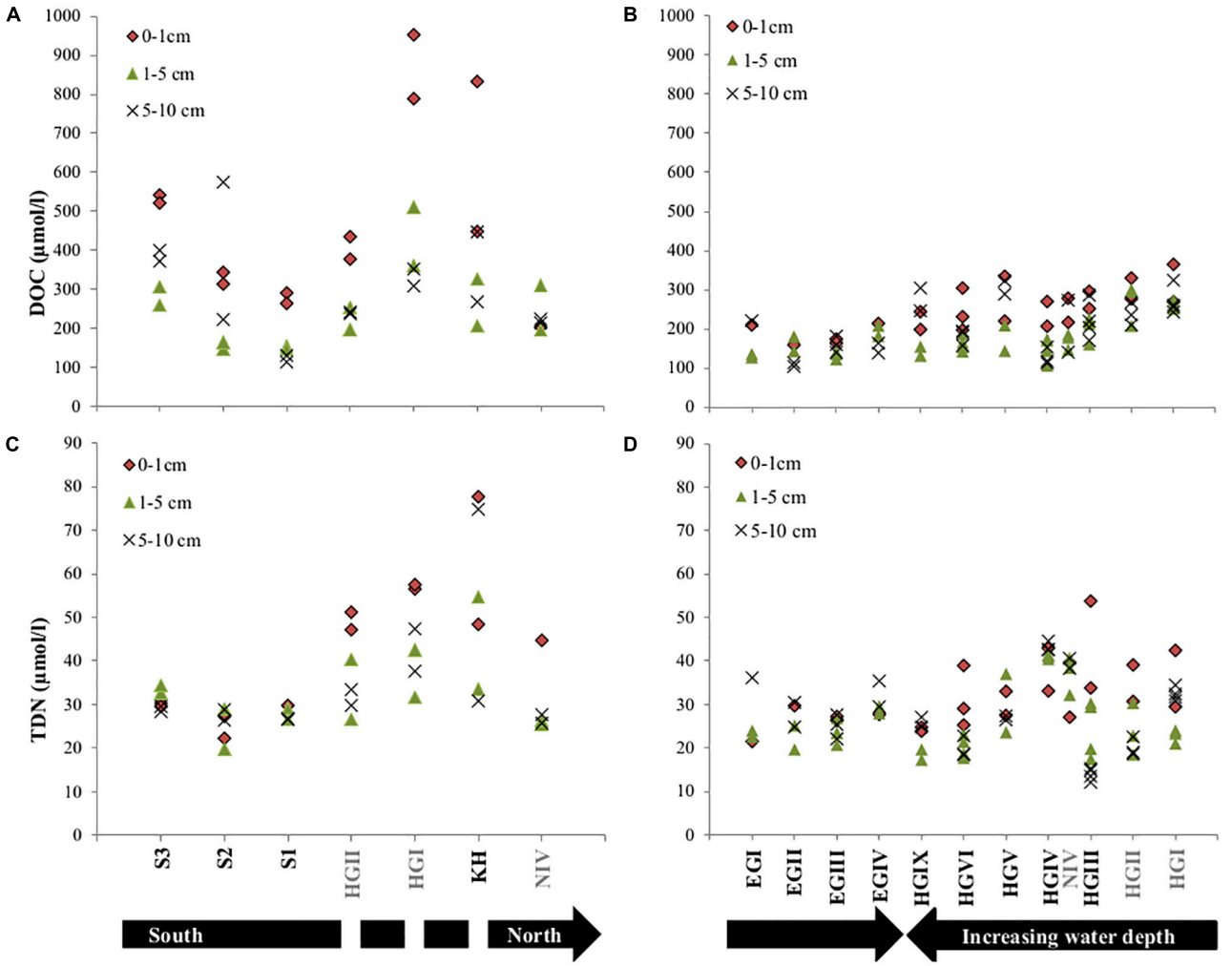

FIGURE 3 | Concentrations of dissolved organic carbon (DOC) and total dissolved nitrogen (TDN) in all analyzed porewaters for the years 2013 **(A,C)** and 2014 **(B,D)**. Note that sampling in 2013 displays latitudinal variations and 2014 longitudinal trends. The discontinuity in the black arrow in **(C)**, indicates that HGII, HGI, KH are at a similar latitude. Stations written in gray font were sampled in both years.

export of DOC from surface sediments to the overlying bottom water (DOC efflux) was observed for all sampling stations (**Supplementary Table S1**). Along with the general trend in DOC efflux, spatial and temporal variations were also observed. The average DOC efflux was two-fold lower on average for the western stations compared to similar water depths in the eastern Fram Strait (**Supplementary Table S1**). Furthermore, southern stations had higher DOC efflux than further north (**Supplementary Table S1**). Also, eastern stations displayed higher DOC efflux in 2013 than in 2014 (**Supplementary Table S1**).

Comparing bottom water, surface porewater (0–1 cm) and deeper porewater (1–5 and 5–10 cm) samples on a molecular level, bottom water DOM had a lower number of formulas compared to surface and deeper porewaters (**Figure 4**). Most of these formulas were shared and only 2, 3, and 22% of each pool were represented by unique formulas (**Figure 4**). On a compositional level, shared formulas among the three DOM pools were represented by more degraded DOM, with more than half of them associated with highly unsaturated formulas (**Figure 4**). Nevertheless, fresh molecular indicators (molecular categories previously associated with phytodetritus input; Rossel et al., 2016) such as unsaturated aliphatics and unsaturated-N also contributed to the shared fraction with 27% (**Figure 4**).

Comparing porewater with bottom water, it was found that less formulas in surface porewater were absent in bottom water compared to those in deeper porewater. Consequently, bottom water was more similar to surface porewater than to deeper porewater (see shared formulas between two pools, **Figure 4**). The main difference between bottom water, surface and deeper porewaters was the increase of unique formulas associated with highly unsaturated formulas toward the deeper porewater (**Figure 4**).

Dissolved organic matter in surface porewater was represented by 58% of highly unsaturated, 14% of unsaturated aliphatics and

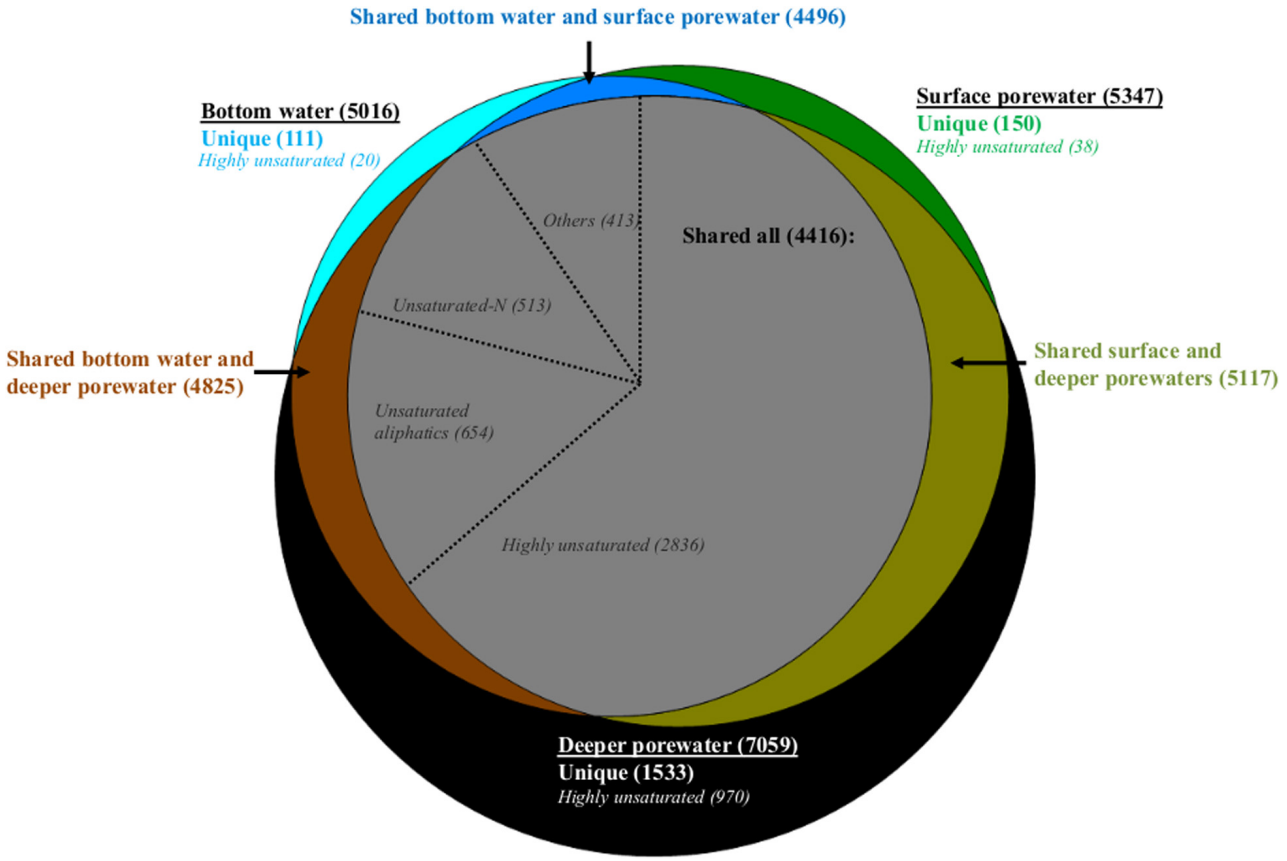

FIGURE 4 | Venn diagram with molecular formulas identified in the whole dataset. Number of formulas detected in bottom water, surface (0–1 cm) and deeper porewater (1–5, 5–10 cm) pools are indicated in bold inside the parentheses. Number of unique formulas in each pool and those shared between two or all pools are color coded and displayed in parentheses. Number of formulas contributing to specific molecular categories are indicated in italics also in parentheses. In the gray circle (with formulas shared between the three pools) "others" represent the sum of aromatics, polyphenols and sugars.

13% of unsaturated-N formulas, of which 10, 11, and 23% were not detected in bottom water, respectively. In deeper porewaters a smaller fraction was absent (2, 8, and 10%, respectively). Consequently, more formulas in surface porewater (associated with both degraded and fresh OM) were absent from bottom water than from deeper porewater.

The higher number of unsaturated-N formulas in surface porewaters compared to bottom waters was also reflected in a higher relative abundance of these formulas as indicated by higher freshness indices, such as MLBwl and $I_{bioprod}$, observed in surface porewaters compared to bottom waters (**Supplementary Table S5**). Despite the higher number of highly unsaturated formulas in surface porewater compared to bottom water, which could indicate more degraded DOM in the former pool, only minor differences were detected for the calculated degradation index, I_{Deg} (**Supplementary Table S5**). This could be related to the fact that the I_{Deg} index was established for water column samples (see section "Discussion"). Also, DOM in bottom waters was generally characterized as more unsaturated (DBE_{wa}), had higher molecular weight (MW_{wa}), but lower relative abundances of aromatics (especially polyphenols) compared to surface porewater (**Supplementary Tables S4**, **S5**).

Similar to bulk data, the DOM composition also displayed longitudinal differences. Although bottom water from the western and eastern Fram Strait shared similar number of formulas with their surface porewaters, more unique formulas were observed in bottom waters of the western compared to the eastern Fram Strait (**Supplementary Figures S5a,b**, respectively). These unique formulas in the western Fram Strait, which were in the central area of the van Krevelen diagram (**Supplementary Figure S5a**), were predominantly CRAM-like (**Supplementary Figure S1**). Additionally, the lower relative abundance of aromatics detected in bottom water compared to surface porewater was more pronounced, especially for polyphenols, at eastern stations (HGI-HGIV) compared to similar water depths in the western Fram Strait (EGI-EGIV, **Supplementary Table S5**). Other molecular categories that behaved differently along the longitudinal transect (**Supplementary Table S5**) were unsaturated aliphatic O-rich formulas. These formulas were only significantly higher ($p < 0.05$ for paired sample t-test) in surface porewaters compared to bottom waters at the eastern stations (HGI-HGIV), but not at the western stations (EGI-EGIV; **Supplementary Table S5**).

Temporal variations indicated higher numbers of shared formulas between surface porewater and respective bottom waters in 2013 than in 2014 (HGI-II comparison, **Supplementary Figures S5c,d**). Of the shared formulas in 2013, 25% were not detected in bottom water in 2014 with more than half of them in the higher H/C region of the van Krevelen diagram (**Supplementary Figure S5c**), commonly associated with fresh molecular indicators such as unsaturated aliphatics and unsaturated-N (**Supplementary Figure S1**). This is consistent with a higher relative abundance of unsaturated aliphatic O-rich and unsaturated-N formulas in bottom waters in 2013 compared to 2014 (**Supplementary Table S5**).

Molecular Composition of Porewater DOM

In sediment porewaters (0–10 cm) from HAUSGARTEN, variations in the relative abundance of molecular categories were related to differences between eastern and western regions of the Strait, evaluated based on 2014 data, and with interannual variability for stations in the eastern part that were sampled in both years. At stations with similar water depths, mainly polyphenols displayed significant differences ($p < 0.05$ for paired sample *t*-test) between western (EGI-IV) and eastern (HGI-IV) Fram Strait, with higher contribution in the latter location (**Supplementary Table S5**).

At stations with similar water depths in the western and eastern Fram Strait, fresh molecular indicators such as unsaturated aliphatics O-rich and O-poor displayed different trends. Unsaturated aliphatics O-poor were significantly higher ($p < 0.05$) in the western Fram Strait, while O-rich aliphatics were similar at both locations ($p = 0.3$). However, comparing both sampling years, unsaturated aliphatics O-rich were two-fold higher in 2013 than in 2014 (HGI-II, **Supplementary Table S5**). Also, the contribution of unsaturated-N formulas was significantly higher ($p < 0.05$) in the western Fram Strait. However, the contribution of unsaturated-N formulas was two-fold higher during 2013 than in 2014 (HGI-HGII). The contribution of unsaturated-N formulas to the total N-containing compounds was on avg. $14 \pm 6\%$ and $10 \pm 4\%$ for western and eastern stations of similar water depths, respectively, and $19 \pm 4\%$ for HGI-HGII in 2013.

To assess the role of the environment on the molecular DOM composition of HAUSGARTEN porewaters, two partial least squares (PLS) analyses were performed: The first PLS included all porewater samples (i.e., 0–1, 1–5, 5–10 cm) and the second only evaluated surface porewaters (0–1 cm, **Supplementary Table S1**) to assess the role of benthic parameters in shaping the composition of surface porewater DOM (see first paragraph of section "Results").

Based on the first PLS analysis (**Supplementary Tables S6**, **S7**), DOM composition was explained by two axes (**Figure 5**). The first axis, factor 1, explained 48% of the environmental (X loadings) and 11% of the DOM molecular data (Y loadings) variability, while factor 2 explained 18% and 5%, respectively (**Figure 5**). Factor 1 was scaled with DOC and TDN concentrations, which negatively correlated with sea ice cover and the distance to the ice margin. DOC and sea ice variables significantly influenced DOM composition (uncertainty test <2 Std. based on cross validation; **Figure 5D**). Samples with higher DOC concentrations were mainly collected in 2013 and from eastern Fram Strait (KH, HGI-HGII $\leq$ 1500 m water depth, **Figures 5B,C**). These stations were characterized by higher abundance of fresher DOM (higher relative abundance of unsaturated-N and unsaturated aliphatic O-rich formulas and higher indexes of lability MLBwl, and lower degradation, I_{deg}, **Figure 5D**). Furthermore, longitude also significantly influenced the DOM composition of porewaters, separating eastern (mainly KH, HGI-HGII) and western Fram Strait (EGI-EGIII) samples along both axes (factor 1 and 2; **Figure 5B**). Along the first axis, eastern (HGI, HGII, and KH) and western Fram Strait (EGI-EGIII) were separated, due to the higher abundance of oxygen-rich compounds (higher O/C_{wa}), polyphenols and higher number of formulas in eastern compared to western porewaters (**Figure 5D**). The second axis was mainly associated with sediment and water depth, which did not significantly influence the DOM composition of the porewaters beyond the surface layer, i.e., 1–5 and 5–10 cm porewater overlapped, and its DOM was overall more degraded, more aromatic and had higher molecular weight (higher I_{deg}, $AImod_{wa}$, MW_{wa}) and abundance of CRAM-like formulas (**Figures 5A,D**).

Based on the second PLS analysis including only DOM from surface porewaters in relation to benthic environmental parameters (**Supplementary Tables S8**, **S9**), DOM composition was explained by two axes (**Figure 6**). The first axis, factor 1, explained 49% of the environmental (X loadings) and 18% of the DOM molecular data (Y loadings) variability, while factor 2 explained 17 and 8%, respectively (**Figure 6**). Similar to the first PLS (**Figure 5**), the first axis was influenced by DOC and TDN concentrations, which also correlated with phytodetritus concentrations (CPE, Chl *a* and phaeopigments) (TDN and phytodetritus proxies significantly influenced surface porewater composition; uncertainty test <2 Std. based on cross validation; **Figure 6D**). Surface porewater DOM composition was mainly separated between those samples collected in 2013 at shallower stations of the eastern Fram Strait (KH, HI-HGII) and those collected in 2014 at deeper stations of the bathymetric transect (HGV, VI and HGIX) and in the western Fram Strait (especially EGI-EGIII) (**Figures 6B,D**). This separation was due to the higher concentrations of DOC, TDN and phytodetritus at the eastern stations in 2013. Higher phytodetritus concentrations were accompanied by higher protein, TOC and phospholipid content and enzymatic activity in the sediments, as well as higher numbers of formulas, and higher relative abundances of CHON and unsaturated aliphatic O-rich formulas in porewater DOM (**Figures 6D**, **7A**). The second axis was influenced by water depth, and prokaryotic abundance and biomass. Abundance and biomass were higher at the eastern (HGI collected in 2014) and southern stations (S2-S3, collected in 2013; **Supplementary Table S1**). These stations were characterized by porewater DOM that had higher molecular weight (MW_{wa}) compared to the DOM from shallower but permanently ice-covered stations (EGI-III, **Figure 6D**). Porewater DOM from deeper stations in the eastern Fram Strait (HGV, HGVI, and HGIX) was more

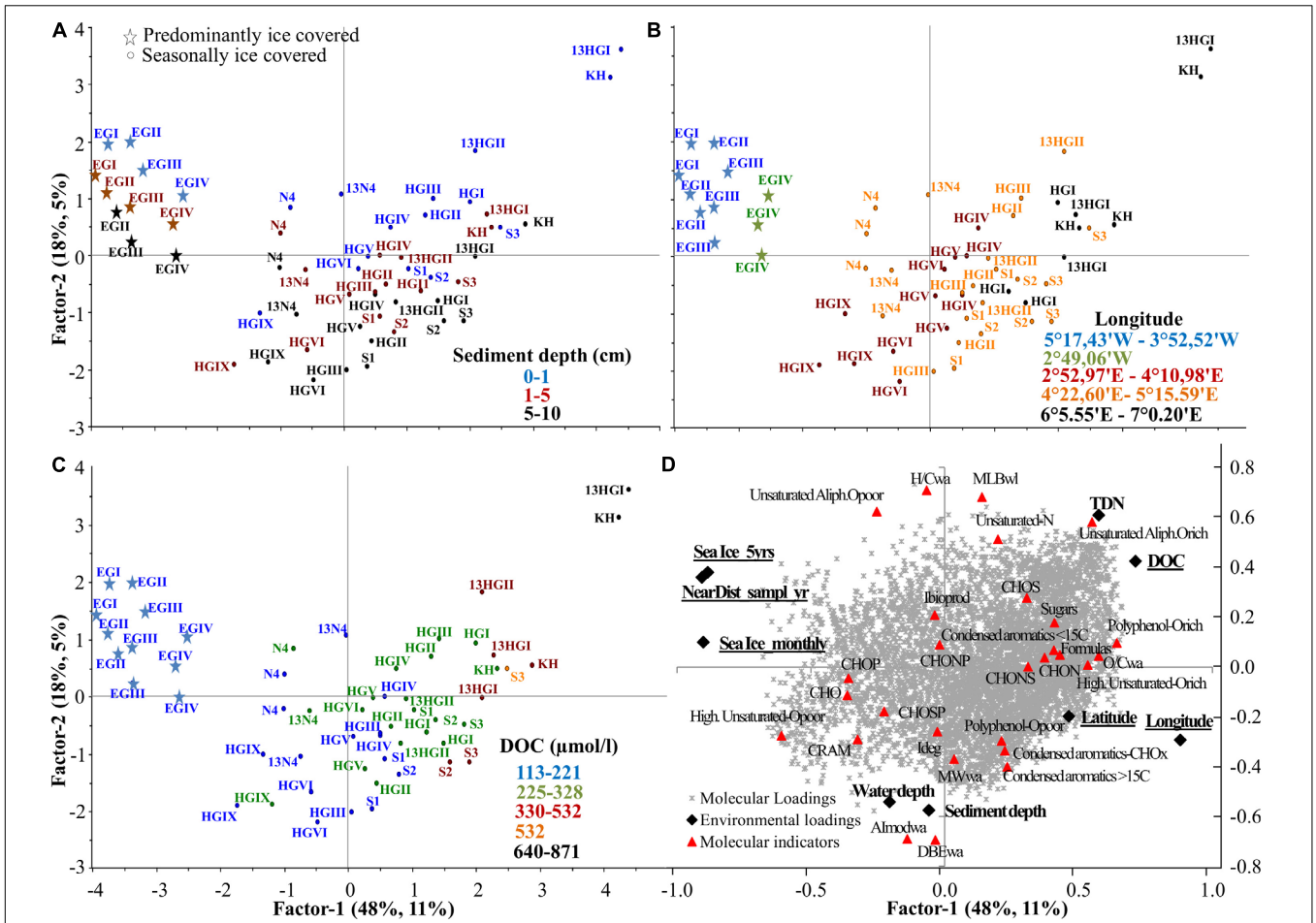

FIGURE 5 | Partial Least Square (PLS) analysis of all porewater samples with factor 1 explaining 48 and 11% of the environmental and molecular variability, respectively, and factor 2 explaining 18 and 5%. **(A)** Scores plot (samples indicated by the name of the station, **Supplementary Table S1**) color coded with sediment depth, **(B)** longitude and **(C)** DOC concentration, and **(D)** correlation of environmental (X loadings) and molecular loadings (Y loadings), passively displaying the evaluated molecular categories, ratios and indices (see molecular indicators in **Supplementary Figure S1** and **Supplementary Table S2**). Underlined environmental variables significantly influence porewater DOM composition. Sea ice variables: Sea Ice_montly, Sea Ice_5yrs and NearDist_sampl_yr, stand for sea ice monthly average, 5 years average and nearest distance to the ice margin (see section "Sea Ice Conditions," **Supplementary Table S1**).

aromatic than at shallower stations in the same region (higher AImod$_{wa}$; **Figure 7B**).

DISCUSSION

Regional and Interannual Differences in Productivity and OM Availability Are Reflected in Benthic DOM Fluxes and Composition in Fram Strait

Environmental conditions at the LTER HAUSGARTEN in Fram Strait differed between regions and years. While the eastern Strait off Svalbard is mostly ice free during the year, the western part off Greenland is characterized by sea ice coverage of over 50%. This influences the input of POM to the seafloor, which was also reflected in CPE concentrations in surface sediments, with much higher values in the East compared to the West (**Figure 1**). This trend was also reflected in other benthic parameters, e.g., sediment TOC, phospholipids and protein content. An exception to the trends observed in the eastern Fram Strait was the deepest station (HGIX), consistent with the funnel-like topography of this station that facilitates accumulation of phytodetrital matter (Cathalot et al., 2015). In 2014 both regions were sampled, and while the eastern Fram Strait exhibited post-bloom conditions at the time of sampling, the western Fram Strait was likely still in a pre-bloom stage; the estimated productivity since winter was twice as high in the East when compared to the West (Fadeev et al., 2018). Regionally, the two parts of the Strait thus clearly differ in productivity and the amount of POM that is received by the seafloor, in agreement with previous reports (Fadeev et al., 2018; Hoffmann et al., 2018; Käss et al., 2019). In addition, there were also temporal differences between 2013 and 2014. The higher productivity indicated by satellite-derived chlorophyll concentrations in 2013 may have been supported by different hydrographical features, namely by the presence of nutrient-rich

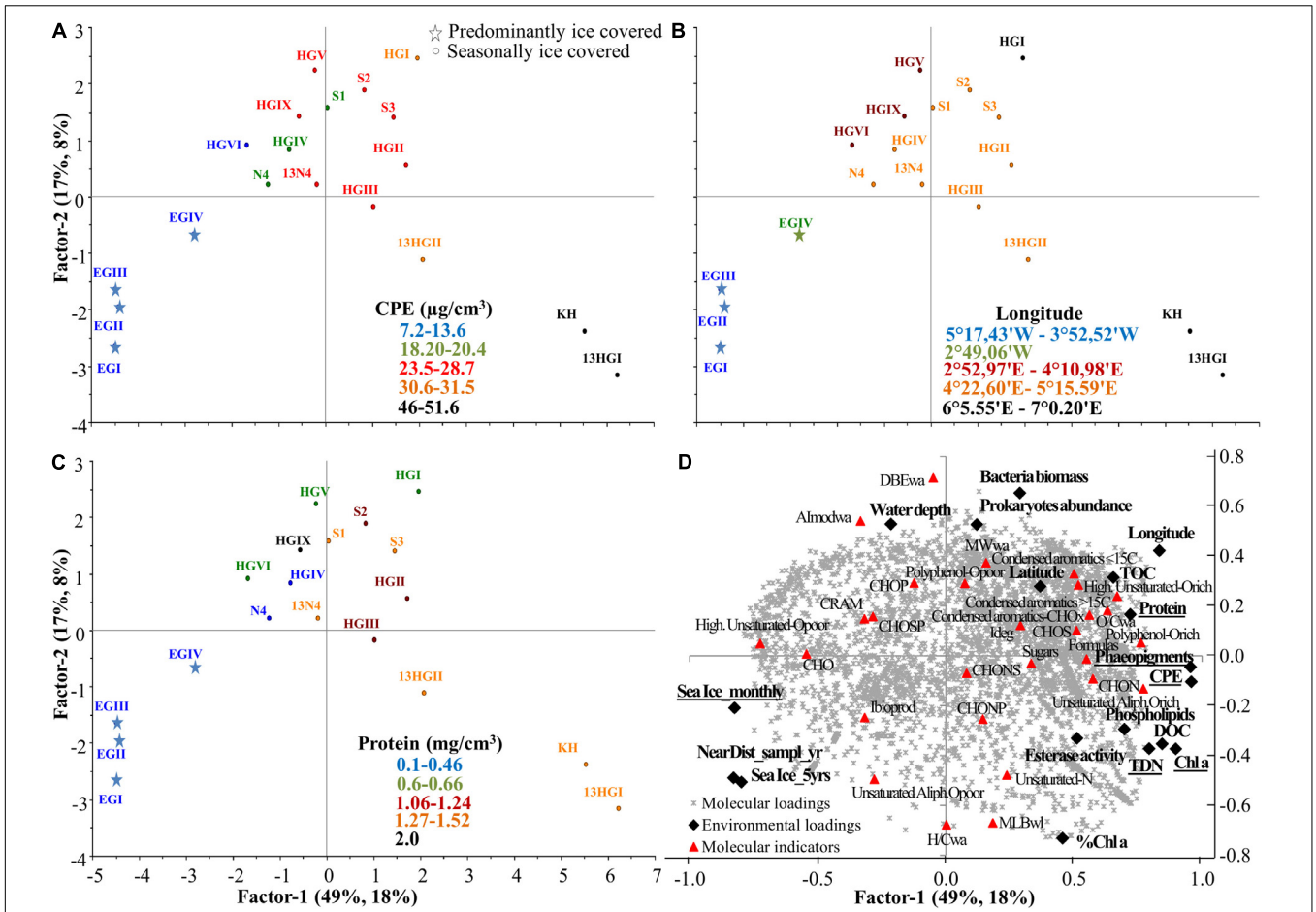

FIGURE 6 | Partial Least Square (PLS) analysis of surface porewater (0–1 cm) samples with factor 1 explaining 49 and 18% of the environmental and molecular variability, respectively, and factor 2 explaining 17 and 8%. **(A)** Scores plot (samples indicated by the name of the station, **Supplementary Table S1**) color coded with CPE, **(B)** longitude and **(C)** protein content, and **(D)** correlation of environmental (X loadings) and molecular loadings (Y loadings), passively displaying the evaluated molecular categories, ratios and indices (see molecular indicators in **Supplementary Figure S1** and **Supplementary Table S2**). Underlined environmental variables are significantly influencing surface porewater DOM composition. Sea ice variables: Sea Ice_montly, Sea Ice_5yrs and NearDist_sampl_yr, stand for sea ice monthly average, 5 years average and nearest distance to the ice margin (**Supplementary Table S1**).

Atlantic waters at the surface of HGI and less ice and thus higher light availability at N4. Higher productivity in 2013 was followed by about three times higher POC export from the upper water column. The larger export event in 2013 may have also resulted in a faster input of fresher phytodetritus to the seafloor, which is supported by higher surface sediment CPE concentrations and chlorophyll *a* proportions in 2013 compared to 2014. All of these variations were well reflected in porewater DOC concentrations, which were higher in the eastern compared to the western Fram Strait and higher in 2013 compared to 2014, in agreement with the higher OM availability (assessed with chlorophyll pigment content) in those regions and year.

Also, DOM composition in porewaters from sediments collected at the LTER HAUSGARTEN differed regionally (East vs. West), as well as interannually (2013 vs. 2014). Porewaters from stations sampled in 2013 from shallower water depth (≤1500 m) and seasonally ice-covered regions (KH, HGI-II, located in the eastern Fram Strait), were associated with fresher DOM signals (higher number of formulas, and abundance of aliphatics formulas and N-containing compounds). Higher contribution of this "fresh" DOM concurs with higher benthic biomass (phospholipids and protein content), enzymatic activity, TOC and phytodetritus proxies in surface sediments of the eastern Fram Strait. On the contrary, the DOM composition of porewaters collected in 2014 at deeper water depths in the eastern Strait were associated with higher abundances of more degraded compound classes (CRAM-like, highly unsaturated oxygen-poor molecular formulas and more aromatic compounds), in agreement with the influence of water depth on benthic remineralization mainly in the eastern Fram Strait (Hoffmann et al., 2018). In the western Fram Strait (EGI-EGIII) porewater DOM was dominated by oxygen-poor compounds (lower O/C_{wa}) in agreement with their association with more degraded material and a lower contribution of fresh material at these permanently ice-covered locations. The observed differences in the sediment DOM pool are in agreement with surface water conditions at the

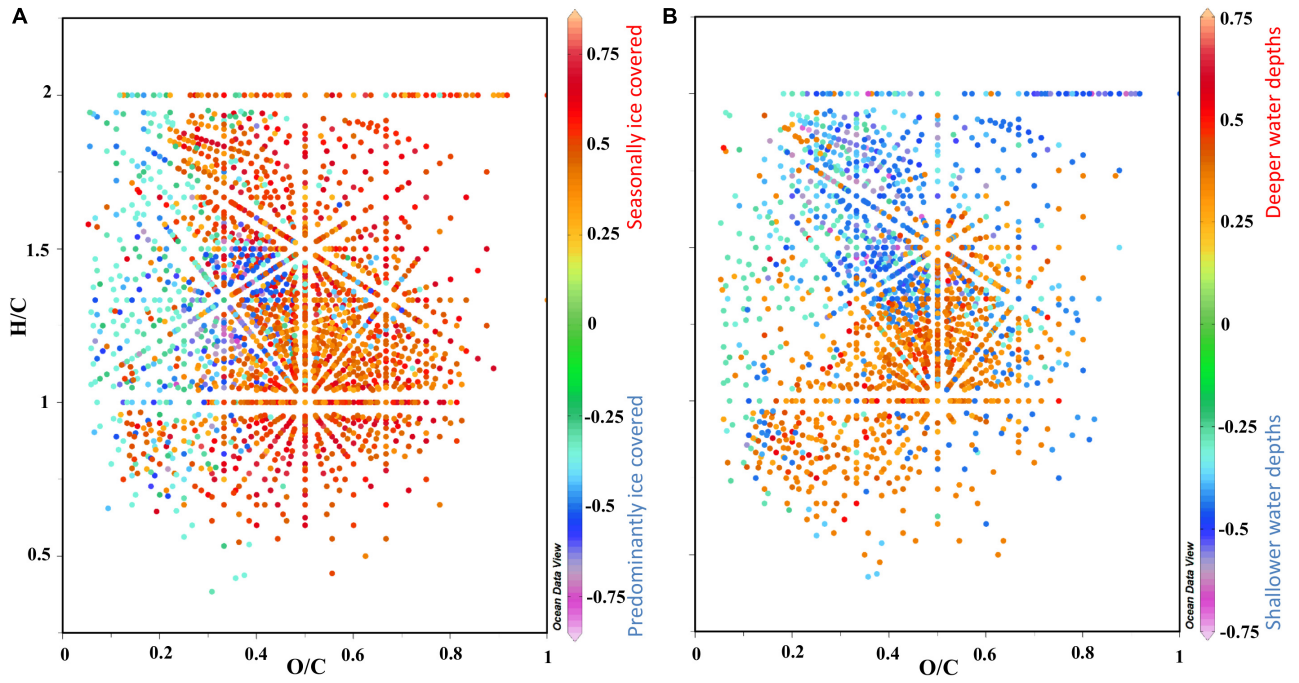

FIGURE 7 | van Krevelen diagrams (VKD) of H/C and O/C ratios using the PLS molecular loadings from **Figure 6D** to summarize the main trends in the molecular composition of surface porewater. **(A)** VKD with factor 1 loadings and **(B)** factor 2 loadings in the *z* axis indicated in the color bar to the right, where the relationship to sea ice cover and water depth are indicated (see **Figure 6**). For definition and location on the VKD of discussed molecular categories see section "Molecular Analysis of DOM via FT-ICR-MS," **Supplementary Figure S1** and **Supplementary Table S2**.

time of sampling during 2014. Because the eastern Fram Strait was characterized by post-bloom conditions (Fadeev et al., 2018) and peak fluxes of POC had already occurred in April, there was likely already an input of fresh organic material to stations in the East, which resulted in higher DOC concentrations and fresh DOM signals due to the breakdown of fresh POM by benthic communities. In contrast, western stations had likely not received (as much) fresh organic material and receive lower inputs of organic material in general, due to the higher ice cover, resulting in a more degraded DOM pool. Differences in DOM composition between north and south were minor compared to those between western and eastern Fram Strait.

Different Productivity Regimes Cause Spatial Differences in OM Availability, DOM Fluxes and Composition Across Ocean Basins

Compared to the central Arctic basins which are permanently ice-covered and strongly nutrient limited, the Fram Strait is much more productive. Overall, surface sediment CPE concentrations at HAUSGARTEN were between 10 to 400-fold higher compared to the Arctic continental slope and the central Arctic (Boetius and Damm, 1998; Rossel et al., 2016), indicating a much larger input of OM in this region. Proportions of chlorophyll *a* (% chl *a* relative to all pigments) were similar between the eastern and western regions, indicating similarly "fresh" material, although overall pigment concentrations differed considerably. Chlorophyll *a* proportions at HAUSGARTEN sediments were higher compared to similar water depths at the Arctic continental slope (Boetius and Damm, 1998), but in a similar range or lower than those previously reported from multiyear ice-covered stations and ice margin stations in the central Arctic (12 and 20%, respectively; Rossel et al., 2016). These values, however, significantly depend on the type of OM that is exported (e.g., quality, fast sinking vs. slow sinking), as well as the timing between deposition at the seafloor and subsequent sampling, and are thus difficult to compare directly.

Bottom water DOC and TDN concentrations in both years were in the range of those reported for the central Arctic (Rossel et al., 2016). Concentrations of DOC were higher in surface sediments than in bottom waters and were in the higher range of those reported for ice margin stations in the central Arctic (Rossel et al., 2016), reflecting the higher OM input especially in the eastern Fram Strait in concert with higher CPE and TOC concentrations in the sediments. Compared to the central Arctic, porewater DOC concentrations in the western Fram Strait were similar to those reported at multiyear ice-covered stations, while those at the eastern side were similar or higher than those at the ice margin (avg. ± SD of 134 ± 34 and 212 ± 78 μmol/L, respectively; Rossel et al., 2016). Compared to other marine systems, DOC concentrations in Arctic porewaters of Fram Strait were in the lower range, and those of the Central Arctic substantially lower than that of other oceans (Burdige and Komada, 2015; Schmidt et al., 2017; Fox et al., 2018; Loginova et al., 2020). Nonetheless,

the gradients between bottom water and porewater are in line with previous reports indicating at least one magnitude higher DOC concentration in porewater compared to bottom water, supporting the role of POM diagenesis in surface sediments for the production of DOC and flux to overlying bottom water (Schmidt et al., 2011; Burdige and Komada, 2015; Loginova et al., 2020).

DOC fluxes from the sediment followed the trends observed for surface porewater DOC concentrations, with higher fluxes in the eastern Strait and in 2013, in agreement with previously reported higher bacterial benthic remineralization in the East, especially at shallower stations (Hoffmann et al., 2018). The calculated DOC flux values from eastern Fram Strait were two to six-fold higher (except for station N4 in the north) than the values reported for ice margin stations in the central Arctic (Rossel et al., 2016). Please note that we re-calculated efflux values for the Central Arctic from this earlier paper to match the model of DOC flux applied for HAUSGARTEN sediments, i.e., assuming fluxes in the sediment rather than across the diffusive boundary layer (see section "DOC Efflux From Porewater Gradients" and **Supplementary Table S10**). Compared to other deep-sea sediments from the Atlantic (ca. 4500 m water depth) and Antarctic Ocean (<2500 m water depth), DOC fluxes in the western Fram Strait were in the lower range, while DOC fluxes in the eastern Fram Strait (HG, S1-3 and N4 stations) were up to 9 fold higher (37–259 and 66 mmol/m^2/yr for Weddell Sea and for Atlantic, respectively; Hulth et al., 1997; Hall et al., 2007). DOC fluxes from Arctic shelves located far from our sampling area, and from productive systems were similar or higher than those from the eastern shallower stations in our study (Hulthe et al., 1997; Loginova et al., 2020), supporting the hypothesis of strong links to productivity regimes and the availability of OM at the seafloor.

HAUSGARTEN porewaters (0–10 cm) displayed similar contributions of highly unsaturated formulas compared to those reported for ice margin stations in the central Arctic (Rossel et al., 2016). Of these formulas, 73% were CRAM-like compounds, slightly lower than the values reported for central Arctic porewaters (79%; Rossel et al., 2016). However, much higher contributions of polyphenols were detected at HAUSGARTEN compared to the central Arctic (polyphenols ranged between 1.9–3.6%; Rossel et al., 2016). According to previously reported relationships between polyphenols and terrigenous OM (Seidel et al., 2015b), our results suggest a higher contribution of terrigenous material in the Fram Strait (increasing from the western to the eastern side) compared to the central Arctic (Rossel et al., 2016), in agreement with the location of HAUSGARTEN and with the increase of terrestrial biomarkers nearby the Svalbard Archipelago (Lalande et al., 2016).

Molecular formulas of unsaturated aliphatics O-rich and unsaturated-N, previously associated with fresh material, displayed similar to lower contributions compared to ice margin stations in the central Arctic (unsaturated aliphatics O-rich and unsaturated-N avg. 1.6 ± 0.7 and 7.6 ± 8.7, respectively; Rossel et al., 2016). Nevertheless, the contribution of unsaturated-N formulas to the total N-containing compounds was similar or lower at HAUSGARTEN than in the central Arctic (unsaturated-N formulas at the ice margin and multiyear ice stations avg. 40 ± 19% and 17 ± 6%, Rossel et al., 2016). This difference may indicate that at HAUSGARTEN some organic N is stored in compounds that may be less accessible for microorganisms or that less fresh material reaches the benthos at these locations. Indeed, proportions of chlorophyll *a* were slightly higher at ice margin stations in the central Arctic, probably due to the input of fast-sinking algae aggregates at the time of sampling (Boetius et al., 2013). Although the abundance of unsaturated-N formulas was lower at HAUSGARTEN than in the central Arctic, higher proportions were observed in 2013 than in 2014, favoring the idea that an increase in phytodetritus would increase the contribution of unsaturated-N formulas in porewater.

Contrary to previous observations in the central Arctic (Rossel et al., 2016), sediment depth (top 10 cm) was not a main driving force of porewater DOM composition, but rather spatial (east and west differences) and temporal variability in OM input. The lack of clear gradients in DOM molecular patterns with sediment depth is likely due to more active bioturbation at HAUSGARTEN sediments compared to the central Arctic (Soltwedel et al., 2019).

Overall, the associations between porewater DOM composition and food availability (i.e., phytodetritus proxies) were similar to ones previously reported for central Arctic sediments (Rossel et al., 2016). Porewater DOM composition in surface sediments at HAUSGARTEN was, based on our multivariate statistical analysis, correlated to enzymatic activity, and phospholipid and protein content, but not with bacterial abundance and biomass, which did not show large differences between eastern and western Fram Strait. Furthermore, porewater DOM composition in the Arctic Ocean may rather be related to the composition of bacterial groups than to their total abundance, in agreement with previous observations in coastal seafloor (Oni et al., 2015) and deep-sea sediments (Jessen et al., 2017; Pop Ristova et al., 2017).

Molecular Variability in Surface Porewater and Bottom Water Reflects Sources and Sinks of DOM

The molecular composition of bottom water DOM was characterized as more unsaturated and with higher molecular weight (DBE_{wa} and MW_{wa}) compared to surface porewater, in agreement with previous observations in central Arctic sediments (Rossel et al., 2016). However, in the Black Sea generally larger and more unsaturated formulas are accumulated in the porewater compared to bottom water (Schmidt et al., 2011), which may result from a different composition of the OM reaching the seafloor in oxic and anoxic ocean basins. Furthermore, bottom water is reported to display a lower richness of molecular formulas and N-containing compounds compared to porewater (Schmidt et al., 2011, 2017), in agreement with our observations in the Arctic Ocean (Rossel et al., 2016; and this study). For this study, we found that only 2% of the formulas present in bottom water were unique to this pool. However, more formulas in surface (16% of the formulas) and deep porewater (32% of the formulas) were absent or below detection in bottom water. Because 84% of the DOM formulas in surface porewater were also found in the bottom water,

overlying bottom water reflects surface porewater composition due to an exchange across the sediment-water interface. This observation aligns with the DOC efflux and a more similar composition between bottom water and surface porewater DOM than between bottom water and subsurface porewater (Schmidt et al., 2017; and this study). However, even a higher number of formulas in surface porewater DOM (96% of its formulas) were shared with the subsurface (here defined as 1–10 cm). Therefore, surface sediment DOM is a source for bottom water and subsurface sediments, but the bacterial communities appear to filter specific components of DOM in surface sediments, and allowed less molecular formulas to escape into the bottom water (16% of it) than to subsurface sediments (4%). In the subsurface, overall DOM composition was most diverse (the number of unique formulas increased from bottom water to subsurface porewater), especially due to the presence of more degraded DOM (highly unsaturated formulas). Thus, the bacterial communities in surface and subsurface sediments reworked DOM, affecting its composition substantially. The calculated average diffusion time for a DOM molecule in the sediment is 0.01 yr per 1 cm. The DOM composition in the upper 10 cm of sediments suggests that the signal of recent phytodetritus was restricted to surface sediment porewaters, indicating that the signal is rapidly lost after deposition, due to porewater DOM alteration by the bacterial communities in the sediment. Our observations are in agreement with the increase of more refractory DOM with increasing sediment depth detected by nuclear magnetic resonance (Fox et al., 2018) and optical properties (Loginova et al., 2020) of porewater DOM in other marine sediments.

Unsaturated-N formulas, which have previously been associated with fresh OM input, were higher in surface porewaters than bottom water (also referred to as peptide formulas; Rossel et al., 2016; Schmidt et al., 2011, 2017). Unsaturated-N contributions were in agreement with other molecular indicators in surface porewater (higher MLBwl and $I_{bioprod}$), which suggests a higher contribution of fresh and bioproduced material in surface porewaters compared to bottom waters. This observation is in line with the deposition and accumulation of OM at the seafloor, where the bulk degradation of OM is mediated by microbial communities in surface sediments by a wider spectrum of active enzymes (Arnosti, 2011; Middelburg, 2018). However, the calculated degradation index, I_{Deg}, did not reflect differences in composition between bottom water and surface porewaters. This may indicate that the application of this index, which was defined based on the correlation of molecular formulas to radiocarbon age for water column DOM (Flerus et al., 2012), cannot be used to compare overlying bottom water and surface porewater due to the exchange of DOM across their interface.

Unsaturated aliphatic O-rich formulas, which have also been reported to be higher in central Arctic sediments than in their overlying bottom waters (Rossel et al., 2016), only followed this trend in the eastern Fram Strait in agreement with their relation to higher phytodetritus input at this location. Although higher contribution of these compounds was observed in surface porewater, molecular indicators associated with fresh material (unsaturated aliphatics O-rich and unsaturated-N) were also higher in bottom water in 2013 compared to 2014, in agreement with higher OM input and DOC efflux in the former year. Nevertheless, a comparison of bottom waters from eastern and western Fram Strait indicated that the latter had higher abundances of unique CRAM-like compounds (absent in their surface porewaters) compared to the East, consistent with less input of fresh material at these permanently ice-covered stations. These data suggest that Arctic sediments are a source of CRAM and fresh DOM to the overlying bottom water, whose contributions vary depending on the quality and quantity of the OM deposited, as previously suggested for other environments (Fox et al., 2018; Loginova et al., 2020).

CONCLUSION

In this study, we show that regional and interannual differences in the production and deposition of OM are reflected in the DOM pool (DOC concentration and DOM composition) of deep-sea surface sediment porewaters, both regionally as well as across ocean basins. The permanent ice cover in the western Fram Strait limits productivity and OM input to the sediment, resulting in a porewater DOM composition that is characterized as more degraded. In contrast, porewater DOM in the eastern Fram Strait has a stronger signal of fresh phytodetrital matter, which decreased with increasing water depth. In this regard, the FT-ICR-MS method and the DOM freshness indicators used were generally able to resolve local and regional differences in surface productivity, export fluxes and OM availability which varied by at least 40, 70, and 30%, respectively, between years and regions. By comparing our results of Fram Strait to data from the Central Arctic basins, the Atlantic and Black Sea, the study also shows that differences between ocean basin productivity and export regimes are captured in the molecular composition of DOM in pore- and bottom waters. Furthermore, we find evidence for the production of a considerable fraction of DOM formulas related to degradation of OM in subsurface sediments, and a differential export from surface sediments to the bottom water and subsurface layers, indicating the substantial role of surface-sediment bacteria for the transformation of DOM. Although this study only provides a snapshot, our results stress the potential impact of changes in primary productivity and OM export on OM composition and benthic fluxes. In the future, more studies should aim to investigate the temporal scales at which these processes are relevant. A better understanding of seasonal variations will help to contrast these against changes resulting from longer-term environmental shifts. Furthermore, surface porewater DOM composition (which was related to enzymatic activity and the content of protein and phospholipids) was not associated with bacterial abundance and biomass, rather suggesting a coupling at the level of bacterial community composition/function. Therefore, studies exploring the interplay between microbial community composition/function and DOM molecular diversity are necessary to identify key microorganisms involved in the first steps of OM decomposition and production of DOM in porewater.

DATA AVAILABILITY STATEMENT

The data were stored in the Data Publisher for Earth and Environmental Science PANGAEA (www.pangaea.de). Details for 2013 and 2014 data from the LTER observatory HAUSGARTEN and from this study (Bacterial cell counts and cell volume, DOC and TDN, DOM composition, etc.) are reported in the reference list.

AUTHOR CONTRIBUTIONS

PR, CB, and AB designed the study. CB performed the sampling. PR analyzed the data and wrote the manuscript with contributions from CB, AB, LH, and TD.

FUNDING

This work has received funding from the European Research Council (ERC) under the European Union's Seventh Framework Program (FP7/2007-2013) research project ABYSS (Grant No. 294757) to AB. This publication is Eprint ID 50429 of the Alfred Wegener Institute Helmholtz Center for Polar and Marine research, Bremerhaven, Germany. We are grateful for the funding by the Hanse Institute for Advanced Studies (HWK), the Deutsche Forschungsgemeinschaft (DFG, German Research Foundation No. 422798570) and the Geochemical Society, which made the workshop "Marine Organic Biogeochemistry" at HWK possible.

ACKNOWLEDGMENTS

We thank the captain and crew and chief scientists of the RV Maria S Merian expedition MSM29 and RV Polarstern expedition PS85, as well as S. Becker, J. Rapp, and K. Hoffmann for support with sampling on board. We thank M. Friebe, I. Ulber, and K. Klaproth for support during sample analysis. V. Schourup-Kristensen provided chlorophyll maps, and C. Lorenzen and E.-M. Nöthig POC flux data. We also thank F. Wenzhöfer for support with carbon flux calculations, and Wilken-Jon von Appen for advice on interpreting hydrographical data. The work was carried out in the framework of the HGF Infrastructure Program FRAM of the Alfred-Wegener-Institute Helmholtz Center for Polar and Marine Research.

SUPPLEMENTARY MATERIAL

The Supplementary Material for this article can be found online at: https://www.frontiersin.org/articles/10.3389/fmars.2020.00428/full#supplementary-material

REFERENCES

Arnarson, T. S., and Keil, R. G. (2001). Organic–mineral interactions in marine sediments studied using density fractionation and X-ray photoelectron spectroscopy. *Org. Geochem.* 32, 1401–1415. doi: 10.1016/s0146-6380(01)00114-0

Arnosti, C. (2011). Microbial extracellular enzymes and the marine carbon cycle. *Annu. Rev. Mar. Sci.* 3, 401–425. doi: 10.1146/annurev-marine-120709-142731

Aufdenkampe, A. K., Hedges, J. I., Richey, J. E., Krusche, A. V., and Llerena, C. A. (2001). Sorptive fractionation of dissolved organic nitrogen and amino acids onto fine sediments within the Amazon Basin. *Limnol. Oceanogr.* 46, 1921–1935. doi: 10.4319/lo.2001.46.8.1921

Bauerfeind, E., Nöthig, E.-M. M., Beszczynska, A., Fahl, K., Kaleschke, L., Kreker, K., et al. (2009). Particle sedimentation patterns in the eastern Fram Strait during 2000–2005: results from the Arctic long-term observatory HAUSGARTEN. *Deep Sea Res. Part I Oceanogr. Res. Pap.* 56, 1471–1487. doi: 10.1016/j.dsr.2009.04.011

Beszczynska-Moller, A., Fahrbach, E., Schauer, U., and Hansen, E. (2012). Variability in Atlantic water temperature and transport at the entrance to the Arctic Ocean, 1997-2010. *ICES J. Mar. Sci.* 69, 852–863. doi: 10.1093/icesjms/fss056

Bienhold, C. (2019). *Prokaryotic Cell Abundance and Biomass Measured During Maria S Merian Cruise MSM29 and Polarstern Cruise PS85 to the Fram Strait*. Bremerhaven: PANGAEA. doi: 10.1594/PANGAEA.908130

Bienhold, C., Boetius, A., and Ramette, A. (2012). The energy–diversity relationship of complex bacterial communities in Arctic deep-sea sediments. *ISME J.* 6, 724–732. doi: 10.1038/ismej.2011.140

Boetius, A., Albrecht, S., Bakker, K., Bienhold, C., Felden, J., Fernandez-Mendez, M., et al. (2013). Export of algal biomass from the melting Arctic sea ice. *Science* 339, 1430–1432. doi: 10.1126/science.1231346

Boetius, A., and Damm, E. (1998). Benthic oxygen uptake, hydrolytic potentials and microbial biomass at the Arctic continental slope. *Deep Sea Res. Part I Oceanogr. Res. Pap.* 45, 239–275. doi: 10.1016/s0967-0637(97)00052-6

Boetius, A., and Lochte, K. (1994). Regulation of microbial enzymatic degradation of organic matter in deep-sea sediments. *Mar. Ecol. Prog. Ser.* 104, 299–307. doi: 10.3354/meps104299

Børsheim, K. Y., Bratbak, G., and Heldal, M. (1990). Enumeration and biomass estimation of planktonic bacteria and viruses by transmission electron microscopy. *Appl. Environ. Microbiol.* 56, 352–356. doi: 10.1128/aem.56.2.352-356.1990

Boudreau, B. B. (1997). *Diagenetic Models and their Implementation: Modelling Transport and Reactions in Aquatic Sediments*. Heidelberg: Springer.

Burdige, D., Berelson, W., and Coale, K. H. (1999). Fluxes of dissolved organic carbon from California continental margin sediments. *Geochim. Cosmochim. Acta* 63, 1507–1515. doi: 10.1016/s0016-7037(99)00066-6

Burdige, D. J. (2006). *Geochemistry of Marine Sediments. Xviii*. Princeton, NJ: Princeton University Press.

Burdige, D. J., Alperin, M. J., Homstead, J., and Martens, C. S. (1992). The role of benthic fluxes of dissolved organic carbon in oceanic and sedimentary carbon cycling. *Geophys. Res. Lett.* 19, 1851–1854. doi: 10.1029/92GL02159

Burdige, D. J., and Komada, T. (2015). "Sediment pore waters," in *Biogeochemistry of Marine Dissolved Organic Matter*, 2nd Edn, eds D. A. Hansell and C. A. Carlson (Boston: Academic Press), 535–577. doi: 10.1016/B978-0-12-405940-5.00012-1

Buttigieg, P. L., and Ramette, A. (2014). A guide to statistical analysis in microbial ecology: a community-focused, living review of multivariate data analyses. *FEMS Microbiol. Ecol.* 90, 543–550. doi: 10.1111/1574-6941.12437

Cathalot, C., Rabouille, C., Sauter, E., Schewe, I., and Soltwedel, T. (2015). Benthic oxygen uptake in the Arctic Ocean margins - A case study at the deep-sea observatory HAUSGARTEN (Fram Strait). *PLoS One* 10:e0138339. doi: 10.1371/journal.pone.0138339

D'Andrilli, J., Cooper, W. T., Foreman, C. M., and Marshall, A. G. (2015). An ultrahigh-resolution mass spectrometry index to estimate natural organic matter lability. *Rapid Commun. Mass Spectrom.* 29, 2385–2401. doi: 10.1002/rcm.7400

de Steur, L., Hansen, E., Gerdes, R., Karcher, M., Fahrbach, E., and Holfort, J. (2009). Freshwater fluxes in the East Greenland Current: a decade

of observations. *Geophys. Res. Lett.* 36, 2–6. doi: 10.1029/2009gl041278

Dittmar, T., Koch, B., Hertkorn, N., and Kattner, G. (2008). A simple and efficient method for the solid-phase extraction of dissolved organic matter (SPE-DOM) from seawater. *Limnol. Oceanogr. Methods* 6, 230–235. doi: 10.4319/lom.2008.6.230

Dittmar, T., and Stubbins, A. (2014). "Dissolved organic matter in aquatic systems," in *Treatise on Geochemistry*, eds H. D. Holland and K. K. Turekian (Amsterdam: Elsevier), 125–156. doi: 10.1016/B978-0-08-095975-7.01010-X

Dobricic, S., Vignati, E., and Russo, S. (2016). Large-scale atmospheric warming in winter and the arctic sea ice retreat. *J. Clim.* 29, 2869–2888. doi: 10.1175/JCLI-D-15-0417.1

Donis, D., McGinnis, D. F., Holtappels, M., Felden, J., and Wenzhoefer, F. (2016). Assessing benthic oxygen fluxes in oligotrophic deep sea sediments (HAUSGARTEN observatory). *Deep Sea Res. Part I Oceanogr. Res. Pap.* 111, 1–10. doi: 10.1016/j.dsr.2015.11.007

Engel, A., Bracher, A., Dinter, T., Endres, S., Grosse, J., Metfies, K., et al. (2019). Inter-annual variability of organic carbon concentration in the eastern Fram strait during summer (2009–2017). *Front. Mar. Sci.* 6:187. doi: 10.3389/fmars.2019.00187

Fadeev, E., Salter, I., Schourup-Kristensen, V., Nöthig, E.-M., Metfies, K., Engel, A., et al. (2018). Microbial communities in the East and West Fram strait during sea ice melting season. *Front. Mar. Sci.* 5:429. doi: 10.3389/fmars.2018.00429

Fahrbach, E., Rohardt, G., Shauer, U., Meincke, J., Osterhus, S., and Verduin, J. (2001). Direct measurements of heat and mass transport through Fram Strait. *Polar Res.* 20, 217–224. doi: 10.3402/polar.v20i2.6520

Findlay, R. H., King, G. M., and Watling, L. (1989). Efficacy of phospholipid analysis in determining microbial biomass in sediments. *Appl. Environ. Microbiol.* 55, 2888–2893. doi: 10.1128/aem.55.11.2888-2893.1989

Flerus, R., Lechtenfeld, O. J., Koch, B. P., McCallister, S. L., Schmitt-Kopplin, P., Benner, R., et al. (2012). A molecular perspective on the ageing of marine dissolved organic matter. *Biogeosciences* 9, 1935–1955. doi: 10.5194/bg-9-1935-2012

Fox, C. A., Abdulla, H. A., Burdige, D. J., Lewicki, J. P., and Komada, T. (2018). Composition of dissolved organic matter in pore waters of anoxic marine sediments analyzed by 1H nuclear magnetic resonance spectroscopy. *Front. Mar. Sci.* 5:172. doi: 10.3389/fmars.2018.00172

Grebmeier, J. M., Overland, J. E., Moore, S. E., Farley, E. V., Carmack, E. C., Cooper, L. W., et al. (2006). A major ecosystem shift in the northern Bering Sea. *Science* 311, 1461–1464. doi: 10.1126/science.1121365

Greiser, N., and Faubel, A. (1989). "Biotic factors," in *Introduction to the Study of Meiofauna*, eds R. P. Higgens and H. Thiel (London: Smithsonian Institution Press), 79–114.

Hall, P. O. J., Brunnega, J., Hulthe, G., Martin, W. R., Stahl, H., and Tengberg, A. (2007). Dissolved organic matter in abyssal sediments?: core recovery artifacts. *Limnol. Oceanogr.* 52, 19–31. doi: 10.4319/lo.2007.52.1.0019

Hawkes, J. A., Patriarca, C., Sjöberg, P. J. R., Tranvik, L. J., and Bergquist, J. (2018). Extreme isomeric complexity of dissolved organic matter found across aquatic environments. *Limnol. Oceanogr. Lett.* 3, 21–30. doi: 10.1002/lol2.10064

Hertkorn, N., Benner, R., Frommberger, M., Schmitt-kopplin, P., Witt, M., Kaiser, K., et al. (2006). Characterization of a major refractory component of marine dissolved organic matter. *Geochim. Cosmochim. Acta* 70, 2990–3010. doi: 10.1016/j.gca.2006.03.021

Hoffmann, K., Hassenrück, C., Salman-Carvalho, V., Holtappels, M., and Bienhold, C. (2017). Response of bacterial communities to different detritus compositions in arctic deep-sea sediments. *Front. Microbiol.* 8:266. doi: 10.3389/fmicb.2017.00266

Hoffmann, R., Braeckman, U., Hasemann, C., and Wenzhöfer, F. (2018). Deep-sea benthic communities and oxygen fluxes in the Arctic Fram Strait controlled by sea-ice cover and water depth. *Biogeosciences* 15, 4849–4869. doi: 10.5194/bg-15-4849-2018

Hulth, S., Tengberg, A., Landén, A., and Hall, P. O. J. (1997). Mineralization and burial of organic carbon in sediments of the southern Weddell Sea (Antarctica). *Deep Sea Res. Part I Oceanogr. Res. Pap.* 44, 955–981. doi: 10.1016/s0967-0637(96)00114-8

Hulthe, G., Hall, P., and Damm, E. (1997). Benthic carbon fluxes – DOC versus ?CO2 in shelf, slope and deep-sea environments, and relation to oxygen fluxes. *Rep. Polar Res.* 226, 115–116.

Iversen, N., and Jorgensen, B. B. (1993). Diffusion coefficients of sulfate and methane in marine sediments: influence of porosity. *Geochim. Cosmochim. Acta* 57, 571–578. doi: 10.1016/0016-7037(93)90368-7

Jacob, M., Soltwedel, T., Boetius, A., and Ramette, A. (2013). Biogeography of deep-sea benthic bacteria at regional scale (LTER HAUSGARTEN, Fram Strait, Arctic). *PLoS One* 8:e72779. doi: 10.1371/journal.pone.0072779

Jessen, G. L., Lichtschlag, A., Ramette, A., Pantoja, S., Rossel, P. E., Schubert, C. J., et al. (2017). Hypoxia causes preservation of labile organic matter and changes seafloor microbial community composition (Black Sea). *Sci. Adv.* 3:e1601897. doi: 10.1126/sciadv.1601897

Jones, D. O. B., Yool, A., Wei, C. L., Henson, S. A., Ruhl, H. A., Watson, R. A., et al. (2014). Global reductions in seafloor biomass in response to climate change. *Glob. Change Biol.* 20, 1861–1872. doi: 10.1111/gcb.12480

Jorgensen, B. B. (2006). "Bacteria and marine biogeochemistry," in *Marine Geochemistry*, eds H. D. Schulz and M. Zabel (Berlin: Springer), 169–206. doi: 10.1007/3-540-32144-6_5

Käss, M., Vedenin, A., Hasemann, C., Brandt, A., and Soltwedel, T. (2019). Community structure of macrofauna in the deep Fram Strait: a comparison between two bathymetric gradients in ice-covered and ice-free areas. *Deep Sea Res. Part I Oceanogr. Res. Pap.* 152:103102. doi: 10.1016/j.dsr.2019.103102

Kêdra, M., Moritz, C., Choy, E. S., David, C., Degen, R., Duerksen, S., et al. (2015). Status and trends in the structure of Arctic benthic food webs. *Polar Res.* 34:23775. doi: 10.3402/polar.v34.23775

Klages, M., Boetius, A., Christensen, J. P., Deubel, H., Piepenburg, D., Schewe, I., et al. (2004). "The benthos of Arctic seas and its role for the organic carbon cycle at the seafloor," in *The Organic Carbon Cycle in the Arctic Ocean*, eds R. W. Stein and R. Macdonald (Berlin: Springer), 139–167. doi: 10.1007/978-3-642-18912-8_6

Koch, B. P., and Dittmar, T. (2006). From mass to structure?: an Aromaticity index for high-resolution mass data of natural organic matter. *Rapid Commun. Mass Spectrom.* 20, 926–932. doi: 10.1002/rcm.2386

Koch, B. P., and Dittmar, T. (2016). Erratum of: from mass to structure: an Aromaticity index for high-resolution mass data of natural organic matter. *Rapid Commun. Mass Spectrom.* 30:250. doi: 10.1002/rcm.7433

Kortsch, S., Primicerio, R., Beuchel, F., Renaud, P. E., Rodrigues, J., Lonne, O. J., et al. (2012). Climate-driven regime shifts in Arctic marine benthos. *Proc. Natl. Acad. Sci. U.S.A.* 109, 14052–14057. doi: 10.1073/pnas.1207509109

Köster, M., Jensen, P., and Meyer-Reil, L.-A. (1991). "Hydrolytic activities of organisms and biogenic structures in deep-sea sediments," in *Microbial Enzymes in Aquatic Environments*, ed. R. J. Chróst (New York, NY: Springer), 298–310. doi: 10.1007/978-1-4612-3090-8_19

Krumpen, T. (2017). *Sea Ice and Amtospheric Conditions at HAUSGARTEN Between 2000-2016 (Daily Resolution), Link to Model Results*. Bremerhaven: PANGAEA. doi: 10.1594/PANGAEA.878244

Kwok, R., and Rothrock, D. A. (2009). Decline in Arctic sea ice thickness from submarine and ICESat records: 1958-2008. *Geophys. Res. Lett.* 36, 1–5. doi: 10.1029/2009GL039035

Lalande, C., Bauerfeind, E., Nöthig, E.-M., and Beszczynska-Möller, A. (2013). Impact of a warm anomaly on export fluxes of biogenic matter in the eastern Fram Strait. *Prog. Oceanogr.* 109, 70–77. doi: 10.1016/j.pocean.2012.09.006

Lalande, C., Nöthig, E.-M., Bauerfeind, E., Hardge, K., Beszczynska-Möller, A., and Fahl, K. (2016). Lateral supply and downward export of particulate matter from upper waters to the seafloor in the deep eastern Fram Strait. *Deep Sea Res. Part I Oceanogr. Res. Pap.* 114, 78–89. doi: 10.1016/j.dsr.2016.04.014

Lalande, C., Nöthig, E.-M., Somavilla, R., Bauerfeind, E., Shevchenko, V., and Okolodkov, Y. (2014). Variability in under-ice export fluxes of biogenic matter in the Arctic Ocean. *Glob. Biogeochem. Cycles* 28, 571–583. doi: 10.1002/2013GB004735

Leu, E., Søreide, J. E., Hessen, D. O., Falk-Petersen, S., and Berge, J. (2011). Consequences of changing sea-ice cover for primary and secondary producers in the European Arctic shelf seas: timing, quantity, and quality. *Prog. Oceanogr.* 90, 18–32. doi: 10.1016/j.pocean.2011.02.004

Linkhorst, A., Dittmar, T., and Waska, H. (2017). Molecular fractionation of dissolved organic matter in a shallow subterranean estuary: the role of the iron curtain. *Environ. Sci. Technol.* 51, 1312–1320. doi: 10.1021/acs.est.6b03608

Loginova, A. N., Dale, A. W., LeMoigne, F. A. C., Thomsen, S., Sommer, S., Wallmann, K., et al. (2020). Sediment release of dissolved organic matter to the oxygen minimum zone off Peru. *Biogeosci. Discuss.* 2020, 1–30.

Magnusson, A. (2010). *gmt: Interface Between GMT Map-Making Software and R*. Available online at: https://CRAN.R-project.org/package=gmt

McLafferty, F. W., and Turecek, F. (1994). *Interpretation of Mass Spectra*, 4th Edn, ed. W. Vetter (Hoboken, NJ: John Wiley & Sons, Ltd). doi: 10.1002/bms.1200230614

Middelburg, J. J. (2018). Reviews and syntheses: to the bottom of carbon processing at the seafloor. *Biogeosciences* 15, 413–427. doi: 10.5194/bg-15-413-2018

Nöthig, E. M., Bracher, A., Engel, A., Metfies, K., Niehoff, B., Peeken, I., et al. (2015). Summertime plankton ecology in Fram strait-a compilation of long-and short-term observations. *Polar Res.* 34:23349. doi: 10.3402/polar.v34.23349

Notz, D., and Stroeve, J. (2016). Observed Arctic sea-ice loss directly follows anthropogenic CO2 emission. *Science* 354, 747–750. doi: 10.1126/science.aag2345

Oksanen, J. (2017). *vegan: Community Ecology Package. R package version 2.4–5*.

Oni, O. E., Schmidt, F., Miyatake, T., Kasten, S., Witt, M., Hinrichs, K.-U., et al. (2015). Microbial communities and organic matter composition in surface and subsurface sediments of the Helgoland mud area, North Sea. *Front. Microbiol.* 6:1290. doi: 10.3389/fmicb.2015.01290

Osterholz, H., Niggemann, J., Giebel, H.-A., Simon, M., and Dittmar, T. (2015). Inefficient microbial production of refractory dissolved organic matter in the ocean. *Nat. Commun.* 6:7422. doi: 10.1038/ncomms8422

Overland, J. E., and Wang, M. (2013). When will the summer Arctic be nearly sea ice free? *Geophys. Res. Lett.* 40, 2097–2101. doi: 10.1002/grl.50316

Paquette, R. G., Bourke, R. H., Newton, J. F., and Perdue, W. F. (1985). The East Greenland polar front in autumn. *J. Geophys. Res. Oceans* 90, 4866–4882. doi: 10.1029/JC090iC03p04866

Peng, G., and Meier, W. N. (2018). Temporal and regional variability of Arctic sea-ice coverage from satellite data. *Ann. Glaciol.* 59, 191–200. doi: 10.1017/aog.2017.32

Pohlabeln, A. M., Gomez-Saez, G. V., Noriega-Ortega, B. E., and Dittmar, T. (2017). Experimental evidence for abiotic sulfurization of marine dissolved organic matter. *Front. Mar. Sci.* 4:364. doi: 10.3389/fmars.2017.00364

Polyakov, I. V., Pnyushkov, A. V., Alkire, M. B., Ashik, I. M., Baumann, T. M., Carmack, E. C., et al. (2017). Greater role for Atlantic inflows on sea-ice loss in the Eurasian Basin of the Arctic Ocean. *Science* 356, 285–291. doi: 10.1126/science.aai8204

Pop Ristova, P., Bienhold, C., Wenzhöfer, F., Rossel, P. E., and Boetius, A. (2017). Temporal and spatial variations of bacterial and faunal communities associated with deep-sea wood falls. *PLoS One* 12:e0169906. doi: 10.1371/journal.pone.0169906

Rabe, B., von Appen, W.-J., Latarius, K., and Wisotzki, A. (2014). *Physical Oceanography During POLARSTERN Cruise PS85 (ARK-XXVIII/2)*. Bremerhaven: PANGAEA. doi: 10.1594/PANGAEA.837425

Ramette, A. (2007). Multivariate analyses in microbial ecology. *FEMS Microbiol. Ecol.* 62, 142–160. doi: 10.1111/j.1574-6941.2007.00375.x

Randelhoff, A., Reigstad, M., Chierici, M., Sundfjord, A., Ivanov, V., Cape, M., et al. (2018). Seasonality of the physical and biogeochemical hydrography in the inflow to the Arctic Ocean through Fram Strait. *Front. Mar. Sci.* 5:224. doi: 10.3389/fmars.2018.00224

Riedel, T., and Dittmar, T. (2014). A method detection limit for the analysis of natural organic matter via Fourier Transform Ion Cyclotron Resonance Mass Spectrometry. *Anal. Chem.* 86, 8376–8382. doi: 10.1021/ac501946m

Rossel, P. E., Bienhold, C., Boetius, A., and Dittmar, T. (2016). Dissolved organic matter in pore water of Arctic Ocean sediments: environmental influence on molecular composition. *Organ. Geochem.* 97, 41–52. doi: 10.1016/j.orggeochem.2016.04.003

Rossel, P. E., and Dittmar, T. (2019a). *Dissolved Organic Carbon and Total Dissolved Organic Nitrogen in Sediment Porewater and Overlying Bottom Water Collected During Maria S Merian Cruise MSM29 and Polarstern Cruise P85 to the Fram Strait*. Bremerhaven: PANGAEA. doi: 10.1594/PANGAEA.908702

Rossel, P. E., and Dittmar, T. (2019b). *Normalized Peak Intensities from Solid Phase Extracted Dissolved Organic Matter from Porewater and Overlying Bottom Water Collected During Maria S Merian Cruise MSM29 and Polarstern Cruise PS85 to the Fram Strait*. Bremerhaven: PANGAEA. doi: 10.1594/PANGAEA.909107

Rossel, P. E., Stubbins, A., Rebling, T., Koschinsky, A., Hawkes, J. A., and Dittmar, T. (2017). Thermally altered marine dissolved organic matter in hydrothermal fluids. *Organ. Geochem.* 110, 73–86. doi: 10.1016/j.orggeochem.2017.05.003

Rossel, P. E., Vähätalo, A. V., Witt, M., and Dittmar, T. (2013). Molecular composition of dissolved organic matter from a wetland plant (*Juncus effusus*) after photochemical and microbial decomposition (1.25 yr): common features with deep sea dissolved organic matter. *Organ. Geochem.* 60, 62–71. doi: 10.1016/j.orggeochem.2013.04.013

RStudio Team (2015). *RStudio: Integrated Development Environment for R*. Available online at: http://www.rstudio.com/

Schewe, I. (2018). *Biochemical Investigation of Multicorer Sediment Profile MSM29_432-2*. Bremerhaven: PANGAEA. doi: 10.1594/PANGAEA.885304

Schewe, I. (2019). *Biochemical Investigation of Multicorer Sediment Profile PS85/436-1*. Bremerhaven: PANGAEA. doi: 10.1594/PANGAEA.903935

Schewe, I., and Soltwedel, T. (2003). Benthic response to ice-edge-induced particle flux in the Arctic Ocean. *Polar Biol.* 26, 610–620. doi: 10.1007/s00300-003-0526-8

Schmidt, F., Elvert, M., Koch, B. P., Witt, M., and Hinrichs, K.-U. (2009). Molecular characterization of dissolved organic matter in pore water of continental shelf sediments. *Geochim. Cosmochim. Acta* 73, 3337–3358. doi: 10.1016/j.gca.2009.03.008

Schmidt, F., Koch, B. P., Elvert, M., Schmidt, G., Witt, M., and Hinrichs, K. (2011). Diagenetic transformation of dissolved organic nitrogen compounds under contrasting sedimentary redox conditions in the Black Sea. *Environ. Sci. Technol.* 45, 5223–5229. doi: 10.1021/es2003414

Schmidt, F., Koch, B. P., Goldhammer, T., Elvert, M., Witt, M., Lin, Y. S., et al. (2017). Unraveling signatures of biogeochemical processes and the depositional setting in the molecular composition of pore water DOM across different marine environments. *Geochim. Cosmochim. Acta* 207, 57–80. doi: 10.1016/j.gca.2017.03.005

Schmidt, F., Koch, B. P., Witt, M., and Hinrichs, K. (2014). Extending the analytical window for water-soluble organic matter in sediments by aqueous Soxhlet extraction. *Geochim. Cosmochim. Acta* 141, 83–96. doi: 10.1016/j.gca.2014.06.009

Schulz, H. D. (2000). "Quantification of early diagenesis: dissolved constituents in marine pore water," in *Marine Geochemistry*, eds H. D. Schulz and M. Zabel (Berlin: Springer), 85–128. doi: 10.1007/978-3-662-04242-7_3

Seibt, M. (2017). *The Molecular Geography of Dissolved Organic Matter in the Atlantic and Southern Ocean*. Ph.D. thesis, University of Oldenburg, Oldenburg.

Seidel, M., Beck, M., Greskowiak, J., Riedel, T., Waska, H., Suryaputra, I. N. A., et al. (2015a). Benthic-pelagic coupling of nutrients and dissolved organic matter composition in an intertidal sandy beach. *Mar. Chem.* 176, 150–163. doi: 10.1016/j.marchem.2015.08.011

Seidel, M., Yager, P. L., Ward, N. D., Carpenter, E. J., Gomes, H. R., Krusche, A. V., et al. (2015b). Molecular-level changes of dissolved organic matter along the Amazon River-to-ocean continuum. *Mar. Chem.* 177, 218–231. doi: 10.1016/j.marchem.2015.06.019

Seidel, M., Beck, M., Riedel, T., Waska, H., Suryaputra, I. G. N. A., Schnetger, B., et al. (2014). Biogeochemistry of dissolved organic matter in an anoxic intertidal creek bank. *Geochim. Cosmochim. Acta* 140, 418–434. doi: 10.1016/j.gca.2014.05.038

Shuman, F. R., and Lorenzen, C. J. (1975). Quantitative degradation of chlorophyll by a marine herbivore. *Limnol. Oceanogr.* 20, 580–586. doi: 10.4319/lo.1975.20.4.0580

Sinninghe Damste, J. S., and de Leeuw, J. W. (1990). Analysis, structure and geochemical significance of organically-bound sulphur in the geosphere: state of the art and future research. *Organ. Geochem.* 16, 1077–1101. doi: 10.1016/0146-6380(90)90145-P

Smith, K. L., Ruhl, H. A., Bett, B. J., Billett, D. S. M., Lampitt, R. S., and Kaufmann, R. S. (2009). Climate, carbon cycling, and deep-ocean ecosystems. *Proc. Natl. Acad. Sci. U.S.A.* 106, 19211–19218. doi: 10.1073/pnas.0908322106

Soltwedel, T., Bauerfeind, E., Bergmann, M., Bracher, A., Budaeva, N., Busch, K., et al. (2016). Natural variability or anthropogenically-induced variation? Insights from 15 years of multidisciplinary observations at the arctic marine LTER site HAUSGARTEN. *Ecol. Indic.* 65, 89–102. doi: 10.1016/j.ecolind.2015.10.001

Soltwedel, T., Hasemann, C., Vedenin, A., Bergmann, M., Taylor, J., and Krauß, F. (2019). Bioturbation rates in the deep Fram strait: results from in situ experiments at the arctic LTER observatory HAUSGARTEN. *J. Exp. Mar. Biol. Ecol.* 511, 1–9. doi: 10.1016/j.jembe.2018.11.001

Stein, R. (2008). *Arctic Ocean Sediments: Processes, Proxies, and Paleoenvironment: Processes, Proxies, and Paleoenvironment*. Amsterdam: Elsevier.

Stubbins, A., and Dittmar, T. (2012). Low volume quantification of dissolved organic carbon and dissolved nitrogen. *Limnol. Oceanogr. Methods* 10, 347–352. doi: 10.4319/lom.2012.10.347

Sun, L., Perlwitz, J., and Hoerling, M. (2016). What caused the recent "Warm Arctic, Cold Continents" trend pattern in winter temperatures? *Geophys. Res. Lett.* 43, 5345–5352. doi: 10.1002/2016GL069024.Received

Thiel, H. (1982). Zoobenthos of the CINECA area and other upwelling regions. *Rapp. Proc. Verb. Réun. Cons. Int. Explor. Mer* 180, 323–334.

Wassmann, P., and Reigstad, M. (2011). Future Arctic Ocean seasonal ice zones and implications for pelagic-benthic coupling. *Oceanography* 24, 220–231. doi: 10.5670/oceanog.2011.74

Wenzhöfer, F., Bauerfeind, E., and Rohardt, G. (2013). *Physical Oceanography During Maria S. Merian Cruise MSM*29. Bremerhaven: PANGAEA. doi: 10.1594/PANGAEA.819391

Wohlers, J., Engel, A., Zollner, E., Breithaupt, P., Jurgens, K., Hoppe, H.-G., et al. (2009). Changes in biogenic carbon flow in response to sea surface warming. *Proc. Natl. Acad. Sci. U.S.A.* 106, 7067–7072. doi: 10.1073/pnas.0812743106

Zark, M., Christoffers, J., and Dittmar, T. (2017). Molecular properties of deep-sea dissolved organic matter are predictable by the central limit theorem: evidence from tandem FT-ICR-MS. *Mar. Chem.* 191, 9–15. doi: 10.1016/j.marchem.2017.02.005

Zhang, C., Dang, H., Azam, F., Benner, R., Legendre, L., Passow, U., et al. (2018). Evolving paradigms in biological carbon cycling in the ocean. *Natl. Sci. Rev.* 5, 481–499. doi: 10.1093/nsr/nwy074

Conflict of Interest: The authors declare that the research was conducted in the absence of any commercial or financial relationships that could be construed as a potential conflict of interest.

frontiers in Marine Science

MINI REVIEW
published: 26 June 2020
doi: 10.3389/fmars.2020.00518

Particulate Organic Carbon Deconstructed: Molecular and Chemical Composition of Particulate Organic Carbon in the Ocean

Jenan J. Kharbush[1], Hilary G. Close[2], Benjamin A. S. Van Mooy[3], Carol Arnosti[4], Rienk H. Smittenberg[5], Frédéric A. C. Le Moigne[6], Gesine Mollenhauer[7,8], Barbara Scholz-Böttcher[9], Igor Obreht[8], Boris P. Koch[7], Kevin W. Becker[10], Morten H. Iversen[7,8] and Wiebke Mohr[11]*

[1] Department of Earth and Environmental Science, University of Michigan, Ann Arbor, MI, United States, [2] Rosenstiel School of Marine and Atmospheric Science, University of Miami, Miami, FL, United States, [3] Department of Marine Chemistry and Geochemistry, Woods Hole Oceanographic Institution, Woods Hole, MA, United States, [4] Department of Marine Sciences, University of North Carolina at Chapel Hill, Chapel Hill, NC, United States, [5] Department of Geological Sciences, Stockholm University, Stockholm, Sweden, [6] Mediterranean Institute of Oceanography (UM 110, MIO), CNRS, IRD, Aix Marseille Université, Marseille, France, [7] Alfred Wegener Institute for Polar and Marine Research, Bremerhaven, Germany, [8] MARUM-Center for Marine Environmental Sciences, University of Bremen, Bremen, Germany, [9] Institute for Chemistry and Biology of the Marine Environment (ICBM), Carl von Ossietzky University of Oldenburg, Oldenburg, Germany, [10] GEOMAR Helmholtz Centre for Ocean Research Kiel, Kiel, Germany, [11] Department of Biogeochemistry, Max Planck Institute for Marine Microbiology, Bremen, Germany

OPEN ACCESS

Edited by:
Marius Nils Müller, Federal University of Pernambuco, Brazil

Reviewed by:
Frank Pavia, California Institute of Technology, United States
Tom Trull, Commonwealth Scientific and Industrial Research Organisation (CSIRO), Australia

***Correspondence:**
Jenan J. Kharbush
jenanjk@umich.edu

Specialty section:
This article was submitted to Marine Biogeochemistry, a section of the journal Frontiers in Marine Science

Received: *09 March 2020*
Accepted: *05 June 2020*
Published: *26 June 2020*

Citation:
Kharbush JJ, Close HG, Van Mooy BAS, Arnosti C, Smittenberg RH, Le Moigne FAC, Mollenhauer G, Scholz-Böttcher B, Obreht I, Koch BP, Becker KW, Iversen MH and Mohr W (2020) Particulate Organic Carbon Deconstructed: Molecular and Chemical Composition of Particulate Organic Carbon in the Ocean. Front. Mar. Sci. 7:518. doi: 10.3389/fmars.2020.00518

The dynamics of the particulate organic carbon (POC) pool in the ocean are central to the marine carbon cycle. POC is the link between surface primary production, the deep ocean, and sediments. The rate at which POC is degraded in the dark ocean can impact atmospheric CO_2 concentration. Therefore, a central focus of marine organic geochemistry studies is to improve our understanding of POC distribution, composition, and cycling. The last few decades have seen improvements in analytical techniques that have greatly expanded what we can measure, both in terms of organic compound structural diversity and isotopic composition, and complementary molecular omics studies. Here we provide a brief overview of the autochthonous, allochthonous, and anthropogenic components comprising POC in the ocean. In addition, we highlight key needs for future research that will enable us to more effectively connect diverse data sources and link the identity and structural diversity of POC to its sources and transformation processes.

Keywords: marine particles, water column, phytoplankton, marine microbes, structural analysis, organic matter characterization, biomarkers

INTRODUCTION

Particulate organic carbon (POC) is operationally defined as all combustible, non-carbonate carbon that can be collected on a filter. The oceanographic community has historically used a variety of filters and pore sizes, most commonly 0.7, 0.8, or 1.0 μm glass or quartz fiber filters. The biomass of living zooplankton is intentionally excluded from POC through the use of a pre-filter or specially designed sampling intakes that repel swimming organisms. Sub-micron particles, including most ocean prokaryotes, which are 0.2–0.8 μm in diameter, are often not captured but should be considered part of POC rather than dissolved organic carbon (DOC, recently reviewed

in Wagner et al., 2020), which is usually operationally defined as < 0.2 μm. Here, we consider POC to contain suspended and sinking particles ≥ 0.2 μm in size, which therefore includes biomass from living microbial cells, detrital material including dead cells, fecal pellets, other aggregated material, and terrestrially-derived organic matter. Some studies further divide POC operationally based on its sinking rate (Riley et al., 2012) or size, with ≥ 51 μm particles sometimes equated to the sinking fraction (e.g., Lam et al., 2011). Both DOC and POC play major roles in the carbon cycle, but POC is the major pathway by which OC produced by phytoplankton is exported -mainly by gravitational settling – from the surface to the deep ocean and eventually to sediments, and is thus a key component of the biological pump (Eppley and Peterson, 1979; Volk and Hoffert, 1985; Boyd and Trull, 2007; Cavan et al., 2015; Boyd et al., 2019; Le Moigne, 2019).

Accurately modeling the ocean carbon cycle requires both quantitative and qualitative understanding of POC production, composition, transformation, and cycling. Decades of measurements and modeling efforts have made significant progress toward this understanding, but persistent questions remain: How much POC is in the oceans? What determines POC spatial distribution and molecular composition? What is the residence time of POC? What regulates exchange between POC and DOC? What processes control the delivery of POC from surface waters to the mesopelagic? What controls degradation and preservation of POC delivered to marine sediments (Arnosti et al., 2019, this issue)?

Many marine organic geochemical investigations attempt to answer these questions from the bottom up, through characterization and quantification of the molecules that make up POC. Notably, because POC encompasses most living cells in the ocean, a considerable proportion of POC (particularly "fresh" POC collected in the upper ocean) is identifiable at the biomolecular level. This contrasts with DOC and sedimentary organic matter, which are predominantly non-cellular and molecularly uncharacterizable (Hedges et al., 2000; Kujawinski, 2011; Hansell, 2013), and implies that molecular-level understanding of POC can provide both qualitative and quantitative information. Major ocean surveys in the 1980s (VERTEX) and 1990s (JGOFS) demonstrated that the biochemical composition of POC was more dynamic and informative than expected from analysis of bulk POC data alone (Wakeham et al., 1984, 1997, 2000). Since then, improvements in analytical techniques have resulted in increasingly detailed studies of POC components in efforts to unmask what Hedges et al. (2000) called biogeochemical "trump cards" hidden by a lack of detailed structural knowledge. Regardless, structural understanding of POC has yet to be translated into parameterizations for carbon cycle models; global biogeochemical ocean models vary widely in their formulation of POC composition and reactivity (e.g., Bendtsen et al., 2015; Weber et al., 2016).

Importantly, there are various scientific motivations for studying POC that determine which organic compounds are characterized in specific studies. For example, biological oceanography or microbial ecology studies examining living components or biological responses are more likely to target labile compounds and small size classes of POC. Chemical oceanography or carbon cycle studies, on the other hand, often consider POC as a bulk, non-living material sinking through the water column, and are therefore more likely to target compounds that may indicate bulk POC sources and lability, and to sample sinking particles. Paleoceanography or "modern analog" approaches may be unconcerned about the bulk properties of POC and instead focus on specific recalcitrant compounds that can be preserved in sediments and serve as indicators of environmental conditions. Still other studies are focused on anthropogenic impacts, and therefore target anthropogenic compounds like plastics, often without contextualizing their quantity in relation to naturally occurring materials in POC. Though seemingly very different, these applications all fall within the framework of organic geochemistry of POC.

Overall, a molecular-level view of POC enables us to explore the biological, chemical, and metabolic processes that underlie carbon cycling in the ocean (**Figure 1**), in order to better understand OC reactivity, its relationship to food web composition and dynamics, how and why the composition of POC changes with depth in the water column, and the types and quantity of carbon exported to sediments. In this overview based on discussions from a recent workshop[1], we briefly highlight the current understanding, recent developments, and knowledge gaps for the major components of POC. We discuss autochthonous sources of POC produced mostly by phytoplankton in surface waters as well as allochthonous material exported from terrestrial environments.

AUTOCHTHONOUS COMPONENTS OF POC

Lipids

All living cells and many viruses contain lipids, which we define here as molecules that are insoluble in water but extractable by non-polar solvents such as chloroform, dichloromethane, and hexane (McNaught and Wilkinson, 1997; Killops and Killops, 2005; Luo et al., 2019). Under this definition, lipids comprise hundreds of thousands of distinct molecules including photosynthetic pigments, hydrocarbons, and glycerol esters/ethers. Functions range from the foundation of cell membrane structure to energy storage, electron transport, signaling, reactive oxygen species scavenging, and light harvesting. Lipids comprise ∼20% of OC in living cells but are usually only a small percentage of sedimentary OC (Wakeham et al., 1997; Wang and Druffel, 2001), and may therefore contribute to the formation of recalcitrant molecularly uncharacterized organic matter (MUC, section "The Molecularly Uncharacterized Component (MUC) of POC"; Hwang and Druffel, 2003). Recent analytical advancements allow us to take advantage of lipid structural diversity to connect organismal ecology and physiology with POC cycling, through both targeted

[1]"Future Directions in Marine Organic Biogeochemistry" held at the Hanse Institute for Advanced Study, Delmenhorst, Germany; April 27–30, 2019.

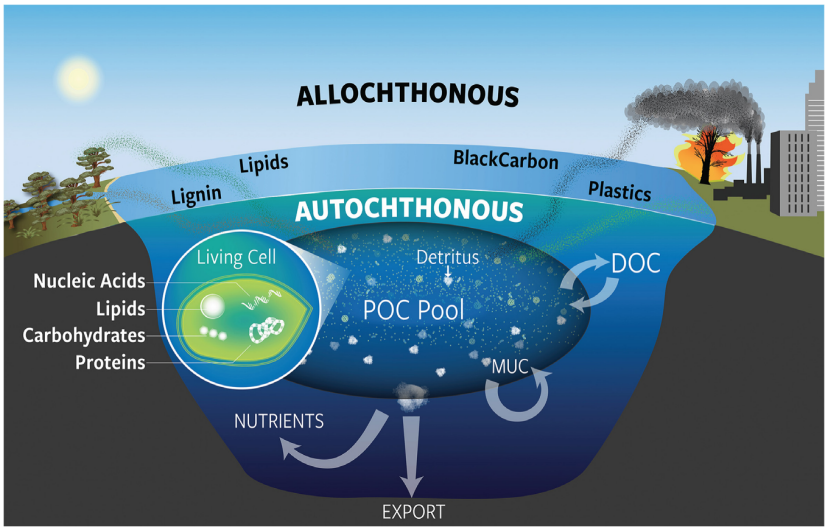

FIGURE 1 | Conceptual overview of marine particulate organic carbon (POC) in the ocean. POC includes components of living cells as well as dead material (detritus), and originates from both allochthonous and autochthonous sources. The POC pool can also exchange material with the dissolved OC (DOC) pool through aggregation and disaggregation of particles. This process and others may be involved in the formation of the molecularly uncharacterized component (MUC), which may incorporate both autochthonous and allochthonous OC.

studies of specific lipid biomarkers and untargeted surveys of the entire POC lipidome (Kharbush et al., 2016; Becker et al., 2018; Sollai et al., 2019).

Lipids and pigments are commonly employed as biomarkers because many of them are synthesized by specific organisms, allowing their sources to be traced within POC pools. Recalcitrant lipid biomarkers have been heavily pursued within POC as indicators that can be exported to sediments and therefore preserve a geologic snapshot of water column metabolisms. For example, pigments like chlorophylls, carotenoids, and their degradation products are used to track phytoplankton-derived POC through the water column (Repeta and Gagosian, 1984; Llewellyn and Mantoura, 1996). Sterol lipid biomarkers exist for a range of planktonic organisms (Wakeham and Beier, 1991; Volkman, 2016). Ladderane lipids are specific to anaerobic ammonia-oxidizing bacteria and thus identify the presence of this metabolism (Sinninghe Damsté et al., 2002). Fatty acids are the non-polar core components of glycerol-based membrane lipids in bacteria and eukaryotes and have long been characterized in POC, and isoprenoid biphytane lipids compose the non-polar core of archaeal membranes. Core lipids are relatively recalcitrant, and some are structurally distinct enough to be used as biomarkers, especially when combined with compound-specific isotope analysis (CSIA, Ingalls et al., 2006; Popendorf et al., 2011; Close et al., 2014). Preserved core lipids in sediments can also be proxies for past environmental conditions (Prahl and Wakeham, 1987; Schouten et al., 2002; Belt et al., 2007), but interpreting these proxies requires thoroughly understanding lipid production, transformation, and diagenesis processes (e.g., Hurley et al., 2016; Ding et al., 2019).

Studying the living components of POC often involves sampling microbial size classes (>0.2 μm) and targeting more specific, labile structures. For instance, analyzing glycerolipids with their polar headgroups still intact (i.e., intact polar lipids, IPLs) using high-resolution mass spectrometry added a new dimension to the development of lipidomic "fingerprints" for specific microbes and their metabolic status. The microbial lipidome can reflect adjustments made in response to changes in external variables like temperature, pH, or nutrient concentrations. Under low phosphorus (P) conditions, sulfur or nitrogen-containing lipids can be used in place of phospholipids (Van Mooy et al., 2009), making these non-P-containing IPLs useful for studying carbon cycling under P-limitation (Kharbush et al., 2016; Schubotz et al., 2018). The molecular distribution of glycerol-dialkyl(dibiphytane)-glycerol tetraethers (GDGTs) produced by pelagic archaea also appear to reflect environmental factors, including temperature (Elling et al., 2015; Zhou et al., 2020). It is often assumed that IPLs degrade rapidly upon cell death and that they can be used to study *in situ* activity of the living microbial component separately from non-living detrital POC. This assumption, however, rests on limited experimental evidence (White et al., 1979; Harvey et al., 1986) and should be revisited (e.g., Logemann et al., 2011), as defining the fraction of living and detrital POC is of urgent importance for understanding POC export to the deep-sea and sediment.

Lipid biomarkers are especially useful in investigating oceanographic processes that impact POC and the biological pump; for example, as indicators for the degradation state of POC, or which microbial groups are contributing to POC production, degradation, or export. The development and increased access to high-resolution mass spectrometry has resulted in the identification of many more biomarker structures, providing increased statistical power in lipidomics studies (e.g., Becker et al., 2018). An additional frontier is devising approaches to rigorously link lipidomics and other types of data. For example, lipid and genetic biomarkers were recently combined

with satellite data to show that viral infection of coccolithophore blooms enhances vertical flux and export of POC (Laber et al., 2018). Becker et al. (2018) discovered that daily oscillations in triacylglycerol concentrations accounted for about 6% of primary production, and used metatranscriptomics to implicate specific lineages of phytoplankton as sources of these lipids. These examples show that although lipids make up a minor component of total biomass and POC, their source-specificity can be capitalized upon to elucidate novel POC cycling and export pathways, particularly when lipid data are combined with other omics data.

Amino Acids and Proteins

Hydrolyzable amino acids (AAs) are the most abundant identifiable component of marine POC (Wakeham et al., 1997) and have been studied for decades. AA sources in POC include living autotrophic and heterotrophic cells, as well as detritus, and the relative contribution of each of these varies with depth (Kawasaki et al., 2011). While the same protein-forming L-amino acids are found in all living things, heterotrophic organisms both remineralize AAs and alter the relative concentration of individual AAs during export to depth (Van Mooy et al., 2002; Engel et al., 2017). These compositional changes have been developed into "degradation indices" (e.g., Dauwe et al., 1999) that are used are indicators of OC freshness. Similarly, the enantiomeric (D/L) AA composition of POC is used to estimate the heterotrophic bacterial contribution to POC, as certain D-AA derive exclusively from bacterial cell walls. Using this method, the total contribution from living and detrital bacterial cells in open-ocean surface waters was estimated to be between 15 and 25% of suspended POC (Kaiser and Benner, 2008; Kawasaki et al., 2011; Tremblay et al., 2015).

The stable isotope ratios of C and N in different AAs form patterns related to the biosynthetic source and/or history of passage through heterotrophic metabolisms. Compound specific isotope analysis of AAs (CSIA-AA) thus is beginning to provide unique insights into the cycling of POC and sedimentary AAs (Batista et al., 2014; Sabadel et al., 2019). Nitrogen CSIA-AA is frequently used to estimate trophic position (e.g., Chikaraishi et al., 2009), and alongside other AA degradation indices can trace heterotrophic bacterial activity (Calleja et al., 2013). Carbon CSIA-AA has been used to differentiate various phytoplankton, heterotrophic bacterial, and allochthonous terrigenous sources within POC and sediments (Hannides et al., 2013; Larsen et al., 2015; McMahon et al., 2015). However, our understanding of the mechanisms that influence isotope fractionation patterns of AA is still incomplete. Of particular interest is elucidating how various microbial processes affect amino acid isotope values. For instance, heterotrophic bacteria acquire AAs in several ways, including *de novo* synthesis, extracellular uptake, or "re-synthesizing" them from other AAs (Ohkouchi et al., 2017). Each may have different isotope fractionation patterns, and unless these are robustly known it could complicate interpretation of CSIA-AA patterns.

POC also contains identifiable proteins, as components of living cells or preserved in detrital material (Dong et al., 2010; Moore et al., 2012). Marine metaproteomics is an emerging technique that links genetic potential with metabolic function, including in particle-associated microbial communities (Bridoux et al., 2015), although challenges remain for data analysis and interpretation (Saito et al., 2019). Although not yet widely applied in marine systems, protein stable isotope probing approaches could further pinpoint *in situ* metabolic activity, yielding simultaneous determination of both phylogeny and metabolic function of specific organisms. This could be useful in determining the role of heterotrophic microbes in degradation and cycling of phytoplankton-derived POC, or in the formation of MUC.

Carbohydrates

Carbohydrates are important structural components and energy storage compounds in photosynthetic organisms, constituting ∼21–50% of phytoplankton biomass (Biersmith and Benner, 1998), >50% of macroalgal biomass (Mabeau and Kloareg, 1987), and 8–10% of suspended POC and 3–18% of sinking POC (Panagiotopoulos and Sempéré, 2005). A significant fraction of carbohydrates biosynthesized by primary producers is thus transformed and remineralized, but some is preserved as detrital components of OC (Wakeham et al., 1997). What production and transformation processes govern carbohydrate dynamics? What factors distinguish carbohydrates that fuel the food web from carbohydrates that are part of the detrital POM pool? These simple questions have complex answers (Arnosti et al., In press), starting with consideration of carbohydrate structures.

Carbohydrates are structurally highly diverse: individual sugars are monosaccharides, mostly either hexoses or pentoses. Monosaccharides are polymerized into disaccharides (two units), oligosaccharides (∼10 units), and polysaccharides (>10 unites). Monosaccharides are linked via hydroxyl groups in a vast diversity of linkage conformations; in theory, three different hexoses could lead to 128 different disaccharides (Laine, 1994). Oligo- and polysaccharides are often branched or contain sulfate, methyl, or amino groups, adding further structural complexity and frequently requiring "matching" enzymes to remove the sulfate, methyl, or amino groups prior to degradation of the polysaccharide backbone (e.g., Reisky et al., 2019). The structural diversity of carbohydrates thus could be used to link detrital components back to their sources, but only recently has progress been made in analytical techniques to begin to characterize these structures with sufficient resolution.

Carbohydrates are frequently measured using colorimetric techniques, providing bulk quantitative measurements but little structural information. Analysis of carbohydrate monomers that break carbohydrate polymers into monomers is more informative, but, like a collection of bricks without the blueprint of the building, leaves us wondering about the original structure. In addition, polysaccharide hydrolysis can destroy some component monosaccharides and fail to hydrolyze others. A paradox remains: the reactivity of carbohydrates ranges from very rapid, as for glucose or energy storage polysaccharides like laminarin, to very slow, as evidenced by the presence of carbohydrates in turbidites over 140,000 years old (Cowie et al., 1995). Carbohydrates constitute a substantial fraction of POC, but without the techniques to determine

specific structures, we have few means to read the messages they could convey. Fortunately, emerging analytical approaches may provide additional structural information: for example, improved chromatographic separations allow compound-specific isotope analysis of individual carbohydrates (Nouara et al., 2019), and specific polysaccharide-hydrolyzing enzymes enable quantification of laminarin in POC (Becker et al., 2017, 2020). Use of carbohydrate microarrays provides new insights into the presence and structure of specific complex carbohydrates in marine samples (Salmeán et al., 2018; Koch et al., 2019). Such techniques can enable us to decipher the specific structures – and therefore the origins, transformations, and relative reactivity – of more of the substantial carbohydrate-containing fraction of POC.

Nucleic Acids

Nucleic acids are the ultimate biomarkers for the living or recently living components of POC, as they can reveal the taxonomic identities and metabolic potential of both photosynthetic producers of POC and heterotrophic organisms that transform POC. Free-living microbial communities are captured as small particles and particle-attached communities are associated with larger suspended and sinking particles (DeLong et al., 1993); investigating these communities can provide critical insight into POC production, export, and attenuation processes. RNA and DNA can distinguish between living, active cells and dead or dormant material, respectively, and enable identification of organisms that are difficult to culture or observe microscopically. Studies can focus on specific genes or use untargeted omics approaches. Commonly applied phylogenetic markers are the 16S (prokaryotic) and 18S (eukaryotic) rRNA genes, used to examine the phylogenetic composition of POC-associated communities and how they change with depth, environmental conditions, and over time (DeLong et al., 2006; Duret et al., 2019; Thiele et al., 2019; Preston et al., 2020).

16S/18S rRNA and other single functional gene approaches reveal "who" is there, but not much insight into "what" they are doing or "how." Metagenomics/transcriptomics can provide focused insight into the metabolic capabilities of the whole community, and also of distinct community members using metagenomics-assembled genomes (Krüger et al., 2019). Major progress has been made through concerted study of spring phytoplankton blooms (Teeling et al., 2012, 2016) as well as global ocean surveys of microbial communities (e.g., Tara Oceans, Bork et al., 2015), and patterns pertaining to POC cycling are beginning to emerge (Guidi et al., 2016). Future advances depend on continuing these international sampling efforts to incorporate biological and chemical measurements across multiple temporal and spatial scales (e.g., Biogeoscapes)[2].

Though challenging, integrating molecular omics approaches with organic geochemistry is important to link the chemical composition of POC with biological processes, which are likely very important in regulating exchange between POC and DOC pools, and in determining the amount of POC ultimately delivered to marine sediments vs. remineralized vs. sequestered as refractory DOC (the "microbial carbon pump," Jiao et al., 2010; Legendre et al., 2015). However, so far we lack sufficient data on both biological as well as chemical composition of different types of particles across varying temporal and spatial scales. To address this knowledge gap some recent studies have begun to examine the relationship of particle size/type with microbial community composition and metabolism using next-generation omics techniques. For example, metagenomics and transcriptomics were recently used to infer the metabolic activities of prokaryotic and eukaryotic communities on sinking particles in the deep sea, which indicated considerable mid-water trophic processing of sinking POC by deep water protists and animals (Boeuf et al., 2019). Additionally, distinct prokaryotic assemblages were associated with suspended vs. sinking particles (Duret et al., 2019), and between different particle size classes (Mestre et al., 2017, 2018). This may suggest that particle compositions foster different metabolisms or modes of colonization, but remains hypothetical without concurrent chemical data.

ALLOCHTHONOUS COMPONENTS OF POC

Lignin and Terrestrial Plant Biomarkers

Vascular-plant derived molecules are used as quantitative tracers of terrestrially derived OC. Long-chain *n*-alkanes and fatty acids are synthesized by vascular plants as a component of leaf waxes, which are most abundant in coastal areas, but can be transported into the ocean with atmospheric dust or through riverine inputs. Lignin, a group of phenolic polymers, is probably the most well-studied terrestrial biomarker, as it is only produced by vascular plants and comprises one third of their biomass on average. Lignin is relatively stable in marine environments and has been used to quantify the amount of POC and DOC derived from plants and to determine plant tissue type and degradation state (Gordon and Goñi, 2004; Hernes and Benner, 2006). In the open ocean lignin is usually a minor component of POC, possibly because it is photo-oxidized, microbially degraded, or transformed into refractory molecules such as chromophoric DOC (CDOM, e.g., McDonald et al., 2019). However, higher concentrations of lignin and lignin phenols have been observed in POM in deep water masses, suggesting that terrestrial OM may be a quantitatively important component of POM in the bathypelagic (Hernes and Benner, 2002, 2006). Lignin-derived molecules are also important for tracing and quantifying terrestrial carbon import and export in coastal ecosystems, especially "blue carbon" ecosystems like salt marshes, mangrove forests and seagrass meadows. So far it has been difficult to quantify how much different sources of terrestrial carbon contribute to marine POC and DOC pools, and how much is sequestered in estuaries and coastal sediments (reviewed in Cragg et al., 2020). Recent studies are making progress in separating distinct terrestrial contributions to POC by combining ^{13}C and radiocarbon CSIA of lignin and other biomarkers (e.g., Tao et al., 2015), and in identifying biological degradation pathways (Woo and Hazen, 2018).

[2]www.biogeoscapes.org

Black Carbon

Black carbon (BC) is produced from incomplete combustion during wildfires and burning fossil fuels, and is found in both dissolved (DBC) and particulate (PBC) pools in the ocean (see Wagner et al., 2018 for detailed review of DBC). Marine PBC is primarily attributed to the absorption of DBC to POC. It spans a range of forms and reactivities, from slightly charred plant material to highly refractory, graphitized soot (the "combustion continuum," Hedges et al., 2000). PBC is enriched in carbon relative to its biological sources and is difficult to characterize structurally because it is dominated by polyaromatic structures, is insoluble, and resists chemical degradations. This is likely why PBC is refractory and decomposes slowly; radiocarbon data show that marine PBC can be tens of thousands of years old (Coppola et al., 2018). PBC represents a significant part of global carbon budgets, and in some locations comprises up to 20% of total POC and up to 50% of the MUC pool in POC (e.g., Gulf of Maine, Flores-Cervantes et al., 2009).

Because of its recalcitrance, PBC may contribute significantly to OC sequestration in marine sediments, however, this quantity is difficult to estimate because PBC reactivity and loss processes are poorly known. Recent work suggests that DBC in the open ocean may not originate from riverine transport, but from another, unidentified source, as its $\delta^{13}C$ values differ from riverine DBC (Wagner et al., 2019), and there are low concentrations of other terrigenous compounds in the open ocean (Hedges et al., 1997). Further isotopic studies could constrain potential sources (e.g., aerosols, autochthonous OC, hydrothermal vents) and reveal photo-oxidative or other degradative alteration processes.

Microplastics

Plastics are a recent but now widespread anthropogenic addition to marine POC (Law, 2017). Plastic particles between 1 μm and 5 mm in size are termed microplastics (MPs). MPs $>$ 100 μm are the most commonly studied; however, the number of plastic particles increases exponentially with decreasing particle size. Because most POC is also $<$ 100 μm in size, the contribution of MP to total POC is poorly known.

Physical forms of MPs include pellets, fragments, fibers, and foils, representing either their originally manufactured size range or alteration during physical and photochemical processes that fragment larger into smaller pieces. Depending on polymer density, MPs may float, sink, or be suspended at intermediate depths. Over time the physical and chemical properties of MPs can also be altered by weathering, embrittlement, fragmentation, and microbial colonization (Bryant et al., 2016).

MPs have been found across all oceans, from the surface to deep sea trenches (Peng et al., 2020). In sediments MPs are accumulating at rates that may leave a stratigraphic signal of the Anthropocene in the geological record (Zalasiewicz et al., 2016). However, the abundance of MPs throughout the marine environment is heterogeneous and inadequately quantified across varying spatial scales, and the processes that distribute MPs among surface, water column, and sediments are poorly understood. Many plastics also contain chemical additives, and their effects on marine species are not well studied.

These knowledge gaps will need to be addressed before we can assess the effects of MPs on marine ecosystems, but new research suggests that MPs could affect the biological pump. For example, laboratory experiments showed that MPs could be ingested by zooplankton, changing the density and sinking rates of their fecal pellets (Cole et al., 2016). In addition, incorporation of MPs can alter particle structure and density, and affect sinking and remineralization rates or influence POC aggregation/disaggregation (Chen et al., 2018; Porter et al., 2018).

THE MOLECULARLY UNCHARACTERIZED COMPONENT (MUC) OF POC

A large fraction of POC is considered "uncharacterizable" because it cannot be separated and identified using traditional chromatography-based molecular analyses. This appropriately abbreviated "MUC" increases in concentration relative to characterizable POC components with increasing depth in the water column, even as the overall flux of POC decreases (Wakeham et al., 1997, 2000; Hedges et al., 2000). This observation suggests that MUC is either produced from transformation of characterizable surface-derived material during export (possibly lipids, Hwang and Druffel, 2003) or from incorporation of DOC deeper in the water column, or, alternatively, that our analytical methods do not adequately identify biomolecules whose presence is obscured in some manner (Hedges et al., 2001). Despite the analytical advancements of the last two decades, the formation and sources of MUC are still poorly understood; hypothesized mechanisms include degradative formation of geo- or bio-macromolecules, incorporation of detrital material and/or black carbon, and interactions with inorganic mineral material. Other analytical methods applied to characterize bulk chemical features of MUC include advanced solid-state NMR and infrared spectroscopy techniques (e.g., Liu et al., 2009; Tremblay et al., 2011). In addition, bulk isotope ratios of POC are one of the few measurements that capture the entire POC pool, including MUC. Some studies have found spatial variations in bulk $\delta^{13}C$ and $\Delta^{14}C$ values of POC that suggest a substantial contribution to POC from ^{14}C-depleted material not immediately derived from surface primary production, possibly from resuspended sediment, black carbon, or incorporation of "old" water column DOC (Roland et al., 2008; Hwang et al., 2010).

Identifying MUC sources and cycling is an area that merits further attention, but may be better addressed in the future through application of high-resolution or ultra-high-resolution mass spectrometry, as well as high-resolution solid-state NMR (Mao et al., 2011), which have the potential to expand the analytical window to simultaneously examine the molecular diversity of important compound classes (e.g., lipids), and also to identify novel structures or functional groups. Within DOC, new analytical tools and workflows are enabling structural information to be assigned for a growing number of molecular features (e.g., Petras et al., 2017), and metabolomics approaches also are beginning to be applied to POC (Johnson et al., 2020).

CONCLUDING REMARKS

The development of new and improved analytical techniques now enables analysis of marine POC in greater molecular detail than ever before, with the potential to greatly expand our current catalog of organic biomarkers and other organic proxies and gain insight into the big questions about POC. However, studies of POC cycling in the ocean are fundamentally challenged by a long-standing limitation of established organic geochemical approaches: the most information-rich compounds or proxies tend to compose only tiny fractions of the bulk POC pool. In other words, using biomarkers to infer sources or cycling of more significant portions of POC necessarily involves making many assumptions about the consistencies of the relative initial ratios of biomarker to POC, and their relative reactivity. These assumptions become increasingly tenuous as POC is cycled and distanced from its source. Overcoming this tension between POC chemotaxonomy and biogeochemistry will mark a new era in the use of biomarkers to study POC.

The VERTEX (Martin et al., 1987) and JGOFS (Bowles and Livingston, 1997) ocean surveys were important first steps in understanding the nature and variability of POC composition but predated oceanographic omics data. On the other hand, the Tara Oceans expedition (Bork et al., 2015) successfully assembled a global metagenome of upper ocean biology but with the exception of pigments did not analyze molecular composition. In order to mechanistically tie together organic compositional information with the fate of the bulk POC pool we need more studies that make simultaneous omics, geochemical, and molecular measurements. Still in the planning stage, Biogeoscapes[2] is one new global effort that proposes to do this across multiple temporal and spatial scales, with the ultimate goal of understanding how metabolic feedbacks and interactions underpin biogeochemistry and structure ocean ecosystems. A multi-dimensional global dataset of POC, analyzed using improved analytical methods and integrated with omics, physiological, and nutrient data, would be invaluable for addressing many of the still-unanswered questions about POC, including how to integrate POC composition into new modeling platforms or even machine learning approaches.

In summary, several areas are promising frontiers for the study of POC: (1) Leveraging the power of structural diversity to identify sources and metabolic processes, (2) Effectively integrating omics and geochemical techniques, (3) Improving methods to characterize unidentified components of POC, (4) coupling isotopic ($\delta^{13}C$ and $\Delta^{14}C$) and molecular investigations of POC and DOC. While future work aimed at these issues will undoubtedly require field surveys, we also emphasize that controlled laboratory and mesocosm experiments are essential to construct mechanistic interpretations of environmental observations and should not be neglected.

AUTHOR CONTRIBUTIONS

JK, BV, HC, CA, and RS wrote the manuscript based on the discussions and notes taken at the workshop, with input from all co-authors. All authors contributed to the article and approved the submitted version.

FUNDING

We thank the Hanse Institute for Advanced Studies (HWK) and the Deutsche Forschungsgemeinschaft (DFG, German Research Foundation) project number 422798570, as well as the Geochemical Society, for funding which made the workshop possible. CA was additionally supported by OCE-1736772. BV was additionally supported by NSF OCE-1756254.

ACKNOWLEDGMENTS

We would like to thank HWK staff for coordinating and organizing the logistics of the workshop, including travel, accommodations, and food services, which greatly enhanced the meeting experience and the outcomes.

REFERENCES

Arnosti, C., Hinrichs, K. U., Coffinet, S., Wilkes, H., and Pantoja, S. (2019). The enduring questions: what's for dinner? Where's my knife? and Can I use my fingers? (Unanswered) questions related to organic matter and microbes in marine sediments. *Front. Mar. Sci.* 6:629. doi: 10.3389/fmars.2019.00629

Arnosti, C., Wietz, M., Brinkhoff, T., Hehemann, J.-H., Probandt, D., Zeugner, L., et al. (in press). The biogeochemistry of marine polysaccharides: sources, inventories, and bacterial drivers of the carbohydrate cycle. *Ann. Rev. Mar. Sci.* 13.

Batista, F. C., Ravelo, A. C., Crusius, J., Casso, M. A., and McCarthy, M. D. (2014). Compound specific amino acid δ15N in marine sediments: a new approach for studies of the marine nitrogen cycle. *Geochim. Cosmochim. Acta* 142, 553–569. doi: 10.1016/j.gca.2014.08.002

Becker, K. W., Collins, J. R., Durham, B. P., Groussman, R. D., White, A. E., Fredricks, H. F., et al. (2018). Daily changes in phytoplankton lipidomes reveal mechanisms of energy storage in the open ocean. *Nat. Commun.* 9:5179. doi: 10.1038/s41467-018-07346-z

Becker, S., Scheffel, A., Polz, M. F., and Hehemann, J. H. (2017). Accurate quantification of laminarin in marine organic matter with enzymes from marine microbes. *Appl. Environ. Microbiol.* 83, 1–14. doi: 10.1128/AEM.03389-3316

Becker, S., Tebben, J., Coffinet, S., Wiltshire, K., Iversen, M. H., Harder, T., et al. (2020). Laminarin is a major molecule in the marine carbon cycle. *Proc. Natl. Acad. Sci. U.S.A.* 117, 6599–6607. doi: 10.1073/pnas.1917001117

Belt, S. T., Massé, G., Rowland, S. J., Poulin, M., Michel, C., and LeBlanc, B. (2007). A novel chemical fossil of palaeo sea ice: IP25. *Org. Geochem.* 38, 16–27. doi: 10.1016/j.orggeochem.2006.09.013

Bendtsen, J., Hilligsøe, K. M., Hansen, J. L. S., and Richardson, K. (2015). Analysis of remineralisation, lability, temperature sensitivity and structural composition of organic matter from the upper ocean. *Prog. Oceanogr.* 130, 125–145. doi: 10.1016/j.pocean.2014.10.009

Biersmith, A., and Benner, R. (1998). Carbohydrates in phytoplankton and freshly produced dissolved organic matter. *Mar. Chem.* 63, 131–144. doi: 10.1016/S0304-4203(98)00057-57

Boeuf, D., Edwards, B. R., Eppley, J. M., Hu, S. K., Poff, K. E., Romano, A. E., et al. (2019). Biological composition and microbial dynamics of sinking particulate

organic matter at abyssal depths in the oligotrophic open ocean. *Proc. Natl. Acad. Sci. U.S.A.* 116, 11824–11832. doi: 10.1073/pnas.1903080116

Bork, P., Bowler, C., De Vargas, C., Gorsky, G., Karsenti, E., and Wincker, P. (2015). Tara Oceans studies plankton at planetary scale. *Science* 348:873. doi: 10.1126/science.aac5605

Bowles, M. C., and Livingston, H. D. (1997). *U.S. Joint Global Ocean Flux Study*. Available online at: http://usjgofs.whoi.edu/overview.html (accessed May 25 2020).

Boyd, P. W., Claustre, H., Levy, M., Siegel, D. A., and Weber, T. (2019). Multi-faceted particle pumps drive carbon sequestration in the ocean. *Nature* 568, 327–335. doi: 10.1038/s41586-019-1098-1092

Boyd, P. W., and Trull, T. W. (2007). Progress in Oceanography Understanding the export of biogenic particles in oceanic waters: is there consensus? *Cell* 72, 276–312. doi: 10.1016/j.pocean.2006.10.007

Bridoux, M. C., Neibauer, J., Ingalls, A. E., Nunn, B. L., and Keil, R. G. (2015). Suspended marine particulate proteins in coastal and oligotrophic waters. *J. Mar. Syst.* 143, 39–48. doi: 10.1016/j.jmarsys.2014.10.014

Bryant, J. A., Clemente, T. M., Viviani, D. A., Fong, A. A., Thomas, K. A., Kemp, P., et al. (2016). Diversity and activity of communities inhabiting plastic debris in the North Pacific Gyre. *mSystems* 1, 1–19. doi: 10.1128/msystems.00024-16

Calleja, M. L., Batista, F., Peacock, M., Kudela, R., and McCarthy, M. D. (2013). Changes in compound specific δ15N amino acid signatures and D/L ratios in marine dissolved organic matter induced by heterotrophic bacterial reworking. *Mar. Chem.* 149, 32–44. doi: 10.1016/j.marchem.2012.12.001

Cavan, E. L., Le Moigne, F. A. C., Poulton, A. J., Tarling, G. A., Ward, P., Daniels, C. J., et al. (2015). Attenuation of particulate organic carbon flux in the Scotia Sea, Southern Ocean, is controlled by zooplankton fecal pellets. *Geophys. Res. Lett.* 42, 821–830. doi: 10.1002/2014GL062744

Chen, C. S., Le, C., Chiu, M. H., and Chin, W. C. (2018). The impact of nanoplastics on marine dissolved organic matter assembly. *Sci. Total Environ.* 634, 316–320. doi: 10.1016/j.scitotenv.2018.03.269

Chikaraishi, Y., Ogawa, N. O., Kashiyama, Y., Takano, Y., Suga, H., Tomitani, A., et al. (2009). Determination of aquatic food-web structure based on compound-specific nitrogen isotopic composition of amino acids. *Limnol. Oceanogr. Methods* 7, 740–750. doi: 10.4319/lom.2009.7.740

Close, H. G., Wakeham, S. G., and Pearson, A. (2014). Lipid and 13C signatures of submicron and suspended particulate organic matter in the Eastern Tropical North Pacific: implications for the contribution of Bacteria. *Deep. Res. Part I Oceanogr. Res. Pap.* 85, 15–34. doi: 10.1016/j.dsr.2013.11.005

Cole, M., Lindeque, P. K., Fileman, E., Clark, J., Lewis, C., Halsband, C., et al. (2016). Microplastics alter the properties and sinking rates of zooplankton faecal pellets. *Environ. Sci. Technol.* 50, 3239–3246. doi: 10.1021/acs.est.5b05905

Coppola, A. I., Wiedemeier, D. B., Galy, V., Haghipour, N., Hanke, U. M., Nascimento, G. S., et al. (2018). Global-scale evidence for the refractory nature of riverine black carbon. *Nat. Geosci.* 11, 584–588. doi: 10.1038/s41561-018-0159-158

Cowie, G. L., Hedges, J. I., Prahl, F. G., and de Lance, G. J. (1995). Elemental and major biochemical changes across an oxidation front in a relict turbidite: an oxygen effect. *Geochim. Cosmochim. Acta* 59, 33–46. doi: 10.1016/0016-7037(94)00329-K

Cragg, S. M., Friess, D. A., Gillis, L. G., Trevathan-Tackett, S. M., Terrett, O. M., Watts, J. E. M., et al. (2020). Vascular plants are globally significant contributors to marine carbon fluxes and sinks. *Ann. Rev. Mar. Sci.* 12, 469–497. doi: 10.1146/annurev-marine-010318-095333

Dauwe, B., Middelburg, J. J., Herman, P. M. J., and Heip, C. H. R. (1999). Linking diagenetic alteration of amino acids and bulk organic matter reactivity. *Limnol. Oceanogr.* 44, 1809–1914.

DeLong, E. F., Franks, D., and Alldredge, A. (1993). Phylogenetic diversity of aggregate-attached vs. free-living marine bacterial assemblages. *Limnol. Oceanogr.* 38, 924–934. doi: 10.2307/2838082

DeLong, E. F., Preston, C. M., Mincer, T., Rich, V., Hallam, S. J., Frigaard, N.-U., et al. (2006). Community genomics among stratified microbial assemblages in the ocean's interior. *Science* 311, 496–503. doi: 10.1126/science.1120250

Ding, Y., Bi, R., Sachs, J., Chen, X., Zhang, H., Li, L., et al. (2019). Lipid biomarker production by marine phytoplankton under different nutrient and temperature regimes. *Org. Geochem.* 131, 34–49. doi: 10.1016/j.orggeochem.2019.01.008

Dong, H. P., Wang, D. Z., Dai, M., and Hong, H. S. (2010). Characterization of particulate organic matters in the water column of the South China Sea using a shotgun proteomic approach. *Limnol. Oceanogr.* 55, 1565–1578. doi: 10.4319/lo.2010.55.4.1565

Duret, M. T., Lampitt, R. S., and Lam, P. (2019). Prokaryotic niche partitioning between suspended and sinking marine particles. *Environ. Microbiol. Rep.* 11, 386–400. doi: 10.1111/1758-2229.12692

Elling, F. J., Könneke, M., Mußmann, M., Greve, A., and Hinrichs, K. U. (2015). Influence of temperature, pH, and salinity on membrane lipid composition and TEX86 of marine planktonic thaumarchaeal isolates. *Geochim. Cosmochim. Acta* 171, 238–255. doi: 10.1016/j.gca.2015.09.004

Engel, A., Wagner, H., Le Moigne, F. A. C., and Wilson, S. T. (2017). Particle export fluxes to the oxygen minimum zone of the eastern tropical North Atlantic. *Biogeosciences* 14, 1825–1838. doi: 10.5194/bg-14-1825-2017

Eppley, R. W., and Peterson, B. J. (1979). Particulate organic matter flux and planktonic new production in the deep ocean. *Nature* 282, 677–680. doi: 10.1038/282677a0

Flores-Cervantes, D. X., Plata, D. L., MacFarlane, J. K., Reddy, C. M., and Gschwend, P. M. (2009). Black carbon in marine particulate organic carbon: inputs and cycling of highly recalcitrant organic carbon in the Gulf of Maine. *Mar. Chem.* 113, 172–181. doi: 10.1016/j.marchem.2009.01.012

Gordon, E. S., and Goñi, M. A. (2004). Controls on the distribution and accumulation of terrigenous organic matter in sediments from the Mississippi and Atchafalaya river margin. *Mar. Chem.* 92, 331–352. doi: 10.1016/j.marchem.2004.06.035

Guidi, L., Chaffron, S., Bittner, L., Eveillard, D., Larhlimi, A., Roux, S., et al. (2016). Plankton networks driving carbon export in the oligotrophic ocean. *Nature* 532, 465–470. doi: 10.1038/nature16942

Hannides, C. C. S., Popp, B. N., Anela Choy, C., and Drazen, J. C. (2013). Midwater zooplankton and suspended particle dynamics in the North Pacific subtropical gyre: a stable isotope perspective. *Limnol. Oceanogr.* 58, 1931–1936. doi: 10.4319/lo.2013.58.6.1931

Hansell, D. A. (2013). Recalcitrant dissolved organic carbon fractions. *Ann. Rev. Mar. Sci.* 5, 421–445. doi: 10.1146/annurev-marine-120710-100757

Harvey, H. R., Fallon, R. D., and Patton, J. S. (1986). The effect of organic matter and oxygen on the degradation of bacterial membrane lipids in marine sediments. *Geochim. Cosmochim. Acta* 50, 795–804. doi: 10.1016/0016-7037(86)90355-90358

Hedges, J. I., Baldock, J. A., Gélinas, Y., Lee, C., Peterson, M., and Wakeham, S. G. (2001). Evidence for non-selective preservation of organic matter in sinking marine particles. *Nature* 409, 801–804. doi: 10.1038/35057247

Hedges, J. I., Eglinton, G., Hatcher, P. G., Kirchman, D. L., Arnosti, C., Derenne, S., et al. (2000). The molecularly-uncharacterized component of nonliving organic matter in natural environments. *Org. Geochem.* 31, 945–958. doi: 10.1016/S0146-6380(00)00096-96

Hedges, J. I., Keil, R. G., and Benner, R. (1997). What happens to terrestrial organic matter in the ocean? *Org. Geochem.* 27, 195–212. doi: 10.1016/S0146-6380(97)00066-61

Hernes, P. J., and Benner, R. (2002). Transport and diagenesis of dissolved and particulate terrigenous organic matter in the North Pacific Ocean. *Deep. Res. Part I Oceanogr. Res. Pap.* 49, 2119–2132. doi: 10.1016/S0967-0637(02)00128-120

Hernes, P. J., and Benner, R. (2006). Terrigenous organic matter sources and reactivity in the North Atlantic Ocean and a comparison to the Arctic and Pacific oceans. *Mar. Chem.* 100, 66–79. doi: 10.1016/j.marchem.2005.11.003

Hurley, S. J., Elling, F. J., Könneke, M., Buchwald, C., Wankel, S. D., Santoro, A. E., et al. (2016). Influence of ammonia oxidation rate on thaumarchaeal lipid composition and the TEX86 temperature proxy. *Proc. Natl. Acad. Sci. U.S.A.* 113, 7762–7767. doi: 10.1073/pnas.1518534113

Hwang, J., and Druffel, E. R. M. (2003). Lipid-like material as the source of the uncharacterized organic carbon in the ocean? *Science* 299, 881–884. doi: 10.1126/science.1078508

Hwang, J., Druffel, E. R. M., and Eglinton, T. I. (2010). Widespread influence of resuspended sediments on oceanic particulate organic carbon: insights from radiocarbon and aluminum contents in sinking particles. *Global Biogeochem. Cycles* 24:GB4016. doi: 10.1029/2010GB003802

Ingalls, A. E., Shah, S. R., Hansman, R. L., Aluwihare, L. I., Santos, G. M., Druffel, E. R. M., et al. (2006). Quantifying archaeal community autotrophy in the mesopelagic ocean using natural radiocarbon. *Proc. Natl. Acad. Sci. U.S.A.* 103, 6442–6447. doi: 10.1073/pnas.0510157103

Jiao, N., Herndl, G. J., Hansell, D. A., Benner, R., Kattner, G., Wilhelm, S. W., et al. (2010). Microbial production of recalcitrant dissolved organic matter: long-term carbon storage in the global ocean. *Nat. Rev. Microbiol.* 8, 593–599. doi: 10.1038/nrmicro2386

Johnson, W. M., Longnecker, K., Kido Soule, M. C., Arnold, W. A., Bhatia, M. P., Hallam, S. J., et al. (2020). Metabolite composition of sinking particles differs from surface suspended particles across a latitudinal transect in the South Atlantic. *Limnol. Oceanogr.* 65, 111–127. doi: 10.1002/lno.11255

Kaiser, K., and Benner, R. (2008). Major bacterial contribution to the ocean reservoir of detrital organic carbon and nitrogen. *Limnol. Oceanogr.* 53, 99–112. doi: 10.4319/lo.2008.53.3.1192

Kawasaki, N., Sohrin, R., Ogawa, H., Nagata, T., and Benner, R. (2011). Bacterial carbon content and the living and detrital bacterial contributions to suspended particulate organic carbon in the North Pacific Ocean. *Aquat. Microb. Ecol.* 62, 165–176. doi: 10.3354/ame01462

Kharbush, J. J., Allen, A. E., Moustafa, A., Dorrestein, P. C., and Aluwihare, L. I. (2016). Intact polar diacylglycerol biomarker lipids isolated from suspended particulate organic matter accumulating in an ultraoligotrophic water column. *Org. Geochem.* 100, 29–41. doi: 10.1016/j.orggeochem.2016.07.008

Killops, S., and Killops, V. (2005). *Introduction To Organic Geochemistry*, 2nd Edn, Hoboken, NJ: Blackwell Publishing.

Koch, H., Dürwald, A., Schweder, T., Noriega-Ortega, B., Vidal-Melgosa, S., Hehemann, J. H., et al. (2019). Biphasic cellular adaptations and ecological implications of *Alteromonas macleodii* degrading a mixture of algal polysaccharides. *ISME J.* 13, 92–103. doi: 10.1038/s41396-018-0252-254

Krüger, K., Chafee, M., Ben Francis, T., Glavina del Rio, T., Becher, D., Schweder, T., et al. (2019). In marine Bacteroidetes the bulk of glycan degradation during algae blooms is mediated by few clades using a restricted set of genes. *ISME J.* 13, 2800–2816. doi: 10.1038/s41396-019-0476-y

Kujawinski, E. B. (2011). The impact of microbial metabolism on marine dissolved organic matter. *Ann. Rev. Mar. Sci.* 3, 567–599. doi: 10.1146/annurev-marine-120308-181003

Laber, C. P., Hunter, J. E., Carvalho, F., Collins, J. R., Hunter, E. J., Schieler, B. M., et al. (2018). *Coccolithovirus facilitation* of carbon export in the North Atlantic. *Nat. Microbiol.* 3, 537–547. doi: 10.1038/s41564-018-0128-124

Laine, R. A. (1994). A calculation of all possible oligosaccharide isomers both branched and linear yields 1.*05* × 10^12 structures for a reducing hexasaccharide: the "isomer barrier" to development of single-method saccharide sequencing or synthesis systems. *Glycobiology* 4, 759–767. doi: 10.1093/glycob/4.6.759

Lam, P. J., Doney, S. C., and Bishop, J. K. B. (2011). The dynamic ocean biological pump: insights from a global compilation of particulate organic carbon, CaCO 3, and opal concentration profiles from the mesopelagic. *Global Biogeochem. Cycles* 25, 1–14. doi: 10.1029/2010GB003868

Larsen, T., Bach, L. T., Salvatteci, R., Wang, Y. V., Andersen, N., Ventura, M., et al. (2015). Assessing the potential of amino acid 13C patterns as a carbon source tracer in marine sediments: effects of algal growth conditions and sedimentary diagenesis. *Biogeosciences* 12, 4979–4992. doi: 10.5194/bg-12-4979-2015

Law, K. L. (2017). Plastics in the marine environment. *Ann. Rev. Mar. Sci.* 9, 205–229. doi: 10.1146/annurev-marine-010816-060409

Le Moigne, F. A. C. (2019). Pathways of organic carbon downward transport by the oceanic biological carbon pump. *Front. Mar. Sci.* 6:634. doi: 10.3389/fmars.2019.00634

Legendre, L., Rivkin, R. B., Weinbauer, M. G., Guidi, L., and Uitz, J. (2015). The microbial carbon pump concept: potential biogeochemical significance in the globally changing ocean. *Prog. Oceanogr.* 134, 432–450. doi: 10.1016/j.pocean.2015.01.008

Liu, Z., Mao, J., Peterson, M. L., Lee, C., Wakeham, S. G., and Hatcher, P. G. (2009). Characterization of sinking particles from the northwest Mediterranean Sea using advanced solid-state NMR. *Geochim. Cosmochim. Acta* 73, 1014–1026. doi: 10.1016/j.gca.2008.11.019

Llewellyn, C. A., and Mantoura, R. F. C. (1996). Pigment biomarkers and particulate carbon in the upper water column compared to the ocean interior of the northeast Atlantic. *Deep. Res. Part I Oceanogr. Res. Pap.* 43, 1165–1184. doi: 10.1016/0967-0637(96)00043-X

Logemann, J., Graue, J., Köster, J., Engelen, B., Rullkötter, J., and Cypionka, H. (2011). A laboratory experiment of intact polar lipid degradation in sandy sediments. *Biogeosciences* 8, 2547–2560. doi: 10.5194/bg-8-2547-2011

Luo, G., Yang, H., Algeo, T. J., Hallmann, C., and Xie, S. (2019). Lipid biomarkers for the reconstruction of deep-time environmental conditions. *Earth Sci. Rev.* 189, 99–124. doi: 10.1016/j.earscirev.2018.03.005

Mabeau, S., and Kloareg, B. (1987). Isolation and analysis of the cell walls of brown algae: *Fucus spiralis*, *F. ceranoides*, *F. vesiculosus*, *F. serratus*, *Bifurcaria bifurcata* and *Laminaria digitata*. *J. Exp. Bot.* 38, 1573–1580. doi: 10.1093/jxb/38.9.1573

Mao, J., Tremblay, L., and Gagné, J. P. (2011). Structural changes of humic acids from sinking organic matter and surface sediments investigated by advanced solid-state NMR: insights into sources, preservation and molecularly uncharacterized components. *Geochim. Cosmochim. Acta* 75, 7864–7880. doi: 10.1016/j.gca.2011.09.044

Martin, J. H., Knauer, G. A., Karl, D. M., and Broenkow, W. W. (1987). VERTEX: carbon cycling in the northeast Pacific. *Deep. Res.* 34, 267–285. doi: 10.1016/0198-0149(87)90086-0

McDonald, N., Achterberg, E. P., Carlson, C. A., Gledhill, M., Liu, S., Matheson-Barker, J. R., et al. (2019). The role of heterotrophic bacteria and archaea in the transformation of lignin in the open ocean. *Front. Mar. Sci.* 6:743. doi: 10.3389/fmars.2019.00743

McMahon, K. W., McCarthy, M. D., Sherwood, O. A., Larsen, T., and Guilderson, T. P. (2015). Millennial-scale plankton regime shifts in the subtropical North Pacific Ocean. *Science* 350, 1530–1533. doi: 10.1126/science.aaa9942

McNaught, A. D., and Wilkinson, A. (eds) (1997). "International union of pure and applied," in *Compendium of Chemical Terminology (the Gold Book)*, 2nd Edn (Oxford: Blackwell Scientific Publications).

Mestre, M., Ferrera, I., Borrull, E., Ortega-Retuerta, E., Mbedi, S., Grossart, H. P., et al. (2017). Spatial variability of marine bacterial and archaeal communities along the particulate matter continuum. *Mol. Ecol.* 26, 6827–6840. doi: 10.1111/mec.14421

Mestre, M., Ruiz-González, C., Logares, R., Duarte, C. M., Gasol, J. M., and Sala, M. M. (2018). Sinking particles promote vertical connectivity in the ocean microbiome. *Proc. Natl. Acad. Sci. U.S.A.* 115, E6799–E6807. doi: 10.1073/pnas.1802470115

Moore, E. K., Nunn, B. L., Goodlett, D. R., and Harvey, H. R. (2012). Identifying and tracking proteins through the marine water column: insights into the inputs and preservation mechanisms of protein in sediments. *Geochim. Cosmochim. Acta* 83, 324–359. doi: 10.1016/j.gca.2012.01.002

Nouara, A., Panagiotopoulos, C., Balesdent, J., Violaki, K., Bard, E., Fagault, Y., et al. (2019). Liquid chromatographic isolation of individual carbohydrates from environmental matrices for stable carbon analysis and radiocarbon dating. *Anal. Chim. Acta* 1067, 137–146. doi: 10.1016/j.aca.2019.03.028

Ohkouchi, N., Chikaraishi, Y., Close, H. G., Fry, B., Larsen, T., Madigan, D. J., et al. (2017). Advances in the application of amino acid nitrogen isotopic analysis in ecological and biogeochemical studies. *Org. Geochem.* 113, 150–174. doi: 10.1016/j.orggeochem.2017.07.009

Panagiotopoulos, C., and Sempéré, R. (2005). Analytical methods for the determination of sugars in marine samples: a historical perspective and future directions. *Limnol. Oceanogr. Methods* 3, 419–454. doi: 10.4319/lom.2005.3.419

Peng, G., Bellerby, R., Zhang, F., Sun, X., and Li, D. (2020). The ocean's ultimate trashcan: hadal trenches as major depositories for plastic pollution. *Water Res.* 168, 115121. doi: 10.1016/j.watres.2019.115121

Petras, D., Koester, I., Da Silva, R., Stephens, B. M., Haas, A. F., Nelson, C. E., et al. (2017). High-resolution liquid chromatography tandem mass spectrometry enables large scale molecular characterization of dissolved organic matter. *Front. Mar. Sci.* 4:405. doi: 10.3389/fmars.2017.00405

Popendorf, K. J., Lomas, M. W., and Van Mooy, B. A. S. (2011). Microbial sources of intact polar diacylglycerolipids in the Western North Atlantic Ocean. *Org. Geochem.* 42, 803–811. doi: 10.1016/j.orggeochem.2011.05.003

Porter, A., Lyons, B. P., Galloway, T. S., and Lewis, C. (2018). Role of marine snows in microplastic fate and bioavailability. *Environ. Sci. Technol.* 52, 7111–7119. doi: 10.1021/acs.est.8b01000

Prahl, F. G., and Wakeham, S. G. (1987). Calibration of unsaturation patterns in long-chain ketone compositions for palaeotemperature assessment. *Nature* 330, 367–369. doi: 10.1038/330367a0

Preston, C. M., Durkin, C. A., and Yamahara, K. M. (2020). DNA metabarcoding reveals organisms contributing to particulate matter flux to abyssal depths in the North East Pacific ocean. *Deep. Res. Part II Top. Stud. Oceanogr.* 173:104708. doi: 10.1016/j.dsr2.2019.104708

Reisky, L., Préchoux, A., Zühlke, M. K., Bäumgen, M., Robb, C. S., Gerlach, N., et al. (2019). A marine bacterial enzymatic cascade degrades the algal polysaccharide ulvan. *Nat. Chem. Biol.* 15, 803–812. doi: 10.1038/s41589-019-0311-319

Repeta, D. J., and Gagosian, R. B. (1984). Transformation reactions and recycling of carotenoids and chlorins in the Peru upwelling region (15°S, 75°W). *Geochim. Cosmochim. Acta* 48, 1265–1277. doi: 10.1016/0016-7037(84)90061-90069

Riley, J. S., Sanders, R., Marsay, C., Le Moigne, F. A. C., Achterberg, E. P., and Poulton, A. J. (2012). The relative contribution of fast and slow sinking particles to ocean carbon export. *Global Biogeochem. Cycles* 26, 1–10. doi: 10.1029/2011GB004085

Roland, L. A., McCarthy, M. D., and Guilderson, T. (2008). Sources of molecularly uncharacterized organic carbon in sinking particles from three ocean basins: a coupled Δ14C and δ13C approach. *Mar. Chem.* 111, 199–213. doi: 10.1016/j.marchem.2008.05.010

Sabadel, A. J. M., Van Oostende, N., Ward, B. B., Woodward, E. M., Van Hale, R., and Frew, R. D. (2019). Characterization of particulate organic matter cycling during a summer North Atlantic phytoplankton bloom using amino acid C and N stable isotopes. *Mar. Chem.* 214:103670. doi: 10.1016/j.marchem.2019.103670

Saito, M. A., Bertrand, E. M., Duffy, M. E., Gaylord, D. A., Held, N. A., Hervey, W. J., et al. (2019). Progress and challenges in ocean metaproteomics and proposed best practices for data sharing. *J. Proteome Res.* 18, 1461–1476. doi: 10.1021/acs.jproteome.8b00761

Salmeán, A. A., Guillouzo, A., Duffieux, D., Jam, M., Matard-Mann, M., Larocque, R., et al. (2018). Double blind microarray-based polysaccharide profiling enables parallel identification of uncharacterized polysaccharides and carbohydrate-binding proteins with unknown specificities. *Sci. Rep.* 8, 1–11. doi: 10.1038/s41598-018-20605-20609

Schouten, S., Hopmans, E. C., Schefuß, E., and Sinninghe-Damsté, J. S. (2002). Distributional variations in marine crenarchaeotal membrane lipids: a new tool for reconstructing ancient sea water temperatures? *Earth Planet Sci. Lett.* 204, 265–274. doi: 10.1016/s0012-821x(02)00979-2

Schubotz, F., Xie, S., Lipp, J. S., Hinrichs, K. U., and Wakeham, S. G. (2018). Intact polar lipids in the water column of the eastern tropical North Pacific: abundance and structural variety of non-phosphorus lipids. *Biogeosciences* 15, 6481–6501. doi: 10.5194/bg-15-6481-2018

Sinninghe Damsté, J. S., Strous, M., Rijpstra, W. I. C., Hopmans, E. C., Geenevasen, J. A. J., Van Duin, A. C. T., et al. (2002). Linearly concatenated cyclobutane lipids form a dense bacterial membrane. *Nature* 419, 708–712. doi: 10.1038/nature01128

Sollai, M., Villanueva, L., Hopmans, E. C., Reichart, G. J., and Sinninghe Damsté, J. S. (2019). A combined lipidomic and 16S rRNA gene amplicon sequencing approach reveals archaeal sources of intact polar lipids in the stratified Black Sea water column. *Geobiology* 17, 91–109. doi: 10.1111/gbi.12316

Tao, S., Eglinton, T. I., Montluçon, D. B., McIntyre, C., and Zhao, M. (2015). Pre-aged soil organic carbon as a major component of the yellow river suspended load: regional significance and global relevance. *Earth Planet. Sci. Lett.* 414, 77–86. doi: 10.1016/j.epsl.2015.01.004

Teeling, H., Fuchs, B. M., Becher, D., Klockow, C., Gardebrecht, A., Bennke, C. M., et al. (2012). Substrate-controlled succession of marine bacterioplankton populations induced by a phytoplankton bloom. *Science* 336, 608–611. doi: 10.1126/science.1218344

Teeling, H., Fuchs, B. M., Bennke, C. M., Krüger, K., Chafee, M., Kappelmann, L., et al. (2016). Recurring patterns in bacterioplankton dynamics during coastal spring algae blooms. *eLife* 5:11888. doi: 10.7554/eLife.11888

Thiele, S., Basse, A., Becker, J. W., Lipski, A., Iversen, M. H., and Mollenhauer, G. (2019). Microbial communities in the nepheloid layers and hypoxic zones of the canary current upwelling system. *Microbiologyopen* 8, 1–13. doi: 10.1002/mbo3.705

Tremblay, L., Alaoui, G., and Léger, M. N. (2011). Characterization of aquatic particles by direct FTIR analysis of filters and quantification of elemental and molecular compositions. *Environ. Sci. Technol.* 45, 9671–9679. doi: 10.1021/es202607n

Tremblay, L., Caparros, J., Leblanc, K., and Obernosterer, I. (2015). Origin and fate of particulate and dissolved organic matter in a naturally iron-fertilized region of the Southern Ocean. *Biogeosciences* 12, 607–621. doi: 10.5194/bg-12-607-2015

Van Mooy, B. A. S., Fredricks, H. F., Pedler, B. E., Dyhrman, S. T., Karl, D. M., Koblízek, M., et al. (2009). Phytoplankton in the ocean use non-phosphorus lipids in response to phosphorus scarcity. *Nature* 458, 69–72. doi: 10.1038/nature07659

Van Mooy, B. A. S., Keil, R. G., and Devol, A. H. (2002). Impact of suboxia on sinking particulate organic carbon: enhanced carbon flux and preferential degradation of amino acids via denitrification. *Geochim. Cosmochim. Acta* 66, 457–465. doi: 10.1016/S0016-7037(01)00787-786

Volk, T., and Hoffert, M. I. (1985). "Ocean carbon pumps: analysis of relative strengths and efficiencies in ocean-driven atmospheric CO_2 changes," in *The Carbon Cycle and Atmospheric CO2: Natural Variations Archean to Present*, eds E. Sundquist and W. Broecker (Washington, DC: American Geophysical Union), 99–110. doi: 10.1029/gm032p0099

Volkman, J. (2016). "Sterols in microalgae," in *The Physiology of Microalgae*, eds M. Borowitzka, J. Beardall, and J. Raven (Berlin: Springer), 485–505. doi: 10.1007/978-3-319-24945-2_19

Wagner, S., Brandes, J., Spencer, R. G. M., Ma, K., Rosengard, S. Z., Moura, J. M. S., et al. (2019). Isotopic composition of oceanic dissolved black carbon reveals non-riverine source. *Nat. Commun.* 10, 1–8. doi: 10.1038/s41467-019-13111-13117

Wagner, S., Jaffé, R., and Stubbins, A. (2018). Dissolved black carbon in aquatic ecosystems. *Limnol. Oceanogr. Lett.* 3, 168–185. doi: 10.1002/lol2.10076

Wagner, S., Schubotz, F., Kaiser, K., Hallmann, C., Waska, H., Rossel, P. E., et al. (2020). Soothsaying DOM: a current perspective on the future of oceanic dissolved organic carbon. *Front. Mar. Sci.* 7:341. doi: 10.3389/fmars.2020.00341

Wakeham, S. G., and Beier, J. A. (1991). Fatty acid and sterol biomarkers as indicators of particulate matter source and alteration processes in the Black Sea. *Deep. Res. Part A* 38, S943–S968. doi: 10.1016/s0198-0149(10)80018-80014

Wakeham, S. G., Lee, C., Farrington, J. W., and Gagosian, R. B. (1984). Biogeochemistry of particulate organic matter in the oceans: results from sediment trap experiments. *Deep Sea Res. Part A. Oceanogr. Res. Pap.* 31, 509–528. doi: 10.1016/0198-0149(84)90099-90092

Wakeham, S. G., Lee, C., and Hedges, J. I. (2000). "Fluxes of major biochemicals in the equatorial Pacific Ocean," in *Dynamics and Characterization of Marine Organic Matter*, eds N. Handa, E. Tanoue, and T. Hama (Dordrecht: Springer), 117–140. doi: 10.1007/978-94-017-1319-1_6

Wakeham, S. G., Lee, C., Hedges, J. I., Hernes, P. J., and Peterson, M. L. (1997). Molecular indicators of diagenetic status in marine organic matter. *Geochim. Cosmochim. Acta* 61, 5363–5369. doi: 10.1016/S0016-7037(97)00312-318

Wang, X. C., and Druffel, E. R. M. (2001). Radiocarbon and stable carbon isotope compositions of organic compound classes in sediments from the NE Pacific and Southern Oceans. *Mar. Chem.* 73, 65–81. doi: 10.1016/S0304-4203(00)00090-96

Weber, T., Cram, J. A., Leung, S. W., DeVries, T., and Deutsch, C. (2016). Deep ocean nutrients imply large latitudinal variation in particle transfer efficiency. *Proc. Natl. Acad. Sci. U.S.A.* 113, 8606–8611. doi: 10.1073/pnas.1604414113

White, D. C., Davis, W. M., Nickels, J. S., King, J. D., and Bobbie, R. J. (1979). Determination of the sedimentary microbial biomass by extractible lipid phosphate. *Oecologia* 40, 51–62. doi: 10.1007/bf00388810

Woo, H. L., and Hazen, T. C. (2018). Enrichment of bacteria from Eastern Mediterranean Sea involved in lignin degradation via the phenylacetyl-CoA pathway. *Front. Microbiol.* 9:922. doi: 10.3389/fmicb.2018.00922

Zalasiewicz, J., Waters, C. N., Ivar do Sul, J. A., Corcoran, P. L., Barnosky, A. D., Cearreta, A., et al. (2016). The geological cycle of plastics and their use as a stratigraphic indicator of the anthropocene. *Anthropocene* 13, 4–17. doi: 10.1016/j.ancene.2016.01.002

Zhou, A., Weber, Y., Chiu, B. K., Elling, F. J., Cobban, A. B., Pearson, A., et al. (2020). Energy flux controls tetraether lipid cyclization in *Sulfolobus acidocaldarius*. *Environ. Microbiol.* 22, 343–353. doi: 10.1111/1462-2920.14851

Conflict of Interest: The authors declare that the research was conducted in the absence of any commercial or financial relationships that could be construed as a potential conflict of interest.

frontiers in Marine Science

ORIGINAL RESEARCH
published: 26 June 2020
doi: 10.3389/fmars.2020.00476

Tracks in the Snow – Advantage of Combining Optical Methods to Characterize Marine Particles and Aggregates

Thor N. Markussen[1†], Christian Konrad[2,3], Christoph Waldmann[3], Marius Becker[4], Gerhard Fischer[3,5] and Morten H. Iversen[2,3,5]*

[1] Department of Geosciences and Natural Resource Management, Faculty of Science, University of Copenhagen, Copenhagen, Denmark, [2] Helmholtz Young Investigator Group SeaPump, Alfred Wegener Institute for Polar and Marine Research, Bremerhaven, Germany, [3] MARUM Center for Marine Environmental Sciences, University of Bremen, Bremen, Germany, [4] Institute of Geosciences, Faculty of Mathematics and Natural Sciences, University of Kiel, Kiel, Germany, [5] Geosciences Department, University of Bremen, Bremen, Germany

OPEN ACCESS

Edited by:
Cindy Lee,
Stony Brook University, United States

Reviewed by:
Adrian Benedict Burd,
University of Georgia, United States
Emilia Trudnowska,
Institute of Oceanology, PAN, Poland

***Correspondence:**
Morten H. Iversen
miversen@marum.de;
morten.iversen@awi.de

†Present address:
Thor N. Markussen,
Jardin Jolivet, Cronat, France

Specialty section:
This article was submitted to Marine Biogeochemistry, a section of the journal Frontiers in Marine Science

Received: 07 March 2020
Accepted: 28 May 2020
Published: 26 June 2020

Citation:
Markussen TN, Konrad C, Waldmann C, Becker M, Fischer G and Iversen MH (2020) Tracks in the Snow – Advantage of Combining Optical Methods to Characterize Marine Particles and Aggregates. Front. Mar. Sci. 7:476. doi: 10.3389/fmars.2020.00476

Settling marine aggregates, such as zooplankton fecal pellets and marine snow, transport organic matter from the surface ocean to the deep sea and are largely responsible for the ocean's sequestration of carbon. However, our understanding of the functioning of the biological pump and the distribution of particulate organic matter in the water column often hinge on limited bulk data from sediment traps, large volume filtration or instantaneous snap-shots from *in situ* optical systems that only see a small part of the particle and aggregate spectra. We evaluated the added value of combining different optical systems to detect a range of organic and inorganic particle types during a case-study in the Cape Blanc upwelling region. Laboratory calibrations showed that one camera system detected large organic aggregates well and *in situ* data showed that it correlated positively with fluorescence. The other camera was better at detecting small, mainly inorganic particles which were not seen by the first camera and correlated positively with turbidity. The combined deployments of the two optical systems together with fluorescence and turbidity sensors showed potentials for added insights into spatial (depth) and temporal (diurnal) particle dynamics. The case study exemplified the different efficiencies of two camera systems to detect particles of different types in marine waters. From this, the results highlighted the importance of discriminating between qualitative and quantitative ranges of imaging systems, in order to understand the quantitative range of sizes as well as types of particles detected by a given system. This is especially important when optical systems are used to estimate carbon fluxes and particulate organic matter distribution in the water column from vertical profiles of particle size-distribution and abundance.

Keywords: optical systems, particle and aggregate dynamics, marine snow, fecal pellets, spatial and temporal data

INTRODUCTION

The formation, distribution and transport of organic particles and aggregates from the surface ocean to the deep sea drives the biological carbon pump and, ultimately, the sequestration of organic matter at the seafloor. The magnitude and efficiency of organic matter export from the surface layers of the ocean is determined by the attenuation processes in the epipelagic zone, the upper roughly 200 m of the water column (Stemmann et al., 2004; Iversen and Ploug, 2010; Jackson and Checkley, 2011). However, our knowledge about particle and aggregate transport and transformation in the epipelagic zone is very limited. This is due to the heterogeneous nature of *in situ* aggregates, where one pool of particles and aggregates at any depth consists of different types with different age, origin, composition and sinking velocities (Iversen and Ploug, 2010). Hence, particles and aggregates at a specific depth may be a cluster of small single-celled phytoplankton and individual mineral particles, as well as large marine snow and fecal pellets formed from a mixture of organic and inorganic particles (e.g., lithogenic material). These particles and aggregates may range in size from μm to cm and generally sink between one to several hundred m per day (Simon et al., 2002; Iversen and Ploug, 2010; Turner, 2015). Furthermore, they may be from days to weeks old with origins in the surface ocean directly above or hundreds of km away (e.g., Siegel and Deuser, 1997; Iversen et al., 2010; Wekerle et al., 2018). This complicates our understanding of transport and transformation of settling organic matter, especially when studying bulk samples and averaging across all particle and aggregate types.

Inclusion of lithogenic and biogenic minerals within marine snow and fecal pellets has been shown to increase their density and size-specific sinking velocities (Passow and De La Rocha, 2006; De La Rocha et al., 2008; Iversen and Ploug, 2010; van der Jagt et al., 2018, Many et al., 2019). However, incorporation of mineral particles into marine snow can cause them to fragment into small and dense aggregates (Passow and De La Rocha, 2006; Engel et al., 2009) with higher size-specific sinking velocities than similar sized non-ballasted aggregates (Ploug et al., 2008; Iversen and Ploug, 2010; Iversen and Robert, 2015). This suggests that similar sized aggregates at any given depth in the water column may consist of a mixture of aggregates of widely different composition, densities, and sinking velocities, showing that size alone is a poor measure for aggregate settling and dynamics. While *in situ* camera systems are good at capturing sizes and abundance of particles and aggregates through the water column, they provide little direct information about aggregate composition and density. It is therefore difficult to extract information about mass and sinking velocities of the aggregates, which, however, is required to determine and understand the downward vertical flux of matter in the ocean.

Recent studies have combined *in situ* camera systems with sediment trap measurements to estimate regional and seasonal particulate organic carbon flux (e.g., Guidi et al., 2008; Iversen et al., 2010; McDonnell and Buesseler, 2010; Nowald et al., 2015; Fender et al., 2019). However, this is biased by the fact that sediment traps and camera systems may capture different particles and aggregates. A sediment trap collects all settling particles and aggregates at one depth over time and area, while a camera system determines instantaneous concentrations of both settling and suspended particles through the water column. Thus, the size-range of captured particles differs between camera systems and sediment traps. Minimum particle sizes captured by camera systems are determined by their optical resolution, while the capture efficiency of small particles by sediment traps are determined by the sinking velocities of the particles. Since large particles and aggregates are often rare in the water column, the maximum particle sizes captured by camera systems is determined by their concentrations in relation to the volume of water imaged by the camera systems and the duration of sampling by the sediment traps (Jackson and Checkley, 2011). Furthermore, conventional sediment traps lack information about individual particles but allow bulk biogeochemical analyses. In contrast, traps filled with viscous gels preserve the shape, size, and structure of each individual particle collected (Lundsgaard, 1995; Waite and Nodder, 2001; Ebersbach and Trull, 2008; Thiele et al., 2015). It is therefore difficult to evaluate if sediment traps and camera systems deployed at the same depth and region will capture similar particle and aggregate types.

Camera systems differ in configurations and, consequently, captured particle size ranges are not the same. More importantly, the configurations of individual camera systems also affect the particle types that the systems detect. For instance, holographic cameras can capture transparent particles (e.g., Bochdansky et al., 2013), Optical Laser Diffraction Instruments (e.g., LISST, Sequoia Sci) can size and count small particles (e.g., Graham et al., 2012; Markussen and Andersen, 2014; Gillard et al., 2019), while more traditional camera systems require particles that either shadow or reflect light, depending on whether the illumination is provided from the back, sides, or front (e.g., Ratmeyer and Wefer, 1996; Davis et al., 2005; Picheral et al., 2010; Lombard et al., 2019). Knowing the advantages and limitations of each applied system and using combinations of different optical systems together with sediment traps may allow detection of a wider range of particle types and provide information about aggregate and particle composition and dynamics (Jackson et al., 1997).

We evaluated two camera systems (Pcam and IRcam) in the laboratory and could show that they detected different particle types. Subsequently, we carried out a case study in which we combined several *in situ* optical systems (the two different camera systems, images of gel traps plus a CTD with a turbidity and fluorescence sensor) with drifting gel trap collections in the upper 250 m of the water column off Cape Blanc, Mauritania. The camera systems were deployed both as profiling from the ship's winch system and drifting on a sediment trap array. We show examples of the added value of combining optical systems, but also highlight a few but important pitfalls and caveats when working with such systems.

MATERIALS AND METHODS

Instruments Used

We tested the added value of simultaneously using two complementary camera systems which detected different particle types. The first camera system, the Pcam, was designed to detect and focus on lithogenic particles while the second camera system, the IRcam, images large, potentially organic, aggregates. The camera systems were calibrated in controlled laboratory settings prior to *in situ* deployment during the case study in the Cape Blanc upwelling region. The calibrations and comparisons between the Pcam and IRcam were made for different aggregate types and the size-detections by the two systems were calibrated against Coulter Counter measurements of the same particles. In the case study, both camera systems were deployed in a profiling mode in concert with a SeaBird SBE-19 CTD equipped with an oxygen sensor, a CHELSEA-fluorometer, and a WETLABS turbidity sensor, as well as in a drifting mode on sediment trap arrays together with gel traps.

Pcam

The Pcam consisted of a Canon D70 digital SLR camera with a 60 mm Canon EF-S macro lens inside a pressure housing rated to a depth of 300 m. The pixel size was 4.1 μm with a 1:1 aspect ratio, and a field of view of 22 × 15 × 5 mm (W×H×D). This provided a measuring volume of 1.69×10^{-3} L. The light source was a green (520 nm) 120 mW (max. output) laser with the beam collimated and spread to a sheet using line generating optics. The Pcam was originally designed and calibrated for use in highly turbid estuarine environments, where a strong and very precise light source is needed (Markussen et al., 2016). However, the laser sheet has two different positions to adjust to different particle concentrations, one position 2 mm from the pressure housing, and one position 10 mm from the house. The second position was used in this study, due to the relatively low particle concentrations in open marine waters. The camera was expected to quantitatively measure particles with equivalent spherical diameters (ESDs) between 10 and 1500 μm. Images were stored on an SD card in the camera and downloaded to a computer through a Raspberry Pi in the camera system. Processing of Pcam images was carried out using the ParChar code (Markussen, 2016).

IRcam

The IRcam consisted of an infrared camera (Basler) connected to a Raspberry Pi and equipped with a fixed focal length lens (16 mm Edmund Optics). The illumination was provided by an infrared LED (wavelength between 700–1000 nm) that was equipped as backlight, providing shadow images of the particle and aggregates. The IRcam captured two-three images per second. Each image had a field of view of 35 × 26.4 × 10 mm (W×H×D), yielding a measuring volume of 9.24×10^{-3} L. The pixel size was 27.8 μm and the camera was expected to quantitatively capture aggregates and particles with ESDs between 50 and 6000 μm. All images were stored on a hard drive and downloaded to a computer after each deployment via an Ethernet connection through the pressure housing. The same Ethernet connection was used to program the camera system before deployment. The image analyses were performed using the Image Processing Toolbox in MatLab (The MathWorks) using a method resembling that of the ParChar code (Markussen, 2016). Each image was converted into gray scale and the background was removed by applying a threshold value. The pixel numbers for each projected particle area was determined, and converted into ESD using the pixels to mm ratio. If particles were porous (contained holes), these areas would not be included as part of the particle area, i.e., we did not apply a 'fill hole' function, and all optical methods in this study would not include those areas as part of the particle when calculating the ESDs. Calibrations were done in the laboratory before field deployments by comparing the frequency size distribution of different particle types to Coulter Counter measurements. Since we excluded pore-spaces in our ESD calculations, the ESD should be considered as solid mass diameter, which is similar to how a Coulter Counter considers sizes (e.g., Jackson et al., 1997).

Both camera systems were deployed simultaneously on one frame. The size of a particle was determined from its area and converted into ESD. Detected particles were sorted into 50 logarithmically spaced size bins based on their ESDs. The particle size distributions (n_C) were calculated from the particle number concentration (ΔN_C) within a given size range (Δd) of each image:

$$n_C = \frac{\Delta N_C}{\Delta d} \quad [\#cm^{-3}\, cm^{-1}] \tag{1}$$

Sediment Gel Traps

Settling particles were collected at three depths using surface-tethered, freely drifting sediment traps filled with a viscous gel. The drifting traps were deployed as a drifting array that consists of a surface buoy equipped with a GPS satellite transmitter, four surface floats and 12 small buoyancy balls serving as wave breakers to reduce the hydrodynamic effects on the traps. Four gimbal mounted collection trap cylinders (100 × 10.4 cm) were deployed at 150, 200, and 400 m, respectively. At each depth, one of the collection cylinders was equipped with a gel-insert that was filled with 200 ml of a viscous gel (Tissue-Tek®, O.C.T.™ COMPOUND, Sakura) to intercept and preserve settling particles without destroying their original size and structure. Upon recovery, we allowed the particles a settling period of 12 h before we removed the gel-inserts from trap cylinders. The two *in situ* camera systems were deployed as part of the drifting array at 100 m depth and thus, in this study, we only focus on the gel trap collection from 150 m.

After retrieval, the gels were photographed using a Canon EOS Rebel T2i and a Sigma 105 mm Macro Lens. The images were illuminated with an even backlight. Each image had a field of view of 29.8 × 19.9 mm and a resolution of 5.75 μm per pixel and was expected to detect particles with ESDs from 10 μm to 3000 μm. The image analyses were again performed with a routine written in Matlab (The Mathworks). The obtained particle sizes for each gel trap were divided into 50 logarithmically spaced size bins. These bins were used to calculate the particle flux size spectrum (f) as a function of diameter (d), by dividing the flux of particles

(ΔN_F) in a given small size range (Δd) from the collection interval (Δt) (Jackson et al., 2005):

$$f = \frac{\Delta N_F}{\Delta d \Delta t} \quad [\#cm^{-2}\ cm^{-1}\ min^{-1}] \tag{2}$$

Acoustic Doppler Current Profiler (ADCP)

An ADCP (RDI, 600 kHz) was mounted on a frame and deployed from the ship in down-looking configuration at 50 m depth during the night of the drifting deployment. The cell size was set to 4 m and the time between pings to 30 s. In this study, we only used the acoustic backscatter profile. Backscatter (dB) was derived from the raw echo intensities (counts) correcting for beam spreading and water absorption (Mullison, 2017). Analysis was based on relative backscatter and the instrumental constant was omitted. The absorption coefficient (0.17 dB/m) was calculated according to Ainslie and McColm (1998) using average values for salinity and temperature, obtained from CTD data. The near-field correction was performed following Downing et al. (1994).

Case Study Region Off Cape Blanc, Mauritania

The Atlantic Ocean region off Cape Blanc in Mauritania, NW Africa, served as a case study site to evaluate the added value of deploying different optical systems simultaneously (**Figure 1**). This region is part of the Canary Current System, which is one of the four major Eastern Boundary Upwelling Ecosystems with a primary productivity of ∼0.33 Gt per year (Carr, 2002). This high production is supported by the year-round coastal upwelling of nutrient-rich deep water (Gabric et al., 1993; Cropper et al., 2014). Furthermore, this region has high dust deposition (Mahowald et al., 1999; Jickells et al., 2005). The combination of high productivity and high dust deposition makes this region optimal for our case study of the combined optical systems optimized for organic and lithogenic material. Numerous particle and export studies have been conducted in the region, including long-term sediment trap moorings that have measured seasonal fluxes since 1998 (Karakaş et al., 2006, 2009; Fischer and Karakaş, 2009; Fischer et al., 2009, 2016; Iversen et al., 2010; Nowald et al., 2015), as well as several studies combining optical measurements using camera systems and vertical flux measurements using sediment traps (Karakaş et al., 2009; Iversen et al., 2010; Nowald et al., 2015). Generally, these studies have shown large flux attenuation in the upper 250 m of the water column off Cape Blanc, suggesting that these depths have the highest rates of particle transformation and turnover (Iversen et al., 2010).

Field Sampling

The case study was done during the R/V Poseidon cruise POS481 from the 15th of February to the 3rd of March, 2015. The data presented here consisted of two vertical profiles and one 18 h drifting deployment. One profile location was in an off-shore, open ocean setting and the other profile location was closer to the coast at the shelf-slope (**Figure 1** and **Table 1**). The drifting deployment was launched from the location of the off-shore, open ocean station.

RESULTS

Laboratory Evaluation of Particle Detection by the Two Camera Systems

We compared the detection of different particle types for the Pcam and the IRcam in the laboratory. Three calibrations are presented based on two different particles types; inorganic lithogenic material (sand and sediment) and transparent particles (glass spheres). The results from the cameras were tested against distributions measured by a Coulter Counter. The IRcam primarily detected grains with sizes larger than 150 μm and, thus, under detected the finer sand and silt grains, when comparing to the results of the Coulter Counter and visually evaluating the images (**Figures 2**, **3**). The Pcam detected grains in the range from 10 to 600 μm, more in accordance with the Coulter Counter. Contrary, the Pcam underestimated the sizes of the glass beads and found a maximum size of 250 μm (**Figures 2**, **3**). The IRcam captured glass beads in the size-range between 500 and 800 μm with a mean size of 650 ± 50 μm and returned similar size-distributions and mean size as those we measured with the Coulter Counter (**Figures 2**, **3**). Finally, we formed porous organic aggregates from diatoms in roller tanks in the laboratory (see method in Iversen and Ploug, 2010). Visual comparison showed that the IRcam was reliably detecting organic, porous diatom aggregates, while the Pcam only detected parts of the aggregates (**Figure 3**).

Evaluation of *in situ* Particle Size-Spectra

We deployed the two camera systems as part of the drifting trap array during a diurnal deployment at the open ocean station (**Figure 1**). The IRcam only stored images until midnight while the Pcam stored images for the full diurnal deployment. There were differences in the concentration particle size-spectra observed by the Pcam and the IRcam, due to their different detection efficiencies for different types of particles. Comparing the Pcam and IRcam, we measured higher abundance of particles smaller than 200 μm with the Pcam compared to the IRcam and vice versa for particles larger than 500 μm. In contrast, the gel trap is considered to be equally ideal for detection of all sizes of particles, our camera system allowed a quantifiable size-range between 10 and 2000 μm for the gel trap (lower and upper size-range determined by (*i*) the optical resolution and (*ii*) the trap area and deployment time, respectively). Combined, the two camera systems spanned a particle size-range similar to that collected in the gel trap (**Figure 4**). Note that the particle size spectra from the camera systems and the gel trap cannot be directly compared for two reasons: (*i*) the camera systems collect concentration particle size-spectra (i.e., # cm^{-4}), while the gel traps collect flux particle size-spectra (i.e., # $cm^{-3}\ min^{-1}$) and (*ii*) the camera systems observe both suspended and settling particles while the gel traps only collect settling particles. However, by comparing the patterns of the flux and concentration particle size-spectra, it can be inferred that the Pcam and IRcam detected all settling particles in the size-range between 20 and 2000 μm and between 200 to 2000 μm,

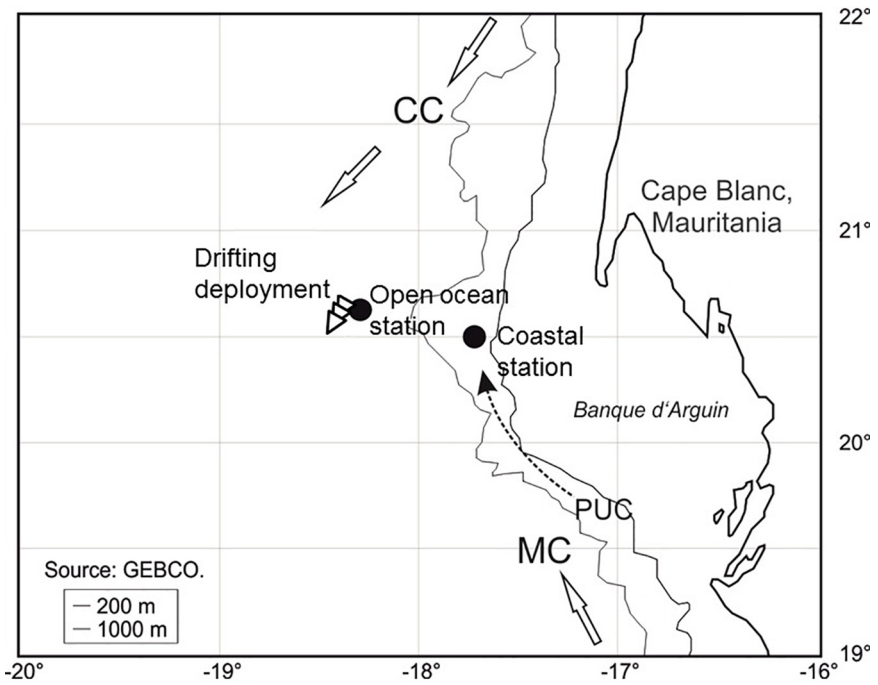

FIGURE 1 | Location of the drifting deployment and the two profiling stations during POS cruise 481 (see **Table 1** for more information). The three arrows show the direction and trajectory of the drifting deployment. CC, Canary Current; MC, Mauritanian Current; PUC, Poleward Undercurrent (=slope current).

TABLE 1 | Overview and metadata of the three deployments, including Station identification (Station I.D.), station name, date, time, full water depth, latitude (Lat. N) and longitude (Long. W).

Station I.D.	Station name	Date	Time (UTC + 1)	Water depth (m)	Lat. N	Long. W
Open ocean station	GeoB19405-1	26/02/15	16:30	1355	20°40.03′	18°19.99′
Drifter deployment	GeoB19405-2	26/02/15	19:00	1345	20°39.97′	18°19.54′
Drifter recovery	GeoB19405-10	27/02/15	13:00	1275	20°34.76′	18°22.48′
Coastal station	GeoB19406-3	27/02/15	20:30	307	20°30.03′	17°45.00′

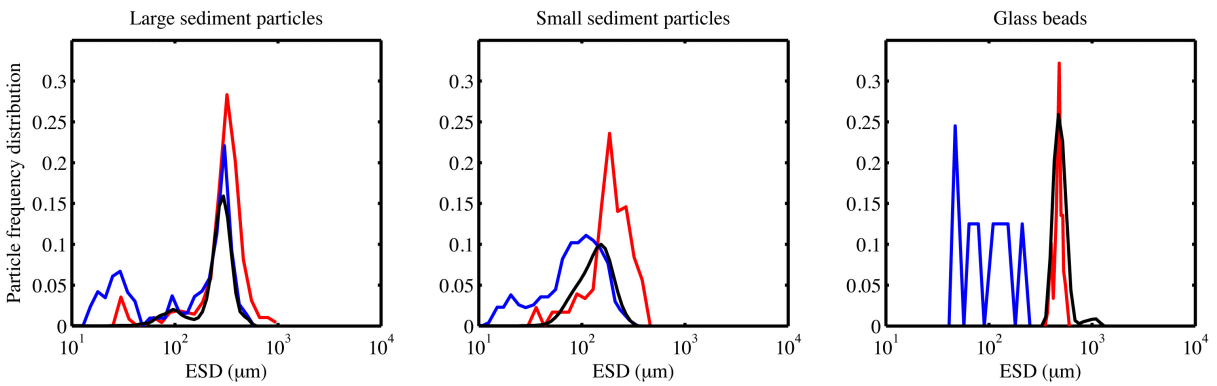

FIGURE 2 | The frequency distribution shows the size-distribution in a sample pool, i.e., the number fraction a certain size-class makes up of the total particle pool. Frequency distributions from the laboratory calibrations using two different sediment types and glass beads. The frequency distribution for Pcam is presented by blue lines, the frequency distribution for the IRcam is presented in red lines, and the frequency distribution measured by the Coulter Counter is presented in black lines.

respectively (**Figure 4**). Additionally, it seems that the IRcam detected suspended particles larger than 500 μm, which were not observed by either the Pcam or the gel trap (**Figure 4**). From the particles collected in the gel trap, we found that 19 ± 2% of the total particle volume was made of by zooplankton fecal pellets in the size-classes between 20 and 200 μm, while fecal pellets

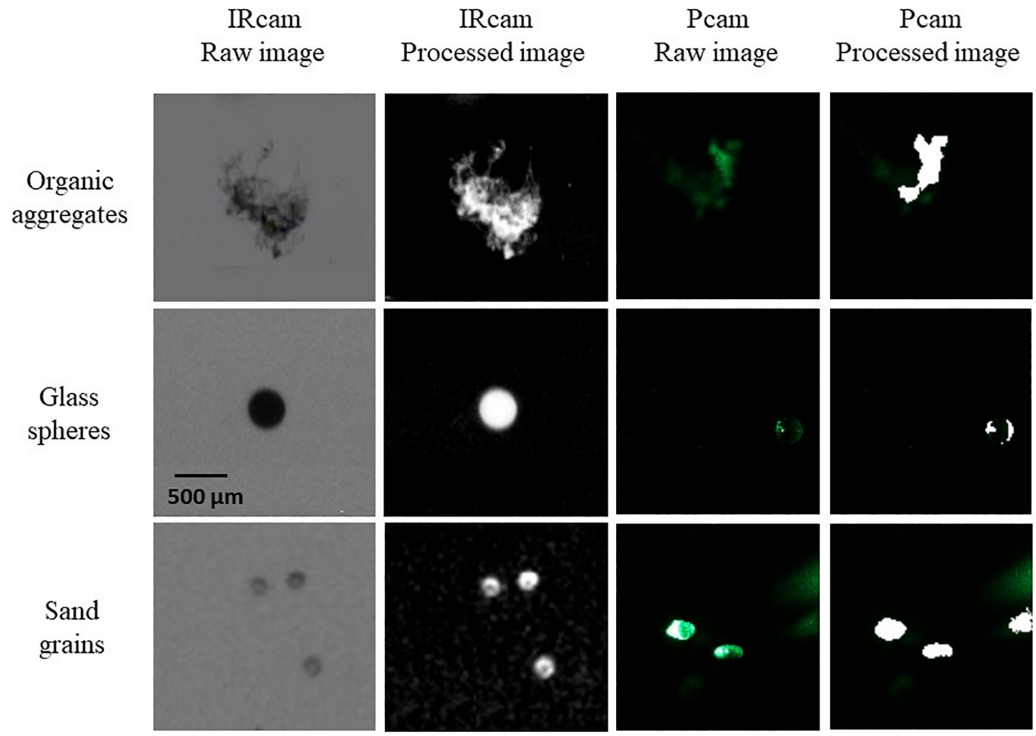

FIGURE 3 | Examples of particles imaged by the two cameras, showing unprocessed IRcam particles (raw images, left column), processed IRcam particles (processed images, second column from left), unprocessed Pcam particles (raw images, third column from left) and processed Pcam particles (processed images, right column). The top row shows examples of marine snow aggregates (organic aggregates), the middle row shows glass beads (glass spheres), and the bottom row shows sediment particles (sand grains). The scale bar in panel is valid for all panels.

made up 32% of the intermediate-sized aggregates (200–500 μm), and 36% of aggregates between 500 and 1000 μm (**Figure 4B**). We did not observe any fecal pellets larger than 1000 μm or smaller than 20 μm (**Figure 4B**). The fecal pellets were primarily produced by copepods.

Diurnal Particle Dynamics

We used a diurnal deployment to exemplify potentials of combining optical systems over time. The Pcam detected higher particle abundance and total volume during evening and morning compared to night-time (**Figure 5** and **Table 2**). The decrease in both total volume and abundance of particles started after 21:00 and lasted until midnight, after which the values remained low and stable throughout the night. At 09:00 a rapid increase in abundance and volume occurred, but remained only 72% of the total particle volume observed during the previous evening (**Figure 5** and **Table 2**). Despite some small variations in the average ESD throughout the deployment, the overall average ESD measured by the Pcam remained at roughly 120 μm. The average ESD measured by the IRcam was twofold higher than that of the Pcam and showed a slight increase at midnight. The total volumes measured by the IRcam were more than 20 times higher than those of the Pcam. However, IRcam values of abundance were lower than those of the Pcam until the last hour before midnight, with mean values in the evening (hours 20–22) being just two thirds of the abundances measured by the Pcam. The ADCP showed an almost constant backscattering signal at 50–70 m depth, higher at this depth than below, from the time of deployment until 07:30 in the morning. At this time, a strong downward directed signal was seen to a depth of 110 m at 08:00 (**Figure 5**).

Vertical Particle Size-Distribution and Abundance

Particle abundance, total particle volume, turbidity and fluorescence decreased with increasing depth at the open ocean station (**Figure 6**). In contrast, there was little coherence between particle abundance and total volume at the coastal station, where the Pcam showed increasing particle abundances with increasing depth while the IRcam showed constant particle abundance with increasing depth and an order of magnitude lower than those observed with the Pcam (**Figure 6**). The abundances of large particles (>200 μm) were in the same order of magnitude at both stations (**Figure 7**). At the open ocean station the Pcam and IRcam detected roughly the same amount of both small and large particles, while the Pcam detected an order of magnitude higher abundance of small particles (<200 μm) compared to the IRcam at the coastal station.

There was a positive significant correlation between turbidity and fluorescence at the open ocean station and a negative significant correlation at the coastal station (**Table 3**). The open ocean station had positive significant correlations of turbidity

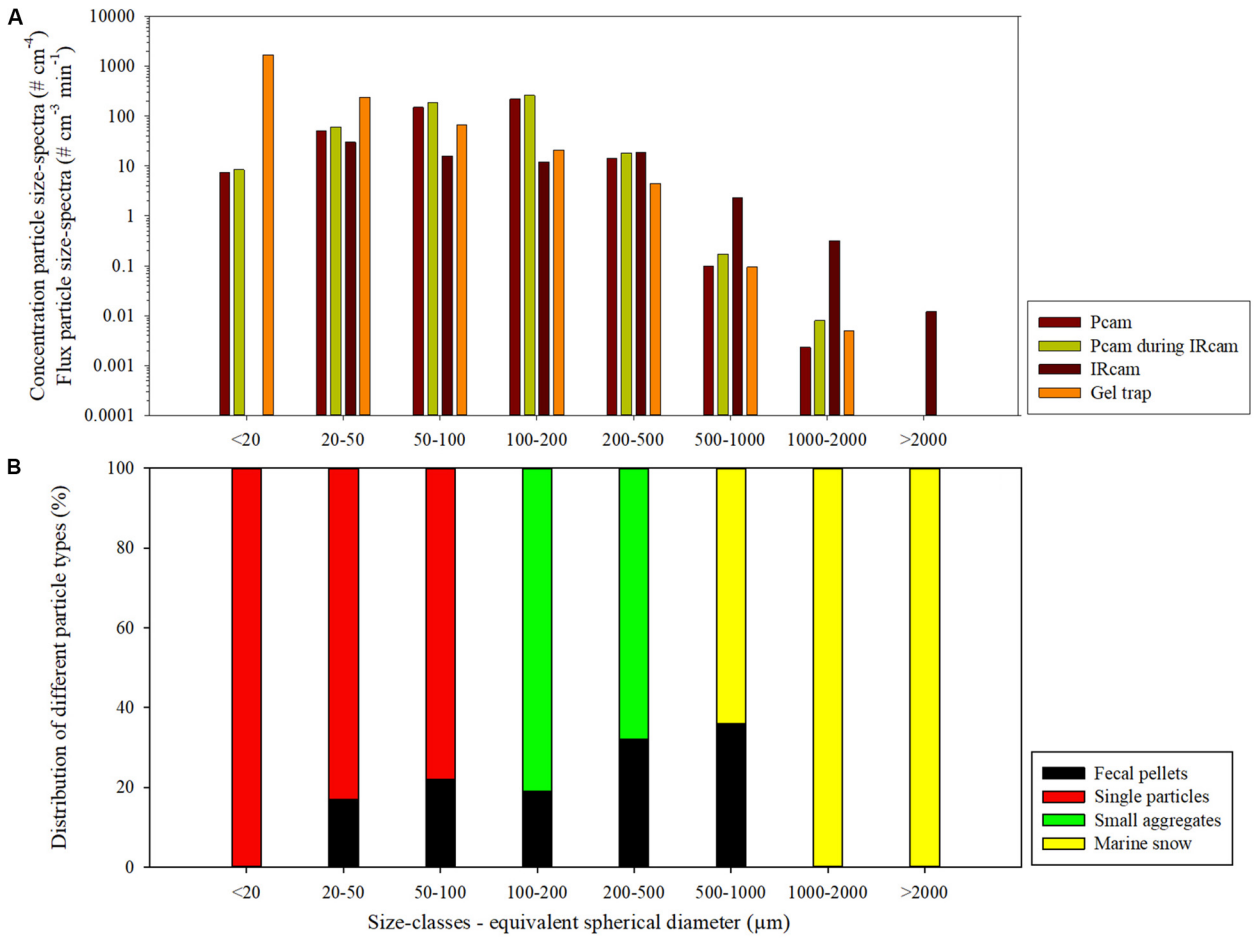

FIGURE 4 | Particle size-spectra for the drifting deployment for the Pcam, IRcam, and gel trap. **(A)** The data from Pcam and the IRcam are presented as concentration particle size-spectra (# cm^{-3} cm^{-1}) and the data from the gel trap is presented as flux particle size-spectra (# cm^{-2} cm^{-1} min^{-1}). The particle size-spectra for all three measuring instruments are divided into eight size classes (*x*-axis, panel **A**). The number particle size-spectra for the Pcam is for the entire deployment period (dark blue) and for the period where the IRcam captured images (light blue). The concentration particle size-spectra for the IRcam data (yellow) and the flux particle size-spectra from the gel trap (dark red). The unit of the concentration particle size-spectra of the Pcam and the IRcam are in numbers of particles per cm^4, the unit of flux particle size-spectra for the gel trap is as numbers of particles per cm^3 per minute. **(B)** The particles types were identified from the gel trap and presented as percentage of fecal pellets, single phytoplankton and lithogenic particles, small aggregates, and marine snow for each size class.

and fluorescence to particle abundances and volumes for both Pcam and IRcam, with the strongest correlations between fluorescence and IRcam abundance and volumes (**Table 3**). This shows that the particles at the open ocean station were dominated by phytoplankton, which was also observed from the presence of fecal pellets and phytoplankton aggregates in the gel trap (**Figure 4**). Hence, the particles and aggregates at the open ocean station were predominantly of organic origin. Note that we have not performed any corrections for non-photochemical quenching of the fluorescence signal near the surface, but the majority of the data are from depths with little influence from solar irradiation. At the coastal station, only Pcam particle abundance and IRcam volumes were significantly correlated to turbidity (positive correlations) and to fluorescence (negative correlation) (**Table 3**). This suggested that the particles at the coastal station were predominantly of inorganic origin, which was also observed during previous studies off Cape Blanc where nepheloid layers (Nowald et al., 2006) could be modeled by "releasing" particles from the shallow shelf area and allowing them to be advected off-shore (Karakaş et al., 2006; Fischer et al., 2009). It is therefore likely that the observed inorganic particles at the costal station were resuspended shelf sediment.

DISCUSSION

The use of high magnification and a thin laser sheet made the Pcam optimal for detection of dense and small lithogenic particles, while transparent and/or porous organic aggregates were underrepresented during the laboratory calibrations (**Figures 2**, **3**). The IRcam captured the full size of glass spheres and organic aggregates during the laboratory calibrations (**Figures 2**, **3**). This was due to the use of backlight which imaged

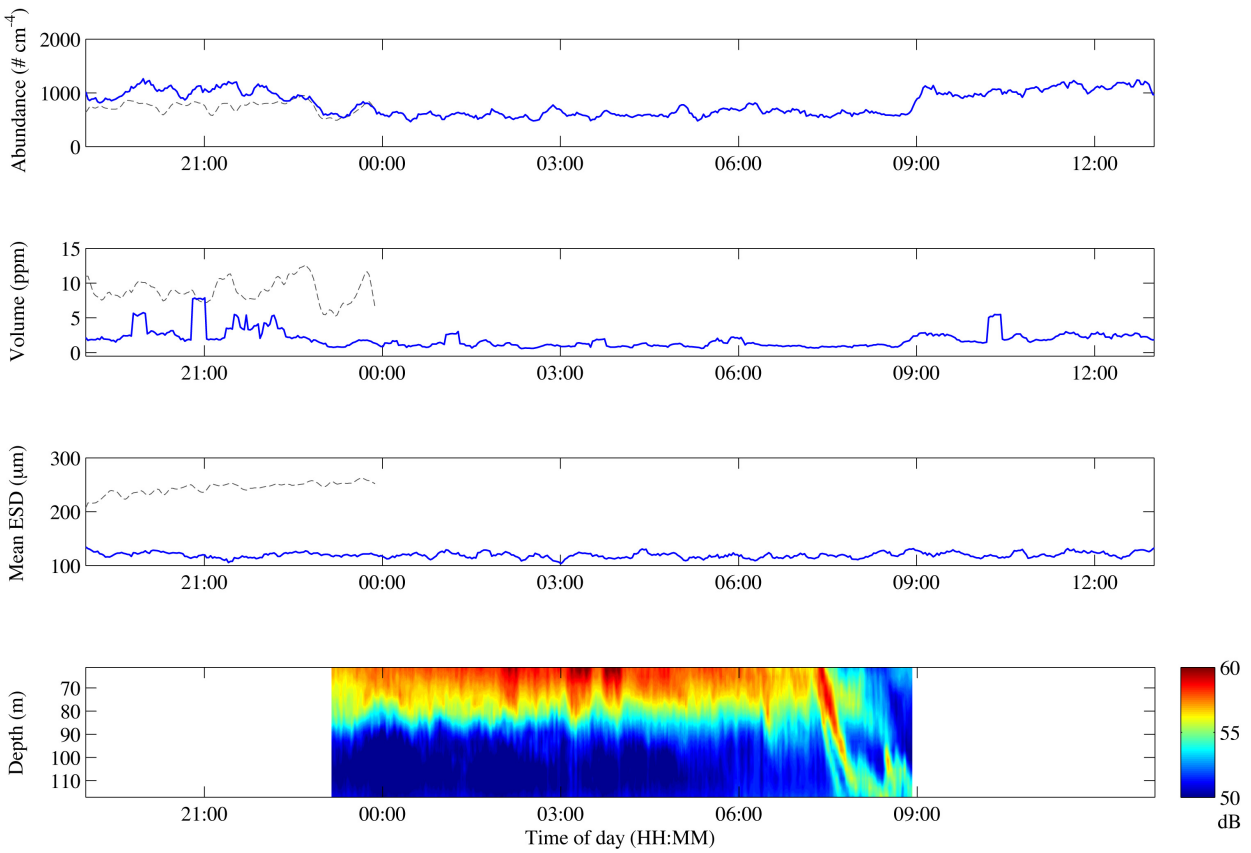

FIGURE 5 | Change in particle abundance **(A)**, particle volume **(B)**, mean ESD **(C)** and ADCP backscatter over depth **(D)** over the course of the drifting deployment. Gray lines represent IRcam data, blue lines represent Pcam data. The time zone is UTC + 1.

TABLE 2 | Mean values of selected camera data for the three periods (evening, night, and morning) of the drifting deployment with standard deviations in brackets.

	Evening	Night	Morning
Total particle volume	3.45 (±2.9) // [87.4 (±14.7)]	1.15 (±1.2)	2.49 (±0.9)
Total particle abundance	1070 (±211) // [750 (±88)]	609 (±158)	1060 (±197)
Mean ESD	118 (±12) // [234 (±8)]	118 (±13)	120 (±11)

All data is from the Pcam, except for in the evening when values from the IRcam is also shown in square brackets after the Pcam data. Evening is from 20 to 22, night is from 00 to 08 and morning is from 10 to 12, all times in UTC + 1, see text for explanation.

large and/or transparent particles well. Fine sand (<200 µm) and silt grains were underrepresented by the IRcam due to the low magnification chosen for this study, whereas the Pcam seemed to capture the entire spectra and potentially even at a finer detail in the low size range than the Coulter Counter. The low detection efficiency of the large organic aggregates by the Pcam is an example of the potential issues with the narrow laser sheet, as it sometimes limits large aggregates from being fully illuminated.

Generally, the Pcam was better at detecting particles smaller than 200 µm while the IRcam was better at detecting particles larger than 500 µm. This shows that our expected size-ranges for the two camera systems were different from the actual quantifiable size-ranges detected during field and laboratory measurements. This highlights a necessity to distinguish the qualitative size limit of a certain camera system from the quantitative size limit of the same system. Further, the differences between the coastal and the open ocean stations showed that even within one region, marine particles consisted of a wide range of types and sizes of inorganic and organic origin. Therefore, when using *in situ* camera systems to quantify particles and aggregates, it is important to understand and consider both the size-range and types of particles, that the applied systems can capture. To this end, combinations of different optical sensors, e.g., fluorescence and turbidity sensors in combination with *in situ* camera systems, can aide in the understanding of particle characteristics, as also shown by Jackson et al. (1997). Thus, it is important to base interpretations on data from instruments that are designed and adapted to the environment and particles that are being investigated. Specific optical instruments may detect different particle types (e.g., organic particles) better than others (e.g., inorganic particles) and therefore only capture a subset of the total *in situ* particles pool. This is further complicated by changes in the particle pool occurring on short temporal and spatial scales. For example, regions with nepheloid layers

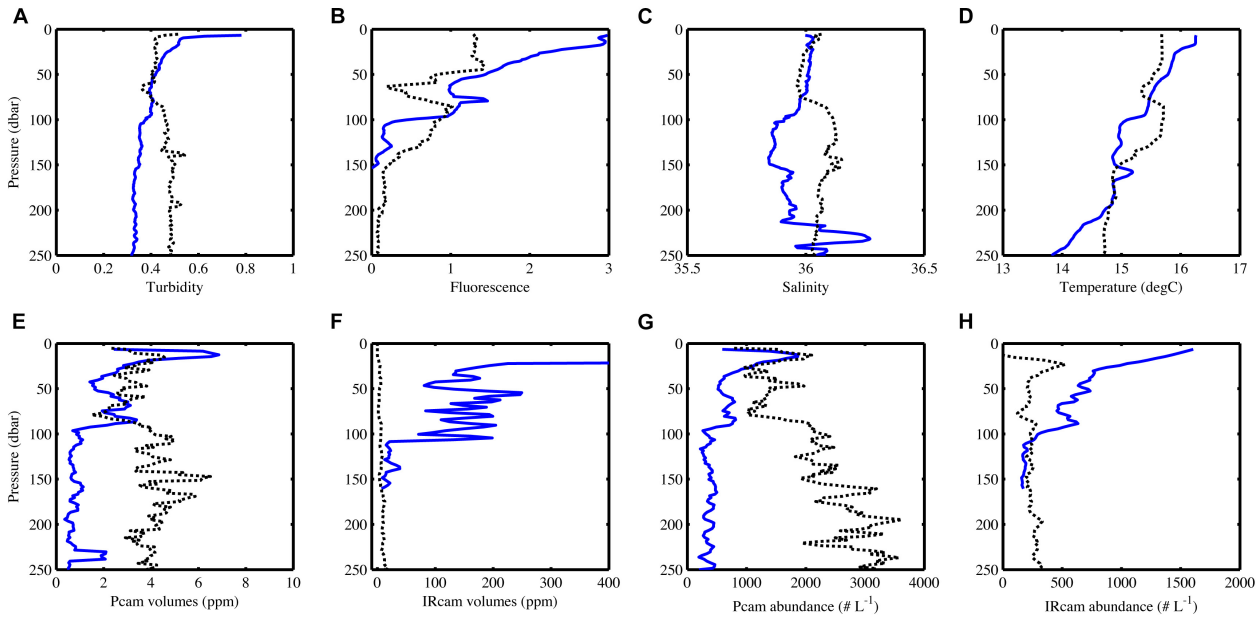

FIGURE 6 | CTD-data **(A–D)** and camera data **(E–H)** changes with depth, blue lines are from the open ocean station and black dots are from the coastal station. Note the different x-axes on **(E)** and **(F)** and that the x-axis in **(F)** does not show the full range of values at the open ocean station. The volume decreases linearly from 11300 ppm at 10 m depth to what is shown on the graph. The IRcam only worked down to 150 m at the open ocean station. Data has been binned in 5 m depth bins. For station metadata, see **Table 1**.

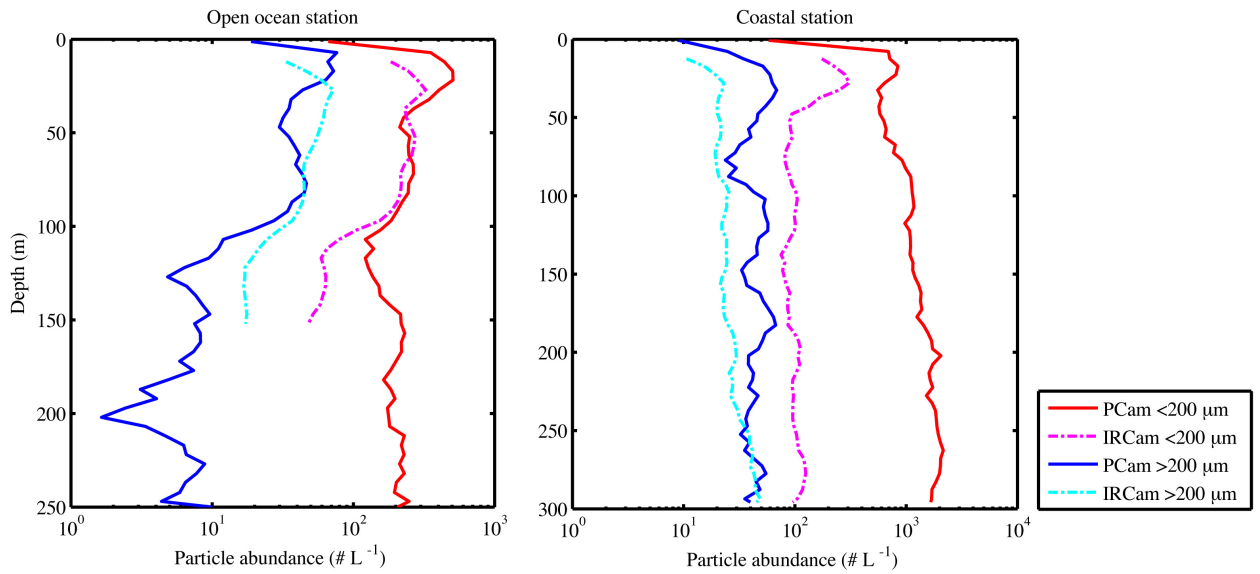

FIGURE 7 | Particle abundances over depth when profiling, showing the open ocean station **(Left)** and the coastal station **(Right)**, the particles are split in two size groups and shown for both camera systems (see legend). All measurements are from the upcast part of the profile and are binned in 5 m depth bins.

may have a water layer dominated by inorganic, lithogenic particles while shallower and deeper layers are dominated by organic aggregates (e.g., Karakaş et al., 2006; Seifert et al., 2019), which may or may not be detected by the camera system used to determine vertical profiles of particle size-distribution and abundances.

Combining Optical Systems

The different particle dynamics observed by the Pcam during the drifting deployment is an example of diurnal changes in particle characteristics. The high particle abundance and total volume observed during evening and morning compared to night-time, despite constant average particle sizes through the

TABLE 3 | Pearson correlation coefficients for selected parameters of the two profiling stations.

		Abundance, Pcam	Abundance, IRcam	Volume, Pcam	Volume, IRcam	Turbidity
Open ocean	Turbidity	*0.735*	*0.961*	*0.654*	*0.514*	–
	Fluorescence	*0.737*	*0.966*	*0.663*	*0.496*	*0.783*
Coastal	Turbidity	*0.466*	0.148	0.227	*0.364*	–
	Fluorescence	*−0.538*	−0.067	−0.179	*−0.428*	*−0.529*

Numbers in italics show statistically significant correlations ($p < 0.001$).

whole deployment period, suggested a particle loss across all particle sizes during night. The morning total volume was only 72% of that observed during the previous evening and may be explained by the time required for growth of new phytoplankton to a threshold level where aggregates formed and sank to the depth of the camera (Jackson and Kiørboe, 2008; Iversen et al., 2010). The low night-time particle abundance and total volume occurred while the ADCP backscatter was high in the water layers above the camera and after an increase in mean ESDs were observed by the IRcam. This suggests a shift toward larger particles during night, possibly vertically migrating zooplankton (Lavery et al., 2009), which would suggest that zooplankton migrated to the upper water column during night and were feeding on the particles. Related to this is the fact that particles were lost across the whole quantifiable size range, which points toward flux feeding from organisms intercepting sinking particles (Jackson, 1993). This would be in accordance with previous studies off Cape Blanc, where changes in particle size distributions through the water column was best described by flux feeding (Iversen et al., 2010). However, this data set is too limited to make any clear conclusions about the mechanisms governing the observed particle and aggregate dynamics, but it does show the potential added value from combining several optical measurements with other methods such as sediment traps, zooplankton and phytoplankton sampling, and hydroacoustics.

We notice that the lower qualitative size limit of the IRcam of 50 μm was not sufficient to capture the smallest particles that were caught in the gel trap (sizes down to 10 μm). When considering the quantitative minimum size limit being closer to 200 μm for the IRcam, this discrepancy between sediment traps and the optical system becomes even larger. Looking at the other end of the size-spectra, the largest particles caught in the gel traps were in the order of 2000 μm whereas the IRcam imaged particles with sizes up to 6000 μm. When comparing the gel trap and the IRcam, we have to consider that the trap only collected settling particles while the IRcam 'saw' both settling and suspended particles. The gel trap collected settling particles for an area of 85 cm^2 during 18 h while the IRcam imaged a total water volume of 333 L during 5 h (9.24 mL per image and a capture frequency of two images per second). If we assume an average settling velocity of 50 m d^{-1}, which is typical for small particles in this region (Iversen et al., 2010), then the gel trap sampled a similar volume (0.43 m^3) as the IRcam (0.33 m^3), suggesting that the additional large particles observed by the IRcam were suspended. The particle sizes quantified by the Pcam fitted well to those collected with the gel trap. However, since we now know that the Pcam underestimates the volume and abundance of organic particles, it is likely that the large suspended particles that were only detected by the IRcam were of organic origin. This once again highlights the importance of being aware of not only size-ranges of imaging systems, but also particle types imaged. Moreover, it becomes especially important when optical systems are used to estimate carbon fluxes from vertical profiles of particles size-distribution and abundance.

Our evaluations showed that the two camera systems detected different particle types. Additionally, when combining data from different optical systems, we gain added insights into spatial (depth) and temporal (diurnal) particle dynamics and compositions. Based on our data, we find that even in marine environments it is important to also focus on relatively small particles (ESD < 200 μm), which primarily consisted of inorganic particles in our study area. Our study suggests that drifting deployments of optical systems together with sediment traps and an ADCP can provide a link between short-term (scale of minutes) particle interactions and transformation to longer-term (scale of hours, possibly days) export and attenuation processes, which has been called for in the past as well (e.g., Hebbeln et al., 2014). However, we need to be careful when interpreting such results and ensure that the applied camera systems overlap well with the sediment traps in terms of types and sizes of detected and captured particles and aggregates in order to be able to calculate, for instance, reliable export carbon fluxes. Combining different optical systems with long-term deployment of instruments, such as sediment traps and acoustic backscattering devices on moorings and landers, has the potential to improve our understanding of the biological carbon pump and oceanic carbon sequestration, throughout all seasons, as well as in different regions, without the necessity of ship access.

In recent years many camera systems have been developed and deployed successfully to observe suspended and sinking particles in the water column, including inorganic lithogenic particles, phytoplankton, zooplankton, jellyfish, fish, and settling aggregates such as marine snow and fecal pellets (see Lombard et al., 2019). Several studies have reviewed these existing optical devices and methods (e.g., Boss et al., 2015; Lombard et al., 2019; Giering et al., 2020), however, there is still a lack of direct comparisons between different optical systems deployed simultaneously. Considering the rapid developments in optical devices, it is now essential for the scientific community to come together to continue comparing different systems to optimize ways in which they can be combined. In this way, we will be able to design platforms with multiple systems that allow us to constrain the full range of particles and organisms that are

present in the oceans, and therefore gain better insights into the driving parameters for ecosystem structure and functioning. Such efforts are currently being undertaken in several international scientific networks focusing on optical methods and organic matter transport and transformation in the ocean, for example the SCOR working group TOMCAT[1] and the Joint Exploration of the Twilight ZoneOcean Network JETZON[2].

DATA AVAILABILITY STATEMENT

The raw data supporting the conclusions of this article will be made available by the authors, without undue reservation, to any qualified researcher.

AUTHOR CONTRIBUTIONS

All authors apart from MB took part in field sampling. MB analyzed ADCP data. TM and MI analyzed all other data, and wrote the manuscript with input from all other authors.

[1] www.tomcat-scor.org

[2] www.jetzon.org

FUNDING

This study was supported by the Helmholtz Association, the Alfred Wegener Institute Helmholtz Centre for Polar and Marine Research and the DFG-Research Center/Cluster of Excellence "The Ocean in the Earth System" at MARUM. This publication was supported by the HGF Young Investigator Group SeaPump "Seasonal and regional food web interactions with the biological pump": VH-NG-1000.

ACKNOWLEDGMENTS

We thank Cindy Lee, Stuart Wakeham, Kai-Uwe Hinrichs, Carol Arnosti, Anne Pearson, and Thorsten Dittmar for organizing the Marine Organic Biogeochemistry workshop held at the Hanse-Wissenschaftskolleg, Delmenhorst, Germany, April 27 – 30th 2019. We thank the crew of F.S. Poseidon cruise 481 for their assistance during the cruises. Thanks to Götz Ruhland, Marco Klann, and Helga van der Jagt for assistance during sediment trap deployments. We thank the reviewers for their valuable input and improvements.

REFERENCES

Ainslie, M. A., and McColm, J. G. (1998). A simplified formula for viscous and chemical absorption in sea water. *J. Acoust. Soc. Am.* 103, 1671–1672. doi: 10.1121/1.421258

Bochdansky, A. B., Jericho, M. H., and Herndl, G. J. (2013). Development and deployment of a point-source digital inline holographic microscope for the study of plankton and particles to a depth of 6000 m. *Limnol. Oceanogr.Methods* 11, 28–40. doi: 10.4319/lom.2013.11.28

Boss, E., Guidi, L., Richardson, M. J., Stemmann, L., Gardner, W., Bishop, J. K. B., et al. (2015). Optical techniques for remote and in-situ characterization of particles pertinent to GEOTRACES. *Prog. Oceanogr.* 133, 43–54. doi: 10.1016/j.pocean.2014.09.007

Carr, M. E. (2002). Estimation of potential productivity in Eastern Boundary Currents using remote sensing. *Deep Sea Res. II Top. Stud. Oceanogr.* 49, 59–80. doi: 10.1016/s0967-0645(01)00094-7

Cropper, T. E., Hanna, E., and Bigg, G. R. (2014). Spatial and temporal seasonal trends in coastal upwelling off Northwest Africa, 1981-2012. *Deep Sea Res. I Oceanogr. Res. Pap.* 86, 94–111. doi: 10.1016/j.dsr.2014.01.007

Davis, C. S., Thwaites, F. T., Gallager, S. M., and Hu, Q. (2005). A three-axis fast-tow digital Video Plankton Recorder for rapid surveys of plankton taxa and hydrography. *Limnol. Oceanogr.-Methods* 3, 59–74. doi: 10.4319/lom.2005.3.59

De La Rocha, C. L., Nowald, N., and Passow, U. (2008). Interactions between diatom aggregates, minerals, particulate organic carbon, and dissolved organic matter: further implications for the ballast hypothesis. *Glob. Biogeochem. Cycles* 22:GB4005. doi: 10.1029/2007GB003156

Downing, A., Thorne, P. D., and Vincent, C. E. (1994). Backscattering from a suspension in the near field of a piston transducer. *J. Acoust. Soc. Am.* 97, 1614–1620. doi: 10.1121/1.412100

Ebersbach, F., and Trull, T. W. (2008). Sinking particle properties from polyacrylamide gels during the KErguelen Ocean and Plateau compared Study (KEOPS): zooplankton control of carbon export in an area of persistent natural iron inputs in the Southern Ocean. *Limnol. Oceanogr.* 53, 212–224. doi: 10.4319/lo.2008.53.1.0212

Engel, A., Szlosek, J., Abramson, L., Liu, Z. F., and Lee, C. (2009). Investigating the effect of ballasting by CaCO3 in Emiliania huxleyi: I. Formation, settling velocities and physical properties of aggregates. *Deep Sea Res. II Top. Stud. Oceanogr.* 56, 1396–1407. doi: 10.1016/j.dsr2.2008.11.027

Fender, C. K., Kelly, T. B., Guidi, L., Ohman, M. D., Smith, M. C., and Stukel, M. R. (2019). Investigating particle size-flux relationships and the biological pump across a range of plankton ecosystem states from coastal to oligotrophic. *Front. Mar. Sci.* 6:603. doi: 10.3389/fmars.2019.00603

Fischer, G., and Karakaş, G. (2009). Sinking rates and ballast composition of particles in the Atlantic Ocean: implications for the organic carbon fluxes to the deep ocean. *Biogeosciences* 6, 85–102. doi: 10.5194/bg-6-85-2009

Fischer, G., Karakaş, G., Blaas, M., Ratmeyer, V., Nowald, N., Schlitzer, R., et al. (2009). Mineral ballast and particle settling rates in the coastal upwelling system off NW Africa and the South Atlantic. *Int. J. Earth Sci.* 98, 281–298. doi: 10.1007/s00531-007-0234-7

Fischer, G., Romero, O., Merkel, U., Donner, B., Iversen, M. H., Nowald, N., et al. (2016). Deep ocean mass fluxes in the coastal upwelling off Mauritania from 1998 to 2012: variability on seasonal to decadal timescales. *Biogeosciences* 13, 3071–3090. doi: 10.5194/bg-13-3071-2016

Gabric, A. J., Garcia, L., Vancamp, L., Nykjaer, L., Eifler, W., and Schrimpf, W. (1993). Offshore Export of Shelf Production in the Cape Blanc (Mauritania) Giant Filament as Derived from Coastal Zone Color Scanner Imagery. *J. Geophys. Res. Oceans* 98, 4697–4712. doi: 10.1029/92jc01714

Giering, S. L. C., Cavan, E. L., Basedow, S. L., Briggs, N., Burd, A. B., Darroch, L. J., et al. (2020). Sinking organic particles in the ocean—flux estimates from in situ optical devices. *Front. Mar. Sci.* 6:834. doi: 10.3389/fmars.2019.00834

Gillard, B., Purkiani, K., Chatzievangelou, D., Vink, A., Iversen, M. H., and Thomsen, L. (2019). Physical and hydrodynamic properties of deep sea mining-generated, abyssal sediment plumes in the Clarion Clipperton Fracture Zone (eastern-central Pacific). *Elementa* 7:5. doi: 10.1525/elementa.343

Graham, G. W., Davies, E. J., Nimmo-Smith, W. A. M., Bowers, D. G., and Braithwaite, K. M. (2012). Interpreting LISST-100X measurements of particles with complex shape using digital in-line holography. *J. Geophys. Res. Oceans* 117:C05034. doi: 10.1029/2011JC007613

Guidi, L., Jackson, G. A., Stemmann, L., Miquel, J. C., Picheral, M., and Gorsky, G. (2008). Relationship between particle size distribution and flux in the mesopelagic zone. *Deep Sea Res. I* 55, 1364–1374. doi: 10.1016/j.dsr.2008.05.014

Hebbeln, D., Wienberg, C., Wintersteller, P., Freiwald, A., Becker, M., Beuck, L., et al. (2014). Environmental forcing of the Campeche cold-water coral province, southern Gulf of Mexico. *Biogeosciences* 11, 1799–1815. doi: 10.5194/bg-11-1799-2014

Iversen, M. H., Nowald, N., Ploug, H., Jackson, G. A., and Fischer, G. (2010). High resolution profiles of vertical particulate organic matter export off Cape Blanc, Mauritania: degradation processes and ballasting effects. *Deep Sea Res. I* 57, 771–784. doi: 10.1016/j.dsr.2010.03.007

Iversen, M. H., and Ploug, H. (2010). Ballast minerals and the sinking carbon flux in the ocean: carbon-specific respiration rates and sinking velocities of marine snow aggregates. *Biogeosciences* 7, 2613–2624. doi: 10.5194/bg-7-2613-2010

Iversen, M. H., and Robert, M. L. (2015). Ballasting effects of smectite on aggregate formation and export from a natural plankton community. *Mar. Chem.* 175, 18–27. doi: 10.1016/j.marchem.2015.04.009

Jackson, G. A. (1993). Flux feeding as a mechanism for zooplankton grazing and its implications for vertical particulate flux. *Limnol. Oceanogr.* 38, 1328–1331. doi: 10.4319/lo.1993.38.6.1328

Jackson, G. A., and Checkley, D. M. Jr. (2011). Particle size distribution in the upper 100 m water column and their implications for animal feeding in the plankton. *Deep Sea Res. I* 58, 283–297. doi: 10.1016/j.dsr.2010.12.008

Jackson, G. A., and Kiørboe, T. (2008). Maximum phytoplankton concentrations in the sea. *Limnol. Oceanogr.* 53, 395–399. doi: 10.4319/lo.2008.53.1.0395

Jackson, G. A., Maffione, R., Costello, D. K., Alldredge, A. L., Logan, B. E., and Dam, H. G. (1997). Particle size spectra between 1 μm and 1 cm at Monterey Bay determined using multiple instruments. *Deep Sea Res. I* 44, 1739–1767. doi: 10.1016/s0967-0637(97)00029-0

Jackson, G. A., Waite, A. M., and Boyd, P. W. (2005). Role of algal aggregation in vertical carbon export during SOIREE and in other low biomass environments. *Geophys. Res. Lett.* 32:L13607. doi: 10.1029/2005GL023180

Jickells, T. D., An, Z. S., Andersen, K. K., Baker, A. R., Bergametti, G., Brooks, N., et al. (2005). Global iron connections between desert dust, ocean biogeochemistry, and climate. *Science* 308, 67–71. doi: 10.1126/science.1105959

Karakaş, G., Nowald, N., Blaas, M., Marchesiello, P., Frickenhaus, S., and Schlitzer, R. (2006). High-resolution modeling of sediment erosion and particle transport across the northwest African shelf. *J. Geophys. Res.* 111:C06025. doi: 10.1029/2005JC003296

Karakaş, G., Nowald, N., Schafer-Neth, C., Iversen, M., Barkmann, W., Fischer, G., et al. (2009). Impact of particle aggregation on vertical fluxes of organic matter. *Prog. Oceanogr.* 83, 331–341. doi: 10.1016/j.pocean.2009.07.047

Lavery, A. C., Chu, D., and Moum, J. N. (2009). Measurements of acoustic scattering from zooplankton and oceanic microstructure using a broadband echosounder. *ICES J. Mar. Sci.* 67, 1–16.

Lombard, F., Boss, E., Waite, A. M., Uitz, J., Stemmann, L., Sosik, H. M., et al. (2019). Globally consistent quantitative observations of planktonic ecosystems. *Front. Mar. Sci.* 6:196. doi: 10.3389/fmars.2019.00196

Lundsgaard, C. (1995). "Use of a high viscosity medium in studies of aggregates," in *Sediment Trap Studies in the Nordic Countries*, eds S. Floderus, A. S. Heisakanen, M. Oleson, and P. Wassmann (Nurmijarvi: Nurmiprint Oy).

Mahowald, N., Kohfeld, K., Hansson, M., Balkanski, Y., Harrison, S. P., Prentice, I. C., et al. (1999). Dust sources and deposition during the last glacial maximum and current climate: a comparison of model results with paleodata from ice cores and marine sediments. *J. Geophys. Res. Atmos.* 104, 15895–15916. doi: 10.1029/1999jd900084

Many, G., Durrieu de Madron, X., Verney, R., Bourrin, F., Renosh, P. R., Jourdin, F., et al. (2019). Geometry, fractal dimension and settling velocity of flocs during flooding conditions in the Rhône ROFI. *Estuar. Coast. Shelf Sci.* 219, 1–13. doi: 10.1016/j.ecss.2019.01.017

Markussen, T. N. (2016). ParChar - Characterization of suspended particles through image processing in Matlab. *J. Open Res. Softw.* 4:p.e26. doi: 10.5334/jors.114

Markussen, T. N., and Andersen, T. J. (2014). Flocculation and floc break-up related to tidally induced turbulent shear in a low-turbidity, microtidal estuary. *J. Sea Res.* 89, 1–11. doi: 10.1016/j.seares.2014.02.001

Markussen, T. N., Elberling, B., Winter, C., and Andersen, T. J. (2016). Flocculated meltwater particles control Arctic land-sea fluxes of labile iron. *Sci. Rep.* 6:24033.

McDonnell, A. M. P., and Buesseler, K. O. (2010). Variability in the average sinking velocity of marine particles. *Limnol. Oceanogr.* 55, 2085–2096. doi: 10.4319/lo.2010.55.5.2085

Mullison, J. (2017). "Backscatter estimation using broadband acoustic doppler current profilers - updated," in *Proceedings of the ASCE Hydraulic Measurements & Experimental Methods Conference*, Durham, NH.

Nowald, N., Iversen, M. H., Fischer, G., Ratmeyer, V., and Wefer, G. (2015). Time series of in-situ particle properties and sediment trap fluxes in the coastal upwelling filament off Cape Blanc, Mauritania. *Prog. Oceanogr.* 137, 1–11. doi: 10.1016/j.pocean.2014.12.015

Nowald, N., Karakaş, G., Ratmeyer, V., Fischer, G., Schlitzer, R., Davenport, R., et al. (2006). Distribution and transport processes of marine particulate matter off Cape Blanc (NW-Africa): results from vertical camera profiles. *Ocean Sci. Discuss.* 3, 903–938. doi: 10.5194/osd-3-903-2006

Passow, U., and De La Rocha, C. L. (2006). Accumulation of mineral ballast on organic aggregates. *Glob. Biogeochem. Cycles* 20:GB1013.

Picheral, M., Guidi, L., Stemmann, L., Karl, D. M., Iddaoud, G., and Gorsky, G. (2010). The Underwater Vision Profiler 5: an advanced instrument for high spatial resolution studies of particle size spectra and zooplankton. *Limnol. Oceanogr. Methods* 8, 462–473. doi: 10.4319/lom.2010.8.462

Ploug, H., Iversen, M. H., and Fischer, G. (2008). Ballast, sinking velocity, and apparent diffusivity within marine snow and zooplankton fecal pellets: implications for substrate turnover by attached bacteria. *Limnol. Oceanogr.* 53, 1878–1886. doi: 10.4319/lo.2008.53.5.1878

Ratmeyer, V., and Wefer, G. (1996). A high resolution camera system (ParCa) for imaging particles in the ocean: system design and results from profiles and a three-month deployment. *J. Mar. Res.* 54, 589–603. doi: 10.1357/0022240963213565

Seifert, M., Hoppema, M., Burau, C., Friedrichs, A., Geuer, J. K., John, U., et al. (2019). Influence of glacial meltwater on summer biogeochemical cycles in Scoresby Sund, East Greenland. *Front. Mar. Sci.* 6:412. doi: 10.3389/fmars.2019.00412

Siegel, D. A., and Deuser, W. G. (1997). Trajectories of sinking particles in the Sargasso Sea: modeling of statistical funnels above deep-ocean sediment traps. *Deep Sea Res. I* 44, 1519–1541. doi: 10.1016/s0967-0637(97)00028-9

Simon, M., Grossart, H. P., Schweitzer, B., and Ploug, H. (2002). Microbial ecology of organic aggregates in aquatic ecosystems. *Aquat. Microb. Ecol.* 28, 175–211. doi: 10.3354/ame028175

Stemmann, L., Jackson, G. A., and Gorsky, G. (2004). A vertical model of particle size distributions and fluxes in the midwater column that includes biological and physical processes; Part II, Application to a three year survey in the NW Mediterranean Sea. *Deep Sea Res. I* 51, 885–908. doi: 10.1016/j.dsr.2004.03.002

Thiele, S., Fuchs, B. M., Amann, R., and Iversen, M. H. (2015). Colonization in the photic zone and subsequent changes during sinking determine bacterial community composition in Marine Snow. *Appl. Environ. Microbiol.* 81, 1463–1471. doi: 10.1128/aem.02570-14

Turner, J. T. (2015). Zooplankton fecal pellets, marine snow, phytodetritus and the ocean's biological pump. *Prog. Oceanogr.* 130, 205–248. doi: 10.1016/j.pocean.2014.08.005

van der Jagt, H., Friese, C. A., Stuut, J.-B. W., Fischer, G., and Iversen, M. I. (2018). The ballasting effect of Saharan dust deposition on aggregate dynamics and carbon export: aggregation, settling, and scavenging potential of marine snow. *Limnol. Oceanogr.* 63, 1386–1394. doi: 10.1002/lno.10779

Waite, A. M., and Nodder, S. D. (2001). The effect of *in situ* iron addition on the sinking rates and export flux of Southern Ocean diatoms. *Deep Sea Res. II Top. Stud. Oceanogr.* 48, 2635–2654. doi: 10.1016/s0967-0645(01)00012-1

Wekerle, C., Krumpen, T., Dinter, T., von Appen, W.-J., Iversen, M. H., and Salter, I. (2018). Properties of sediment trap catchment areas in Fram Strait: results from lagrangian modeling and remote sensing. *Front. Mar. Sci.* 5:407. doi: 10.3389/fmars.2018.00407

Conflict of Interest: The authors declare that the research was conducted in the absence of any commercial or financial relationships that could be construed as a potential conflict of interest.

The reviewer AB declared a past co-authorship with one of the authors MI to the handling editor.

frontiers in Marine Science

MINI REVIEW
published: 14 July 2020
doi: 10.3389/fmars.2020.00517

Radiocarbonscapes of Sedimentary Organic Carbon in the East Asian Seas

Rui Bao[1,2,3]* *and Thomas M. Blattmann*[3,4]*

[1] Frontiers Science Center for Deep Ocean Multispheres and Earth System, and Key Laboratory of Marine Chemistry Theory and Technology, Ministry of Education/Institute for Advanced Ocean Studies, Ocean University of China, Qingdao, China, [2] Laboratory for Marine Ecology and Environmental Science, Qingdao National Laboratory for Marine Science and Technology, Qingdao, China, [3] Department of Earth Sciences, Geological Institute, ETH Zürich, Zurich, Switzerland, [4] Biogeochemistry Program, Research Institute for Marine Resources Utilization, Japan Agency for Marine-Earth Science and Technology, Yokosuka, Japan

Natural abundance radiocarbon (^{14}C) is an increasingly widely used tool for investigating the organic carbon (OC) cycle in the contemporary ocean. Recent studies have provided extensive information on the ^{14}C characteristics of organic matter (OM) in sinking particles and sediments in the East Asian Seas including studies from the Bohai Sea, Yellow Sea, East China Sea, South China Sea, Japan Sea, and Japan Trench. ^{14}C investigations have provided insights into biogeochemical processes controlling the fate of sedimentary OM in these settings. Here, we highlight these insights from oceanic landscapes stretching across deltas, shelves, abyssal oceans, and the hadal zones of the East Asian Seas; share our perspectives on the source-to-sink dynamics of sedimentary OM in the ocean; and outline the challenges that need to be faced to make the most out of interpreting ^{14}C signals in sedimentary OC.

Keywords: ^{14}C, sediment, source-to-sink, shelf, margin, abyssal, hadal, turbidite

OPEN ACCESS

Edited by:
Cindy Lee,
Stony Brook University, United States

Reviewed by:
Ann P. McNichol,
Woods Hole Oceanographic Institution, United States
Gesine Mollenhauer,
Alfred Wegener Institute, Helmholtz Center for Polar and Marine Research, Germany

***Correspondence:**
Rui Bao
baorui@ouc.edu.cn
Thomas M. Blattmann
blattmannt@jamstec.go.jp

Specialty section:
This article was submitted to Marine Biogeochemistry, a section of the journal Frontiers in Marine Science

Received: *13 January 2020*
Accepted: *05 June 2020*
Published: *14 July 2020*

Citation:
Bao R and Blattmann TM (2020) Radiocarbonscapes of Sedimentary Organic Carbon in the East Asian Seas. Front. Mar. Sci. 7:517. doi: 10.3389/fmars.2020.00517

INTRODUCTION

The net amount of carbon that is reduced and buried in the form of sedimentary organic carbon (OC) is one key flux controlling global biogeochemical cycles over geologic timescales (Berner, 1990). The journey begins with fixation by autotrophs incorporating the radiocarbon (^{14}C) signature of their sources. This carbon propagates through the food web until it is respired or enters non-living pools of marine OC, which are subject to ^{14}C radioactive decay. Expressed as a large spread in ^{14}C patterns in the ocean, sedimentary OC contains a spectrum of pools at varying states of (radioactive) decay (McNichol and Aluwihare, 2007). The cosmogenic origin and ^{14}C decay provide insight into the timescales of source-to-sink carbon dynamics and the response of the carbon cycle to perturbations (Eglinton and Repeta, 2014). Natural abundance ^{14}C has established itself as a cornerstone for assessing sources and processes governing the fate of sedimentary OC in the oceans (Williams et al., 1992; Wang et al., 1996; Eglinton et al., 1997; Masiello and Druffel, 1998; Drenzek et al., 2009; Griffith et al., 2010). Recent technical developments in accelerator mass spectrometry reducing sample size requirements (Synal et al., 2007; Xu et al., 2016; Yamane et al., 2019) and increasing throughput by interfacing with direct CO_2 intake systems by elemental analyzers (McIntyre et al., 2017) or gas bench-type systems (Wacker et al., 2013) are poised to continue this progress.

In marine environments, interpretations of ^{14}C in sedimentary OC often require going beyond a straightforward chronological approach and are convoluted owing to a series of factors. Across the vast expanses of oceanic landscapes stretching deltas, shelves, abyssal plains, and hadal trenches, "radiocarbonscapes" (here, defined as spatiotemporal variations, characteristics, and patterns of radiocarbon) of sedimentary OC are markedly different, providing insight into the stories that carbon has to tell as it traverses from sedimentary source to sink. The East Asian Seas host natural laboratories characterized by a range of depositional environments from vast shelves spanning hundreds of kilometers to the deepest trenches scarring the face of our planet. To date, extensive ^{14}C datasets exist for these natural laboratories with starkly contrasting underpinning controls, which we divide into four different themes shaping radiocarbonscapes including (A) provenance, (B) hydrodynamic processes, (C) event-driven sedimentation, and (D) organic matter (OM)–mineral interactions. In this contribution, we highlight several OC ^{14}C studies from the East Asian Seas and review these distinct radiocarbonscapes from the perspectives of these four themes.

DISCUSSION

Provenance

The East Asian marginal seas receive continentally derived sedimentary OM exported from some of the world's largest rivers including the Yangtze, Yellow, and Pearl Rivers (Wang et al., 2012; Tao et al., 2015; Wu et al., 2018; Lin et al., 2019). After fixation from the atmosphere, terrigenous OC may undergo long storage times on land, reducing its ^{14}C content. For example, particulate OM from the Yellow River contains a higher percentage of aged OC (Tao et al., 2015, 2016; Yu et al., 2019); hence, the corresponding deltaic area shows lower ^{14}C content than elsewhere in the Bohai Sea (Bao et al., 2016; **Figure 1A**). Similarly, based on cluster analysis of combined sedimentary OC content and its ^{14}C concentration across the vast expanses of the East China Sea, the radiocarbonscape emanating from the Yangtze River reflects heavy terrestrial influence (Van der Voort et al., 2018). An extreme case of provenance-dominated oceanic radiocarbonscape is exemplified by the export of ^{14}C-free OC of petrogenic origin (i.e., kerogen) (Kao and Liu, 1996; Hilton et al., 2008; Lin et al., 2020). Surrounding Taiwan island, these contributions of petrogenic OC appear as anomalously low ^{14}C signatures in sedimentary OC (**Figure 1A**; Bao et al., 2016; Zheng et al., 2017). Therefore, low ^{14}C concentrations in sedimentary OC of deltaic and land-proximal settings may reflect a provenance-based effect with the addition of pre-aged sedimentary OM from terrestrial sources to recently synthesized marine OM (see also South China Sea investigation by Mollenhauer et al., 2005).

Hydrodynamic Processes

Often, the ^{14}C content of sedimentary OC is to a first-order determined by provenance; however, when viewing spatiotemporal patterns in radiocarbon contents of sedimentary OC (**Figure 1A**), it is apparent that highly variable ^{14}C contents in distal shelf settings are prevalent. Sedimentary redistribution processes (e.g., resuspension and dispersal) affect particles with different hydrodynamic properties differently, resulting in these highly variable patterns. Thus, there is size-dependent redistribution, as well as lateral transport time, recorded by the ^{14}C "clock," leading to a highly variable radiocarbonscape dependent on transport pathways (Bao et al., 2018c). Resuspension remobilizes aged sedimentary OM associated especially with intermediate grain size fractions in shallow inner-shelf settings, whereas in deeper regions and erosional areas, bedload transport exerts the strongest influence on redistribution of aged sedimentary OM, especially for the coarser fractions (Bao et al., 2016; **Figure 1B**). The aged sedimentary OM spreads into deep-sea settings that receive sedimentary input from these areas. In the East Asian Seas, based on ^{14}C analyses of specific compounds and OM thermal decomposition windows on specific grain size fractions, lateral transport of sedimentary OM over millennial year timescales is evident across hundreds of kilometers' distance in the Bohai, Yellow Sea, and East China Sea (Bao et al., 2018c, 2019a,b). Such contributions of aged sedimentary OM are also apparent in deeper waters adjacent to and receiving detrital input from East Asian shelves, such as for aged suspended sedimentary OM arriving in the Okinawa trough (Honda et al., 2000). Laterally derived aged suspended sedimentary OM is also observed in the lower water column of the Japan Sea (Kim et al., 2017, 2020). Hydrodynamic processes redistribute sedimentary OM with aged ^{14}C signatures, thereby overprinting ^{14}C of OC in surface sediments into which redeposition takes place leading to considerable spatial variability in radiocarbonscapes and uncertainty in ^{14}C age-related information.

Event-Driven Sedimentation

Mass wasting events such as those triggered by earthquakes and typhoons mobilize enormous pulses of sediments into the deep sea (Carter et al., 2012; Kioka et al., 2019), carrying with it vast amounts of OM (Tsai et al., 2010; Liu et al., 2013). The heavily incised active margin shelves along the Japan Trench offer little accommodation space for sediment storage, facilitating landslides triggered by tectonic events. This old sedimentary OM, which is mobilized, a consequence of protracted storage in intermediate reservoirs on land (e.g., soils) and/or on the continental margin, strongly influences the ^{14}C contents of OC in the hadal zone such as the Japan Trench (∼8,000-m water depth; Bao et al., 2018b). Such events blanket the seafloor with turbidites containing aged OM (**Figure 1C**; see also Nakamura et al., 1990). Similarly, within the Gaoping canyon, directly south of Taiwan, event-driven sedimentary inputs of terrestrial OC to the ocean are common. In the case of typhoons, hyperpycnal flow conditions directly export large contributions of land-derived biospheric and petrogenic OC into the South China Sea via submarine canyons (Hilton et al., 2008; Kao et al., 2014; Zheng et al., 2017; Lin et al., 2020). Over hundreds of kilometers' distance, sedimentary OC is carried by turbidites (Zhang et al., 2018) or entrained in eddies (Zhang et al., 2014), reflecting an event-driven overlay observed

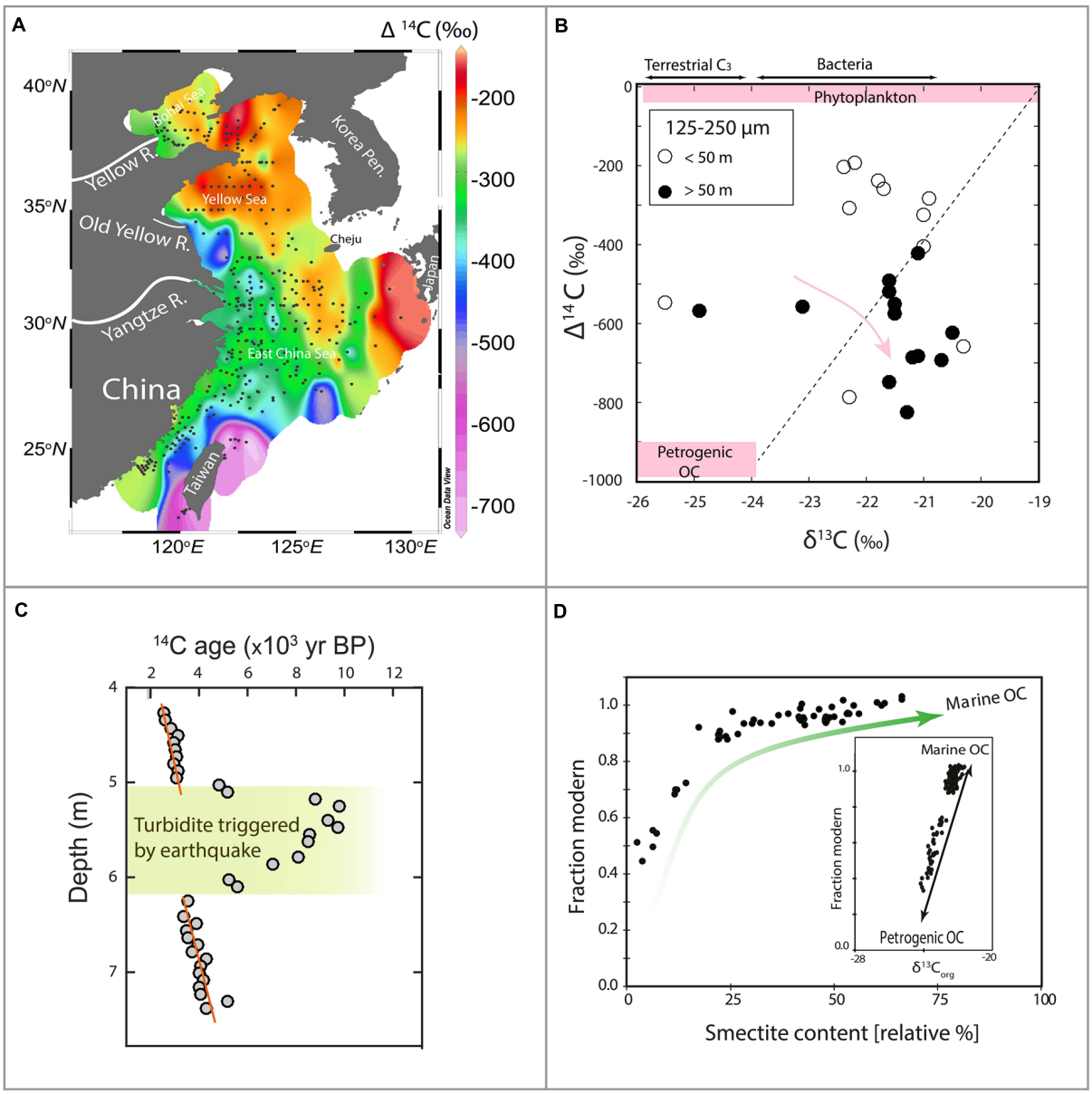

FIGURE 1 | ^{14}C study highlights from East Asian Seas with **(A)** illustrating the spatial distribution of ^{14}C concentration in sedimentary OC in the Bohai, Yellow, East China Seas (Bao et al., 2016). **(B)** Shows the ^{14}C concentrations of sedimentary OC in 125–250-µm grain size fractions of surface sediments in the East China Sea, with the dashed line separating the result of mixing of OC sources on the left from the effect of sedimentary reworking on the right (water depth >50 m; Bao et al., 2019a). **(C)** Illustrates a sedimentary profile in the Japan trench showing the ^{14}C imprint on sedimentary OC in a turbidite deposit triggered by one earthquake (after Bao et al., 2018b). **(D)** Shows the relationship between ^{14}C content of sedimentary OC and phyllosilicate composition in abyssal South China Sea sinking particles with modern marine OM associated with soil-derived smectite (after Blattmann et al., 2019).

over time series of sinking particles (Blattmann et al., 2018). Therefore, these episodic aged or even petrogenic OM exports, triggered by events such as earthquakes and typhoons, exert large-scale control on radiocarbonscapes in the deep ocean.

OM–Mineral Interactions

Mineral ballast exerts key control over the sedimentary transport and deposition of OM in aquatic environments (Ittekkot et al., 1990; Wakeham et al., 2009). Investigations have revealed the association of marine OM with lithogenic minerals (Keil et al., 1997; Kennedy and Wagner, 2011), which is also observed in the sinking particles of the South China Sea, which impart a strong effect on ^{14}C contents of sedimentary OC (Blattmann et al., 2018). The systematic radiocarbonscapes with contrasting modern and ancient forms of sedimentary OM (see insert in **Figure 1D**), representing marine and petrogenic OM forms, respectively, display strong relationships with mineralogical composition, revealing mineral-specific behavior

on the retention and release of terrestrial OM in the marine environment by loss-and-replacement reactions (**Figure 1D**; Blattmann et al., 2019). Smectite, a pedogenic mineral, loses its association with pedogenic OM and associates with marine OM in distal marine settings. By way of this mechanism, sedimentary OM sourced from land is desorbed and/or degraded, leaving marine OM with a straightforward source-to-sink trajectory to repopulate the particulate phase (c.f., Zhang et al., 2019). Organic matter–mineral interactions impart a systematic effect on the fate of sedimentary OM in the ocean and govern the type of OM that is stabilized, thereby changing the overall radiocarbonscape.

SYNTHESIS AND PERSPECTIVES

^{14}C is a one-dimensional value traditionally used to express age based on its decay constant (Libby et al., 1949). Rather than ^{14}C expressing a single property (i.e., age, which is commonly assumed), sedimentary OC in oceanic settings integrates an overlay of processes, which contribute to an overall radiocarbonscape. Delineating the manifold processes involved given the scalar nature of this measurement often arrives at a non-unique set of solutions. Toward resolving these ambiguities by extending ^{14}C into multidimensional space, sedimentary OM can be dissected into different physical fractions [e.g., density (Wakeham et al., 2009); grain size (Bao et al., 2019a), and hydrodynamic (Coppola et al., 2007)], reactivity pools [e.g., chemical oxidation (Ohkouchi and Eglinton, 2006), thermal treatment (Hemingway et al., 2019; Bao et al., 2018a)], and individual compounds that can be targeted (e.g., Eglinton et al., 1997; Tao et al., 2016). Based on the evidence accumulated thus far, the "radiocarbonscapes" of the East Asian Seas are controlled by a combination of (A) provenance, (B) hydrodynamics, (C) event-driven sedimentation, (D) OM–mineral interactions, and/or other potentially important and less-well understood processes. ^{14}C is a tracer that intersects with all of these themes, and it is apparent that we need to continue our efforts to deconvolve the complex tapestry of radiocarbonscapes in the marine environment to resolve basic questions including the following:

1. How do the four themes provenance, hydrodynamics, event-driven sedimentation, and OM–mineral interactions weigh against each other in shaping radiocarbonscapes?
2. How can quantitative information on these four themes be extracted from radiocarbonscapes?

Based on the East Asian Sea natural laboratories, we have developed our own perspectives toward answering these questions and judged the relative influences of the four themes on seafloor radiocarbonscapes (**Figure 2**). It appears that the relative importance of these four themes varies greatly across delta to deep-sea transects for active and passive margin settings (c.f., Blair and Aller, 2012), with provenance-based influence strongest in deltas and more diffuse across passive margins with hydrodynamic processes, leading to extensive imprints on radiocarbonscapes on wide, high-energy shelf settings. In contrast, event-driven sedimentation markedly impacts radiocarbonscapes across active margin settings where episodic mobilization and redistribution of vast amounts of sediment occur along with a pronounced inheritance of a provenance signal. With their areas of greatest influence difficult to pinpoint, OM–mineral interactions control loss and replacement of terrestrial with marine OM, thereby rewriting the organic geochemical fingerprint of sedimentary OM. Based on individual case studies of the East Asian Seas natural laboratories, the operation of these four themes crystallizes out of radiocarbonscape patterns. However, quantitative approaches for disentangling

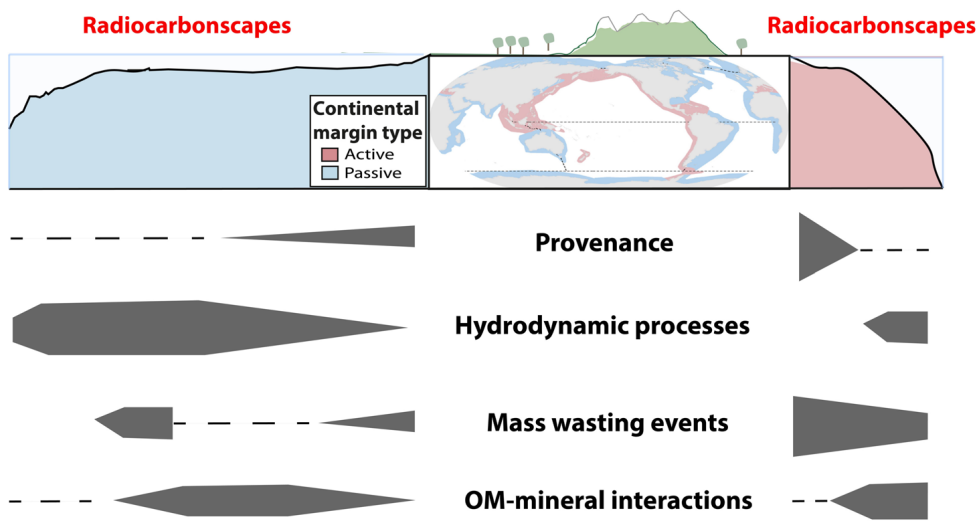

FIGURE 2 | Radiocarbonscapes of sedimentary OC are influenced by several underpinning controls, with their relative influence represented by the thickness of the tapered bars across source-to-sink sediment pathways as hypothesized by the authors. Top panel is modified from Bao et al. (2018d) and Blair and Aller (2012).

radiocarbonscapes are needed where these four themes are more intertwined, ultimately key for understanding marine biogeochemical cycles.

AUTHOR CONTRIBUTIONS

RB and TB contributed equally to discussion and writing. Both authors contributed to the article and approved the submitted version.

FUNDING

The authors acknowledge funding from Stockholm University, Harvard University, JAMSTEC, Ocean University of China (No. 862001013124), and ETH Zürich. Additional financial support from the Hanse-Wissenschaftskolleg, the Geochemical Society, and the Deutsche Forschungsgemeinschaft (DFG, German Research Foundation) project number 422798570 made this publication possible.

ACKNOWLEDGMENTS

The authors are deeply indebted to Timothy Eglinton for his many years of tutelage and gracious support and we are thankful for the stimulating and dedicated reviews we received from GM and AM that have greatly improved this contribution. We thank the organizers and attendees of the Marine Organic Geochemistry workshop held in Delmenhorst, Germany for inspiring discussions.

REFERENCES

Bao, R., Blattmann, T. M., McIntyre, C., Zhao, M., and Eglinton, T. I. (2019a). Relationships between grain size and organic carbon ^{14}C heterogeneity in continental margin sediments. *Earth Planet. Sci. Lett.* 505, 76–85. doi: 10.1016/j.epsl.2018.10.013

Bao, R., Zhao, M., McNichol, A., Galy, V., McIntyre, C., Haghipour, N., et al. (2019b). Temporal constraints on lateral organic matter transport along a coastal mud belt. *Organic Geochem.* 128, 86–93. doi: 10.1016/j.orggeochem.2019.01.007

Bao, R., McIntyre, C., Zhao, M., Zhu, C., Kao, S.-J., and Eglinton, T. I. (2016). Widespread dispersal and aging of organic carbon in shallow marginal seas. *Geology* 44, 791–794. doi: 10.1130/g37948.1

Bao, R., McNichol, A. P., Hemingway, J. D., Lardie Gaylord, M. C., and Eglinton, T. I. (2018a). Influence of different acid treatments on the radiocarbon content spectrum of sedimentary organic matter determined by rpo/accelerator mass spectrometry. *Radiocarbon* 61, 395–413. doi: 10.1017/rdc.2018.125

Bao, R., Strasser, M., McNichol, A. P., Haghipour, N., McIntyre, C., Wefer, G., et al. (2018b). Tectonically-triggered sediment and carbon export to the Hadal zone. *Nat. Commun.* 9:121. doi: 10.1038/s41467-017-02504-1

Bao, R., Uchida, M., Zhao, M., Haghipour, N., Montlucon, D., McNichol, A., et al. (2018c). Organic carbon aging during across-shelf transport. *Geophys. Res. Lett.* 45, 8425–8434. doi: 10.1029/2018gl078904

Bao, R., van der Voort, T. S., Zhao, M., Guo, X., Montluçon, D. B., McIntyre, C., et al. (2018d). Influence of hydrodynamic processes on the fate of sedimentary organic matter on continental margins. *Global Biogeochem. Cycles* 32, 1420–1432. doi: 10.1029/2018gb005921

Berner, R. A. (1990). Atmospheric carbon dioxide levels over phanerozoic time. *Science* 249, 1382–1386. doi: 10.1126/science.249.4975.1382

Blair, N. E., and Aller, R. C. (2012). The fate of terrestrial organic carbon in the marine environment. *Annu. Rev. Mar. Sci.* 4, 401–423. doi: 10.1146/annurev-marine-120709-142717

Blattmann, T. M., Liu, Z., Zhang, Y., Zhao, Y., Haghipour, N., Montluçon, D. B., et al. (2019). Mineralogical control on the fate of continentally derived organic matter in the ocean. *Science* 366, 742–745. doi: 10.1126/science.aax5345

Blattmann, T. M., Zhang, Y., Zhao, Y., Wen, K., Lin, S., Li, J., et al. (2018). Contrasting fates of petrogenic and biospheric carbon in the South China Sea. *Geophys. Res. Lett.* 45, 9077–9086. doi: 10.1029/2018gl079222

Carter, L., Milliman, J. D., Talling, P. J., Gavey, R., and Wynn, R. B. (2012). Near-synchronous and delayed initiation of long run-out submarine sediment flows from a record-breaking river flood, offshore Taiwan. *Geophys. Res. Lett.* 39:L12603. doi: 10.1029/2012GL051172

Coppola, L., Gustafsson, Ö, Andersson, P., Eglinton, T. I., Uchida, M., and Dickens, A. F. (2007). The importance of ultrafine particles as a control on the distribution of organic carbon in Washington Margin and Cascadia Basin sediments. *Chem. Geol.* 243, 142–156. doi: 10.1016/j.chemgeo.2007.05.020

Drenzek, N. J., Hughen, K. A., Montluçon, D. B., Southon, J. R., dos Santos, G. M., Druffel, E. R., et al. (2009). A new look at old carbon in active margin sediments. *Geology* 37, 239–242. doi: 10.1130/g25351a.1

Eglinton, T. I., Benitez-Nelson, B. C., Pearson, A., McNichol, A. P., Bauer, J. E., and Druffel, E. R. M. (1997). Variability in radiocarbon ages of individual organic compounds from marine sediments. *Science* 277, 796–799. doi: 10.1126/science.277.5327.796

Eglinton, T. I., and Repeta, D. J. (2014). "Organic matter in the contemporary ocean," in *Treatise on Geochemistry*, eds H. D. Holland and K. K. Turekian (Oxford: Elsevier), 151–189. doi: 10.1016/b978-0-08-095975-7.00606-9

Griffith, D. R., Martin, W. R., and Eglinton, T. I. (2010). The radiocarbon age of organic carbon in marine surface sediments. *Geochim. Cosmochim. Acta* 74, 6788–6800. doi: 10.1016/j.gca.2010.09.001

Hemingway, J. D., Rothman, D. H., Grant, K. E., Rosengard, S. Z., Eglinton, T. I., Derry, L. A., et al. (2019). Mineral protection regulates long-term global preservation of natural organic carbon. *Nature* 570, 228–231. doi: 10.1038/s41586-019-1280-6

Hilton, R. G., Galy, A., Hovius, N., Chen, M.-C., Horng, M.-J., and Chen, H. (2008). Tropical-cyclone-driven erosion of the terrestrial biosphere from mountains. *Nat. Geosci.* 1, 759–762. doi: 10.1038/ngeo333

Honda, M. C., Kusakabe, M., Nakabayashi, S., and Katagiri, M. (2000). Radiocarbon of sediment trap samples from the Okinawa trough: lateral transport of ^{14}C-poor sediment from the continental slope. *Mar. Chem.* 68, 231–247. doi: 10.1016/s0304-4203(99)00080-8

Ittekkot, V., Haake, B., and Wiesner, M. G. (1990). Organic-mineral interactions in the sea: implications for atmospheric CO_2-transfer to the deep ocean. *Mitteilun. Geol. Paläontol. Inst. Univ. Hamburg* 69, 167–175.

Kao, S.-J., Hilton, R. G., Selvaraj, K., Dai, M., Zehetner, F., Huang, J.-C., et al. (2014). Preservation of terrestrial organic carbon in marine sediments offshore Taiwan: mountain building and atmospheric carbon dioxide sequestration. *Earth Surface Dyn.* 2, 127–139. doi: 10.5194/esurf-2-127-2014

Kao, S.-J., and Liu, K.-K. (1996). Particulate organic carbon export from a subtropical mountainous river (Lanyang Hsi) in Taiwan. *Limnol. Oceanogr.* 41, 1749–1757. doi: 10.4319/lo.1996.41.8.1749

Keil, R. G., Mayer, L. M., Quay, P. D., Richey, J. E., and Hedges, J. I. (1997). Loss of organic matter from riverine particles in deltas. *Geochim. Cosmochimi. Acta* 61, 1507–1511. doi: 10.1016/s0016-7037(97)00044-6

Kennedy, M. J., and Wagner, T. (2011). Clay mineral continental amplifier for marine carbon sequestration in a greenhouse ocean. *Proc. Natl. Acad. Sci. U.S.A.* 108, 9776–9781. doi: 10.1073/pnas.1018670108

Kim, M., Hwang, J., Rho, T., Lee, T., Kang, D.-J., Chang, K.-I., et al. (2017). Biogeochemical properties of sinking particles in the southwestern part of the East Sea (Japan Sea). *J. Mar. Syst.* 167, 33–42. doi: 10.1016/j.jmarsys.2016.11.001

Kim, M., Kim, Y.-I., Hwang, J., Choi, K. Y., Kim, C. J., Ryu, Y., et al. (2020). Influence of sediment resuspension on the biological pump of the Southwestern East Sea (Japan Sea). *Front. Earth Sci.* 8:144. doi: 10.3389/feart.2020.00144

Kioka, A., Schwestermann, T., Moernaut, J., Ikehara, K., Kanamatsu, T., McHugh, C. M., et al. (2019). Megathrust earthquake drives drastic organic carbon supply to the hadal trench. *Sci. Rep.* 9:1553. doi: 10.1038/s41598-019-38834-x

Libby, W. F., Anderson, E. C., and Arnold, J. R. (1949). Age determination by radiocarbon content - world-wide assay of natural radiocarbon. *Science* 109, 227–228. doi: 10.1126/science.109.2827.227

Lin, B., Liu, Z., Eglinton, T. I., Kandasamy, S., Blattmann, T. M., Haghipour, N., et al. (2019). Perspectives on provenance and alteration of suspended and sedimentary organic matter in the subtropical Pearl River system. South China. *Geochim. Cosmochim. Acta* 259, 270–287. doi: 10.1016/j.gca.2019.06.018

Lin, B., Liu, Z., Eglinton, T. I., Kandasamy, S., Blattmann, T. M., Haghipour, N., et al. (2020). Island-wide variation in provenance of riverine sedimentary organic carbon: a case study from Taiwan. *Earth Planet. Sci. Lett.* 539:116238. doi: 10.1016/j.epsl.2020.116238

Liu, J. T., Kao, S.-J., Huh, C.-A., and Hung, C.-C. (2013). gravity flows associated with flood events and carbon burial: taiwan as instructional source area. *Annu. Rev. Mar. Sci.* 5, 47–68. doi: 10.1146/annurev-marine-121211-172307

Masiello, C. A., and Druffel, E. R. M. (1998). Black carbon in deep-sea sediments. *Science* 280, 1911–1913. doi: 10.1126/science.280.5371.1911

McIntyre, C. P., Wacker, L., Haghipour, N., Blattmann, T. M., Fahrni, S., Usman, M., et al. (2017). Online ^{13}C and ^{14}C gas measurements by EA-IRMS–AMS at ETH Zürich. *Radiocarbon* 59, 893–903. doi: 10.1017/rdc.2016.68

McNichol, A. P., and Aluwihare, L. I. (2007). The power of radiocarbon in biogeochemical studies of the marine carbon cycle: Insights from studies of dissolved and particulate organic carbon (DOC and POC). *Chem. Rev.* 107, 443–466. doi: 10.1021/cr050374g

Mollenhauer, G., Kienast, M., Lamy, F., Meggers, H., Schneider, R. R., Hayes, J. M., et al. (2005). An evaluation of ^{14}C age relationships between co-occurring foraminifera, alkenones, and total organic carbon in continental margin sediments. *Paleoceanography* 20:A1016. doi: 10.1029/2004PA001103

Nakamura, T., Shiki, T., and Nakai, N. (1990). Variations in ^{14}C ages of various organic fractions in a turbidite sediment core from Suruga Trough. *Geochem. J.* 24, 47–56. doi: 10.2343/geochemj.24.47

Ohkouchi, N., and Eglinton, T. I. (2006). Radiocarbon constraint on relict organic carbon contributions to Ross Sea sediments. *Geochem. Geophys. Geosyst.* 7:Q04012. doi: 10.1029/2005GC001097

Synal, H.-A., Stocker, M., and Suter, M. (2007). MICADAS: a new compact radiocarbon AMS system. *Nuclear Instrum. Methods Phys. Res. Section BBeam Interact. Mater. Atoms* 259, 7–13. doi: 10.1016/j.nimb.2007.01.138

Tao, S., Eglinton, T. I., Montluçon, D. B., McIntyre, C., and Zhao, M. (2015). Pre-aged soil organic carbon as a major component of the Yellow River suspended load: regional significance and global relevance. *Earth Planet. Sci. Lett.* 414, 77–86. doi: 10.1016/j.epsl.2015.01.004

Tao, S., Eglinton, T. I., Montluçon, D. B., McIntyre, C., and Zhao, M. (2016). Diverse origins and pre-depositional histories of organic matter in contemporary Chinese marginal sea sediments. *Geochim. Cosmochim. Acta* 191, 70–88. doi: 10.1016/j.gca.2016.07.019

Tsai, F., Hwang, J.-H., Chen, L.-C., and Lin, T.-H. (2010). Post-disaster assessment of landslides in southern Taiwan after 2009 Typhoon Morakot using remote sensing and spatial analysis. *Nat. Hazards Earth Syst. Sci.* 10, 2179–2190. doi: 10.5194/nhess-10-2179-2010

Van der Voort, T. S., Mannu, U., Blattmann, T. M., Bao, R., Zhao, M., and Eglinton, T. I. (2018). Deconvolving the fate of carbon in coastal sediments. *Geophys. Res. Lett.* 45, 4134–4142. doi: 10.1029/2018gl077009

Wacker, L., Fahrni, S. M., Hajdas, I., Molnar, M., Synal, H. A., Szidat, S., et al. (2013). A versatile gas interface for routine radiocarbon analysis with a gas ion source. *Nuclear Instrum. Methods Phys. Res. Section BBeam Interact. Mater. Atoms* 294, 315–319. doi: 10.1016/j.nimb.2012.02.009

Wakeham, S. G., Canuel, E. A., Lerberg, E. J., Mason, P., Sampere, T. P., and Bianchi, T. S. (2009). Partitioning of organic matter in continental margin sediments among density fractions. *Mar. Chem.* 115, 211–225. doi: 10.1016/j.marchem.2009.08.005

Wang, X., Ma, H., Li, R., Song, Z., and Wu, J. (2012). Seasonal fluxes and source variation of organic carbon transported by two major Chinese Rivers: the yellow river and changjiang (Yangtze) River. *Global Biogeochem. Cycles* 26:GB2025. doi: 10.1029/2011GB004130

Wang, X.-C., Druffel, E. R. M., and Lee, C. (1996). Radiocarbon in organic compound classes in particulate organic matter and sediment in the deep northeast Pacific Ocean. *Geophys. Res. Lett.* 23, 3583–3586. doi: 10.1029/96gl03423

Williams, P. M., Robertson, K. J., Soutar, A., Griffin, S. M., and Druffel, E. R. M. (1992). Isotopic signatures (^{14}C, ^{13}C, ^{15}N) as tracers of sources and cycling of soluble and particulate organic matter in the Santa Monica Basin. California. *Prog. Oceanogr.* 30, 253–290. doi: 10.1016/0079-6611(92)90015-r

Wu, Y., Eglinton, T. I., Zhang, J., and Montlucon, D. B. (2018). Spatiotemporal variation of the quality, origin, and age of particulate organic matter transported by the Yangtze River (Changjiang). *J. Geophys. Res. Biogeosci.* 123, 2908–2921. doi: 10.1029/2017jg004285

Xu, X., Gao, P., and Salamanca, E. G. (2016). Ultra small-mass graphitization by sealed tube zinc reduction method for AMS ^{14}C Measurements. *Radiocarbon* 55, 608–616. doi: 10.1017/s0033822200057751

Yamane, M., Yokoyama, Y., Hirabayashi, S., Miyairi, Y., Ohkouchi, N., and Aze, T. (2019). Small- to ultra-small-scale radiocarbon measurements using newly installed single-stage AMS at the University of Tokyo. *Nuclear Instrum. Methods Phys. Res. Section BBeam Interact. Mater. Atoms* 455, 238–243. doi: 10.1016/j.nimb.2019.01.035

Yu, M., Eglinton, T. I., Haghipour, N., Montluçon, D. B., Wacker, L., Wang, Z., et al. (2019). Molecular isotopic insights into hydrodynamic controls on fluvial suspended particulate organic matter transport. *Geochim. Cosmochim. Acta* 262, 78–91. doi: 10.1016/j.gca.2019.07.040

Zhang, J., Li, H., Xuan, J., Wu, Z., Yang, Z., Wiesner, M. G., et al. (2019). Enhancement of mesopelagic sinking particle fluxes due to upwelling, aerosol deposition, and monsoonal influences in the northwestern South China Sea. *J. Geophys. Res. Oceans* 124, 99–112. doi: 10.1029/2018jc014704

Zhang, Y., Liu, Z., Zhao, Y., Colin, C., Zhang, X., Wang, M., et al. (2018). Long-term in situ observations on typhoon-triggered turbidity currents in the deep sea. *Geology* 46, 675–678. doi: 10.1130/g45178.1

Zhang, Y., Liu, Z., Zhao, Y., Wang, W., Li, J., and Xu, J. (2014). Mesoscale eddies transport deep-sea sediments. *Sci. Rep.* 4:5937. doi: 10.1038/srep05937

Zheng, L.-W., Ding, X., Liu, J. T., Li, D., Lee, T.-Y., Zheng, X., et al. (2017). Isotopic evidence for the influence of typhoons and submarine canyons on the sourcing and transport behavior of biospheric organic carbon to the deep sea. *Earth Planet. Sci. Lett.* 465, 103–111. doi: 10.1016/j.epsl.2017.02.037

Conflict of Interest: The authors declare that the research was conducted in the absence of any commercial or financial relationships that could be construed as a potential conflict of interest.

The reviewer AM declared a past co-authorship with one of the authors RB to the handling editor.

frontiers in Marine Science

ORIGINAL RESEARCH
published: 22 July 2020
doi: 10.3389/fmars.2020.00533

Fermentation and Anaerobic Oxidation of Organic Carbon in the Oxygen Minimum Zone of the Upwelling Ecosystem Off Concepción, in Central Chile

Benjamín M. Srain[1,2,3], Marcus Sobarzo[1,4], Giovanni Daneri[2,5], Humberto E. González[6], Giovanni Testa[6,7], Laura Farías[1,7], Alex Schwarz[8], Norma Pérez[8†] and Silvio Pantoja-Gutiérrez[1,2]*

[1] Departamento de Oceanografía, Universidad de Concepción, Concepción, Chile, [2] Centro de Investigación Oceanográfica COPAS Sur-Austral, Universidad de Concepción, Concepción, Chile, [3] Programa de Postgrado en Oceanografía, Departamento de Oceanografía, Universidad de Concepción, Concepción, Chile, [4] Centro Interdisciplinario para la Investigación Acuícola (INCAR), Concepción, Chile, [5] Centro de Investigación en Ecosistemas de la Patagonia, Coyhaique, Chile, [6] Centro de Investigacion Dinámica de Ecosistemas Marinos de Altas Latitudes (IDEAL) and Universidad Austral de Chile, Valdivia, Chile, [7] Centro de Ciencia del Clima y la Resiliencia (CR2), Concepción, Chile, [8] Departamento de Ingeniería Civil, Universidad de Concepción, Concepción, Chile

We studied the dynamics of fermentation and anaerobic degradation of organic matter at a fixed station in the Oxygen Minimum Zone (OMZ) within the Humboldt Current System off Concepción, central Chile. Products of the main anaerobic microbial reactions [fermentation, denitrification, and reduction of $Fe(OH)_3$ and SO_4^{2-}] were analyzed during laboratory incubations of OMZ waters. Fermentation of glucose and amino acids resulted in the production of volatile fatty acids, mainly acetate; these compounds were detected year-round in *in situ* water samples and were associated with high primary production rates and presence of O_2-deficient waters at the sampling site. In contrast, whilst ethanol was produced from glucose fermentation by OMZ water microorganisms under laboratory conditions, it was not detected in the water column during the annual cycle. Evidence of acetate oxidation (which is thermodynamically feasible), with $Fe(OH)_3$ as an electron acceptor, suggests that microbial activity could reduce solid-phase Fe carried by rivers using fermented metabolites in oxygen-depleted water, thus releasing dissolved bioavailable Fe. Here we present evidence for productivity-driven seasonality of biogeochemical cycles in the Humboldt system, supported by fermentation and anaerobic consumption of fermentation products oxidized by a variety of electron acceptors including NO_3^-, $Fe(OH)_3$, and SO_4^{2-}. Our results suggest that products of fermentation in the OMZ may provide a source of labile organics for advection to oxygenated waters of subantarctic origin during austral winter. Fermentation, anaerobic oxidation and associated advection of fermentation products are likely to be enhanced during the twenty-first century due both to temperature increase and decrease in dissolved O_2 in the water column.

Keywords: fermentation, oxygen minimum zone, anaerobic respiration, volatile fatty acids, acetate, Chile, South East Pacific

OPEN ACCESS

Edited by:
Stuart Wakeham, University of Georgia, United States

Reviewed by:
Doug LaRowe, University of Southern California, United States
Mary I. Scranton, Stony Brook University, United States
Rainer M. W. Amon, Texas A&M University, United States

***Correspondence:**
Silvio Pantoja-Gutiérrez
spantoja@udec.cl

†Present address:
Norma Pérez, Departamento de Acuicultura, Universidad Católica del Norte, Coquimbo, Chile

Specialty section:
This article was submitted to Marine Biogeochemistry, a section of the journal Frontiers in Marine Science

Received: *05 August 2019*
Accepted: *11 June 2020*
Published: *22 July 2020*

Citation:
Srain BM, Sobarzo M, Daneri G, González HE, Testa G, Farías L, Schwarz A, Pérez N and Pantoja-Gutiérrez S (2020) Fermentation and Anaerobic Oxidation of Organic Carbon in the Oxygen Minimum Zone of the Upwelling Ecosystem Off Concepción, in Central Chile. Front. Mar. Sci. 7:533. doi: 10.3389/fmars.2020.00533

INTRODUCTION

Hypoxic zones within the marine water column appear to be expanding due to warming and eutrophication (Diaz and Rosenberg, 2008; Rabalais et al., 2014; Schmidtko et al., 2017). These processes will enhance fermentative production of semi-reduced metabolites that act as substrates for anaerobic microbial oxidation of organic matter (Oremland and Polcin, 1982; Megonigal et al., 2004*)* through, for example, NO_3^- (denitrification) and SO_4^{2-} reduction, and methanogenesis (Sansone and Martens, 1981; Jørgensen, 1982). Presently, O_2-depleted marine environments are typically found in sediments, enclosed or semi-enclosed water bodies, coastal ocean dead zones, and areas referred to as Oxygen Minimum Zones or OMZs (Helly and Levin, 2004; Diaz and Rosenberg, 2008). These OMZs can be hundreds of meters in depth, and are characterized by suboxic and anoxic levels of O_2 typically in the productive, weakly ventilated waters of the eastern Pacific and southeastern Atlantic Oceans, and the Arabian Sea (Wyrtki, 1962; Kamykowski and Zentara, 1990; Helly and Levin, 2004; Ulloa et al., 2012; Löscher et al., 2016; Pizarro-Koch et al., 2019). On a global scale, OMZs are significant sinks (via N_2O and N_2) for oceanic N (Codispoti et al., 2001), and are zones hosting active S cycling (Canfield et al., 2010) through diverse communities of anaerobic microbes (Fossing et al., 1995; Ward et al., 2009; Ulloa et al., 2012; Wright et al., 2012; Srain et al., 2015).

In low-oxygen environments, acetate is a major energy substrate for sulfate-reducing bacteria in lake (e.g., Skyring, 1988), estuarine (e.g., Suzuki et al., 2007) and marine sediments (e.g., Sørensen et al., 1981; Skyring et al., 1983; Parkes et al., 1989), and in the marine water column (Albert et al., 1995; Ho et al., 2002). Fermentation (incomplete oxidation of organics in the absence of external electron acceptors) is required to generate intermediate organic products for anaerobic oxidizers, whilst producing soluble molecules and gases that can circulate back into more oxygenated regions (Schmitz et al., 2006). The biological mechanisms, kinetics, and ecological role of fermentation have been extensively studied in rumen, sewage, soils and sediments (e.g., Sabine and Johnson, 1964; Hungate, 1965; Sansone and Martens, 1982; Shaw et al., 1984; Oremland, 1988; Conrad et al., 1989; Wagner et al., 1997; Moser-Engeler et al., 1998; Finke and Jørgensen, 2008; Bourke et al., 2017), but the occurrence and significance of this metabolic pathway has received less attention in suboxic and anoxic zones within the marine water column (e.g., Albert et al., 1995; Wu et al., 1997; Ho et al., 2002; González and Quiñones, 2009; Zhuang et al., 2019). Interest in fermentative reactions is becoming more relevant in light of expansion of OMZs (Breitburg et al., 2018), and the increasing concentrations of N (Howarth, 2008), P (Bennett et al., 2001), and organic carbon (Berner, 1982) associated with eutrophication and deoxygenation of the coastal ocean (Rabalais et al., 2014).

In the present study, we examined chemical dynamics of the water column within the OMZ off Concepción, Chile (∼36^{o}S). This is a coastal area where intense seasonal upwelling (Sobarzo et al., 2001, 2007) of high-nutrient subsurface waters – depleted in dissolved O_2 –supports high rates of primary production of up to 20 g C m^{-2} d^{-1} in near surface waters (Montero et al., 2007; Testa et al., 2018). The area off Concepción constitutes the most southerly extent of the OMZ in the eastern South Pacific (Fuenzalida et al., 2009), the fourth largest (by volume) of the six permanent hypoxic regions in the world oceans (Schneider et al., 2006). At this latitude on the continental shelf, the OMZ is located beneath surface waters of subantarctic origin (eastern South Pacific Transition Water, ESPTW) and is fed by poorly oxygenated subsurface waters (Equatorial Subsurface Water, ESSW) which upwell toward the coast driven by favorable winds during austral spring and summer (i.e., from September–October to March–April). During austral winter, northerly converging winds generate coastal downwelling and offshore bottom Ekman transport, which removes ESSW from the shelf and replaces it with ESPTW throughout most of the water column (Sobarzo et al., 2007).

The goal of the present study was to reveal relevant microbial pathways within OMZ waters [fermentation, and reduction of NO_3^-, $Fe(OH)_3$ and SO_4^{2-}]. A series of controlled incubations of OMZ microbial assemblages, supplemented with high concentrations of substrates, was interpreted in the context of anaerobic processes within the water column during an annual cycle. The study aimed to describe annual patterns within the water column of vertical distribution of volatile fatty acids (VFA), mainly acetate, and other indicators of anaerobic metabolism of OMZ. A further aim was to evaluate potential export of these indicators to oxygenated waters of subantarctic origin.

MATERIALS AND METHODS

Sampling

Cruises were carried out within the framework of the project "Microbial Initiative in Low Oxygen off Concepción and Oregon" (MILOCO), and as a part of the Time Series at Oceanographic Station 18 (33 km from the coast, 90 m depth, 36°29.94′S, 73°07.8′W) conducted by the COPAS Center for Oceanographic Research in the eastern South Pacific (FONDAP CONICYT Chile) in the upwelling ecosystem off Concepción in central Chile (**Figure 1**). Water samples were collected monthly aboard L/C Kay-Kay II between November 2009 and January 2011, encompassing two austral springs, one austral fall, one austral winter, and two austral summers. Ancillary water column measurements of dissolved O_2, fluorescence, temperature, salinity, and nutrients were provided by the database of the COPAS Center and the MILOCO Project. Data for hourly coastal winds were collected by the meteorological station at Carriel Sur Airport (36°47′S; 73°04′W), located less than 10 km from the coast of Concepcion.

Water samples for chemical measurements and incubations were collected with Niskin bottles (10 L) at six depths (0, 10, 30, 50, 65, 80 m) stored in acid-washed carboys in the dark at ca. 10°C. For VFA, ethanol, and CO_2 measurements, 50 mL aliquots of seawater (in triplicate) were removed on board and dispensed into glass bottles in a N_2 saturated chamber using

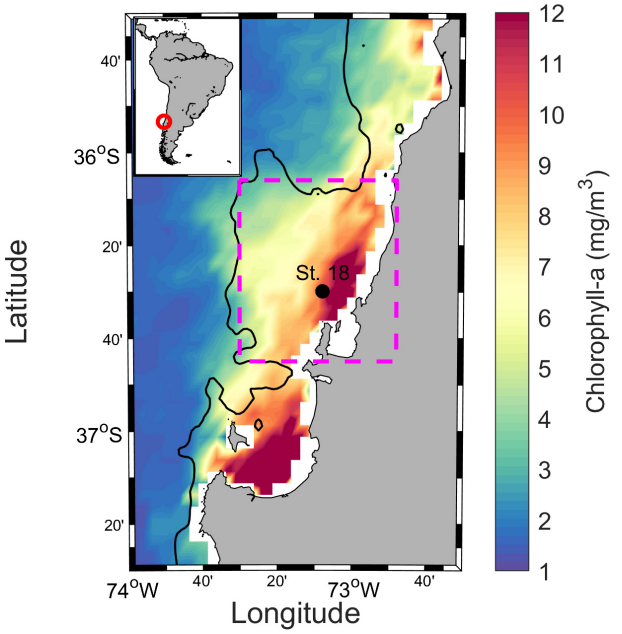

FIGURE 1 | The geographical location of the study site at Station 18, off Concepción in central Chile. Color scale represents the average chlorophyll-*a* concentration observed between November 2009 and January 2011. The black solid line shows the 200 m isobath and the magenta dashed square represents the area analyzed for Net Primary Production estimates. The map was generated using Ocean Data View (Schlitzer, 2010).

glove bags (Aldrich® AtmosBag) and immediately poisoned with $HgCl_2$ (0.001%). Gas-tight bottles were sealed with butyl rubber stoppers, crimped, and then stored in the dark at 10°C. In the laboratory (within 12 h), 1 L seawater per depth was filtered through pre-combusted 0.7 μm glass fiber filters (Whatman GF/F); filtrates and filters were kept at −20°C prior to analyses of dissolved amino acids, and elemental analysis of C and N and natural abundance of ^{13}C and ^{15}N in particulate material.

On November 29, 2010, inocula of seawater for laboratory incubations were taken from 65 m depth (10.2°C, 34.6 PSU, 8.4 μM O_2), and transferred to 10 mL serum vacuum-tubes BD®. Tubes were stored at 10°C in darkness until arrival at laboratory.

Dissolved inorganic N anomalies – defined as a linear combination of nitrate and phosphate – were used in order to determine the role and distribution of nitrogen fixation and denitrification in the water column. The parameter N* was estimated following Hansell et al. (2004, $N^* = [NO_3^-] + [NO_2^-] + [NH_4^+] - 16\,[PO_4^{+3}] + 2.9$). N*values lower than −3 μmol kg^{-1} are indicative of denitrification while values higher than 2 μmol kg^{-1} denotes nitrogen fixation (Gruber and Sarmiento, 1997).

Laboratory Incubations

Artificial seawater for incubations was prepared according to Lovley (2006). To remove O_2, water was autoclaved, capped, and gently bubbled with N_2 for 15 min in a laminar flow hood LABCONCO Class II Type IIA. In addition to those measures, O_2-sensitive methylene blue (Resazurin 0.0001%, Wolfe, 2011) was added to incubation vessels to detect unwanted traces of O_2 (higher than 700 nM).

Incubations were conducted in darkness in a Shell-Lab incubator (Sheldon Manufacturing, United States) at 10°C for 7 days (glucose fermentation), 8 days (amino acids fermentation), and 35 days (acetate oxidation). Subsamples of 2 mL were removed and filtered through 0.22 μm filters (MILLEX GV™ filter unit) every ca. 24 h for analyses of amino acids, and pH (pH–indicator paper Neutralit, pH 5.5–9.0, Merck Millipore). Measurements of $Fe^{2+}{}_{aq}$ were carried out by removing 500 μL of water at the beginning and the end of the incubations, and amending with $Fe(OH)_3$ as electron acceptor. For CO_2 and HS^- measurements, 500 μL of gas was removed from the headspace at each subsampling time. Control treatments were prepared without inocula. Filtration of solutions (0.22 μm MILLEX GV™), bubbling with N_2, and the addition of substrates and inocula were conducted under a N_2 saturated chamber.

Fermentation of Glucose and Amino Acids

Aliquots of 30 mL artificial seawater were transferred into gas-tight bottles (60 mL, in triplicate) containing 3 mL inocula of seawater, and then amended with glucose or the amino acids alanine, leucine, threonine, phenylalanine, glutamic acid, and ornithine to final concentrations of 40 mM glucose and 10 mM of each amino acid. Such high substrate concentrations are four orders of magnitude higher than natural DOC concentrations and were intended to provide a culture medium not limited by substrate in order to achieve quick-start of microbial growth and short incubation times. Consequently, no inferences were made regarding reaction rates from these incubations because of the transient nature of zero-order reactions; however, the experiments do reveal potential reactions within OMZ waters. Incubation vessels were treated with 200 μM molybdate to prevent consumption of fermentative products by SO_4^{2-} reduction (Oremland and Capone, 1988), and with 200 μM *N*-guanyl-1,7-diaminoheptane (GC_7) to stop acetotrophic methanogenesis (Jansson et al., 2000). Bottles were capped with pre-sterilized butyl-caps and aluminum seals, and then incubated as described.

Anaerobic Oxidation of Acetate by Reduction of NO_3^-, $Fe(OH)_3$ and SO_4^{2-}

Anoxic incubations (35 days) and inoculations were conducted as described above in the glucose fermentation section. NO_3^- ($NaNO_3$, 60 mM), 250 mM of poorly crystalline ferrihydrite-iron oxyhydroxide (Schwertmann and Cornell, 1991), $Fe(OH)_3$, and SO_4^{2-} (Na_2SO_4, 50 mM) were added to incubations as electron acceptors, and acetate ($NaCH_3COO$, 40 mM) supplemented as C source. Artificial seawater with 5% v/v of reducing solution ($Na_2O_2S \times 5H_2O$ and cysteine) was used in the experiments for acetotrophic SO_4^{2-} reduction. $Fe^{2+}{}_{aq}$ concentrations were measured with the 1,10 Phenanthroline method, using kit HACH (Hach Lange GmbH) and a spectrophotometer HACH DR-4000 (Method 8146, DOC316.53.01049). The detection limit of the assay was 3.5 ± 0.3 μM.

Analyses of VFA, Ethanol, HS^- and CO_2 by Gas Chromatography Coupled to Mass Spectrometry (GC–MS)

Acetate, propionate, isobutyrate, butyrate isovalerate, valerate, and ethanol were extracted from headspaces of both ambient samples and incubation vessels using solid-phase micro-extraction. Equilibrium partition between the aqueous phase and headspace was estimated by sonicating standard solutions of VFA (0.1, 1, 5 μM) in gas-tight bottles containing synthetic seawater at 30°C for 15 min, followed by adsorption of analytes from the gaseous phase on 85 μm CarboxenTM/PDMS Stable Flex micro-extraction fibers (SUPELCO). An adsorption fiber was inserted through the septum in the headspace and maintained for 5 min under continuous stirring, followed by desorption for 5 min at 250°C in the injection port of the gas chromatograph Agilent 6890N series coupled to a mass spectrometer Agilent 5973 Network. Compounds were separated with an HP-Plot/Q column 30 m (0.32 mm diameter, 0.20 μm film thickness), using He as the gas carrier.

The mass spectrometer was operated in electron impact mode (70 eV) and spectra of standards and incubations were acquired in full scan mode (m/z 40-600, 2.6 s^{-1}). Spectra of environmental samples were acquired by selective ion monitoring (SIM): acetate (m/z 43-45-60), propionate (m/z 28-45-74), isobutyrate (m/z 43-73-88), butyrate (m/z 41-60-73), isovalerate (m/z 43-60-87), valerate (m/z 41-60-73), and ethanol (m/z 31-45). An example of a peak ID is shown in **Supplementary Figure 1**.

Concentrations of the above compounds were determined using calibration curves ($R^2 > 0.998$), with a VFA mixture (Supelco 46975-U), and ethanol (HPLC grade, Fisher) added to artificial seawater in the range 5 nmol L^{-1} to 1 μmol L^{-1} of acetate, isobutyrate and ethanol (Fisher HPLC grade). Concentrations of VFA and ethanol in the gas phase were calculated as $C_{HS} = C_{ap}/[K + (V_{HS}/V_S)]$ with the partition coefficient $K = C_{AP}/C_{HS}$ (C_{HS} is the concentration in the headspace, C_{AP} is the concentration in the aqueous phase, and V_{HS} and V_S are headspace and sample volume, Slack et al., 2003). This resulted in partition coefficients K of 1.2 for acetate, 1 for isobutyrate, and 1.4 for ethanol.

HS^- and CO_2 were measured in incubation bottles by removing 500 μL of gas from the headspace of either incubation or ambient sample with a Hamilton gas-tight syringe. The gas sample was injected into the GC-MS and detected in SIM mode (m/z 32-33 and 34 for HS^- and m/z 28 and 44 for CO_2). CO_2 was quantified by comparing sample chromatographic areas with those of a CH_4 reference internal standard co-injected (1 ppm) as a surrogate (1750, NOAA). Henry's Law was used to calculate aqueous concentrations from partial pressure. HS^- is reported as percent of maximum abundance since we lacked an appropriate standard.

Detection limits were calculated from slopes of calibration curves, and residual standard deviations were derived from linear regressions of calibration curves (three times residual error times slope, Shrivastava and Gupta, 2011). Detection limits were 40 nmol L^{-1} for acetate, 10 nmol L^{-1} for isobutyrate, 50 nmol L^{-1} for ethanol, and 10 μmol L^{-1} for CO_2.

Analyses of Dissolved Free Amino Acids (DFAA) by High-Pressure Liquid Chromatography (HPLC) With Fluorescence Detection

Concentrations of DFAA from incubations, and from Station 18, were quantified as OPA-derivatized adducts (Lindroth and Mopper, 1979) with a Shimadzu LC-10AT HPLC coupled to a Shimadzu RF-10Axl fluorescence detector (set at excitation/emission of 340/450 nm), column oven CTO 10As and autosampler (Shimadzu SIL 10 ADvp). Aliquots of 600 μL sample, mixed with 400 μL methanol, were derivatized in the autosampler with 60 μL ortho-phthalaldehyde/2-mercaptoethanol reagent (OPT, Lindroth and Mopper, 1979) and 100 μL sodium acetate buffer 0.1 N, pH 5, and injected (50 μL) into the HPLC. Fifteen amino acids (asp, glu, ser, his, gly, thr, arg, ala, tyr, val, met, phe, ile, leu, lys) were separated using an Alltima C18 (5 μm, 250 × 4.6 mm) column kept at 40°C, with a mobile phase of 5% tetrahydrofuran in 25 mM sodium acetate and methanol, and at a flow rate of 1 mL min^{-1}. A gradient of 25–30% methanol in 35 min, 30–50% in 7 min, 50–60% in 18 min, 60–100% in 12 min was used. Initial conditions were restored in 7 min, and the column was equilibrated for 10 min between injections. Amino acids were identified and quantified by comparison with chromatograms of a standard amino acid mix (Pierce 20088) run under the same conditions every 10 injections. The coefficient of variation for quantification of duplicate samples was 9.4%.

Concentrations and Stable Isotope Composition of Particulate Organic C and N

Particulate samples were acid-fumed to remove carbonate (Nieuwenhuize et al., 1994), dried at 60°C for 24 h, wrapped in tin capsules, and analyzed using continuous-flow isotope ratio mass spectrometry (IRMS, Finnigan Delta Plus) interfaced with an elemental analyzer Carlo Erba NC2500. Reproducibility of standard acetanilide was greater than 0.11% for ^{13}C, and 0.005‰ for ^{15}N. Isotope ratios were expressed as per mil (‰) deviations of isotopic values relative to PDB (^{13}C) or atmospheric N_2 (^{15}N).

Satellite-Derived Chlorophyll-*a* and Net Primary Production Estimates

We examined chlorophyll-*a* estimates (monthly averages at 4 km resolution) from the Aqua Moderate-Resolution Imaging Spectroradiometer (MODIS) mission between November 2009 and January 2011, extracting data from the CoastWatch project[1]. Net primary production (NPP) estimates were made using the standard Vertically Generalized Production Model (Behrenfeld and Falkowski, 1997, Ocean Productivity Home Page[2]), previously validated for the upwelling ecosystem off central Chile (Testa et al., 2018). We analyzed satellite estimates within boundaries of 72°48′-73°30′ W, 36°6′-36°45′ S over the

[1]https://coastwatch.noaa.gov

[2]http://www.science.oregonstate.edu/ocean.productivity/

continental shelf surrounding Station 18 (**Figure 1**). Data were averaged every 8 days between 2009 and 2011 (at least 33% of pixels) at a spatial resolution of ca. 9 km and integrating to the depth of euphotic zone (11–51 m).

Export Flux of POC

We calculated export flux of carbon through the photic zone by deriving an empirical relation (**Supplementary Figure 2**) based on simultaneous *in situ* determinations of gross primary production (GPP), and of the fraction of GPP sinking through 50 m depth at station 18 between April 2004 and May 2005. GPP experiments and drifting sediment trap deployments were conducted quasi-monthly from April 2004 to May 2005 (González et al., 2009).

Data Analysis

Both homogeneity of variances (Levene test) and normality of variables (Shapiro–Wilk test) were not fulfilled; therefore, we also tested for significant differences among environmental data using the non-parametric Kruskal–Wallis ANOVA test, and differences among experimental results using the paired sample Wilcoxon Signed Rank test. Correlations were examined using Spearman R coefficients.

Thermodynamic Calculations

Estimates of Gibbs Energy (ΔG) values for proposed metabolic reactions in the suboxic water column were calculated using substrate and product activities, temperature, and pH resembling suboxic water column in spring at the sampling site. The following data and sources were used: temperature (10.2°C), O_2 (8.4 μM), NO_3^- (25 μM) from the COPAS Center Oceanographic Time Series database (W Schneider, curator), acetate (430 nM, November 2010, 65 m, this study), dissolved free amino acids (100 nM, this study), glucose (90 nM, Sempéré et al., 2008), $Fe^{2+}{}_{aq}$ (400 nM, Achterberg et al., 2001); Iron hydroxide Fe(III)s (50 μM, Schoemann et al., 1998), SO_4^{2-} and HCO_3^- (28 and 2 mM, Pilson, 2012), N_2 (389 μM, Craig et al., 1967), HS^- (1 μM, Lavik et al., 2009; Schunck et al., 2013), and H_2 (0.06 mM, Seiler and Schmidt, 1974). Thermodynamic calculations were carried out using Thermodyn© software (Damgaard and Hanselmann, 1991).

RESULTS

Fermentation of Glucose and Amino Acids and Anaerobic Oxidation of Acetate During Laboratory Incubations

The microbial degradations of glucose, amino acids, and acetate were detected during laboratory incubations under excess concentration of substrates (millimolar range) in the absence of O_2 (**Figure 2**). Production of acetate (from 0 to 1 mM), ethanol (from 0 to 2 mM), CO_2 (from 0 to 4 mM), and H^+ (pH from 8 to 5) indicated fermentation of glucose during the 7 days incubation period (**Figure 2A**). Fermentation of the amino acid mix containing alanine, leucine, threonine, phenylalanine, glutamic acid, and ornithine (decrease from ca. 60 mM to ca. 6 mM) resulted in the production of VFA, acetate, propionate, isobutyrate, butyrate, isovalerate, and valerate (from 0 to ca.7.5 mM) during 8 days of incubation (**Figure 2B** and **Supplementary Figure 3**).

No decay of fermentation products (acetate, ethanol) was detected in 7 days of incubation likely due either to the absence of external electron acceptors for anaerobic oxidation in the culture media, the thermodynamically unfavorable conditions caused by buildup of fermentation products, or the slow growth rates of acetate consumers suggested by comparing decay of amino acids (90% in near 2 days, **Figure 2B**) with decay of acetate (90% in near 30 days, **Figures 2C–E**).

Microbial oxidation of acetate with excess NO_3^- (**Figure 2C**), $Fe(OH)_3$ (**Figure 2D**), and SO_4^{2-} as electron acceptors was detected in the inocula treatments of OMZ water incubated under anaerobic conditions (**Figure 2E**). In control incubations, decrease in acetate concentration was not detected (**Supplementary Figure 3d**) and CO_2 was always below the detection limit. Estimated Gibbs Energy (ΔG) for fermentation of glucose and amino acids, and anaerobic oxidation of acetate with NO_3^-, $Fe(OH)_3$, and SO_4^{2-} were in the range of −73 to −3777 kJ mol^{-1} suggesting that these reactions were exergonic (**Table 1**).

Dissolved inorganic N anomalies ($NO_3^- + NO_2^- + NH_4^+$; N*) showed the year-round extent of NO_3^- deficit in the area. Ranges of −40 to 5 ESSW, −5 to 25 ESPTW (summer) and −20 to −10 ESPTW (winter) (**Supplementary Table 1** and **Figure 3**) were observed, with $\delta^{15}N$ of particulate organic nitrogen (PON) enriched to values of 20–35‰ (ESSW); 10–15‰ (ESPTW summer); and 5–10‰ (ESPTW winter) (**Supplementary Table 1** and **Figure 3**).

Variability in the Structure of the Water Column

During the spring-summer, upwelling-favorable winds (southerlies) predominated in the study area (**Figure 4A**, positive values are indicative of upwelling favorable winds) and contributed to lift the 11°C isotherm, the oxycline, and more saline waters (34.4–34.6) to depths shallower than 30 m (**Figures 4B–D**). This near-surface layer above 30 m tends to gain heat at this time of year. During austral autumn-winter, downwelling favorable winds (northerlies) prevailed and were associated with the deepening of the 11–11.5°C isotherm, the 34.4–34.6 isohalines, and the oxycline (**Figures 4A–D**). In these seasons, the upper 30 m was diluted by the continental contribution from rivers (**Figure 4C**), as previously shown by Sobarzo et al. (2007). In particular, O_2 concentrations in surface waters exceeded 150 μM throughout the year, with a hypoxic boundary layer of 22.5 μM O_2 located at ca. 30 m depth in austral spring and summer, but below 70 m depth during winter (**Figure 4D**, white line). Anomalous bottom cooling (10–11°C) was observed during July 2010 in the absence of upwelling favorable winds (**Figures 4A,B**). Temporal and

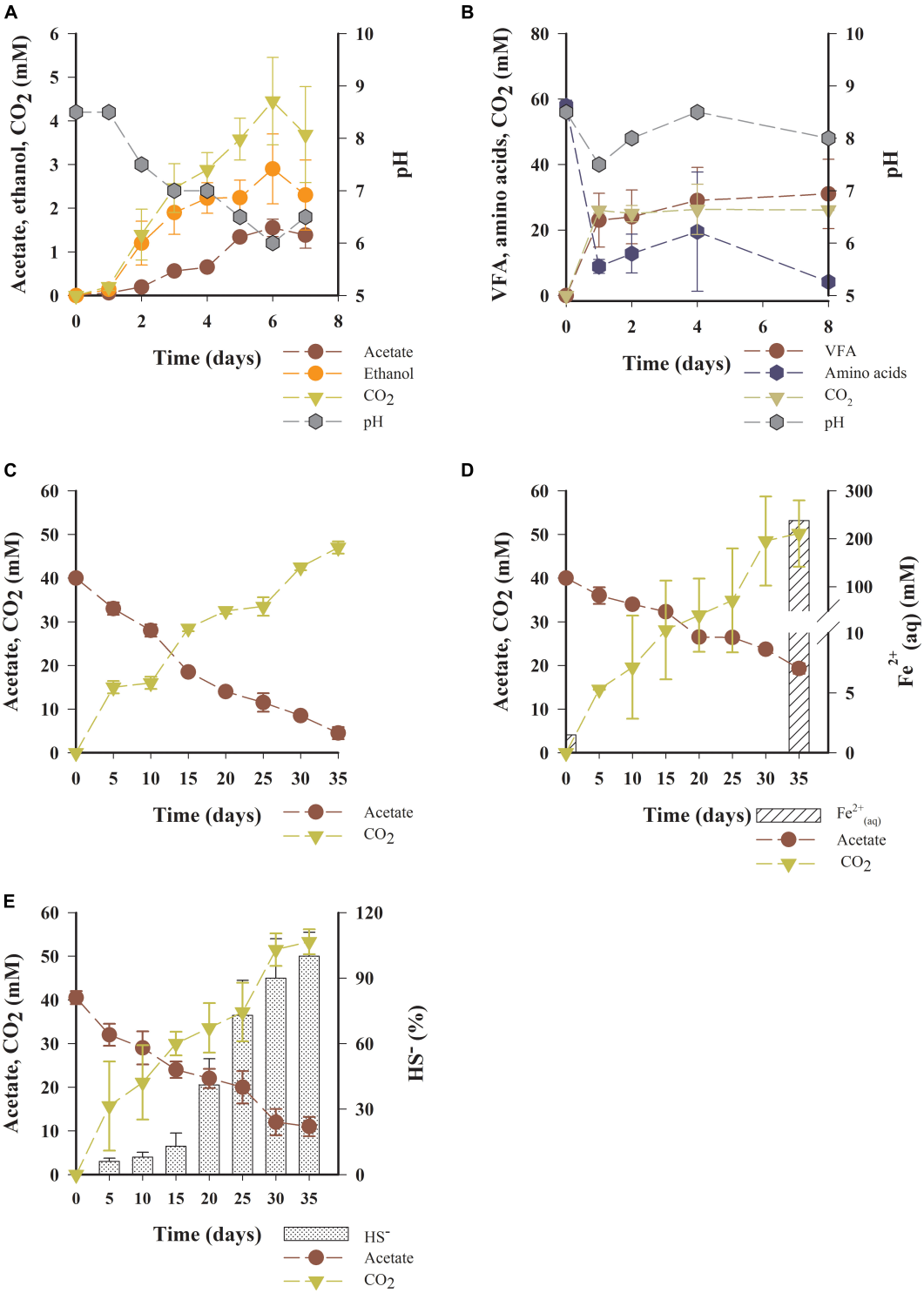

FIGURE 2 | Fermentation of glucose and amino acids during incubations. **(A)** Changes in concentration of acetate, ethanol, CO_2, and H^+ (measured as pH) during fermentation of glucose, **(B)** Decay of amino acid mixed substrate (alanine, leucine, threonine, phenylalanine, ornithine, glutamic acid), and changes in concentration of VFA (sum of acetate, propionate, isobutyrate, butyrate, isovalerate, and valerate), CO_2 and H^+ during amino acid fermentation. Anaerobic terminal oxidation of acetate. The decay of acetate and increase in concentration of CO_2, $Fe^{2+}{}_{aq}$ and HS^- under induced conditions of **(C)** denitrification (excess NO_3^-, 60 mM), **(D)** dissimilative iron reduction [excess $Fe(OH)_3$, 250 mM], and **(E)** dissimilative sulfate reduction (excess SO_4^{2-}, 50 mM). Values shown represent the average ± standard deviation. Relative abundance of HS^- is shown as percent of maximum production.

TABLE 1 | Summary of metabolic reactions and chemical equations in incubations of suboxic waters collected in November 2010 at Station 18 off Concepción.

Metabolic reaction and substrate	Chemical equation	ΔG (kJ/mol substrate)	$\Delta G^{0'}$ (kJ/mol substrate (Froelich et al., 1979)
(1) Glucose fermentation to acetate (**Figure 2A**)	$C_6H_{12}O_6 + 4H_2O = 2\ CH_3COO^- + 2HCO_3^- + H^+ + 7H_2$	–217	–350
(2) Glucose fermentation to ethanol (**Figure 2A**)	$C_6H_{12}O_6 + H_2O = 2C_2H_5OH + 2HCO_3^- + 2H^+$	–534	–350
(3) Stickland fermentation of alanine (oxidation) and glycine (reduction) to acetate (**Figure 2B**)	$2C_3H_7NO_2 + H_2O = 3CH_3COO^- + 2\ NH_4^+ + H^+$ $C_2H_5NO_2 + H_2 = 3CH_3COO^- + 2\ NH_4^+$	–252	–350
(4) Acetate oxidation by denitrification (**Figure 2C**)	$5\ CH_3COO^- + 8NO_3^- + 3H^+ = 10HCO_3^- + 4N_2 + 4H_2O$	–3777	–2750
(5) Acetate oxidation by dissimilative iron reduction (**Figure 2D**)	$CH_3COO^- + 8Fe(OH)_3 + 15H^+ = 2HCO_3^- + 8Fe^{2+}{}_{aq} + 20H_2O$	–77	–1370
(6) Acetate oxidation by dissimilative sulfate reduction (**Figure 2E**)	$CH_3COO^- + SO_4{}^{2-} = HS^- + 2HCO_3^-$	–73	–380

Gibbs energy (ΔG) was calculated assuming substrate and product activities, temperature, and pH typical of suboxic water column conditions for spring at the sampling site. For comparison, Standard Gibbs energy ($\Delta G^{0'}$) of a Redfield-type substrate $(CH_2O)_{106}(NH_3)_{16}(H_3PO_4)$ under standard biological conditions are shown [as calculated by Froelich et al. (1979)].

spatial distributions of hydrographic properties confirm the presence of two distinct water masses during the study period, with mid and bottom layers on the continental shelf occupied by ESSW with low preformed O_2 concentration (<45 μM, ca. 1 mL L^{-1}), high salinity (34.5) and low temperature <11.5°C. During austral spring-summer, the core of this water mass (indicated by isopycnal 26.5) rose to near 30 m depth (**Figures 4B–D**, white line) while during winter it was confined to 50–70 m depth.

The surface layer was dominated by ESPTW originating from Subantarctic Water (SAW) from the subantarctic front (Schneider et al., 2003), with cold and low salinity waters during austral winter and higher temperature and moderate salinity during austral summer (**Figures 4B,C**).

Variability in the Chemistry of the Water Column

Chlorophyll-*a* concentration increased from ∼2 to >10 mg m^{-3} during spring and throughout the productive summer season (**Figure 5A**). Concentrations of POC and PN averaged 27 ± 46 mmol C m^{-3}, and 4 ± 8 mmol N m^{-3}, corresponding to an average C/N ratio of ∼ 7, with maximum values of C and N occurring during the productive season (**Figures 5B,C**). $PO_4{}^{3-}$ concentrations were higher below 30-m depth than in surface waters throughout the year, and a pronounced depletion of surface $PO_4{}^{3-}$ occurred in surface water during austral summer (**Figure 5D**). The annual cycle of NO_3^- generally followed expected patterns, with concentrations typically lower in near-surface waters, and higher in deeper waters. Concentrations were substantially higher throughout the water column (>10 μM) during austral winter and summer 2011, with a conspicuous depletion below 50-m depth, suggesting microbial consumption (**Figure 5E**). Satellite-based estimates of primary production varied from 30 mmol C m^{-2} d^{-1} (0.4 g C m^{-2} d^{-1}) during winter to over 600 mmol C m^{-2} d^{-1} (7 g C m^{-2} d^{-1}) during spring-summer (**Figure 5F**).

Our sampling coverage for NH_4^+ concentrations were rather limited but showed accumulation of up to 2.5 μM NH_4^+ in both the deeper and subsurface layers during austral spring and summer (**Figure 6A**). A surface maximum of ca. 1 μM NH_4^+ was detected in the surface oxygenated ESPTW water mass, but otherwise, concentrations were below 0.5 μM (**Figure 6A**). NO_2^- concentrations were generally less than 1.5 μM NO_2^- throughout the water column, except for measurements of up to 7 μM during the productive season in austral summer in suboxic ESSW below 50 m depth (**Figure 6B**).

The concentrations of VFA (ca. 66% acetate, ca. 33% isobutyrate, and <1% isovalerate) ranged from 0.05 to 4 μM throughout the year, with higher concentrations observed under low O_2 conditions below 50 m depth (Kruskal–Wallis Test, $p < 0.05$, $N = 52$, **Figure 6C**). VFA concentrations of over 2 μM were observed in the water column during suboxic conditions, peaking in austral fall 2009, austral spring 2010, and austral summer 2011. VFA correlated positively with NH_4^+ concentrations (Spearman $r = 0.2$, $p < 0.05$, $N = 78$) and negatively with dissolved O_2 (Spearman $r = -0.3$, $p < 0.05$, $N = 78$) and temperature (Spearman $r = -0.3$, $p < 0.05$, $N = 78$). Concentrations of dissolved free amino acids (DFAA) reached up to ∼0.5 μM and generally decreased with depth during upwelling months (austral spring and summer). In contrast, concentrations of DFAA lower than 0.1 μM were observed throughout the water column in winter months (**Figure 6D**). Concentrations of DFAA and VFA were higher in ESSW during the upwelling season than in ESPTW during winter (**Figures 6C,D**).

DISCUSSION

Fermentation of Glucose and Amino Acids and Anaerobic Oxidation of Acetate

In our experiments with excess concentrations of substrates (millimolar range), the fermentation of glucose produced acetate and ethanol, and the fermentation of DFAA, alanine, leucine, threonine, phenylalanine glutamic acid, and ornithine produced acetate, propionate, isobutyrate, butyrate, isovalerate and valerate. Along with sugars, DFAA are considered to be suitable substrates for microbial heterotrophic metabolism; this

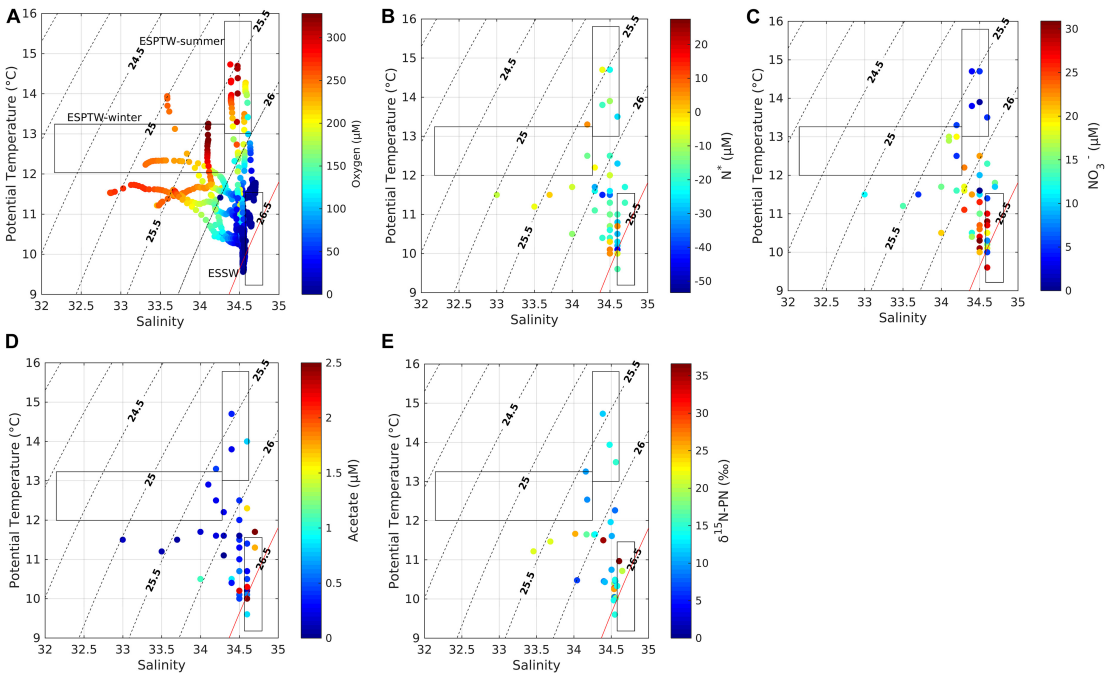

FIGURE 3 | Potential temperature/salinity diagram from depth profiles taken at Station 18, off Concepción; data points are color coded (see color bar) for the following measurements **(A)** oxygen, **(B)** N*, **(C)** NO_3^-, **(D)** acetate, **(E)** δ^{15}N-PN. N* = [NO_3^- + NO_2^- + NH_4^+] – 16 [PO_4^{+3}] + 2.9 (Hansell et al., 2004), PN, particulate nitrogen. Rectangles indicate temperature and salinity ranges for Equatorial Subsurface Water (ESSW), and Eastern South Pacific Transition Water (ESPTW) in austral winter and summer. Dotted lines represent isopycnals as sigma-t and red line corresponds to sigma-t of 26.5 in the core of ESSW.

would explain why their concentration was maintained lower than 100 nM in the water column, since their removal rates are coupled to their production (Webb and Johannes, 1967; Crawford et al., 1974; Fuhrman, 1987). In the absence of O_2, amino acids are known to undergo anaerobic degradation (Barker, 1981) as observed in our incubations of microbial assemblages from OMZ waters. Our observations are also consistent with the Stickland catabolic pathway (Stickland, 1934; Nisman, 1954; Barker, 1981), a process that couples anaerobic reduction and oxidation of amino acids and produces VFA, CO_2, and NH_4^+. In Stickland fermentation, an electron-donating amino acid is oxidized to a VFA that is shorter by one carbon (Stickland, 1934; Nisman, 1954; Barker, 1981); thus, acetate can be produced by alanine oxidation, propionate by threonine, butyrate by glutamic acids, and valerate by leucine. An electron-accepting amino acid is reduced to a VFA of the same number of carbons (Stickland, 1934; Nisman, 1954; Barker, 1981) as in the reduction of threonine to butyrate, and of leucine to caproic acid. In the present study, incubation media remained mildly alkaline (**Figure 2B**), likely because of NH_4^+ formation during fermentation of amino acids (Prüss et al., 1994; Wolfe, 2005).

In our experiments under induced conditions of denitrification and dissimilative $Fe(OH)_3$ and SO_4^{2-} reductions, anaerobic terminal oxidation of acetate was detected together with CO_2 production (**Figures 2C–E** and **Table 1**, reaction 4–6). This experimental evidence of thermodynamically feasible acetate oxidation – with $Fe(OH)_3$ as an electron acceptor –reveals the potential ability of microbes to reduce solid-phase iron which is carried by rivers in the region, using the fermented metabolites produced in oxygen-depleted water. This process would release dissolved bioavailable Fe for utilization by phytoplankton and chemolithotrophic microbes (Segovia-Zavala et al., 2013), and metalloenzymes required for reduction of nitrate and nitrite (Milligan and Harrison, 2000). In support of this working hypothesis, bacterial reduction of solid-phase metals associated with oxidation of acetate has in fact been detected in the Baltic Sea (Berg et al., 2013). We suggest that our data provides evidence that acetate, and likely other VFA such as butyric acid, represents a principal intermediate of anaerobic metabolism in OMZ waters on the Concepción shelf.

Twice as much ethanol than acetate was produced during incubations of inocula from OMZ waters (**Figure 2A**, Wilcoxon Signed Rank test $p < 0.05$, $n = 8$), but ethanol was not detected in any sample from the water column. The observed production of ethanol could be an experimental artifact resulting in selection for ethanologenic copiotroph microorganisms, or because of acidification in enclosed vessels (which would normally be buffered to some extent by alkalinity in natural seawater) promoting microbial excretion of neutral molecules such as ethanol (Michels et al., 1979; Wolfe, 2005). These processes may explain the observed onset of ethanol production when pH begins to drop in the experimental vessels, preventing further decrease (**Figure 2A**). Alternatively, the absence of detectable ethanol could be a result of microbial consumption and fast turnover times in the water column, which would preclude its accumulation. In fact, the activity of the enzyme ethanol

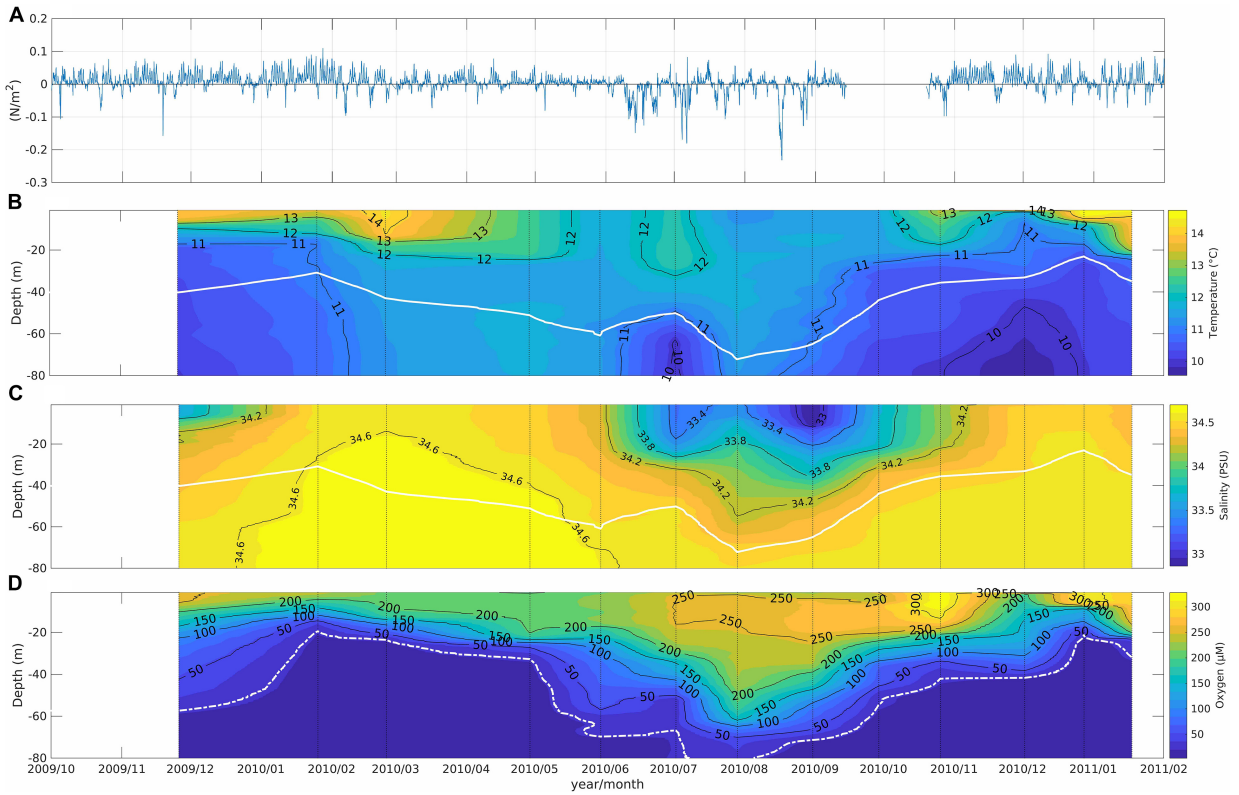

FIGURE 4 | Time series data from November 2009 through January 2011. **(A)** wind stress at Carriel Sur airport, Concepción (positive values represent upwelling-favorable winds); **(B)** temperature, **(C)** salinity, **(D)** concentration of O_2 in the water column at Station 18 off Concepción. The white lines in **(B,C)** represent isopycnal of 26.5 in the core of ESSW and dotted line in **(D)** is the isoline of 22 μM O_2 (ca. 0.5 mL O_2 L^{-1}, often considered the limit of suboxia).

dehydrogenase has been previously detected in OMZ waters on the Concepción shelf (González and Quiñones, 2009), thus providing evidence the potential for ethanologenic fermentation triggered by the high concentration of organic carbon and reduced pH in these waters.

Chemical and Physical Variability in the Water Column

General hydrographic patterns detected during this study were consistent with previous research in this area (Schneider et al., 2003, 2017; Escribano and Schneider, 2007; Sobarzo et al., 2007; Letelier et al., 2009; Escribano and Morales, 2012). The surface layer was dominated by ESPTW which originates from Subantarctic Water (SAW) from the subantarctic front (Schneider et al., 2003), and which is characterized by cold and low salinity waters during austral winter and higher temperature and moderate salinity during austral summer. While ESPTW is transported northward along the rim of the Subtropical Gyre, ESSW is transported southward by the Peru-Chile Undercurrent off central Chile, constituting the water source for coastal upwelling (Sobarzo et al., 2007; Silva et al., 2009). The fundamental mechanisms proposed to explain seasonal variations in predominance of these two water masses on the continental shelf have been coastal upwelling, and downwelling induced by alongshore winds (Sobarzo et al., 2007; Schneider et al., 2017). Other processes, such as wind curl, coastally trapped waves, or topographic upwelling, have been less studied at these latitudes. These processes could explain a seemingly anomalous bottom cooling detected in July 2010 that could not be attributable to upwelling favorable wind.

As expected, upwelling favorable southerly winds resulted in a shallowing of the nutricline and upwelling of subsurface nutrient rich waters (up to ∼15 μM NO_3^- and ∼1.5 μM PO_4^{2-}) closer to the surface, leading to the fertilization of the photic zone, as has been previously documented (Sobarzo et al., 2007; Farías et al., 2015). Satellite-based estimates of primary production during spring-summer 2009 and 2010 showed a three-fold increase in rates of primary production and significant increases in the concentrations of chlorophyll-*a*, POC and PN. The seasonal pattern of phytoplankton activity in surface waters, generally followed previously described annual patterns of primary production (e.g., Montero et al., 2007; Testa et al., 2018) during spring-summer 2009 and 2010. Sinking POC fluxes however did not follow the seasonal pattern of phytoplankton activity. Fluxes of POC sinking to 50-m depth averaged 23 ± 4 mmol C m^{-2} d^{-1} throughout the year, varying between 25 ± 3 mmol C m^{-2} d^{-1} during the upwelling seasons and 19 ± 1 mmol C m^{-2} d^{-1} in austral winter. Variation in sinking fluxes of POC at 50-m depth did not closely reflect the

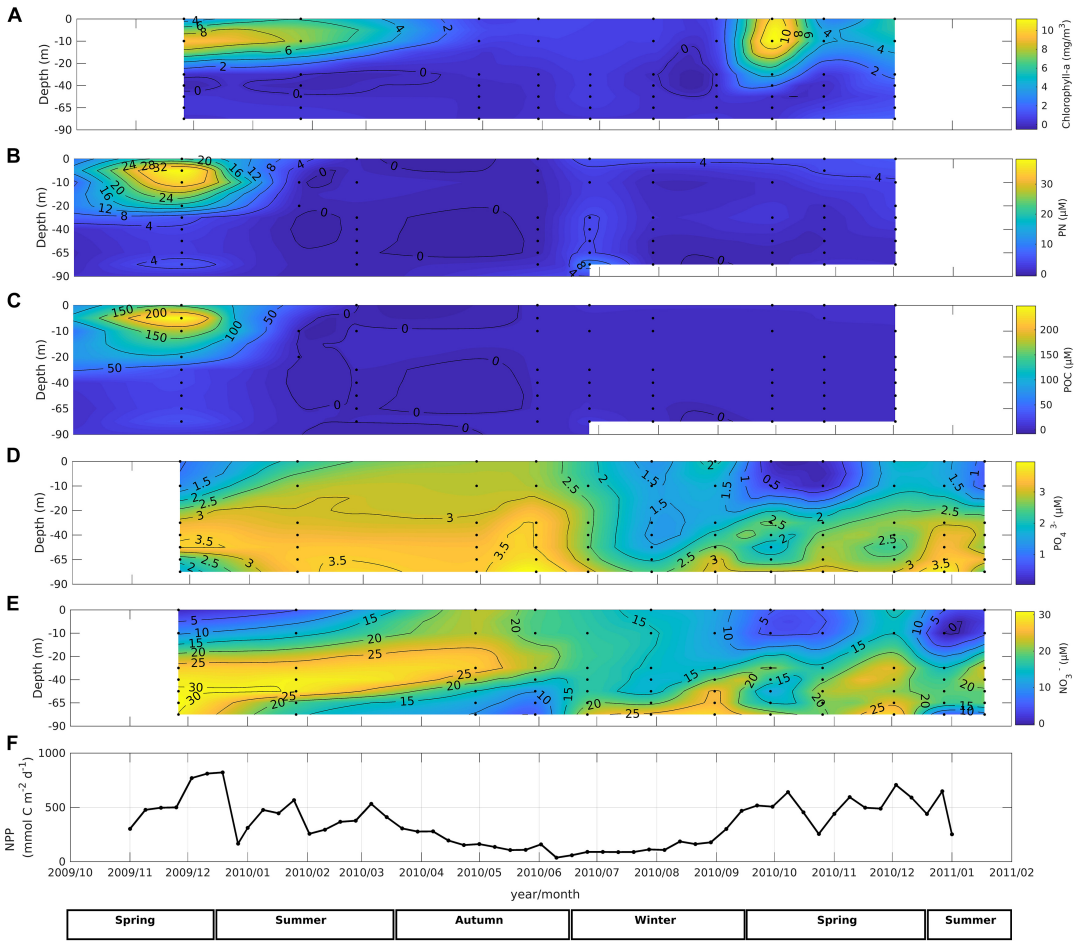

FIGURE 5 | Time series data from November 2009 through January 2011 in the water column at Station 18 off Concepción; **(A)** chlorophyll-*a*, **(B)** particulate nitrogen, **(C)** particulate organic carbon, **(D)** phosphate concentration, **(E)** nitrate concentration, **(F)** rate of depth integrated net primary production (NPP).

threefold increase in primary production observed in both water masses between winter and upwelling conditions. These sinking fluxes were therefore rather similar throughout the year (P_{sink} upwelling ESSW/P_{sink} winter ESPTW = 1.3), in good agreement with the low seasonal variability in export production previously detected (3–10% of surface waters PP production) for this area (González et al., 2009).

In a modeling study, Pizarro-Koch et al. (2019) concluded that the southern extension and seasonality of the OMZ at Station 18 is driven more by changes in the undercurrent transport and mesoscale eddy fluxes than by mixing and local input. Similar year-round sinking carbon fluxes reported here appear to support this conclusion.

At Station 18 off Concepción, elevated concentrations of VFA and NH_4^+ were concurrently observed (**Figures 6A,C**), suggesting fermentation of amino acids and production of NH_4^+ in the water column through the Stickland fermentation reaction. In the OMZ off Peru, the stoichiometric production of NH_4^+ from fermentation of amino acids could explain previously unaccounted NH_4^+ requirements of up to 17 mmol NH_4^+ m^{-2} d^{-1} for anammox bacteria (Lam et al., 2009). Our monthly field determinations in the water column off Concepción show that both VFA and NH_4^+ concurrently increased during November–March 2010 (austral spring-summer) whereas decay of VFA occurred during intrusion of oxygenated ESPTW in March–July (austral winter). In contrast, NH_4^+ was depleted much later in July–November (austral autumn), a likely consequence of a slow build-up of anaerobic NH_4^+ oxidizers (anammox) bacteria with relatively low growth rates (Kuenen, 2008; Kartal et al., 2013). Anammox reaction rates (ca. 0.4 nmol L^{-1} h^{-1}, Canfield et al., 2010) are about 20 times lower than suboxic rates of degradation of amino acids (ca. 10 nmol L^{-1} h, Pantoja et al., 2009) in the OMZ off the northern Chilean coast, implicating that Stickland fermentation could be a source of NH_4^+ for anammox in OMZ waters.

Anaerobic Metabolism of OMZ Waters and the Role of Acetate

Changes in water column biogeochemistry in OMZ waters are driven by the relative contribution of diverse metabolic processes, including reduction of NO_3^- (e.g., Naqvi et al., 2000; Bange et al.,

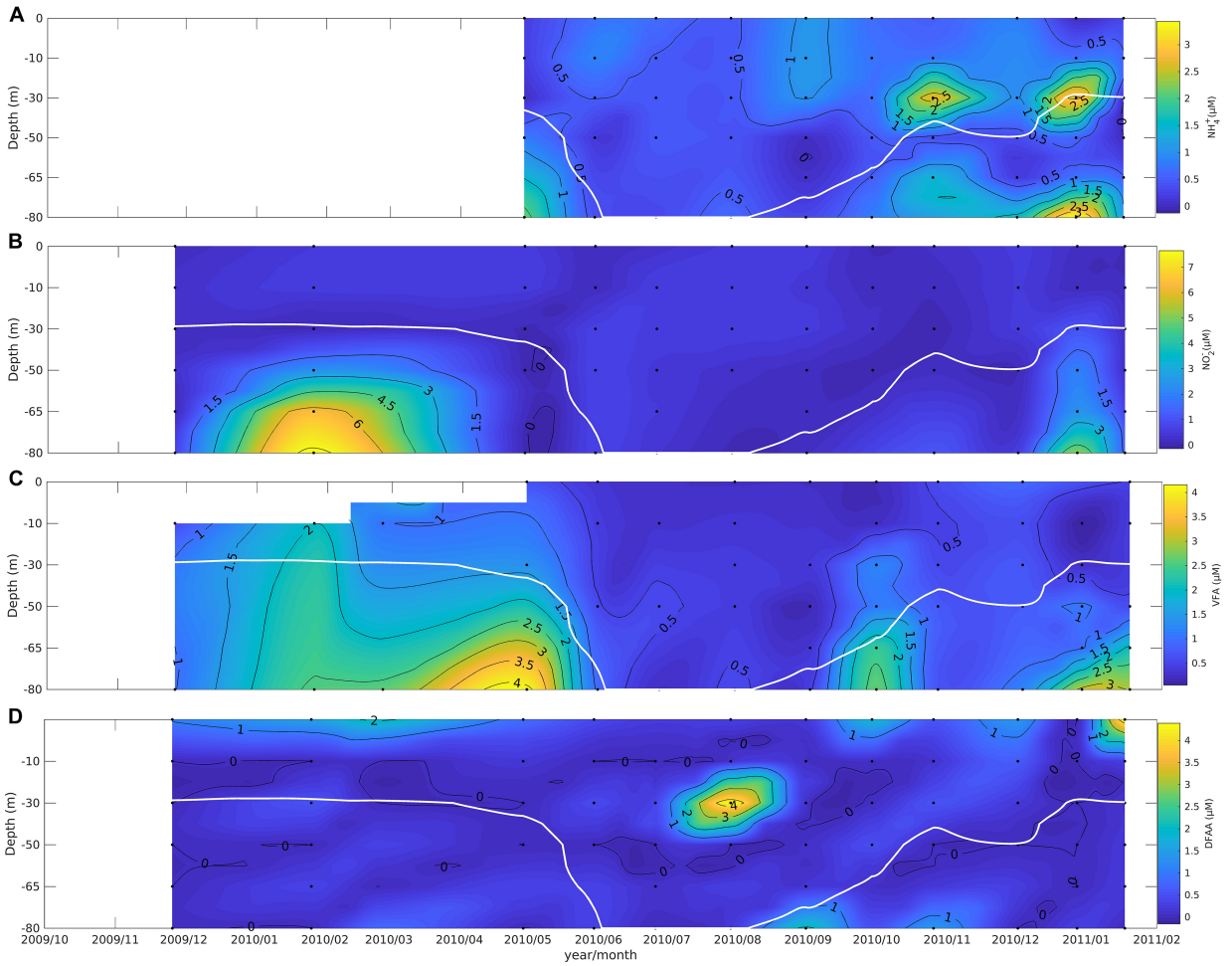

FIGURE 6 | Time series data from November 2009 through January 2011 in the water column at Station 18 off Concepción; **(A)** ammonium, **(B)** nitrite, **(C)** Volatile Fatty Acids, VFA **(D)** Dissolved Free Amino Acids, DFAA. The white line represents isopycnal of 26.5 in the core of ESSW.

2001; Farías et al., 2009; Dalsgaard et al., 2014), Fe(III) (e.g., Bruland, 2006; Moffett et al., 2007), and SO_4^{2-} (e.g., Dugdale et al., 1977; Canfield et al., 2010), production of CH_4 (e.g., Farías et al., 2009; Naqvi et al., 2010; Chronopoulou et al., 2017), and N_2O (e.g., Cohen and Gordon, 1978; Farías et al., 2009; Naqvi et al., 2010; Kock et al., 2016), and anaerobic cycling of NO_2^- and NH_4^+ (e.g., Lipschultz et al., 1990; Molina et al., 2005; Lam et al., 2009; Fernandez and Farías, 2012). For reactions to occur, enzymatic hydrolysis of high molecular weight DOC (e.g., Hoppe et al., 1988; Chróst, 1990; Pantoja et al., 2009) by extracellular enzymes of marine bacteria (e.g., Arnosti, 2011; Arnosti et al., 2012) and fungi (Gutiérrez et al., 2011) produces low molecular weight substrates – such as amino acids and sugars – that are transported across cell-membranes (Weiss et al., 1991) and subsequently degraded. In the absence of metazoans in hypoxic waters (e.g., Vaquer-Sunyer and Duarte, 2008; Cavan et al., 2017), anaerobic microbes rely on low molecular weight organic substrates (acetate and other VFA) for dissimilative reduction of NO_3^-, Fe(III) and SO_4^{2-} and for methanogenesis (Megonigal et al., 2004).

Dissolved inorganic N anomalies (NO_3^- + NO_2^- + NH_4^+; N*) are probably associated with water column nitrogen cycle microaerophilic and anaerobic metabolism. N* showed a year-round NO_3^- deficit in the study area, with similar negative N* values that have been previously recorded in the area from 21 to 33°S (De Pol-Holz et al., 2009; Galán et al., 2014; Galán et al., 2017), and have been attributed to denitrification and anammox. Under conditions of NO_3^- depletion, ^{15}N enrichment of remaining NO_3^- would be expected in these low O_2 waters. Upwelled water with isotopically heavy NO_3^- may result in the enrichment of $\delta^{15}N$ of particulate organic nitrogen (PON). This mechanism is consistent with $\delta^{15}N$-PON values of up to 35‰ found during this study. The similarity of the isotopic range of PON found in both OMZ and subantarctic water masses during the winter, can be explained by enhanced mixing of both water masses at that time of the year. Similar conclusions were reported by De Pol-Holz et al. (2009) analyzing $\delta^{15}N$-NO_3^- for this study area, and by Cline and Kaplan (1975), Liu and Kaplan (1989), Castro et al. (2001), and Sigman et al. (2003) for the California Current System.

Since OMZ waters (ESSW) are pushed offshore by SAW during austral winter, waters enriched in δ^{15}N-PON and acetate, and with negative N*, mix with the more oxygenated waters of subantarctic origin, thus imprinting a signal of anaerobic activity on ESPTW. Calculations using the mixing triangle shows that, even during austral winter, 50% of ESSW is located at depths as shallow as 50 m (the ESSW can be present at 25-m and above during austral summer). Concentrations of acetate (>1.5 μM) in ESSW were higher than in surface ESPTW, both during summer (0.01–0.8 μM) and winter (<0.2 μM). Mixing of water masses allows the byproducts of anaerobic metabolism to spread beyond the boundaries of OMZ source waters, thus providing labile and low molecular weight dissolved organics to surrounding oxygenated ESPTW.

Acetate, isobutyrate, and isovalerate were present at significant levels within the OMZ and surrounding waters as biomarkers for fermentative activity. Twice as much acetate (range 0.1–2.5 μM) was present in the water column during upwelling seasons than observed in winter (Kruskal–Wallis Test, $p < 0.05$, $N = 52$), and showed a similar trend to isobutyrate which ranged from 0.9–1.5 μM. Elevated concentrations of acetate (up to 10–60 μM) have been detected in the anoxic Black Sea (Mopper and Kieber, 1991; Albert et al., 1995), the Pettaquamscutt River Estuary (*ca.* 7 μM, Wu and Scranton, 1994), and at *ca.* 10 μM in anoxic waters of the Cariaco Basin (Ho et al., 2002). In more oxic waters, acetate concentrations have been detected in the range 0.01–2.4 μM at the Chemotaxis Dock in Woods Hole (Lee, 1992), surface waters of the Cariaco Basin (Ho et al., 2002), in Long Island Sound (Wu et al., 1997), and the Gulf of Mexico (Zhuang et al., 2019). Acetate concentrations in suboxic waters off Concepción were generally within the ranges in the oxic and anoxic waters described above, and were likely enhanced by higher rates of primary production (**Figure 5F**) than observed in the Cariaco Basin, Long Island Sound and the Gulf of Mexico. Higher concentration of isobutyrate observed off Concepción (up to 1.5 μM) – associated with anaerobic degradation of iso-leucine (Mueller-Harvey and John Parkes, 1987) – cannot be readily compared with those of other coastal environments because of lack of measurements in the water column. As a reference, Sansone and Martens (1982) measured iso-butyrate in the eutrophic sediments of Cape Lookout Bight within the range < 0.5–6 μmole per liter sediment, and concentrations of up to 8 μM have been determined in pore waters at several coastal sites (Finke et al., 2006).

Enhanced water column concentrations of VFA up to 4 μM were detected during austral spring, summer, and fall throughout the water column (dominated by ESSW, **Supplementary Figures 4A,B** and **Figures 3**, **6C**). Intruding oxygenated ESPTW of subantarctic origin during winter contains up to 0.5 μM VFA that can be attributed to the fermentation of organic matter by ambient microbial assemblages within OMZ waters.

CONCLUSION

We identified several products of the main anaerobic microbial reactions (fermentation, denitrification, and reduction of $FeOH_3$ and SO_4^{2-}) during laboratory incubations of OMZ waters, and we related these products to the annual cycle in water column chemistry within the upwelling ecosystem on the continental margin off Concepción, central Chile. Degradation of organic matter in anoxic systems relies on fermentation products and these can then be transported to neighboring oxygenated waters as labile substrates for microbial respiration. Within OMZ waters, acetate produced by fermentation is a major substrate for SO_4^{2-} reducers (Megonigal et al., 2004; Jørgensen and Kasten, 2006), and was shown to be active even in the presence of NO_2^- and NO_3^- (Canfield et al., 2010). The reduction of SO_4^{2-}, with acetate as electron donor, is thermodynamically feasible in OMZ waters (**Table 1**) when the inhibitor HS^- remains in low concentrations (Arndt et al., 2013). A group of Gammaproteobacteria affiliated to HS^- oxidizers have been identified in OMZ waters off the Chilean coast (Canfield et al., 2010), and a SO_4^{2-}-reducing microorganism has been isolated from the OMZ in Peruvian coastal waters (Finster and Kjeldsen, 2010); these observations provide support for the findings shown here.

Implications of HS^-, SO_4^{2-}, amino acids, and acetate cycling are evident in cycling of N and C in OMZ waters. Fermentation of amino acids could conceivably fuel the NH_4^+ requirements of anammox bacteria because degradation of organic matter by denitrification is insufficient to account for observed anammox rates in OMZ waters (Thamdrup et al., 2006; Lam et al., 2009). The potential production of NH_4^+ through Stickland fermentation of amino acids in the OMZ could have implications for our understanding of the biogeochemistry of C and N, and could elucidate sources of NH_4^+ for the microaerophilic NH_4^+ oxidizers *Thaumarchaeota* (Venter et al., 2004; Könneke et al., 2005; Francis et al., 2005) and anammox bacteria (Kuypers et al., 2005; Dalsgaard et al., 2005; Thamdrup et al., 2006); these microbes have been unexplored to date.

DATA AVAILABILITY STATEMENT

The datasets generated for this study are available on request to the corresponding author.

AUTHOR CONTRIBUTIONS

BS and SP-G initiated and planned the study. BS conducted the field campaigns. BS, SP-G, GD, HG, LF, AS, and NP provided the chemical and isotopic analyses. GT and MS provided the satellite and physical analyses. All the authors contributed to the data analysis and writing of the manuscript based on an initial version written by BS and SP-G.

FUNDING

This research was funded by the Center for Oceanographic Research COPAS Sur-Austral CONICYT PIA PFB31 and APOYO CCTE AFB170006, and the Gordon and Betty Moore Foundation (MI_LOCO Oregon_Concepción, grant # 1661).

We thank the Hanse-Wissenschaftskolleg Delmenhorst, Germany, for sponsoring the "Marine Organic Biogeochemistry" workshop in April 2019. The workshop was funded by the Deutsche Forschungsgemeinschaft (DFG, German Research Foundation), grant # 422798570.

ACKNOWLEDGMENTS

We acknowledge the support provided by the COPAS Oceanographic Time-Series Station 18 off Concepción maintained by the Center for Oceanographic Research in the eastern South Pacific (FONDAP COPAS Center). We would particularly thank Prof. Dr. Wolfgang Schneider for validating data used in this study. Prof. Dr. Donald Canfield is acknowledged for providing insightful comments to an earlier version of this manuscript, and Dr. David Crawford for valuable comments. We are also grateful to UdeC personnel Lilian Núñez, Víctor Acuña, and Eduardo Tejos of the Marine Organic Geochemistry Laboratory, as well as Captain Sergio Marileo and the crew of L/C *Kay-Kay II* for valuable help during sampling and laboratory work. BS acknowledges the support provided by a student fellowship from the Gordon and Betty Moore Foundation, and valuable insights on thermodynamics and microbial metabolism from Prof. Dr. Kurt Hanselmann and international graduate courses ECODIM (Concepción, Chile) and Geobiology (Santa Catalina Island, United States). GT acknowledges the supports provided by a student fellowship (CONICYT-PFCHA/Doctorado Nacional/2017-21170561). **Figure 1** was produced using Ocean Data View software developed by Reiner Schlitzer (http://www.awi-bremerhaven.de/GEO/ODV).

SUPPLEMENTARY MATERIAL

The Supplementary Material for this article can be found online at: https://www.frontiersin.org/articles/10.3389/fmars.2020.00533/full#supplementary-material

REFERENCES

Achterberg, E. P., Holland, T. W., Bowie, A. R., Mantoura, R. F. C., and Worsfold, P. J. (2001). Determination of iron in seawater. *Anal. Chim. Acta* 442, 1–14. doi: 10.1016/S0003-2670(01)01091-1

Albert, D. B., Taylor, C., and Martens, C. S. (1995). Sulfate reduction rates and low molecular weight fatty acid concentrations in the water column and surficial sediments of the Black Sea. *Deep Sea Res. Part I* 42, 1239–1260. doi: 10.1016/0967-0637(95)00042-5

Arndt, S., Jørgensen, B. B., LaRowe, D. E., Middelburg, J. J., Pancost, R. D., and Regnier, P. (2013). Quantifying the degradation of organic matter in marine sediments: a review and synthesis. *Earth Sci. Rev.* 123, 53–86. doi: 10.1016/j.earscirev.2013.02.008

Arnosti, C. (2011). Microbial extracellular enzymes and the marine carbon cycle. *Annu. Rev. Mar. Sci.* 3, 401–425. doi: 10.1146/annurev-marine-120709-142731

Arnosti, C., Fuchs, B. M., Amann, R., and Passow, U. (2012). Contrasting extracellular enzyme activities of particle-associated bacteria from distinct provinces of the north Atlantic Ocean. *Front. Microbiol.* 3:425. doi: 10.3389/fmicb.2012.00425

Bange, H. W., Rapsomanikis, S., and Andreae, M. O. (2001). Nitrous oxide cycling in the Arabian Sea. *J. Geophys. Res. Oceans* 106, 1053–1065. doi: 10.1029/1999JC000284

Barker, H. A. (1981). Amino acid degradation by anaerobic bacteria. *Annu. Rev. Biochem.* 50, 23–40. doi: 10.1146/annurev.bi.50.070181.000323

Behrenfeld, M. J., and Falkowski, P. G. (1997). Photosynthetic rates derived from satellite-based chlorophyll concentration. *Limnol. Oceanogr.* 42, 1–20. doi: 10.4319/lo.1997.42.1.0001

Bennett, E. M., Carpenter, S. R., and Caraco, N. F. (2001). Human impact on erodable phosphorus and eutrophication: a global perspective. *BioScience* 51, 227–234. doi: 10.1641/0006-35682001051[0227:hioepa]2.0.co;2

Berg, C., Beckmann, S., Jost, G., Labrenz, M., and Jürgens, K. (2013). Acetate-utilizing bacteria at an oxic-anoxic interface in the Baltic Sea. *FEMS Microbiol. Ecol.* 85, 251–261. doi: 10.1111/1574-6941.12114

Berner, R. A. (1982). Burial of organic carbon and pyrite sulfur in the modern ocean; its geochemical and environmental significance. *Am. J. Sci.* 282, 451–473. doi: 10.2475/ajs.282.4.451

Bourke, M. F., Marriott, P. J., Glud, R. N., Hasler-Sheetal, H., Kamalanathan, M., Beardall, J., et al. (2017). Metabolism in anoxic permeable sediments is dominated by eukaryotic dark fermentation. *Nat. Geosci.* 10, 30–35. doi: 10.1038/ngeo2843

Breitburg, D., Levin, L. A., Oschlies, A., Grégoire, M., Chavez, F. P., Conley, D. J., et al. (2018). Declining oxygen in the global ocean and coastal waters. *Science* 359:eaam7240. doi: 10.1126/science.aam7240

Bruland, K. W. (2006). A review of the chemistries of redox sensitive elements within suboxic zones of oxygen minimun regions. *Gayana* 70, 6–13. doi: 10.4067/s0717-65382006000300003

Canfield, D. E., Stewart, F. J., Thamdrup, B., De Brabandere, L., Dalsgaard, T., Delong, E. F., et al. (2010). A cryptic sulfur cycle in oxygen-minimum-zone waters off the Chilean coast. *Science* 30, 1375–1378. doi: 10.1126/science.1196889

Castro, C. G., Chavez, F. P., and Collins, C. A. (2001). Role of the California undercurrent in the export of denitrified waters from the eastern tropical North Pacific. *Glob. Biogeochem. Cycles* 15, 819–830. doi: 10.1029/2000GB001324

Cavan, E. L., Trimmer, M., Shelley, F., and Sanders, R. (2017). Remineralization of particulate organic carbon in an ocean oxygen minimum zone. *Nat. Commun.* 8:14847. doi: 10.1038/ncomms14847

Chronopoulou, P. M., Shelley, F., Pritchard, W. J., Maanoja, S. T., and Trimmer, M. (2017). Origin and fate of methane in the Eastern Tropical North Pacific oxygen minimum zone. *ISME J.* 11, 1386–1399. doi: 10.1038/ismej.2017.6

Chróst, R. J. (1990). "Microbial ectoenzymes in aquatic environments," in *Aquatic Microbial Ecology. Brock/Springer Series in Contemporary Bioscience*, eds J. Overbeck and R. J. Chróst (New York, NY: Springer).

Cline, J. D., and Kaplan, I. R. (1975). Isotopic fractionation of dissolved nitrate during denitrification in the eastern tropical north pacific ocean. *Mar. Chem.* 3, 271–299. doi: 10.1016/0304-4203(75)90009-2

Codispoti, L. A., Brandes, J. A., Christensen, J. P., Devol, A. H., Naqvi, S. W. A., Paerl, H. W., et al. (2001). The oceanic fixed nitrogen and nitrous oxide budgets: moving targets as we enter the anthropocene? *Sci. Mar.* 65, 85–105. doi: 10.3989/scimar.2001.65s285

Cohen, Y., and Gordon, L. I. (1978). Nitrous oxide in the oxygen minimum of the eastern tropical North Pacific: evidence for its consumption during denitrification and possible mechanisms for its production. *Deep Sea Res.* 25, 509–524. doi: 10.1016/0146-6291(78)90640-9

Conrad, R., Bak, F., Seitz, H. J., Thebrath, B., Mayer, H. P., and Schütz, H. (1989). Hydrogen turnover by psychrotrophic homoacetogenic and mesophilic methanogenic bacteria in anoxic paddy soil and lake sediment. *FEMS Microbiol. Lett.* 62, 285–293. doi: 10.1016/0378-1097(89)90010-4

Craig, H., Weiss, R. F., and Clarke, W. B. (1967). Dissolved gases in the equatorial and south Pacific Ocean. *J. Geophys. Res.* 72, 6165–6181. doi: 10.1029/jz072i024p06165

Crawford, C. C., Hobbie, J. E., and Webb, K. L. (1974). The utilization of dissolved free amino acids by estuarine microorganisms. *Ecology* 55, 551–563. doi: 10.2307/1935146

Dalsgaard, T., Stewart, F. J., Thamdrup, B., De Brabandere, L., Revsbech, N. P., Ulloa, O., et al. (2014). Oxygen at nanomolar levels reversibly suppresses process rates and gene expression in anammox and denitrification in the oxygen minimum zone off Northern Chile. *mBio* 5:e01966-14. doi: 10.1128/mBio.01966-14

Dalsgaard, T., Thamdrup, B., and Canfield, D. E. (2005). Anaerobic ammonium oxidation (anammox) in the marine environment. *Res. Microbiol.* 156, 457–464. doi: 10.1016/j.resmic.2005.01.011

Damgaard, L. R., and Hanselmann, K. (1991). Thermodyn© -A spread sheet for the calculation of free reaction energies under actual conditions. Based on K.W. Hanselmann. Microbial energetics applied to waste repositories. *Experientia* 47, 645–687.

De Pol-Holz, R., Robinson, R. S., Hebbeln, D., Sigman, D. M., and Ulloa, O. (2009). Controls on sedimentary nitrogen isotopes along the Chile margin. *Deep Sea Res. II Top. Stud. Oceanogr.* 56, 1042–1054. doi: 10.1016/j.dsr2.2008.09.014

Diaz, R. J., and Rosenberg, R. (2008). Spreading dead zones and consequences for marine ecosystems. *Science* 321, 926–929. doi: 10.1126/science.1156401

Dugdale, R. C., Goering, J. J., Barber, R. T., Smith, R. L., and Packard, T. T. (1977). Denitrification and hydrogen sulfide in the Peru upwelling region during 1976. *Deep Sea Res.* 24, 601–608. doi: 10.1016/0146-6291(77)90530-6

Escribano, R., and Morales, C. E. (2012). Spatial and temporal scales of variability in the coastal upwelling and coastal transition zones off central-southern Chile (35-40°S). *Prog. Oceanogr.* 92, 1–7. doi: 10.1016/j.pocean.2011.07.019

Escribano, R., and Schneider, W. (2007). The structure and functioning of the coastal upwelling system off central/southern Chile. *Prog. Oceanogr.* 75, 343–347. doi: 10.1016/j.pocean.2007.08.020

Farías, L., Besoain, V., and García-Loyola, S. (2015). Presence of nitrous oxide hotspots in the coastal upwelling area off central Chile: an analysis of temporal variability based on ten years of a biogeochemical time series. *Environ. Res. Lett.* 10:044017. doi: 10.1088/1748-9326/10/4/044017

Farías, L., Fernández, C., Faúndez, J., Cornejo, M., and Alcaman, M. E. (2009). Chemolithoautotrophic production mediating the cycling of the greenhouse gases N2O and CH4 in an upwelling ecosystem. *Biogeosciences* 6, 3053–3069. doi: 10.5194/bg-6-3053-2009

Fernandez, C., and Farías, L. (2012). Assimilation and regeneration of inorganic nitrogen in a coastal upwelling system: ammonium and nitrate utilization. *Mar. Ecol. Prog. Ser.* 451, 1–14. doi: 10.3354/meps09683

Finke, N., and Jørgensen, B. B. (2008). Response of fermentation and sulfate reduction to experimental temperature changes in temperate and Arctic marine sediments. *ISME J.* 2, 815–829. doi: 10.1038/ismej.2008.20

Finke, N., Vandieken, V., and Jørgensen B. B. (2006). Acetate, lactate, propionate, and isobutyrate as electron donors for iron and sulfate reduction in Arctic marine sediments, Svalbard. *FEMS Microbiol. Ecol.* 59, 10–22. doi: 10.1111/j.1574-6941.2006.00214.x

Finster, K. W., and Kjeldsen, K. U. (2010). Desulfovibrio oceani subsp. oceani sp. nov., subsp. nov. and Desulfovibrio oceani subsp. galateae subsp. nov., novel sulfate-reducing bacteria isolated from the oxygen minimum zone off the coast of Peru. *Antonie van Leeuwenhoek* 97, 221–229. doi: 10.1007/s10482-009-9403-y

Fossing, H., Gallardo, V. A., Jørgensen, B. B., Hüttel, M., Nielsen, L. P., Schulz, H., et al. (1995). Concentration and transport of nitrate by the mat-forming sulphur bacterium Thioploca. *Nature* 374, 713–715. doi: 10.1038/374713a0

Francis, C. A., Roberts, K. J., Beman, J. M., Santoro, A. E., and Oakley, B. B. (2005). Ubiquity and diversity of ammonia-oxidizing archaea in water columns and sediments of the ocean. *Proc. Natl. Acad. Sci. U.S.A.* 102, 14683–14688. doi: 10.1073/pnas.0506625102

Froelich, P. N., Klinkhammer, G. P., Bender, M. L., Luedtke, N. A., Heath, G. R., Cullen, D., et al. (1979). Early oxidation of organic matter in pelagic sediments of the eastern equatorial Atlantic: suboxic diagenesis. *Geochim. Cosmochim. Acta* 43, 1075–1090. doi: 10.1016/0016-7037(79)90095-4

Fuenzalida, R., Schneider, W., Garcés-Vargas, J., Bravo, L., and Lange, C. (2009). Vertical and horizontal extension of the oxygen minimum zone in the eastern South Pacific Ocean. *Deep Sea Res. II Top. Stud. Oceanogr.* 56, 992–1003. doi: 10.1016/j.dsr2.2008.11.001

Fuhrman, J. (1987). Close coupling between release and uptake of dissolved free amino acids in seawater studied by an isotope dilution approach. *Mar. Ecol. Prog. Ser.* 37, 45–52. doi: 10.3354/meps037045

Galán, A., Fauñdez, J., Thamdrup, B., Santibáñez, J. F., and Farías, L. (2014). Temporal dynamics of nitrogen loss in the coastal upwelling ecosystem off central chile: evidence of autotrophic denitrification through sulfide oxidation. *Limnol. Oceanogr.* 59, 1865–1878. doi: 10.4319/lo.2014.59.6.1865

Galán, A., Thamdrup, B., Saldías, G. S., and Farías, L. (2017). Vertical segregation among pathways mediating nitrogen loss (N2 and N2O production) across the oxygen gradient in a coastal upwelling ecosystem. *Biogeosciences* 14, 4795–4813. doi: 10.5194/bg-14-4795-2017

González, H. E., Daneri, G., Iriarte, J. L., Yannicelli, B., Menschel, E., Barría, C., et al. (2009). Carbon fluxes within the epipelagic zone of the Humboldt Current System off Chile: the significance of euphausiids and diatoms as key functional groups for the biological pump. *Prog. Oceanogr.* 83, 217–227. doi: 10.1016/j.pocean.2009.07.036

González, R. R., and Quiñones, R. A. (2009). Common catabolic enzyme patterns in a microplankton community of the Humboldt Current System off northern and central-south Chile: malate dehydrogenase activity as an index of water-column metabolism in an oxygen minimum zone. *Deep Sea Res. II Top. Stud. Oceanogr.* 56, 1095–1104. doi: 10.1016/j.dsr2.2008.09.012

Gruber, N., and Sarmiento, J. L. (1997). Global patterns of marine nitrogen fixation and denitrification. *Glob. Biogeochem. Cycles* 11, 235–266. doi: 10.1029/97GB00077

Gutiérrez, M. H., Pantoja, S., Tejos, E., and Quiñones, R. A. (2011). The role of fungi in processing marine organic matter in the upwelling ecosystem off Chile. *Mar. Biol.* 158, 205–219. doi: 10.1007/s00227-010-1552-z

Hansell, D. A., Bates, N. R., and Olson, D. B. (2004). Excess nitrate and nitrogen fixation in the North Atlantic Ocean. *Mar. Chem.* 84, 243–265. doi: 10.1016/j.marchem.2003.08.004

Helly, J. J., and Levin, L. A. (2004). Global distribution of naturally occurring marine hypoxia on continental margins. *Deep Sea Res.* 51, 1159–1168. doi: 10.1016/j.dsr.2004.03.009

Ho, T. Y., Scranton, M. I., Taylor, G. T., Varela, R., Thunell, R. C., and Muller-Karger, F. (2002). Acetate cycling in the water column of the Cariaco Basin: seasonal and vertical variability and implication for carbon cycling. *Limnol. Oceanogr.* 47, 1119–1128. doi: 10.4319/lo.2002.47.4.1119

Hoppe, H. G., Kim, S. J., and Gocke, K. (1988). Microbial decomposition in aquatic environments: combined process of extracellular enzyme activity and substrate uptake. *Appl. Environ. Microbiol.* 54, 784–790.

Howarth, R. W. (2008). Coastal nitrogen pollution: a review of sources and trends globally and regionally. *Harmful Algae* 8, 14–20. doi: 10.1016/j.hal.2008.08.015

Hungate, R. E. (1965). "Quantitative aspects of the rumen fermentations," in *Physiology of Digestion in the Ruminant*, ed. R. W. Dougherty (Washington, D.C: Butterworths), 311–321.

Jansson, B. P. M., Malandrin, L., and Johansson, H. E. (2000). Cell cycle arrest in archaea by the hypusination inhibitor N1-guanyl- 1,7-diaminoheptane. *J. Bacteriol.* 182, 1158–1161. doi: 10.1128/JB.182.4.1158-1161.2000

Jørgensen, B. B. (1982). Mineralization of organic matter in the sea bed–the role of sulphate reduction. *Nature* 296, 643–645. doi: 10.1038/296643a0

Jørgensen, B. B., and Kasten, S. (2006). "Sulfur cycling and methane oxidation," in *Marine Geochemistry*, eds H. D. Schulz and M. Zabel (Berlin: Springer), 271–309.

Kamykowski, D., and Zentara, S. J. (1990). Hypoxia in the world ocean as recorded in the historical data set. *Deep Sea Res. A Oceanogr. Res. Pap.* 37, 1861–1874. doi: 10.1016/0198-0149(90)90082-7

Kartal, B., De Almeida, N. M., Maalcke, W. J., Op den Camp, H. J. M., Jetten, M. S. M., and Keltjens, J. T. (2013). How to make a living from anaerobic ammonium oxidation. *FEMS Microbiol. Rev.* 37, 428–461. doi: 10.1111/1574-6976.12014

Kock, A., Arevalo-Martinez, D. L., Loscher, C. R., and Bange, H. W. (2016). Extreme N2O accumulation in the coastal oxygen minimum zone off Peru. *Biogeosciences* 13, 827–840. doi: 10.5194/bg-13-827-2016

Könneke, M., Bernhard, A. E., De La Torre, J. R., Walker, C. B., Waterbury, J. B., and Stahl, D. A. (2005). Isolation of an autotrophic ammonia-oxidizing marine archaeon. *Nature* 437, 543–546. doi: 10.1038/nature03911

Kuenen, J. G. (2008). Anammox bacteria: from discovery to application. *Nat. Rev. Microbiol.* 6, 320–326. doi: 10.1038/nrmicro1857

Kuypers, M. M. M., Lavik, G., Woebken, D., Schmid, M., Fuchs, B. M., Amann, R., et al. (2005). Massive nitrogen loss from the Benguela upwelling system through anaerobic ammonium oxidation. *Proc. Natl. Acad. Sci.* 102, 6478–6483. doi: 10.1073/pnas.0502088102

Lam, P., Lavik, G., Jensen, M. M., van de Vossenberg, J., Schmid, M., Woebken, D., et al. (2009). Revising the nitrogen cycle in the Peruvian oxygen minimum zone. *Proc. Natl. Acad. Sci.* 106, 4752–4757. doi: 10.1073/pnas.0812444106

Lavik, G., Stührmann, T., Brüchert, V., Van Der Plas, A., Mohrholz, V., Lam, P., et al. (2009). Detoxification of sulphidic African shelf waters by blooming chemolithotrophs. *Nature* 457, 581–584. doi: 10.1038/nature07588

Lee, C. (1992). Controls on organic carbon preservation: the use of stratified water bodies to compare intrinsic rates of decomposition in oxic and anoxic systems. *Geochim. Cosmochim. Acta* 56, 3323–3335. doi: 10.1016/0016-7037(92)90308-6

Letelier, J., Pizarro, O., and Nuñez, S. (2009). Seasonal variability of coastal upwelling and the upwelling front off central Chile. *J. Geophys. Res. Oceans* 114:C12009. doi: 10.1029/2008JC005171

Lindroth, P., and Mopper, K. (1979). High performance liquid chromatographic determination of subpicomole amounts of amino acids by precolumn fluorescence derivatization with o-phthaldialdehyde. *Anal. Chem.* 51, 1667–1674. doi: 10.1021/ac50047a019

Lipschultz, F., Wofsy, S. C., Ward, B. B., Codispoti, L. A., Friedrich, G., and Elkins, J. W. (1990). Bacterial transformations of inorganic nitrogen in the oxygen-deficient waters of the Eastern Tropical South Pacific Ocean. *Deep Sea Res. A* 37, 1513–1541. doi: 10.1016/0198-0149(90)90060-9

Liu, K. K., and Kaplan, I. R. (1989). The eastern tropical Pacific as a source of 15N-enriched nitrate in seawater off southern California. *Limnol. Oceanogr.* 34, 820–830. doi: 10.4319/lo.1989.34.5.0820

Löscher, C. R., Bange, H. W., Schmitz, R. A., Callbeck, C. M., Engel, A., Hauss, H., et al. (2016). Water column biogeochemistry of oxygen minimum zones in the eastern tropical North Atlantic and eastern tropical South Pacific oceans. *Biogeosciences* 13, 3585–3606. doi: 10.5194/bg-13-3585-2016

Lovley, D. (2006). "Dissimilatory Fe(III)- and Mn(IV)-Reducing prokaryotesin," in *The Prokaryotes*, eds M. Dworkin, S. Falkow, E. Rosenberg, K.-H. Schleifer, and E. Stackebrandt (Berlin: Springer-Verlag), 287–308.

Megonigal, J. P., Mines, M. E., and Visscher, P. T. (2004). "Linkages to trace gases and aerobic processes," in *Biogeochemistry*, ed. W. H. Schlesinger (Oxford, UK: Elsevier-Pergamon), 317–424.

Michels, P. A. M., Michels, J. P. J., Boonstra, J., and Konings, W. N. (1979). Generation of an electrochemical proton gradient in bacteria by the excretion of metabolic end products. *FEMS Microbiol. Lett.* 5, 357–364. doi: 10.1111/j.1574-6968.1979.tb03339.x

Milligan, A. J., and Harrison, P. J. (2000). Effects of non-steady-state iron limitation on nitrogen assimilatory enzymes in the marine diatom *Thalassiosira weissflogii* (Bacillariophyceae). *J. Phycol.* 36, 78–86. doi: 10.1046/j.1529-8817.2000.99013.x

Moffett, J. W., Goepfert, T. J., and Naqvi, S. W. A. (2007). Reduced iron associated with secondary nitrite maxima in the Arabian Sea. *Deep Sea Res. I* 54, 1341–1349. doi: 10.1016/j.dsr.2007.04.004

Molina, V., Farías, L., Eissler, Y., Cuevas, L. A., Morales, C. E., and Escribano, R. (2005). Ammonium cycling under a strong oxygen gradient associated with the Oxygen Minimum Zone off northern Chile (23°S). *Mar. Ecol. Prog. Ser.* 288, 35–43. doi: 10.3354/meps288035

Montero, P., Daneri, G., Cuevas, L. A., González, H. E., Jacob, B., Lizárraga, L., et al. (2007). Productivity cycles in the coastal upwelling area off Concepción: the importance of diatoms and bacterioplankton in the organic carbon flux. *Prog. Oceanogr.* 75, 518–530. doi: 10.1016/j.pocean.2007.08.013

Mopper, K., and Kieber, D. J. (1991). Distribution and biological turnover of dissolved organic compounds in the water column of the Black Sea. *Deep Sea Res. A* 38, 1021–1047. doi: 10.1016/s0198-0149(10)80022-6

Moser-Engeler, R., Udert, K. M., Wild, D., and Siegrist, H. (1998). Products from primary sludge fermentation and their suitability for nutrient removal. *Water Sci. Technol.* 38, 265–273. doi: 10.1016/S0273-1223(98)00411-9

Mueller-Harvey, I., and John Parkes, R. (1987). Measurement of volatile fatty acids in pore water from marine sediments by HPLC. *Estua. Coast. Shelf Sci.* 25, 567–579. doi: 10.1016/0272-7714(87)90115-6

Naqvi, S. W. A., Bange, H. W., Farías, L., Monteiro, P. M. S., Scranton, M. I., and Zhang, J. (2010). Marine hypoxia/anoxia as a source of CH 4 and N 2O. *Biogeosciences* 7, 2159–2190. doi: 10.5194/bg-7-2159-2010

Naqvi, S. W. A., Jayakumar, D. A., Narvekar, P. V., Naik, H., Sarma, V. V. S. S., D'Souza, W., et al. (2000). Increased marine production of N2O due to intensifying anoxia on the Indian continental shelf. *Nature* 408, 346–349. doi: 10.1038/35042551

Nieuwenhuize, J., Maas, Y. E. M., and Middelburg, J. J. (1994). Rapid analysis of organic carbon and nitrogen in particulate materials. *Mar. Chem.* 45, 217–224. doi: 10.1016/0304-4203(94)90005-1

Nisman, B. (1954). The Stickland reaction. *Bacteriol. Rev.* 18, 16–42. doi: 10.1201/9781351071505-3

Oremland, R. S. (1988). "Biogeochemistry of methanogenic bacteria," in *Biology of Anaerobic Microorganisms*, ed. A. J. B. Zehnder (Hoboken, NJ: John Wiley & Sons), 641–705.

Oremland, R. S., and Capone, D. G. (1988). "Use of 'Specific' inhibitors in biogeochemistry and microbial ecology," in *Advances in Microbial Ecology*, ed. K. C. Marshall (Boston, MA: Springer).

Oremland, R. S., and Polcin, S. (1982). Methanogenesis and sulfate reduction: competitive and noncompetitive substrates in estuarine sediments. *Appl. Environ. Microbiol.* 44, 1270–1276. doi: 10.1128/aem.44.6.1270-1276.1982

Pantoja, S., Rossel, P., Castro, R., Cuevas, L. A., Daneri, G., and Córdova, C. (2009). Microbial degradation rates of small peptides and amino acids in the oxygen minimum zone of Chilean coastal waters. *Deep Sea Res. II Top. Stud. Oceanogr.* 56, 1055–1062. doi: 10.1016/j.dsr2.2008.09.007

Parkes, R. J., Gibson, G. R., Mueller-Harvey, I., Buckingham, W. J., and Herbert, R. A. (1989). Determination of the substrates for sulphate-reducing bacteria within marine and esturaine sediments with different rates of sulphate reduction. *Microbiology* 135, 175–187. doi: 10.1099/00221287-135-1-175

Pilson, M. E. Q. (2012). *An Introduction to the Chemistry of the Sea*. Cambridge, MA: Cambridge University Press.

Pizarro-Koch, M., Pizarro, O., Dewitte, B., Montes, I., Ramos, M., Paulmier, A., et al. (2019). Seasonal variability of the southern tip of the oxygen minimum zone in the Eastern South Pacific (30°-38°S): a modeling study. *J. Geophys. Res. Oceans* 124, 8574–8604. doi: 10.1029/2019JC015201

Prüss, B. M., Nelms, J. M., Park, C., and Wolfe, A. J. (1994). Mutations in NADH: ubiquinone oxidoreductase of *Escherichia coli* affect growth on mixed amino acids. *J. Bacteriol.* 176, 2143–2150.

Rabalais, N., Cai, W.-J., Carstensen, J., Conley, D., Fry, B., Hu, X., et al. (2014). Eutrophication-driven deoxygenation in the Coastal Ocean. *Oceanography* 27, 172–183. doi: 10.5670/oceanog.2014.21

Sabine, J. R., and Johnson, B. C. (1964). Acetate metabolism in the ruminant. *J. Biol. Chem.* 239, 89–93.

Sansone, F. J., and Martens, C. S. (1981). Determination of volatile fatty acid turnover rates in organic-rich marine sediments. *Mar. Chem.* 10, 233–247. doi: 10.1016/0304-4203(81)90044-X

Sansone, F. J., and Martens, C. S. (1982). Volatile fatty acid cycling in organic-rich marine sediments. *Geochim. Cosmochim. Acta* 46, 1575–1589. doi: 10.1016/0016-7037(82)90315-5

Schlitzer, R. (2010). *Ocean Data View Version 4.3.6*. Bremerhaven: Alfred Wegener Institute. Available online at: http://odv.awi.de/

Schmidtko, S., Stramma, L., and Visbeck, M. (2017). Decline in global oceanic oxygen content during the past five decades. *Nature* 542, 335–339. doi: 10.1038/nature21399

Schmitz, R. A., Daniel, R., Deppenmeier, U., and Gottschalk, G. (2006). "The anaerobic way of life," in *The Prokaryotes*, eds E. Rosenberg, E. F. DeLong, S. Lory, E. Stackebrandt, and F. Thompson (Berlin: Springer).

Schneider, W., Donoso, D., Garcés-Vargas, J., and Escribano, R. (2017). Water-column cooling and sea surface salinity increase in the upwelling region off central-south Chile driven by a poleward displacement of the South Pacific High. *Prog. Oceanogr.* 151, 38–48. doi: 10.1016/j.pocean.2016.11.004

Schneider, W., Fuenzalida, R., Garcés-Vargas, J., Bravo, L., and Lange, C. (2006). Vertical and horizontal extension of the oxygen minimum zone in the easterns south Pactific Ocean. *Gayana* 70(Suppl.1), 79–82. doi: 10.4067/s0717-65382006000300016

Schneider, W., Fuenzalida, R., Rodríguez-Rubio, E., Garcés-Vargas, J., and Bravo, L. (2003). Characteristics and formation of Eastern South Pacific intermediate water. *Geophys. Res. Lett.* 30:1581. doi: 10.1029/2003GL017086

Schoemann, V., De Baar, H. J. W., De Jong, J. T. M., and Lancelot, C. (1998). Effects of phytoplankton blooms on the cycling of manganese and iron in coastal waters. *Limnol. Oceanogr.* 43, 1427–1441. doi: 10.4319/lo.1998.43.7.1427

Schunck, H., Lavik, G., Desai, D. K., Großkopf, T., Kalvelage, T., Löscher, C. R., et al. (2013). Giant hydrogen sulfide plume in the oxygen minimum zone off peru supports chemolithoautotrophy. *PLoS One* 8:e68661. doi: 10.1371/journal.pone.0068661

Schwertmann, U., and Cornell, R. M. (1991). *Iron Oxides in the Laboratory: Preparation and characterization*. Weinheim: VCH.

Segovia-Zavala, J. A., Delgadillo-Hinojosa, F., Huerta-Díaz, M. Á, Muñoz-Barbosa, A., Galindo-Bect, M. S., Hernández-Ayón, J. M., et al. (2013). Concentración de hierro disuelto en la zona del mínimo de oxígeno frente al umbral de San Esteban, golfo de California. *Ciencias Mar.* 39, 231–237. doi: 10.7773/cm.v39i2.2199

Seiler, W., and Schmidt, U. (1974). "Dissolved nonconservative gases in seawater," in *The Sea*, ed. E. D. Goldberg (New York, NY: Wiley lnterscience), 219–244.

Sempéré, R., Tedetti, M., Panagiotopoulos, C., Charrière, B., and Van Wambeke, F. (2008). Distribution and bacterial availability of dissolved neutral sugars in the South East Pacific. *Biogeosciences* 5, 1165–1173. doi: 10.5194/bg-5-1165-2008

Shaw, D. G., Alperin, M. J., Reeburgh, W. S., and McIntosh, D. J. (1984). Biogeochemistry of acetate in anoxic sediments of Skan Bay, Alaska. *Geochim. Cosmochim. Acta* 48, 1819–1825. doi: 10.1016/0016-7037(84)90035-8

Shrivastava, A., and Gupta, V. (2011). Methods for the determination of limit of detection and limit of quantitation of the analytical methods. *Chron. Young Sci.* 2, 15–21. doi: 10.4103/2229-5186.79345

Sigman, D. M., Robinson, R., Knapp, A. N., Van Geen, A., McCorkle, D. C., Brandes, J. A., et al. (2003). Distinguishing between water column and sedimentary denitrification in the Santa Barbara Basin using the stable isotopes of nitrate. *Geochem. Geophys. Geosyst.* 4:1040. doi: 10.1029/2002GC000384

Silva, N., Rojas, N., and Fedele, A. (2009). Water masses in the Humboldt Current system: properties, distribution, and the nitrate deficit as a chemical water mass tracer for Equatorial Subsurface Water off Chile. *Deep Sea Res. II Top. Stud. Oceanogr.* 56, 1004–1020.

Skyring, G. W. (1988). Acetate as the main energy substrate for the sulfate-reducing bacteria in Lake Eliza (South Australia) hypersaline sediments. *FEMS Microbiol. Lett.* 4, 87–93. doi: 10.1016/0378-1097(88)90016-X

Skyring, G. W., Chambers, L. A., and Bauld, J. (1983). Sulfate reduction in sediments colonized by cyanobacteria, spencer gulf, south australia. *Mar. Freshw. Res.* 34, 359–374. doi: 10.1071/MF9830359

Slack, G. C., Snow, N. H., and Kou, D. (2003). "Extraction of volatile organic compounds from solids and liquids," in *Sample Preparation Techniques in Analytical Chemistry*, ed. S. Mitra (Canada: John Wiley & Sons).

Sobarzo, M., Bravo, L., Donoso, D., Garcés-Vargas, J., and Schneider, W. (2007). Coastal upwelling and seasonal cycles that influence the water column over the continental shelf off central Chile. *Prog. Oceanogr.* 75, 363–382. doi: 10.1016/j.pocean.2007.08.022

Sobarzo, M., Figueroa, M., and Djurfeldt, L. (2001). Upwelling of subsurface water into the rim of the Biobío submarine canyon as a response to surface winds. *Continent. Shelf Res.* 21, 279–299. doi: 10.1016/S0278-4343(00)00082-0

Sørensen, J., Christensen, D., and Jørgensen, B. B. (1981). Volatile fatty acids and hydrogen as substrates for sulfate-reducing bacteria in anaerobic marine sediment. *Appl. Environ. Microbiol.* 42, 5–11. doi: 10.1128/aem.42.1.5-11.1981

Srain, B., Sepúlveda, J., Pantoja, S., Summons, R. E., Quiñones, R. A., and Levipan, H. A. (2015). Archaeal and bacterial assemblages in the Oxygen Minimum Zone of the upwelling ecosystem off Central Chile as determined by organic biomarkers. *Gayana* 79, 26–44. doi: 10.4067/s0717-65382015000100005

Stickland, L. H. (1934). The chemical reactions by which C. sporogenes obtains its energy. *Biochem. J.* 28, 1746–1759.

Suzuki, D., Ueki, A., Amaishi, A., and Ueki, K. (2007). *Desulfobulbus japonicus* sp. nov., a novel Gram-negative propionate-oxidizing, sulfate-reducing bacterium isolated from an estuarine sediment in Japan. *Int. J. Syst. Evol. Microbiol.* 57(Pt 4), 849–855. doi: 10.1099/ijs.0.64855-0

Testa, G., Masotti, I., and Farías, L. (2018). Temporal variability in net primary production in an upwelling area off Central Chile (36°S). *Front. Mar. Sci.* 5:179. doi: 10.3389/fmars.2018.00179

Thamdrup, B., Dalsgaard, T., Jensen, M. M., Ulloa, O., Farías, L., and Escribano, R. (2006). Anaerobic ammonium oxidation in the oxygen-deficient waters off northern Chile. *Limnol. Oceanogr.* 51, 2145–2156. doi: 10.4319/lo.2006.51.5.2145

Ulloa, O., Canfield, D. E., DeLong, E. F., Letelier, R. M., and Stewart, F. J. (2012). Microbial oceanography of anoxic oxygen minimum zones. *Proc. Natl. Acad. Sci.U.S.A.* 109, 15996–16003. doi: 10.1073/pnas.1205009109

Vaquer-Sunyer, R., and Duarte, C. M. (2008). Thresholds of hypoxia for marine biodiversity. *Proc. Natl. Acad. Sci. U.S.A.* 105, 15452–15457. doi: 10.1073/pnas.0803833105

Venter, J. C., Remington, K., Heidelberg, J. F., Halpern, A. L., Rusch, D., Eisen, J. A., et al. (2004). Environmental genome shotgun sequencing of the sargasso Sea. *Science* 304, 66–74. doi: 10.1126/science.1093857

Wagner, R. D., Warner, T., Roberts, L., Farmer, J., and Balish, E. (1997). Colonization of congenitally immunodeficient mice with probiotic bacteria. *Infect. Immun.* 65, 3345–3351. doi: 10.1128/iai.65.8.3345-3351.1997

Ward, B. B., Devol, A. H., Rich, J. J., Chang, B. X., Bulow, S. E., Naik, H., et al. (2009). Denitrification as the dominant nitrogen loss process in the Arabian Sea. *Nature* 461, 78–81. doi: 10.1038/nature08276

Webb, K. L., and Johannes, R. E. (1967). Studies of the release of dissolved free amino acids by marine zooplankton. *Limnol. Oceanogr.* 12, 376–382. doi: 10.4319/lo.1967.12.3.0376

Weiss, M. S., Abele, U., Weckesser, J., Welte, W., Schiltz, E., and Schulz, G. E. (1991). Molecular architecture and electrostatic properties of a bacterial porin. *Science* 254, 1627–1630. doi: 10.1126/science.1721242

Wolfe, A. J. (2005). The acetate switch. *Microbiol. Mol. Biol. Rev.* 69, 12–50. doi: 10.1128/mmbr.69.1.12-50.2005

Wolfe, R. S. (2011). Techniques for cultivating methanogens. *Methods Enzymol.* 494, 1–22. doi: 10.1016/B978-0-12-385112-3.00001-9

Wright, J. J., Konwar, K. M., and Hallam, S. J. (2012). Microbial ecology of expanding oxygen minimum zones. *Nat. Rev. Microbiol.* 10, 381–394. doi: 10.1038/nrmicro2778

Wu, H., Green, M., and Scranton, M. I. (1997). Acetate cycling in the water column and surface sediment of Long Island Sound following a bloom. *Limnol. Oceanogr.* 42, 705–713. doi: 10.4319/lo.1997.42.4.0705

Wu, H., and Scranton, M. I. (1994). Cycling of some low molecular weight volatile fatty acids in a permanently anoxic estuarine basin. *Mar. Chem.* 47, 97–113. doi: 10.1016/0304-4203(94)90102-3

Wyrtki, K. (1962). The oxygen minima in relation to ocean circulation. *Deep Sea Res. Oceanogr. Abstr.* 9, 11–23. doi: 10.1016/0011-7471(62)90243-7

Zhuang, G. C., Peña-Montenegro, T. D., Montgomery, A., Montoya, J. P., and Joye, S. B. (2019). Significance of acetate as a microbial carbon and energy source in the water column of gulf of Mexico: implications for marine carbon cycling. *Glob. Biogeochem. Cycles* 33, 223–235. doi: 10.1029/2018GB006129

Conflict of Interest: The authors declare that the research was conducted in the absence of any commercial or financial relationships that could be construed as a potential conflict of interest.

frontiers in Marine Science

ORIGINAL RESEARCH
published: 20 August 2020
doi: 10.3389/fmars.2020.00675

Influence of Algal Production and Decomposition on the Carbon Isotope Signature of Labile Particulate Organic Matter on a Productive Continental Shelf Under the Stress of Coastal Hypoxia

*Zixiang Yang[1,2], Han Zhang[3], Peihong Kang[1,2], Yangyang Zhao[1,2] and Tiantian Tang[1,2]**

[1] State Key Laboratory of Marine Environmental Science, Xiamen University, Xiamen, China, [2] College of Ocean and Earth Sciences, Xiamen University, Xiamen, China, [3] Key Laboratory of Urban Environment and Health, Institute of Urban Environment, Chinese Academy of Sciences, Xiamen, China

OPEN ACCESS

Edited by:
Stuart Wakeham,
University of Georgia, United States

Reviewed by:
Ying Wu,
East China Normal University, China
Hilary G. Close,
University of Miami, United States

***Correspondence:**
Tiantian Tang
tiantian.tang@xmu.edu.cn

Specialty section:
This article was submitted to Marine Biogeochemistry, a section of the journal Frontiers in Marine Science

Received: 29 February 2020
Accepted: 24 July 2020
Published: 20 August 2020

Citation:
Yang Z, Zhang H, Kang P, Zhao Y and Tang T (2020) Influence of Algal Production and Decomposition on the Carbon Isotope Signature of Labile Particulate Organic Matter on a Productive Continental Shelf Under the Stress of Coastal Hypoxia. Front. Mar. Sci. 7:675. doi: 10.3389/fmars.2020.00675

To better understand the sources and recycling of labile organic matter in coastal water, we studied the carbon isotope signature of particulate organic carbon (POC) and particulate amino acids, a major group of labile organic compounds, on the shelf of the northern South China Sea. In addition, we were able to compare effects of hypoxia on labile organic matter at one station on the shelf. We found that carbon-weighted average $\delta^{13}C$ values of particulate amino acids (*w*AA$\delta^{13}C$) were generally higher at more productive offshore stations than nearshore stations. This amino acid $\delta^{13}C$ distribution suggests that the labile fraction of organic matter in coastal water originated primarily from local primary production. In contrast, bulk POC $\delta^{13}C$ (PO^{13}C) values showed little spatial variation on the NSCS shelf. The different patterns of *w*AA$\delta^{13}C$ and PO^{13}C distributions indicate a combined effect of POM lability and physical processes on the isotopic distribution of organic materials on this productive shelf. Moreover, the amino acid $\delta^{13}C$ in coastal hypoxic water suggests local primary production as the most likely source of labile organic matter that drives hypoxia on the NSCS shelf. No clear difference was observed in particulate amino acid $\delta^{13}C$ distribution between hypoxic and oxic waters.

Keywords: hypoxia, continental shelf, labile organic carbon, amino acids, compound specific isotope analysis (CSIA)

INTRODUCTION

Usually, algal organic carbon is depleted in ^{13}C relative to its inorganic carbon source, i.e., dissolved CO_2 in seawater (Freeman, 2001). This RuBisCo catalyzed isotope fractionation has a linear relationship with the ratio of growth rate (μ) over [CO_2] (μ/[CO_2], Laws et al., 1995; Popp et al., 1998; Burkhardt et al., 1999). The carbon fixed by cells is used to synthesize biomolecules

through diverse metabolic pathways, which results in intracellular isotope fractionations among biomolecules (Hayes, 2001). Thus, carbon isotope signatures of individual organic compounds are determined by the inorganic carbon source, the RuBisCo catalyzed isotope fractionation, and the intracellular isotope fractionation that occurs during compound synthesis.

Amino acids (AA) are a major class of cellular compounds in algae. In the marine environment, AA are considered to be a biomarker of labile organic carbon because AA can be preferentially decomposed (Wakeham et al., 1997; Benner and Amon, 2015; Wakeham and Lee, 2019). The rapid development of compound specific isotopic analysis of individual AA has provided a new tool to investigate geochemical behavior of these labile organic carbon compounds (Close, 2019). AA carbon isotopes are used to determine the metabolic origins of organic matter from terrestrial organisms, microalgae, bacteria, even the same species grown in different metabolic patterns (Larsen et al., 2009, 2013, 2015; Tang et al., 2017b). In marine environments, the carbon isotope ratios of AA are subject to decompositional modification. Bacterial reworking of AA carbon isotopes has been identified in estuarine sediments, particles, and dissolved organic matter (Keil et al., 2001; McCarthy et al., 2004; Hannides et al., 2013). However, there is little information on the AA carbon isotope distribution in productive coastal oceans, particularly in areas under the stress of coastal hypoxia. Hypoxic waters have microbial communities and metabolisms that are very different from those of oxic seawater (e.g., Liu et al., 2017). We don't presently know how AA carbon isotopes respond to the characteristic hypoxic metabolism found in coastal environment.

The ocean, particularly the coastal ocean, has experienced a decline in oxygen concentrations and an increase of hypoxia (usually defined as DO <2 mg L^{-1}, or <65 μmol kg^{-1}) over the past century, primarily due to anthropogenic activity (Breitburg et al., 2018). Both natural and anthropogenic terrestrial sources bring abundant nutrients and organic carbon into coastal waters; decomposition of both terrestrial organic matter and the organic matter formed during local primary production can lower oxygen concentrations (Kemp et al., 1992; Rabalais et al., 2014). More frequent summer hypoxia has been documented on the shallow shelf of the northern South China Sea (NSCS) due to increasing loading of nutrients and organic carbon from the adjacent Pearl River system (Su et al., 2017; Lu et al., 2018; Zhao et al., 2020). Even though hypoxia is related to the remineralization of excess organic carbon, not all organic matter can be quickly or easily remineralized because of the varying reactivity and bioavailability of the organic compounds that make up organic matter (Benner and Amon, 2015). AA and other labile organic compounds can be easily decomposed into CO_2. Therefore, accumulation and subsequent decomposition of labile organic matter can effectively cause hypoxia in a short time. Labile organic carbon on the NSCS shelf comes mainly from two sources: *in situ* growth of phytoplankton on the shelf (Zhang and Li, 2010) and discharge from the Pearl River. The relative contribution of these two sources to the spreading summer hypoxia at the mouth of the Pearl River Estuary (PRE) is currently not clear.

Here we used AA carbon isotope signatures (AA $\delta^{13}C$) in particulate matter to investigate the sources and recycling of labile organic carbon in coastal waters along a transect across the inner shelf of the NSCS in the summer of 2018. At this time, oxygen concentrations were generally lower in bottom waters, but bottom hypoxia was observed at one site near the transect. After a tropical storm passed through our study area, we revisited that station, which had been replenished with oxygen, so that a comparison between hypoxic and oxic conditions was possible. Below, we present the general distribution of carbon isotope signatures of particulate AA and organic carbon along the transect, which provides the first set of information on isotopic geochemistry of labile organic carbon on this productive shelf system.

MATERIALS AND METHODS

Sample Collection

During a cruise on the R/V Haike 68, a transect across the inner NSCS shelf was surveyed seaward from the mouth of the PRE on July 12, 2018 (station information are shown in **Figure 1** and **Supplementary Table 1**). All sampling from Sta. A8–A14 was taken within a 14-h period while tidal movement was offshore. Water samples were collected from the surface (S, 1 m) and bottom (B, 12–25 m) of the water column using a Niskin Rosette sampler with a CTD profiler attached. Water samples were also collected beneath the surface mixed layer (M, 7–15 m) where temperature and salinity profiles showed strong stratification. Bottom hypoxia had been observed at station F303 (F303H) near transect A on July 11, 2018. The cruise was interrupted by Tropical Storm Son-Tinh which landed on Hainan Island on July 18, 2018. After the storm, we resampled Sta. F303 (F303O) on July 19, when the bottom water had been replenished with oxygen.

Particulate matter was collected by filtering the water samples of about 1 L through precombusted GFF filters, and then storing them at −20°C. Two filters were collected for each water sample, one for bulk organic carbon analysis, the other for compound specific analysis of AA. Salinity, temperature and bottle depth were provided by a CTD profiler (SBE21, Seabird). The concentrations of dissolved oxygen were measured on board by the Winkler method (Pai et al., 1993). The chl*a* concentrations were measured by a fluorometer after extracting filters with acetone.

Bulk Organic Carbon Concentrations and Bulk $PO^{13}C$ Values

Bulk organic carbon concentration on filters was analyzed following the method of Kao et al. (2012). Before analysis of bulk $PO^{13}C$, filters were dried overnight at 60°C and acidified with drops of 1 N HCl to remove any carbonate. The acidified filters were dried again overnight at 60°C, and placed in precombusted nickel cups. Organic carbon on the filters was converted to CO_2 on an Elemental analyzer (EA, Isoprime 500). The $^{13}CO_2/^{12}CO_2$ ratios were measured by coupled isotopic ratio mass spectrometry (EA-IRMS, Isoprime 500). The stable isotope standards glutamic acid (USGS-40) and acetanilide (Merck) were used to calibrate the $\delta^{13}C$ ratios and concentrations of bulk organic carbon samples, with a standard deviation of 0.09‰

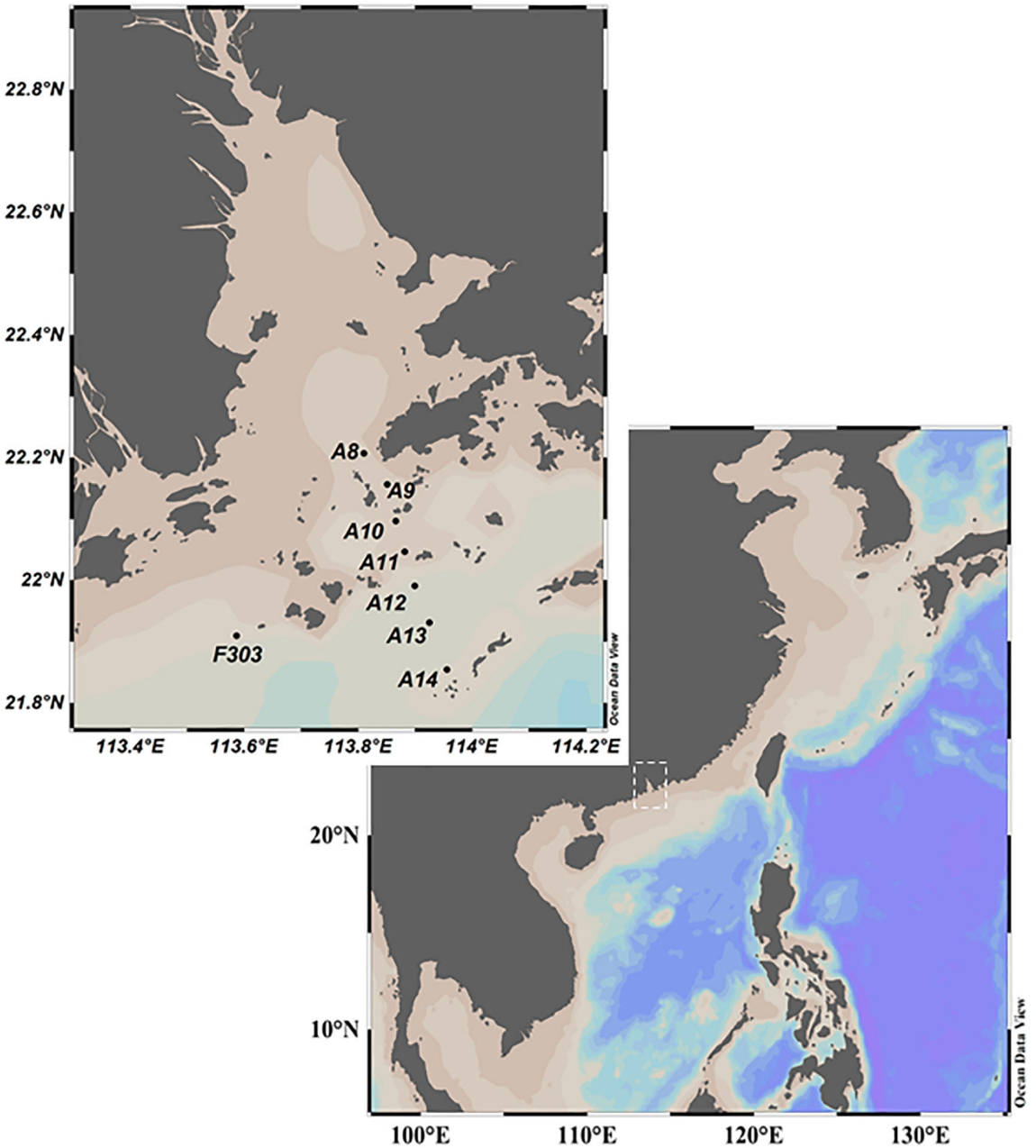

FIGURE 1 | Location of sampling sites on the shelf of the northern South China Sea (NSCS) in July 2018. Figure was produced using Ocean Data View (version 5.1.7).

(n = 14) for $\delta^{13}C$ ratios and a relative standard deviation of 2.9% (n = 13) for concentrations.

Amino Acid Concentrations and $\delta^{13}C$ Values

Amino acid $\delta^{13}C$ ratios were analyzed following a modification (Tang et al., 2017b) of Silfer et al. (1991). Combined AA were released by hydrolyzing filters in 6 N HCl (trace-metal clean, Sigma-Aldrich) for 20 h at 110°C. The hydrolyzate was purified following Takano et al. (2010). Briefly, the hydrolyzate was dried with a stream of N_2 gas, redissolved in 0.1 N HCl, and loaded onto a pipette column that had been packed with Dowex 50WX8 cation exchange resin (Sigma-Aldrich) and preconditioned with 1 N HCl and 1 N NaOH. The column was rinsed with 0.1 N HCl, and then the purified AA were eluted using 1.5 N aqueous ammonium hydroxide. The eluate was dried under N_2, resuspended into acidified isopropanol (20% acetyl chloride), and esterified at 110°C for 1 h. The reaction was stopped by freezing the sample at −20°C. After rinsing with

CH_2Cl_2, samples were acylated with trifluoroacetic anhydride in CH_2Cl_2 at 100°C for 15 min. Ten AAs, alanine (ALA), glycine (GLY), threonine (THR), leucine (LEU), valine (VAL), isoleucine (ILE), proline (PRO), aspartic acid (ASP), glutamic acid (GLU), and phenylalanine (PHE), were separated by gas chromatography (60 m × 0.25 mm, 0.25 μm, HP-5MS) and oxidized to CO_2 online with a combustion oven at 1,000°C. Concentrations of the purified $^{13}CO_2$ and $^{12}CO_2$ were determined by the coupled IRMS (GC-C-IRMS, Thermo Delta V Advantage). The peak of each AA was identified by GC-MS (Pegasus 4D, LECO USA). Norleucine with a known $\delta^{13}C$ value was added to samples before hydrolysis as an internal standard. A mixture of AA standards was derivatized and analyzed in parallel to the samples. The $\delta^{13}C$ ratios of individual AA standards were determined by EA-IRMS. AA concentrations were determined by comparing the peak areas of AA and added norleucine in both samples and external standards as in McCarthy et al. (2013). Triplicate samples were analyzed, and the $\delta^{13}C$ values of AA were corrected for the carbon added during the derivatization process using the external standards. The analytical standard deviation of AA $\delta^{13}C$ values ranged from 0.5 to 1.4‰. A carbon weighted mean of AA $\delta^{13}C$ (*w*AA $\delta^{13}C$) was calculated in a given sample as the sum of individual AA $\delta^{13}C$ value multiplied by its relative carbon molar concentration to total AA carbon molar concentration.

Statistical Analysis

Principal component analysis (PCA) as in Tang et al. (2017a) was applied to normalized AA $\delta^{13}C$ values relative to *w*AA $\delta^{13}C$. The loadings of the first three principal components (PCs) were plotted with the site scores for all the samples measured. The site scores were divided by eight for better visualization. The PCA analysis was carried out using RStudio (version 0.99.902).

Linear discriminant function analysis (LDA) was applied to the $\delta^{13}C$ values of essential AA (ILE, LEU, PHE, THR, and VAL) in shelf particles (Larsen et al., 2013). The data training set came from Larsen et al. (2009, 2013).

The normalized $\delta^{13}C$ values of leucine and isoleucine in shelf particles were linearly regressed using a standardized dataset that included bacteria, forest bacteria, microalgae and open ocean suspended particles following the work by Sabadel et al. (2019).

RESULTS

Input of River Water and Formation of Hypoxia on the NSCS Shelf

A transect across the inner NSCS shelf was surveyed seaward from the mouth of the PRE (station numbers are shown in **Figure 1**). The input of river water was observed in the upper 10 m of most stations with salinity less than 30 (e.g., Stas. A8–A13) (**Figures 2A,B**). More saline waters from the adjacent South China Sea basin clearly occupied bottom waters at more seaward stations (A11–A14). Stratification was much stronger at the seaward end (**Figures 2A,B**), and was also observed at Sta. F303H where freshwater overlies SCS basin water (**Figure 2B**). However, the storm disrupted the stratification, and a well-mixed water column was found when the site was resampled (F303O; **Figures 2A,B**).

Stratification limits the resupply of oxygen from the atmosphere to the bottom of the NSCS shelf, but OC export from the surface continues with subsequent consumption of oxygen during OC decomposition. As a result, lower dissolved oxygen concentrations ranging from 2.0 to 6.5 mg L^{-1} were observed in the mid-depth and bottom water along the transect, in contrast to the saturated surface water (**Figures 2C**, **4B**). The lowest DO was at the bottom of A12, while the highest bottom water DO was at the most seaward station A14, suggesting more exchange of offshore bottom water with open ocean water. The lowest DO concentration of 0.1 mg L^{-1} was found at the bottom of F303H, which is the only surveyed location where hypoxia was observed. This hypoxic bottom water was replenished after the storm (**Figure 2C**). Surface maxima of chl*a* were observed in most stations except the most offshore sta. A14 and sta. F303O after the storm. The highest chl*a* concentrations were in the middle stations of the transect, and they rapidly decreased with depth (A9, A10, and A12; **Figures 2D**, **4A**). The hypoxic station F303H had the lowest chl*a* both before and after the storm.

Distribution of Amino Acid and Bulk Organic Carbon on the NSCS Shelf

The highest particulate organic carbon (POC) concentrations of 100–200 μmol L^{-1} were observed at the nearer shore stations A8 and A9 (**Figure 3A**). These high POC concentrations rapidly decreased seaward. Except for these near shore stations, POC was generally higher in the surface than in the middle and bottom waters. The highest surface POC in the more seaward stations was found at A13, while the lowest was at A14, reflecting the influence of oligotrophic water from the SCS basin.

Particulate AA concentrations ranging from 1.1 to 37.0 μmolC L^{-1} were observed along the surveyed transect (**Figure 3B**). The ratio of AAC/POC was much smaller at Sta. A8–A10 than at more seaward stations (**Supplementary Table 1**).

At more seaward stations (A11–A14), the AA vertical distribution was generally similar to the bulk POC distributions, high at the surface and decreasing with depth. A surface AA maximum of up to 37.0 μmolC L^{-1} at Sta. A13 with the POC maximum there, consistent with a phytoplankton-dominated source of both labile and bulk OC across the shelf. In addition, the AA carbon yield in POC along the transect was lower in nearshore water (2.8%), and increased to 68.1% at the seaward stations (**Supplementary Table 1**). This difference in AA carbon yield is consistent with previous reports of AA carbon yield in the PRE (Chen et al., 2004).

Lower POC and AA concentrations were found at F303 than at the transect stations for both visits to F303 (O and H) (**Figures 3A,B**). The lower POC and AA concentrations were observed at F303O than F303H. The differences in POC and AA between surface and bottom samples were smaller at Sta. F303H, and these differences were even less at F303 after the storm had mixed the entire water column. The AA carbon yield was slightly lower at F303O than at F303H, most likely indicating a decrease in phytoplankton biomass after the storm.

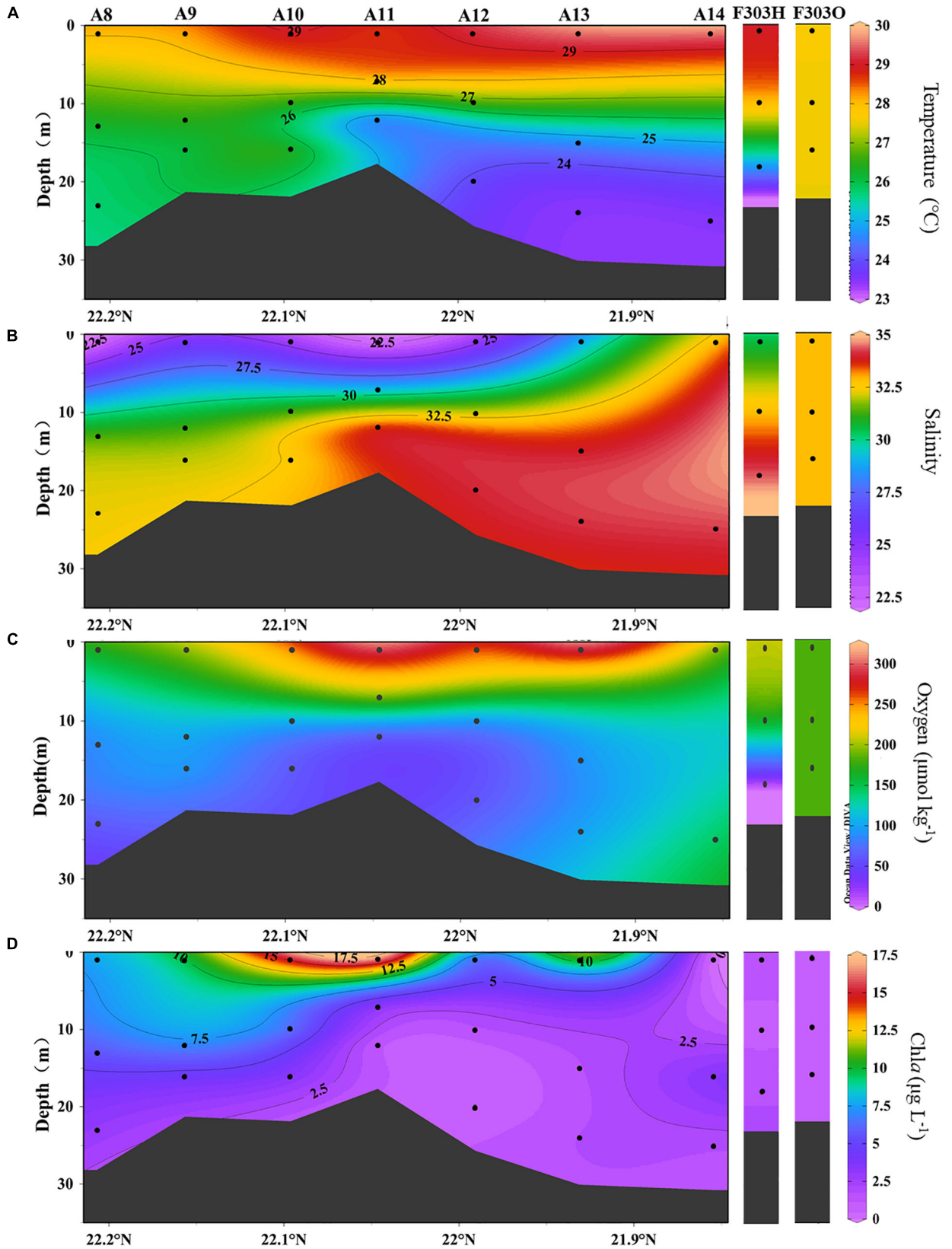

FIGURE 2 | Distribution of **(A)** temperature, **(B)** salinity, **(C)** dissolved oxygen, and **(D)** chl*a* at transect A and station F303 on the NSCS shelf. Station F303H and F303O are the two visits to station F303 before and after Tropical Storm Son-Tinh, respectively.

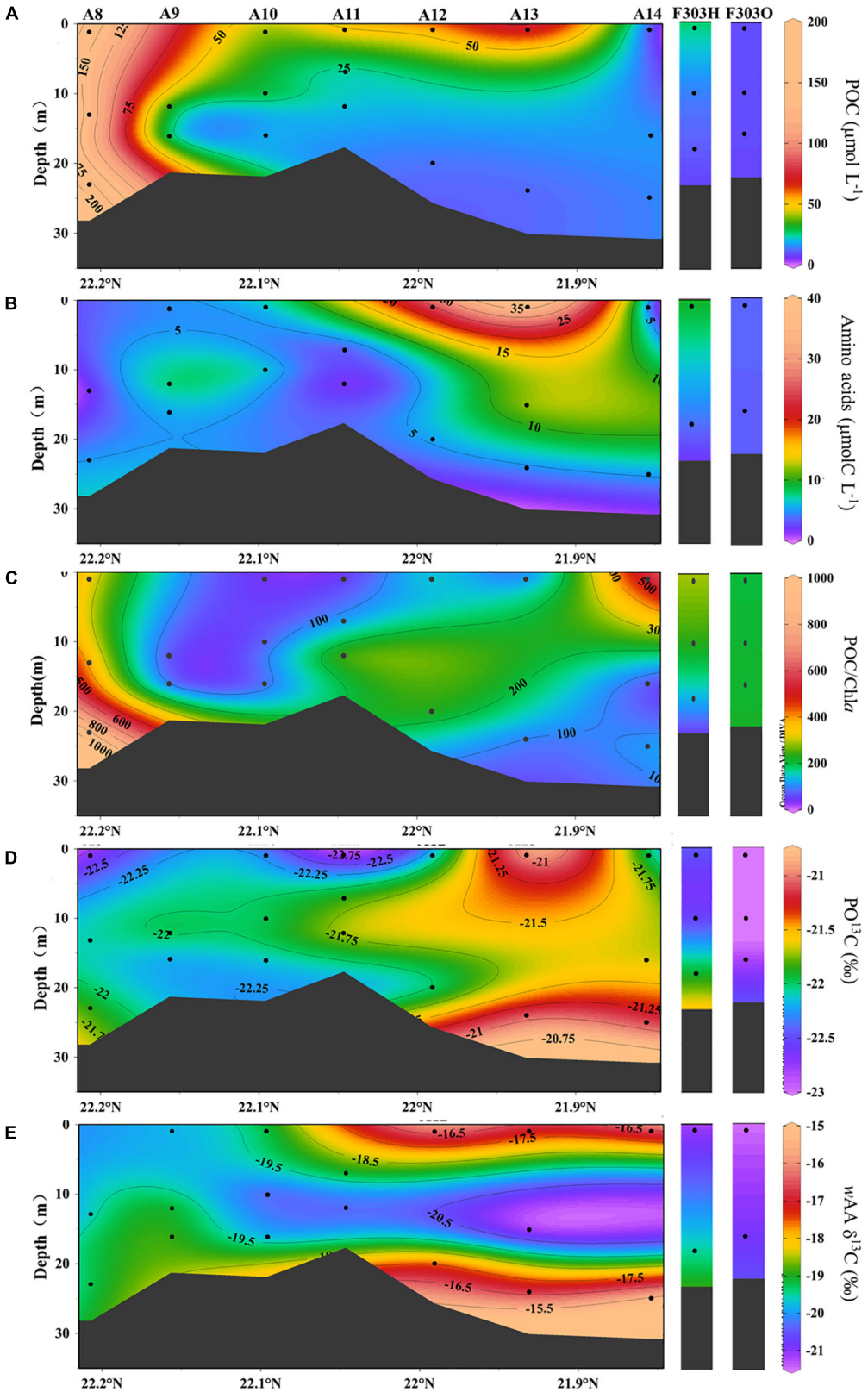

FIGURE 3 | Concentrations of particulate organic carbon **(A)**, amino acids **(B)** and POC/Chl*a* **(C)**, particulate organic carbon $\delta^{13}C$, $PO^{13}C$ **(D)** and carbon-weighted mean of amino acid $\delta^{13}C$, *w*AA $\delta^{13}C$ **(E)** from transect A and station F303 on the NSCS shelf. Station F303H and F303O are the two visits to station F303 before and after Tropical Storm Son-Tinh, respectively.

Distributions of Bulk POC and Amino Acid $\delta^{13}C$

The $\delta^{13}C$ values in POC were relatively constant across all the stations studied, ranging between −23.1 and −21.1‰ (**Figures 3C,D**, **4A,B**). The seaward station $PO^{13}C$ ratios (A12–A14) were somewhat higher than those nearer the coast (A8–A11). This spatial difference among stations was usually larger than the vertical difference between surface and bottom waters at the same station. Carbon-weighted means of AA $\delta^{13}C$ ratios (*w*AA $\delta^{13}C$) ranged from −21.2 to −15.3‰ (**Figures 3D**, **4B**), and were always higher than corresponding $PO^{13}C$ ratios. $PO^{13}C$ and *w*AA $\delta^{13}C$ shared a similar spatial distribution pattern, lower at nearshore stations than at seaward stations. For most stations, surface and bottom particle *w*AA $\delta^{13}C$ ratios were similar, but a slightly lower *w*AA $\delta^{13}C$ was observed at mid-depths.

Individual AA in each sample showed a larger range in $\delta^{13}C$ values, from −30.0‰ in valine to −5.9‰ in glycine. This range agrees with previous reports of AA carbon isotope distribution in estuarine sediments, and both suspended and sinking particles in the open ocean as well as in phytoplankton cells (Keil et al., 2001; McCarthy et al., 2004; Hannides et al., 2013; Larsen et al., 2013, 2015). Among the 10 AAs we studied, isoleucine and leucine showed the least individual variation in $\delta^{13}C$ values, −19.3 ± 1.3‰ and −26.2 ± 1.0‰, respectively (**Figures 4C**, **5A,B**), while valine and glycine showed much larger individual variations, -23.7 ± 4.8‰ and −12.6 ± 3.6‰, respectively (**Figures 4D**, **5C,D**). A decrease in $\delta^{13}C$ value of both LEU and ILE was observed in mid-depth particles of the offshore stations (A10–A12; **Figures 5A,B**). This decrease was not observed in VAL and GLY $\delta^{13}C$; instead, a progressive increase of VAL and GLY $\delta^{13}C$ was observed with depth (**Figures 4D**, **5C,D**).

Although the salinity at F303H/O was somewhat higher than most other stations on the transect, more negative $PO^{13}C$ and *w*AA $\delta^{13}C$ values were observed at F303H/O than at any other stations (**Figures 3C,D**). $PO^{13}C$ and *w*AA $\delta^{13}C$ values were even more negative at F303O than at F303H. Hypoxic bottom water (F303H) has slightly more positive $PO^{13}C$ and *w*AA $\delta^{13}C$ than the overlying surface water. This bottom enrichment in ^{13}C disappeared after the storm (F303O). The ILE $\delta^{13}C$ ratios at F303 decreased slightly after the storm (**Figure 5A**).

Statistical Analysis of Amino Acid $\delta^{13}C$ Values

The first three PCs (PC1, PC2, and PC3) of individual AA normalized $\delta^{13}C$ values ($\delta^{13}C$ values of individual AA relative to *w*AA $\delta^{13}C$ values) for all samples measured are shown in **Figure 6**. PC1, PC2, and PC3 explained 34.6, 17.6, and 12.8% of the variation. LEU had the highest loadings of PC1, while VAL had the lowest loading. Loadings of GLY and GLU were the highest and lowest of PC2, respectively. Loadings of PRO and GLY were the highest and lowest of PC3, respectively. Samples across the NSCS shelf clustered into two groups as seen in **Figure 6A** (PC1 vs PC2): samples from offshore stations clustered at the bottom left, while samples from nearshore stations were at the upper right. In **Figure 6B** (PC1 vs PC3), surface samples (upper) were separated from mid-depth and bottom water samples (bottom). The hypoxic bottom water at Sta. F303 (F303HB) showed no difference from other bottom water samples. Both before and after the storm, Sta. F303H/F303O clustered with the nearshore stations.

DISCUSSION

Source and Recycling of Labile Organic Matter on the NSCS Shelf

Continental shelves and river deltas contain the largest oceanic organic carbon pool found in marine sediments, and 80% of the organic carbon in sediments is buried there (Hedges and Keil, 1995; Gattuso et al., 1998). POC above and on shelf sediments is highly dynamic due to diverse inputs from local primary production and terrestrial sources, exchange with the open ocean, and rapid recycling by water column and benthic micro and macrobiota (Lee and Wakeham, 1988; Bianchi et al., 2013). The POC from these different sources is highly diverse in molecular composition, and has a large span of reactivity and bioavailability (Benner and Amon, 2015). Among the organic compounds on the shelf, labile molecules like AA are most readily recycled (Benner and Amon, 2015). AA, in either particulate or dissolved phase, are widely distributed in coastal areas (e.g., recently by Chen et al., 2004; Liu et al., 2010; Shen et al., 2016; Tang et al., 2017a; Li et al., 2018). The distribution of AA on the shelf is also determined by the sources mentioned above, and the relative abundance of AA to bulk OC varies greatly among the sources (Chen et al., 2004). The removal of shelf AA (and other labile compounds) is usually faster than that of bulk OC because AA degrade faster (Benner and Amon, 2015; Wakeham and Lee, 2019).

Local Primary Production

Hot spots with high dissolved AA concentrations have been found on the coastal shelf of the Gulf of Mexico in response to rapid growth of phytoplankton (Shen et al., 2016). Similarly, on the NSCS shelf, *in situ* primary production can be high, as it is supported by high nutrient inputs from the PRE and from wind driven coastal upwelling (Han et al., 2012). Along our surveyed transect in the summer of 2018, particulate AAs were found to account for up to 68.1% of the bulk POC. This is an even higher percentage than the average cellular content of phytoplankton in estuaries (25–50%; Canuel and Hardison, 2016). The generally higher AA carbon yield across the transect (except at A8) suggests that POC on the NSCS shelf comes mainly from freshly produced phytoplankton, in contrast to terrestrial organic matter or resuspended sediment with its lower AA carbon yield (e.g., A8), as will be discussed later. The vertical decrease in AA and POC concentrations with depth observed at most surveyed stations mirrored the declining chl*a* in the water column. A relatively constant $PO^{13}C$ of −22.0 ± 0.6‰ throughout the surveyed stations agrees with the typical surface $PO^{13}C$ found in the SCS basin (Liu et al., 2007), suggesting that POM on the shelf originates from primary production in seawater.

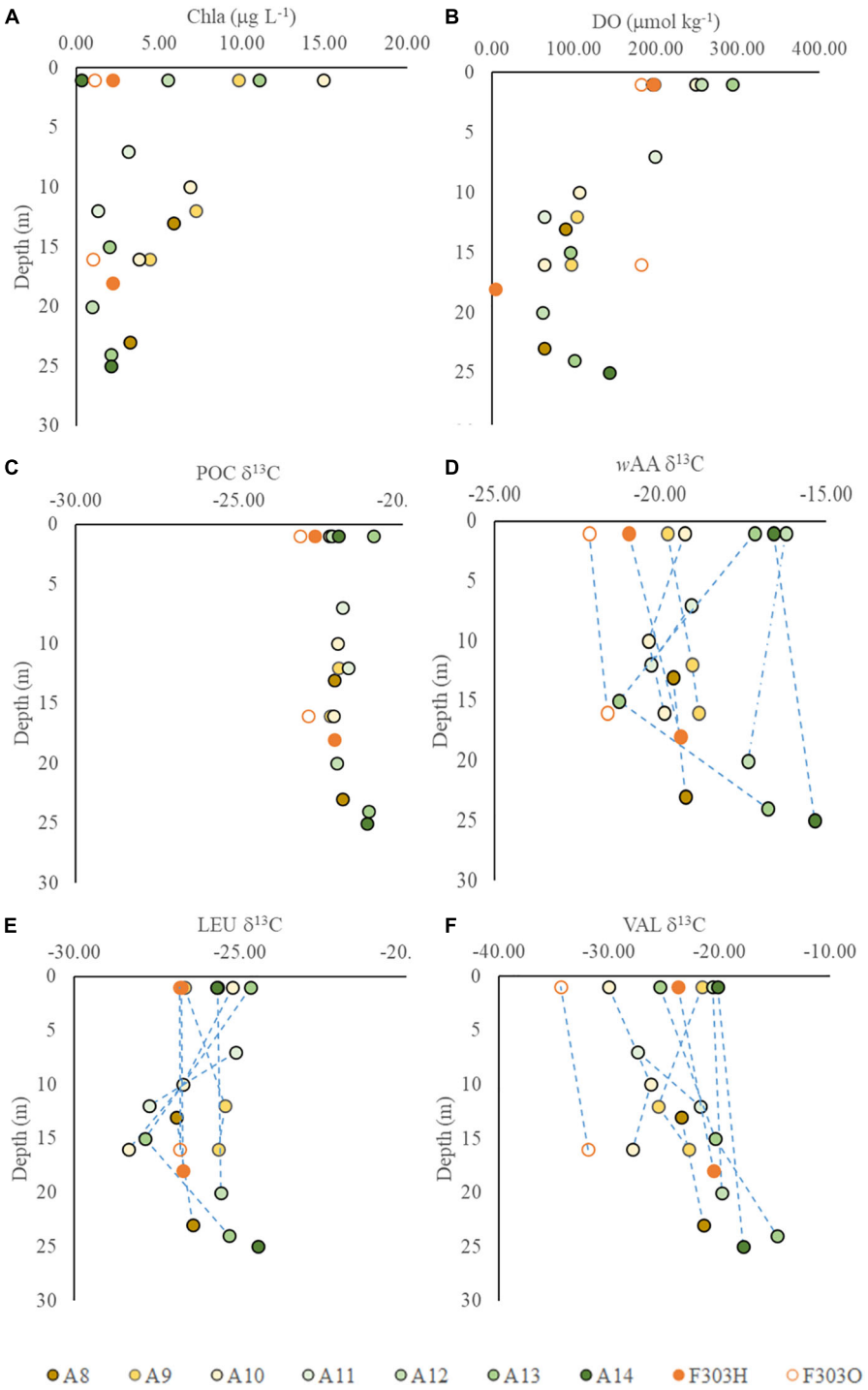

FIGURE 4 | Vertical profiles of $\delta^{13}C$ values in particles from transect A and station F303 on the NSCS shelf: **(A)** Chl*a*; **(B)** DO concentrations; **(C)** particulate organic carbon $\delta^{13}C$, $PO^{13}C$; **(D)** carbon-weighted mean of amino acid $\delta^{13}C$, *w*AA $\delta^{13}C$; **(E)** leucine $\delta^{13}C$; and **(F)** valine $\delta^{13}C$. Station F303H and F303O are the two visits to station F303 before and after Tropical Storm Son-Tinh respectively.

In surface waters of the NSCS shelf, *w*AA$\delta^{13}C$ values varied from −22.2 to −16.2‰, but generally agree with observations of bulk AA $\delta^{13}C$ in phytoplankton (−18.2‰), sinking particles (−16.7‰), and sediment (−17.2 to −19.0‰) from the northeastern Pacific (Wang and Duffel, 1996; Wang et al., 1998), supporting the idea that local primary production is the dominant source of labile organic carbon. Variations in *w*AA$\delta^{13}C$ might be due to either variations in inorganic carbon source

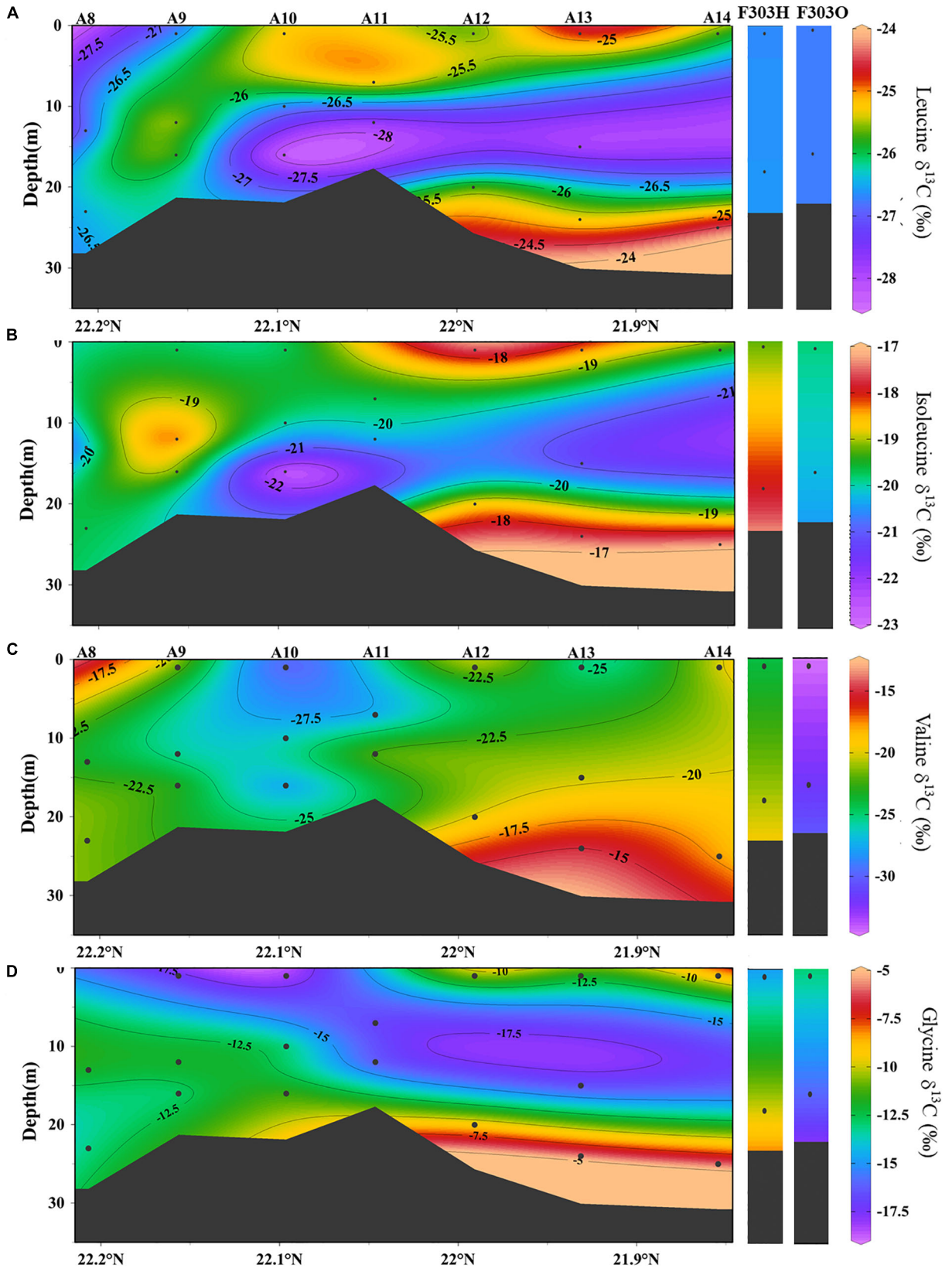

FIGURE 5 | The distribution of $\delta^{13}C$ values in particles from transect A and station F303 on the NSCS shelf: **(A)** leucine $\delta^{13}C$, **(B)** isoleucine $\delta^{13}C$, **(C)** valine $\delta^{13}C$, and **(D)** glycine $\delta^{13}C$. Station F303H and F303O are the two visits to station F303 before and after the Typhon Son-Tinh, respectively.

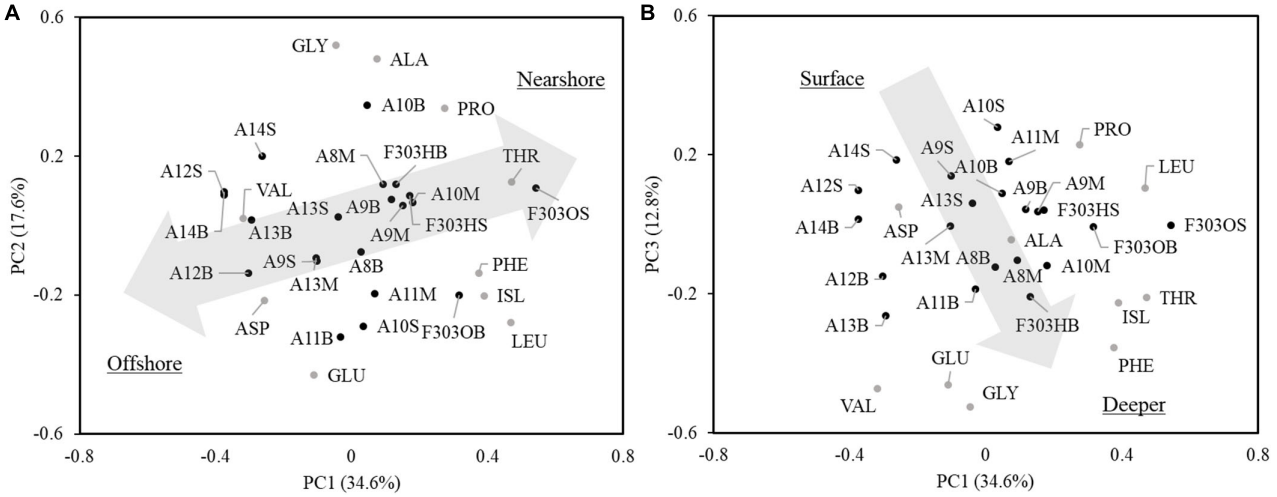

FIGURE 6 | Principal component analysis of amino acid $\delta^{13}C$ values in particles from transect A and station F303. The site scores were divided by eight for better visualization. The first three principal components account for 34.6, 17.6, and 12.8% of the variations. PC1 and PC2 **(A)** clusters the samples into offshore (bottom left) and nearshore (upper right) samples. PC1 and PC3 **(B)** clusters the samples into surface samples (upper) and samples in depth (bottom). Letters behind the station represent depth of the sample, the "S", "M," and "B" indicates surface, middle, and bottom water, respectively. Station F303H and F303O are the two visits to station F303 before and after the Tropical Storm Son-Tinh, respectively.

or isotope fractionation during photosynthesis. A variation of $DI^{13}C$ ranging from −4.0‰ (at A8) to −0.5‰ (at A14) was reported previously on the NSCS shelf in the summer of 2017, with the lowest value at the mouth of the PRE (Zhao et al., 2020). This variation in $DI^{13}C$ ratio might explain the lower *w*AA$\delta^{13}C$ and $PO^{13}C$ in nearshore surface water (F303, A9, A10; **Figure 3**) compared to offshore stations (A12–A14). However, *w*AA $\delta^{13}C$ in offshore surface waters of up to −16.2‰ are even larger than the highest values reported for surface particles of the open ocean (−16.7 to −18.2%; Wang and Duffel, 1996; Wang et al., 1998). These higher values of *w*AA$\delta^{13}C$ in surface particles suggest that the AA $\delta^{13}C$ may also be influenced by isotope fractionation during photosynthesis. Offshore stations had higher AA carbon yields than nearshore stations. It is possible that the elevated AA $\delta^{13}C$ values result from smaller RuBisCo-catalyzed isotope fractionation in more productive shelf surface waters where growth rates are higher (Laws et al., 1995; Popp et al., 1998; Burkhardt et al., 1999). However, phytoplankton growth is inhibited in the open ocean due to a limited supply of nutrients; thus AA $\delta^{13}C$ values in surface waters of the open ocean are lower as RuBisCo-catalyzed isotope fractionations increase (Wang and Duffel, 1996; Wang et al., 1998).

Local primary production could also explain the lower *w*AA$\delta^{13}C$ values in mid-depth waters than those in the surface. Although the nutrient supply was adequate on the shelf, primary production likely decreased with depth due to lower light intensity. As a result, decreased phytoplankton growth rates in the darker mid-depth waters may have led to a change in isotope fractionation (Popp et al., 1998), and a subsequent negative shift in AA $\delta^{13}C$ ratios. *In situ* production may have contributed to some extent to the mid-depth decrease in *w*AA$\delta^{13}C$, but not bottom samples, where diminished photosynthesis is reflected in the low concentration of Chl*a* across the transect.

Isotope ratios of individual compounds reflect not only the inorganic carbon source and the isotope fractionation in photosynthesis, but also the isotope fractionation caused during biosynthesis of individual compounds (Hayes, 2001). The $\delta^{13}C$ values of the total AA and bulk POC are determined by the relative abundance and the $\delta^{13}C$ of the individual molecules present. The $\delta^{13}C$ of individual AA showed different linear relationships with $PO^{13}C$ and had varied slopes (ranging from 0.6373 in ILE to 3.1949 in VAL; **Supplementary Figure 1**), indicating a changing isotope fractionation among individual compounds from the same source (local primary production). This different response of individual AA $\delta^{13}C$ to $PO^{13}C$ agrees with previous findings in algal cultures where isotope fractionations varied among lipid biomarkers from the same species under changing growth rates (Wilkes et al., 2017, 2018). The first two PCs of the PCA cluster the samples surveyed into offshore and nearshore stations (**Figure 6**), supporting the idea that *in situ* primary production is the dominant factor regulating the $\delta^{13}C$ signature of individual AA. This is also supported by the LDA and comparison of normalized leucine and isoleucine (**Figure 7**), where shelf POM clustered with bacteria and microalgae, indicating that shelf AA may predominantly originate from microalgae, and that bacteria may also contribute to the AA $\delta^{13}C$, either by autotrophic carbon fixation, or by heterotrophic decomposition.

A Combined Effect of Lability and Physical Mixing

For many of the bottom samples (A8B, A9M, A9B, A13B, A14B, F303OB, and F303HB), *w*AA$\delta^{13}C$ values were generally similar or slightly more positive than the corresponding surface

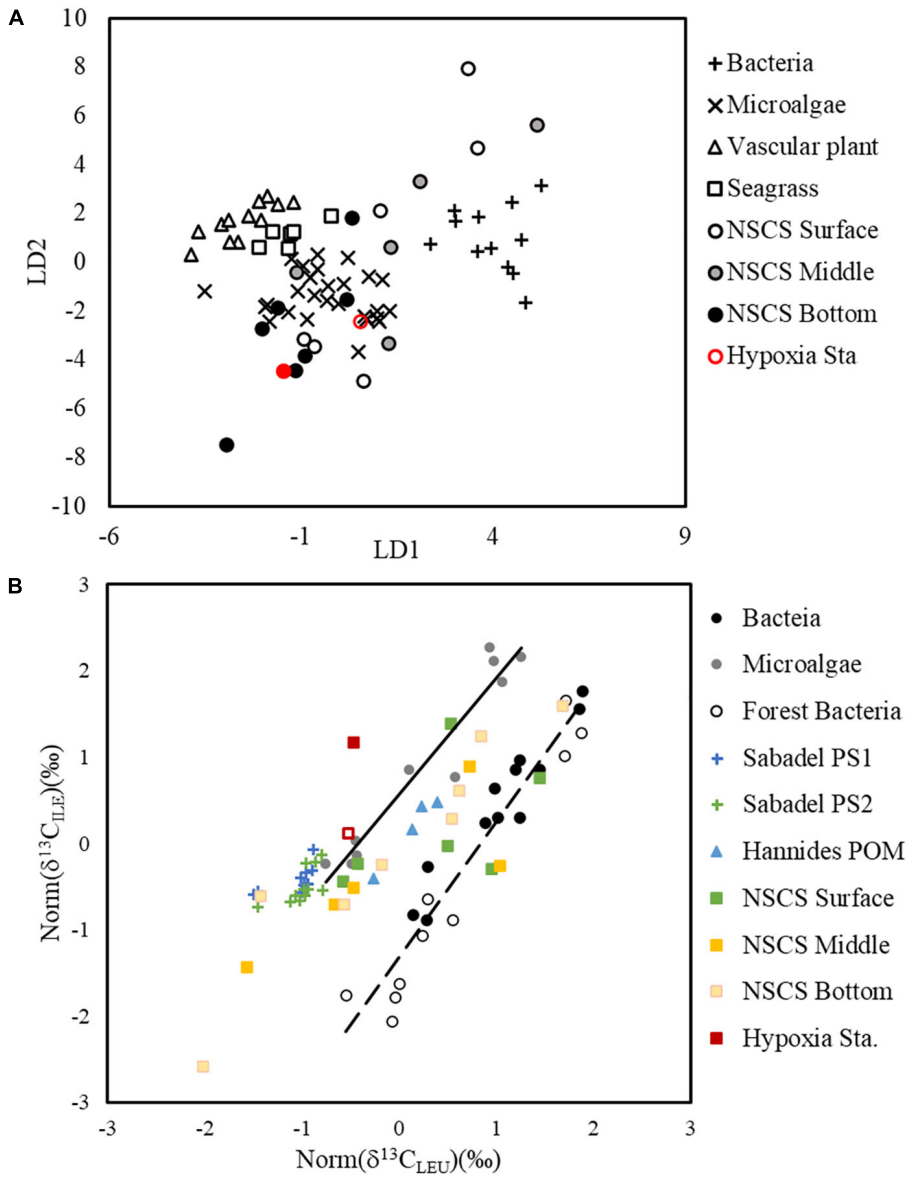

FIGURE 7 | Linear discriminant analysis of essential amino acid $\delta^{13}C$ values from surface, mid-depth, and bottom particles sampled on the NSCS shelf as well as particles from the hypoxic station F303H **(A)**. The training dataset of bacteria, microalgae, vascular plant, and seagrass are from Larsen et al. (2009), Larsen et al. (2013). Normalized $\delta^{13}C$ values of leucine and isoleucine **(B)**. The bacteria (Larsen et al., 2013, 2015), forest bacteria (Larsen et al., 2009), microalgae (Larsen et al., 2013, 2015), Atlantic POM (Sabadel et al., 2019), and Pacific POM (Hannides et al., 2013) were used as a combined dataset for the standardization. The $\delta^{13}C$ values were normalized accordingly in particles from the surface, mid-depth and bottom of the NSCS shelf. The solid and dashed lines are regression lines of microalgae and bacteria.

samples (**Figures 3E**, **4D**). Thus, the *w*AA$\delta^{13}C$ values in the water column showed a spatial variation between nearshore and offshore waters. This *w*AA$\delta^{13}C$ distribution generally follows the transport of two water masses, river input from the nearshore and seawater offshore, respectively (**Figures 1A,B**), indicating physical mixing as the primary forcing regulating the *w*AA$\delta^{13}C$ distribution on NSCS shelf. In contrast to spatial variation of the *w*AA$\delta^{13}C$ across the shelf, $PO^{13}C$ ratios showed a much more constant $\delta^{13}C$ distribution among stations (**Figures 3D**, **4C**). One exception was observed in $PO^{13}C$ at F303O, where a much more negative surface $PO^{13}C$ was observed, which might result from the stronger vertical mixing and increased river discharge after the storm. The different patterns of *w*AA$\delta^{13}C$ and $PO^{13}C$ distributions could result from a number of processes and may be related to a combination of the difference in greater biological lability of AA compared to POC, and also biological and physical processes in this highly dynamic area. As part of labile organic matter, AA are subject to rapid decomposition; thus if AA

are present in the water column, they are probably be more recently produced than the more refractory OM in bulk POC, which has more complicated origins and potentially is more influenced by physical movement. The NSCS shelf around the PRE plume is extensively affected by tides (Dai et al., 2014), which results in diurnal horizontal movement of shelf water. Horizontal transport of suspended particles with tidal movement or other physical processes may contribute to the homogenized $PO^{13}C$ distribution, but less so to AA $\delta^{13}C$, which varies among stations.

Decomposition of POM can also influence the AA isotopic signatures, either by selective remineralization of labile POM to inorganic carbon, and/or degradational modification to other compounds. The influence of bacterial reworking on AA $\delta^{13}C$ in coastal sediment has also been suggested for coastal sediments of phytoplankton origin (Keil et al., 2001), although bulk organic carbon isotopes are thought to be subject to little degradational modification (Freeman, 2001). Because aerobic decomposition consumes oxygen, the extent of decomposition may be partially linked to the DO concentrations in the water column. Along the transect surveyed, lower mid-depth *w*AA$\delta^{13}C$ values (A13M, A12B, A11M, A11B, A10M, and A10B) were found at stations with lower bottom DO concentration (61–105 $\mu mol\ kg^{-1}$) (**Figures 2C**, **4B**), implying that enhanced decomposition may contribute to the decrease of *w*AA$\delta^{13}C$ in these mid-depth particles. This may be due to the selective reworking of certain AA or to the changes in isotopic fractionation during heterotrophic biosynthesis, which is supported by the varied vertical distributions of individual AA $\delta^{13}C$ in the water column (**Figures 4**, **5**). For example, glycine and valine showed increasing $\delta^{13}C$ values from the surface to bottom, while leucine and isoleucine showed decreased $\delta^{13}C$ values in mid-depth (**Figures 4E,F**). However, the influence of decomposition to AA $\delta^{13}C$ is hard to be distinguished from other processes, particularly on this highly dynamic shelf system.

Terrestrial Input and Sediment Resuspension

There is considerable terrestrial input to the NSCS shelf (Dai et al., 2014); the PRE delivers about $3.26 \times 10^{11}\ m^3$ of fresh water (with its associated DOC and POC) to the shelf annually (Cao et al., 2011). In general, river discharge can carry large amounts of terrestrial OM from vascular plant debris and soil leachates (Bianchi, 2011). In addition, studies suggest local phytoplankton production can also be an important contributor of estuarine labile organic components, e.g., fatty acid and Chl*a* (Qian et al., 1996; Bianchi and Bauer, 2011). The rapid turnover of labile components may limit export of this material to the continental shelf. This is supported by a major contribution of local primary production to OM on NSCS shelf based on the carbon isotope signature of POM, sediment OM and DIC (Chen et al., 2008; Zhao et al., 2020). Thus terrestrially derived organic matter may contribute a small proportion to the shelf particulate AA. Differences in *w*AA $\delta^{13}C$ and individual AA $\delta^{13}C$ were observed between nearshore and seaward stations. Based on the first two PCs (**Figure 6**), the samples surveyed roughly cluster into seaward or nearshore samples, but the clusters do not clearly separate from each other. This difference in AA $\delta^{13}C$ may relate more to the $DI^{13}C$ difference between offshore and nearshore stations instead of terrestrial OM input. This is also supported by the constant $PO^{13}C$ values across the transect.

Resuspended sediments can also affect the proportion of labile material reaching shelf sediments. Shallow water depths and highly dynamic water movement can result in resuspending large amounts of sediment OM (accumulated at the sediment-water interface) back to the water column, and this would be greater at nearshore stations. Compared to the particles in the water column, sediment OM is usually older organic matter that is more resistant to further decomposition (Cowie et al., 1995; Wang and Duffel, 1996; Wang et al., 1998; Sheridan et al., 2002). Along the surveyed transect, a mismatch was found between the AA and POC distribution. POC was higher at the most nearshore station (A8), but the AA concentration at A8 was among the lowest measured. This mismatch resulted in a lower AA carbon yield at nearshore stations adjacent to the mouth of the PRE. This may result from either the input of recalcitrant terrestrial OM or resuspension of sediment OM. However, it is difficult to distinguish sediment OM from either terrestrial OM or local primary production due to the complicated origins of sediment OM.

Effect of Coastal Hypoxia on Particulate Organic Carbon

Coastal hypoxia on the NSCS shelf results from the stress of increasing nutrient and terrestrial OM inputs. From June to September, the Southwest monsoon brings 80% of the annual precipitation to the SCS (Su, 2004). As a response, freshwater discharge from the PRE usually reaches a maximum in summer. This high flux of freshwater usually covers the more saline seawater from the SCS basin. Under the influence of these two water masses, the NSCS shelf becomes more stratified in the summer. This stratification is clearly illustrated by the sharp gradient of temperature and salinity with depth at Sta. A10–A12 (**Figures 2A,B**). Continued input of warmer and lower salinity surface water blocks oxygen replenishment of the bottom waters of the NSCS shelf. Hypoxia are formed when this stratification lasts for a longer period of time (Lu et al., 2018), and hypoxia can frequently be observed surrounding the mouth of the PRE at these times. Subtropical summer storms frequently visit the SCS and effectively break up this stratification and resupply the bottom waters with oxygen. Therefore, coastal hypoxia cannot be sustained for a long period of time (usually less than a month) (Qian et al., 2018). However, with increasing inputs of nutrients from the PRE, phytoplankton growth has been gradually increasing (Gan et al., 2010), and has resulted in more frequently observed coastal hypoxia on the NSCS shelf in the summer. At the beginning of our survey, low oxygen bottom water was found to spread around the PRE, with Sta. F303H as the center of hypoxia. This is likely due to the long-lasting stratification driven by calm weather that occurred at that time. The low oxygen bottom water might also have resulted from limited bottom water exchange due to the higher topography in this area. After the tropical storm, the strong wind disturbance

mixed the water column so that all physical and biogeochemical parameters we measured exhibited constant values throughout the water column at F303O.

Although hypoxia is directly related to the loading of OM in the water column, OM from different sources contributes differently to the formation of hypoxia on the NSCS shelf. A major contribution of OM from marine sources was suggested as the major cause of hypoxic water in the lower reaches of the PRE by Su et al. (2017). Our results also support the idea that local primary production is the most likely source of OM driving hypoxia on the NSCS shelf, as seen in the more positive $PO^{13}C$ and $wAA\delta^{13}C$ ratios in the bottom hypoxic water (F303H) compared to those at the surface of F303H and F303O as well as the bottom of F303O. Compared with other nearshore stations (A8–A11), F303 had a higher AA carbon yield, implying that accumulation of labile organic matter may contribute to the rapid consumption of oxygen in hypoxic areas.

A decline in oxygen can influence recycling of shelf OC, particularly labile OC, in two ways. First, labile organic matter can accumulate in the hypoxic bottom water because of increased supply of freshly produced organic matter from the surface, or decreased decomposition in the hypoxic bottom waters, particularly decomposition related to zooplankton consumption (Jessen et al., 2017). Surface AA concentrations at F303 were lower than at the more productive offshore stations (A12, A13). This suggests that OM supply was not the limiting factor for hypoxia to form since primary production was overall very high on the NSCS shelf, while hypoxic waters were found only near Sta. F303. On the other hand, the similar AA carbon yields across the water column might suggest that degradation rates of sinking particles were slower at F303, thus labile OM might accumulate in the bottom waters. Second, the microbial community in low oxygen water probably uses a different metabolic strategy to decompose labile organic matter from that in oxic waters (Liu et al., 2013, 2017). However, if such a metabolic difference occurred at F303H, it does not appear to have influenced individual AA $\delta^{13}C$ values. In the PCA of AA $\delta^{13}C$ (**Figure 6**), hypoxic bottom water at F303H cannot be differentiated from other bottom samples, but is somewhat different from the surface samples. The weak difference between surface samples and bottom samples (**Figure 6**) implies that decompositional modification shifts the AA $\delta^{13}C$ of deeper particles away from the freshly produced surface particles, but this modification did not appear to be influenced by oxygen concentration. This supports findings by Liu et al. (2017) that peptide hydrolysis rates are equally fast in both oxic and hypoxic waters. It is also possible that the short lifetime of most coastal hypoxia events cannot support extensive anaerobic decompositional modification of shelf labile OM $\delta^{13}C$ distributions.

CONCLUSION

Overall, our observations on the NSCS shelf provide new information on the source and recycling of labile organic matter in coastal water under the stress of hypoxia. The $\delta^{13}C$ distribution of AA on the shelf suggests that the labile organic carbon on the NSCS shelf is primarily being regulated by *in situ* production by shelf phytoplankton. Higher $wAA\delta^{13}C$ in offshore water than nearshore might be due to either variations in inorganic carbon source or to isotope fractionation during photosynthesis, both of which are strongly influenced by the physical mixing of river water and offshore seawater. The change of AA $\delta^{13}C$ in the surface particles can be also be observed in the particles beneath the surface water. The contribution of terrestrial input and resuspended sediment to AA may be less important and only limited at the most nearshore stations.

In contrast to the dynamic distribution of $AA\delta^{13}C$, bulk $PO^{13}C$ showed little spatial variation on the NSCS shelf. The different patterns of $AA\delta^{13}C$ and $PO^{13}C$ distribution may result from a combined effect of POM lability and physical processes, which contribute to the homogenized $PO^{13}C$ distribution, but less so to AA $\delta^{13}C$, which varies among stations. Decompositional modification of particles caused a lower wAA $\delta^{13}C$ in some mid-depth particles, although individual AA behaved differently: glycine and valine showed increasing $\delta^{13}C$ from the surface to bottom, while leucine and isoleucine showed lower $\delta^{13}C$ at mid-depth. Our study suggests that the AA $\delta^{13}C$ distribution is better than the bulk POC in distinguishing sources of newly produced organic matter and their recent cycling in the marine environments.

The more positive $PO^{13}C$ and $wAA\delta^{13}C$ values we measured in the bottom hypoxic water (F303H) compared to the water column above or after the storm support the idea that local primary production may be the most likely source of OM driving hypoxia on the NSCS shelf. Based on the comparison of AA $\delta^{13}C$ pattern in oxic and hypoxic waters, it appears that the influence of decomposition may be similar in both the hypoxic and oxic waters we observed on the NSCS shelf.

DATA AVAILABILITY STATEMENT

All datasets generated for this study are included in the article/**Supplementary Material**.

AUTHOR CONTRIBUTIONS

ZY collected and analyzed the samples and prepared the manuscript. HZ set up the analytical method for CSIA analysis. PK helped in sample measurement and data analysis. YZ contributes to the sample collection and provided DO and Chl*a* data. TT organized the experiment and wrote the manuscript. All authors contributed to the article and approved the submitted version.

FUNDING

This work is supported by the National Natural Science Foundation of China (Project Nos. 41976035, 41703070) and the Research Grants Council of the Hong Kong Special Administrative Region, China (Project No. T21-602/16R). This work was presented at a workshop on "Marine Organic Biogeochemistry" (April 2019) funded by the Deutsche

Forschungsgemeinschaft (DFG project number 422798570) and the Hanse-Wissenschaftskolleg, and the Geochemical Society.

ACKNOWLEDGMENTS

We thank J. Li, K. Uthaipan, Z. Q. Liu, Z. M. Lu, and D. Li for sample collection. We appreciate H. B. Liu to provide the Chl*a* data. We thank L. Tian and W. B. Zou for assistance with EA-IRMS analysis. Y. Y. Li and X. H. Wang for assistance with GC-MS analysis. We thank C. Lee and Z. Q. Liu for their help in reviewing the manuscript. We appreciate the help of the captain and crew of R/V Haike 68.

SUPPLEMENTARY MATERIAL

The Supplementary Material for this article can be found online at: https://www.frontiersin.org/articles/10.3389/fmars.2020.00675/full#supplementary-material

REFERENCES

Benner, R., and Amon, R. M. W. (2015). The size-reactivity continuum of major bioelements in the Ocean. *Ann. Rev. Mar. Sci.* 7, 185–205. doi: 10.1146/annurev-marine-010213-135126

Bianchi, T., Allison, M., and Cai, W. (eds) (2013). *Biogeochemical Dynamics at Major River-Coastal Interfaces: Linkages With Global Change*. Cambridge: Cambridge University Press, doi: 10.1017/CBO9781139136853

Bianchi, T. S. (2011). The role of terrestrially derived organic carbon in the coastal ocean: a changing paradigm and the priming effect. *Proc. Natl. Acad. Sci. U.S.A.* 108, 19473–19481. doi: 10.1073/pnas.1017982108

Bianchi, T. S., and Bauer, J. E. (2011). Particulate organic carbon cycling and transformation. *Treat. Estuar. Coast. Sci.* 5, 67–117. doi: 10.1016/B978-0-12-374711-2.00503-9

Breitburg, D., Levin, L. A., Oschlies, A., Grégoire, M., Chavez, F. P., Conley, D. J., et al. (2018). Declining oxygen in the global ocean and coastal waters. *Science* 359:eaam7240. doi: 10.1126/science.aam7240

Burkhardt, S., Riebesell, U., and Zondervan, I. (1999). Effects of growth rate, CO2 concentration, and cell size on the stable carbon isotope fractionation in marine phytoplankton. *Geochim. Cosmochim. Acta* 63, 3729–3741. doi: 10.1016/s0016-7037(99)00217-3

Canuel, E. A., and Hardison, A. K. (2016). Sources, ages, and alteration of organic matter in estuaries. *Ann. Rev. Mar. Sci.* 8, 409–434. doi: 10.1146/annurev-marine-122414-034058

Cao, Z., Dai, M., Zheng, N., Wang, D., Li, Q., Zhai, W., et al. (2011). Dynamics of the carbonate system in a large continental shelf system under the influence of both a river plume and coastal upwelling. *J. Geophys. Res. Biogeosci.* 116, 1–14. doi: 10.1029/2010JG001596

Chen, F., Zhang, L., Yang, Y., and Zhang, D. (2008). Chemical and isotopic alteration of organic matter during early diagenesis: evidence from the coastal area off-shore the Pearl River estuary, south China. *J. Mar. Syst.* 74, 372–380. doi: 10.1016/j.jmarsys.2008.02.004

Chen, J., Li, Y., Yin, K., and Jin, H. (2004). Amino acids in the Pearl River Estuary and adjacent waters: Origins, transformation and degradation. *Cont. Shelf Res.* 24, 1877–1894. doi: 10.1016/j.csr.2004.06.013

Close, H. G. (2019). Compound-specific isotope geochemistry in the ocean. *Ann. Rev. Mar. Sci.* 11, 10.1–10.30. doi: 10.1146/annurev-marine-121916-063634

Cowie, G. L., Hedges, J. I., Prahl, F. G., and de Lance, G. J. (1995). Elemental and major biochemical changes across an oxidation front in a relict turbidite: An oxygen effect. *Geochim. Cosmochim. Acta* 59, 33–46. doi: 10.1016/0016-7037(94)00329-k

Dai, M., Gan, J. P., Han, A., Kung, H. S., and Yin, Z. (2014). "Physical dynamics and biogeochemistry of the Pearl River plume," in *Biogeochemical Dynamics at Major River-Coastal Interfaces: Linkages with Global Change*, eds T. Bianchi, M. Allison, and W.-J. Cai (Cambridge: Cambridge University Press), 321–352. doi: 10.1017/cbo9781139136853.017

Freeman, K. H. (2001). "Isotopic biogeochemistry of marine organic carbon," in *Stable Isotope Geochemistry*, *Reviews in Mineralogy and Geochemistry*, Vol. 43, eds J. W. Valley and D. R. Cole (Berlin: De Gruyter), 579–605. doi: 10.2138/gsrmg.43.1.579

Gan, J., Lu, Z., Dai, M., Cheung, A. Y. Y., Liu, H., and Harrison, P. (2010). Biological response to intensified upwelling and to a river plume in the northeastern South China Sea: a modeling study. *J. Geophys. Res. Ocean* 115, 1–19. doi: 10.1029/2009JC005569

Gattuso, J. P., Frankignoulle, M., and Wollast, R. (1998). Carbon and carbonate metabolism in coastal aquatic ecosystems. *Annu. Rev. Ecol. Syst.* 29, 405–434. doi: 10.1146/annurev.ecolsys.29.1.405

Han, A., Dai, M., Kao, S., Gan, J., Li, Q., Wang, L., et al. (2012). Nutrient dynamics and biological consumption in a large continental shelf system under the influence of both a river plume and coastal upwelling. *Limnol. Oceanogr.* 57, 486–502. doi: 10.4319/lo.2012.57.2.0486

Hannides, C. C. S., Popp, B. N., AnelaChoy, C., and Drazen, J. C. (2013). Midwater zooplankton and suspended particle dynamics in the North Pacific Subtropical Gyre: a stable isotope perspective. *Limnol. Oceanogr.* 58, 1931–1936. doi: 10.4319/lo.2013.58.6.1931

Hayes, J. M. (2001). Fractionation of carbon and hydrogen isotopes in biosynthetic processes. *Rev. Mineral. Geochemistry* 43, 225–277. doi: 10.2138/gsrmg.43.1.225

Hedges, J. I., and Keil, R. G. (1995). Sedimentary organic matter preservation: an assessment and speculative synthesis. *Mar. Chem.* 49, 81–115. doi: 10.1016/0304-4203(95)00008-F

Jessen, G. L., Lichtschlag, A., Ramette, A., Pantoja, S., Rossel, P. E., Schubert, C. J., et al. (2017). Hypoxia causes preservation of labile organic matter and changes seafloor microbial community composition (Black Sea). *Sci. Adv.* 3:e1601897. doi: 10.1126/sciadv.1601897

Kao, S. J., Terence Yang, J. Y., Liu, K. K., Dai, M., Chou, W. C., Lin, H. L., et al. (2012). Isotope constraints on particulate nitrogen source and dynamics in the upper water column of the oligotrophic South China Sea. *Global. Biogeochem. Cycles* 26:GB2033. doi: 10.1029/2011gb004091

Keil, R. G., Fogel, M. L., Keill, R. G., and Fogel, L. (2001). Reworking of amino acid in marine sediments: stable carbon isotopic composition of amino acids in sediments along the Washington Coast *Limnol. Oceanogr.* 46, 14–23. doi: 10.4319/lo.2001.46.1.0014

Kemp, W. M., Sampou, P. A., Garber, J., Tuttle, J., and Boynton, W. R. (1992). Seasonal depletion of oxygen from bottom waters of Chesapeake Bay: roles of benthic and planktonic respiration and physical exchange processes. *Mar. Ecol. Prog. Ser.* 85, 137–152. doi: 10.2307/24829928

Larsen, T., Kiel, C., Bach, L. T., Wang, Y. V., Kiel, C., Ventura, M., et al. (2015). Assessing the potential of amino acid 13C patterns as a carbon source tracer in marine sediments: effects of algal growth conditions and sedimentary diagenesis. *Biogeosciences* 12, 4979–4992. doi: 10.5194/bg-12-4979-2015

Larsen, T., Taylor, D. L., Leigh, M. B., and O'Brien, D. M. (2009). Stable isotope fingerprinting: a novel method for identifying plant, fungal, or bacterial origins of amino acids. *Ecology* 90, 3526–3535. doi: 10.1890/08-1695.1

Larsen, T., Ventura, M., Andersen, N., O'Brien, D. M., Piatkowski, U., and McCarthy, M. D. (2013). Tracing carbon sources through aquatic and terrestrial food webs using amino acid stable isotope fingerprinting. *PLoS One* 8:e73441. doi: 10.1371/journal.pone.0073441

Laws, E. A., Popp, B. N., Bidigare, J. R. R., Kennicutt, M. C., and Macko, S. A. (1995). Dependence of phytoplankton carbon isotopic composition on growth rate and [CO2]aq: theoretical considerations and experimental results. *Geochim. Cosmochim. Acta* 59, 1131–1138. doi: 10.1016/0016-7037(95)00030-4

Lee, C., and Wakeham, S. G. (1988). "Organic matter in seawater: Biogeochemical processes," in *Chemical Oceanography*, Vol. 9, ed. J. P. Riley (Cambridge, MA: Academic Press), 1–51.

Li, X., Liu, Z., Chen, W., Wang, L., He, B., Wu, K., et al. (2018). Production and transformation of dissolved and particulate organic matter as indicated by

amino acids in the Pearl River Estuary. *China. J. Geophys. Res. Biogeosci.* 123, 1–15. doi: 10.1029/2018JG004690

Liu, K. K., Kao, S. J., Hu, H. C., Chou, W. C., Hung, G. W., and Tseng, C. M. (2007). Carbon isotopic composition of suspended and sinking particulate organic matter in the northern South China Sea-From production to deposition. *Deep. Res. Part II* 54, 1504–1527. doi: 10.1016/j.dsr2.2007.05.010

Liu, S., Wawrik, B., and Liu, Z. (2017). Different bacterial communities involved in peptide decomposition between normoxic and hypoxic coastal waters. *Front. Microbiol.* 8:353. doi: :10.3389/fmicb.2017.00353

Liu, Z., Kobiela, M. E., McKee, G. A., Tang, T., Lee, C., Mulholland, M. R., et al. (2010). The effect of chemical structure on the hydrolysis of tetrapeptides along a river-to-ocean transect: AVFA and SWGA. *Mar. Chem.* 119, 108–120. doi: 10.1016/j.marchem.2010.01.005

Liu, Z., Liu, S., Liu, J., and Gardner, W. S. (2013). Differences in peptide decomposition rates and pathways between hypoxic and oxic coastal environments. *Mar. Chem.* 157, 67–77. doi: 10.3389/fmicb.2017.00353

Lu, Z., Gan, J., Dai, M., Liu, H., and Zhao, X. (2018). Joint effects of extrinsic biophysical fluxes and intrinsic hydrodynamics on the formation of hypoxia west off the Pearl River estuary. *J. Geophys. Res. C Ocean* 123, 6241–6259. doi: 10.1029/2018JC014199

McCarthy, M. D., Benner, R., Lee, C., Hedges, J. I., and Fogel, M. L. (2004). Amino acid carbon isotopic fractionation patterns in oceanic dissolved organic matter: an unaltered photoautotrophic source for dissolved organic nitrogen in the ocean? *Mar. Chem.* 92, 123–134. doi: 10.1016/j.marchem.2004.06.021

McCarthy, M. D., Lehman, J., and Kudela, R. (2013). Compound-specific amino acid δ15N patterns in marine algae: tracer potential for cyanobacterial vs. eukaryotic organic nitrogen sources in the ocean. *Geochim. Cosmochim. Acta* 103, 104–120. doi: 10.1016/j.gca.2012.10.037

Pai, S. C., Gong, G. C., and Liu, K. K. (1993). Determination of dissolved oxygen in seawater by direct spectrophotometry of total iodine. *Mar. Chem.* 41, 343–351. doi: 10.1016/0304-4203(93)90266-q

Popp, B. N., Laws, E. A., Bidigare, R. R., Dore, J. E., Hanson, K. L., and Wakeham, S. G. (1998). Effect of phytoplankton cell geometry on carbon isotopic fractionation. *Geochim. Cosmochim. Acta* 62, 69–77. doi: 10.1016/s0016-7037(97)00333-5

Qian, W., Gan, J., Liu, J., He, B., Lu, Z., Guo, X., et al. (2018). Current status of emerging hypoxia in a eutrophic estuary: the lower reach of the Pearl River Estuary. *China. Estuar. Coast. Shelf Sci.* 205, 58–67. doi: 10.1016/j.ecss.2018.03.004

Qian, Y., Kennicutt, M. C., Svalberg, J., Macko, S. A., Bidigare, R. R., and Walker, J. (1996). Suspended particulate organic matter (SPOM) in Gulf of Mexico estuaries: Compound-specific isotope analysis and plant pigment compositions. *Org. Geochem.* 24, 875–888. doi: 10.1016/S0146-6380(96)00072-1

Rabalais, N. N., Cai, W.-J., Carstensen, J., Conley, D. J., Fry, B., Hu, X., et al. (2014). Eutrophication-driven deoxygenation in the coastal ocean. *Oceanography* 27, 172–183. doi: 10.5670/oceanog.2014.21

Sabadel, A. J. M., Van Oostende, N., Ward, B. B., Woodward, E. M. S., Van Hale, R., and Frew, R. D. (2019). Characterization of particulate organic matter cycling during a summer North Atlantic phytoplankton bloom using amino acid C and N stable isotopes. *Mar. Chem.* 214:103670. doi: 10.1016/j.marchem.2019.103670

Shen, Y., Fichot, C. G., Liang, S. K., Benner, R., Fichot, G., Liang, S. K., et al. (2016). Biological hot spots and the accumulation of marine dissolved organic matter in a highly productive ocean margin. *Limnol. Oceanogr.* 61, 1287–1300. doi: 10.5670/oceanog.2014.21

Sheridan, C. C., Lee, C., Wakeham, S. G., and Bishop, J. K. B. (2002). Suspended particle organic composition and cycling in surface and midwaters of the equatorial Pacific Ocean. *Deep Sea Res. Part I* 49, 1983–2008. doi: 10.1016/s0967-0637(02)00118-8

Silfer, J. A., Engel, M. H., Limited, V. G. I., Way, A., and Oht, C. C. (1991). Stable carbon isotope analysis of amino acid enantiomers by conventional isotope ratio mass spectrometry and combined gas chromatography isotope ratio mass spectrometry. *Anal. Chem.* 63, 370–374. doi: 10.1021/ac00004a014

Su, J. (2004). Overview of the South China Sea circulation and its influence on the coastal physical oceanography outside the Pearl River Estuary. *Cont. Shelf Res.* 24, 1745–1760. doi: 10.1016/j.csr.2004.06.005

Su, J., Dai, M., He, B., Wang, L., Gan, J., Guo, X., et al. (2017). Tracing the origin of the oxygen-consuming organic matter in the hypoxic zone in a large eutrophic estuary: The lower reach of the Pearl River Estuary, China. *Biogeosciences* 14, 4085–4099. doi: 10.5194/bg-14-4085-2017

Takano, Y., Kashiyama, Y., Ogawa, N. O., Chikaraishi, Y., and Ohkouchi, N. (2010). Isolation and desalting with cation-exchange chromatography for compound-specific nitrogen isotope analysis of amino acids: application to biogeochemical samples. *Rapid Commun. Mass Spectrom.* 24, 2317–2323. doi: 10.1002/rcm.4651

Tang, T., Filippino, K. C., Liu, Z., Mulholland, M. R., and Lee, C. (2017a). Peptide hydrolysis and uptake of peptide hydrolysis products in the James River estuary and lower Chesapeake Bay. *Mar. Chem.* 197, 52–63. doi: 10.1016/j.marchem.2017.10.002

Tang, T., Mohr, W., Sattin, S. R., Rogers, D. R., Girguis, P. R., and Pearson, A. (2017b). Geochemically distinct carbon isotope distributions in *Allochromatium vinosum* DSM 180 T grown photoautotrophically and photoheterotrophically. *Geobiology* 15, 324–339. doi: 10.1111/gbi.12221

Wakeham, S. G., and Lee, C. (2019). Limits of our knowledge, part 2: Selected frontiers in marine organic biogeochemistry. *Mar. Chem.* 212, 16–46. doi: 10.1016/j.marchem.2019.02.005

Wakeham, S. G., Lee, C., Hedges, J. I., Hernes, P. J., and Peterson, M. L. J. (1997). Molecular indicators of diagenetic status in marine organic matter. *Geochim. Cosmochim. Acta* 61, 5363–5369. doi: 10.1016/S0016-7037(97)00312-8

Wang, X., and Duffel, E. R. M. (1996). Radiocarbon in organic compound classes in particulate organic matter and sediment in the deep northeast Pacific Ocean. *Geophys. Res. Lett.* 23, 3583–3586. doi: 10.1029/96gl03423

Wang, X. C., Druffel, E. R. M., Griffin, S., Lee, C., and Kashgarian, M. (1998). Radiocarbon studies of organic compound classes in plankton and sediment of the northeastern Pacific Ocean. *Geochim. Cosmochim. Acta* 62, 1365–1378. doi: 10.1016/S0016-7037(98)00074-X

Wilkes, E. B., Carter, S. J., and Pearson, A. (2017). CO2 -dependent carbon isotope fractionation in the dinoflagellate *Alexandrium tamarense*. *Geochim. Cosmochim. Acta* 212, 48–61. doi: 10.1016/j.gca.2017.05.037

Wilkes, E. B., Lee, R. B. Y., McClelland, H. L. O., Rickaby, R. E. M., and Pearson, A. (2018). Carbon isotope ratios of coccolith–associated polysaccharides of Emiliania huxleyi as a function of growth rate and CO2 concentration. *Org. Geochem.* 119, 1–10. doi: 10.1016/j.orggeochem.2018.02.006

Zhang, H., and Li, S. (2010). Effects of physical and biochemical processes on the dissolved oxygen budget for the Pearl River Estuary during summer. *J. Mar. Syst.* 79, 65–88. doi: 10.1016/j.jmarsys.2009.07.002

Zhao, Y., Liu, J., Uthaipan, K., Song, X., Xu, Y., He, B., et al. (2020). Dynamics of inorganic carbon and pH in a large subtropical continental shelf system: Interaction between eutrophication, hypoxia, and ocean acidification. *Limnol. Oceanogr.* 65, 1359–1379. doi: 10.1002/lno.11393

Conflict of Interest: The authors declare that the research was conducted in the absence of any commercial or financial relationships that could be construed as a potential conflict of interest.

frontiers in Marine Science

REVIEW
published: 02 September 2020
doi: 10.3389/fmars.2020.00718

Analytical and Computational Advances, Opportunities, and Challenges in Marine Organic Biogeochemistry in an Era of "Omics"

*Andrew D. Steen[1], Stephanie Kusch[2], Hussain A. Abdulla[3], Nevenka Cakić[4], Sarah Coffinet[5], Thorsten Dittmar[4,6], James M. Fulton[7], Valier Galy[8], Kai-Uwe Hinrichs[5], Anitra E. Ingalls[9], Boris P. Koch[10], Elizabeth Kujawinski[8], Zhanfei Liu[11], Helena Osterholz[12], Darci Rush[13], Michael Seidel[4], Julio Sepúlveda[14] and Stuart G. Wakeham[15]**

[1] Department of Microbiology and Department of Earth and Planetary Sciences, The University of Tennessee, Knoxville, Knoxville, TN, United States, [2] CologneAMS, University of Cologne, Köln, Germany, [3] Department of Physical and Environmental Sciences, Texas A&M University-Corpus Christi, Corpus Christi, TX, United States, [4] Institute for Chemistry and Biology of the Marine Environment (ICBM), Carl von Ossietzky University of Oldenburg, Oldenburg, Germany, [5] MARUM – Center for Marine Environmental Sciences, University of Bremen, Bremen, Germany, [6] Helmholtz Institute for Functional Marine Biodiversity (HIFMB), University of Oldenburg, Oldenburg, Germany, [7] Department of Geosciences, Baylor University, Waco, TX, United States, [8] Department of Marine Chemistry and Geochemistry, Woods Hole Oceanographic Institution, Woods Hole, MA, United States, [9] School of Oceanography, University of Washington, Seattle, WA, United States, [10] Alfred-Wegener-Institut Helmholtz-Zentrum für Polar- und Meeresforschung, Bremerhaven, Germany, [11] Marine Science Institute, University of Texas at Austin, Port Aransas, TX, United States, [12] Department of Marine Chemistry, Leibniz Institute for Baltic Sea Research, Rostock, Germany, [13] Department of Marine Microbiology and Biogeochemistry, NIOZ Royal Netherlands Institute for Sea Research and Utrecht University, Den Burg, Netherlands, [14] Department of Geological Sciences and Institute of Arctic and Alpine Research (INSTAAR), University of Colorado Boulder, Boulder, CO, United States, [15] Skidaway Institute of Oceanography, University of Georgia, Savannah, GA, United States

OPEN ACCESS

Edited by:
Christian Lønborg, Aarhus University, Denmark

Reviewed by:
Elise Sabina Morrison, University of Florida, United States
Daniel Petras, University of California, San Diego, United States

***Correspondence:**
Stuart G. Wakeham
stuart.g.wakeham@gmail.com

Specialty section:
This article was submitted to Marine Biogeochemistry, a section of the journal Frontiers in Marine Science

Received: *21 March 2020*
Accepted: *06 August 2020*
Published: *02 September 2020*

Citation:
Steen AD, Kusch S, Abdulla HA, Cakić N, Coffinet S, Dittmar T, Fulton JM, Galy V, Hinrichs K-U, Ingalls AE, Koch BP, Kujawinski E, Liu Z, Osterholz H, Rush D, Seidel M, Sepúlveda J and Wakeham SG (2020) Analytical and Computational Advances, Opportunities, and Challenges in Marine Organic Biogeochemistry in an Era of "Omics". Front. Mar. Sci. 7:718. doi: 10.3389/fmars.2020.00718

Advances in sampling tools, analytical methods, and data handling capabilities have been fundamental to the growth of marine organic biogeochemistry over the past four decades. There has always been a strong feedback between analytical advances and scientific advances. However, whereas advances in analytical technology were often the driving force that made possible progress in elucidating the sources and fate of organic matter in the ocean in the first decades of marine organic biogeochemistry, today process-based scientific questions should drive analytical developments. Several paradigm shifts and challenges for the future are related to the intersection between analytical progress and scientific evolution. Untargeted "molecular headhunting" for its own sake is now being subsumed into process-driven targeted investigations that ask new questions and thus require new analytical capabilities. However, there are still major gaps in characterizing the chemical composition and biochemical behavior of macromolecules, as well as in generating reference standards for relevant types of organic matter. Field-based measurements are now routinely complemented by controlled laboratory experiments and *in situ* rate measurements of key biogeochemical processes. And finally, the multidisciplinary investigations that are becoming more common generate large and diverse datasets, requiring innovative computational tools

to integrate often disparate data sets, including better global coverage and mapping. Here, we compile examples of developments in analytical methods that have enabled transformative scientific advances since 2004, and we project some challenges and opportunities in the near future. We believe that addressing these challenges and capitalizing on these opportunities will ensure continued progress in understanding the cycling of organic carbon in the ocean.

Keywords: chemometrics, natural marine organic matter, FT-ICR-MS, analytical challenges, HR-NMR, marine organic biogeochemistry

INTRODUCTION

The growth of marine organic biogeochemistry over the past several decades has been largely driven by advances in sampling tools, analytical methods and data handling capabilities. Max Blumer, one of the founding fathers of marine organic biogeochemistry, suggested in 1975 that limitations of analytical techniques are the major roadblock to understanding the chemical complexities of nature (Blumer, 1975). He asked whether we can conduct "realistic studies of nature that acknowledge the limitations of our present analytical powers and gaps in our understanding." It is therefore not surprising that every symposium, workshop or review on marine organic biogeochemistry since (reviewed by Wakeham and Lee, 2019) has repeated one theme – *continuing development of analytical capabilities is necessary to affect progress in the future*.

There has always been a strong feedback between analytical advances and scientific advances, but analytical technology should not be the driving force. Rather, process-based scientific questions should drive analytical developments. Several of the challenges identified at the 2004 symposium honoring the late John Hedges (Lee et al., 2004) remain. At the same time, the impressive growth of 'omics technologies since 2004 have changed the context in which marine organic biogeochemistry operates. For our purposes, we define 'omics as the set of analytical technologies and associated algorithms and databases that shine light on the internal workings of ecosystems via the sequences of biological molecules such as DNA, RNA, and protein, and the concentrations and structures of lipids and small organic molecules that are essential to life. Accordingly, we used the following themes to guide the discussions of this working group on analytical methodologies:

(i) Multidisciplinary investigations generating diverse data. Integration of disparate data sets, including better global coverage and mapping, is critical to understanding processes in the ocean.
(ii) "Molecular headhunting," or attempts to characterize the structures present in marine organic matter for their own sake, are being subsumed into process-driven targeted investigations requiring new analytical capabilities.
(iii) There are still major gaps in characterizing the composition and behavior of macromolecules – the molecularly uncharacterized component of marine organic matter after Hedges et al. (2000).
(iv) Improvements are needed in protocols for making *in situ* rate measurements of key biogeochemical processes.

Here, we present a perspective review on advances in analytical methods since 2004 derived from a 2019 Hanse-Wissenschaftskolleg Workshop on Marine Organic Geochemistry, and on some pressing analytical needs for the next decade or two. We do not attempt to create a totally comprehensive review of advances and needs; such an effort would require a book. Rather, we highlight advances and needs that workshop participants found particularly important, exciting, or underappreciated, as summarized in **Figure 1**. We hope that this review will serve as a guide and inspiration to those attempting to expand the limits of analytical chemistry to better understand the cycling of organic matter in the ocean.

ADVANCES IN ANALYTICAL INSTRUMENTATION

Nano-Elemental Analysis

Advances in continuous flow elemental analysis-isotope ratio mass spectrometry (EA-IRMS) have facilitated the tandem isotopic analysis of carbon and nitrogen in suspended, sinking, and sedimentary organic matter for describing C and N cycling processes in the ocean. Modifications to EA-IRMS systems allow for small samples of ca. 10–100 nmol, termed "nano-EA" (Polissar et al., 2009; Ogawa et al., 2010; Langel and Dyckmans, 2014), and have been applied to the study of isolated biomarker compounds (Junium et al., 2015; Fulton et al., 2018; Isaji et al., 2020) and samples with low content of organic matter (Junium et al., 2018; Cui et al., 2019; Murray et al., 2019).

Other techniques to minimize sample size include the spooling wire microcombustion (SWiM) method. SwiM has been applied to the C isotope analysis of sorted microbial cells (Eek et al., 2007), biomarkers (Pearson et al., 2016), and diatoms from sediments (Hansman and Sessions, 2016). The "denitrifier method" (Sigman et al., 2001) has been applied to the N isotopic analysis of biomarker compounds, phytoplankton, and dissolved organic matter (Robinson et al., 2004; Knapp et al., 2005; Higgins et al., 2009).

Chromatography

Gas chromatography (GC) and high-performance liquid chromatography (HPLC) are common in the analysis

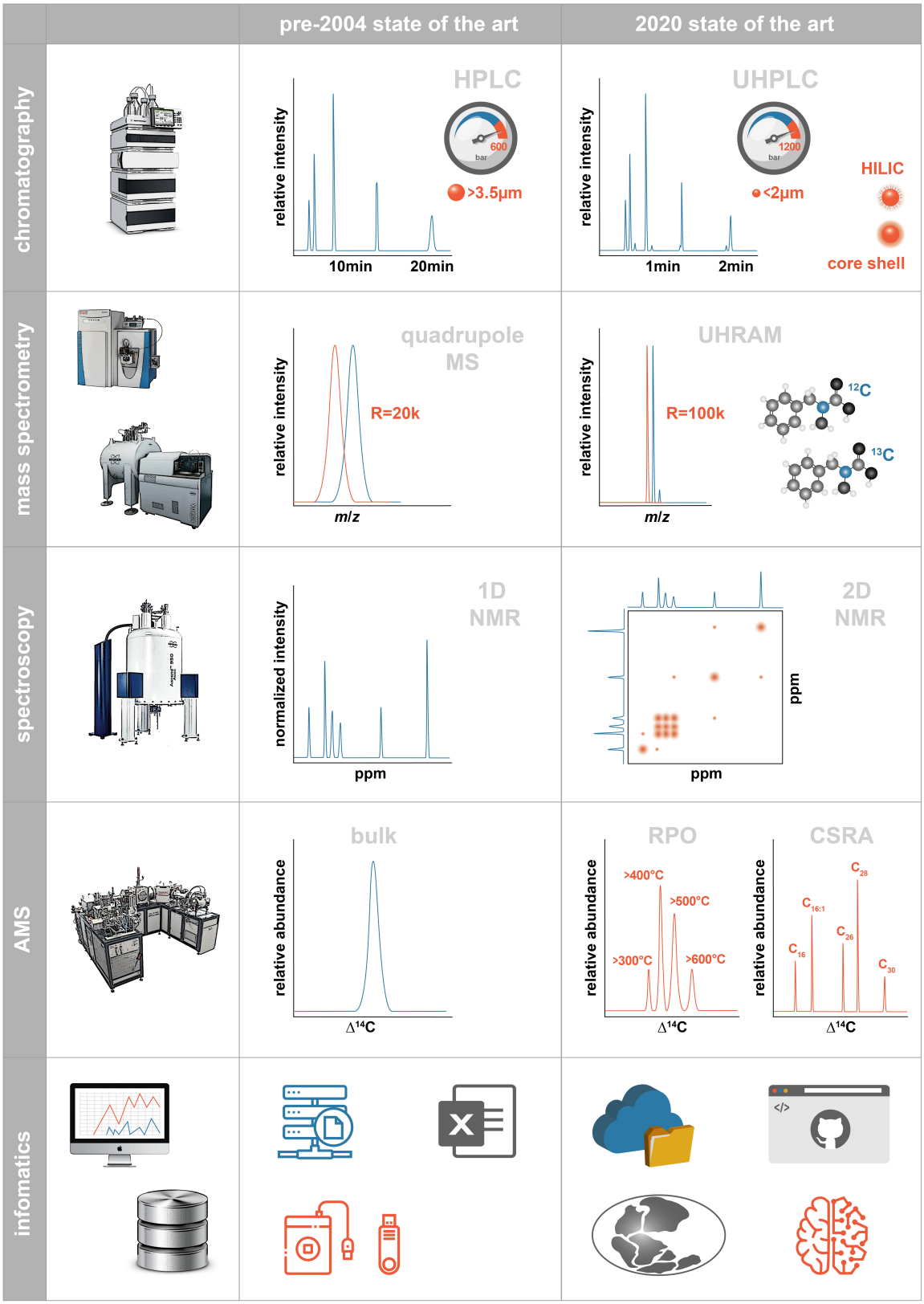

FIGURE 1 | Schematic illustrating the state of analytical methodologies available for marine organic biogeochemistry prior to 2004 and at present. Abbreviations are described in the text.

of molecular biomarkers in marine biogeochemistry (Wakeham et al., 2007, 2009). GC and HPLC systems are coupled to a range of detectors, but most compound identifications are made by mass spectrometry (MS). Chromatographic methods generally target specific compound classes useful in biogeochemical proxy development, and recent developments have increased the analytical capacity to resolve previously intractable components. Comprehensive two-dimensional GC (GC × GC) has been applied to biomarker studies and unresolved complex mixtures in petroleomics (reviewed by Eiserbeck et al., 2014) and non-targeted marine contaminant research (Hoh et al., 2012). It also has great potential in the study of metabolomics (Higgins Keppler et al., 2018).

Relatively large (m/z 500-2000) polar molecules (pigments and intact polar lipids) are most effectively separated by HPLC, with some of the most recent analytical advances summarized by Wörmer et al. (2015). Garrido et al. (2012) reviewed methods for pigment analysis, and Higgins et al. (2012) summarized pigment-based phytoplankton chemotaxonomy. Intact polar lipid analysis by HPLC is used in environmental proxy development (e.g., Rütters et al., 2002; Sturt et al., 2004; Van Mooy et al., 2009; Hopmans et al., 2016; Schubotz et al., 2018), and the range of compounds that can be detected during an individual analysis has expanded (Collins et al., 2016). Underivatized small polar metabolites are also analyzed by HPLC (Genta-Jouve et al., 2014; Johnson et al., 2017). Most of the recent technical improvements include Ultra-HPLC (UHPLC or UPLC) systems operating at higher pressure than conventional HPLC systems to rapidly resolve molecular peaks, in addition to chromatographic columns containing sub-2-μm solid-core particles that enable large increases in efficiency. UHPLC has been applied to the analysis of pigments (Zhang et al., 2016), intact polar lipids (Besseling et al., 2020), lipid biomarkers in temperature proxy calculations (de Bar et al., 2017), and organic ligands (Wichard, 2016).

The introduction of hydrophilic interaction liquid chromatography (HILIC) columns resulted in enhanced peak resolution and reduced analysis time of IPLs using normal-phase chromatography, which separates molecules according to their polar headgroups (Wörmer et al., 2013). On the other hand, intact polar lipid (IPL) analysis using reverse-phase chromatography provides compound separation by alkyl chain hydrophobicity (Wörmer et al., 2013), which improves the separation of compounds with the same headgroup and slight differences in the core lipid structure, and also allows for the simultaneous analysis of less polar compounds such as glycerol dialkyl glycerol tetraethers (GDGTs), pigments, alkenones, bacteriohopanepolyols (BHPs), and quinones. Core and intact archaeal isoprenoidal GDGTs can be now analyzed in a single run using reversed-phase chromatography (Zhu et al., 2013), while the analysis of core bacterial and archaeal GDGTs has been improved by the use of ethylene bridged hybrid (BEH) HILIC columns (Hopmans et al., 2016). The detection of BHPs has been improved by the analysis of non-derivatized compounds using either atmospheric pressure chemical ionization (APCI) (Talbot et al., 2016) or electrospray ionization (ESI) (Rush et al., 2019).

Fourier-Transform Ion Cyclotron Resonance Mass Spectrometry (FT-ICR-MS)

Fourier-transform ion cyclotron resonance mass spectrometry (FT-ICR-MS), with its unsurpassed mass resolution and mass accuracy (UHRMS – ultrahigh-resolution MS), provides the primary tool to study the composition of complex mixtures of organic compounds not accessible *via* other methods (Comisarow and Marshall, 1974; Kujawinski et al., 2004; Koch et al., 2005; Marshall and Chen, 2015). FT-ICR-MS provides elemental formulae, involving primarily C, H, and O and lesser amounts of N, S, and P. Elemental formulae may be converted into molecular formulae, and elemental compositions are visualized in van Krevelen plots of H/C and O/C ratios where they may be compared with the same ratios in potential biochemical precursors (lipids, proteins, carbohydrates), between samples, and across various spatial scales. H/C and O/C ratios that diverge from precursors indicate organic matter (OM) that has been degraded or transformed. FT-ICR-MS as a semi-quantitative fingerprinting method can be combined with targeted assays quantifying specific fractions of the natural organic matter (NOM) pool such as amino acids, carbohydrates or lipids. The unconventional type of information derived from FT-ICR-MS analyses – relative intensities of up to tens of thousands of peaks – warrants the use and development of new tools for data evaluation and interpretation. We discuss these needs in more detail below, in the section labeled "Untargeted high-resolution analysis: FT-ICR-MS and Orbitrap."

FT-ICR-MS has enabled detailed analysis of dissolved organic matter (DOM) composition across gradients from marine to freshwater biomes (Medeiros et al., 2015; Osterholz et al., 2016) and ocean basins (Lechtenfeld et al., 2014; Hansman et al., 2015; Martínez-Pérez et al., 2017) to sediment porewaters (Schmidt et al., 2011; Seidel et al., 2014) to understand its biotic and abiotic turnover. The detection limit below femto-or even sub-attomolar concentrations enabled the description of bacterial metabolites (Kujawinski, 2011; Schwedt et al., 2015; Noriega-Ortega et al., 2019; see further description below), trace metal-DOM complexes (Lechtenfeld et al., 2011; Waska et al., 2015), or anthropogenic contaminants (Wagner et al., 2015b; Powers and Gonsior, 2019).

A critical caveat for FT-ICR-MS analysis is that a single chemical formula could represent structurally distinct compounds, which may potentially exhibit divergent chemical properties. The extent to which this is a problem in practice is a subject of substantial controversy. Coupling FT-ICR-MS to trapped ion mobility mass spectrometry (TIMS-FT-ICR-MS) provides new insights into the presumed high structural diversity of DOM. Lower limits of isomeric diversity could be established (Tose et al., 2018; Leyva et al., 2019), while upper limit estimates still range widely and are dependent on detection limit and resolving power.

Orbitrap Mass Spectrometers

Orbitraps, a new type of Fourier-transform MS (Hu et al., 2005), use an electrostatic field rather than the superconducting

magnets of FT-ICR-MS. These are available to a much wider range of labs than FT-ICR-MS because purchase prices as well as maintenance expenses are much lower than for FT-ICR-MS. Although maximum mass accuracy is slightly lower for Orbitraps than for FT-ICR-MS, acquisition rates are faster (15 Hz vs. 1 Hz), compatible with LC resolution allowing detection of multiple mass spectra across a chromatographic peak. This provides (ultra-) high-resolution accurate mass (HRAM) determination with resolution of up to 1,000,000 at m/z 200 and mass accuracies of <1 ppm and can be used for targeted and untargeted analyses. Extended mass range Orbitrap systems now have analytical windows of up to m/z 20,000 allowing, for example, for intact protein analysis. Orbitrap also offers superior resolving power at the low m/z end of the analytical window in comparison to other HRAM instruments such as quadrupole time-of-flight (Q-TOF), important for structural elucidation in metabolomics and lipidomics. Thus, Orbitrap mass spectrometers provide the potential to greatly expand the number of labs that can use high-resolution mass spectrometry to characterize marine OM. Coupled with UHPLC and ESI, Orbitrap technology has proven to be a very powerful tool for proteomics, metabolomics, and lipidomics in marine organic geochemical research (Poulson-Ellestad et al., 2014; Saito et al., 2014; Hunter et al., 2015; Cantarero et al., in press) and allows the deconvolution of isotopic patterns of all common stable isotopes (compound-specific isotope analysis; CSIA) and position-specific isotope analysis (PSIA) of molecular fragment ions including multiply substituted isotopologues (Eiler et al., 2017). PSIA holds promise to intensively increase our understanding of biogeochemical pathways, cell physiology and metabolic state, dietary patterns, and degradation effects among other potential applications.

Analysis of Polar, Biologically Labile Organic Molecules

A central goal of organic biogeochemistry has been to track the composition of biologically relevant molecules as they are produced, consumed or transformed by small and large marine organisms (Moran et al., 2016). These molecules can be categorized according to the major biochemicals within cells (i.e., lipids, proteins, carbohydrates, and nucleic acids), their monomeric counterparts (i.e., amino acids, sugars, and nucleobases) and other metabolic intermediates. Small polar intermediates in this last biochemical class have received attention in the last 5 years as advances in sample acquisition, liquid chromatography, and mass spectrometry have expanded the analytical window of marine organic compounds. These compounds can be detected and quantified in both dissolved (Johnson et al., 2017) and particulate (Durham et al., 2019; Johnson et al., 2020) pools, and include molecules such as growth substrates, metabolic cofactors, and signaling molecules (the collective is often referred to as "metabolites," inferring a biological origin and sink).

Methods for metabolite analysis couple liquid chromatography to high-resolution mass spectrometry (LC/MS), thus targeting molecules that are polar and soluble in aqueous solution. The two most popular LC-column materials are reversed-phase C_{18} (or C_8) and hydrophilic-interaction liquid chromatography (HILIC) and can be used in parallel to detect the largest suite of compounds within a single sample (Boysen et al., 2018). Detection limits with triple-quadrupole or Orbitrap mass spectrometry fall within the femtogram to picogram range (per 5–10 μL injection). Thus, reasonable signals are achievable with a few hundred mL to a few L of seawater for both dissolved and particulate metabolites. Smaller volumes can be used for metabolite analysis by gas chromatography (GC) MS (Sogin et al., 2019) but fewer molecules are accessible to the derivatization required for GC analysis.

Targeted and untargeted analyses of polar metabolites generate large, complex data sets that require novel tools to analyze. Many of these tools cross disciplinary boundaries from biomedicine to marine science. Of interest to the marine science community will be advances in programs for chromatographic data analysis (MS-DIAL, Lai et al., 2018; MZmine, Pluskal et al., 2010; XCMS, Smith et al., 2006), programs to make existing tools easier to use (Li and Li, 2019; McLean and Kujawinski, 2019), and improvements in websites used to search and store mass spectrometry data (METLIN, Guijas et al., 2018; MetaboLights, Haug et al., 2020; the Metabolomics Workbench, Sud et al., 2016; MassIVE-KB, Wang et al., 2018). Several computational tools increase our ability to identify unknown compounds through searches and *in silico* calculations (CSI:FingerID, Dührkop et al., 2019; ClassyFire, Feunang et al., 2016; MetFrag, Ruttkies et al., 2019). The structural similarities in MS^2 spectra have proven especially useful in identifying compounds (MolNetEnhancer, Ernst et al., 2019; MetDNA, Shen et al., 2019; MS2LDA, van der Hooft et al., 2020), which is evident in the expanded list of tools now available at Global Natural Products Social Networking (Wang et al., 2016; Aron et al., 2020). For example, users can search mass spectrometry data using MASST (Wang et al., 2020) and reuse publicly available data via ReDU (Jarmusch et al., 2019). Collectively, these tools allow marine scientists to expand our understanding of OM in seawater (Kharbush et al., 2016; Hartmann et al., 2017; Longnecker and Kujawinski, 2017; Petras et al., 2017).

Metabolite analyses offer a strong connection to genome-based assessments of community metabolism, both potential (diversity analysis or metagenomics) and realized (metatranscriptomics or metaproteomics). Metabolic capabilities can be inferred from diversity analysis while metabolic pathways can be identified through metagenomics. Pathway activity can be monitored through metatranscriptomics and metaproteomics and their end result within elemental cycles can be tracked through metabolomics. Early studies have used diversity analysis to connect culture-based metabolic inferences with metabolite analyses (Allen et al., 2008; Johnson et al., 2016; Heal et al., 2017). Field studies are connecting community composition (and inferred metabolic potential) with metabolite concentrations to postulate microbe-microbe interactions (Durham et al., 2019) and OM-related processes (Johnson et al., 2020). This field is rapidly expanding with new method developments presented at major conferences; significant advances in our understanding of

microbe–microbe interactions through chemical exchange are likely in the near future.

Nuclear Magnetic Resonance (NMR)

Nuclear magnetic resonance spectroscopy (NMR) is a group of analytical techniques that rely on measuring how NMR-active nuclei (i.e., ^{13}C, ^{1}H, ^{15}N, ^{31}P) resonate in the presence of a strong magnetic field. Within the same nucleus (e.g., ^{13}C), the resonance frequency differs slightly based on shielding of local electrons, deshielding from adjacent chemical functional groups, and coupling with other nuclei. These differences in resonance allow identification of the chemical functional groups in which nuclei reside, and in some cases larger-scale structural information.

In the 1980s and 1990s, cross-polarization (CP) and magic angle spinning (MAS) techniques were coupled to allow characterization of functional group abundance in marine DOM isolate fractions such as XAD-resin-extracted DOM, ultrafiltered DOM (Benner et al., 1992; Abdulla et al., 2010a,b), and DOM concentrated by reverse osmosis–electrodialysis (Koprivnjak et al., 2009), as well as ultrafiltered particulate organic matter (POM) (particles 0.1–60 μm; Sannigrahi et al., 2005) and sinking particles (Liu et al., 2009). One of the major drawbacks of CP-^{13}C NMR is underestimating de-protonated carbons (e.g., carbonyl and substituted aromatic carbon), especially in the presence of paramagnetic iron, which makes it a semi-quantitative technique (Pfeffer et al., 1984; Mao et al., 2000; Abdulla et al., 2010a). Direct polarization (DP-MAS-^{13}C NMR) is more quantitative, and has been used to measure changes in the composition of DOM isolated from coastal and open oceans sites (Helms et al., 2015; Cao et al., 2018). However, DP- ^{13}C NMR requires a longer acquisition time and its spectrum has a lower signal to noise (S/N) ratio relative to CP-^{13}C NMR.

Recently, many sophisticated solid-state spectra-editing techniques (e.g., ^{13}C chemical shift anisotropy filter, CH selection, CH_2 selection) have been applied to resolve overlapping peaks within marine DOM (Helms et al., 2015; Cao et al., 2018). Two-dimensional correlation spectroscopy analysis techniques on CP-MAS-^{13}C NMR spectra have been used to track the changes of different DOM components under different perturbations and to correlate ^{13}C NMR with other spectroscopy techniques such as Fourier-transform infrared spectroscopy (FTIR) and FT-ICR-MS (Abdulla et al., 2010b, 2013a,b).

DOM has also been characterized by ^{1}H NMR, but this technique can be challenging due to interference from ^{1}H in water. Therefore, ^{1}H NMR has typically required extraction, drying, and redissolution in D_2O (e.g., Repeta et al., 2002). However, recent advances in high magnetic field NMR (currently up to 900 MHz or 21 Tesla) and the development of water suppression techniques allow analysis of marine DOM using ^{1}H NMR techniques without any isolation or pretreatment on open ocean and sediment pore water samples (Lam and Simpson, 2008; Zheng and Price, 2012; Fox et al., 2018).

Fewer studies have reported marine DOM and POM spectra for ^{31}P and ^{15}N (McCarthy et al., 1997; Clark et al., 1998; Kolowith et al., 2001; Aluwihare et al., 2005; Maie et al., 2006; Sannigrahi et al., 2006). Chemical shifts from multiple nuclei are measured in two-dimensional (2D) NMR spectroscopy techniques, which allows resolution of overlapping peaks, verification of the interpretation of the chemical shifts, and identification of specific structures. These 2D-NMR techniques include correlation spectroscopy (COSY), total correlation spectroscopy (TOCSY), heteronuclear single-quantum correlation spectroscopy (HSQC), heteronuclear multiple-bond correlation spectroscopy (HMBC) and ^{1}H-^{13}C heteronuclear correlation (HETCOR) (e.g., Repeta et al., 2002; Hertkorn et al., 2006, 2013; Cao et al., 2018).

Natural-Level Radiocarbon Analysis

Advancements in accelerator mass spectrometry (AMS) technology have dramatically reduced the cost and sample size required for ^{14}C analysis. It is now possible to measure natural abundance ^{14}C in samples containing as low as a few tens to hundred μg C rather than the routine 1 mg C (Pearson et al., 1998; Santos et al., 2007; Shah and Pearson, 2007). Compact low energy AMS systems (e.g., the Mini Carbon Dating System; Synal et al., 2007) represent a milestone toward (ultra-) small-scale ^{14}C analyses (<10 μg C at a precision of ±2‰ for modern samples Wacker et al., 2010). At this point, ^{14}C measurements are analytically no longer size-limited, but rather by the sample pre-treatment methods and the associated blank C contamination (Santos et al., 2010). These improvements in sample size requirements have also allowed for natural-level compound-specific radiocarbon analysis, which has improved our understanding of carbon metabolisms of marine organisms, sedimentary processes in the ocean, and continental carbon cycling (Wakeham and McNichol, 2014; Druffel et al., 2016; Van der Voort et al., 2018). Methods allowing for the isolation of individual compounds, mostly based on preparative gas chromatography or preparative liquid chromatography, continue to be developed for multiple compound classes. Compound classes for which compound-specific radiocarbon analytic protocols have been established include alkanes, alkanoic acids (Eglinton et al., 1996), benzene polycarboxylic acids (BPCAs) (Gierga et al., 2014), PAHs (Reddy et al., 2002) and phospholipid fatty acids (Druffel et al., 2010; Wakeham and McNichol, 2014), aliphatic alcohols, sterols and hopanols (Pearson et al., 2001), lignin phenols (Hou et al., 2010; Ingalls et al., 2010), GDGTs (Ingalls et al., 2006; Birkholz et al., 2013), amino acids (Bour et al., 2016; Ishikawa et al., 2018), pigments (Kusch et al., 2010), and diatom bound organic compounds (Ingalls et al., 2004).

Several recent developments suggest further improvements to natural abundance ^{14}C analysis. New CO_2-accepting ion sources allow peripheral instruments, such as elemental analyzers, other oxidation or hydrolysis systems and potentially gas chromatography, to interface directly to AMS (Bronk Ramsey et al., 2004; Ruff et al., 2010; Haghipour et al., 2019). This eliminates the need for an offline graphitization step, which is labor-intensive and potentially introduces ^{14}C contamination. Moreover, positive ion mass spectrometry (PIMS) uses an electron cyclotron resonance (ECR) plasma ion source generating high ion beam currents, which may allow further reductions in sample size. Finally, saturated absorption cavity ring-down spectroscopy (SCAR), a technique based on optical absorption of

CO_2 gas, is now capable of measuring ^{14}C at natural abundance levels (Galli et al., 2016). The accuracy (±3%) and sample size required (6 mg) are not currently acceptable for most marine organic geochemical applications, but because this technique is inherently simpler than mass spectrometry, it has the potential to dramatically reduce the cost of natural abundance ^{14}C analysis.

Improvements have also focused on peripheral instrumentation. Ramped pyrolysis/oxidation (RPO) involves progressively heating OM to 685°C under helium, then oxidizing the pyrolysis products to CO_2 (Rosenheim et al., 2008). This procedure exploits differences in stability of organic molecules to quantify and characterize different pools of OM. Coupled with radiocarbon dating, RPO is used to independently measure the age and reactivity distribution of fresh autochthonous OC and diagenetically stabilized allochthonous OM in terrestrial and marine settings. Recent applications of RPO include studies of riverine organic carbon (OC) (Rosenheim and Galy, 2012), oil-spill impacted sediments (Pendergraft et al., 2013), permafrost OC cycling in the Arctic (Zhang et al., 2017), weathering and recycling of petrogenic OC (Hemingway et al., 2018), the fate of terrestrial OC in the marine environment (Bao et al., 2019), soil OC preservation (Grant et al., 2019) and a global assessment of the controls on OC persistence in the environment (Hemingway et al., 2019). Because it characterizes the reactivity and age distribution of the entire OC pool, RPO is complementary to compound-specific ^{14}C, which is much more specific but characterizes only a small portion of the bulk OC. Serial UV oxidation protocols aim at the separation of distinct DOC subpools for ^{14}C analysis (Beaupré et al., 2007; Beaupré and Druffel, 2012). In both RPO and UV-oxidation, sample size limits have been pushed in recent years and more attention has been put toward minimizing potential blank C contamination.

Enzyme Assays

Field measurements along spatial and temporal gradients have been the mainstay for characterizing OM cycling in the ocean. However, process-based measurements, such as on-deck or laboratory incubations, are essential to deconvolute environmental factors affecting OM decomposition, or to quantify rates of distinct processes, although these rates should be regarded as "potential." An essential step along the pathway from POM to DOM is extracellular enzymatic hydrolysis, in which high molecular weight DOM is cleaved into fragments smaller than ∼600–1000 Da, allowing for microbial uptake (Arnosti, 2011). Various simple substrate proxies, often fluorogenic or with a fluorescent tag, are utilized to evaluate hydrolytic rates in different aquatic environments (e.g., Hoppe, 1983; Somville and Billen, 1983). Interpreting results requires caution since natural OM is far more complex than these simple proxies in terms of its structural diversity and three-dimensional conformation and organic matter uptake mechanisms are complex (Reintjes et al., 2017). Nevertheless, these simple substrates integrate the activities of diverse enzymes reasonably well (Steen et al., 2015). Substrate proxies better resembling NOM in terms of structural complexity, such as polysaccharides and peptides with fluorescent tags, provide further insight (Arnosti, 1995; Pantoja et al., 1997). Extracellular enzymatic hydrolysis is often instant and can outpace the uptake of hydrolysis products by microbes (Arnosti, 2004; Liu et al., 2013), and hydrolysis rate is highly dependent on substrate structure and environment (Liu et al., 2010; Arnosti et al., 2011). These methods collectively provide a bridge between genome/proteome-based methods to understand microbial metabolism and methods for the analysis of organic carbon composition.

Advances in Data Processing

The mandate for scientists to describe experiments in sufficient detail that they could be reproduced by others dates to at least the 17th century (Stodden, 2010). With respect to obtaining and physically processing samples, clearly written descriptions of analytical methods in manuscripts can suffice to make methods reproducible. However, many of the new analytical systems described above generate large quantities of data which must be extensively transformed and reduced prior to presentation, frequently requiring custom-written computer code. Accordingly, an increasing number of analytical chemists have learned to become programmers on the side. While this opens exciting new opportunities for discovery, it also places new burdens on analytical chemists to clearly describe the computational methods by which we obtain our results. Such descriptions are as essential to reproducibility as are descriptions of the chemical conditions by which a sample was analyzed.

Fortunately, several trends have facilitated reproducible data analysis. First, (relatively) user-friendly, free and open-source software languages such as R and python, and to some extent Julia, have been developed into sophisticated analytical platforms, complete with packages for almost any type of statistical analysis that is common in the literature and high-quality integrated development environments. These languages have rapidly gained popularity compared to closed-source platforms such as SAS and SPSS (Muenchen, 2019).

Second, tools to integrate code with text, such as the R Markdown document specification and JupyterLab allow seamless integration of text, code, and code results (Baumer and Udwin, 2015; Perkel, 2016, 2018). This makes it easy to relate code to the results that it produces, and to annotate code and results with a plain-language explanation of why the analysis was done in the way that it was. Such tools have long been available (Knuth, 1984; Ramsey, 1994; Leisch, 2002) but used the cumbersome TeX/LaTeX document preparation system (Knauff and Nejasmic, 2014) and did not support the languages most often used for data analysis.

Third, the availability of version control systems such as git and mercurial encourage integration of version control into the process of writing data analysis scripts and packages. Version control encourages a systematic approach to updating documents and tracking contributions by multiple authors, a key aspect of project management that scientists often manage informally (Cham, 2012). Associated hosting services such as GitHub and GitLab, each of which are commercial services that offer a free tier, make it easy to share and collaborate on code. These tools collectively take some time to learn (and can be frustrating even for experienced users; Munroe, 2015) but once adopted, they improve research productivity (Wilson, 2006; Ram, 2013).

Fourth, systems to facilitate the preservation and sharing of raw data have developed considerably. Repositories such as PANGAEA, National Centers for Environmental Information (NCEI), and Biological-Chemical Oceanography Data Management Office (BCO-DMO) have grown rapidly over the past decade. As of early 2020, PANGAEA has over 392,000 unique, publicly available data sets (Grobe et al., 2006). Concurrently, academics have developed best-practices and principles for data sharing and preservation, although there is disagreement in the literature as to how best to reconcile ideals of how best to share and preserve data with the practicalities of doing so with limited time and resources (Wilkinson et al., 2016; Tierney and Ram, 2020).

Finally, a broad ecosystem of support services for the above three developments has emerged. Evidence-based short courses such as Software Carpentry and Data Carpentry offer low-cost, evidence-based lessons in computational skills aimed specifically at scientific researchers (Wilson, 2014). Websites such as stackoverflow.com host questions about programming, and provide incentives for users to provide clear, accurate answers. Integrated Development Environments such as R Studio and JupyterLab, which are explicitly designed for data analysists, make the process of code development and debugging much easier (Gandrud, 2013). These trends have led to the development of a range of open-source tools that are valuable for marine organic geochemistry, particularly instruments that generate large quantities of data such as ultra-high resolution mass spectrometers, for instance XCMS (Smith et al., 2006) and LOBSTAHS (Collins et al., 2016), and many of the tools listed in the "Analysis of polar, biologically labile organic molecules" section.

All of these trends have deep roots in computer science. For instance, Donald Knuth coined the term "literate programming" to describe the practice of mixing explanatory text with computer code in 1984 (Knuth, 1984) and the idea of reproducible data analysis has a long history in the computer science literature (as reviewed in Stodden, 2010). The main advances since 2004 have stemmed from the fact that the tools for reproducible data analysis have become much more widespread and accessible to researchers, such as marine organic geochemists, whose primary expertise lies outside of computer science. The new accessibility of these tools, combined with an increased need for them to be used by marine organic geochemists, suggests a bright future for reproducible data analysis in our community. In any case, increased transparency in data analysis is far preferable to what Rossini et al. (2003) identified as the alternative: "blind faith in our colleagues' programming skills."

Drawing From Other Fields

Progress in adjacent fields has also led to improved understanding of marine organic geochemistry. Most notably, the explosive progress in DNA and RNA sequencing technology, coupled with advances in bioinformatic tools to process those data, have led to a phase shift in our ability to draw inferences from biological sequence data. Hedges et al. (2000) predicted that "fast-developing capabilities [to identify marine microbes by taxonomy] should help compensate for our inability to culture most microorganisms." Microbial taxonomy does offer some insight into environmental function, but this insight is severely limited (Royalty and Steen, 2019). However, it is now routine for individual labs to assemble incomplete or even complete, closed genomes of the most abundant microbes in a marine environment, in the context of a single project. Given microbial genomes, researchers can make reasonable predictions about broad nature of microbial interactions with organic matter (Rinke et al., 2013; Bird et al., 2019). It remains the case that bacterial and archaeal cells in seawater and sediments are only distantly related to microbes that have been grown in culture (Lloyd et al., 2018), and that the most common method of determining microbial abundance, surveys of primer-amplified 16S gene abundance, are biased toward taxa represented in culture collections (Steen et al., 2019). However, new culturing techniques and a renewed focus on culturing previously uncultured taxa have led to the culturing of quite a few abundant, environmentally important marine microbes (Könneke et al., 2005; Katayama et al., 2019; Imachi et al., 2020). Studies of microbes in pure culture act as "ground truthing" for inferences based on culture-independent techniques.

Other fields of ocean science have also impacted marine organic geochemistry. Improved understanding of the importance of mesoscale eddies to ocean physics have led biogeochemists to look for, and discover, differences in OM cycling in mesoscale eddies, for instance differences in D:L-amino acid transformation rates apparently due to different microbial communities within vs. outside of eddies (e.g., Zhang et al., 2009; Sarma et al., 2019). Remote sensing techniques have advanced substantially since 2001, due to improvements in sensors, the recent availability of inexpensive research drones, and improvements in the algorithms used to remove the overprint of the atmosphere on light reaching satellites from the ocean (e.g., Werdell et al., 2013). Coupled with improved understanding of DOM optical characteristics (Coble, 2007; Helms et al., 2008), this permits more accurate and robust measurements of parameters such as DOC concentration, chromophoric dissolved organic matter (CDOM) content, and even indirect estimations of parameters such as methylmercury concentrations (Fichot et al., 2016; Slonecker et al., 2016).

CHALLENGES AND OPPORTUNITIES FOR THE NEXT DECADE(S)

The technical advances described create new challenges and opportunities for the next decade-plus of marine organic geochemistry research (**Table 1**). While a few of these challenges and opportunities are specific to individual technologies, for the most part they rely on integrating advances from different analytical techniques and fields of knowledge. Below, we describe some directions for future research that our working group found most exciting.

New Lipid Biomarkers and New Uses of Old Lipid Biomarkers

Biomarker lipids show the presence of particular source organisms or biosynthetic pathways and can be proxies for past environmental parameters, including temperature, pH, and input

TABLE 1 | Summary of future challenges and opportunities.

Future challenge	Opportunity
New lipid biomarkers	Increase use of compound-specific isotope analysis
	Increase spatial sample resolution and analytical sensitivity
	Innovate software for high-throughput analysis
	Expand use of new chromatographic front-ends (e.g., HILIC, 2D-HPLC)
	Improve interpretation by better understanding feedbacks between microbial physiology and the environment
Data comparisons	Expand repositories for raw and processed data
	Further multi-lab intercalibration studies for specific technologies
Untargeted high-resolution analysis: mass spectrometry	Improve extraction and ionization methods for specific analytes and matrices; better tailor these methods for specific research questions
	Expand use of multi-dimensional chromatographic separation and fragment analysis
	Improve algorithms to assign formulae
Untargeted high-resolution analysis: coupled NMR-MS	Expand use of water suppression in ^{1}H-NMR
	Improve algorithms to compare NMR and mass spectrometric data
Coupling untargeted chemical and microbiological assays	Expand stable isotope probing in coupled chemical and microbiological assays
	Expand use of coupled NMR and ultrahigh-resolution mass spectrometry in bioassay experiments
Consensus reference materials	Better consensus on what constitutes appropriate chemical and biological reference materials
	Reference materials beyond bulk marine DOM: e.g., marine POM, sedimentary OM
	References designed for specific techniques, e.g., molecular fingerprinting

of soil organic matter to marine systems. Lipid chemical stability enables their preservation in the geological record and thus, their extensive use as paleo-indicators. Novel HPLC-MS techniques have greatly widened the range of compounds amenable for analysis, both in terms of size and polarity (Schouten et al., 2000; Sturt et al., 2004), revealing a large diversity of microbial lipids in their intact (polar) forms in marine environments (e.g., Van Mooy and Fredricks, 2010; Schubotz et al., 2018) and make possible environmental proxies (e.g., the GDGT-based TEX_{86} sea surface temperature proxy; see Schouten et al., 2013b). These techniques facilitate quantification of microbial intact polar lipids, which provide high taxonomic resolution (Schubotz et al., 2009), and which can yield insight into microbial processes such as ammonia oxidation rates (Hurley et al., 2016). Adding compound-specific isotope analysis in the context of natural isotope abundances (e.g., Schubotz et al., 2009; Pearson et al., 2016) or tracer experiments (e.g., Kellermann et al., 2016) can give further insight into elemental flow within ancient or currently active communities.

However, analytical refinements, along with extensive large-scale environmental and laboratory-based surveys, have highlighted the complexity in interpreting the biomarker record solely from a single influencing parameter point of view (Hurley et al., 2016; Sollai et al., 2019). Recent advances have focused on increasing the resolution and sensitivity of lipid analysis. Wörmer et al. (2014) introduced, for example, the use of direct laser-ablation of lipids from sediment core surfaces drastically improving spatial sampling resolution. High resolution mass spectrometry technology, such as orbitraps, has decreased detection limits and shown value as a tool to characterize and identify novel lipid structures (Moore et al., 2016; see also below). The identification of carboxyl-rich alicyclic material (CRAM; Hertkorn et al., 2006; see also below), carotenoid degradation products (CDP; Arakawa et al., 2017) and material derived from linear terpenoids (MDLT; Woods et al., 2011; Arakawa and Aluwihare, 2015) have shone a light on some of the most abundant classes of recalcitrant NOM in seawater. Although these structures have been inferred from NMR and ultrahigh-resolution mass spectrometry, and they appear related to biologically produced source molecules, there is not yet direct proof of how those molecules are produced, whether biotically or abiotically. Fractionation of DOM through hydrophilic interaction chromatography (HILIC) and multidimensional separation (2-D HPLC) coupled with ultrahigh-resolution mass spectrometry or conjunction with NMR experiments (Woods et al., 2011; Spranger et al., 2019) represent promising tools to determine if these materials might be useful as biomarkers or indicators of biogeochemical processes. At the same time, the data produced by these high-resolution instruments have highlighted the lack of pipelines for 'omics' data that are available for environmental lipidomic work.

To fully exploit the potential of these techniques, high-throughput methods need to be developed. For example, LOBSTAHS is an open-source lipidomics workflow, written in R, for high-throughput annotation and putative identification of lipids in high-mass-accuracy HPLC-MS data that can identify thousands of compounds (>14,000 unique entries) in a sample (Collins et al., 2016). In our view, the improved accessibility to high-resolution mass spectrometers and lipidomics workflow for high-throughput annotation and putative identification of lipids, not only enhance the number of structures that scientists can identify for targeted lipidomics, but they also allow us to explore the patterns of unknown compounds in sample sets with contrasting conditions. The latter has the potential of enhancing the amount of biologically and biogeochemically relevant information obtained from non-targeted, exploratory lipidomic analysis.

Future challenges require better comprehension of the biomarker producers, through understanding the environmental constraints and the biosynthetic origin of lipid biomarkers. For example, targeting the diversity of lipid biosynthetic genes has already helped us identify limitations of using long-established hopane biomarkers (Welander et al., 2010). Lipid isotope

probing assays, recently adapted to use radiotracer applications (Evans et al., 2018), hold high promise in revealing lipid biosynthetic pathways in pure cultures, but also in environmental settings. By working together with microbiologists in the future, we will fulfill the need for a better grasp of the effects of microbial physiology on biomarker synthesis.

More and Improved Data Comparisons

State-of-the-art analytical techniques allow rapid chemical measurements of small samples. Some of these techniques, such as FT-ICR-MS, allow rapid measurements from small samples that can generate large amounts of data, with greater efficiency. Consequently, the amount of data available is expanding, presenting new challenges for data analysis, integration and intercalibration. Additionally, small variations in sample collection, physicochemical experiments, extraction protocols, fractionations, mass spectrometry analysis and data processing can lead to challenges in intercomparing data from multiple studies.

Differences in data processing algorithms can also impact acquired data files. As described above, computational methods to transform raw data should be understood as part of the analytical method, not as something downstream of the analysis. For example, comparison of three software tools and their parameters for processing mass spectral data showed large differences in the results depending on the tools and parameters chosen, specifically for the degree of false positive or negative peak detections (Cajka and Fiehn, 2016). This is especially important in the area of peak picking and identification in untargeted mass spectrometry analysis. There is a need to build on existing, successful data intercomparison (Schouten et al., 2013a) and sharing of information. Strengthened international cooperation and connections between diverse research fields could play a pivotal role in standardizing protocols and advancing understanding in the field of marine organic biogeochemistry.

Untargeted High-Resolution Analysis: Ultrahigh-Resolution Mass Spectrometry

Advances in sample preparation, analysis and interpretation for FT-ICR-MS of NOM are ongoing and will aid in further deciphering the structural diversity of NOM. Molecular analysis of DOM from marine samples is hindered by the salt matrix in which the compounds are present. Extraction with commercially available PPL columns (Dittmar et al., 2008) and analysis of the obtained methanol extract in ESI-negative mode represent the most widely applied combination. Different isolation techniques with variable efficiency have been proposed and compared (e.g., Sleighter and Hatcher, 2008; Green et al., 2014; Schmidt et al., 2014; Li et al., 2017; Stücheli et al., 2018). Because ESI primarily ionizes polar to semi-polar compounds and in itself represents a complex technique affecting compounds differently based on polarity, molecular size, acid/base character and concentration, no single ionization method captures the whole suite of compounds present in NOM (Ohno and Bro, 2006; Hertkorn et al., 2008; Reemtsma, 2009). Accordingly, extraction and ionization methods need to be tailored to the scientific question (Kido Soule et al., 2010; Sleighter et al., 2012).

FT-ICR-MS analyzers provide the highest accuracy and resolving power (>1,000,000 at m/z 400, Junot et al., 2014) for exact molecular formula determination. Direct infusion techniques are able to produce detailed information on sample composition in relatively short time, allowing fingerprinting of complex mixtures in high throughput studies. As one molecular formula can represent an unknown number of isomers (Hertkorn et al., 2008; Zark et al., 2017) and co-suppression of signals may occur when analyzing highly complex mixtures of organics such as (marine) DOM (Patriarca et al., 2018). Chemical separation techniques, such as liquid chromatography or electrophoresis, are applied prior to sample injection to overcome these issues and to provide more detailed structural information behind molecular formula assignments (Hawkes et al., 2018). While these techniques are commonly used in conjunction with tandem mass spectrometers including Orbitrap, we expect one-dimensional as well as multi-dimensional chromatographic separations prior to FT-ICR-MS analysis to become more prevalent in the future (Ghaste et al., 2016). However, the relatively slow acquisition rates of FT-ICR-MS instruments limit their applicability to hyphenated approaches often used in metabolomics and lipidomics research (Junot et al., 2010). Coupling FT-ICR-MS to trapped ion mobility mass spectrometry (TIMS-FT-ICR-MS) provided new insights into the presumed high structural diversity of DOM. Lower limits of isomeric diversity have been established (Tose et al., 2018; Leyva et al., 2019), while upper limit estimates still range widely and are dependent on detection limit and resolving power. Additionally, fragmentation approaches have been applied to confirm molecular formula attributions and to elucidate the structural diversity of DOM (Wagner et al., 2015a; Kujawinski et al., 2016; Zark et al., 2017).

The complex, high-dimensional information provided by ultrahigh-resolution MS requires development of new mathematical tools. The first, fundamental step is the assignment of unique molecular formulas. All tools in one way or another use mathematical transformations to improve resolving power, mass accuracy and sensitivity (e.g., Kilgour et al., 2013), or apply chemical and stochastic rules (Dittmar and Koch, 2006; Kind and Fiehn, 2007). After formula assignment, elemental ratios, molecular mass or mass defect analyses (Hughey et al., 2001) can provide first insights into NOM composition. Due to the high number of molecular formulae and increasing sample throughput, the application of multivariate statistics has been established in the field (Kujawinski et al., 2009; Sleighter et al., 2010; Longnecker and Kujawinski, 2016).

Untargeted High-Resolution Analysis: Coupled NMR and Ultrahigh-Resolution Mass Spectrometry

The alliance of NMR and ultrahigh-resolution mass spectrometry will continue to provide valuable insights into the sources of a refractory DOM components (Hertkorn et al., 2006; Aluwihare and Meador, 2008; Abdulla et al., 2013b; DiDonato and Hatcher, 2017). For example, combined NMR and FT-ICR-MS analyses

show that the major components of the polysaccharide fraction of HMW-DOM are acylated polysaccharides (APS; *N*-acyl amino acids bound with neutral and amino sugars and non-acylated heteropolysaccharides) and CRAM (Hertkorn et al., 2006) with smaller amounts of aromatics and aromatic *N*-heterocyclics. CRAM is the most abundant identified component of DOM. Increasing depth in the water column conserves increasingly branched CRAM and heteroatom-containing components at the expense of carbohydrates, contributing to the resistance of DOM to biodegradation (Hertkorn et al., 2013).

Additional information may be gained by utilizing different NMR techniques. Higher magnetic field NMR instruments will likely not advance solid-state NMR techniques. This is because higher magnetic fields require a higher spinning speed for the sample rotor to remove the spinning sideband, which is not currently feasible (see Mopper et al., 2007 for a more complete explanation). However, higher magnetic field NMR and NMR Cryoprobes may allow the use of water suppression ^{1}H NMR techniques to analyze the entire marine DOM composition even in the deep ocean (Lam and Simpson, 2008; Fox et al., 2018). Diffusion ordered spectroscopy (DOSY) and 2D-NMR techniques (^{1}H-^{1}H-TOCSY and ^{1}H-^{1}H-COSY) estimate the molecular weight of DOM components, resolve overlapping peaks, confirm the interpretation of the chemical shifts, and help to identify the structures of specific DOM components. Coupling ^{1}H NMR techniques with offline chromatography and high-resolution mass spectrometry techniques will advance our understanding of the entire marine DOM transformation and cycling characterization of marine DOM (Simpson et al., 2004).

Chemometric statistical methods allow combining NMR data with mass spectrometry data using multivariate statistics, for example to identify structural components and pathways of metabolic perturbations or to determine the biotransformation of metabolites on short timescales (Jaeger and Aspers, 2014). These methods use the intrinsic covariance between signal intensities in the same and related molecules measured by different techniques across great numbers of samples (Crockford et al., 2006). Another approach identifies single metabolites by generating theoretical NMR and MS/MS spectra for possible chemical structures and by comparing them directly against experimental NMR and ultrahigh-resolution MS^2 spectra of the unknowns (Boiteau et al., 2018). This approach does not require identified compounds from experimental metabolomics databases, providing means for the identification of unknown and uncatalogued metabolites in natural DOM. Further development of chemometric tools will be needed in the future.

Coupling Untargeted Chemical and Microbiological Assays

Information on microbial metabolite transformations will enhance our understanding of carbon cycling in the oceans. Parallel trends between the complex, but closely connected non-living and living worlds are established by combining chemical with, e.g., untargeted microbiological assessments (Kujawinski, 2011; Osterholz et al., 2016). The application of stable isotope tracers will enable the delineation of causal links (e.g., Biddle et al., 2006; Orsi et al., 2018; Seyler et al., 2018). Understanding structural diversity as a meaningful property of DOM adds a new facet to the interpretation of UHRMS data. Borrowing on traditional ecological concepts, this approach may increase the understanding of the long-term stability of carbon compounds dissolved in the ocean, sustaining highly diverse microbial communities (Dittmar, 2015; Osterholz et al., 2016). Likewise, bioassay experiments employing metabolic profiling via NMR and FT-ICR-MS show that bacterial DOM has a chemical composition and structural diversity similar to refractory natural DOM in seawater (Lechtenfeld et al., 2015). In the future, including DOM fingerprint information into numeric models such as ocean circulation models can provide mechanistic explanations to observations and may enable us to better place our findings within the bigger picture of global carbon cycling.

Consensus Reference Materials

A broad range of chemical reference materials for ocean sciences remains elusive, despite the recognition that accuracy of data depends on calibration and intercomparison over time and among laboratories. To that end, the US National Research Council prepared a report identifying the most critically needed reference materials and recommending the most appropriate approaches for their development, with an emphasis on organic materials (Committee on Reference Materials for Ocean Science, 2002). Some of the recommendations of this committee remain unfulfilled.

The marine DOC community has adopted the consensus reference material available from D. Hansell's lab (University of Miami) to determine reproducibility and accuracy of oceanic DOC analyses (Sharp et al., 2002). When several researchers promoted the need for a collection of humic and fulvic acids to be made available to the scientific community, the International Humic Substances Society (IHSS) was organized in 1981. Since then, NOM research has benefited significantly from sharing common standard and reference materials with known elemental and stable isotopic ratios. Intercomparison of UHRMS data is challenging, as the "true" result is not known. A first interlaboratory comparison including 17 different high-resolution mass spectrometers and NOM reference material from the IHSS showed that while differences exist, common trends in elemental ratios are reproduced (Hawkes et al., 2020). Efforts such as this one will lead to the development of consensus values for quality control of the complex analyses. However, a marine reference material similar to the freshwater-sourced NOM from IHSS suitable also for fingerprinting techniques such as FT-ICR-MS or Orbitrap is missing to date, calling upon the community to establish such a material.

Reference materials for biological, particulate, and sedimentary OM are also conspicuously absent, in part because of logistical difficulties in preparing and certifying them, and perhaps more complex, a lack of consensus as to what would best constitute an appropriate reference material and what organic parameters should be targeted. Intercomparison

exercises have been conducted for organic contaminants in biological tissues (mussel) and sediments (New York/New Jersey estuary) in the marine environment (Schantz et al., 2008), but comparable exercises for marine biogeochemical materials have generally not been carried out. These difficulties are partially alleviated by targeting specific biomarkers or ratios of biomarkers. Two successful small-scale round-robin laboratory intercomparison exercises, in which a few kilograms of sediment or extracts/isolates were distributed to a limited number of laboratories, are the alkenone intercomparison (Rosell-Melé et al., 2001) and the GDGT intercomparison (Schouten et al., 2013a). It should be noted that in both of these round robin exercises, the targeted parameters were biomarker ratios ($U^{K'}_{37}$ and TEX_{86} and BIT, respectively) rather than a rigorous assessment of absolute concentrations. Nonetheless, the marine organic biogeochemical community needs to address this shortfall.

CONCLUDING REMARKS

Marine organic biogeochemistry has made significant contributions toward a better understanding of the fundamental processes that affect element cycles in the ocean, especially for carbon and nitrogen. As new questions arise and new paradigms are developed, there is a never-ending need for novel analytical methodologies, ranging from advanced instrumentation, cross-disciplinary field observations and experimentation, to new thinking about how the massive amounts of data generated by biogeochemists is handled and interpreted (**Figure 1**). This review has summarized the state of the art with respect to analytical instrumentation in use by marine organic biogeochemists (e.g., chromatography, mass spectrometry, NMR spectroscopy, radiocarbon analysis, enzyme assays) and chemometrics for data handling. Key challenges for the future are also highlighted. These include identifying new biomarkers, employing advanced high-resolution mass spectrometry and NMR spectroscopy for characterizing dissolved organic matter and its behavior, and coupling chemical analyses with microbiological assays. The review concludes with a plea to move forward in the long-standing but as yet unrealized effort to develop and distribute reference materials – whether certified standard reference materials (SRMs) for intercalibration exercises or consensus reference materials for intercomparisons – to the biogeochemical community. Identifying and preparing reference materials, while not an easy task, is critical to guarantee that data generated by laboratories worldwide will truly be applicable and useable worldwide.

AUTHOR CONTRIBUTIONS

SW conceived the workshop and convened the group of authors. AS, SK, and SW organized the manuscript and lead the writing. SK created the figure. All co-authors contributed text and ideas. All authors listed have made a substantial, direct and intellectual contribution to the work, and approved it for publication.

FUNDING

The Hanse-Wissenschaftskolleg Delmenhorst, Germany, sponsored the "Marine Organic Biogeochemistry" workshop in April 2019, of which this working group report was a part. The workshop was funded by the Deutsche Forschungsgemeinschaft (DFG, German Research Foundation) – project number: 422798570. The Geochemical Society provided additional funding for the conference. AS was supported by DOE grant DE-SC0020369.

REFERENCES

Abdulla, H. A. N., Minor, E. C., Dias, R. F., and Hatcher, P. G. (2010a). Changes in the compound classes of dissolved organic matter along an estuarine transect: a study using FTIR and ^{13}C NMR. *Geochim. Cosmochim. Acta* 74, 3815–3838. doi: 10.1016/j.gca.2010.04.006

Abdulla, H. A. N., Minor, E. C., Dias, R. F., and Hatcher, P. G. (2013a). Transformations of the chemical compositions of high molecular weight DOM along a salinity transect: using two dimensional correlation spectroscopy and principal component analysis approaches. *Geochim. Cosmochim. Acta* 118, 231–246. doi: 10.1016/j.gca.2013.03.036

Abdulla, H. A. N., Minor, E. C., and Hatcher, P. G. (2010b). Using two-dimensional correlations of ^{13}C NMR and FTIR to investigate changes in the chemical composition of dissolved organic matter along an estuarine transect. *Environ. Sci. Technol.* 44, 8044–8049. doi: 10.1021/es100898x

Abdulla, H. A. N., Sleighter, R. L., and Hatcher, P. G. (2013b). Two dimensional correlation analysis of Fourier transform ion cyclotron resonance mass spectra of dissolved organic matter: a new graphical analysis of trends. *Anal. Chem.* 85, 3895–3902. doi: 10.1021/ac303221j

Allen, A. E., LaRoche, J., Maheswari, U., Lommer, M., Schauer, N., Lopez, P. J., et al. (2008). Whole-cell response of the pennate diatom Phaeodactylum tricornutum to iron starvation. *Proc. Natl. Acad. Sci. U.S.A.* 105, 10438–10443. doi: 10.1073/pnas.0711370105

Aluwihare, L. I., and Meador, T. (2008). Chemical composition of marine dissolved organic nitrogen. *Nitrogen Mar. Environ.* 95–140. doi: 10.1016/b978-0-12-372522-6.00003-7

Aluwihare, L. I., Repeta, D. J., Pantoja, S., and Johnson, C. G. (2005). Two chemically distinct pools of organic nitrogen accumulate in the ocean. *Science* 308, 1007–1010. doi: 10.1126/science.1108925

Arakawa, N., and Aluwihare, L. (2015). Direct identification of diverse alicyclic terpenoids in suwannee river fulvic acid. *Environ. Sci. Technol.* 49, 4097–4105. doi: 10.1021/es5055176

Arakawa, N., Aluwihare, L. I., Simpson, A. J., Soong, R., Stephens, B. M., and Lane-Coplen, D. (2017). Carotenoids are the likely precursor of a significant fraction of marine dissolved organic matter. *Sci. Adv.* 3:e1602976. doi: 10.1126/sciadv.1602976

Arnosti, C. (1995). Measurement of depth- and site-related differences in polysaccharide hydrolysis rates in marine sediments. *Geochim. Cosmochim. Acta* 59, 4247–4257. doi: 10.1016/0016-7037(95)00247-W

Arnosti, C. (2004). Speed bumps and barricades in the carbon cycle: substrate structural effects on carbon cycling. *Mar. Chem.* 92, 263–273. doi: 10.1016/j.marchem.2004.06.030

Arnosti, C. (2011). Microbial extracellular enzymes and the marine carbon cycle. *Ann. Rev. Mar. Sci.* 3, 401–425. doi: 10.1146/annurev-marine-120709-142731

Arnosti, C., Steen, A. D., Ziervogel, K., Ghobrial, S., Jeffrey, W. H. W. H., and Wanunu, M. (2011). Latitudinal gradients in degradation of marine

dissolved organic carbon. *PLoS One* 6:e28900. doi: 10.1371/journal.pone.0028900

Aron, A. T., Gentry, E. C., McPhail, K. L., Nothias, L.-F., Nothias-Esposito, M., Bouslimani, A., et al. (2020). Reproducible molecular networking of untargeted mass spectrometry data using GNPS. *Nat. Protoc.* 15, 1954–1991.

Bao, R., Zhao, M., McNichol, A., Wu, Y., Guo, X., Haghipour, N., et al. (2019). On the origin of aged sedimentary organic matter along a river-shelf-deep ocean transect. *J. Geophys. Res. Biogeosci.* 124, 2582–2594. doi: 10.1029/2019JG005107

Baumer, B., and Udwin, D. (2015). R Markdown. *Wiley Interdiscip. Rev. Comput. Stat.* 7, 167–177. doi: 10.1002/wics.1348

Beaupré, S. R., and Druffel, E. R. M. (2012). Photochemical reactivity of ancient marine dissolved organic carbon. *Geophys. Res. Lett.* 39:L18602. doi: 10.1029/2012GL052974

Beaupré, S. R., Druffel, E. R. M., and Griffin, S. (2007). A low-blank photochemical extraction system for concentration and isotopic analyses of marine dissolved organic carbon. *Limnol. Oceanogr. Methods* 5, 174–184. doi: 10.4319/lom.2007.5.174

Benner, R., Pakulski, J. D., McCarthy, M., Hedges, J. I., and Hatcher, P. G. (1992). Bulk chemical characteristics of dissolved organic matter in the ocean. *Science* 255, 1561–1564. doi: 10.1126/science.255.5051.1561

Besseling, M. A., Hopmans, E. C., Bale, N. J., Schouten, S., Damsté, J. S. S., and Villanueva, L. (2020). The absence of intact polar lipid-derived GDGTs in marine waters dominated by Marine Group II: implications for lipid biosynthesis in Archaea. *Sci. Rep.* 10:294.

Biddle, J. F., Lipp, J. S., Lever, M. A., Lloyd, K. G., Sørensen, K. B., Anderson, R., et al. (2006). Heterotrophic Archaea dominate sedimentary subsurface ecosystems off Peru. *Proc. Natl. Acad. Sci. U.S.A.* 103, 3846–3851. doi: 10.1073/pnas.0600035103

Bird, J. T., Tague, E. D., Zinke, L., Schmidt, J. M., Steen, A. D., Reese, B. K., et al. (2019). Uncultured microbial phyla suggest mechanisms for multi-thousand-year subsistence in Baltic Sea sediments. *mBio* 10:e02376-18.

Birkholz, A., Smittenberg, R. H., Hajdas, I., Wacker, L., and Bernasconi, S. M. (2013). Isolation and compound specific radiocarbon dating of terrigenous branched glycerol dialkyl glycerol tetraethers (brGDGTs). *Org. Geochem.* 60, 9–19. doi: 10.1016/j.orggeochem.2013.04.008

Blumer, M. (1975). Organic compounds in nature: limits of our knowledge. *Angew. Chemie Int. Ed. Engl.* 14, 507–514. doi: 10.1002/anie.197505071

Boiteau, R. M., Hoyt, D. W., Nicora, C. D., Kinmonth-Schultz, H. A., Ward, J. K., and Bingol, K. (2018). Structure elucidation of unknown metabolites in metabolomics by combined NMR and MS/MS prediction. *Metabolites* 8:8. doi: 10.3390/metabo8010008

Bour, A. L., Walker, B. D., Broek, T. A. B., and McCarthy, M. D. (2016). Radiocarbon analysis of individual amino acids: carbon blank quantification for a small-sample high-pressure liquid chromatography purification method. *Anal. Chem.* 88, 3521–3528. doi: 10.1021/acs.analchem.5b03619

Boysen, A. K., Heal, K. R., Carlson, L. T., and Ingalls, A. E. (2018). Best-matched internal standard normalization in liquid chromatography-mass spectrometry metabolomics applied to environmental samples. *Anal. Chem.* 90, 1363–1369. doi: 10.1021/acs.analchem.7b04400

Bronk Ramsey, C., Ditchfield, P., and Humm, M. (2004). Using a gas ion source for radiocarbon AMS and GC-AMS. *Radiocarbon* 46, 25–32. doi: 10.1017/s003382220003931x

Cajka, T., and Fiehn, O. (2016). Toward merging untargeted and targeted methods in mass spectrometry-based metabolomics and lipidomics. *Anal. Chem.* 88, 524–545. doi: 10.1021/acs.analchem.5b04491

Cantarero, S., Henríquez-Castillo, C., Dildar, N., Vargas, C., von Dassow, P., Cornejo-D'Ottone, M., et al. (in press). Size-fractionated contribution of microbial biomass to suspended organic matter in the Eastern Tropical South Pacific oxygen minimum zone. *Front. Mar. Sci*. doi: 10.3389/fmars.2020.540643

Cao, X., Aiken, G. R., Butler, K. D., Huntington, T. G., Balch, W. M., Mao, J., et al. (2018). Evidence for major input of riverine organic matter into the ocean. *Org. Geochem.* 116, 62–76. doi: 10.1016/j.orggeochem.2017.11.001

Cham, J. (2012). *Piled Higher and Deeper Comics*. Available online at: http://phdcomics.com/comics/archive.php?comicid=1531 (accessed July 1, 2020).

Clark, L. L., Ingall, E. D., and Benner, R. (1998). Marine phosphorus is selectively remineralized. *Nature* 393:426. doi: 10.1038/30881

Coble, P. G. (2007). Marine optical biogeochemistry: the chemistry of ocean color. *Chem. Rev.* 107, 402–418. doi: 10.1021/cr050350

Collins, J. R., Edwards, B. R., Fredricks, H. F., and Van Mooy, B. A. S. S. (2016). LOBSTAHS: an adduct-based lipidomics strategy for discovery and identification of oxidative stress biomarkers. *Anal. Chem.* 88, 7154–7162. doi: 10.1021/acs.analchem.6b01260

Comisarow, M. B., and Marshall, A. G. (1974). Fourier transform ion cyclotron resonance spectroscopy. *Chem. Phys. Lett.* 25, 282–283.

Committee on Reference Materials for Ocean Science (2002). *Chemical Reference Materials: Setting the Standards for Ocean Science*. Washington, DC: The National Academies Press.

Crockford, D. J., Holmes, E., Lindon, J. C., Plumb, R. S., Zirah, S., Bruce, S. J., et al. (2006). Statistical heterospectroscopy, an approach to the integrated analysis of NMR and UPLC-MS data sets: application in metabonomic toxicology studies. *Anal. Chem.* 78, 363–371. doi: 10.1021/ac051444m

Cui, L., Wang, X., and Feng, L. (2019). Determination of nitrogen isotopes on samples with tens of nmol of N using the combination of an elemental analyzer, a GasBench interface and an isotope ratio mass spectrometer: an evaluation of blank N contributions and blank-correction. *Rapid Commun. Mass Spectrom.* 33, 74–80. doi: 10.1002/rcm.8309

de Bar, M. W., Hopmans, E. C., Verweij, M., Dorhout, D. J. C., Damsté, J. S. S., and Schouten, S. (2017). Development and comparison of chromatographic methods for the analysis of long chain diols and alkenones in biological materials and sediment. *J. Chromatogr. A* 1521, 150–160. doi: 10.1016/j.chroma.2017.09.037

DiDonato, N., and Hatcher, P. G. (2017). Alicyclic carboxylic acids in soil humic acid as detected with ultrahigh resolution mass spectrometry and multi-dimensional NMR. *Org. Geochem.* 112, 33–46. doi: 10.1016/j.orggeochem.2017.06.010

Dittmar, T. (2015). "Reasons behind the long-term stability of dissolved organic matter," in *Biogeochemistry of Marine Dissolved Organic Matter*, eds D. A. Hansell and C. A. Carlson (New York, NY: Elsevier Inc), 369–385. doi: 10.1016/B978-0-12-405940-5.00007-8

Dittmar, T., Koch, B., Hertkorn, N., and Kattner, G. (2008). A simple and efficient method for the solid-phase extraction of dissolved organic matter (SPE-DOM) from seawater. *Limnol. Oceanogr. Methods* 6, 230–235. doi: 10.4319/lom.2008.6.230

Dittmar, T., and Koch, B. P. (2006). Thermogenic organic matter dissolved in the abyssal ocean. *Mar. Chem.* 102, 208–217. doi: 10.1016/j.marchem.2006.04.003

Druffel, E. R. M., Beaupré, S. R., and Ziolkowski, L. A. (2016). "Radiocarbon in the oceans," in *Radiocarbon and Climate Change: Mechanisms, Applications and Laboratory Techniques*, eds E. Schuur, E. Druffel, and S. Trumbore (Cham: Springer), 139–166. doi: 10.1007/978-3-319-25643-6_5

Druffel, E. R. M., Zhang, D., Xu, X., Ziolkowski, L. A., Southon, J. R., Dos Santos, G. M., et al. (2010). Compound-specific radiocarbon analyses of phospholipid fatty acids and n-alkanes in Ocean sediments. *Radiocarbon* 52, 1215–1223. doi: 10.1017/S0033822200046294

Dührkop, K., Fleischauer, M., Ludwig, M., Aksenov, A. A., Melnik, A. V., Meusel, M., et al. (2019). SIRIUS 4: a rapid tool for turning tandem mass spectra into metabolite structure information. *Nat. Methods* 16, 299–302. doi: 10.1038/s41592-019-0344-8

Durham, B. P., Boysen, A. K., Carlson, L. T., Groussman, R. D., Heal, K. R., Cain, K. R., et al. (2019). Sulfonate-based networks between eukaryotic phytoplankton and heterotrophic bacteria in the surface ocean. *Nat. Microbiol.* 4, 1706–1715. doi: 10.1038/s41564-019-0507-5

Eek, K. M., Sessions, A. L., and Lies, D. P. (2007). Carbon-isotopic analysis of microbial cells sorted by flow cytometry. *Geobiology* 5, 85–95. doi: 10.1111/j.1472-4669.2006.00094.x

Eglinton, T. I., Aluwihare, L. I., Bauer, J. E., Druffel, E. R. M., and McNichol, A. P. (1996). Gas chromatographic isolation of individual compounds from complex matrices for radiocarbon dating. *Anal. Chem.* 68, 904–912. doi: 10.1021/ac9508513

Eiler, J., Cesar, J., Chimiak, L., Dallas, B., Grice, K., Griep-Raming, J., et al. (2017). Analysis of molecular isotopic structures at high precision and accuracy by Orbitrap mass spectrometry. *Int. J. Mass Spectrom.* 422, 126–142. doi: 10.1016/j.ijms.2017.10.002

Eiserbeck, C., Nelson, R. K., Reddy, C. M., and Grice, K. (2014). *Advances in Comprehensive Two-Dimensional Gas Chromatography (GC× GC)*. London: Royal Society of Chemistry.

Ernst, M., Kang, K. B., Caraballo-Rodríguez, A. M., Nothias, L.-F., Wandy, J., et al. (2019). MolNetEnhancer: enhanced molecular networks by integrating metabolome mining and annotation tools. *Metabolites* 9:144. doi: 10.3390/metabo9070144

Evans, T. W., Könneke, M., Lipp, J. S., Adhikari, R. R., Taubner, H., Elvert, M., et al. (2018). Lipid biosynthesis of Nitrosopumilus maritimus dissected by lipid specific radioisotope probing (lipid-RIP) under contrasting ammonium supply. *Geochim. Cosmochim. Acta* 242, 51–63. doi: 10.1016/j.gca.2018.09.001

Feunang, Y. D., Eisner, R., Knox, C., Chepelev, L., Hastings, J., Owen, G., et al. (2016). ClassyFire: automated chemical classification with a comprehensive, computable taxonomy. *J. Cheminform.* 8:61.

Fichot, C. G., Downing, B. D., Bergamaschi, B. A., Windham-Myers, L., Marvin-Dipasquale, M., Thompson, D. R., et al. (2016). High-resolution remote sensing of water quality in the san francisco bay-delta estuary. *Environ. Sci. Technol.* 50, 573–583. doi: 10.1021/acs.est.5b03518

Fox, C. A., Abdulla, H. A., Burdige, D. J., Lewicki, J. P., and Komada, T. (2018). Composition of dissolved organic matter in pore waters of anoxic marine sediments analyzed by 1H nuclear magnetic resonance spectroscopy. *Front. Mar. Sci.* 5:172. doi: 10.3389/fmars.2018.00172

Fulton, J. M., Arthur, M. A., Thomas, B., and Freeman, K. H. (2018). Pigment carbon and nitrogen isotopic signatures in euxinic basins. *Geobiology* 16, 429–445. doi: 10.1111/gbi.12285

Galli, I., Bartalini, S., Ballerini, R., Barucci, M., Cancio, P., De Pas, M., et al. (2016). Spectroscopic detection of radiocarbon dioxide at parts-per-quadrillion sensitivity. *Optica* 3, 385–388. doi: 10.1364/OPTICA.3.000385

Gandrud, C. (2013). *Reproducible Research with R and R Studio*. Boca Raton, FL: CRC Press.

Garrido, J. L., Airs, R. L., Rodríguez, F., van Heukelem, L., and Zapata, M. (2012). "New HPLC separation techniques," in *Phytoplankton Pigments*, eds S. Roy and C. A. Llewellyn (Cambridge: Cambridge University Press), 165–194. doi: 10.1017/cbo9780511732263.008

Genta-Jouve, G., Croué, J., Weinberg, L., Cocandeau, V., Holderith, S., Bontemps, N., et al. (2014). Two-dimensional ultra high pressure liquid chromatography quadrupole/time-of-flight mass spectrometry for semi-targeted natural compounds identification. *Phytochem. Lett.* 10, 318–323. doi: 10.1016/j.phytol.2014.10.029

Ghaste, M., Mistrik, R., and Shulaev, V. (2016). Applications of fourier transform ion cyclotron resonance (FT-ICR) and orbitrap based high resolution mass spectrometry in metabolomics and lipidomics. *Int. J. Mol. Sci.* 17:816. doi: 10.3390/ijms17060816

Gierga, M., Schneider, M. P. W., Wiedemeier, D. B., Lang, S. Q., Smittenberg, R. H., Hajdas, I., et al. (2014). Purification of fire derived markers for μg scale isotope analysis ($\delta^{13}C$, $\Delta^{14}C$) using high performance liquid chromatography (HPLC). *Org. Geochem.* 70, 1–9. doi: 10.1016/j.orggeochem.2014.02.008

Grant, K. E., Galy, V. V., Chadwick, O. A., and Derry, L. A. (2019). Thermal oxidation of carbon in organic matter rich volcanic soils: insights into SOC age differentiation and mineral stabilization. *Biogeochemistry* 144, 291–304. doi: 10.1007/s10533-019-00586-1

Green, N. W., Perdue, E. M., Aiken, G. R., Butler, K. D., Chen, H., Dittmar, T., et al. (2014). An intercomparison of three methods for the large-scale isolation of oceanic dissolved organic matter. *Mar. Chem.* 161, 14–19. doi: 10.1016/j.marchem.2014.01.012

Grobe, H., Diepenbroek, M., Dittert, N., Reinke, M., and Sieger, R. (2006). "Archiving and distributing earth-science data with the PANGAEA information system," in *Antarctica*, eds D. K. Fütterer, D. Damaske, G. Kleinschmidt, H. Miller, and F. Tessensohn (Berlin: Springer-Verlag), 403–406. doi: 10.1007/3-540-32934-x_51

Guijas, C., Montenegro-Burke, J. R., Domingo-Almenara, X., Palermo, A., Warth, B., Hermann, G., et al. (2018). METLIN: a technology platform for identifying knowns and unknowns. *Anal. Chem.* 90, 3156–3164. doi: 10.1021/acs.analchem.7b04424

Haghipour, N., Ausin, B., Usman, M. O., Ishikawa, N., Wacker, L., Welte, C., et al. (2019). Compound-specific radiocarbon analysis by elemental analyzer-accelerator mass spectrometry: precision and limitations. *Anal. Chem.* 91, 2042–2049. doi: 10.1021/acs.analchem.8b04491

Hansman, R. L., Dittmar, T., and Herndl, G. J. (2015). Conservation of dissolved organic matter molecular composition during mixing of the deep water masses of the northeast Atlantic Ocean. *Mar. Chem.* 177, 288–297. doi: 10.1016/j.marchem.2015.06.001

Hansman, R. L., and Sessions, A. L. (2016). Measuring the in situ carbon isotopic composition of distinct marine plankton populations sorted by flow cytometry. *Limnol. Oceanogr. Methods* 14, 87–99. doi: 10.1002/lom3.10073

Hartmann, A. C., Petras, D., Quinn, R. A., Protsyuk, I., Archer, F. I., Ransome, E., et al. (2017). Meta-mass shift chemical profiling of metabolomes from coral reefs. *Proc. Natl. Acad. Sci. U.S.A.* 114, 11685–11690. doi: 10.1073/pnas.1710248114

Haug, K., Cochrane, K., Nainala, V. C., Williams, M., Chang, J., Jayaseelan, K. V., et al. (2020). MetaboLights: a resource evolving in response to the needs of its scientific community. *Nucleic Acids Res.* 48, D440–D444.

Hawkes, J. A., D'Andrilli, J., Agar, J. N., Barrow, M. P., Berg, S. M., Catalán, N., et al. (2020). An international laboratory comparison of dissolved organic matter composition by high resolution mass spectrometry: are we getting the same answer? *Limnol. Oceanogr. Methods* 18, 235–258. doi: 10.1002/lom3.10364

Hawkes, J. A., Patriarca, C., Sjöberg, P. J. R., Tranvik, L. J., and Bergquist, J. (2018). Extreme isomeric complexity of dissolved organic matter found across aquatic environments. *Limnol. Oceanogr. Lett.* 3, 21–30. doi: 10.1002/lol2.10064

Heal, K. R., Qin, W., Ribalet, F., Bertagnolli, A. D., Coyote-Maestas, W., Hmelo, L. R., et al. (2017). Two distinct pools of B12 analogs reveal community interdependencies in the ocean. *Proc. Natl. Acad. Sci. U.S.A.* 114, 364–369. doi: 10.1073/pnas.1608462114

Hedges, J., Eglinton, G., Hatcher, P., Kirchman, D., Arnosti, C., Derenne, S., et al. (2000). The molecularly-uncharacterized component of nonliving organic matter in natural environments. *Org. Geochem.* 31, 945–958. doi: 10.1016/s0146-6380(00)00096-6

Helms, J. R., Mao, J., Chen, H., Perdue, E. M., Green, N. W., Hatcher, P. G., et al. (2015). Spectroscopic characterization of oceanic dissolved organic matter isolated by reverse osmosis coupled with electrodialysis. *Mar. Chem.* 177, 278–287. doi: 10.1016/j.marchem.2015.07.007

Helms, J. R., Stubbins, A., Ritchie, J. D., Minor, E. C., Kieber, D. J., and Mopper, K. (2008). Absorption spectral slopes and slope rations as indicators of molecular weight, source, and photoleaching of chromophoric dissolved organic matter. *Limnol. Oceanogr.* 53, 955–969. doi: 10.4319/lo.2008.53.3.0955

Hemingway, J. D., Hilton, R. G., Hovius, N., Eglinton, T. I., Haghipour, N., Wacker, L., et al. (2018). Microbial oxidation of lithospheric organic carbon in rapidly eroding tropical mountain soils. *Science* 360, 209–212. doi: 10.1126/science.aao6463

Hemingway, J. D., Rothman, D. H., Grant, K. E., Rosengard, S. Z., Eglinton, T. I., Derry, L. A., et al. (2019). Mineral protection regulates long-term global preservation of natural organic carbon. *Nature* 570, 228–231. doi: 10.1038/s41586-019-1280-6

Hertkorn, N., Benner, R., Frommberger, M., Schmitt-Kopplin, P., Witt, M., Kaiser, K., et al. (2006). Characterization of a major refractory component of marine dissolved organic matter. *Geochim. Cosmochim. Acta* 70, 2990–3010. doi: 10.1016/j.gca.2006.03.021

Hertkorn, N., Frommberger, M., Witt, M., Koch, B. P., Schmitt-Kopplin, P., and Perdue, E. M. (2008). Natural organic matter and the event horizon of mass spectrometry. *Anal. Chem.* 80, 8908–8919. doi: 10.1021/ac800464g

Hertkorn, N., Harir, M., Koch, B. P., Michalke, B., and Schmitt-Kopplin, P. (2013). High-field NMR spectroscopy and FTICR mass spectrometry: powerful discovery tools for the molecular level characterization of marine dissolved organic matter. *Biogeosciences* 10, 1583–1624. doi: 10.5194/bg-10-1583-2013

Higgins, H. W., Wright, S. W., and Schlüter, L. (2012). "Quantitative interpretation of chemotaxonomic pigment data," in *Phytoplankton Pigments*, eds S. Roy and C. A. Llewellyn (Cambridge: Cambridge University Press), 257–313. doi: 10.1017/cbo9780511732263.010

Higgins, M. B., Robinson, R. S., Casciotti, K. L., McIlvin, M. R., and Pearson, A. (2009). A method for determining the nitrogen isotopic composition of porphyrins. *Anal. Chem.* 81, 184–192. doi: 10.1021/ac8017185

Higgins Keppler, E. A., Jenkins, C. L., Davis, T. J., and Bean, H. D. (2018). Advances in the application of comprehensive two-dimensional gas chromatography in metabolomics. *TrAC Trends Anal. Chem.* 109, 275–286. doi: 10.1016/j.trac.2018.10.015

Hoh, E., Dodder, N. G., Lehotay, S. J., Pangallo, K. C., Reddy, C. M., and Maruya, K. A. (2012). Nontargeted comprehensive two-dimensional gas chromatography/time-of-flight mass spectrometry method and software

for inventorying persistent and bioaccumulative contaminants in marine environments. *Environ. Sci. Technol.* 46, 8001–8008. doi: 10.1021/es30 1139q

Hopmans, E. C., Schouten, S., and Sinninghe Damsté, J. S. (2016). The effect of improved chromatography on GDGT-based palaeoproxies. *Org. Geochem.* 93, 1–6. doi: 10.1016/j.orggeochem.2015.12.006

Hoppe, H.-G. (1983). Significance of exoenzymatic activities in the ecology of brackish water: measurements by means of methylumbelliferyl-substrates. *Mar. Ecol. Prog. Ser.* 11, 299–308. doi: 10.3354/meps011299

Hou, J., Huang, Y., Brodsky, C., Alexandre, M. R., McNichol, A. P., King, J. W., et al. (2010). Radiocarbon dating of individual lignin phenols: a new approach for establishing chronology of late quaternary lake sediments. *Anal. Chem.* 82, 7119–7126. doi: 10.1021/ac100494m

Hu, Q., Noll, R. J., Li, H., Makarov, A., Hardman, M., and Graham Cooks R. (2005). The Orbitrap: a new mass spectrometer. *J. Mass Spectrom.* 40, 430–443. doi: 10.1002/jms.856

Hughey, C. A., Hendrickson, C. L., Rodgers, R. P., Marshall, A. G., and Qian, K. (2001). Kendrick mass defect spectrum: a compact visual analysis for ultrahigh-resolution broadband mass spectra. *Anal. Chem.* 73, 4676–4681. doi: 10.1021/ac010560w

Hunter, J. E., Frada, M. J., Fredricks, H. F., Vardi, A., and Van Mooy, B. A. S. (2015). Targeted and untargeted lipidomics of Emiliania huxleyi viral infection and life cycle phases highlights molecular biomarkers of infection, susceptibility, and ploidy. *Front. Mar. Sci.* 2:81. doi: 10.3389/fmars.2015.00081

Hurley, S. J., Elling, F. J., Könneke, M., Buchwald, C., Wankel, S. D., Santoro, A. E., et al. (2016). Influence of ammonia oxidation rate on thaumarchaeal lipid composition and the TEX86 temperature proxy. *Proc. Natl. Acad. Sci. U.S.A.* 113, 7762–7767. doi: 10.1073/pnas.1518534113

Imachi, H., Nobu, M. K., Nakahara, N., Morono, Y., Ogawara, M., Takaki, Y., et al. (2020). Isolation of an archaeon at the prokaryote–eukaryote interface. *Nature* 577, 519–525.

Ingalls, A. E., Anderson, R. F., and Pearson, A. (2004). Radiocarbon dating of diatom-bound organic compounds. *Mar. Chem.* 92, 91–105. doi: 10.1016/j.marchem.2004.06.019

Ingalls, A. E., Ellis, E. E., Santos, G. M., McDuffee, K. E., Truxal, L., Keil, R. G., et al. (2010). HPLC purification of higher plant-dervied lignin phenols for compound specific radiocarbon analysis. *Anal. Chem.* 82, 8931–8938. doi: 10.1021/ac1016584

Ingalls, A. E., Shah, S. R., Hansman, R. L., Aluwihare, L. I., Santos, G. M., Druffel, E. R. M., et al. (2006). Quantifying archaeal community autotrophy in the mesopelagic ocean using natural radiocarbon. *Proc. Natl. Acad. Sci. U.S.A.* 103, 6442–6447. doi: 10.1073/pnas.0510157103

Isaji, Y., Ogawa, N. O., Boreham, C. J., Kashiyama, Y., and Ohkouchi, N. (2020). Evaluation of $\delta^{13}C$ and $\delta^{15}N$ uncertainties associated with the compound-specific isotope analysis of geoporphyrins. *Anal. Chem.* 92, 3152–3160. doi: 10.1021/acs.analchem.9b04843

Ishikawa, N. F., Itahashi, Y., Blattmann, T. M., Takano, Y., Ogawa, N. O., Yamane, M., et al. (2018). Improved method for isolation and purification of underivatized amino acids for radiocarbon analysis. *Anal. Chem.* 90, 12035–12041. doi: 10.1021/acs.analchem.8b02693

Jaeger, M., and Aspers, R. (2014). Chapter Five - Covariance NMR and small molecule applications. *Annu. Rep. NMR Spectrosc.* 83, 271–349. doi: 10.1016/b978-0-12-800183-7.00005-8

Jarmusch, A. K., Wang, M., Aceves, C. M., Advani, R. S., Aguire, S., Aksenov, A. A., et al. (2019). Repository-scale co-and re-analysis of tandem mass spectrometry data. *bioRxiv* [Preprint]. doi: 10.1101/750471

Johnson, W. M., Kido Soule, M. C., and Kujawinski, E. B. (2016). Evidence for quorum sensing and differential metabolite production by a marine bacterium in response to DMSP. *ISME J.* 10, 2304–2316. doi: 10.1038/ismej.2016.6

Johnson, W. M., Kido Soule, M. C., and Kujawinski, E. B. (2017). Extraction efficiency and quantification of dissolved metabolites in targeted marine metabolomics: matrix effects in marine metabolomics. *Limnol. Oceanogr. Methods* 15, 417–428. doi: 10.1002/lom3.10181

Johnson, W. M., Longnecker, K., Kido Soule, M. C., Arnold, W. A., Bhatia, M. P., Hallam, S. J., et al. (2020). Metabolite composition of sinking particles differs from surface suspended particles across a latitudinal transect in the South Atlantic. *Limnol. Oceanogr.* 65, 111–127. doi: 10.1002/lno.11255

Junium, C. K., Arthur, M. A., and Freeman, K. H. (2015). Compound-specific $\delta^{15}N$ and chlorin preservation in surface sediments of the Peru Margin with implications for ancient bulk δ15N records. *Geochim. Cosmochim. Acta* 160, 306–318. doi: 10.1016/j.gca.2014.12.018

Junium, C. K., Dickson, A. J., and Uveges, B. T. (2018). Perturbation to the nitrogen cycle during rapid Early Eocene global warming. *Nat. Commun.* 9:3186. doi: 10.1038/s41467-018-05486-w

Junot, C., Fenaille, F., Colsch, B., and Bécher, F. (2014). High resolution mass spectrometry based techniques at the crossroads of metabolic pathways. *Mass Spectrom. Rev.* 33, 471–500. doi: 10.1002/mas.21401

Junot, C., Madalinski, G., Tabet, J. C., and Ezan, E. (2010). Fourier transform mass spectrometry for metabolome analysis. *Analyst* 135, 2203–2219. doi: 10.1039/c0an00021c

Katayama, T., Nobu, M. K., Kusada, H., Meng, X.-Y., Yoshioka, H., Kamagata, Y., et al. (2019). Membrane-bounded nucleoid discovered in a cultivated bacterium of the candidate phylum 'Atribacteria.'. *bioRxiv* [Preprint]. doi: 10.1101/728279

Kellermann, M. Y., Yoshinaga, M. Y., Wegener, G., Krukenberg, V., and Hinrichs, K. U. (2016). Tracing the production and fate of individual archaeal intact polar lipids using stable isotope probing. *Org. Geochem.* 95, 13–20. doi: 10.1016/j.orggeochem.2016.02.004

Kharbush, J. J., Allen, A. E., Moustafa, A., Dorrestein, P. C., and Aluwihare, L. I. (2016). Intact polar diacylglycerol biomarker lipids isolated from suspended particulate organic matter accumulating in an ultraoligotrophic water column. *Org. Geochem.* 100, 29–41. doi: 10.1016/j.orggeochem.2016.07.008

Kido Soule, M. C., Longnecker, K., Giovannoni, S. J., Kujawinski, E. B., Soule, M. C. K., Longnecker, K., et al. (2010). Impact of instrument and experiment parameters on reproducibility of ultrahigh resolution ESI FT-ICR mass spectra of natural organic matter. *Org. Geochem.* 41, 725–733. doi: 10.1016/j.orggeochem.2010.05.017

Kilgour, D. P. A. A., Wills, R., Qi, Y., O'Connor, P. B., and O'Connor, P. B. (2013). Autophaser: an algorithm for automated generation of absorption mode spectra for FT-ICR MS. *Anal. Chem.* 85, 3903–3911. doi: 10.1021/ac303289c

Kind, T., and Fiehn, O. (2007). Seven Golden Rules for heuristic filtering of molecular formulas obtained by accurate mass spectrometry. *BMC Bioinformatics* 8:105. doi: 10.1186/1471-2105-8-105

Knapp, A. N., Sigman, D. M., and Lipschultz, F. (2005). N isotopic composition of dissolved organic nitrogen and nitrate at the Bermuda Atlantic Time-series study site. *Global Biogeochem. Cycles* 19, 1–15. doi: 10.1029/2004GB002320

Knauff, M., and Nejasmic, J. (2014). An efficiency comparison of document preparation systems used in academic research and development. *PLoS One* 9:e115069. doi: 10.1371/journal.pone.0115069

Knuth, D. E. (1984). Literate programming. *Comput. J.* 27, 97–111. doi: 10.1093/COMJNL/27.2.97

Koch, B., Witt, M., Engbrodt, R., Dittmar, T., and Kattner, G. (2005). Molecular formulae of marine and terrigenous dissolved organic matter detected by electrospray ionization Fourier transform ion cyclotron resonance mass spectrometry. *Geochim. Cosmochim. Acta* 69, 3299–3308. doi: 10.1016/j.gca.2005.02.027

Kolowith, L. C., Ingall, E. D., and Benner, R. (2001). Composition and cycling of marine organic phosphorus. *Limnol. Oceanogr.* 46, 309–320. doi: 10.4319/lo.2001.46.2.0309

Könneke, M., Bernhard, A. E., De La Torre, J. R., Walker, C. B., Waterbury, J. B., and Stahl, D. A. (2005). Isolation of an autotrophic ammonia-oxidizing marine archaeon. *Nature* 437, 543–546. doi: 10.1038/nature03911

Koprivnjak, J.-F., Pfromm, P. H., Ingall, E., Vetter, T. A., Schmitt-Kopplin, P., Hertkorn, N., et al. (2009). Chemical and spectroscopic characterization of marine dissolved organic matter isolated using coupled reverse osmosis–electrodialysis. *Geochim. Cosmochim. Acta* 73, 4215–4231. doi: 10.1016/j.gca.2009.04.010

Kujawinski, E. B. (2011). The impact of microbial metabolism on marine dissolved organic matter. *Ann. Rev. Mar. Sci.* 3, 567–599. doi: 10.1146/annurev-marine-120308-081003

Kujawinski, E. B., Del Vecchio, R., Blough, N. V., Klein, G. C., Marshall, A. G., Delvecchio, R., et al. (2004). Probing molecular-level transformations of dissolved organic matter: insights on photochemical degradation and protozoan modification of DOM from electrospray ionization Fourier

transform ion cyclotron resonance mass spectrometry. *Mar. Chem.* 92, 23–37. doi: 10.1016/j.marchem.2004.06.038

Kujawinski, E. B., Longnecker, K., Barott, K. L., Weber, R. J. M., and Kido Soule, M. C. (2016). Microbial community structure affects marine dissolved organic matter composition. *Front. Mar. Sci.* 3:45. doi: 10.3389/fmars.2016.00045

Kujawinski, E. B., Longnecker, K., Blough, N. V., Del Vecchio, R., Finlay, L., Kitner, J. B., et al. (2009). Identification of possible source markers in marine dissolved organic matter using ultrahigh resolution mass spectrometry. *Geochim. Cosmochim. Acta* 73, 4384–4399. doi: 10.1016/j.gca.2009.04.033

Kusch, S., Kashiyama, Y., Ogawa, N. O., Altabet, M., Butzin, M., Friedrich, J., et al. (2010). Implications for chloro-and pheopigment synthesis and preservation from combined compound-specific $\delta^{13}C$, $\delta^{15}N$, and $\Delta^{14}C$ analysis. *Biogeosci. Discuss.* 7, 6265–6294.

Lai, Z., Tsugawa, H., Wohlgemuth, G., Mehta, S., Mueller, M., Zheng, Y., et al. (2018). Identifying metabolites by integrating metabolome databases with mass spectrometry cheminformatics. *Nat. Methods* 15, 53–56. doi: 10.1038/nmeth.4512

Lam, B., and Simpson, A. J. (2008). Direct ^{1}H NMR spectroscopy of dissolved organic matter in natural waters. *Analyst* 133, 263–269. doi: 10.1039/b713457f

Langel, R., and Dyckmans, J. (2014). Combined ^{13}C and ^{15}N isotope analysis on small samples using a near-conventional elemental analyzer/isotope ratio mass spectrometer setup. *Rapid Commun. Mass Spectrom.* 28, 1019–1022. doi: 10.1002/rcm.6878

Lechtenfeld, O. J., Hertkorn, N., Shen, Y., Witt, M., and Benner, R. (2015). Marine sequestration of carbon in bacterial metabolites. *Nat. Commun.* 6:6711. doi: 10.1038/ncomms7711

Lechtenfeld, O. J., Kattner, G., Flerus, R., McCallister, S. L., Schmitt-Kopplin, P., and Koch, B. P. (2014). Molecular transformation and degradation of refractory dissolved organic matter in the Atlantic and Southern Ocean. *Geochim. Cosmochim. Acta* 126, 321–337. doi: 10.1016/j.gca.2013.11.009

Lechtenfeld, O. J., Koch, B. P., Geibert, W., Ludwichowski, K. U., and Kattner, G. (2011). Inorganics in organics: quantification of organic phosphorus and sulfur and trace element speciation in natural organic matter using HPLC-ICPMS. *Anal. Chem.* 83, 8968–8974. doi: 10.1021/ac201765a

Lee, C., Wakeham, S. G., and Benner, R. H. (2004). Symposium on new approaches in marine organic biogeochemistry: a tribute to the life and science of John I. Hedges. *Mar. Chem.* 92, 1–3. doi: 10.1016/j.marchem.2004.06.013

Leisch, F. (2002). "Sweave: dynamic generation of statistical reports using literate data analysis," in *Compstat*, eds W. Härdle and B. Rönz (Heidelberg: Physica-Verlag HD), 575–580. doi: 10.1007/978-3-642-57489-4_89

Leyva, D., Tose, L. V., Porter, J., Wolff, J., Jaffé, R., and Fernandez-Lima, F. (2019). Understanding the structural complexity of dissolved organic matter: Isomeric diversity. *Faraday Discuss.* 218, 431–440. doi: 10.1039/c8fd00221e

Li, Y., Harir, M., Uhl, J., Kanawati, B., Lucio, M., Smirnov, K. S., et al. (2017). How representative are dissolved organic matter (DOM) extracts? A comprehensive study of sorbent selectivity for DOM isolation. *Water Res.* 116, 316–323. doi: 10.1016/j.watres.2017.03.038

Li, Y., and Li, L. (2019). Mass accuracy check using common background peaks for improving metabolome data quality in chemical isotope labeling LC-MS. *J. Am. Soc. Mass Spectrom.* 30, 1733–1741. doi: 10.1007/s13361-019-02248-w

Liu, Z., Kobiela, M. E., McKee, G. A., Tang, T., Lee, C., Mulholland, M. R., et al. (2010). The effect of chemical structure on the hydrolysis of tetrapeptides along a river-to-ocean transect: AVFA and SWGA. *Mar. Chem.* 119, 108–120. doi: 10.1016/j.marchem.2010.01.005

Liu, Z., Liu, S., Liu, J., and Gardner, W. S. (2013). Differences in peptide decomposition rates and pathways between hypoxic and oxic coastal environments. *Mar. Chem.* 157, 67–77. doi: 10.1016/j.marchem.2013.08.003

Liu, Z., Mao, J., Peterson, M. L., Lee, C., Wakeham, S. G., and Hatcher, P. G. (2009). Characterization of sinking particles from the northwest Mediterranean Sea using advanced solid-state NMR. *Geochim. Cosmochim. Acta* 73, 1014–1026. doi: 10.1016/j.gca.2008.11.019

Lloyd, K. G., Steen, A. D., Ladau, J., Yin, J., and Crosby, L. (2018). Phylogenetically novel uncultured microbial cells dominate earth microbiomes. *mSystems* 3:e00055-18. doi: 10.1128/mSystems.00055-18

Longnecker, K., and Kujawinski, E. B. (2016). Using network analysis to discern compositional patterns in ultrahigh-resolution mass spectrometry data of dissolved organic matter. *Rapid Commun. Mass Spectrom.* 30, 2388–2394. doi: 10.1002/rcm.7719

Longnecker, K., and Kujawinski, E. B. (2017). Mining mass spectrometry data: using new computational tools to find novel organic compounds in complex environmental mixtures. *Org. Geochem.* 110, 92–99. doi: 10.1016/j.orggeochem.2017.05.008

Maie, N., Parish, K. J., Watanabe, A., Knicker, H., Benner, R., Abe, T., et al. (2006). Chemical characteristics of dissolved organic nitrogen in an oligotrophic subtropical coastal ecosystem. *Geochim. Cosmochim. Acta* 70, 4491–4506. doi: 10.1016/j.gca.2006.06.1554

Mao, J. D., Hu, W. G., Schmidt-Rohr, K., Davies, G., Ghabbour, E. A., and Xing, B. (2000). Quantitative characterization of humic substances by solid-state carbon-13 nuclear magnetic resonance. *Soil Sci. Soc. Am. J.* 64, 873–884. doi: 10.2136/sssaj2000.643873x

Marshall, A. G., and Chen, T. (2015). 40 years of Fourier transform ion cyclotron resonance mass spectrometry. *Int. J. Mass Spectrom.* 377, 410–420. doi: 10.1016/j.ijms.2014.06.034

Martínez-Pérez, A. M., Osterholz, H., Nieto-Cid, M., Álvarez, M., Dittmar, T., and Álvarez-Salgado, X. A. (2017). Molecular composition of dissolved organic matter in the Mediterranean Sea. *Limnol. Oceanogr.* 62, 2699–2712. doi: 10.1002/lno.10600

McCarthy, M., Pratum, T., Hedges, J., and Benner, R. (1997). Chemical composition of dissolved organic nitrogen in the ocean. 390, 150–154. doi: 10.1038/36535

McLean, C., and Kujawinski, E. B. (2019). AutoTuner: high fidelity, robust, and rapid parameter selection for metabolomics data processing. *bioRxiv* [Preprint]. doi: 10.1101/812370

Medeiros, P. M., Seidel, M., Ward, N. D., Carpenter, E. J., Gomes, H. R., Niggemann, J., et al. (2015). Fate of the Amazon River dissolved organic matter in the tropical Atlantic Ocean. *Glob. Biogeochem. Cycles* 29, 677–690. doi: 10.1002/2015GB005115

Moore, E. K., Hopmans, E. C., Rijpstra, W. I. C., Villanueva, L., and Damsté, J. S. S. (2016). Elucidation and identification of amino acid containing membrane lipids using liquid chromatography/high-resolution mass spectrometry. *Rapid Commun. Mass Spectrom.* 30, 739–750. doi: 10.1002/rcm.7503

Mopper, K., Stubbins, A., Ritchie, J. D., Bialk, H. M., and Hatcher, P. G. (2007). Advanced instrumental approaches for characterization of marine dissolved organic matter: extraction techniques, mass spectrometry, and nuclear magnetic resonance spectroscopy. *Chem. Rev.* 107, 419–442. doi: 10.1021/cr050359b

Moran, M. A., Kujawinski, E. B., Stubbins, A., Fatland, R., Aluwihare, L. I., Buchan, A., et al. (2016). *Deciphering Ocean Carbon in a Changing World. National Academy of Sciences*. Available online at: http://www.pnas.org/content/113/12/3143.abstract (accessed March 13, 2017).

Muenchen, R. (2019). *The Popularity of Data Science Software*. Available online at: http://r4stats.com/articles/popularity/ (accessed July 5, 2020).

Munroe, R. (2015). *xkcd: Git*. Available online at: https://xkcd.com/1597/ (Accessed July 1, 2020).

Murray, J., Prouty, N. G., Peek, S., and Paytan, A. (2019). Coral Skeleton δ 15 N as a tracer of historic nutrient loading to a coral reef in Maui, Hawaii. *Sci. Rep.* 9:5579.

Noriega-Ortega, B. E., Wienhausen, G., Mentges, A., Dittmar, T., Simon, M., and Niggemann, J. (2019). Does the chemodiversity of bacterial exometabolomes sustain the chemodiversity of marine dissolved organic matter? *Front. Microbiol.* 10:215. doi: 10.3389/fmicb.2019.00215

Ogawa, N. O., Nagata, T., Kitazato, H., and Ohkouchi, N. (2010). "Ultra-sensitive elemental analyzer/isotope ratio mass spectrometer for stable nitrogen and carbon isotope analyses," in *Earth Life Isotopes*, eds N. Ohkouchi, I. Tayasu, and K. Koba (Kyoto: Kyoto University Press), 339–353.

Ohno, T., and Bro, R. (2006). Dissolved organic matter characterization using multiway spectral decomposition of fluorescence landscapes. *Soil Sci. Soc. Am. J.* 70, 2028–2037. doi: 10.2136/sssaj2006.0005

Orsi, W. D., Wilken, S., del Campo, J., Heger, T., James, E., Richards, T. A., et al. (2018). Identifying protist consumers of photosynthetic picoeukaryotes in the surface ocean using stable isotope probing. *Environ. Microbiol.* 20, 815–827. doi: 10.1111/1462-2920.14018

Osterholz, H., Kirchman, D. L., Niggemann, J., and Dittmar, T. (2016). Environmental drivers of dissolved organic matter molecular composition in the Delaware Estuary. *Front. Earth Sci.* 4:95. doi: 10.3389/feart.2016.00095

Pantoja, S., Lee, C., and Marecek, J. F. (1997). Hydrolysis of peptides in seawater and sediment. *Mar. Chem.* 57, 25–40. doi: 10.1016/s0304-4203(97)00003-0

Patriarca, C., Bergquist, J., Sjöberg, P. J. R., Tranvik, L., and Hawkes, J. A. (2018). Online HPLC-ESI-HRMS method for the analysis and comparison of different dissolved organic matter samples. *Environ. Sci. Technol.* 52, 2091–2099. doi: 10.1021/acs.est.7b04508

Pearson, A., Hurley, S. J., Walter, S. R. S., Kusch, S., Lichtin, S., and Zhang, Y. G. (2016). Stable carbon isotope ratios of intact GDGTs indicate heterogeneous sources to marine sediments. *Geochim. Cosmochim. Acta* 181, 18–35. doi: 10.1016/j.gca.2016.02.034

Pearson, A., McNichol, A. P., Benitez-Nelson, B. C., Hayes, J. M., and Eglinton, T. I. (2001). Origins of lipid biomarkers in Santa Monica Basin surface sediment: a case study using compound-specific Δ^{14}C analysis. *Geochim. Cosmochim. Acta* 65, 3123–3137. doi: 10.1016/s0016-7037(01)00657-3

Pearson, A., McNichol, A. P., Schneider, R. J., von Reden, K. F., and Zheng, Y. (1998). Microscale AMS ^{14}C measurement at NOSAMS. *Radiocarbon* 40, 61–75. doi: 10.1017/s0033822200017902

Pendergraft, M. A., Dincer, Z., Sericano, J. L., Wade, T. L., Kolasinski, J., and Rosenheim, B. E. (2013). Linking ramped pyrolysis isotope data to oil content through PAH analysis. *Environ. Res. Lett.* 8:44038.

Perkel, J. (2016). Democratic databases: science on GitHub. *Nature* 538, 127–128. doi: 10.1038/538127a

Perkel, J. M. (2018). Why Jupyter is data scientists' computational notebook of choice. *Nature* 563, 145–147.

Petras, D., Koester, I., Da Silva, R., Stephens, B. M., Haas, A. F., Nelson, C. E., et al. (2017). High-resolution liquid chromatography tandem mass spectrometry enables large scale molecular characterization of dissolved organic matter. *Front. Mar. Sci.* 4:405.

Pfeffer, P. E., Gerasimowicz, W. V., and Piotrowski, E. G. (1984). Effect of paramagnetic iron on quantitation in carbon-13 cross polarization magic angle spinning nuclear magnetic resonance spectrometry of heterogeneous environmental matrixes. *Anal. Chem.* 56, 734–741. doi: 10.1021/ac00268a032

Pluskal, T., Castillo, S., Villar-Briones, A., and Orešiè, M. (2010). MZmine 2: modular framework for processing, visualizing, and analyzing mass spectrometry-based molecular profile data. *BMC Bioinformatics* 11:395. doi: 10.1186/1471-2105-11-395

Polissar, P. J., Fulton, J. M., Junium, C. K., Turich, C. C., and Freeman, K. H. (2009). Measurement of 13C and 15N isotopic composition on nanomolar quantities of C and N. *Anal. Chem.* 81, 755–763. doi: 10.1021/ac801370c

Poulson-Ellestad, K. L., Jones, C. M., Roy, J., Viant, M. R., Fernández, F. M., Kubanek, J., et al. (2014). Metabolomics and proteomics reveal impacts of chemically mediated competition on marine plankton. *Proc. Natl. Acad. Sci. U.S.A.* 111, 9009–9014. doi: 10.1073/pnas.1402130111

Powers, L., and Gonsior, M. (2019). Non-targeted screening of disinfection by-products in desalination plants using mass spectrometry: a review. *Curr. Opin. Environ. Sci. Health* 7, 52–60. doi: 10.1016/j.coesh.2018.11.001

Ram, K. (2013). Git can facilitate greater reproducibility and increased transparency in science. *Source Code Biol. Med.* 8:7. doi: 10.1186/1751-0473-8-7

Ramsey, N. (1994). Literate programming simplified. *IEEE Softw.* 11, 97–105. doi: 10.1109/52.311070

Reddy, C. M., Pearson, A., Xu, L., McNichol, A. P., Benner, B. A., Wise, S. A., et al. (2002). Radiocarbon as a tool to apportion the sources of polycyclic aromatic hydrocarbons and black carbon in environmental samples. *Environ. Sci. Technol.* 36, 1774–1782. doi: 10.1021/es011343f

Reemtsma, T. (2009). Determination of molecular formulas of natural organic matter molecules by (ultra-) high-resolution mass spectrometry, Status and needs. *J. Chromatogr. A* 1216, 3687–3701. doi: 10.1016/j.chroma.2009.02.033

Reintjes, G., Arnosti, C., Fuchs, B. M., and Amann, R. (2017). An alternative polysaccharide uptake mechanism of marine bacteria. *ISME J.* 11, 1640–1650. doi: 10.1038/ismej.2017.26

Repeta, D. J., Quan, T. M., Aluwihare, L. I., and Accardi, A. M. (2002). Chemical characterization of high molecular weight dissolved organic matter in fresh and marine waters. *Geochim. Cosmochim. Acta* 66, 955–962. doi: 10.1016/s0016-7037(01)00830-4

Rinke, C., Schwientek, P., Sczyrba, A., Ivanova, N. N., Anderson, I. J., Cheng, J. F., et al. (2013). Insights into the phylogeny and coding potential of microbial dark matter. *Nature* 499, 431–437. doi: 10.1038/nature12352

Robinson, R. S., Brunelle, B. G., and Sigman, D. M. (2004). Revisiting nutrient utilization in the glacial Antarctic: evidence from a new method for diatom-bound N isotopic analysis. *Paleoceanography* 19, A3001. doi: 10.1029/2003PA000996

Rosell-Melé, A., Bard, E., Emeis, K. C., Grimalt, J. O., Müller, P., Schneider, R., et al. (2001). Precision of the current methods to measure the alkenone proxy U37K' and absolute alkenone abundance in sediments: results of an interlaboratory comparison study. *Geochem. Geophys. Geosyst.* 2. doi: 10.1029/2000GC000141

Rosenheim, B. E., Day, M. B., Domack, E., Schrum, H., Benthien, A., and Hayes, J. M. (2008). Antarctic sediment chronology by programmed-temperature pyrolysis: Methodology and data treatment: PYROLYSIS OF ANTARCTIC SEDIMENTS. *Geochem. Geophys. Geosyst.* 9:Q04005. doi: 10.1029/2007GC001816

Rosenheim, B. E., and Galy, V. (2012). Direct measurement of riverine particulate organic carbon age structure. *Geophys. Res. Lett.* 39:L19703. doi: 10.1029/2012GL052883

Rossini, A. J., Lumley, T., and Leisch, F. (2003). On the edge: Statistics & computing: Reproducible statistical research. *Chance* 16, 41–45.

Royalty, T., and Steen, A. D. (2019). Partitioning of microbial function among taxonomic ranks across the tree of life. *bioRxiv* [Preprint]. doi: 10.1101/520973

Ruff, M., Fahrni, S., Gäggeler, H. W., Hajdas, I., Suter, M., Synal, H. A., et al. (2010). On-line radiocarbon measurements of small samples using elemental analyzer and MICADAS gas ion source. *Radiocarbon* 52, 1645–1656. doi: 10.1017/S003382220005637X

Rush, D., Talbot, H. M., van der Meer, M. T. J., Hopmans, E. C., Douglas, B., and Sinninghe Damsté, J. S. (2019). Biomarker evidence for the occurrence of anaerobic ammonium oxidation in the eastern Mediterranean Sea during Quaternary and Pliocene sapropel formation. *Biogeosciences* 16, 2467–2479. doi: 10.5194/bg-16-2467-2019

Rütters, H., Sass, H., Cypionka, H., and Rullkötter, J. (2002). Phospholipid analysis as a tool to study complex microbial communities in marine sediments. *J. Microbiol. Methods* 48, 149–160. doi: 10.1016/s0167-7012(01)00319-0

Ruttkies, C., Neumann, S., and Posch, S. (2019). Improving MetFrag with statistical learning of fragment annotations. *BMC Bioinformatics* 20:376. doi: 10.1186/s12859-019-2954-7

Saito, M. A., McIlvin, M. R., Moran, D. M., Goepfert, T. J., DiTullio, G. R., Post, A. F., et al. (2014). Multiple nutrient stresses at intersecting Pacific Ocean biomes detected by protein biomarkers. *Science* 345, 1173–1177. doi: 10.1126/science.1256450

Sannigrahi, P., Ingall, E. D., and Benner, R. (2005). Cycling of dissolved and particulate organic matter at station Aloha: insights from 13C NMR spectroscopy coupled with elemental, isotopic and molecular analyses. *Deep Sea Res. Part I Oceanogr. Res. Pap.* 52, 1429–1444. doi: 10.1016/j.dsr.2005.04.001

Sannigrahi, P., Ingall, E. D., and Benner, R. (2006). Nature and dynamics of phosphorus-containing components of marine dissolved and particulate organic matter. *Geochim. Cosmochim. Acta* 70, 5868–5882. doi: 10.1016/j.gca.2006.08.037

Santos, G. M., Southon, J. R., Drenzek, N. J., Ziolkowski, L. A., Druffel, E., Xu, X., et al. (2010). Blank assessment for ultra-small radiocarbon samples: chemical extraction and separation versus AMS. *Radiocarbon* 52, 1322–1335. doi: 10.1017/S0033822200046415

Santos, G. M., Southon, J. R., Griffin, S., Beaupre, S. R., and Druffel, E. R. M. (2007). Ultra small-mass AMS 14C sample preparation and analyses at KCCAMS/UCI Facility. *Nucl. Inst. Methods Phys. Res. Sect. B Beam Interact. Mater. Atoms* 259, 293–302. doi: 10.1016/j.nimb.2007.01.172

Sarma, V. V. S. S., Yadav, K., and Behera, S. (2019). Role of eddies on organic matter production and f-ratios in the Bay of Bengal. *Mar. Chem.* 210, 13–23. doi: 10.1016/j.marchem.2019.01.006

Schantz, M. M., Parris, R. M., and Wise, S. A. (2008). *NIST Intercomparison Exercise Program for Organic Contaminants in the Marine Environment: Description and Results of the 2007 Organic Intercomparison Exercises*. Gaithersburg, MD: National Institute of Standards and Technology, 1–279.

Schmidt, F., Koch, B. P., Elvert, M., Schmidt, G., Witt, M., and Hinrichs, K. U. (2011). Diagenetic transformation of dissolved organic nitrogen compounds

under contrasting sedimentary redox conditions in the black sea. *Environ. Sci. Technol.* 45, 5223–5229. doi: 10.1021/es2003414

Schmidt, F., Koch, B. P., Witt, M., and Hinrichs, K. U. (2014). Extending the analytical window for water-soluble organic matter in sediments by aqueous Soxhlet extraction. *Geochim. Cosmochim. Acta* 141, 83–96. doi: 10.1016/j.gca.2014.06.009

Schouten, S., Hopmans, E. C., Pancost, R. D., and Damste, J. S. (2000). Widespread occurrence of structurally diverse tetraether membrane lipids: evidence for the ubiquitous presence of low-temperature relatives of hyperthermophiles. *Proc. Natl. Acad. Sci. U.S.A.* 97, 14421–14426. doi: 10.1073/pnas.97.26.14421

Schouten, S., Hopmans, E. C., Rosell-Melé, A., Pearson, A., Adam, P., Bauersachs, T., et al. (2013a). An interlaboratory study of TEX 86 and BIT analysis of sediments, extracts, and standard mixtures. *Geochem. Geophys. Geosystems* 14, 5263–5285. doi: 10.1002/2013GC004904

Schouten, S., Hopmans, E. C., and Sinninghe Damsté, J. S. (2013b). The organic geochemistry of glycerol dialkyl glycerol tetraether lipids: a review. *Org. Geochem.* 54, 19–61. doi: 10.1016/j.orggeochem.2012.09.006

Schubotz, F., Wakeham, S. G., Lipp, J. S., Fredricks, H. F., and Hinrichs, K. U. (2009). Detection of microbial biomass by intact polar membrane lipid analysis in the water column and surface sediments of the Black Sea. *Environ. Microbiol.* 11, 2720–2734. doi: 10.1111/j.1462-2920.2009.01999.x

Schubotz, F., Xie, S., Lipp, J. S., Hinrichs, K.-U., and Wakeham, S. G. (2018). Intact polar lipids in the water column of the eastern tropical North Pacific: abundance and structural variety of non-phosphorus lipids. *Biogeosciences* 15, 6481–6501. doi: 10.5194/bg-15-6481-2018

Schwedt, A., Seidel, M., Dittmar, T., Simon, M., Bondarev, V., Romano, S., et al. (2015). Substrate use of *Pseudovibrio* sp. growing in ultra-oligotrophic seawater. *PLoS One* 10:e0121675. doi: 10.1371/journal.pone.0121675

Seidel, M., Beck, M., Riedel, T., Waska, H., Suryaputra, I. G. N. A., Schnetger, B., et al. (2014). Biogeochemistry of dissolved organic matter in an anoxic intertidal creek bank. *Geochim. Cosmochim. Acta* 140, 418–434. doi: 10.1016/j.gca.2014.05.038

Seyler, L. M., McGuinness, L. R., Gilbert, J. A., Biddle, J. F., Gong, D., and Kerkhof, L. J. (2018). Discerning autotrophy, mixotrophy and heterotrophy in marine TACK archaea from the North Atlantic. *FEMS Microbiol. Ecol.* 94:fiy014.

Shah, S. R., and Pearson, A. (2007). Ultra-Microscale (5–25 μg C) Analysis of Individual Lipids by 14 C AMS: assessment and correction for sample processing blanks. *Radiocarbon* 49, 69–82. doi: 10.1017/s0033822200041904

Sharp, J. H., Carlson, C. A., Peltzer, E. T., Castle-Ward, D. M., Savidge, K. B., and Rinker, K. R. (2002). Final dissolved organic carbon broad community intercalibration and preliminary use of DOC reference materials. *Mar. Chem.* 77, 239–253. doi: 10.1016/s0304-4203(02)00002-6

Shen, X., Wang, R., Xiong, X., Yin, Y., Cai, Y., Ma, Z., et al. (2019). Metabolic reaction network-based recursive metabolite annotation for untargeted metabolomics. *Nat. Commun.* 10:1516.

Sigman, D. M., Casciotti, K. L., Andreani, M., Barford, C., Galanter, M., and Böhlke, J. K. (2001). A bacterial method for the nitrogen isotopic analysis of nitrate in seawater and freshwater. *Anal. Chem.* 73, 4145–4153. doi: 10.1021/ac010088e

Simpson, A. J., Tseng, L. H., Simpson, M. J., Spraul, M., Braumann, U., Kingery, W. L., et al. (2004). The application of LC-NMR and LC-SPE-NMR to compositional studies of natural organic matter. *Analyst* 129, 1216–1222. doi: 10.1039/b408064e

Sleighter, R. L., Chen, H., Wozniak, A. S., Willoughby, A. S., Caricasole, P., and Hatcher, P. G. (2012). Establishing a measure of reproducibility of ultrahigh-resolution mass spectra for complex mixtures of natural organic matter. *Anal. Chem.* 84, 9184–9191. doi: 10.1021/ac3018026

Sleighter, R. L., and Hatcher, P. G. (2008). Molecular characterization of dissolved organic matter (DOM) along a river to ocean transect of the lower Chesapeake Bay by ultrahigh resolution electrospray ionization Fourier transform ion cyclotron resonance mass spectrometry. *Mar. Chem.* 110, 140–152. doi: 10.1016/j.marchem.2008.04.008

Sleighter, R. L., Liu, Z., Xue, J., and Hatcher, P. G. (2010). Multivariate statistical approaches for the characterization of dissolved organic matter analyzed by ultrahigh resolution mass spectrometry. *Environ. Sci. Technol.* 44, 7576–7582. doi: 10.1021/es1002204

Slonecker, E. T., Jones, D. K., and Pellerin, B. A. (2016). The new Landsat 8 potential for remote sensing of colored dissolved organic matter (CDOM). *Mar. Pollut. Bull.* 107, 518–527. doi: 10.1016/j.marpolbul.2016.02.076

Smith, C. A., Want, E. J., O'Maille, G., Abagyan, R., and Siuzdak, G. (2006). XCMS: processing mass spectrometry data for metabolite profiling using nonlinear peak alignment, matching, and identification. *Anal. Chem.* 78, 779–787. doi: 10.1021/ac051437y

Sogin, E. M., Puskás, E., Dubilier, N., and Liebeke, M. (2019). Marine metabolomics: a method for nontargeted measurement of metabolites in seawater by gas chromatography–mass spectrometry. *mSystems* 4:e00638-19.

Sollai, M., Villanueva, L., Hopmans, E. C., Reichart, G. J., and Sinninghe Damsté, J. S. (2019). A combined lipidomic and 16S rRNA gene amplicon sequencing approach reveals archaeal sources of intact polar lipids in the stratified Black Sea water column. *Geobiology* 17, 91–109. doi: 10.1111/gbi.12316

Somville, M., and Billen, G. (1983). A method for determining exoproteolytic activity in natural waters. *Limnol. Oceanogr.* 28, 190–193. doi: 10.4319/lo.1983.28.1.0190

Spranger, T., Van Pinxteren, D., Reemtsma, T., Lechtenfeld, O. J., and Herrmann, H. (2019). 2D liquid chromatographic fractionation with ultra-high resolution MS analysis resolves a vast molecular diversity of tropospheric particle organics. *Environ. Sci. Technol.* 53, 11353–11363. doi: 10.1021/acs.est.9b03839

Steen, A. D., Crits-Christoph, A., Carini, P., DeAngelis, K. M., Fierer, N., Lloyd, K. G., et al. (2019). High proportions of bacteria and archaea across most biomes remain uncultured. *ISME J.* 13, 3126–3130. doi: 10.1038/s41396-019-0484-y

Steen, A. D., Vazin, J. P. J. P., Hagen, S. M. S. M., Mulligan, K. H. K. H., and Wilhelm, S. W. S. W. (2015). Substrate specificity of aquatic extracellular peptidases assessed by competitive inhibition assays using synthetic substrates. *Aquat. Microb. Ecol.* 75, 271–281. doi: 10.3354/ame01755

Stodden, V. (2010). The Scientific Method in Practice: Reproducibility in the Computational Sciences. MIT Sloan Research Paper No. 4773-10. Available online at: https://papers.ssrn.com/sol3/papers.cfm?abstract_id=1550193 (accessed February 9, 2010).

Stücheli, P. E., Niggemann, J., and Schubert, C. J. (2018). Comparison of different solid phase extraction sorbents for the qualitative assessment of dissolved organic nitrogen in freshwater samples using FT-ICR-MS. *J. Limnol.* 77, 400–411.

Sturt, H. F., Summons, R. E., Smith, K., Elvert, M., and Hinrichs, K.-U. (2004). Intact polar membrane lipids in prokaryotes and sediments deciphered by high-performance liquid chromatography/electrospray ionization multistage mass spectrometry—new biomarkers for biogeochemistry and microbial ecology. *Rapid Commun. Mass Spectrom.* 18, 617–628. doi: 10.1002/rcm.1378

Sud, M., Fahy, E., Cotter, D., Azam, K., Vadivelu, I., Burant, C., et al. (2016). Metabolomics Workbench: an international repository for metabolomics data and metadata, metabolite standards, protocols, tutorials and training, and analysis tools. *Nucleic Acids Res.* 44, D463–D470.

Synal, H. A., Stocker, M., and Suter, M. (2007). MICADAS: a new compact radiocarbon AMS system. *Nucl. Inst. Methods Phys. Res. Sect. B Beam Interact. Mater. Atoms* 259, 7–13. doi: 10.1016/j.nimb.2007.01.138

Talbot, H. M., Sidgwick, F. R., Bischoff, J., Osborne, K. A., Rush, D., Sherry, A., et al. (2016). Analysis of non-derivatised bacteriohopanepolyols by ultrahigh-performance liquid chromatography/tandem mass spectrometry. *Rapid Commun. Mass Spectrom.* 30, 2087–2098. doi: 10.1002/rcm.7696

Tierney, N. J., and Ram, K. (2020). *A Realistic Guide to Making Data Available Alongside Code to Improve Reproducibility*. Available online at: http://arxiv.org/abs/2002.11626 (accessed July 1, 2020).

Tose, L. V., Benigni, P., Leyva, D., Sundberg, A., Ramírez, C. E., Ridgeway, M. E., et al. (2018). Coupling trapped ion mobility spectrometry to mass spectrometry: trapped ion mobility spectrometry-time-of-flight mass spectrometry versus trapped ion mobility spectrometry-Fourier transform ion cyclotron resonance mass spectrometry. *Rapid Commun. Mass Spectrom.* 32, 1287–1295. doi: 10.1002/rcm.8165

van der Hooft, J. J. J., Mohimani, H., Bauermeister, A., Dorrestein, P. C., Duncan, K. R., and Medema, M. H. (2020). Linking genomics and metabolomics to chart specialized metabolic diversity. *Chem. Soc. Rev.* 49, 3297–3314. doi: 10.1039/D0CS00162G

Van der Voort, T. S., Mannu, U., Blattmann, T. M., Bao, R., Zhao, M., and Eglinton, T. I. (2018). Deconvolving the fate of carbon in coastal sediments. *Geophys. Res. Lett.* 45, 4134–4142. doi: 10.1029/2018GL077009

Van Mooy, B. A. S., and Fredricks, H. F. (2010). Bacterial and eukaryotic intact polar lipids in the eastern subtropical South Pacific: water-column distribution, planktonic sources, and fatty acid composition. *Geochim. Cosmochim. Acta* 74, 6499–6516. doi: 10.1016/j.gca.2010.08.026

Van Mooy, B. A. S., Fredricks, H. F., Pedler, B. E., Dyhrman, S. T., Karl, D. M., Koblížek, M., et al. (2009). Phytoplankton in the ocean use non-phosphorus lipids in response to phosphorus scarcity. *Nature* 458, 69–72. doi: 10.1038/nature07659

Wacker, L., Bonani, G., Friedrich, M., Hajdas, I., Kromer, B., Nìmec, M., et al. (2010). MICADAS: routine and high-precision radiocarbon dating. *Radiocarbon* 52, 252–262. doi: 10.1017/S0033822200045288

Wagner, S., Dittmar, T., and Jaffé, R. (2015a). Molecular characterization of dissolved black nitrogen via electrospray ionization Fourier transform ion cyclotron resonance mass spectrometry. *Org. Geochem.* 79, 21–30. doi: 10.1016/j.orggeochem.2014.12.002

Wagner, S., Riedel, T., Niggemann, J., Vähätalo, A. V., Dittmar, T., and Jaffé, R. (2015b). Linking the molecular signature of heteroatomic dissolved organic matter to watershed characteristics in world rivers. *Environ. Sci. Technol.* 49, 13798–13806. doi: 10.1021/acs.est.5b00525

Wakeham, S. G., Amann, R., Freeman, K. H., Hopmans, E. C., Jørgensen, B. B., Putnam, I. F., et al. (2007). Microbial ecology of the stratified water column of the Black Sea as revealed by a comprehensive biomarker study. *Org. Geochem.* 38, 2070–2097. doi: 10.1016/j.orggeochem.2007.08.003

Wakeham, S. G., and Lee, C. (2019). Limits of our knowledge, part 2: selected frontiers in marine organic biogeochemistry. *Mar. Chem.* 212, 16–46. doi: 10.1016/j.marchem.2019.02.005

Wakeham, S. G., Lee, C., Peterson, M. L., Liu, Z., Szlosek, J., Putnam, I. F., et al. (2009). Organic biomarkers in the twilight zone-Time series and settling velocity sediment traps during MedFlux. *Deep. Res. Part II Top. Stud. Oceanogr.* 56, 1437–1453. doi: 10.1016/j.dsr2.2008.11.030

Wakeham, S. G., and McNichol, A. P. (2014). Transfer of organic carbon through marine water columns to sediments-insights from stable and radiocarbon isotopes of lipid biomarkers. *Biogeosciences* 11, 6895–6914. doi: 10.5194/bg-11-6895-2014

Wang, M., Carver, J. J., Phelan, V. V., Sanchez, L. M., Garg, N., Peng, Y., et al. (2016). Sharing and community curation of mass spectrometry data with Global Natural Products Social Molecular Networking. *Nat. Biotechnol.* 34, 828–837.

Wang, M., Jarmusch, A. K., Vargas, F., Aksenov, A. A., Gauglitz, J. M., Weldon, K., et al. (2020). Mass spectrometry searches using MASST. *Nat. Biotechnol.* 38, 23–26.

Wang, M., Wang, J., Carver, J., Pullman, B. S., Cha, S. W., and Bandeira, N. (2018). Assembling the community-scale discoverable human proteome. *Cell Syst.* 7, 412–421.

Waska, H., Koschinsky, A., Ruiz Chancho, M. J., and Dittmar, T. (2015). Investigating the potential of solid-phase extraction and Fourier-transform ion cyclotron resonance mass spectrometry (FT-ICR-MS) for the isolation and identification of dissolved metal-organic complexes from natural waters. *Mar. Chem.* 173, 78–92. doi: 10.1016/j.marchem.2014.10.001

Welander, P. V., Coleman, M. L., Sessions, A. L., Summons, R. E., and Newman, D. K. (2010). Identification of a methylase required for 2-methylhopanoid production and implications for the interpretation of sedimentary hopanes. *Proc. Natl. Acad. Sci. U.S.A.* 107, 8537–8542. doi: 10.1073/pnas.0912949107

Werdell, P. J., Franz, B. A., Bailey, S. W., Feldman, G. C., Boss, E., Brando, V. E., et al. (2013). Generalized ocean color inversion model for retrieving marine inherent optical properties. *Appl. Opt.* 52, 2019–2037. doi: 10.1364/AO.52.002019

Wichard, T. (2016). Identification of metallophores and organic ligands in the chemosphere of the marine Macroalga Ulva (Chlorophyta) and at Land-Sea Interfaces. *Front. Mar. Sci.* 3:131. doi: 10.3389/fmars.2016.00131

Wilkinson, M. D., Dumontier, M., Aalbersberg, I. J., Appleton, G., Axton, M., Baak, A., et al. (2016). Comment: the FAIR Guiding Principles for scientific data management and stewardship. *Sci. Data* 3:160018. doi: 10.1038/sdata.2016.18

Wilson, G. (2006). Software carpentry: getting scientists to write better code by making them more productive. *Comput. Sci. Eng.* 8, 66–69. doi: 10.1109/MCSE.2006.122

Wilson, G. (2014). Software Carpentry: lessons learned. *F1000Res.* 3:62. doi: 10.12688/f1000research.3-62.v2

Woods, G. C., Simpson, M. J., Koerner, P. J., Napoli, A., and Simpson, A. J. (2011). HILIC-NMR: toward the identification of individual molecular components in dissolved organic matter. *Environ. Sci. Technol.* 45, 3880–3886. doi: 10.1021/es103425s

Wörmer, L., Elvert, M., Fuchser, J., Lipp, J. S., Buttigieg, P. L., Zabel, M., et al. (2014). Ultra-high-resolution paleoenvironmental records via direct laser-based analysis of lipid biomarkers in sediment core samples. *Proc. Natl. Acad. Sci. U.S.A.* 111, 15669–15674. doi: 10.1073/pnas.1405237111

Wörmer, L., Lipp, J. S., and Hinrichs, K.-U. (2015). "Comprehensive analysis of microbial lipids in environmental samples through HPLC-MS protocols," in *Hydrocarbon and Lipid Microbiology Protocols*, eds T. McGenity, K. Timmis, and B. Nogales (Berlin: Springer), 289–317. doi: 10.1007/8623_2015_183

Wörmer, L., Lipp, J. S., Schröder, J. M., and Hinrichs, K.-U. (2013). Application of two new LC–ESI–MS methods for improved detection of intact polar lipids (IPLs) in environmental samples. *Org. Geochem.* 59, 10–21. doi: 10.1016/j.orggeochem.2013.03.004

Zark, M., Christoffers, J., and Dittmar, T. (2017). Molecular properties of deep-sea dissolved organic matter are predictable by the central limit theorem: evidence from tandem FT-ICR-MS. *Mar. Chem.* 191, 9–15. doi: 10.1016/j.marchem.2017.02.005

Zhang, J., Liu, D., Cao, P., Wang, Y., Keesing, J. K., Li, J., et al. (2016). A highly sensitive method for analyzing marker phytoplankton pigments: ultra-high-performance liquid chromatography-tandem triple quadrupole mass spectrometry: analyzing marker phytoplankton pigments: UHPLC-MS/MS. *Limnol. Oceanogr. Methods* 14, 623–636. doi: 10.1002/lom3.10117

Zhang, X., Bianchi, T. S., Cui, X., Rosenheim, B. E., Ping, C., Hanna, A. J. M., et al. (2017). Permafrost organic carbon mobilization from the watershed to the colville river delta: evidence from 14 C ramped pyrolysis and lignin biomarkers. *Geophys. Res. Lett.* 44, 11,491–11,500. doi: 10.1002/2017GL075543

Zhang, Y., Sintes, E., Chen, J., Zhang, Y., Dai, M., Jiao, N., et al. (2009). Role of mesoscale cyclonic eddies in the distribution and activity of Archaea and Bacteria in the South China Sea. *Aquat. Microb. Ecol.* 56, 65–79. doi: 10.3354/ame01324

Zheng, G., and Price, W. S. (2012). Direct hydrodynamic radius measurement on dissolved organic matter in natural waters using diffusion NMR. *Environ. Sci. Technol.* 46, 1675–1680. doi: 10.1021/es202809e

Zhu, C., Lipp, J. S., Wörmer, L., Becker, K. W., Schröder, J., and Hinrichs, K.-U. (2013). Comprehensive glycerol ether lipid fingerprints through a novel reversed phase liquid chromatography–mass spectrometry protocol. *Org. Geochem.* 65, 53–62. doi: 10.1016/j.orggeochem.2013.09.012

Conflict of Interest: The authors declare that the research was conducted in the absence of any commercial or financial relationships that could be construed as a potential conflict of interest.

frontiers in Marine Science

MINI REVIEW
published: 08 September 2020
doi: 10.3389/fmars.2020.540165

Open-Ocean Minima in $\delta^{13}C$ Values of Particulate Organic Carbon in the Lower Euphotic Zone

Hilary G. Close and Lillian C. Henderson*

Department of Ocean Sciences, Rosenstiel School of Marine and Atmospheric Science, University of Miami, Miami, FL, United States

Extensive studies in the 1980s–1990s led to the characterization of latitudinal variations in sea surface $\delta^{13}C$ values of particulate organic carbon ($\delta^{13}C_{POC}$), and relationships were found with CO_2 concentrations, temperature, growth rates, and cell geometries. Surprisingly, no large-scale efforts have been made to describe variations in $\delta^{13}C_{POC}$ values over depth in the water column. Here we compile published examples demonstrating a widespread isotopic pattern in particulate organic carbon (POC) of the upper water column. In 51 vertical profiles, $\delta^{13}C_{POC}$ values in the lower euphotic zone on average are 1.4‰ lower than $\delta^{13}C_{POC}$ values in the upper euphotic zone of open ocean settings. In a majority of locations this vertical decrease in $\delta^{13}C_{POC}$ values is >2‰ and up to 5‰, larger than the commonly recognized vertical $\delta^{13}C$ variation in dissolved inorganic carbon over the same depths. We briefly review hypotheses and supporting evidence offered by previous studies of individual water columns: The observed patterns could result from vertical differences in photosynthetic growth rates or community composition, biochemical composition of organic matter due to degradation, isotopic disequilibrium within the dissolved inorganic carbon pool, particle dynamics, or seasonal vertical mixing. Coordinated isotopic, biological, and seawater chemistry data are sparse, and consistent drivers of this widespread isotopic pattern are currently elusive. Further work is needed to adequately characterize the environmental conditions coinciding with this pattern, to test its origins, and to determine if the magnitude of upper water column $\delta^{13}C_{POC}$ variations could be a useful marker of upper ocean carbon cycle dynamics.

Keywords: carbon isotopes, particulate organic carbon, water column, marine organic carbon, phytoplankton

OPEN ACCESS

Edited by:
Cindy Lee,
Stony Brook University, United States

Reviewed by:
Matt McCarthy,
University of California, Santa Cruz, United States
Tom Trull,
Commonwealth Scientific and Industrial Research Organisation (CSIRO), Australia

****Correspondence:***
Hilary G. Close
hclose@rsmas.miami.edu

Specialty section:
This article was submitted to Marine Biogeochemistry, a section of the journal Frontiers in Marine Science

Received: *03 March 2020*
Accepted: *13 August 2020*
Published: *08 September 2020*

Citation:
Close HG and Henderson LC (2020) Open-Ocean Minima in $\delta^{13}C$ Values of Particulate Organic Carbon in the Lower Euphotic Zone. Front. Mar. Sci. 7:540165. doi: 10.3389/fmars.2020.540165

INTRODUCTION

Particulate organic carbon (POC) is the major carrier of carbon from the surface to the deep ocean (the biological pump); therefore, quantifying POC and understanding its origins and degradation are important priorities. POC is defined as all combustible carbon captured on filters of pore size ~0.7 μm and remaining after removal of carbonates by acidification. POC therefore encompasses diverse organic structures contained in the biomass of phytoplankton, heterotrophic and chemoautotrophic microbes, and detrital materials such as dead cells,

cell fragments, fecal pellets, other aggregated material, and terrigenous or resuspended allochthonous organic matter. The naturally occurring stable carbon isotope ratio of POC ($\delta^{13}C_{POC}$) is one of the only chemical characterizations that captures the entire POC pool, since individual, measurable chemical components constitute only a small proportion of the total (Kharbush et al., 2020; this issue). Accordingly, $\delta^{13}C_{POC}$ values preserved in seafloor sediments are important factors in interpreting earth's past carbon cycle (Kump and Arthur, 1999).

$\delta^{13}C_{POC}$ values in the surface ocean have been relatively well-characterized, largely motivated by the possibility of using preserved $\delta^{13}C_{POC}$ values as an indicator of photosynthetic responses to past and evolving sea surface CO_2 concentrations (e.g., Rau et al., 1989; Freeman and Hayes, 1992; Francois et al., 1993; Goericke and Fry, 1994; Young et al., 2013). Open-ocean $\delta^{13}C_{POC}$ values vary from −35‰ at high latitudes to −16‰ at low-mid latitudes (Goericke and Fry, 1994). In contrast, the $\delta^{13}C$ value of dissolved CO_2 used as a substrate for photosynthesis only varies by ∼2‰ across surface waters (Rau et al., 1989). To explain the $\delta^{13}C_{POC}$ variations, the expressed isotopic fractionation (ε_P) between CO_2 ($\delta^{13}C_{CO2}$) and photosynthetic biomass ($\delta^{13}C_P$) (Hayes, 1993, 2001) was found to correlate to some degree with CO_2 concentration, but also with phytoplankton growth rates and cell geometry (Laws et al., 1995; Popp et al., 1998, and others). Additional influence on ε_P can arise from the use of carbon concentrating mechanisms and the active uptake and/or fixation of bicarbonate (see Wilkes and Pearson, 2019).

In contrast, relatively few studies have focused explicitly on vertical patterns of $\delta^{13}C_{POC}$ extending below near-surface depths (Jeffrey et al., 1983; Saino, 1992), and to our knowledge no global data compilation exists. Individually, several studies have noted large (2–5‰) decreases in $\delta^{13}C_{POC}$ values between the near-surface ocean and the lower euphotic zone or upper pycnocline in open ocean settings, a depth range over which the values of $\delta^{13}C_{CO2}$ usually vary by only 0.5–2.0‰ (Schmittner et al., 2013; Meyer et al., 2016). Hypothesized mechanisms for creating vertical $\delta^{13}C_{POC}$ patterns include both photosynthetic and degradative processes. In this short review we compile data from published studies reporting $\delta^{13}C_{POC}$ values in the upper 250 m of open-ocean water columns in order to explore whether global patterns or environmental drivers can be detected, briefly review existing hypotheses for the observed vertical patterns, and make suggestions for future work.

DATA COMPILATION OF GLOBAL OCEAN $\delta^{13}C_{POC}$ PROFILES

Average $\delta^{13}C_{POC}$ Minimum in the Lower Euphotic Zone or Local Pycnocline

We compiled suspended $\delta^{13}C_{POC}$ data from 11 published studies representative of the global open ocean and containing 51 vertical profiles of $\delta^{13}C_{POC}$ extending from near-surface waters to depths of 250 m. Study locations spanned latitudes from −53° to 50° (**Figure 1A** and **Supplementary Tables S1, S2**) in the oligotrophic Atlantic (Pedrosa-Pàmies et al., 2018), equatorial Atlantic (Bishop et al., 1977; Jeffrey et al., 1983), Gulf of Mexico, Caribbean Sea, Eastern Tropical Pacific (Jeffrey et al., 1983), South Atlantic (Hurley et al., 2019), Southern Ocean (O'Leary et al., 2001; Trull et al., 2008), and North Pacific (Saino, 1992; Minagawa et al., 2001; Hernes and Benner, 2002; Druffel et al., 2003). Non-tabulated data points (Saino, 1992) and coordinates locations (Trull et al., 2008) were extracted using a built-in MATLAB function (ginput); data are compiled in **Supplementary Table S2**. We excluded some published studies from our numerical analysis due to a scarcity of depths sampled in the upper water column or due to likelihood of terrigenous inputs, low-oxygen metabolisms, or experimental manipulations (Williams and Gordon, 1970; Eadie and Jeffrey, 1973; Druffel et al., 1996; Benner et al., 1997; Trull and Armand, 2001; Hernes and Benner, 2006; Close et al., 2014; Krishna et al., 2018; Liu et al., 2018). We also did not include data from the Arctic region due to the prevalence of terrigenous or advected POC in these areas (e.g., Griffith et al., 2012; Xiang and Lam, 2020).

To compare across sites, we standardized reported sampling depth in two different ways: as a proportion of total euphotic zone depth, defined as 0.1% surface PAR (E_z, **Figure 1B**), and relative to the monthly and maximum annual mixed layer depths (MLD, **Figure 1C**). For the E_z standardization we retrieved global 1% surface PAR depths from the mapped MODIS-Aqua satellite data product (NASA Goddard Space Flight Center, 2018) produced using the method of Lee et al. (2007); determined to be within ∼14% of *in situ* measured values). The 4 × 4 km grid location closest to each published study site was extracted; results were similar (within 0.3 ± 1.7 m) when using an average of the surrounding data points. E_z was calculated based on first-order attenuation from 1% PAR at each location and ranged from 61 to 187 m. We retrieved monthly and maximum annual MLD from Holte et al. (2017), who compiled data from Argo float profiles and used a hybrid density algorithm to find MLD. We found the nearest points on the resulting 1 × 1° grid and used an average of the values at these points.

To account for known latitudinal variations in absolute values of $\delta^{13}C_{POC}$, the $\delta^{13}C_{POC}$ data for each individual vertical profile were normalized to the minimum $\delta^{13}C_{POC}$ value anywhere within the upper 250 m of the water column, i.e., the local minimum value was subtracted from each data value in an individual profile to calculate $\Delta\delta^{13}C_{POC}$ (**Figures 1B,C**). After depth and isotopic data were normalized, we compiled all data to assess global vertical trends. We compared the distribution of all $\Delta\delta^{13}C_{POC}$ values in the upper 0–50% and lower 50–100% of the E_z and below (**Figure 1B** and **Supplementary Figure S2A**). For the MLD standardization we compared all $\Delta\delta^{13}C_{POC}$ values above the monthly MLD, between the monthly and annual maximum MLD (local pycnocline), and below the annual maximum MLD (maximum pycnocline; **Figure 1C** and **Supplementary Figure S2B**). Due to normalization of the isotopic data to a zero value, the distributions were skewed and statistical tests were chosen accordingly for non-normally distributed data. A Wilcoxon rank sum test was used to assess significance pair-wise between the different depth ranges (**Supplementary Table S3**). $\delta^{13}C_{POC}$ values were found to be significantly lower in the lower euphotic zone

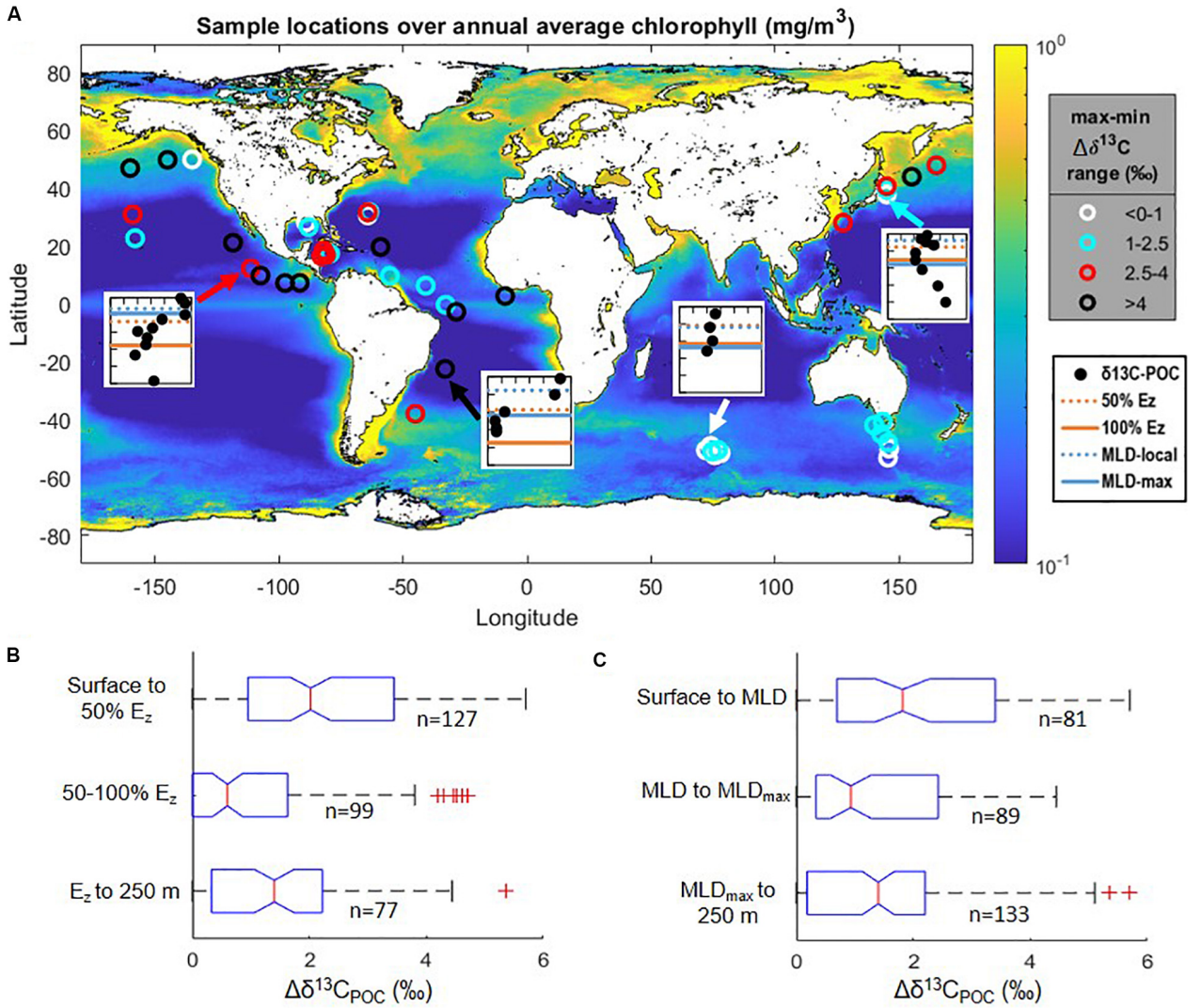

FIGURE 1 | (A) Data locations (open circles) shown over mapped annual climatological surface ocean chlorophyll concentrations from Melin (2013). Symbols are color-coded according to the ranges in $\Delta\delta^{13}C_{POC}$ values observed in the upper 250 m (overlying maximum minus underlying minimum; see **Figure 2**). Insets show examples of four vertical profiles of $\delta^{13}C_{POC}$ values (filled black circles): each inset spans from the surface down to 250 m on the vertical axis and a $\delta^{13}C$ range of −27 to −21‰ on the horizontal axis (see also **Supplementary Figure S1**); horizontal lines indicate depths of the mixed layer and euphotic zone as indicated in the legend. **(B,C)** Normalized $\Delta\delta^{13}C_{POC}$ values among all compiled data: medians (center vertical lines), interquartile range (boxes), 99% intervals (brackets), and outliers (individual points); **(B)** when grouped by standardized euphotic zone depth intervals (100% E_z, depth at which irradiance is 0.1% of surface values); **(C)** when grouped by local mixed layer depth (MLD) and maximum annual mixed layer depth (MLD_{max}). $\Delta\delta^{13}C_{POC}$ indicates $\delta^{13}C_{POC}$ values normalized to the minimum $\delta^{13}C_{POC}$ value found within the upper 250 m at each station, as described in the text. Depth ranges and statistical results are further outlined in **Supplementary Table S3**.

compared to the upper euphotic zone, with a difference in median $\Delta\delta^{13}C_{POC}$ values of 1.4‰ ($p < 10^{-8}$; **Figure 1B** and **Supplementary Table S3**). $\delta^{13}C_{POC}$ values were also significantly lower in depths between the monthly and maximum MLD when compared to those above the monthly MLD, with a difference in median $\Delta\delta^{13}C_{POC}$ values of 0.9‰ ($p < 0.01$; **Figure 1C** and **Supplementary Table S3**).

Generalizing the statistical results above, within the 51 compiled profiles, $\delta^{13}C_{POC}$ values in the lower euphotic zone and/or below the local mixed layer are significantly lower than values in the upper euphotic zone and/or above the local mixed layer. Further, when considering data distribution in relation to the euphotic zone depth, $\delta^{13}C_{POC}$ values in the lower euphotic zone (50–100% of E_z) defined a local minimum; they are lower than $\delta^{13}C_{POC}$ values both above and below this depth range ($p < 0.02$; **Figure 1B** and **Supplementary Table S3**).

Comparison of Individual $\delta^{13}C_{POC}$ Vertical Profiles to Environmental Data

The analysis above considered the compiled global data as a whole and examined differences between median $\delta^{13}C_{POC}$ values

within coarse divisions of the upper water column. We also examined the overall magnitude of variation in $\delta^{13}C_{POC}$ values found within individual water columns, i.e., the upper water column max-min range in $\delta^{13}C_{POC}$ values ($\Delta\delta^{13}C_{POC}$ max-min). We calculated this range as the difference between the minimum $\delta^{13}C_{POC}$ value found anywhere in the upper 250 m of individual water columns and the maximum $\delta^{13}C_{POC}$ value found *above* this depth in order to focus on the pattern of higher $\delta^{13}C_{POC}$ overlying lower $\delta^{13}C_{POC}$ values. We found that 63% of individual water columns had a max-min range > 2‰, with the largest ranges >5‰ (**Figure 2A**). We attempted to assess whether the observed $\Delta\delta^{13}C_{POC}$ max-min range correlated with broad scale environmental features extracted from global datasets. Using linear regressions (MATLAB function polyfit), no correlation was found between the local max-min range and the absolute depth of the euphotic zone, chlorophyll *a*, nor modeled surface phytoplankton size or fecal pellet export (Melin, 2013; Siegel et al., 2014; linear regression, $r^2 < 0.1$). The only linear regressions resulting in $r^2 > 0.15$ were those comparing the local $\Delta\delta^{13}C_{POC}$ max-min range to net primary production (**Figure 2B**) and maximum annual mixed layer depth (**Figure 2C**).

Where possible, we extracted coinciding *in situ* vertical profiles of concentrations of POC, dissolved inorganic carbon (DIC), O_2, chlorophyll, and nutrient concentrations from the published studies, as well as C:N ratios. We also obtained annual climatological DIC concentrations, alkalinity, salinity, pH, and temperature data mapped at 1 × 1° resolution from GLODAP and World Ocean Atlas databases (Key et al., 2004), and we calculated CO_2 concentration profiles for each $\delta^{13}C_{POC}$ data location using the CO2SYS tool (Lewis and Wallace, 1998). We tested for pair-wise correlations between vertical profiles of these variables and $\delta^{13}C_{POC}$ values (both absolute values and $\Delta\delta^{13}C_{POC}$ values) where possible, and we did not find any significant relationships. Measured *in situ* $\delta^{13}C_{DIC}$ values were available from O'Leary et al. (2001) and Hurley et al. (2019). We normalized $\delta^{13}C_{DIC}$ and $\delta^{13}C_{POC}$ to near-surface values, using the data point closest to the surface to account for the known latitudinal variation in surface ocean $\delta^{13}C_{DIC}$ and $\delta^{13}C_{POC}$ values. In the nine individual profiles where this comparison was possible, we found that the vertical range in $\delta^{13}C_{POC}$ values was on average approximately four times larger than the vertical range in $\delta^{13}C_{DIC}$ over the same depths (slope = 4.17, $r^2 = 0.53$, linear regression).

DISCUSSION

Data Availability and Quality

While our compilation of published data here is likely not exhaustive, it is to our knowledge the first global examination of vertical profiles of $\delta^{13}C_{POC}$ in the upper water column. Global mapped 3-dimensional oceanographic data products for $\delta^{13}C_{POC}$ currently do not exist, and most major oceanographic programs do not include vertical $\delta^{13}C_{POC}$ as a standard parameter. Anecdotally, vertical $\delta^{13}C_{POC}$ values might be measured much more frequently than they are published or interpreted (e.g., Bishop et al., 1999). The scarcity of published data and lack of a database for $\delta^{13}C_{POC}$ values were barriers to identifying environmental commonalities underlying the observed patterns. We also note that low vertical resolution in many profiles likely means that the true minimum and maximum $\delta^{13}C_{POC}$ values in a given water column were not captured (**Supplementary Figure S1**).

Of the 11 studies from which we compiled data, 6 collected POC using *in situ* or submersible pumps to filter large volumes of water (>70 L). Jeffrey et al. (1983); Saino (1992), Wu et al. (1999); Minagawa et al. (2001), and Hernes and Benner (2002) instead collected seawater in large volumes (10–30 L) from Niskin bottles and filtered the water shipboard. Filtering POC from large volumes of water helps in obtaining a statistical sampling of the particle population; small sample volumes are subject to interference from the inconsistent capture of sparse large particles as well as a larger proportional blank contribution from dissolved organic matter (DOM) sorbed to the filter when POC loading is low. Discussion of DOM sorption and differential particle retention based on filtration media or pressures has been extensive in terms of effects on POC and pigment concentrations (e.g., Gardner et al., 2003; Nayar and Chou, 2003; Bishop et al., 2012). However, the effects of sampling methods and blank correction on $\delta^{13}C_{POC}$ values are underdiscussed (Lorrain et al., 2003) and are of particular importance in the subsurface where POC concentrations are lower and blank contribution is proportionally higher. In addition, the most common, elemental analysis-based methods for bulk carbon isotope analysis are >99% inefficient, necessitating large sample quantities; broader use of "nano-scale" analytical methods could improve our ability to obtain better three-dimensional data coverage for oceanic $\delta^{13}C_{POC}$ measurements (see Close, 2019).

The size fraction(s) of particles studied also can be important. Most studies described here collected total POC onto 0.45, 0.7, 0.8, or 1.0 μm glass or quartz fiber filters, but the studies of Bishop et al. (1977) and Hurley et al. (2019) in the mid-latitude Atlantic included a prefilter of 53 μm mesh size. In these cases, the observed patterns of $\delta^{13}C_{POC}$ in the lower euphotic zone were a particular feature of small particles (∼0.7–53 μm), which constituted the majority of POC. Trull et al. (2008) included measurements of several particle size classes in a study of the Southern Ocean – where large phytoplankton and particles are more abundant that the above studies – and found heterogeneities in the $\delta^{13}C$ values across both size and depth, possibly relating to a combination of physiological effects on ε_P, different sinking rates, and temporal offsets between surface production and deeper particles (see below).

Photosynthetic Hypotheses for Origins of Low $\delta^{13}C_{POC}$ Values in the Lower Euphotic Zone or Upper Pycnocline

Several physiological, community, and environmental features of *in situ* photosynthesis have been suggested as drivers of systematic variations in $\delta^{13}C_{POC}$ values between the upper

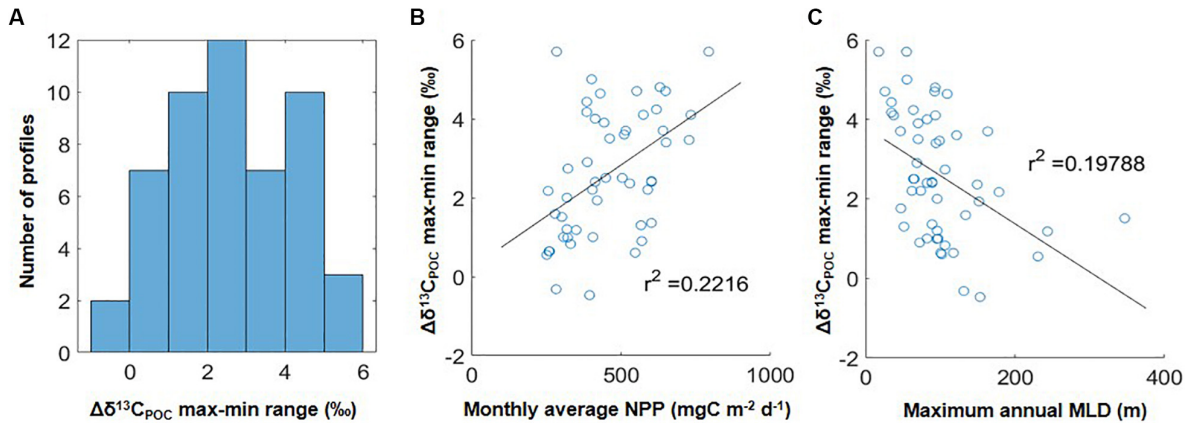

FIGURE 2 | (A) Distribution of upper water column ranges in $\Delta\delta^{13}C_{POC}$ values in the 51 individual water columns in this study, calculated as the overlying maximum $\delta^{13}C_{POC}$ value minus subsurface minimum $\delta^{13}C_{POC}$ value (i.e., maximum values occurring at depths below the minimum are not considered here). Negative values indicate profiles in which the minimum $\delta^{13}C_{POC}$ value was found at the shallowest data point. **(B)** Comparison of $\Delta\delta^{13}C_{POC}$ max-min ranges in **(A)** to climatological net primary production (NPP) at each location. **(C)** Comparison of $\Delta\delta^{13}C_{POC}$ max-min ranges in **(A)** to maximum annual mixed layer depth (MLD_{max}) at each location. One extreme outlier was omitted from **(B)** with an NPP value of 1250 mg m^{-2} d^{-1} and $\Delta\delta^{13}C_{POC}$ max-min range of 1.8‰.

and lower euphotic zones. Saino (1992) noted "a subsurface minimum near the base of the euphotic zone" when examining $\delta^{13}C_{POC}$ values at study sites adjacent to the Kuroshio Current and suggested photosynthetic mechanisms. Models and culture studies (e.g., Popp et al., 1998; Cassar et al., 2006) have demonstrated that ε_P depends on an interplay between the growth rate of an organism and the supply rate of CO_2; higher CO_2 supply rates and/or slower growth rates will lead to a larger ε_P, and therefore lower values of $\delta^{13}C_P$. Saino (1992) suggested that both conditions likely exist in the lower euphotic zone: CO_2 concentrations here are higher than the surface due to the net removal of CO_2 by photosynthesis at the surface and the net respiration of CO_2 in the lower euphotic zone, and growth rates are likely lower due to light limitation. O'Leary et al. (2001) also found low $\delta^{13}C_{POC}$ values in the lower euphotic zone in a study of the subantarctic water column, and their model results pointed to slow photosynthetic growth rates as the cause. Decreases in photosynthetic growth rate with increasing depth in the euphotic zone are frequently observed in the open ocean (e.g., Laws, 2013), and relationships between growth rates and photosynthetic fractionation of carbon isotopes have been demonstrated in culture (Laws et al., 1995; Bidigare et al., 1997; Popp et al., 1998).

A smaller average cell size of phytoplankton in the lower euphotic zone/upper pycnocline than in the upper euphotic zone/mixed layer also is a frequent observation in open-ocean settings (e.g., Poulton et al., 2006; Barone et al., 2015). Trull and Armand (2001) demonstrated that a smaller average cell size (higher surface area: volume ratio) of phytoplankton in the lower euphotic zone could result in lower $\delta^{13}C_{POC}$ values, an isotopic relationship previously established in phytoplankton cultures and models by Rau et al. (1996); Popp et al. (1998), and others, stemming from faster CO_2 diffusion rates.

Conversely, targeted studies of individual photosynthetic taxa or biomarkers have sometimes suggested a pattern of increasing or unchanging $\delta^{13}C$ values over increasing depth in the euphotic zone (Prahl et al., 2005; Popp et al., 2006; Tolosa et al., 2008; Radabaugh et al., 2014). The recent model of Wilkes and Pearson (2019) suggests that increasing $\delta^{13}C$ values over depth could be a phenomenon specific to eukaryotic phytoplankton with intracellular CO_2 partitioning or carbon concentrating strategies, with carbon isotopic fractionation varying according to whether growth is limited by low nutrient concentrations (upper euphotic zone/mixed layer) or other factors such as light [lower euphotic zone/upper pycnocline; also explored by Laws et al. (2002) and Cassar et al. (2006)]. Some phytoplankton also employ active uptake and/or fixation of bicarbonate (HCO_3^-), thereby also complicating relationships between cell size, CO_2 concentrations, and $\delta^{13}C_P$ (e.g., Bentaleb et al., 1998; Cassar et al., 2004). Due to such variations in photosynthetic physiologies, the isotopic sensitivity of a whole phytoplankton community to its local seawater environment (CO_2 concentrations, light and nutrient availability) will depend also on the taxonomic composition of photosynthesizing organisms present (e.g., Leboulanger et al., 1995; Bentaleb et al., 1998; Trull et al., 2008).

Saino (1992) also discussed how slow isotopic equilibrium relative to chemical equilibrium within the DIC system could lead to relatively high values of $\delta^{13}C_{CO2}$ in the mixed layer compared to the lower euphotic zone. Notably, $\delta^{13}C_{CO2}$ usually is calculated from measured $\delta^{13}C_{DIC}$ using constants that assume the system is at both chemical and isotopic equilibrium (Freeman and Hayes, 1992).

Some compound-specific isotope analyses of lipids have supported a photosynthetic origin of low $\delta^{13}C_{POC}$ values in the lower euphotic zone. Close et al. (2014) found that $\delta^{13}C$ values of lipid biomarkers for *in situ* production paralleled $\delta^{13}C_{POC}$ values throughout the euphotic zone in the Eastern Tropical North Pacific, which ruled out the degradative accumulation of lipids

(see section "Degradative or Dynamical Hypotheses for Origins of Low $\delta^{13}C_{POC}$ Values in the Lower Euphotic Zone or Upper Pycnocline") as a driver behind low δ^{13}C values in the lower euphotic zone. Similarly, O'Leary et al. (2001) demonstrated that δ^{13}C values of photosynthetic sterols paralleled vertical profiles of $\delta^{13}C_{POC}$ in subantarctic waters.

Degradative or Dynamical Hypotheses for Origins of Low $\delta^{13}C_{POC}$ Values in the Lower Euphotic Zone or Upper Pycnocline

Equally common in published interpretations of upper water column $\delta^{13}C_{POC}$ variations are hypotheses relating to degradation or alteration processes. Jeffrey et al. (1983) noted that "the upper part of the pycnocline (i.e., below the local mixed layer) is marked by lighter POC-δ^{13}C values at almost all the stations occupied" in a broad-ranging study of the Eastern Tropical North Pacific, Gulf of Mexico, Caribbean, and western south Atlantic. These authors suggested a degradative mechanism, following the interpretations of Eadie and Jeffrey (1973) and based on the results of Degens (1969): below the local mixed layer POC concentrations decrease rapidly due to high rates of respiration. Amino acids and sugars comprise quickly degrading, ^{13}C-enriched components of POC, potentially leaving remaining POC at these depths with a relatively high abundance of ^{13}C-depleted lipids. This explanation was cited by Druffel et al. (2003), who noted relatively low δ^{13}C values of POC in the upper 200 m at study sites in the North Central Pacific and Sargasso Sea.

Bishop et al. (1977) noted "a depletion in ^{13}C of 4‰ over the depth interval between 32 and 50 m," but could not attribute this to the degradative explanation of Eadie and Jeffrey (1973) because a preponderance of lipids should result in an increase in C:N ratios. Instead C:N ratios were invariant over these depths, and the authors suggested that secondary production by bacteria could lead to low δ^{13}C values. However, the proportional contribution of lipids may increase without being accompanied by an increase in C:N, if proteinaceous (low C:N) material is also abundant, as suggested by Pedrosa-Pàmies et al. (2018). There are few broad organic compositional studies of POC that are accompanied by carbon isotopic data. One such study by Sannigrahi et al. (2005) did not find a strong relationship between organic composition and $\delta^{13}C_{POC}$ values in the upper water column at Station ALOHA [isotopic data previously reported by Hernes and Benner (2002)]; in particular the lipid composition was not proportionally higher at the lower euphotic $\delta^{13}C_{POC}$ minimum than it was at shallower depths.

Hernes and Benner (2002, 2006) suggested that low subsurface $\delta^{13}C_{POC}$ values in the oligotrophic subtropical Pacific and Sargasso Sea were the result of an advected source of terrigenous organic matter, based on a correlation with lignin concentration. However, this correlation existed mainly in POM below the euphotic zone. The local minimum in $\delta^{13}C_{POC}$ values observed in the lower euphotic zone did not correlate with the proportional contribution of lignin to total POC at that depth. Advection of POC from adjacent waters often cannot explain the range of $\delta^{13}C_{POC}$ values observed in a single water column (e.g., Lourey et al., 2004), although this is more commonly cited in the Arctic (Griffith et al., 2012; Xiang and Lam, 2020).

Overall, organic compositional effects on $\delta^{13}C_{POC}$ values seem to be more apparent at advanced stages of organic matter degradation that occur below the euphotic zone, in deep mesopelagic and bathypelagic waters. Here decreases in $\delta^{13}C_{POC}$ values are more clearly related to increasing C:N ratios or changing biochemical composition than they are in the upper water column (see Minagawa et al., 2001; Hwang and Druffel, 2003; Sannigrahi et al., 2005). Analogous to the patterns recognized for particulate δ^{15}N values (Altabet et al., 1991), shallower, earlier degradation of macromolecules may lead first to increases in $\delta^{13}C_{POC}$ values as bonds containing ^{12}C are more quickly hydrolyzed or respired in upper mesopelagic waters (e.g., Bishop et al., 1977; Jeffrey et al., 1983; Wu et al., 1999). Accordingly, slightly higher $\delta^{13}C_{POC}$ values were found below E_z compared to the lower euphotic zone in our data compilation (**Figure 1B** and **Supplementary Table S3**), and this pattern is more apparent in individual water column profiles (**Supplementary Figure S1**; see also Cavagna et al., 2013).

Particle, seasonal, and water column dynamics also may lead to vertical variations in $\delta^{13}C_{POC}$. Studies of size-fractionated POC or plankton frequently find size-based differences in δ^{13}C values. Typically large particles are assumed to sink more quickly through the euphotic zone; those originating in the surface can carry their $\delta^{13}C_{POC}$ values below the mixed layer, possibly also being disaggregated into small particles therein. Large phytoplankton often have higher $\delta^{13}C_{POC}$ values than small phytoplankton and therefore would tend to contribute ^{13}C-enriched rather than ^{13}C-depleted material into the subsurface through such a mechanism (Bishop et al., 1977; Fry and Wainright, 1991; Wu et al., 1999; Trull and Armand, 2001; Trull et al., 2008). Heterogeneous sinking rates and δ^{13}C values have also been used to explain temporal offsets in the origins of upper and lower water column $\delta^{13}C_{POC}$ values, especially in locations with strong seasonality. That is, POC in the subsurface may represent export from the surface ocean during growth conditions (growth rates, CO_2 concentrations, phytoplankton community composition) typical of preceding seasons (Lourey et al., 2004; Cavagna et al., 2013). In high latitude areas seasonal changes in MLD can also distribute surface biomass throughout the euphotic zone and create temporal and spatial offsets between the formation and observation of POC (Grenier et al., 2015).

Zooplankton egesta and/or methane production by gut microbiota also have been cited as possibly affecting $\delta^{13}C_{POC}$ values (Cavagna et al., 2013). Fecal pellets can be highly ^{13}C-depleted in comparison to zooplankton diet (Tamelander et al., 2006). In addition, relatively ^{13}C-depleted methane has been observed reaching maximum concentrations in the pycnocline of oxygenated open-ocean water columns (Holmes et al., 2000; Sasakawa et al., 2008), likely linked to bacterial degradation of dissolved organic compounds (Repeta et al., 2016). Bacteria may incorporate this methane into biomass during oxidative metabolism (Sasakawa et al., 2008), but it is unclear if biomass quantities would be sufficient to affect overall $\delta^{13}C_{POC}$ values.

Unique Geochemical Signatures of the Lower Euphotic Zone or Upper Pycnocline: Potential Implications

One objective of this review is to motivate wider measurement and/or reporting of vertically resolved $\delta^{13}C_{POC}$ data. Regardless of the underlying primary or degradative drivers of this pattern, better data coverage – especially at higher vertical resolution – will allow more precise definition of the depths at which $\delta^{13}C_{POC}$ minima occur and the overall magnitude of variation in upper water column $\delta^{13}C_{POC}$ values; both could prove to be a useful diagnostic of underlying ecosystem processes or carbon dynamics as described above.

The current data compilation suggests that there is a widespread pool of POC in the ocean with $\delta^{13}C$ values that are significantly different from those modeled as "source" photosynthetic values in the surface ocean. POC in the lower euphotic zone or upper pycnocline is abundant and serves as a food source for subsurface biota; studies such as Liu et al. (2018) have discussed how variations in $\delta^{13}C_{POC}$ values in deep chlorophyll maxima can influence how $\delta^{13}C$ values are interpreted in food web studies. The depths of the lower euphotic zone or upper pycnocline, which usually include deep chlorophyll maxima when present, can also be a location of net particle formation and export (Kemp et al., 2000; Benitez-Nelson et al., 2001; Umhau et al., 2019). Recognizing subsurface sources for exported material can be important to the interpretation of the sedimentary geochemical record (e.g., Luo et al., 2014; Hurley et al., 2018). Interestingly, an analog exists in terrestrial systems; plant matter growing in the upper canopy of forests consistently has higher $\delta^{13}C$ values than plant matter growing below (the "canopy effect"; Van der Merwe and Medina, 1991). The differential preservation and dietary usage of these two signatures can affect the interpretation of terrestrial soil records and food webs (e.g., Bonafini et al., 2013).

Finally, global biogeochemical models include the carbon isotope fractionation of photosynthetic organisms according to relationships with growth rate and CO_2 concentrations established in culture (Tagliabue and Bopp, 2008; Schmittner et al., 2013). However, it is unclear whether current models already can adequately reproduce observed vertical $\delta^{13}C_{POC}$ patterns; these models have instead focused on validation of surface ocean $\delta^{13}C_{POC}$ values or vertical $\delta^{13}C_{DIC}$ patterns. A more comprehensive dataset of vertical $\delta^{13}C_{POC}$ values could help validate such isotope-enabled carbon cycle models.

CONCLUSION

Existing published works demonstrate that $\delta^{13}C_{POC}$ values can be significantly lower in the lower euphotic zone or upper pycnocline compared to the upper euphotic zone or local surface mixed layer in a wide range of global open-ocean locations. While individual studies have offered hypotheses for the origin of this vertical pattern, a global compilation of $\delta^{13}C_{POC}$ profiles with coinciding oceanographic data is necessary to test whether there are consistent environmental drivers. We suggest that high-quality isotopic data coverage of the global open ocean is needed, particularly with better data density throughout the euphotic zone and with coinciding CO_2 system data, cell size characterization, and $\delta^{13}C_{DIC}$ data. The large water sample volume needed to obtain sufficient material for $\delta^{13}C_{POC}$ measurements is currently a barrier to including this parameter in many global-scale oceanographic programs, but improvements in the efficiency of isotopic measurement could mitigate this issue. Compound-specific isotope approaches, autotrophic and heterotrophic rate measurements (including substrate-specific photosynthetic uptake, bicarbonate vs. CO_2), particle dynamics characterization, and relevant enzyme expression data all would aid in discerning between potential hypothesized mechanisms. Further, we suggest that an isotope-specific database such as the emergent IsoBank (Pauli et al., 2017)[1] would be an appropriate place to aggregate both published and unpublished $\delta^{13}C_{POC}$ data that currently may be dispersed across various oceanographic databases.

AUTHOR CONTRIBUTIONS

HC and LH designed the study. LH conducted the data analysis and contributed to the manuscript. HC wrote the manuscript. Both authors contributed to the article and approved the submitted version.

FUNDING

Publication was funded by the Deutsche Forschungsgemeinschaft (DFG, German Research Foundation) project number 422798570. This work was partially inspired by discussions at a workshop on Marine Organic Biogeochemistry that was held in Delmenhorst, Germany in April 2019 and funded by the Hanse-Wissenschaftskolleg and the Geochemical Society. LH was supported by a University of Miami Fellowship.

ACKNOWLEDGMENTS

We thank Ellen Druffel and Rut Pedrosa-Pámies for providing tabulated data from Druffel et al. (2003) and Pedrosa-Pàmies et al. (2018), Igor Belkin for advice in recovering data from Saino (1992), and David Siegel for providing modeled climatologies from Siegel et al. (2014). We are grateful for comments by MM, Yuan Shen, and TT which resulted in considerable improvements to this mini-review.

SUPPLEMENTARY MATERIAL

The Supplementary Material for this article can be found online at: https://www.frontiersin.org/articles/10.3389/fmars.2020.540165/full#supplementary-material

[1] http://isobank-qa.tacc.utexas.edu/en/

REFERENCES

Altabet, M. A., Deuser, W. G., Honjo, S., and Stienen, C. (1991). Seasonal and depth-related changes in the source of sinking particles in the North Atlantic. *Nature* 354, 136–139. doi: 10.1038/354136a0

Barone, B., Bidigare, R. R., Church, M. J., Karl, D. M., Letelier, R. M., and White, A. E. (2015). Particle distributions and dynamics in the euphotic zone of the North Pacific Subtropical Gyre. *J. Geophys. Res. Oceans* 120, 3229–3247. doi: 10.1002/2015jc010774

Benitez-Nelson, C., Buesseler, K. O., Karl, D. M., and Andrews, J. (2001). A time-series study of particulate matter export in the North Pacific Subtropical Gyre based on 234Th: 238U disequilibrium. *Deep Sea Res. Part I Oceanogr. Res. Pap.* 48, 2595–2611. doi: 10.1016/s0967-0637(01)00032-2

Benner, R., Biddanda, B., Black, B., and McCarthy, M. (1997). Abundance, size distribution, and stable carbon and nitrogen isotopic compositions of marine organic matter isolated by tangential-flow ultrafiltration. *Mar. Chem.* 57, 243–263. doi: 10.1016/s0304-4203(97)00013-3

Bentaleb, I., Fontugne, M., Descolas-Gros, C., Girardin, C., Mariotti, A., Pierre, C., et al. (1998). Carbon isotopic fractionation by plankton in the Southern Indian Ocean: relationship between δ13C of particulate organic carbon and dissolved carbon dioxide. *J. Mar. Syst.* 17, 39–58. doi: 10.1016/s0924-7963(98)00028-1

Bidigare, R. R., Fluegge, A., Freeman, K. H., Hanson, K. L., Hayes, J. M., Hollander, D., et al. (1997). Consistent fractionation of 13C in nature and in the laboratory: growth-rate effects in some haptophyte algae. *Global Biogeochem. Cycles* 11, 279–292. doi: 10.1029/96gb03939

Bishop, J. K., Calvert, S. E., and Soon, M. Y. (1999). Spatial and temporal variability of POC in the northeast Subarctic Pacific. *Deep Sea Res. Part II Top. Stud. Oceanogr.* 46, 2699–2733. doi: 10.1016/s0967-0645(99)00081-8

Bishop, J. K., Edmond, J. M., Ketten, D. R., Bacon, M. P., and Silker, W. B. (1977). The chemistry, biology, and vertical flux of particulate matter from the upper 400 m of the equatorial Atlantic Ocean. *Deep Sea Res.* 24, 511–548. doi: 10.1016/0146-6291(77)90526-4

Bishop, J. K., Lam, P. J., and Wood, T. J. (2012). Getting good particles: accurate sampling of particles by large volume in-situ filtration. *Limnol. Oceanogr. Methods* 10, 681–710. doi: 10.4319/lom.2012.10.681

Bonafini, M., Pellegrini, M., Ditchfield, P., and Pollard, A. (2013). Investigation of the 'canopy effect'in the isotope ecology of temperate woodlands. *J. Archaeol. Sci.* 40, 3926–3935. doi: 10.1016/j.jas.2013.03.028

Cassar, N., Laws, E. A., Bidigare, R. R., and Popp, B. N. (2004). Bicarbonate uptake by Southern Ocean phytoplankton. *Global Biogeochem. Cycles* 18:GB2003.

Cassar, N., Laws, E. A., and Popp, B. N. (2006). Carbon isotopic fractionation by the marine diatom *Phaeodactylum tricornutum* under nutrient-and light-limited growth conditions. *Geochim. Cosmochim. Acta* 70, 5323–5335. doi: 10.1016/j.gca.2006.08.024

Cavagna, A.-J., Dehairs, F., Bouillon, S., Woule-Ebongué, V., Planchon, F., Delille, B., et al. (2013). Water column distribution and carbon isotopic signal of cholesterol, brassicasterol and particulate organic carbon in the Atlantic sector of the Southern Ocean. *Biogeosciences* 10, 2787–2801. doi: 10.5194/bg-10-2787-2013

Close, H. G. (2019). Compound-specific isotope geochemistry in the ocean. *Annu. Rev Mar. Sci.* 11, 27–56. doi: 10.1146/annurev-marine-121916-063634

Close, H. G., Wakeham, S. G., and Pearson, A. (2014). Lipid and 13C signatures of submicron and suspended particulate organic matter in the Eastern Tropical North Pacific: implications for the contribution of Bacteria. *Deep Sea Res. Part I Oceanogr. Res. Pap.* 85, 15–34. doi: 10.1016/j.dsr.2013.11.005

Degens, E. (1969). "Biogeochemistry of stable carbon isotopes," in *Organic Geochemistry*, eds E. Eglington, and M. T. J. Murphy (Berlin: Springer), 304–329. doi: 10.1007/978-3-642-87734-6_14

Druffel, E. R., Bauer, J. E., Griffin, S., and Hwang, J. (2003). Penetration of anthropogenic carbon into organic particles of the deep ocean. *Geophys. Res. Lett.* 30:1744.

Druffel, E. R., Bauer, J. E., Williams, P. M., Griffin, S., and Wolgast, D. (1996). Seasonal variability of particulate organic radiocarbon in the northeast Pacific Ocean. *J. Geophys. Res. Oceans* 101, 20543–20552. doi: 10.1029/96jc01850

Eadie, B. J., and Jeffrey, L. M. (1973). δ13C analyses of oceanic particulate organic matter. *Mar. Chem.* 1, 199–209. doi: 10.1016/0304-4203(73)90004-2

Francois, R., Altabet, M. A., Goericke, R., McCorkle, D. C., Brunet, C., and Poisson, A. (1993). Changes in the δ13C of surface water particulate organic matter across the subtropical convergence in the SW Indian Ocean. *Global Biogeochem. Cycles* 7, 627–644. doi: 10.1029/93gb01277

Freeman, K. H., and Hayes, J. (1992). Fractionation of carbon isotopes by phytoplankton and estimates of ancient CO2 levels. *Global Biogeochem. Cycles* 6, 185–198. doi: 10.1029/92gb00190

Fry, B., and Wainright, S. C. (1991). Diatom sources of 13 C-rich carbon in marine food webs. *Mar. Ecol. Prog. Ser.* 76, 149–157. doi: 10.3354/meps076149

Gardner, W. D., Richardson, M. J., Carlson, C. A., Hansell, D., and Mishonov, A. V. (2003). Determining true particulate organic carbon: bottles, pumps and methodologies. *Deep Sea Res. Part II Top. Stud. Oceanogr.* 50, 655–674. doi: 10.1016/s0967-0645(02)00589-1

Goericke, R., and Fry, B. (1994). Variations of marine plankton δ13C with latitude, temperature, and dissolved CO2 in the world ocean. *Global Biogeochem. Cycles* 8, 85–90. doi: 10.1029/93gb03272

Grenier, M., Della Penna, A., and Trull, T. (2015). Autonomous profiling float observations of the high-biomass plume downstream of the Kerguelen Plateau in the Southern Ocean. *Biogeosciences* 12, 2707–2735. doi: 10.5194/bg-12-2707-2015

Griffith, D. R., McNichol, A. P., Xu, L., McLaughlin, F. A., Brown, K. A., and Eglinton, T. I. (2012). Carbon dynamics in the western Arctic Ocean: insights from full-depth carbon isotope profiles of DIC, DOC, and POC. *Biogeosciences* 9, 1217–1224. doi: 10.5194/bg-9-1217-2012

Hayes, J. (1993). Factors controlling 13C contents of sedimentary organic compounds: principles and evidence. *Mar. Geol.* 113, 111–125. doi: 10.1016/0025-3227(93)90153-m

Hayes, J. M. (2001). Fractionation of carbon and hydrogen isotopes in biosynthetic processes. *Rev. Mineral. Geochem.* 43, 225–277. doi: 10.1515/9781501508745-006

Hernes, P. J., and Benner, R. (2002). Transport and diagenesis of dissolved and particulate terrigenous organic matter in the North Pacific Ocean. *Deep Sea Res. Part I Oceanogr. Res. Pap.* 49, 2119–2132. doi: 10.1016/s0967-0637(02)00128-0

Hernes, P. J., and Benner, R. (2006). Terrigenous organic matter sources and reactivity in the North Atlantic Ocean and a comparison to the Arctic and Pacific oceans. *Mar. Chem.* 100, 66–79. doi: 10.1016/j.marchem.2005.11.003

Holmes, M. E., Sansone, F. J., Rust, T. M., and Popp, B. N. (2000). Methane production, consumption, and air-sea exchange in the open ocean: an evaluation based on carbon isotopic ratios. *Global Biogeochem. Cycles* 14, 1–10. doi: 10.1029/1999gb001209

Holte, J., Talley, L. D., Gilson, J., and Roemmich, D. (2017). An Argo mixed layer climatology and database. *Geophys. Res. Lett.* 44, 5618–5626. doi: 10.1002/2017gl073426

Hurley, S. J., Close, H. G., Elling, F. J., Jasper, C. E., Gospodinova, K., McNichol, A. P., et al. (2019). CO2-dependent carbon isotope fractionation in Archaea, Part II: the marine water column. *Geochim. Cosmochim. Acta* 261, 383–395. doi: 10.1016/j.gca.2019.06.043

Hurley, S. J., Lipp, J. S., Close, H. G., Hinrichs, K.-U., and Pearson, A. (2018). Distribution and export of isoprenoid tetraether lipids in suspended particulate matter from the water column of the Western Atlantic Ocean. *Organ. Geochem.* 116, 90–102. doi: 10.1016/j.orggeochem.2017.11.010

Hwang, J., and Druffel, E. R. (2003). Lipid-like material as the source of the uncharacterized organic carbon in the ocean? *Science* 299, 881–884. doi: 10.1126/science.1078508

Jeffrey, A. W., Pflaum, R. C., Brooks, J. M., and Sackett, W. M. (1983). Vertical trends in particulate organic carbon 13C: 12C ratios in the upper water column. *Deep Sea Res. Part A Oceanogr. Res. Pap.* 30, 971–983. doi: 10.1016/0198-0149(83)90052-3

Kemp, A. E., Pike, J., Pearce, R. B., and Lange, C. B. (2000). The "Fall dump"—a new perspective on the role of a "shade flora" in the annual cycle of diatom production and export flux. *Deep Sea Res. Part II Top. Stud. Oceanogr.* 47, 2129–2154. doi: 10.1016/s0967-0645(00)00019-9

Key, R. M., Kozyr, A., Sabine, C. L., Lee, K., Wanninkhof, R., Bullister, J. L., et al. (2004). A global ocean carbon climatology: results from Global Data Analysis Project (GLODAP). *Global Biogeochem. Cycles* 18:GB4031.

Kharbush, J. J., Van Mooy, B. A., Close, H. G., Arnosti, C., Smittenberg, R. H., Le Moigne, F. A. C., et al. (2020). Particulate organic carbon deconstructed: molecular and chemical composition of particulate organic carbon in the ocean. *Front. Mar. Sci.* 7:518. doi: 10.3389/fmars.2020.00518

Krishna, M., Mukherjee, J., Dalabehera, H., and Sarma, V. (2018). Particulate organic carbon composition in temperature fronts of the northeastern Arabian Sea during winter. *J. Geophys. Res. Biogeosci.* 123, 463–478. doi: 10.1002/2018jg004387

Kump, L. R., and Arthur, M. A. (1999). Interpreting carbon-isotope excursions: carbonates and organic matter. *Chem. Geol.* 161, 181–198. doi: 10.1016/s0009-2541(99)00086-8

Laws, E. A. (2013). Evaluation of *in situ* phytoplankton growth rates: a synthesis of data from varied approaches. *Annu. Rev Mar. Sci.* 5, 247–268. doi: 10.1146/annurev-marine-121211-172258

Laws, E. A., Popp, B. N., Bidigare, R. R., Kennicutt, M. C., and Macko, S. A. (1995). Dependence of phytoplankton carbon isotopic composition on growth rate and [CO2) aq: theoretical considerations and experimental results. *Geochim. Cosmochim. Acta* 59, 1131–1138. doi: 10.1016/0016-7037(95)00030-4

Laws, E. A., Popp, B. N., Cassar, N., and Tanimoto, J. (2002). 13C discrimination patterns in oceanic phytoplankton: likely influence of CO2 concentrating mechanisms, and implications for palaeoreconstructions. *Funct. Plant Biol.* 29, 323–333. doi: 10.1071/pp01183

Leboulanger, C., Descolas-Gros, C., Fontugne, M., Bentaleb, I., and Jupin, H. (1995). Interspecific variability and environmental influence on particulate organic carbon δ13C in cultured marine phytoplankton. *J. Plankton Res.* 17, 2079–2091. doi: 10.1093/plankt/17.11.2079

Lee, Z., Weidemann, A., Kindle, J., Arnone, R., Carder, K. L., and Davis, C. (2007). Euphotic zone depth: its derivation and implication to ocean-color remote sensing. *J. Geophys. Res. Oceans* 112. doi: 10.1029/2006JC003802

Lewis, E., and Wallace, D. (1998). *Program Developed for CO2 System Calculations*. Oak Ridge, TN: US Department of Energy.

Liu, Q., Kandasamy, S., Lin, B., Wang, H., and Chen-Tung, A. C. (2018). Biogeochemical characteristics of suspended particulate matter in deep chlorophyll maximum layers in the southern East China Sea. *Biogeosciences* 15, 2091–2109. doi: 10.5194/bg-15-2091-2018

Lorrain, A., Savoye, N., Chauvaud, L., Paulet, Y.-M., and Naulet, N. (2003). Decarbonation and preservation method for the analysis of organic C and N contents and stable isotope ratios of low-carbonated suspended particulate material. *Anal. Chim. Acta* 491, 125–133. doi: 10.1016/s0003-2670(03)00815-8

Lourey, M. J., Trull, T. W., and Tilbrook, B. (2004). Sensitivity of δ13C of Southern Ocean suspended and sinking organic matter to temperature, nutrient utilization, and atmospheric CO2. *Deep Sea Res. Part I Oceanogr. Res. Pap.* 51, 281–305. doi: 10.1016/j.dsr.2003.10.002

Luo, G., Algeo, T. J., Huang, J., Zhou, W., Wang, Y., Yang, H., et al. (2014). Vertical δ13Corg gradients record changes in planktonic microbial community composition during the end-Permian mass extinction. *Palaeogeogr. Palaeoclimat. Palaeoecol.* 396, 119–131. doi: 10.1016/j.palaeo.2014.01.006

Melin, F. (2013). *GMIS - SeaWiFS Monthly Climatology Sea Surface Chlorophyll-a Concentration (9km) in mg.m^-3*. Available online at: http://data.europa.eu/89h/d6f9abd9-777c-4a0c-a5f7-669612f83307 (accessed July 1, 2020).

Meyer, K., Ridgwell, A., and Payne, J. (2016). The influence of the biological pump on ocean chemistry: implications for long-term trends in marine redox chemistry, the global carbon cycle, and marine animal ecosystems. *Geobiology* 14, 207–219. doi: 10.1111/gbi.12176

Minagawa, M., Ohashi, M., Kuramoto, T., and Noda, N. (2001). δ15N of PON and nitrate as a clue to the origin and transformation of nitrogen in the subarctic North Pacific and its marginal sea. *J. Oceanogr.* 57, 285–300.

NASA Goddard Space Flight Center, Ocean Ecology Laboratory, Ocean Biology Processing Group (2018). *Moderate-Resolution Imaging Spectroradiometer (MODIS) Aqua Euphotic Depth Data; 2018 Reprocessing*. Available online at: https://oceancolor.gsfc.nasa.gov/data/10.5067/AQUA/MODIS/L3M/ZLEE/2018 (accessed January 8, 2020).

Nayar, S., and Chou, L. (2003). Relative efficiencies of different filters in retaining phytoplankton for pigment and productivity studies. *Estuar. Coast. Shelf Sci.* 58, 241–248. doi: 10.1016/s0272-7714(03)00075-1

O'Leary, T., Trull, T., Griffiths, F., Tilbrook, B., and Revill, A. (2001). Euphotic zone variations in bulk and compound-specific δ13C of suspended organic matter in the Subantarctic Ocean, south of Australia. *J. Geophys. Res. Oceans* 106, 31669–31684. doi: 10.1029/2000jc000288

Pauli, J. N., Newsome, S. D., Cook, J. A., Harrod, C., Steffan, S. A., Baker, C. J., et al. (2017). Opinion: why we need a centralized repository for isotopic data. *Proc. Natl. Acad. Sci. U.S.A.* 114, 2997–3001. doi: 10.1073/pnas.1701742114

Pedrosa-Pàmies, R., Conte, M., Weber, J., and Johnson, R. (2018). Carbon cycling in the Sargasso Sea water column: insights from lipid biomarkers in suspended particles. *Prog. Oceanogr.* 168, 248–278. doi: 10.1016/j.pocean.2018.08.005

Popp, B. N., Laws, E. A., Bidigare, R. R., Dore, J. E., Hanson, K. L., and Wakeham, S. G. (1998). Effect of phytoplankton cell geometry on carbon isotopic fractionation. *Geochim. Cosmochim. Acta* 62, 69–77. doi: 10.1016/s0016-7037(97)00333-5

Popp, B. N., Prahl, F. G., Wallsgrove, R. J., and Tanimoto, J. (2006). Seasonal patterns of alkenone production in the subtropical oligotrophic North Pacific. *Paleoceanography* 21:PA1004.

Poulton, A. J., Holligan, P. M., Hickman, A., Kim, Y.-N., Adey, T. R., Stinchcombe, M. C., et al. (2006). Phytoplankton carbon fixation, chlorophyll-biomass and diagnostic pigments in the Atlantic Ocean. *Deep Sea Res. Part II Top. Stud. Oceanogr.* 53, 1593–1610. doi: 10.1016/j.dsr2.2006.05.007

Prahl, F. G., Popp, B. N., Karl, D. M., and Sparrow, M. A. (2005). Ecology and biogeochemistry of alkenone production at Station ALOHA. *Deep Sea Res. Part I Oceanogr. Res. Pap.* 52, 699–719. doi: 10.1016/j.dsr.2004.12.001

Radabaugh, K. R., Malkin, E. M., Hollander, D. J., and Peebles, E. B. (2014). Evidence for light-environment control of carbon isotope fractionation by benthic microalgal communities. *Mar. Ecol. Prog. Ser.* 495, 77–90. doi: 10.3354/meps10559

Rau, G. H., Riebesell, U., and Wolf-Gladrow, D. (1996). A model of photosynthetic 13C fractionation by marine phytoplankton based on diffusive molecular CO2 uptake. *Mar. Ecol. Prog. Ser.* 133, 275–285. doi: 10.3354/meps133275

Rau, G. H., Takahashi, T., and Des Marais, D. J. (1989). Latitudinal variations in plankton δ13C: implications for CO2 and productivity in past oceans. *Nature* 341, 516–518. doi: 10.1038/341516a0

Repeta, D. J., Ferrón, S., Sosa, O. A., Johnson, C. G., Repeta, L. D., Acker, M., et al. (2016). Marine methane paradox explained by bacterial degradation of dissolved organic matter. *Nat. Geosci.* 9, 884–887. doi: 10.1038/ngeo2837

Saino, T. (1992). 15N and 13C natural abundance in suspended particulate organic matter from a Kuroshio warm-core ring. *Deep Sea Res. Part A Oceanogr. Res. Pap.* 39, S347–S362.

Sannigrahi, P., Ingall, E. D., and Benner, R. (2005). Cycling of dissolved and particulate organic matter at station Aloha: insights from 13C NMR spectroscopy coupled with elemental, isotopic and molecular analyses. *Deep Sea Res. Part I Oceanogr. Res. Pap.* 52, 1429–1444. doi: 10.1016/j.dsr.2005.04.001

Sasakawa, M., Tsunogai, U., Kameyama, S., Nakagawa, F., Nojiri, Y., and Tsuda, A. (2008). Carbon isotopic characterization for the origin of excess methane in subsurface seawater. *J. Geophys. Res. Oceans* 113:C03012.

Schmittner, A., Gruber, N., Mix, A. C., Key, R. M., Tagliabue, A., and Westberry, T. K. (2013). Biology and air-sea gas exchange controls on the distribution of carbon isotope ratios (delta C-13) in the ocean. *Biogeosciences* 10, 5793–5816. doi: 10.5194/bg-10-5793-2013

Siegel, D., Buesseler, K., Doney, S., Sailley, S., Behrenfeld, M. J., and Boyd, P. (2014). Global assessment of ocean carbon export by combining satellite observations and food-web models. *Global Biogeochem. Cycles* 28, 181–196. doi: 10.1002/2013gb004743

Tagliabue, A., and Bopp, L. (2008). Towards understanding global variability in ocean carbon-13. *Global Biogeochem. Cycles* 22:GB1025.

Tamelander, T., Søreide, J. E., Hop, H., and Carroll, M. L. (2006). Fractionation of stable isotopes in the Arctic marine copepod *Calanus glacialis*: effects on the isotopic composition of marine particulate organic matter. *J. Exp. Mar. Biol. Ecol.* 333, 231–240. doi: 10.1016/j.jembe.2006.01.001

Tolosa, I., Miquel, J.-C., Gasser, B., Raimbault, P., Goyet, C., and Claustre, H. (2008). Distribution of lipid biomarkers and carbon isotope fractionation in contrasting trophic environments of the South East Pacific. *Biogeosciences* 5, 949–968. doi: 10.5194/bg-5-949-2008

Trull, T., and Armand, L. (2001). Insights into Southern Ocean carbon export from the δ13C of particles and dissolved inorganic carbon during the SOIREE iron release experiment. *Deep Sea Res. Part II Top. Stud. Oceanogr.* 48, 2655–2680. doi: 10.1016/s0967-0645(01)00013-3

Trull, T. W., Davies, D., and Casciotti, K. (2008). Insights into nutrient assimilation and export in naturally iron-fertilized waters of the Southern Ocean from nitrogen, carbon and oxygen isotopes. *Deep Sea Res. Part II Top. Stud. Oceanogr.* 55, 820–840. doi: 10.1016/j.dsr2.2007.12.035

Umhau, B. P., Benitez-Nelson, C. R., Close, H. G., Hannides, C. C., Motta, L., Popp, B. N., et al. (2019). Seasonal and spatial changes in carbon and nitrogen

fluxes estimated using 234Th: 238U disequilibria in the North Pacific tropical and subtropical gyre. *Mar. Chem.* 217:103705. doi: 10.1016/j.marchem.2019.103705

Van der Merwe, N. J., and Medina, E. (1991). The canopy effect, carbon isotope ratios and foodwebs in Amazonia. *J. Archaeol. Sci.* 18, 249–259. doi: 10.1016/0305-4403(91)90064-v

Wilkes, E. B., and Pearson, A. (2019). A general model for carbon isotopes in red-lineage phytoplankton: interplay between unidirectional processes and fractionation by RubisCO. *Geochim. Cosmochim. Acta* 265, 163–181. doi: 10.1016/j.gca.2019.08.043

Williams, P., and Gordon, L. (1970). Carbon-13: carbon-12 ratios in dissolved and particulate organic matter in the sea. *Deep Sea Res. Oceanogr. Abstr.* 17, 19–27. doi: 10.1016/0011-7471(70)90085-9

Wu, J., Calvert, S., Wong, C., and Whitney, F. (1999). Carbon and nitrogen isotopic composition of sedimenting particulate material at Station Papa in the subarctic northeast Pacific. *Deep Sea Res. Part II Top. Stud. Oceanogr.* 46, 2793–2832. doi: 10.1016/s0967-0645(99)00084-3

Xiang, Y., and Lam, P. J. (2020). Size-fractionated compositions of marine suspended particles in the Western Arctic Ocean: lateral and vertical sources. *J. Geophys. Res. Oceans* 125:e2020J16144. doi: 10.1029/2020JC016144

Young, J., Bruggeman, J., Rickaby, R., Erez, J., and Conte, M. (2013). Evidence for changes in carbon isotopic fractionation by phytoplankton between 1960 and 2010. *Global Biogeochem. Cycles* 27, 505–515. doi: 10.1002/gbc.20045

Conflict of Interest: The authors declare that the research was conducted in the absence of any commercial or financial relationships that could be construed as a potential conflict of interest.

frontiers in Marine Science

METHODS
published: 18 September 2020
doi: 10.3389/fmars.2020.539601

Separation of Branched and Isoprenoid Glycerol Dialkyl Glycerol Tetraether (GDGT) Isomers in Peat Soils and Marine Sediments Using Reverse Phase Chromatography

Jayne E. Rattray[1†] and Rienk H. Smittenberg[*]*

Department of Geological Sciences, Stockholm University, Stockholm, Sweden

OPEN ACCESS

Edited by:
Kai-Uwe Hinrichs, University of Bremen, Germany

Reviewed by:
Arnaud Huguet, UMR 7619 Milieux Environnementaux, Transferts et Interactions dans les hydrosystèmes et les Sols (METIS), France
Sabine Kerstin Lengger, University of Plymouth, United Kingdom
Kevin W. Becker, Woods Hole Oceanographic Institution, United States

***Correspondence:**
Jayne E. Rattray
jayne.rattray@ucalgary.ca
Rienk H. Smittenberg
rienk.smittenberg@geo.su.se

†Present address:
Jayne E. Rattray, Department of Biological Sciences, University of Calgary, Calgary, AB, Canada

Specialty section:
This article was submitted to Marine Biogeochemistry, a section of the journal Frontiers in Marine Science

Received: *01 March 2020*
Accepted: *24 August 2020*
Published: *18 September 2020*

Citation:
Rattray JE and Smittenberg RH (2020) Separation of Branched and Isoprenoid Glycerol Dialkyl Glycerol Tetraether (GDGT) Isomers in Peat Soils and Marine Sediments Using Reverse Phase Chromatography. Front. Mar. Sci. 7:539601. doi: 10.3389/fmars.2020.539601

Over the last decade, glycerol dialkyl glycerol tetraethers (GDGTs) have become one of the most investigated lipid classes in marine and terrestrial organic geochemical research. GDGTs are microbial membrane core lipids biosynthesized as multiple homolog series of isoprenoid or methyl-branched isomers [isoprenoid glycerol dialkyl glycerol tetraethers (isoGDGTs) and Branched GDGTs (brGDGTs), respectively], whose relative abundance depend on a range of environmental parameters, including temperature. This has led to the development of GDGT-based temperature proxies. A key aspect in the analysis of GDGTs and the further development of their use as environmental proxies is good chromatographic separation of the full range of structural and stereo-isomers, with potential for discovery of novel GDGT variants. Several HPLC methods have been developed to this extent, but partial co-elution of GDGTs remains an issue despite long run times. In this study, we investigate the effects of different types of reverse phase (RP) chromatography on the separation of GDGT isomers. We found that the use of a Kinetex C18-XB column gives good separation of isoGDGT isomers in comparison to the recently developed double column HILIC analysis operated in normal phase (NP) and has a shorter run time. In marine samples, the regularly reported isoprenoid GDGTs separated in a similar way as in NP, however an earlier eluting group was observed to elute with the crenarchaeol isomer used in the TEX_{86} proxy. In a Swedish peat bog sample, a large range of isoGDGT isomers were observed. We observed a range of brGDGT isomers in several samples often with near baseline separation. Exact identification of all these isomers remained elusive, due to the different mechanism of separation in RP, and the complexity of the brGDGT family. The C18-XB method is rapid and versatile and can be set up on either low-pressure HPLC systems (max 400 bar) with a sample run time of 25 min for brGDGTs and 45 min to include isoGDGTs. On UHPLC-MS systems (>600 bar) the sample run time is reduced to 15 min. Most importantly, the C18-XB method presented here gives unusual separation of both isoprenoid and brGDGTs and could be a useful tool for the further elucidation of the biological sources and environmental factors that play a role in the production of different GDGT isomers.

Keywords: tetraethers, HPLC-MS, isomer resolution, reverse phase, GDGT

INTRODUCTION

Archaea, and more specifically Thaumarchaeota, are an abundant and diverse group of prokaryotes, inhabiting a range of marine, freshwater, terrestrial, and extreme environments (Brochier-Armanet et al., 2012; Könneke et al., 2014). They have a deeply branching phylogeny emanating from ancient hot environments (de la Torre et al., 2008) and have evolved to play a major role in oceanic CO_2 fixation and nitrogen cycling (Könneke et al., 2014; Tolar et al., 2016). Thaumarchaeal cell membranes are predominantly comprised of isoprenoid glycerol dialkyl glycerol tetraether (isoGDGT, **Figure 1A**) lipids which are biosynthetically regulated in response to environmental parameters like temperature, buffering capacity (Elling et al., 2017) and the core lipids are typically recalcitrant after cell death (Kuypers et al., 2001). The relationship between a ratio of sedimentary isoGDGTs and sea surface temperature is described in the TEX_{86} paleotemperature proxy (Schouten et al., 2002). Global calibration of the TEX_{86} ratio in marine core top sediments performed over the temperature range −2 to 30°C indicate that the relationship between the TEX_{86} ratio and temperature is a global phenomenon (Kim et al., 2008). In marine sediment cores TEX_{86} temperatures have been calculated as far back as the early Jurassic (∼194 Ma), making the TEX_{86} an important temperature proxy for understanding ocean warming and global climate change over extended geological time scales (Robinson et al., 2016). However, exceptions to the TEX_{86} temperature response have been found in sediments supporting the anaerobic oxidation of methane (Schouten et al., 2002; Zhang Y. G. et al., 2016) and hot-spring environments (Pearson et al., 2004; Zhang et al., 2006; Schouten et al., 2007). These are not only related to different groups of archaea being metabolically active, but also to the fact that many different structural and stereo-isomers exist. Recently, progress been made regarding the presence and relative abundance of isoGDGT regio-isomers, i.e., the parallel or anti-parallel glycerol configurations (Becker et al., 2013; Liu et al., 2018), in part using selective *sn*2 ether cleavage after fraction collection of the co-eluting isomers (Liu et al., 2019). Also, the cyclopentane moiety adjacent to the cyclohexane ring in crenarchaeol was found to exhibit the unusual *cis* stereochemistry in contrast to the regular *trans* stereochemistry (Sinninghe Damsté et al., 2018). Lastly, structural isomers of isoGDGTs now also include examples with cyclohexane rings (so-called S-GDGTs) and with double bonds instead of rings (Liu et al., 2016). The structural and stereochemical variations found in glycerol dialkyl glycerol tetraethers (GDGTs) affect their packing as membrane lipids, which provide biophysical explanation for their variety.

Branched GDGTs (brGDGTs) (**Figure 1B**) were originally attributed to a terrestrial source as they were hypothesized to be produced by an unknown group of soil bacteria (Weijers et al., 2009). Increasing evidence now shows brGDGTs are also produced *in situ* in aquatic systems (De Jonge et al., 2014a,b; Liu et al., 2014; Zhang Z. H. et al., 2016; Naafs et al., 2017). The distribution of brGDGTs in soils, peats and lacustrine sediments has been found to relate to mean annual air temperature and pH (Weijers et al., 2007; Tierney et al., 2012; Schoon et al., 2013), leading to the development of the terrestrial paleoclimate proxies based on the MBT and CBT ratios (Weijers et al., 2007; De Jonge et al., 2014a). Exactly how other environmental factors like alkalinity, salinity, and euxinity (presence of H_2S) influence the distributions of both isoGDGTs and brGDGTs is yet to be properly understood and can only be investigated efficiently if GDGT isomers are resolved sufficiently by HPLC-MS chromatography.

Glycerol dialkyl glycerol tetraethers have traditionally been analyzed using normal phase (NP) chromatography (Hopmans et al., 2004; Schouten et al., 2013b). The separation of individual isoprenoid GDGTs occurs in the order of increasing cyclopentane rings and the NP chromatography is selective enough to allow separation of the crenarchaeol isomer (*m*/*z* 1292) as a rider peak. More recently developed methods have successfully baseline separated the crenarchaeol isomer from crenarchaeol (Becker et al., 2013; Hopmans et al., 2016). The standard set of isoprenoid GDGTs elutes first in NP followed by H-shaped and hydroxylated GDGTs (OH-GDGTs). In NP chromatography, brGDGTs elute after the isoprenoid GDGTs with the higher masses eluting first. Due to a lack of resolution it was difficult to discriminate between individual methyl-branched isomers. Recently, brGDGTs have been identified as 5-methyl, 6-methyl, and 7-methyl isomers using lengthy HPLC fractionation and subsequent isomer identification using Gas Chromatography/Mass Spectrometry analysis of the hydrocarbons formed after ether cleavage of the GDGTs (Liu et al., 2012b; De Jonge et al., 2013; Ding et al., 2016). Separation of brGDGTs using Cyano columns was then superceded using tandem silica hydrophobic interaction liquid (HILIC) chromatography columns run in NP mode (Hopmans et al., 2016). This method successfully separates the 5- and 6-methyl-brGDGTs isomers but still has the disadvantage of a 90 min (plus 20 min re-equilibration) run time. The improved peak resolution of brGDGT isomers has further evolved the MBT and CBT proxies to include or exclude the 5- and 6-methyl-branched isomers (De Jonge et al., 2014a; Naafs et al., 2017; Russell et al., 2018), but clearly more diversity exists as suggested by co-eluting 5/6 isomers (Liu et al., 2012b; Weber et al., 2015).

Other studies have successfully used RP chromatography columns (ACE3 C18, Agilent Eclipse XDB-C18, Nucleodur C18 ISIS, Waters Acquity UPLC BEH C18, Waters XBridge C18) for separating GDGTs (Wörmer et al., 2013; Zhu et al., 2013, 2014; Liu et al., 2016, 2018, 2019). The wide range of phases available for reverse phase (RP) chromatography gives the possibility to combine with ultra (U)-HPLC conditions (>600 bar), important for high resolution analysis and keeping the cost of analysis low. Different stationary phases potentially allow for a range of interaction mechanisms that can separate GDGT isomers, making this an interesting avenue for further method development in GDGT research. This paper builds on previous research into RP GDGT chromatography (Wörmer et al., 2013; Zhu et al., 2013; Liu et al., 2016, 2018) by investigating GDGT chromatography

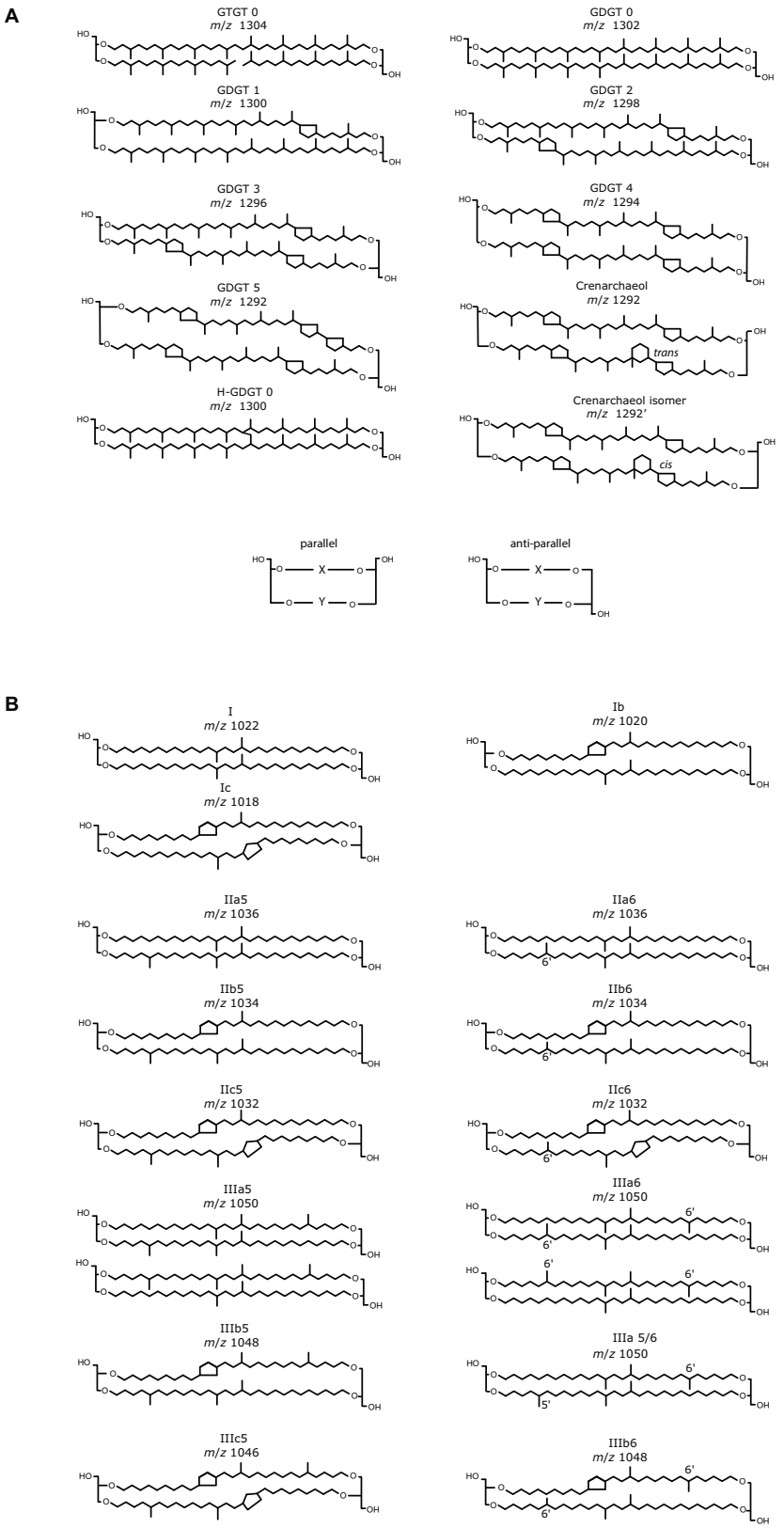

FIGURE 1 | Structures of **(A)** isoprenoid and **(B)** branched GDGTs including masses and common annotation found in the literature (Schouten et al., 2013b; De Jonge et al., 2014a). Note that this overview is not extensive and a large range of additional isomers are not shown (Liu et al., 2012b).

using four different RP core-shell particle column phases; C18-XB, PFP, C8, phenyl-hexyl. Subsequently the optimal RP method using the C18-XB column, hereafter termed C18-XB method, is compared with results from the conventional NP separation using a Cyano column (original GDGT method; Hopmans et al., 2004) and existing literature on RP to better understand GDGT isomer peak separation and distribution.

MATERIALS AND METHODS

Sampling and Lipid Extraction

In this study a total of 12 marine sediments (4 sites), 11 lacustrine sediments (2 sites), 22 peat bog soils (3 sites), and 1 sample of pre-purified GDGTs "Extract E" were used. Sample metadata are listed in **Supplementary Table S1**. Due to the often low quantities of sample extracts, not all samples were analyzed using every type of chromatography or column type, details of what samples are analyzed by the different methods are also found in **Supplementary Table S1**. All sediments were frozen and freeze dried after sampling and stored at −20°C until extraction. For total lipid extraction, solid samples were ground prior to weighing and ultrasonically extracted 3 × using methanol (MeOH), 3 × dichloromethane (DCM)/MeOH (1:1, v:v) and 3 × DCM or using 5 × 2:1 DCM:MeOH. Extracts were combined to produce a total lipid extract which was subsequently dried using a vacuum concentrator or under a stream of N_2. The Black Sea sample was extracted by Automated Solvent Extraction (ASE) as described by Birkholz et al. (2013). Extract E was provided as a pre-purified lipid extract as part of an international calibration study (Schouten et al., 2013a) and was stored at −20°C until analysis. We also tested a British peat and marine extract (**Figures 2**, **3** and **Supplementary Table S1**) provided by David Naafs from the University of Bristol (Naafs et al., 2018). Lastly, we analyzed a sample from the lake sediment of a soda lake in central Myanmar (Taum Pyauk), which was extracted using ultrasonication as described above.

For NP analysis the dried lipid extract was reconstituted in 99:1 v/v Hexane:propan-2-ol and placed in an ultrasonic bath for 10 min to ensure proper mixing. The extract was then filtered using a 0.45 μm, 4 mm diameter PFTE syringe filter. For RP analysis samples were re-dissolved in 9:1 MeOH: DCM (Zhu et al., 2013). Specifically, DCM was added first and vortexed to ensure lipids were brought into solution then MeOH was added. The samples were placed in an ultrasonic bath for 10 min before filtering through 0.45 μm, 13 mm diameter PFTE syringe filters prior to analysis. We tested using ethyl acetate as a cheaper and lower toxicity alternative to DCM (Graeve and Janssen, 2009) by dissolving a Baltic Sea lipid extract aliquots into varying percentages of ethyl acetate and methanol (EtOAc:MeOH 99:1, 9:1, 8:2, and 6:4). The largest crenarchaeol peak area was obtained using either 99:1 or 6:4 EtOAc:MeOH (v/v) solution. However, repeat injections showed there was a large variation in peak area (range 8–15% RSD, n = 3). In comparison, the average crenarchaeol peak area was less using the 9:1 MeOH:DCM solution but reproducibility was significantly higher (range 3–5% RSD, n = 3), therefore we selected this solvent mixture.

Analytical Instrumentation

A Dionex Ultimate 3000RS quaternary pump stack including auto-sampler, column compartment and switching device were coupled via either an atmospheric pressure chemical ionization (APCI) ion source or a heated electrospray ionization interface (HESI used in ESI mode), to a Thermo Scientific TSQ quantum access MAX triple stage quadrupole max mass spectrometer. Both APCI and ESI (electrospray ionization) interfaces were tested and the APCI interface was selected because it gave repeatedly higher signal intensities and a lower background signal (**Supplementary Figure S1**).

The conditions used for APCI-MS were: discharge current 12 μA, vaporizer temperature 384°C, sheath gas 0.4 l/min, ion sweep gas pressure 0.6 l/min, auxiliary gas pressure 1.5 l/min and capillary temperature 250°C. Conditions of ESI-MS were: spray voltage 3 kV, vaporizer temperature 384°C, sheath gas pressure 0.4 l/min, ion sweep gas pressure 0.6 l/min, auxiliary gas pressure 1.5 l/min and capillary temperature 229°C. Branched and isoprenoid GDGTs were detected using positive ion spectra generated by scanning with selective ion monitoring over the following ranges: m/z 741.2-744.8 (in 0.1 s), m/z 1016.5-1023.5 (in 0.2 s), m/z 1030.5-1037.5 (in 0.2 s), m/z 1044.5-1051.1 (in 0.2 s), m/z 1287.2-1304.8 (in 0.5 s).

Reverse Phase Chromatography

An overview of the different analytical parameters of various NP and RP methods are given in **Supplementary Table S2**. To investigate the effect of different core-shell polymer phases on the isomer elution of GDGTs we selected columns from the same manufacturer (Phenomenex) to avoid any variation caused by the type of base silica used in HPLC column assembly. Four phase coatings were chosen for study: (1) A Kinetex C18-XB with iso-butyl side chains and TMS endcapping and a core shell silica solid support, 1.7 μm, 100 Å, 150 × 2.1 mm; (2) A Kinetex C8, 1.7 μm, 100 Å, 150 × 2.1 mm; (3) A Kinetex PFP (pentafluorophenyl), 1.7 μm, 100 Å, 150 × 2.1 mm; (4) A Kinetex phenyl-hexyl, 1.7 μm, 100 Å, 150 × 2.1 mm. The separation of GDGTs was achieved using mobile phase A: MeOH with 0.04% formic acid and mobile phase B: propan-2-ol with 0.04% formic acid (formic acid was used as a solvent additive for both ESI and APCI ionization methods) selected from previously described RP methods (Lanekoff and Karlsson, 2010; Zhu et al., 2013). The method used a flow rate of 0.2 ml/min and gave a typical pressure of around 300 bar at a column oven temperature of 45°C. The initial composition of the mobile phase gradient was 60%:40% A:B was held for 1 min and then ramped to 50% B at 20 min. This mix was held for 15 min then changed back to 40% B for column re-equilibration. The total run time was 45 min An injection volume of 10 μl sample was used and samples were kept at ambient temperature to prevent coagulation of the sample which can cause higher back pressure if injected onto the column. We further created a UHPLC method by increasing the pump pressure and heating the column oven to 60°C. A flow

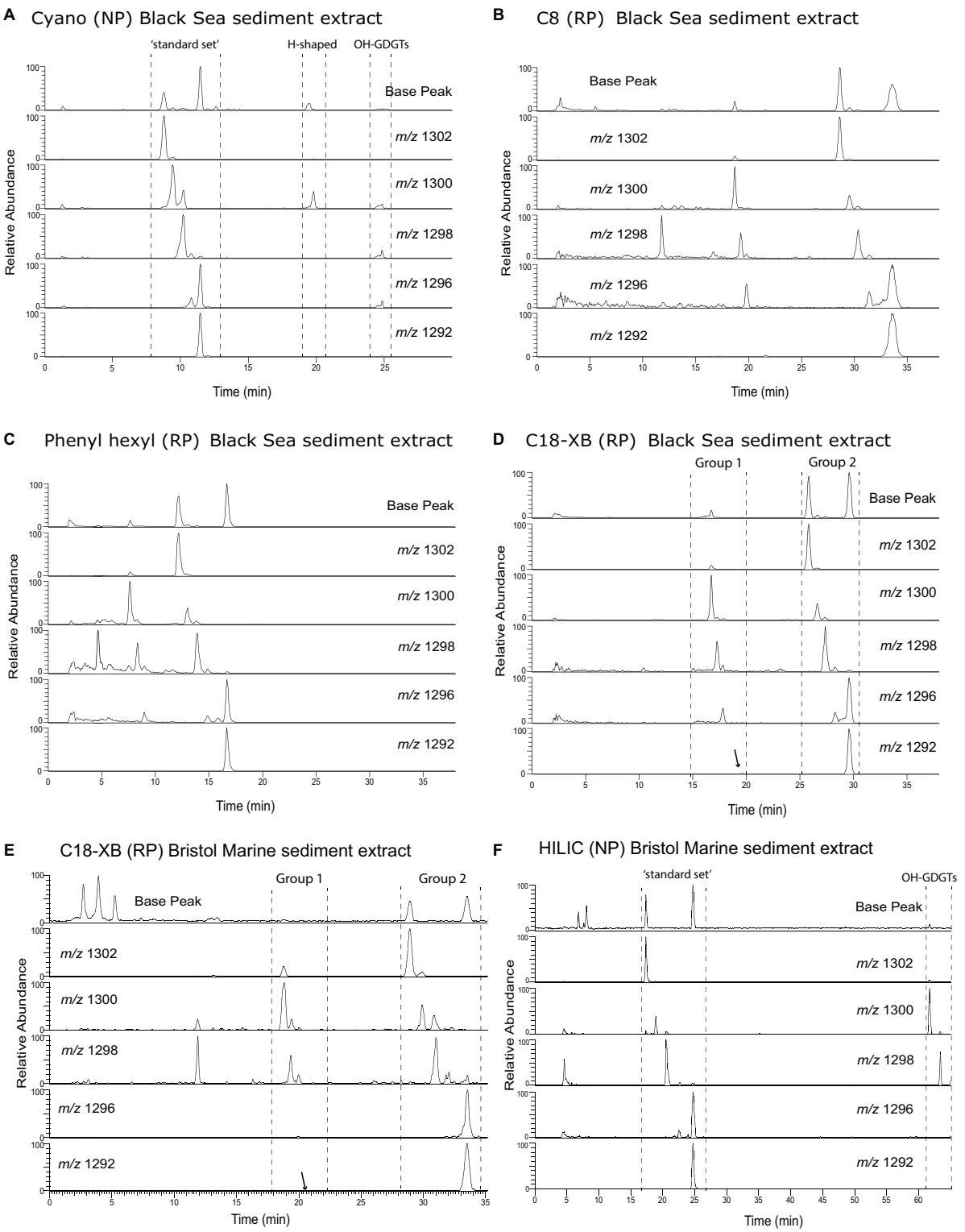

FIGURE 2 | Base peak and selected ion monitoring chromatogram of isoprenoid GDGTs from two marine sediment extracts. The Black Sea extract was analyzed using **(A)** Cyano column, NP; **(B)** C8, RP; **(C)** phenyl hexyl, RP; **(D)** C18-XB, RP columns. Due to a lack of sample material a Bristol marine sediment extract analyzed using **(E)** C18-XB and **(F)** HILIC is also shown. Indicated OH-GDGTs are identified using a combination of an RP fractionation experiment (described in section "Isoprenoid GDGTs in Marine Sediment"), RP and NP retention times found in the literature (see text). For RP, two clear groups can be identified. Note the small peak in the 1292 isomer is indicated by an arrow at 20 min in **(D,E)**. **Supplementary Figure S6A** compares the chromatography of C18-XB and HILIC using the British peat extract.

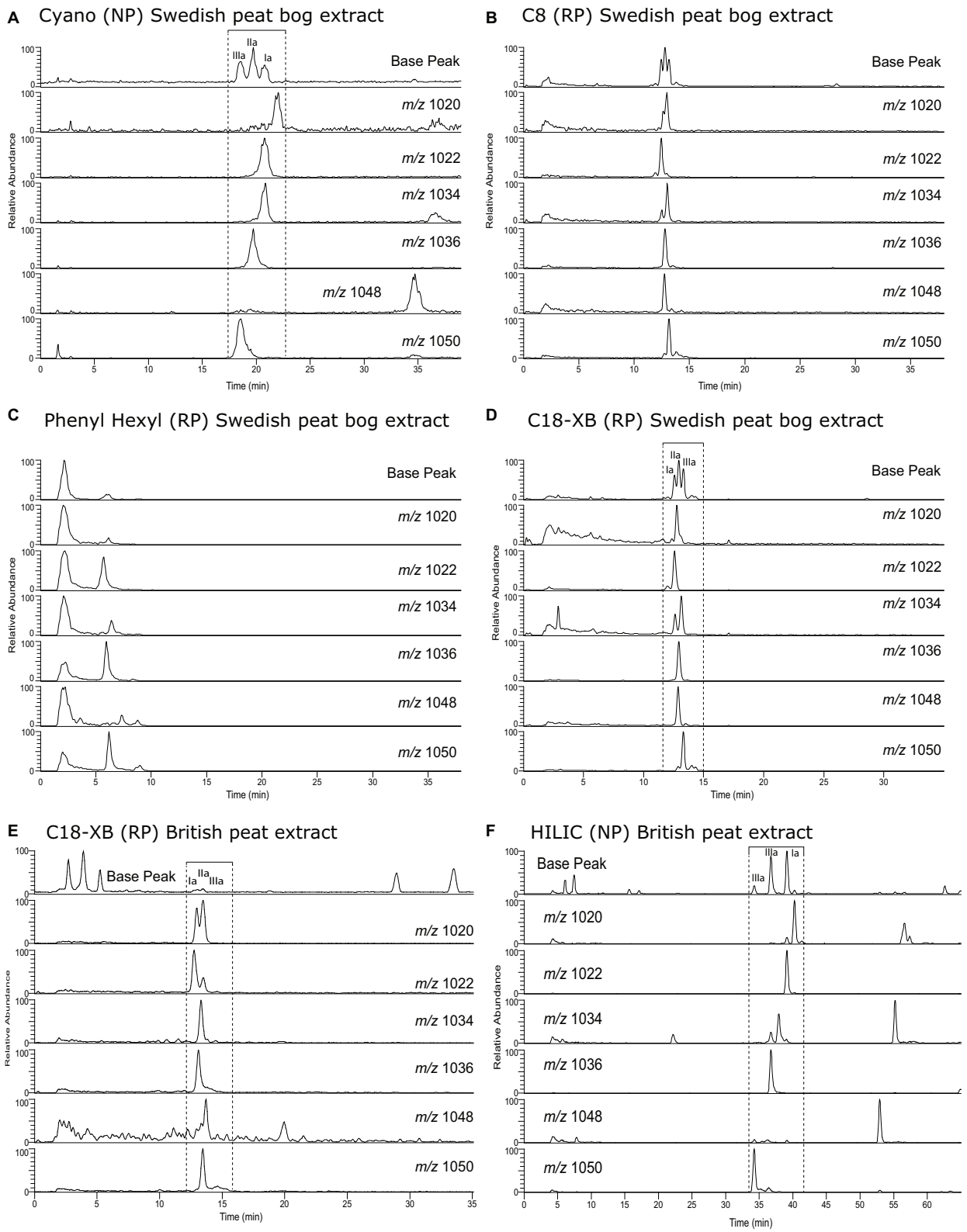

FIGURE 3 | Base peak and selected ion monitoring chromatogram of branched GDGTs from a two peat bog extracts. The Swedish peat extract was analyzed using **(A)** cyano, NP; **(B)** C8, RP; **(C)** phenyl hexyl, RP; **(D)** C18-XB, RP. A British peat extract analyzed was more recently analyzed using C18-XB and HILIC **(E,F)**. Note the reverse order of the tetra (I), penta (II), and hexamethylated (III) GDGTs in NP and RP. **Supplementary Figure S6B** compares the chromatography of C18-XB and HILIC using the British peat extract.

rate of 0.43 ml/min was used which gave a pressure of 600 bar. The initial composition of the mobile phase gradient was 60%:40% A:B, which was held for 1 min and then ramped to 50% B at 10 min. This blend was held for 4 min and decreased back to 40% B. The total run time was 15 min. An injection volume of 2 μl sample was used and samples were kept at ambient temperature during analysis. Lower injection volumes are necessary for UHPLC due to the small (1.7 μm) silica pore size which requires a decreased loading capacity to reach optimal analyte peak shape and retention. Sharp peaks created in UHPLC methods mean a lower limit of detection and quantification can be achieved because small broad peaks are difficult to integrate and discriminate from the baseline.

Normal Phase Chromatography

Normal phase chromatography used a single Grace Prevail Cyano 3 μ column (150 × 2.1 mm; Grace Discovery Sciences, United States) similar to the method described by Hopmans et al. (2004). Gradient chromatography was hexane with 1% propan-2-ol (mobile phase A) followed by a linear gradient to 10% propan-2-ol (mobile phase B) over 45 min using a flow rate of 1 ml/min. After each analysis the column was cleaned by back-flushing hexane/propanol (99:1, v/v) at 1 ml/min for 10 min. The total run time was 60 min with an injection volume of 10 μL, samples were kept at ambient temperature during analysis. In addition, samples were run using a NP HILIC method as described in detail by Hopmans et al. (2016) except that our UHPLC pump was operated at a flow rate of 0.3 ml/min to give a faster gradient and higher backpressure. The system was monitored to ensure optimal peak resolution was achieved with each analysis.

Fraction Collection

To better understand the exact position and type of isoGDGT isomers on the C18-XB column we extracted large amounts of Baltic Sea sediment, for the brGDGT isomers we extracted Nong Thale Prong (NTP) lacustrine sediment and Swedish bog soil. Freeze dried ground soil or sediment (±60 g) was extracted using 5 × 2:1 DCM:MeOH. The total extract was separated over an Al_2O_3 column and the polar fraction eluted with 95:5 DCM:MeOH. The eluent was dried under a constant stream of nitrogen, re-dissolved in 9:1 MeOH:DCM (initially dissolving in DCM and vortexing then adding MeOH and vortexing), and filtered over a 0.45 μm PTFE filter. The polar fraction was separated using a semi-preparative C18-XB column (100 Å, 150 × 2.1 mm 2.6 μm) fitted to a Dionex Ultimate 3000RS HPLC connected to a Dionex AFC-3000 automated fraction collector with splitting device. The flow rate was 0.2 ml/min with the following eluent gradient; 60%:40% A:B for 1 min, linear gradient to 50% B at 20 min. Hold for 15 min then 40% B for 9 min for column re-equilibration. Eluent A is MeOH/HCO_2H (100/0.04 v/v) and B is Propan-2-ol/HCO_2H (100/0.04 v/v). Fractions were collected in 1 min intervals between 5 and 45 min and then re-analyzed for brGDGTs using the RP method. Selected isoGDGT fractions (collected 25–30 min) were also analyzed using the NP method. Where possible, isomers were identified by direct injection of the fractions and performing MS/MS experiments. GDGT fragmentation patterns were compared with those published by Knappy et al. (2009), Liu et al. (2012b), De Jonge et al. (2014a), and Ding et al. (2016).

RESULTS AND DISCUSSION

The Influence of Core-Shell Polymer Coatings on the Analysis of GDGTs

Isomer retention and separation was investigated using repeat injection of GDGT lipids extracted from the Black Sea sediment. An environmental sample was used for column comparison due to the lack of commercially available standards for GDGT analysis and had the advantage of letting us understand environmental sample matrix effects at the start of method development. NP analysis using the cyano column (**Figure 2A**) eluted isoprenoid GDGTs in three separate series and the early eluting series contained peaks with the largest areas. Due to the more recent setup of the NP HILIC method and a lack of sample material, the HILIC method was tested at a later date using the Bristol marine standard extract which elutes the "standard set" of isoprenoid GDGT compounds between 17 and 26 min (**Figure 2E** and **Supplementary Figure S6**). Isoprenoid GDGT isomers in the early eluting "standard set" are used in TEX_{86} proxy calculation. The second eluting group in the NP method consists of H-shaped GDGTs which have an approximately double retention time compared to the regular GDGTs (Naafs et al., 2018), and the third group OH-GDGTs.

On the C8 and PH columns (**Figures 2B,C**), three groups of GDGTs are observed (**Figure 2**), on the C18-XB (**Figure 2D**) two groups are seen, eluting between 17–22 (Group 1), and 27–35 min (Group 2). The PFP column gave no retention of GDGTs so it was excluded from further study. On all three RP columns an undefined hump of non-retained compounds elutes at the start of the run (before 5 min) and gives the largest peak area when using the C8 and PH column methods. After the analysis of different sediment and soils (**Supplementary Table S1**) it was found that non-retained compounds from the sample matrix appeared variable with sample type but elute prior to 2.5 min (in RP) and do not significantly affect the first group of GDGTs. Baseline separation of peaks from each other or undefined humps is essential for proper peak integration. In our experiments the best separation was observed using the C8 and C18-XB columns (**Figures 3B,D**) and the sharpest peaks were observed using the C18-XB column. On the C18-XB column retention time was tested for reproducibility. The standard reproducibility of the retention time of the largest and best resolved peak in the chromatogram (m/z 1292, n = 10) using repeat injections from different vials in the same sequence was 6 s and of repeat injections made in different runs (i.e., on different days) was 37 s (m/z 1292, n = 5). Comparing critical pairs calculated for the main GDGTs used in proxy calculation (**Supplementary Table S3**) shows the C18-XB method gives good separation of isoGDGT isomers in comparison to the recently developed double column HILIC analysis operated in NP.

Branched GDGT chromatography was investigated using a Swedish bog lipid extract. They were found to elute as a single series on all column types (**Figure 3**). Using NP

(**Figure 3A**), brGDGTs elute later than the isoprenoid GDGTs and this is converse for the RP analysis (**Figures 3B–D**) as previously reported by Zhu et al. (2013) for RP chromatography. The tetramethylated (I) elute before the pentamethylated (II) and hexamethylated (III) homologs in RP, in contrast to the NP method where the order is III-II-I. Using a longer NP method gives the largest retention time difference between isomers I-III (De Jonge et al., 2013; Hopmans et al., 2016; **Figure 3F**). The PH column (**Figure 3C**) showed less retention of the brGDGTs and as a result was influenced by the hump of injection material. On both the C8 and C18-XB columns (**Figures 3B,D**) brGDGTs elute at similar retention times

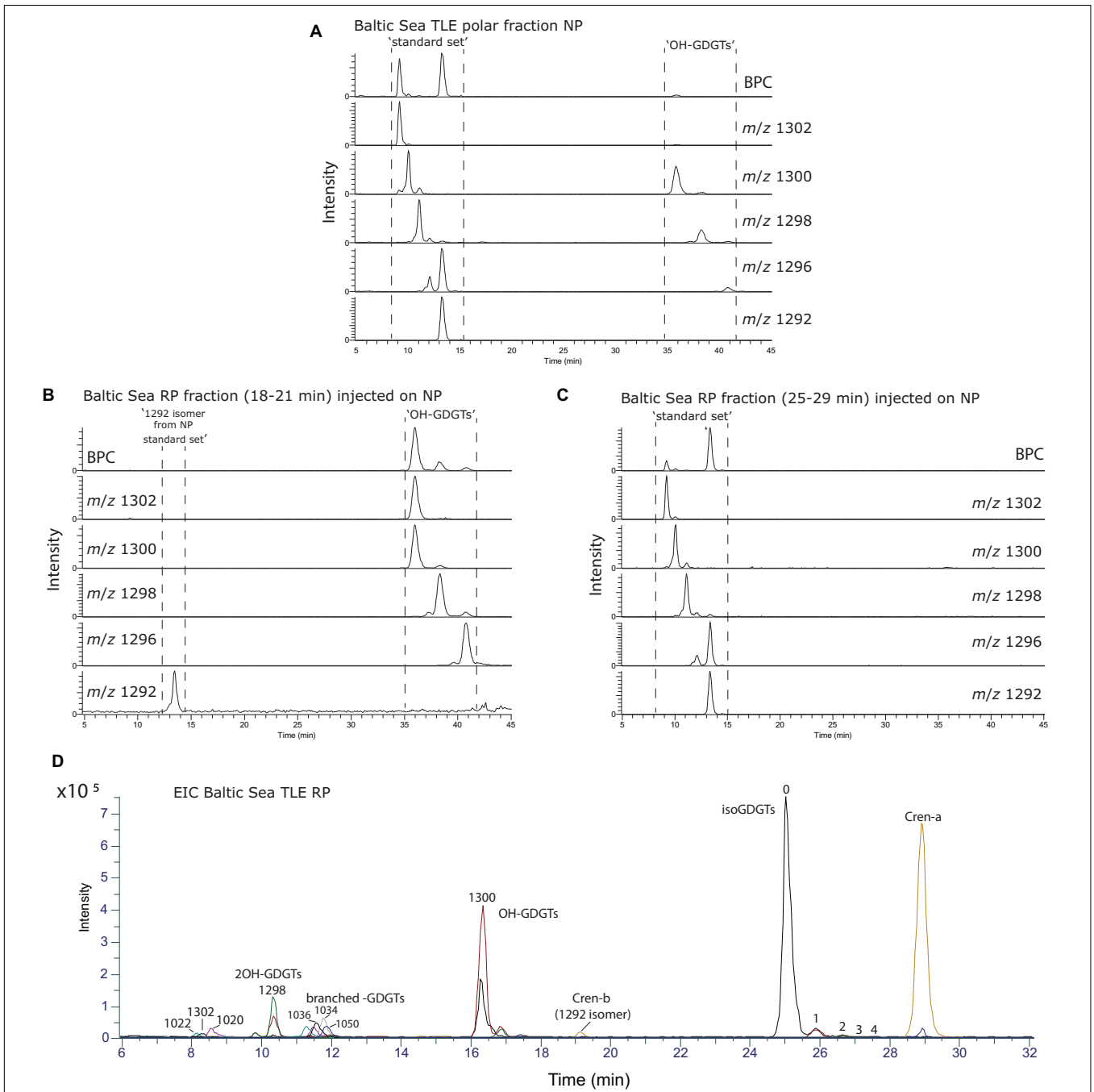

FIGURE 4 | GDGT analyses of a Baltic Sea sediment lipid extract. **(A)** Polar fraction separated using the traditional NP method using a Cyano column. **(B)** The 18–21 min fraction from fraction collection after separation the C18-XB method, again using the Cyano NP method. **(C)** Same as b, but for the 25–29 min fraction. **(D)** Extracted ion chromatogram overview of isoprenoid and branched GDGT isomers both identified and tentatively identified (based on comparison with other RP methods (Zhu et al., 2013; Liu et al., 2019). The various ion chromatograms are overlaid over each other with different colors.

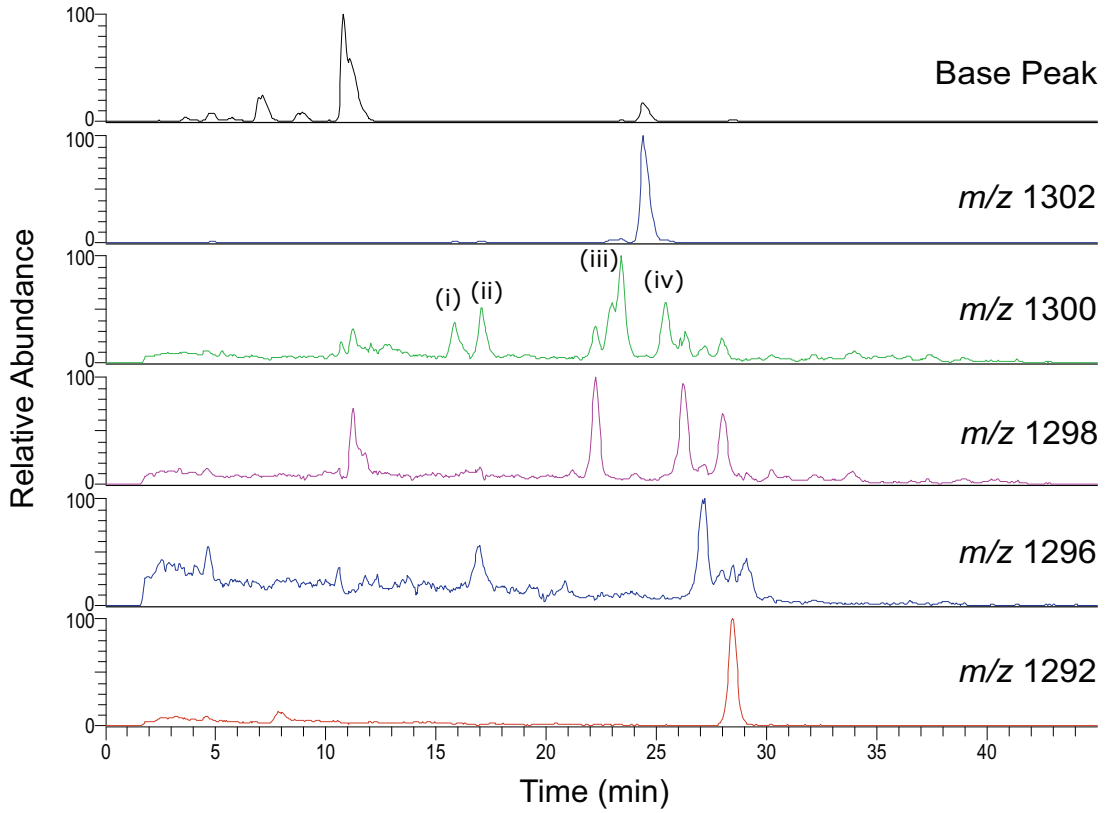

FIGURE 5 | HPLC-MS Single Ion Monitoring chromatograms from a C18-XB analysis of the Swedish peat bog extract, showing multiple isoGDGT isomers.

as sharp peaks which create, in some cases, near baseline separation of a range of isomers. Based on the good isomer separation and the added advantage that it can be used for UHPLC applications, the C18-XB column was selected for further testing.

GDGT and Isomer Separation

Isoprenoid GDGTs in Marine Sediment

To identify the GDGT structures on the C18-XB chromatogram, we fractionated a large quantity of the Baltic Sea total lipid extract using semi-preparative RP chromatography and (re-)injected the total extract (**Figure 4A**) and two fractions (18–21 min and 25–29 min) on the NP cyano column (**Figures 4B,C**). The fraction of isoprenoid GDGTs in group 1 on the C18-XB column (eluting 18–20 min) elute later, between 35 and 40 min, when re-injected on the NP column (**Figure 4B**). The retention of the RP 18–20 min fraction in NP suggests that the *m*/*z* 1300, *m*/*z* 1298, *m*/*z* 1296 are OH-GDGTs (Liu et al., 2012a), however, the inclusion of *m*/*z* 1302 in the series and the placement of the *m*/*z* 1292 isomer at 13 min suggests that these are a mix of OH-GDGTs with stereoisomers or isotopologs of the "regular isoGDGTs" (**Figure 4B**). Comparing the C18-XB elution pattern of the marine sediment isoGDGTs with published GDGT-RP methods (Zhu et al., 2013; Liu et al., 2019) also supports the earlier elution of OH-GDGTs in comparison to the regular set of GDGTs. GDGT group 2 (25–29 min, C18-XB column) elute between 9 and 15 min on the NP column and are the "regular" isoGDGTs used to calculate the TEX_{86} proxy. The *m*/*z* 1292 isomer is not present in the RP 25–29 min fractions as a typical NP shoulder peak where the regular *m*/*z* 1292 elutes at 13 min. Sinninghe Damsté et al. (2018) concluded that the 1292′ isomer is in fact a stereo-isomer of the regular crenarchaeol where the cyclopentane ring next to the characteristic cyclohexane ring has a *cis*-configuration instead of the regular *trans*. This suggests that separation using the C18-XB method is sensitive to structural and stereo-isomeric differences of the biphytanyl chains of the GDGTs, on top of polarity. It also indicates that early eluting (group 2) GDGTs could be stereo-isomers of the regular *trans* isomers. Further work is needed to resolve the exact nature of the early eluting GDGTs on our RP method, although it is clear that the *m*/*z* 1292′ crenarchaeol isomer used in the TEX_{86} elutes at the end of this group. An extracted ion chromatogram overview of isoprenoid and brGDGT isomers both identified and tentatively identified (based on comparison with other RP methods (Zhu et al., 2013; Liu et al., 2019), from the Baltic Sea extract is shown in **Figure 4D**.

Isoprenoid GDGTs in a Peat Bog Lipid Extract

Unusual separation of isoGDGTs was found when analyzing the Swedish peat bog extract using the C18-XB column. Multiple isomers were observed, especially for *m*/*z* 1300, 1298, 1296

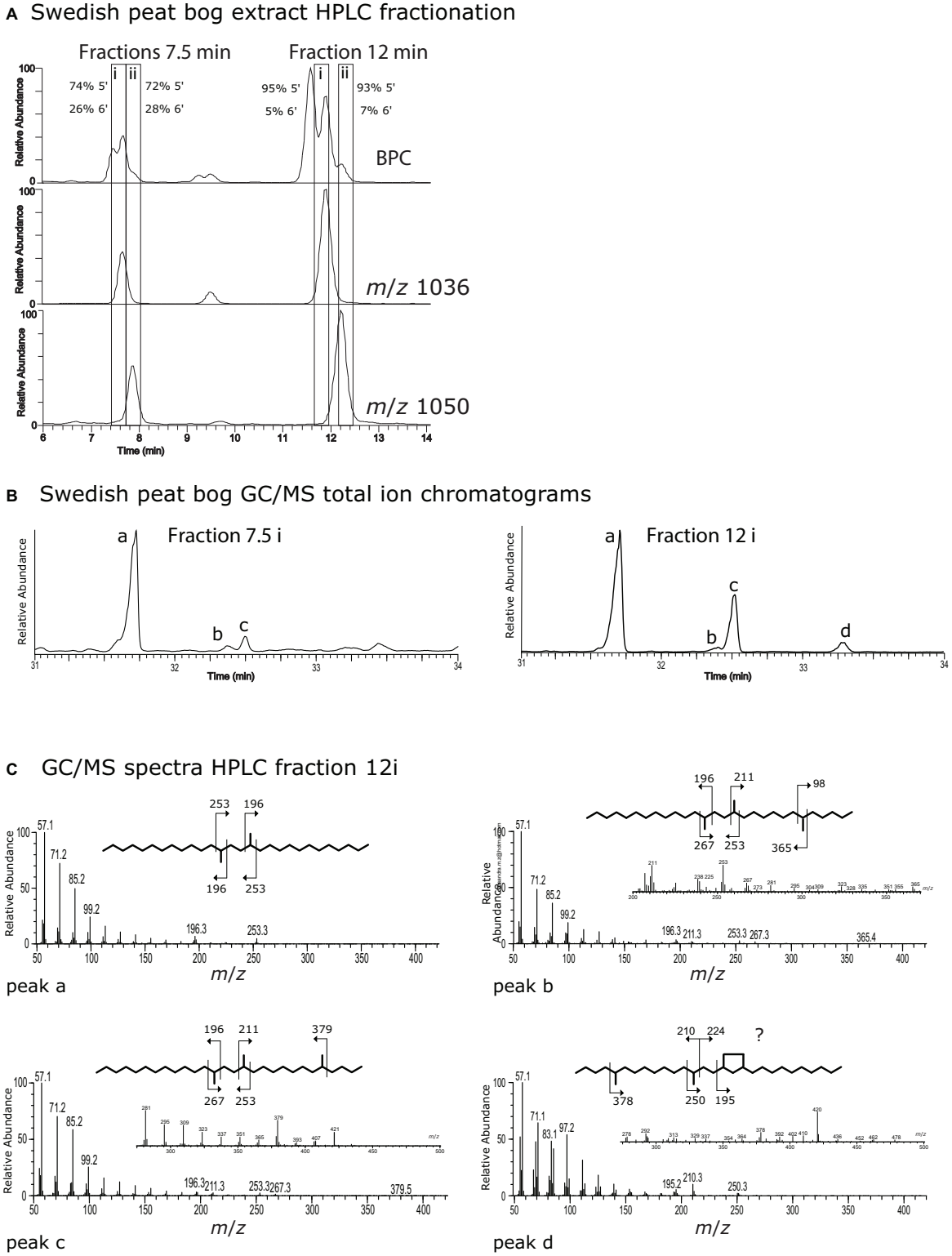

FIGURE 6 | (A) Partial base peak and *m/z* 1036 and *m/z* 1050 chromatograms from a Swedish Bog extract used for RP HPLC fraction collection. Boxes around 7.5 and 12 min show collection time windows where an earlier (i) and later (ii) fraction was taken at each collection time window. Fractions were subsequently ether cleaved and hydrogenated to elucidate the position (5′ or 6′) of the methyl group on the isomers. **(B)** GC-MS total ion chromatogram (TIC) from ether cleaved and hydrogenated HPLC fractions 7.5(i) and 12(i) from the Swedish peat bog. **(C)** GC-MS mass spectra from hydrocarbons a–d afforded from fraction 12(i) after ether cleavage and hydrogenation.

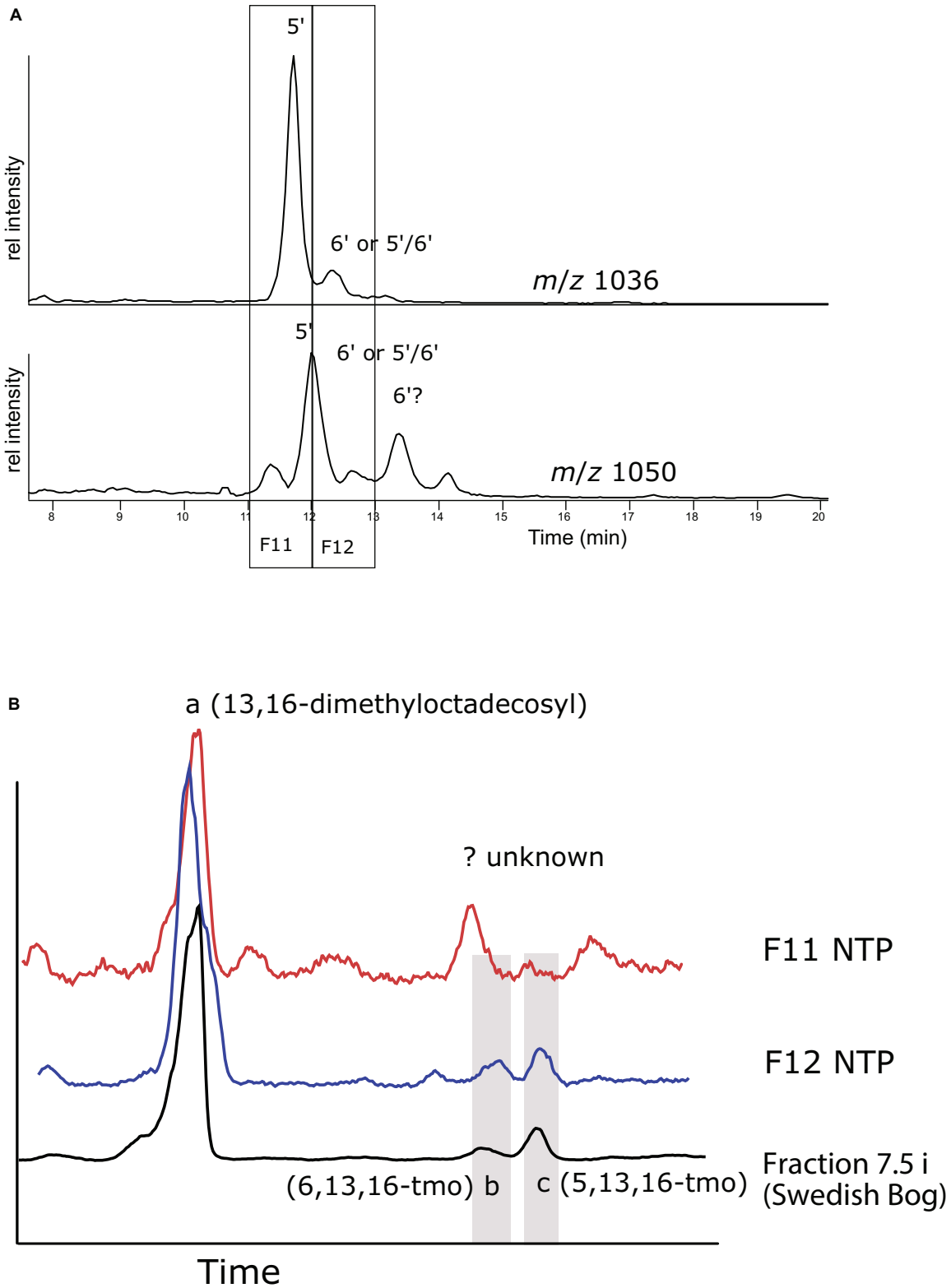

FIGURE 7 | (A) Reverse phase HPLC-MS ion chromatograms showing the distribution of *m/z* 1036 and *m/z* 1050 isomers in the NTP lake sediment extract. Numbers indicate the likely position of the methyl group on the isomers. **(B)** GC-MS total ion chromatogram (TIC) from ether cleaved and hydrogenated HPLC fractions eluting between 11–12 and 12–13 min, compared with the TIC of the 7.5 min fraction from the Swedish peat bog (cf. **Figure 6**). The positions of 5,13,16 (b)- and 6,13,16-trimethyloctasanyl as identified in **Figure 6** are indicated.

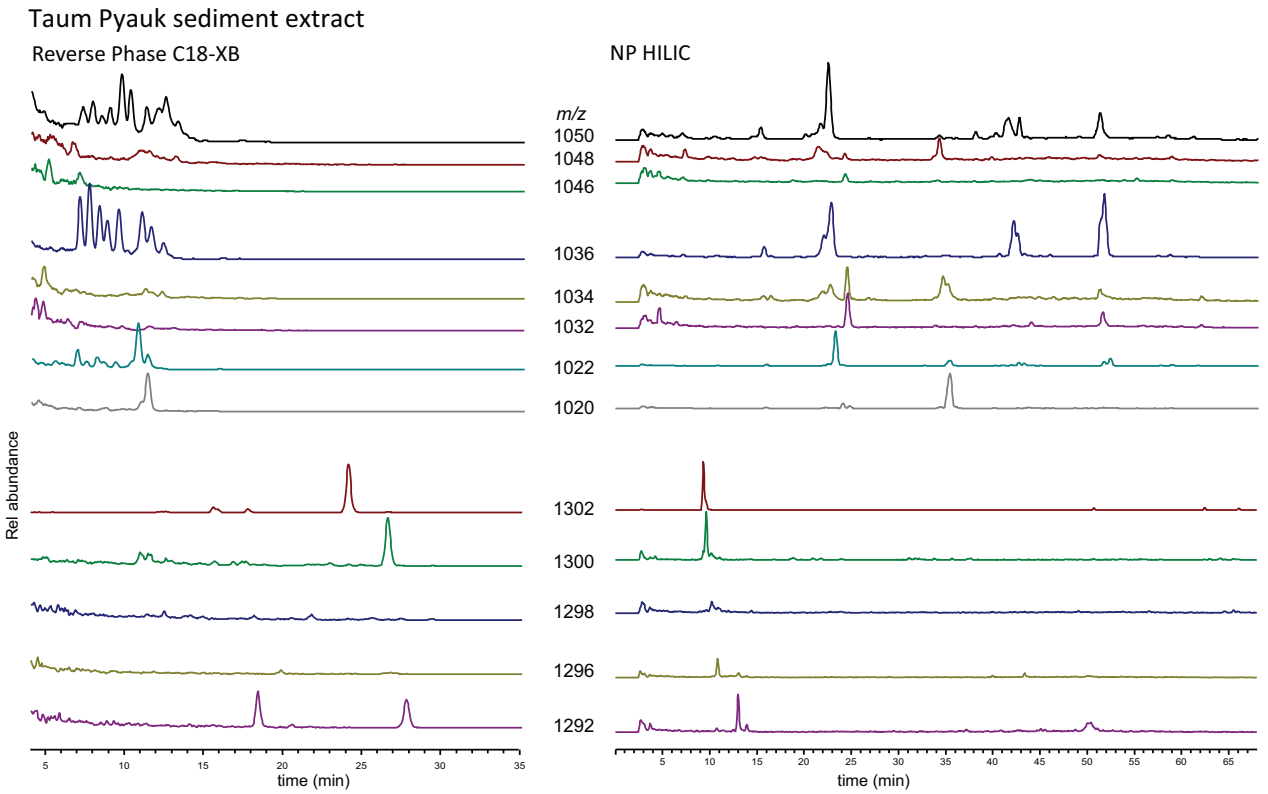

FIGURE 8 | C18-XB (left) and HILIC (right) selected ion chromatograms of branched and isoprenoid GDGTs from Taum Pyauk soda lake, Myanmar. In RP, many isomers can be observed for the branched GDGTs, while these are not clearly visible in NP. The *m/z* 1292 trace shows a clear isomer after the main peak at 13 min in the HILIC run. In RP, *m/z* 1292 exhibits two clear, nearly equally sized peaks.

(**Figure 5** and **Supplementary Figure S2**). The same group 2 observed for the marine sample described above (eluting 25–29 min) corresponds to the regular set of GDGTs. The crenarchaeol isomer *m/z* 1292′ (observed at 19 min in the marine sample), was not detected in the peat bog sample but the lack of crenarchaeol and its isomer has often been observed in peat samples (Schouten et al., 2000; Pancost and Sinninghe Damste, 2003; Weijers et al., 2004; Huguet et al., 2010; Zheng et al., 2015) and is attributed to the low abundance of ammonia-oxidizing Thaumarchaeota. A number of peaks of *m/z* 1300 and *m/z* 1298 were observed between 10 and 24 min. Our results show a similar pattern as those observed by Liu et al. (2016) using a different C18 RP method, who identified series of GDGTs with double bonds, cyclopentyl rings, and cyclohexyl rings ("S-GDGTs") for *m/z* 1300, 1298, and 1296, where more unsaturated bonds generally lead to shorter retention times and cyclohexyl rings to longer ones (Zhu et al., 2014); for structures see Liu et al. (2016). MS/MS fragmentation experiments on the *m/z* 1300 GDGT isomers at 15.8, 17.1, 23.4, 25.4 min (**Supplementary Figure S2**) all showed the typical fragmentation of the intact core GDGT and the product ion (*m/z* 743) formed from the loss of the 1,31-biphytadiene from the main molecule (Knappy et al., 2009). However, fragments <*m/z* 743 in spectra (i-iv) display varied fragmentation patterns, which are suspected to be caused by the structural differences of the various biphytane units within the *m/z* 1300 GDGT family. Our methods did not allow for further elucidation of the various GDGT structures, which requires the use of standards as well as ether cleavage experiments and subsequent analysis of the products by GC-MS. Isomers likely include unsaturated, hydroxyl and ring containing GDGTs as well as stereo-isomers but this needs to be experimentally verified. Liu et al. (2016) investigated the differences of NP and RP GDGT separation in detail. The NP double column method (Becker et al., 2013; Hopmans et al., 2016) gave improved separation of the GDGT isomers in comparison to the RP single column method (Zhu et al., 2013). While the isomers were less resolved using the RP method, an abundance of unusual GDGT isomers were identified, including variants containing unsaturated, cyclopentyl and cyclohexyl moieties.

Branched GDGTs

In order to attempt to identify the position of the brGDGT isomers eluted during the C18-XB method (**Figure 3**) we extracted a large quantity of Swedish bog material and subjected it to fraction collection using a semi-preparative C18-XB column, focusing on the pentamethylated (*m/z* 1036, IIa) and hexamethylated (*m/z* 1050, IIIa) GDGTs, which were most dominant (**Figure 6**). Interestingly there were two different sets with retention times at 7.5 and 12 min (**Figure 6A**). The two sets were collected and at each instance first a fraction

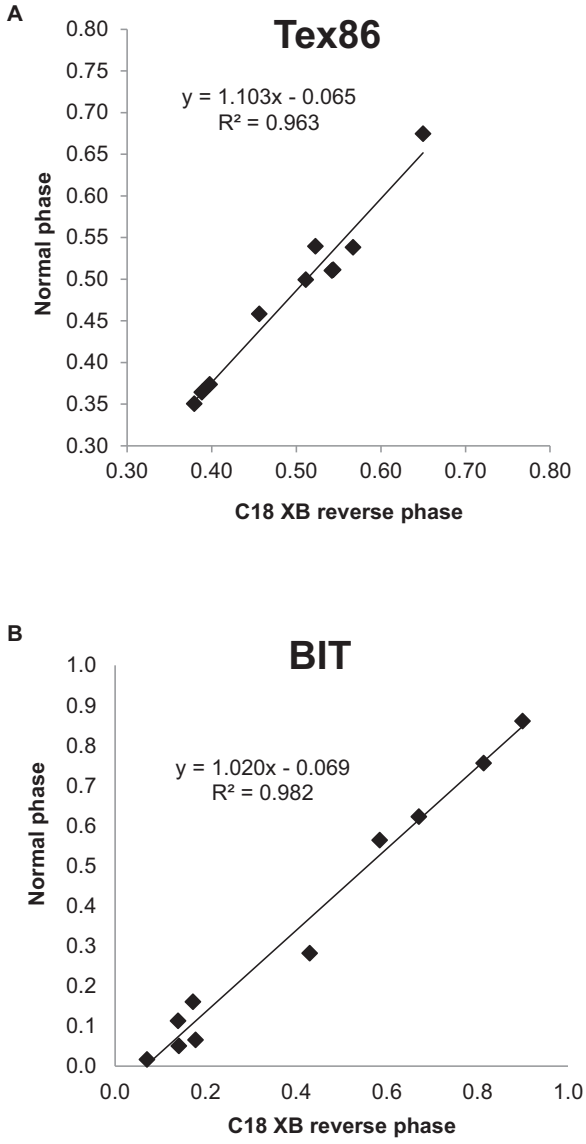

FIGURE 9 | Comparison of **(A)** BIT and **(B)** TEX_{86} values obtained by Normal Phase (Cyano column) and Reverse Phase (C18-XB) chromatography.

containing predominantly IIa (labeled i) and then a fraction with mainly IIIa (labeled ii). Collected fractions were subjected to ether cleavage and hydrogenation, and individual fractions were analyzed by GC/MS. **Figure 6B** shows the partial GC/MS total ion chromatograms of the (i)-fractions collected at 7.5 and 12 min; **Figure 6C**(a–d) and **Supplementary Figures S3, S4** show mass spectra. We compared hydrocarbons a, b, c and d to previously reported chromatographic retention times and mass spectra (De Jonge et al., 2013; Ding et al., 2016). The relative amounts of 5,13,16- and 6,13,16-trimethyloctacosanyl (5-tmo and 6-tmo, respectively) analyzed using GC/MS can be used to back-calculate the relative abundance 5' and 6' isomers of IIa and IIIa within the collected fractions. The mass spectrum of GC/MS peak b contains the pair *m*/*z* 98/365 deriving from 6-tmo, while *m*/*z* 379 indicates 5-tmo for peak c. Peak d shows the characteristic fragments *m*/*z* 210, 250 and 195 indicative the ringed structures observed by Ding et al. (2016), where *m*/*z* 378 indicates that this would be a 5-methyl isomer. However, the series of *m*/*z* 83/97/101 instead of the regular 85/99/103 does not agree with earlier published spectra. Concentrations were too low to further investigate the exact structure of peak d. In both the 7.5 and 12 min group there is one major isomer peak for IIa which, unlike the IIIa, has no small peaks or shoulders eluting prior to or after the main peak. Fractions i and ii eluting around 12 min had a higher percentage of 5-tmo (95% and 93%) than earlier eluting fractions at 7.5 min (74%, 72%). For both collection time windows the initial fraction (i) contained slightly more of the 5-methyl isomer than the subsequent fraction (ii). The ratio of 5-tmo to 6-tmo of IIa at 7.5 min suggests a mixed signal of 5′, 5′/6′ and/or 6′ isomers (i.e., IIa_5, $IIa_{5/6}$, IIa_6) and thus that these isomers are not well separated. Given the large percentage of the 5-tmo in the 12 min fractions, we infer that the here mainly 5-methyl isomers elute, however still with a small admixture of 6′ or 5′/6′ isomers. The question why there are two sets of isomers remains unresolved. Possibly, the earlier eluting set are OH-brGDGT isomers; future analysis using an ESI source could provide evidence for this.

To verify our experimental procedure and to attempt to get more evidence for the elution order of the 5′ and 6′ isomers, HPLC fractions were collected, ether cleaved and hydrogenated from sediments of a tropical lake NTP, southern Thailand. Because of the tropical temperatures, the brGDGT distribution was dominated by the tetramethylated GDGTs (I), while the hexamethylated GDGTs (III) comprised less than 10%. In the base peak chromatogram of the NTP extract IIIa isomers (1050) elute as five near-baseline separated peaks and there are at least two isomers of II (**Figure 7A**). Unfortunately, low recovery of material from the fraction collection experiment gave unsatisfying results but we could still draw some conclusions, also by comparing retention times with those from the peat bog analysis (**Figure 7B**). The fraction collected between 11 and 12 min was dominated by 13,16-dimethyloctadecosyl deriving from I and II. We tentatively assigned one peak to 5,13,16-tmo but 6,13,16-tmo was not detected. Instead we observed another hydrocarbon that likely derived from a variety of I, but this remains speculation as the mass spectra were inconclusive (**Supplementary Figure S5**). The fraction eluting at 12–13 min resulted in peaks both of 5,13,16- and 6,13,16-tmo, the former around twice as large as the latter. This suggests that the largest peak of III (1050) is the 5′ isomer, while the subsequent peak could be the 6′ isomer or even the mixed 5/6 isomer, followed again by the 6′ isomer, in the same order as seen during the HILIC/NP separation (De Jonge et al., 2014a; Ding et al., 2016; Hopmans et al., 2016). For this sample, we clearly show that C18-XB method is capable of separating various structural isomers of the brGDGTs. The laborious method of identifying the exact structures of the alkyl groups complicates identification. Moreover, one needs to count on the possibility of asymmetric brGDGTs, i.e., combinations of di/tetra-methylated octacosanyl chains

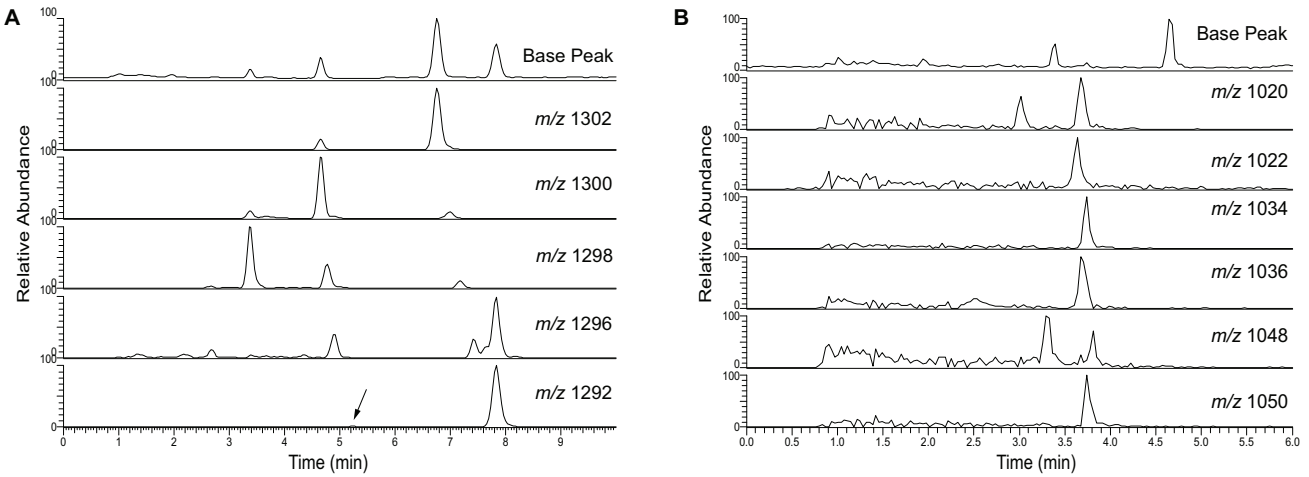

FIGURE 10 | UHPLC analyses of Baltic Sea surface sediment extract showing the base peak chromatogram of **(A)** isoprenoid GDGTs and **(B)** branched GDGTs. The arrow indicates the crenarchaeol isomer.

within the GDGT structures, and the potential for mixed 5/6, 5/7, 6/7 isomers.

As a last test to explore the differences between the RP C18-XB and the NP methods, we analyzed GDGTs extracted from sediment recovered from a soda lake (with a water pH of ca. 10) in Myanmar, using both the HILIC and the C18-XB methods (**Figure 8**). Of note here is that the NP HILIC analysis was performed 2 years after the C18-XB method; the GDGT fractions were stored at −18°C. Also, this sample comes from an extreme environment with reducing (euxinic) conditions at very high pH. With the C18-XB method we found a large suite of brGDGT isomers of especially Ia, IIa and IIIa, eluting between 7 and 14 min, while the NP HILIC method gave some peaks at the "normal" retention time, but also several late eluting peaks. This suggests some of the early eluting brGDGTs (on RP) might be OH-GDGTs, which would elute late with HILIC/NP chromatography. We did not further pursue identification the compounds in this sample.

To conclude, the C18-XB method appears capable of separating a large range of brGDGT isomers, including 5′ and 6′ methyl isomers, although further work is needed to come to conclusive evidence of the exact order or chromatographic separation. Our results clearly indicate that the mixtures of brGDGTs in various settings are highly variable and of different complexity. The RP method presented here provides an additional tool to investigate the family of brGDGTs, a task that clearly is not finished yet.

The Impact of the RP Method on the Calculation of the TEX_{86} and BIT Proxies

TEX_{86} values of multiple environmental samples run on both the C18-XB and the Cyano column compared well (r^2 = 0.96, n = 11, **Figure 9A**). BIT indices measured on a small suite of environmental samples both using RP and NP methods also compared well (r^2 = 0.98, n = 10, **Figure 9B**). Despite tentative assignment of 5-methyl GDGTs, we refrain from discussing the $MBT_{(5Me)}$ and $CBT_{(5Me)}$ proxies as we could not always account for all isomers when comparing our results with the HILIC method. More sample comparisons are needed to further substantiate the transferability of the GDGT-based proxy results between the different methods. However, we argue that final results of any study using GDGT proxies will likely depend more on the choice of calibration, and the extent to which that calibration is evaluated and validated for a particular site or setting, than on the chromatographic method used.

Adaption to UPLC

UHPLC (>600 bar) has the advantages of fast run times and low injection volume, in this case 2 µl, which is essential for creating sharp peaks to improve baseline resolution (**Figure 10**). The run time of the UHPLC method is ultimately limited by the tailing hump of unresolved compounds which is eluting soon after injection. The isoprenoid and brGDGTs elute within 10 min and the total run time is 15 min including column flushing. Comparing **Figure 10** with **Figures 3**, **4** shows that GDGT peak distribution remains the same in the UHPLC and RP 45 min run. The TEX_{86} values calculated for a Black Sea surface sediment after analysis using the NP, RP HPLC, and RP UHPLC methods gave the same results (**Supplementary Table S4**), and corresponded also with the value published by Wakeham et al. (2003). BIT values were also comparable for the three methods (**Supplementary Table S4**) when applied to Extract E from the TEX_{86} and BIT intercalibration study performed by Schouten et al. (2013a). Tentative assignment of the various brGDGTs and subsequent calculation of MBT'_{5Me}, CBT_{5Me} and CBT' proxies gave identical results when comparing the 45 min RP method (see **Supplementary Figure S7** for the HPLC chromatogram) with the 15 min UHPLC method (**Supplementary Table S4**). These initial tests suggest a good agreement of the different proxy calculations indicating that both the RP HPLC and

UHPLC methods provide proxy calculation comparable to the original NP method.

CONCLUSION

The chromatography of four different core-shell polymer phases on the elution of isoprenoidal and brGDGT isomers has been investigated. The C18-XB column was ultimately chosen based on good peak elution, acceptable runtime and the capability to run under UHPLC conditions. The C18-XB column separated isoGDGTs into two groups. The first group consisting of OH-GDGTs appears to contain admixtures of structural isomers of the "normal" isoGDGTs, which predominantly elute in group 2. Surprisingly, the crenarchaeol isomer used in the TEX_{86} proxy eluted at the end of the first group. BrGDGTs elute before the isoGDGTs, which makes the RP chromatography more time efficient for these compounds compared to the regularly used NP methods. Besides a swapped elution order based on mass (i.e., the compound with *m*/*z* 1050 elutes before the *m*/*z* 1036 compound and before the *m*/*z* 1022 compound) compared to NP chromatography (where compounds elute in the order *m*/*z* 1022, *m*/*z* 1036, *m*/*z* 1050), the RP method appears to separate the various structural isomers with different methyl-group positioning on the octacosanyl chains in the same way as NP (i.e., 5-methyl brGDGTs elute before 6-methyl brGDGTs). However, we did not manage to arrive at unequivocal evidence for the exact positioning of these isomers. Moreover, in some samples we found a larger variety of apparent isomers than observed in the regular analytical window of NP chromatography, while in others we found less. Comparison of a limited set of samples run both on the RP method using the C18-XB column, and the traditionally used NP method using a Cyano column, gave virtually the same BIT index values and highly similar TEX_{86} values. Besides being a possible alternative to the existing NP methods, the unusual isoprenoid and brGDGT isomer separation on the C18-XB column could aid further elucidation of the biological sources and environmental factors that play a role in the production of the different GDGT isomers.

DATA AVAILABILITY STATEMENT

The datasets generated for this study are available on request to the corresponding authors.

AUTHOR CONTRIBUTIONS

Both authors carried out analytical work and performed data analysis, interpretation, and manuscript writing.

FUNDING

The research was funded by a start-up grant from the Bolin Centre for Climate Research, Stockholm University (JR) and the Swedish Research Council grant 621-2011-4916 (RS). This article is published as a contribution to the proceedings of the Marine Organic Geochemistry Workshop held in April 2019 in Delmenhorst, funded by the Deutsche Forschungsgemeinschaft (DFG, German Research Foundation) project number 422798570. In addition, the Hanse-Wissenschaftskolleg and the Geochemical Society provided funding for the conference.

ACKNOWLEDGMENTS

We would like to thank Enrique Iñiguez, Kweku Yamoah, and Alan Wiech for laboratory assistance and data analysis. Francesco Muschitiello and Joanna Sawicka provided samples. Mandana Fasth and Sven Josefsson from Phenomenex Sweden provided advice on column selection and chromatography. Three reviewers greatly helped improve an earlier version of this manuscript.

SUPPLEMENTARY MATERIAL

The Supplementary Material for this article can be found online at: https://www.frontiersin.org/articles/10.3389/fmars.2020.539601/full#supplementary-material

REFERENCES

Becker, K. W., Lipp, J. S., Zhu, C., Liu, X. L., and Hinrichs, K. U. (2013). An improved method for the analysis of archaeal and bacterial ether core lipids. *Org. Geochem.* 61, 34–44. doi: 10.1016/j.orggeochem.2013.05.007

Birkholz, A., Smittenberg, R. H., Hajdas, I., Wacker, L., and Bernasconi, S. M. (2013). Isolation and compound specific radiocarbon dating of terrigenous branched glycerol dialkyl glycerol tetraethers (brGDGTs). *Org. Geochem.* 60, 9–19. doi: 10.1016/j.orggeochem.2013.04.008

Brochier-Armanet, C., Gribaldo, S., and Forterre, P. (2012). Spotlight on the Thaumarchaeota. *ISME J.* 6, 227–230. doi: 10.1038/ismej.2011.145

De Jonge, C., Hopmans, E. C., Stadnitskaia, A., Rijpstra, W. I. C., Hofland, R., Tegelaar, E., et al. (2013). Identification of novel penta- and hexamethylated branched glycerol dialkyl glycerol tetraethers in peat using HPLC-MS2, GC-MS and GC-SMB-MS. *Org. Geochem.* 54, 78–82. doi: 10.1016/j.orggeochem.2012.10.004

De Jonge, C., Hopmans, E. C., Zell, C. I., Kim, J. H., Schouten, S., and Sinninghe Damsté, J. S. (2014a). Occurrence and abundance of 6-methyl branched glycerol dialkyl glycerol tetraethers in soils: implications for palaeoclimate reconstruction. *Geochim. Cosmochim. Acta* 141, 97–112. doi: 10.1016/j.gca.2014.06.013

De Jonge, C., Stadnitskaia, A., Hopmans, E. C., Cherkashov, G., Fedotov, A., and Sinninghe Damsté, J. S. (2014b). In situ produced branched glycerol dialkyl glycerol tetraethers in suspended particulate matter from the Yenisei River, Eastern Siberia. *Geochim. Cosmochim. Acta* 125, 476–491. doi: 10.1016/j.gca.2013.10.031

de la Torre, J. R., Walker, C. B., Ingalls, A. E., Könneke, M., and Stahl, D. A. (2008). Cultivation of a thermophilic ammonia oxidizing archaeon synthesizing crenarchaeol. *Environ. Microbiol.* 10, 810–818. doi: 10.1111/j.1462-2920.2007.01506.x

Ding, S., Schwab, V. F., Ueberschaar, N., Roth, V.-N., Lange, M., Xu, Y., et al. (2016). Identification of novel 7-methyl and cyclopentanyl branched glycerol

dialkyl glycerol tetraethers in lake sediments. *Org. Geochem.* 102, 52–58. doi: 10.1016/j.orggeochem.2016.09.009

Elling, F. J., Könneke, M., Nicol, G. W., Stieglmeier, M., Bayer, B., Spieck, E., et al. (2017). Chemotaxonomic characterisation of the thaumarchaeal lipidome. *Environ. Microbiol.* 19, 2681–2700. doi: 10.1111/1462-2920.13759

Graeve, M., and Janssen, D. (2009). Improved separation and quantification of neutral and polar lipid classes by HPLC-ELSD using a monolithic silica phase: application to exceptional marine lipids. *J. Chromatogr. B Anal. Technol. Biomed. Life Sci.* 877, 1815–1819. doi: 10.1016/j.jchromb.2009.05.004

Hopmans, E. C., Schouten, S., and Sinninghe Damsté, J. S. (2016). The effect of improved chromatography on GDGT-based paleoproxies. *Org. Geochem.* 93, 1–6. doi: 10.1016/j.orggeochem.2015.12.006

Hopmans, E. C., Weijers, J. W. H., Schefuss, E., Herfort, L., Sinninghe Damsté, J. S., and Schouten, S. (2004). A novel proxy for terrestrial organic matter in sediments based on branched and isoprenoid tetraether lipids. *Earth Planet. Sci. Lett.* 224, 107–116. doi: 10.1016/j.epsl.2004.05.012

Huguet, A., Fosse, C., Laggoun-Defarge, F., Toussaint, M. L., and Derenne, S. (2010). Occurrence and distribution of glycerol dialkyl glycerol tetraethers in a French peat bog. *Org. Geochem.* 41, 559–572. doi: 10.1016/j.orggeochem.2010.02.015

Kim, J. H., Schouten, S., Hopmans, E. C., Donner, B., and Sinninghe Damsté, J. S. (2008). Global sediment core-top calibration of the TEX86 paleothermometer in the ocean. *Geochim. Cosmochim. Acta* 72, 1154–1173. doi: 10.1016/j.gca.2007.12.010

Knappy, C. S., Chong, J. P. J., and Keely, B. J. (2009). Rapid discrimination of archaeal tetraether lipid cores by liquid chromatography-tandem mass spectrometry. *J. Am. Soc. Mass Spectrom.* 20, 51–59. doi: 10.1016/j.jasms.2008.09.015

Könneke, M., Schubert, D. M., Brown, P. C., Hugler, M., Standfest, S., Schwander, T., et al. (2014). Ammonia-oxidizing archaea use the most energy-efficient aerobic pathway for CO2 fixation. *Proc. Natl. Acad.Sci. U.S.A.* 111, 8239–8244. doi: 10.1073/pnas.1402028111

Kuypers, M. M. M., Blokker, P., Erbacher, J., Kinkel, H., Pancost, R. D., Schouten, S., et al. (2001). Massive expansion of marine archaea during a mid-Cretaceous oceanic anoxic event. *Science* 293, 92–94. doi: 10.1126/science.1058424

Lanekoff, I., and Karlsson, R. (2010). Analysis of intact ladderane phospholipids, originating from viable anammox bacteria, using RP-LC-ESI-MS. *Anal. Bioanal. Chem.* 397, 3543–3551. doi: 10.1007/s00216-010-3913-3

Liu, X. L., Lipp, J. S., Birgel, D., Summons, R. E., and Hinrichs, K. U. (2018). Predominance of parallel glycerol arrangement in archaeal tetraethers from marine sediments: structural features revealed from degradation products. *Org. Geochem.* 115, 12–23. doi: 10.1016/j.orggeochem.2017.09.009

Liu, X. L., Lipp, J. S., Simpson, J. H., Lin, Y. S., Summons, R. E., and Hinrichs, K. U. (2012a). Mono- and dihydroxyl glycerol dibiphytanyl glycerol tetraethers in marine sediments: identification of both core and intact polar lipid forms. *Geochim. Cosmochim. Acta* 89, 102–115. doi: 10.1016/j.gca.2012.04.053

Liu, X. L., Russell, D. A., Bonfio, C., and Summons, R. E. (2019). Glycerol configurations of environmental GDGTs investigated using a selective sn2 ether cleavage protocol. *Org. Geochem.* 128, 57–62. doi: 10.1016/j.orggeochem.2018.12.003

Liu, X. L., Summons, R. E., and Hinrichs, K. U. (2012b). Extending the known range of glycerol ether lipids in the environment: structural assignments based on tandem mass spectral fragmentation patterns. *Rapid Commun. Mass Spectrom.* 26, 2295–2302. doi: 10.1002/rcm.6355

Liu, X. L., Torio, A. D., Bosak, T., and Summons, R. E. (2016). Novel archaeal tetraether lipids with a cyclohexyl ring identified in Fayetteville Green Lake, NY, and other sulfidic lacustrine settings. *Rapid Commun. Mass Spectrom.* 30, 1197–1205. doi: 10.1002/rcm.7549

Liu, X. L., Zhu, C., Wakeham, S. G., and Hinrichs, K. U. (2014). In situ production of branched glycerol dialkyl glycerol tetraethers in anoxic marine water columns. *Mar. Chem.* 166, 1–8. doi: 10.1016/j.marchem.2014.08.008

Naafs, B. D. A., Inglis, G. N., Zheng, Y., Amesbury, M. J., Biester, H., Bindler, R., et al. (2017). Introducing global peat-specific temperature and pH calibrations based on brGDGT bacterial lipids. *Geochim. Cosmochim. Acta* 208, 285–301. doi: 10.1016/j.gca.2017.01.038

Naafs, B. D. A., Mccormick, D., Inglis, G. N., Pancost, R. D., and Collaborators, T. G. P. D. (2018). Archaeal and bacterial H-GDGTs are abundant in peat and their relative abundance is positively correlated with temperature. *Geochim. Cosmochim. Acta* 227, 156–170. doi: 10.1016/j.gca.2018.02.025

Pancost, R. D., and Sinninghe Damste, J. S. (2003). Carbon isotopic compositions of prokaryotic lipids as tracers of carbon cycling in diverse settings. *Chem. Geol.* 195, 29–58. doi: 10.1016/s0009-2541(02)00387-x

Pearson, A., Huang, Z., Ingalls, A. E., Romanek, C. S., Wiegel, J., Freeman, K. H., et al. (2004). Nonmarine crenarchaeol in Nevada hot springs. *Appl. Environ. Microbiol.* 70, 5229–5237. doi: 10.1128/aem.70.9.5229-5237.2004

Robinson, S. A., Ruhl, M., Astley, D. L., Naafs, B. D. A., Farnsworth, A. J., Bown, P. R., et al. (2016). Early jurassic north Atlantic sea-surface temperatures from TEX86 palaeothermometry. *Sedimentology* 64:215. doi: 10.1111/sed.12321

Russell, J. M., Hopmans, E. C., Loomis, S. E., Liang, J., and Sinninghe Damsté, J. S. (2018). Distributions of 5-and 6-methyl branched glycerol dialkyl glycerol tetraethers (brGDGTs) in East African lake sediment: effects of temperature, pH, and new lacustrine paleotemperature calibrations. *Organ. Geochem.*117, 56–69. doi: 10.1016/j.orggeochem.2017.12.003

Schoon, P. L., De Kluijver, A., Middelburg, J. J., Downing, J. A., Sinninghe Damsté, J. S., and Schouten, S. (2013). Influence of lake water pH and alkalinity on the distribution of core and intact polar branched glycerol dialkyl glycerol tetraethers (GDGTs) in lakes. *Org. Geochem.* 60, 72–82. doi: 10.1016/j.orggeochem.2013.04.015

Schouten, S., Hopmans, E. C., Pancost, R. D., and Sinninghe Damsté, J. S. (2000). Widespread occurrence of structurally diverse tetraether membrane lipids: evidence for the ubiquitous presence of low-temperature relatives of hyperthermophiles. *Proc. Natl. Acad. Sci. U.S.A.* 97, 14421–14426. doi: 10.1073/pnas.97.26.14421

Schouten, S., Hopmans, E. C., Schefus, E., and Sinninghe Damsté, J. S. (2002). Distributional variations in marine crenarchaeotal membrane lipids: a new tool for reconstructing ancient sea water temperatures? *Earth Planet. Sci. Lett.* 204, 265–274. doi: 10.1016/s0012-821x(02)00979-2

Schouten, S., Van Der Meer, M. T. J., Hopmans, E. C., Rijpstra, W. I. C., Reysenbach, A. L., Ward, D. M., et al. (2007). Archaeal and bacterial glycerol dialkyl glycerol tetraether lipids in hot springs of yellowstone National Park. *Appl. Environ. Microbiol.* 73, 6181–6191. doi: 10.1128/aem.00630-07

Schouten, S., Hopmans, E. C., Rosell-Melé, A., Pearson, A., Adam, P., Bauersachs, T., et al. (2013a). An interlaboratory study of TEX86 and BIT analysis of sediments, extracts, and standard mixtures. *Geochem. Geophys. Geosyst.* 14, 5263–5285.

Schouten, S., Hopmans, E. C., and Sinninghe Damsté, J. S. (2013b). The organic geochemistry of glycerol dialkyl glycerol tetraether lipids: a review. *Org. Geochem.* 54, 19–61. doi: 10.1016/j.orggeochem.2012.09.006

Sinninghe Damsté, J. S., Rijpstra, W. I. C., Hopmans, E. C., Den Uijl, M. J., Weijers, J. W. H., and Schouten, S. (2018). The enigmatic structure of the crenarchaeol isomer. *Org. Geochem.* 124, 22–28. doi: 10.1016/j.orggeochem.2018.06.005

Tierney, J. E., Schouten, S., Pitcher, A., Hopmans, E. C., and Sinninghe Damsté, J. S. (2012). Core and intact polar glycerol dialkyl glycerol tetraethers (GDGTs) in Sand Pond, Warwick, Rhode Island (USA): insights into the origin of lacustrine GDGTs. *Geochim. Cosmochim. Acta* 77, 561–581. doi: 10.1016/j.gca.2011.10.018

Tolar, B. B., Ross, M. J., Wallsgrove, N. J., Liu, Q., Aluwihare, L. I., Popp, B. N., et al. (2016). Contribution of ammonia oxidation to chemoautotrophy in Antarctic coastal waters. *ISME J.* 10, 2605–2619. doi: 10.1038/ismej.2016.61

Wakeham, S. G., Lewis, C. M., Hopmans, E. C., Schouten, S., and Sinninghe Damsté, J. S. (2003). Archaea mediate anaerobic oxidation of methane in deep euxinic waters of the Black Sea. *Geochim. Cosmochim. Acta* 67, 1359–1374. doi: 10.1016/s0016-7037(02)01220-6

Weber, Y., De Jonge, C., Rijpstra, W. I. C., Hopmans, E. C., Stadnitskaia,. A., Schubert, C. J., et al. (2015). Identification and carbon isotope composition of a novel branched GDGT isomer in lake sediments: evidence for lacustrine branched GDGT production. *Geochim. Cosmochim. Acta* 154, 118–129 doi: 10.1016/j.gca.2015.01.032

Weijers, J. W. H., Panoto, E., Van Bleijswijk, J., Schouten, S., Rijpstra, W. I. C., Balk, M., et al. (2009). Constraints on the biological source(s) of the orphan branched tetraether membrane lipids. *Geomicrobiol. J.* 26, 402–414. doi: 10.1080/01490450902937293

Weijers, J. W. H., Schouten, S., Van Den Donker, J. C., Hopmans, E. C., and Sinninghe Damsté, J. S. (2007). Environmental controls on bacterial tetraether

membrane lipid distribution in soils. *Geochim. Cosmochim. Acta* 71, 703–713. doi: 10.1016/j.gca.2006.10.003

Weijers, J. W. H., Schouten, S., Van Der Linden, M., Van Geel, B., and Sinninghe Damsté, J. S. (2004). Water table related variations in the abundance of intact archaeal membrane lipids in a Swedish peat bog. *FEMS Microbiol. Lett.* 239, 51–56. doi: 10.1016/j.femsle.2004.08.012

Wörmer, L., Lipp, J. S., Schröder, J. M., and Hinrichs, K. U. (2013). Application of two new LC-ESI-MS methods for improved detection of intact polar lipids (IPLs) in environmental samples. *Organ. Geochem.* 59, 10–21. doi: 10.1016/j.orggeochem.2013.03.004

Zhang, C. L., Pearson, A., Li, Y. L., Mills, G., and Wiegel, J. (2006). Thermophilic temperature optimum for crenarchaeol synthesis and its implication for archaeal evolution. *Appl. Environ. Microbiol.* 72, 4419–4422. doi: 10.1128/aem.00191-06

Zhang, Y. G., Pagani, M., and Wang, Z. R. (2016). Ring Index: a new strategy to evaluate the integrity of TEX86 paleothermometry. *Paleoceanography* 31, 220–232. doi: 10.1002/2015pa002848

Zhang, Z. H., Smittenberg, R. H., and Bradley, R. S. (2016). GDGT distribution in a stratified lake and implications for the application of TEX86 in paleoenvironmental reconstructions. *Sci. Rep.* 6:10.

Zheng, Y. H., Li, Q. Y., Wang, Z. Z., Naafs, B. D. A., Yu, X. F., and Pancost, R. D. (2015). Peatland GDGT records of Holocene climatic and biogeochemical responses to the Asian Monsoon. *Org. Geochem.* 87, 86–95. doi: 10.1016/j.orggeochem.2015.07.012

Zhu, C., Lipp, J. S., Wörmer, L., Becker, K. W., Schröder, J., and Hinrichs, K. U. (2013). Comprehensive glycerol ether lipid fingerprints through a novel reversed phase liquid chromatography-mass spectrometry protocol. *Org. Geochem.* 65, 53–62. doi: 10.1016/j.orggeochem.2013.09.012

Zhu, C., Yoshinaga, M. Y., Peters, C. A., Liu, X. L., Elvert, M., and Hinrichs, K. U. (2014). Identification and significance of unsaturated archaeal tetraether lipids in marine sediments. *Rapid Commun. Mass Spectrom.* 28, 1144–1152. doi: 10.1002/rcm.6887

Conflict of Interest: The authors declare that the research was conducted in the absence of any commercial or financial relationships that could be construed as a potential conflict of interest.

frontiers in Marine Science

ORIGINAL RESEARCH
published: 22 September 2020
doi: 10.3389/fmars.2020.540643

Size-Fractionated Contribution of Microbial Biomass to Suspended Organic Matter in the Eastern Tropical South Pacific Oxygen Minimum Zone

Sebastian I. Cantarero[1], Carlos Henríquez-Castillo[2,3], Nadia Dildar[1], Cristian A. Vargas[4,5], Peter von Dassow[4,6], Marcela Cornejo-D'Ottone[4,7] and Julio Sepúlveda[1,4]**

[1] Department of Geological Sciences and Institute of Arctic and Alpine Research, University of Colorado Boulder, Boulder, CO, United States, [2] Laboratorio de Fisiología y Genética Marina (FIGEMA), Centro de Estudios Avanzados de Zonas Áridas (CEAZA), Coquimbo, Chile, [3] Facultad de Ciencias del Mar, Universidad Católica del Norte, Coquimbo, Chile, [4] Millenium Institute of Oceanography, Universidad de Concepción, Concepción, Chile, [5] Coastal Ecosystems and Global Environmental Change Lab, Department of Aquatic Systems, Centre for Environmental Sciences EULA-Chile, Universidad de Concepción, Concepción, Chile, [6] Department of Ecology, Pontificia Universidad Católica de Chile, Santiago, Chile, [7] Escuela de Ciencias del Mar, Pontificia Universidad Católica de Valparaíso, Valparaíso, Chile

OPEN ACCESS

Edited by:
Kai-Uwe Hinrichs,
University of Bremen, Germany

Reviewed by:
Yantao Liang,
Ocean University of China, China
Thomas Evans,
Massachusetts Institute of Technology, United States

***Correspondence:**
Sebastian I. Cantarero
sebastian.cantarero@colorado.edu
Julio Sepúlveda
jsepulveda@colorado.edu

Specialty section:
This article was submitted to Marine Biogeochemistry, a section of the journal Frontiers in Marine Science

Received: 05 March 2020
Accepted: 17 August 2020
Published: 22 September 2020

Citation:
Cantarero SI, Henríquez-Castillo C, Dildar N, Vargas CA, von Dassow P, Cornejo-D'Ottone M and Sepúlveda J (2020) Size-Fractionated Contribution of Microbial Biomass to Suspended Organic Matter in the Eastern Tropical South Pacific Oxygen Minimum Zone. Front. Mar. Sci. 7:540643. doi: 10.3389/fmars.2020.540643

Cell membrane intact polar lipids (IPLs) are chemotaxonomic biomarkers whose abundances and distributions in water column environments reflect the living biomass of *in situ* microbial communities, and can be used to determine the relative contribution of distinct functional and phylogenetic groups to water column carbon stocks. The diversity of IPLs in marine environments is, however, vast, while our knowledge of their biological origins remains limited. Here, we study the distribution of IPLs in size-fractionated suspended organic matter from the oxygen minimum zone (OMZ) of the eastern tropical South Pacific (ETSP) off northern Chile. Canonical correspondence analyses of total IPL abundances and water column physiochemistry demonstrate distinct distributions of microbial sources associated with different geochemical regions in the water column (chlorophyll maximum, upper chemocline, lower chemocline, upper OMZ, core OMZ, and mesopelagic region). Furthermore, the distribution of IPLs in free-living (0.3–2.7 μm) and particle-attached (2.7–53 μm) suspended organic matter differs, suggesting distinct biological sources in each size fraction. While some parallels exist, the diversity and distribution of IPLs in the OMZ system of the ETSP off northern Chile exhibited some unique features compared to other OMZ systems; for instance, we observed a significantly lower contribution of betaine lipids from phytoplanktonic sources, possibly reflecting a physiological response to severe N-limitation in this area. The overall IPL abundance in the two size fractions also indicates a dominance of free-living biomass in the OMZ and mesopelagic regions, suggesting that these areas of the water column could provide additional sources of submicrometer-sized organic

carbon to deeper waters. This study improves the utility of IPLs as chemotaxonomic biomarkers by providing insight into the contrasting distributions of microbial biomass from different life modes (free-living and particle-attached). Our results suggest that microbial production in low oxygen environments may be more important to total water column carbon stocks than previously thought.

Keywords: intact polar lipids, oxygen minimum zone, marine biogeochemistry, biomarker, microbial biomass

INTRODUCTION

Lipids are a class of organic molecules ubiquitous to all forms of known life. The great chemical diversity of cell membrane intact polar lipids (IPLs) provides some phylogenetic specificity, which has been exploited in the mapping of planktonic and microbial communities in marine environments (Wakeham et al., 2007; Popendorf et al., 2011; Brandsma et al., 2012; Rush et al., 2012; Sollai et al., 2015). Given the susceptibility of their polar head groups to hydrolysis after cell death (White et al., 1979; Harvey et al., 1986; Petersen et al., 1991), the abundance of environmental IPLs is commonly interpreted to represent the occurrence of living cells, and is thus used to determine the *in situ* abundances of different metabolic and biosynthetic pathways (e.g., Schubotz et al., 2009; Van Mooy and Fredricks, 2010; Wakeham et al., 2012; Schubotz et al., 2018). While the stability of polar head groups has been questioned in sediments (Schouten et al., 2010; Logemann et al., 2011), the short residence time of particles in water column samples (Moran and Buesseler, 1992) allows the use of IPLs to study microbial abundances and contribution to carbon stocks in suspended particles.

Marine planktonic IPLs are mostly comprised of several distinct classes of amino/betaine, glycol, and phospholipids that are predominantly produced by algae, a combination of cyanobacteria/algae, and bacteria, respectively (Goldfine, 1984; Dembitsky, 1996; Harwood, 1998; Wada and Murata, 1998; Suzumura, 2005). Additionally, the predominance of polyunsaturated fatty acids in eukaryotic cells (Volkman et al., 1989), the preferential synthesis of odd-chain fatty acids in bacterial membranes (Schubotz et al., 2009; Van Mooy and Fredricks, 2010), the presence of isoprenoidal lipids in archaea (Pearson and Ingalls, 2013), as well as the differing stereochemistry of ether and ester linkages between bacterial and archaeal lipids (Weijers et al., 2006; Valentine, 2007), are used to assess distinct biological sources in the environment. Furthermore, empirical relationships between water column chemistry, cell sorting techniques, and IPL concentrations have served useful to determine potential biological sources (Van Mooy and Fredricks, 2010; Wakeham et al., 2012; Schubotz et al., 2018). Other specific IPLs in marine environments include archaeal glyco- and phospho- glycerol dialkyl glycerol tetraethers (GDGTs; Pitcher et al., 2011; Elling et al., 2014; Sollai et al., 2015) as well as anammox bacteria ladderane phospholipids (Sinninghe Damsté et al., 2005; Boumann et al., 2006; Rush et al., 2012).

Microbial activity has significant global effects on the biogeochemical structure of the water column (Arrigo, 2005; Falkowski et al., 2008), particularly via the extensive remineralization of organic matter and the transfer of carbon between the surface and subsurface ocean (termed the "microbial loop" by Pomeroy, 1974; Azam et al., 1983; Azam, 1998). The microbial loop also controls the cycling of nitrogen (Herbert, 1999; Jetten, 2008; Lam and Kuypers, 2011; Thamdrup, 2012), phosphorus (Dyhrman et al., 2007), and sulfur (Sievert et al., 2007; Canfield et al., 2010). Oxygen minimum zones (OMZs) are hot spots of marine microbial diversity (Ulloa et al., 2012; Wright et al., 2012) containing chemoautotrophic processes that can have a significant contribution to carbon fluxes (see Taylor et al., 2001; Lengger et al., 2020). The adsorption of fine organic particles onto ballasted minerals, or the formation of aggregates (marine snow) greatly increases their sinking rates through the water column (Passow and De La Rocha, 2006; De La Rocha et al., 2008; Wilson et al., 2012) thus providing a mechanism for the export of submicron organics to the deep sea. Indeed, previous biomarker work suggests that a significant proportion of exported particulate organic matter (POM) to the mesopelagic region in oligotrophic waters may be from a submicron component (Close et al., 2013). However, POM has historically been collected using 0.7 μm filters, which may not capture all average-sized bacterial cells (0.2–0.6 μm; Pomeroy et al., 2007), and thus underestimate the contribution of microbial organic matter. Lipidomic and metagenomic studies in these systems indicate that the composition and abundance of microbial biomass differs between micron-scale (typically > 1–3 μm) and submicron-scale (ranging from 0.2 to 0.7 μm) POM fractions (Close et al., 2014; Ganesh et al., 2014, 2015; Duret et al., 2015; Matys et al., 2017). Thus, the interpretation of individual IPL sources, and their use to reconstruct microbial distributions in the environment, may be complicated either by the occurrence of distinct metabolic niches in large vs. submicron POM, by multiple biological sources for common compounds, or by the potentially rapid export of particles via ballasting.

The eastern tropical South Pacific (ETSP) harbors one of the largest volumes of hypoxic waters in the world (Helly and Levin, 2004; Paulmier and Ruiz-Pino, 2009). The subsurface waters along the Humboldt Current off northern Chile and Perú are characterized by reduced circulation and ventilation (Czeschel et al., 2011; Thamdrup et al., 2012; Karstensen and Ulloa, 2019) as well as intense aerobic decomposition of detrital organic matter (Pantoja et al., 2004; Canfield et al., 2010) fueled by the upwelling of nutrient-rich water masses and high productivity in surface waters (Daneri et al., 2000). These processes lead to the occurrence of a marked OMZ (<20 μM) between ∼50–100 and 300–400 m (De Pol-Holz et al., 2009; Fuenzalida et al., 2009; Ulloa and Pantoja, 2009) that is functionally anoxic (Thamdrup et al., 2012; Ulloa et al., 2012). The exact depth and structure of the oxycline is determined by a combination of O_2 production via

photosynthesis, stratification and depth of the wind mixed layer, and aerobic respiration rates, in addition to mesoscale physical processes such as eddies that can also replenish the subsurface with O_2 (Ulloa et al., 2012).

Here, we study the differences in distribution and abundance of IPLs in size-fractionated suspended organic matter, a "particle-attached" fraction (2.7–53 μm) and a "free-living" fraction (0.3–2.7 μm), through waters of the OMZ in the ETSP off the coast of northern Chile. While these size fractions may include some overlap between bacterial cells (typically < 1 μm; see Ducklow, 2001; Pomeroy et al., 2007) attached to larger organic substrates, or eukaryotic picoplankton cells contributing to the free-living fraction (~2 μm; see Finkel et al., 2010), this investigation is meant to broadly define differences in the IPL composition between both planktonic life modes. We aim to demonstrate the utility of size-fractionated IPLs distributions in POM to improve the characterization of *in situ* microbial planktonic community composition across strong geochemical gradients, in addition to better quantify their potential contribution to water column carbon stocks. Additionally, we present an exhaustive catalog of predominantly bacterial and eukaryotic IPLs that expands the ever growing database of microbial signatures in marine OMZs.

MATERIALS AND METHODS

Sampling and Physicochemical Water Analyses

Samples of suspended organic matter were collected from two stations off the coast of Iquique, northern Chile (~20°S; **Figure 1**) during the LowpHOX-2 Cruise (February 4–6, 2018) aboard the AGS-61 *Cabo de Hornos*. Samples were collected from a depth profile along a more nearshore station (T3, ~30 km from the coast) where the OMZ exhibited a shallow oxycline (~15–55 m), denoted henceforth as "nearshore station," in addition to a second station further offshore (T5, ~80 km from the coast) with a slightly deeper oxycline (~25–60 m), denoted henceforth as "offshore station." Physicochemical profiles were measured using a Seabird SBE-911 CTD system, equipped with an SBE 43 oxygen sensor and fluorometer, in addition to 24 10-L General Oceanics Niskin Bottles. Chlorophyll *a* concentration was estimated fluorometrically as described by Parsons et al. (1984) and dissolved inorganic N (nitrite, NO_2^- and nitrate, NO_3^-) and phosphate (PO_4^{3-}) were analyzed using protocols established by Grasshoff et al. (2009). Temperature, salinity, oxygen, and fluorescence sensors were calibrated before the cruise by Seabird Scientific®, WA, United States (2nd half of 2017). Onboard, all sensors were carefully maintained after each cast to avoid salt accumulation. Oxygen and fluorescence data were checked and corrected with *in situ* values analyzed through Winkler titration method (Carpenter, 1965) and fluorometric analyses, respectively at standard depths (2, 10, 25, 50, 100, and 250 m). We collected an entire rosette cast (200 L) for IPL analysis at six discrete depths: chlorophyll maximum (~10 m), upper chemocline (~25 m), lower chemocline (~45 m), upper OMZ (~60 m), core OMZ (~250 m), and mesopelagic zone (~750 m). Sea water was transferred to a large, high-density polyethylene drum and then filtered through pre-combusted, 142 mm Sterlitech (D1420) and Advantec glass fiber filters (GF75142MM) of 2.7 and 0.3 μm pore sizes, respectively. Water samples were prefiltered through a 53 μm mesh to remove large organisms. Here, we refer to the 2.7–53 μm size fraction as "particle-attached," and to the 0.3–2.7 μm size fraction as "free-living" microbes, although we recognize that some overlap between both fractions is likely. All samples were wrapped in combusted aluminum foil and shipped frozen to the Organic Geochemistry Laboratory at the University of Colorado, Boulder for IPL extraction and analysis. Additional water column filtrates (1–2 L) were collected for particulate organic carbon (POC) and particulate organic nitrogen (PON) using pre-combusted 25 mm diameter glass fiber filters with a 0.7 μm pore size. The same water was subsequently filtered through 25 mm diameter glass fiber filters with a 0.2 μm pore size for dissolved organic carbon (DOC).

Lipid Extraction and Analysis

Intact polar lipids were extracted from glass fiber filters via a modified version (Wörmer et al., 2013) of the original Bligh and Dyer Extraction method (Bligh and Dyer, 1959). Samples were extracted by ultrasonication a total of five times with three different extraction mixtures. Two extractions were performed using Dichloromethane/Methanol/Phosphate $buffer_{(aq)}$ [1:2:0.8, v:v:v], with the Phosphate buffer adjusted

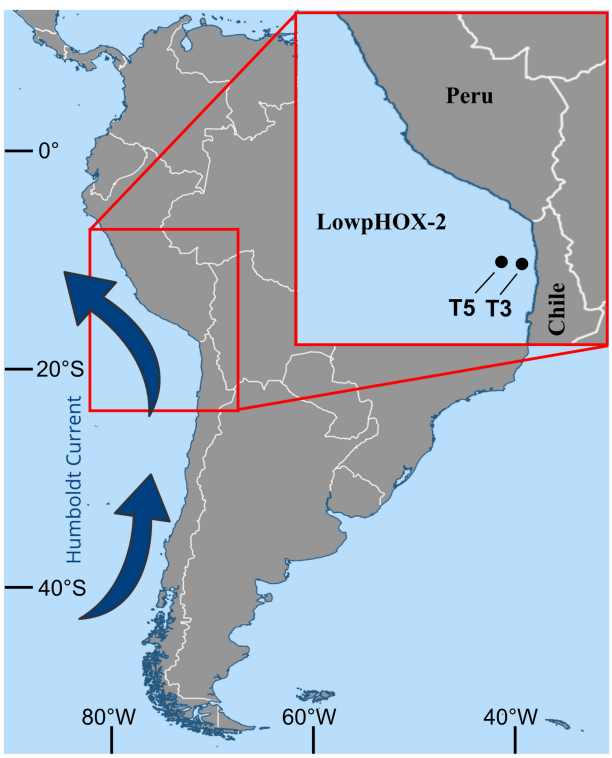

FIGURE 1 | Study area marking the location of Stations T3 (nearshore) and T5 (offshore) along the Humboldt Current in the ETSP off northern Chile.

to a pH of ∼7.4. Two extractions were subsequently prepared with Dichloromethane/Methanol/Trichloroacetic acid buffer$_{(aq)}$ [1:2:0.8, v:v:v] with the 5% Trichloroacetic acid buffer at a final pH of ∼2. A final extraction was prepared with Dichloromethane/Methanol [1:5, v:v]. We added 2 μg of C_{16}PAF (see **Supplementary Table 1**) to each extraction as internal standard. Following extraction, samples were concentrated under a gentle flow of N_2 using a Turbovap, re-dissolved in 9:1 Dichloromethane:Methanol, (v/v), sonicated, vortexed, and then filtered using a 0.45 μm polytetrafluoroethylene (PTFE) syringe filter. Before analysis, an aliquot representative of ∼1% of the total lipid extract (TLE) was transferred into a 2 mL vial with an insert, and re-dissolved in 100 μl of 9:1 Dichloromethane:Methanol, (v/v). The coupled identification and quantification of IPLs was achieved using a Thermo Scientific Ultimate 3000 High Performance Liquid Chromatography interphase to a Q Exactive Focus Orbitrap-Quadrupole High Resolution Mass Spectrometer (HPLC-HRMS) via electrospray ionization (ESI) in positive mode. We used the chromatographic conditions described by Wörmer et al. (2013); i.e., an Acquity BEH Amide 1.7 μm, 2.1 by 150 mm column, flow rate of 0.4 mL/min with two mobile phases. Mobile phase A consisted of Acetonitrile:Dichloromethane [75:25, v:v] with 0.01% formic acid and 0.01% NH_4OH; Mobile phase B consisted of Methanol:H_2O [50:50, v:v] with 0.4% formic acid and 0.4% NH_4OH. Mobile phases were proportioned under the following gradients: 0 min: 1% B, 2.5 min: 1% B, 4 min: 5%, 22.5 min: 25% B, 26.5 min: 40% B, 27.5 min: 40% B. Column temperature was kept at 40°C and samples were injected in Dichloromethane:Methanol [9:1, v:v]. Electrospray ionization settings were optimized for maximum intensity across all measured IPL classes under the following conditions: auxiliary gas heater temperature 425°C, capillary temperature 265°C, spray voltage 3.50 kV, sheath gas flow 35 arbitrary units (AU), aux gas flow 13 AU, S-lens RF level 55.0 AU. The instrument was constantly calibrated for mass resolution and accuracy using the Pierce™ LTQ Velos ESI Positive Ion Calibration Solution (88323). Samples were analyzed in full scan mode to obtain an untargeted screening (or lipidomic profile) of each sample, in addition to targeted MS/MS mode for compound identification via diagnostic fragmentation patterns (Sturt et al., 2004; Schubotz et al., 2009; Wakeham et al., 2012). IPLs were identified by their exact masses, polar head groups, the number of carbon atoms and unsaturation in the core structure, and their retention times. While other studies have analyzed IPLs under both positive and negative ionization modes to determine the fatty acid composition in the core lipid structures, we took advantage of the high resolution of our mass spectrometer to focus on the diversity of head group combinations with total carbon atoms and unsaturation only.

Quantification of IPLs was achieved with a combination of an internal standard (C_{16}PAF, Avanti Lipids) and external calibration standards consisting of 17 different IPL classes (16 IPL-Mix, Avanti Lipids, and Matreya LLC main phospholipid of Thermoplasma acidophilum; see **Supplementary Table 1**). The intensity of each individual IPL identified in the HPLC-ESI-HRMS analysis was calibrated to a linear regression between peak areas and known concentrations of the same lipid class (or the most similar molecular structure) across a 5-point dilution series (0.001–2.5 ng/μl). Samples were also spiked with known concentrations of deuterated IPL standards (Avanti Lipids: d7-PC, d7-PE, d7-PG, and d9-DGTS) to correct for possible sample matrix effects on ionization efficiency, and to check for consistency in retention times.

POC, DOC, and PON Analyses

Filters were dried overnight at 60°C and split for duplicate analyses and packed into tin boats. Total particulate organic carbon and nitrogen was measured using a Thermo Scientific Elemental Analyzer – Isotope Ratio Mass Spectrometer at the CU Boulder Earth Systems Stable Isotope Lab. Purified acetanilide standards were measured for external calibration and drift corrections with a carbon and nitrogen analytical precision between 1.1–2.2% and 0.6–2.2%, respectively, across all analysis runs. Dissolved organic carbon was performed using a modified OI Analytical model 1030 wet TOC analyzer (analytical precision of 1.8%), with a model 1088 autosampler at the Ján Veizer Stable Isotope Laboratory at the University of Ottawa.

DIC, pH_T, and pCO_2

Samples for total alkalinity (A_T) were poisoned with 50 μL of saturated $HgCl_2$ solution and A_T was determined using the open-cell titration method (Dickson et al., 2003) with an automatic Alkalinity Tritrator (Model AS-ALK2 Apollo SciTech). All samples were analyzed at 25°C (±0.1°C) with temperature regulation using a water-bath. DIC samples were collected in 250 mL Wheaton® glass bottles and preserved with 50 μL saturated $HgCl_2$ solution. Samples were acidified with 10% phosphoric acid and the evolved CO_2 measured with a LICOR 6262 non-dispersive infrared gas analyzer. Analytical accuracy was controlled against a certified reference material (CRM, supplied by Andrew Dickson, Scripps Institution of Oceanography, San Diego, CA, United States; Batch #166) and the A_T repeatability averaged 2–3 μmol kg^{-1}. Temperature, salinity, A_T and DIC data were used to calculate pH_T (total scale), aqueous carbon dioxide (CO_2-aq), and partial pressure (pCO_2). Analyses were performed using CO_2SYS software for MS Excel (Pierrot et al., 2006) set with Mehrbach solubility constants (Mehrbach et al., 1973) refitted by Dickson and Millero (1987), the $KHSO_4$ equilibrium constant determined by Dickson (1990) was used for all calculations.

Lipid Diversity and Canonical Correspondence Analysis

Lipid richness through the water column was estimated using the Shannon index based on equal completeness, as described in Chao et al. (2012) using the iNEXT package v2.0.19 in R environment. A canonical correspondence analysis (CCA) was carried out to elucidate the relationships between IPLs distribution and physicochemical conditions (O_2, DOC, DIC, pCO_2, pH, NO_3^-, NO_2^-, PO_4^{3-}, Chl-a). Triplots include sites, response variables (IPL concentrations) and explanatory variables (environmental data). The site scores are weighted sums of IPLs. The distribution of individual compounds within a

given IPL class was also explored via CCAs combining intra-class abundances and water column physiochemistry.

RESULTS

Physicochemical Characterization of the Water Column and IPL Concentrations

Oxygen levels varied from 6 ml/L at the surface to below detection limit (∼0.012 mL/L) in the OMZ (**Figure 2A**). A shallow oxycline (15–50 m) was evident in the nearshore station, while a slightly deeper oxycline (25–60 m) was observed in the offshore station. The functionally anoxic OMZ impinged the euphotic zone and reached a depth of at least 250 m in both stations. Below this depth, waters remained < 0.3 mL/L O_2 until at least 500 m. Chlorophyll concentration varied between 3.12 and 3.85 mg/m^3 in the chlorophyll maximum at ∼10 and 25 m in the nearshore and offshore stations, respectively, and quickly dropped to <0.5 mg/m^3 by a depth of 50 m (**Figure 2A**).

The vertical distribution of nutrient species showed minimum concentrations of NO_3^- (0–0.65 μmol/L), NO_2^- (∼0 μmol/L), and PO_4^{3-} (∼1.0 μmol/L) in the surface and along the chlorophyll maximum (**Figure 2B**). The concentration of these nutrients increased significantly through the oxycline, with PO_4^{3-} maintaining elevated concentrations through the anoxic core and into the mesopelagic region (∼3 μmol/L). NO_3^- increased to 15–20 μmol/L in the oxycline, with a secondary local minimum in the anoxic core (10–15 μmol/L), and maximum concentrations of >35 μmol/L in the mesopelagic region. NO_2^- remained depleted until OMZ waters, reaching maximum concentrations of (5–6 μmol/L) in the anoxic core, and then returning to nearly absent levels in the mesopelagic region. A summary of the water column chemistry data incorporated into statistical analyses is shown in **Supplementary Table 2**.

POC and PON showed maximum concentrations (340–500 μg/L and 68–80 μg/L, respectively) around the chlorophyll maximum (∼10–25 m; **Figure 2C**). The concentrations decreased rapidly through the chemocline and reached minimum values of ∼30 μg/L POC and 2.5-4 μg/L PON in the mesopelagic region. The C/N ratio varied from ∼5 to 7 in the upper 50 m of the water column and increased with depth to maximum values ∼7.5 to 12 between 100 and 750 m (**Figure 2D**).

Total IPL concentrations (normalized by liter of filtered seawater) showed an exponential decay with depth, with maximum values in surface waters (∼4,800–7,100 ng/L) and minimum values in the mesopelagic region (∼140–180 ng/L; **Figure 2E**). The concentration of IPLs normalized by POC (μg IPL/μg POC) showed maximum values in the chemocline (>0.02 μg IPL/μg POC), while the upper and core OMZ exhibited values that are comparable and even larger than those in the chlorophyll maximum (**Figure 2F**). The mesopelagic region, on the other hand, showed the lowest contribution of IPLs to the POC pool (<0.01 μg IPL/μg POC). The relative abundance of IPLs in the free-living fraction relative to the particle-attached fraction ([free-living IPLs]/[total IPLs]) showed generally lower values in the surface ocean (10–25% of total IPLs), and it broadly increased with depth through the OMZ and showed greatest values in the mesopelagic region (∼90% of total IPLs; **Figure 2G**). We also observed spatial variability in free-living fractional abundances among the two stations (**Figure 2G**), with the most contrasting trends observed in the chlorophyll maximum and along the chemocline. Finally, the lipid richness as calculated by the Shannon index indicated greatest IPLs diversity in the surface and secondary maxima in the OMZ (see **Supplementary Table 3**).

CCAs of IPL Class Distribution

The distribution of total IPLs as categorized by polar head group classes remained largely consistent between both stations within individual size fractions aside from some variability within the relative abundances of glycolipid classes in the photic zone (**Figure 3**). The triplot for the CCA showed a spatial structuring in the diversity and distribution of IPLs in response to the environmental constraints (**Figure 4**), with well-defined

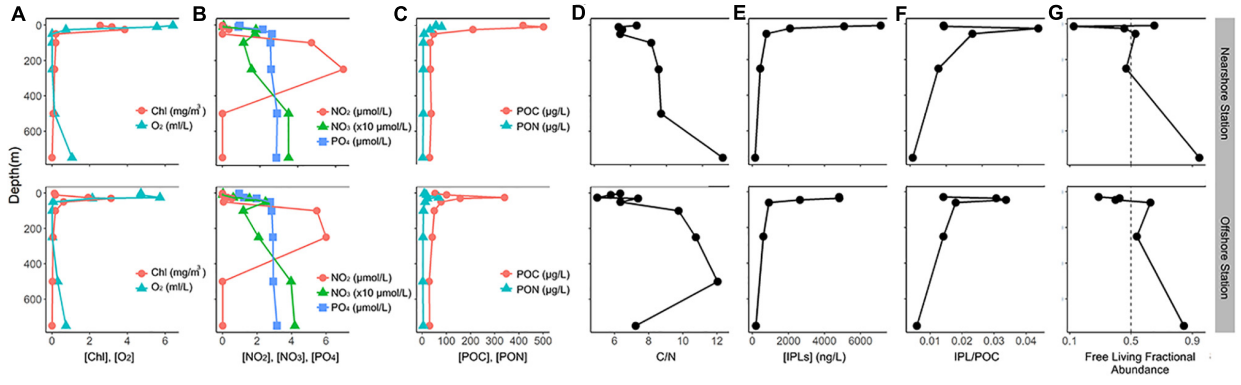

FIGURE 2 | Physicochemical characterization of the water column during the LowpHOX-2 cruise at stations T3 and T5. **(A)** chlorophyll (mg/m^3) and O_2 (mL/L) concentrations; **(B)** nitrate (x10μmol/L), nitrite (μmol/L), and phosphorous (μmol/L)concentrations; **(C)** particulate organic carbon and nitrogen concentrations (μg/L); **(D)** carbon/nitrogen ratios; **(E)** total IPL concentrations; **(F)** POC-normalized IPL concentration (μg/μg); **(G)** relative abundance of free-living IPLs, expressed as [free-living IPLs]/[total IPLs].

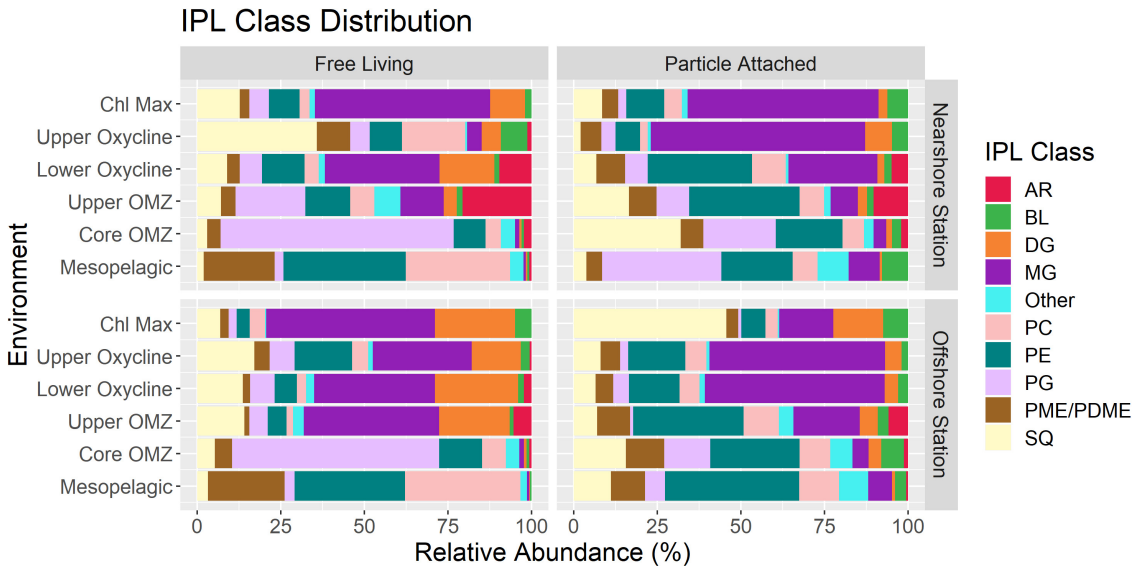

FIGURE 3 | Relative abundance of individual IPL classes in each size fraction and sampling station.

IPL groupings by geochemical regions (**Figures 4**, **5**). This includes (a) a prevalence of glycolipids and betaine lipids with high chlorophyll, pCO_2, and oxygen in surface waters, (b) a predominance of phospholipids associated with high DOC, NO_3^- and PO_4^{3-} in subsurface waters below the chlorophyll maximum, and (c) a predominance of archaeal lipids clustered closely to high NO_2^- concentrations in the lower oxycline and oxygen minimum zone.

Glycolipid Distribution

Particle-associated IPLs in both sites showed significant abundances of glycolipids SQDG (*Sulfoquinovosyldiacylglycerol)* and MGDG (*Monogalactosyldiacylglycerol*) at all depths (∼25–75%; **Figure 3**), with generally higher glycolipid contributions (MG, DG; *Diglycosyldiacylglycerol*, SQ) in the surface and oxycline than at depth. Free-living IPLs showed an even more pronounced dominance of glycolipids (MG, SQ, DG) in the chlorophyll maximum and oxycline (∼70%) and were drastically reduced in the core OMZ and mesopelagic regions (<5%; **Figure 3**).

A total of 20 unique MGDG molecules were detected in the ETSP, which showed greatest relative abundance in the chlorophyll maximum (up to 60% of the total IPL yield) and oxycline in both size fractions. While the particle-attached fraction was comprised of up to 15% MGDGs in the mesopelagic, MGDGs were nearly absent in the free-living fraction from both the core OMZ and mesopelagic regions. One of the most abundant MGDGs (30:1; up to 40% of the total IPL yield, see **Figures 6A,B**) in the particle-attached fraction clusters closely with chlorophyll concentrations, as do most MGDGs (**Figure 7B**). However, in the free-living fraction the clustering of this same molecule (as well as the majority of MGDGs) occurred along high NO_2^- and pCO_2 (**Figure 7A**).

A total of 20 DGDGs in the ETSP contribute up to 25% of the IPL yield, largely confined to the photic zone in both size fractions, and with the greatest contribution found in the free-living fraction of the offshore station (**Figure 3**). The most abundant molecule amongst in the photic zone (DGDG-30:0; **Figures 6A,B**) is closely correlated to chlorophyll and O_2 concentrations amongst free-living IPLs (**Figure 7C**), but in the particle-attached fraction it is associated with high pCO_2 and moderate PO_4^{3-} and NO_2^- concentrations (**Figure 7D**). The core OMZ and mesopelagic region exhibited a low contribution of DGDGs (<2% of total IPLs).

A total of 17 SQDGs were detected in the ETSP, and their relative abundance to the total IPL pool was highly variable (**Figure 3**). The free-living fraction is consistent between stations, with maximum contributions (15–30%) found in the chlorophyll maximum and the upper oxycline. The particle-attached fraction shows more variability between stations. SQDGs make up 55% of the total IPL pool in the offshore station chlorophyll maximum and 40% of the total IPL pool in the nearshore station core OMZ. The 2 most abundant SQDGs in the free-living fraction (28:0 and 30:0; **Figures 6A,B**) are associated with both high chlorophyll and NO_2^- concentrations, but have a negative correlation to chlorophyll in the particle-attached fraction (**Figures 7E,F**). The distribution of SQDGs in both fractions showed an increase in the contribution of SQDG-29:0 at depth (see **Supplementary Figure 1C**) and a strong correlation with NO_2^- (**Figures 7E,F**).

Phospholipid Distribution

Phospholipids (PG; *Phosphatidylglycerol*, PE; *Phosphatidylethanolamine*, PC; *Phosphatidylcholine*, PME/PDME; *Phosphatidyl(di)methylethanolamine*) were prevalent throughout the water column and increased from <10% in surface waters to 75 and 95% of the total IPL pool in the core OMZ and mesopelagic region, respectively.

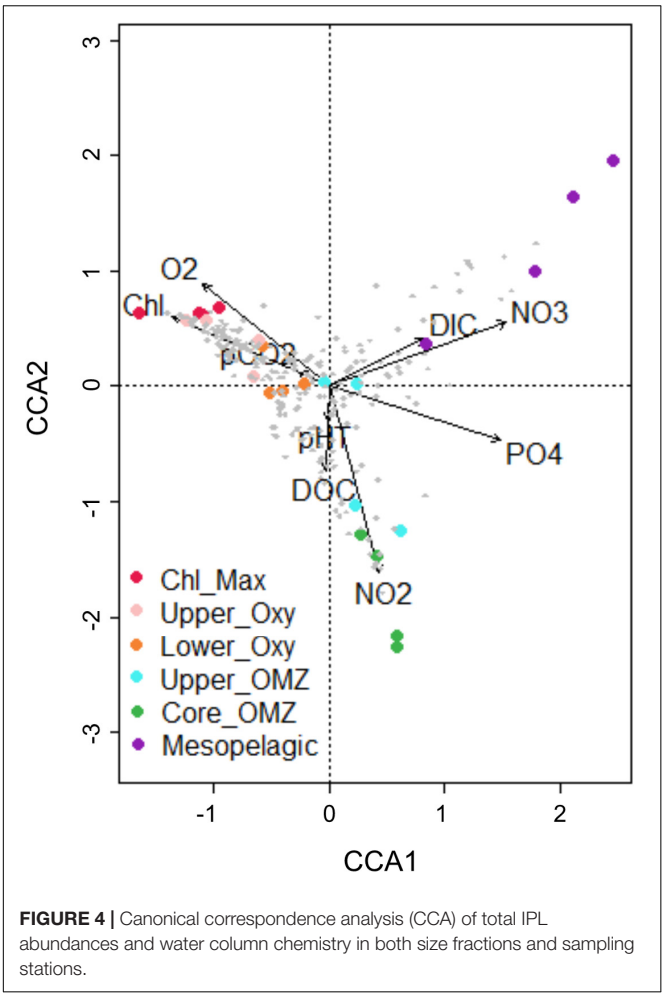

FIGURE 4 | Canonical correspondence analysis (CCA) of total IPL abundances and water column chemistry in both size fractions and sampling stations.

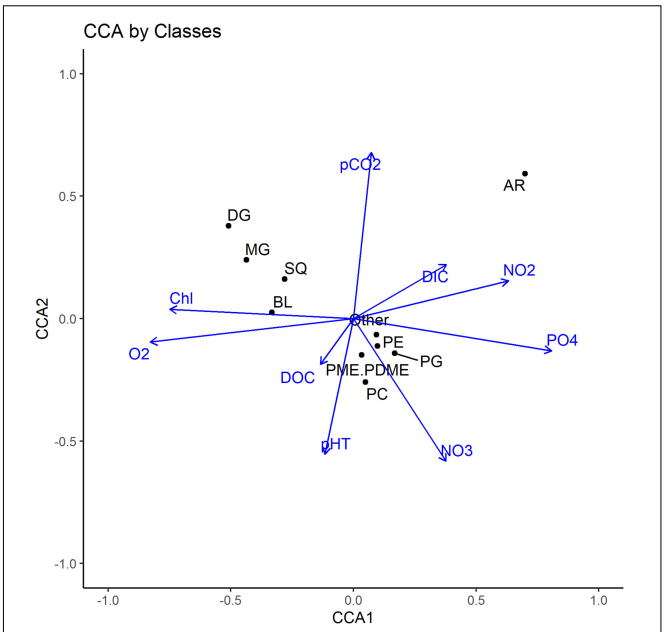

FIGURE 5 | Canonical correspondence analysis (CCA) of total IPL abundances (summed by class) and water column chemistry in both size fractions and sampling stations.

PGs were amongst the least diverse IPL class in the ETSP (13 compounds) molecules detected. Their contribution to the total free-living IPL pool ranged from <5% in the chlorophyll maximum to 60–70% in core OMZ waters and <5% in the mesopelagic region (**Figure 3**). Similarly, the particle-attached fraction demonstrated a significant relative contribution of PGs in the OMZ (∼15–25%) and mesopelagic (5–10%) waters. In addition, of the most abundant PGs in either fraction (i.e., 32:0, 33:1, and 34:3; **Figures 6A,B**) only 32:0 in the free-living fraction showed a strong association with chlorophyll in the surface (**Figures 8A,B**).

A high diversity of PEs were detected in the ETSP (24 compounds; see **Supplementary Figure 2**). PEs made up a small proportion of the total IPL pool in both fractions in the chlorophyll maximum and upper oxycline (5–10%; **Figure 3**), however their relative abundance increased in the oxycline and below, reaching maximum values in OMZ waters (15–25%; **Figure 3**). Notably, the most abundant PEs (31:0 and 33:0; **Figures 6A,B**) in the photic zone were nearly absent in the free-living fraction in the core OMZ (see **Supplementary Figure 2C**) but remained a major contributor in the particle-attached fraction.

The distribution of PCs in the ETSP was highly variable with a <5% contribution to total IPL yields in the chlorophyll maximum, yet ∼40 and 15% in the free-living and particle-attached fractions (respectively) within the mesopelagic region (**Figure 3**). However, the diversity of this lipid class (38 compounds) was high across all depths (**Supplementary Figure 2A**). In the chlorophyll maximum and upper oxycline, the relative abundance of PCs were dominated by PC-30:0, which clustered between O_2 and NO_3^- in a CCA of the free-living fraction (**Figure 8E**), yet it correlated closely with O_2 and chlorophyll in the particle-attached fraction (**Figure 8F**). Most particle-attached PCs correlated to high chlorophyll, or moderate concentrations of both NO_2^- and chlorophyll, while the free-living PCs were largely associated with high NO_2^- concentrations.

PMEs/PDMEs in the ETSP typically contributed less than 10% of the total IPL pool from the photic zone through the core OMZ, with maximum contributions in the free-living fraction of the mesopelagic region (∼20%). The distribution of the 17 molecules detected was largely the same in the particle-attached fraction, but showed variability with depth in the free-living fraction (**Supplementary Figure 3A**). The fractional abundances of PME/PDME indicated a dominance of particle-attached molecules for the entire water column, except in the mesopelagic region (**Supplementary Figures 4, 5**).

Betaine Lipid Distribution

Betaine lipids (BLs) DGTA, DGTS, and DGCC remained minor contributors to the total IPL pool at all depths and fraction sizes (<10%; **Figure 3**), but were amongst the most diverse IPL classes

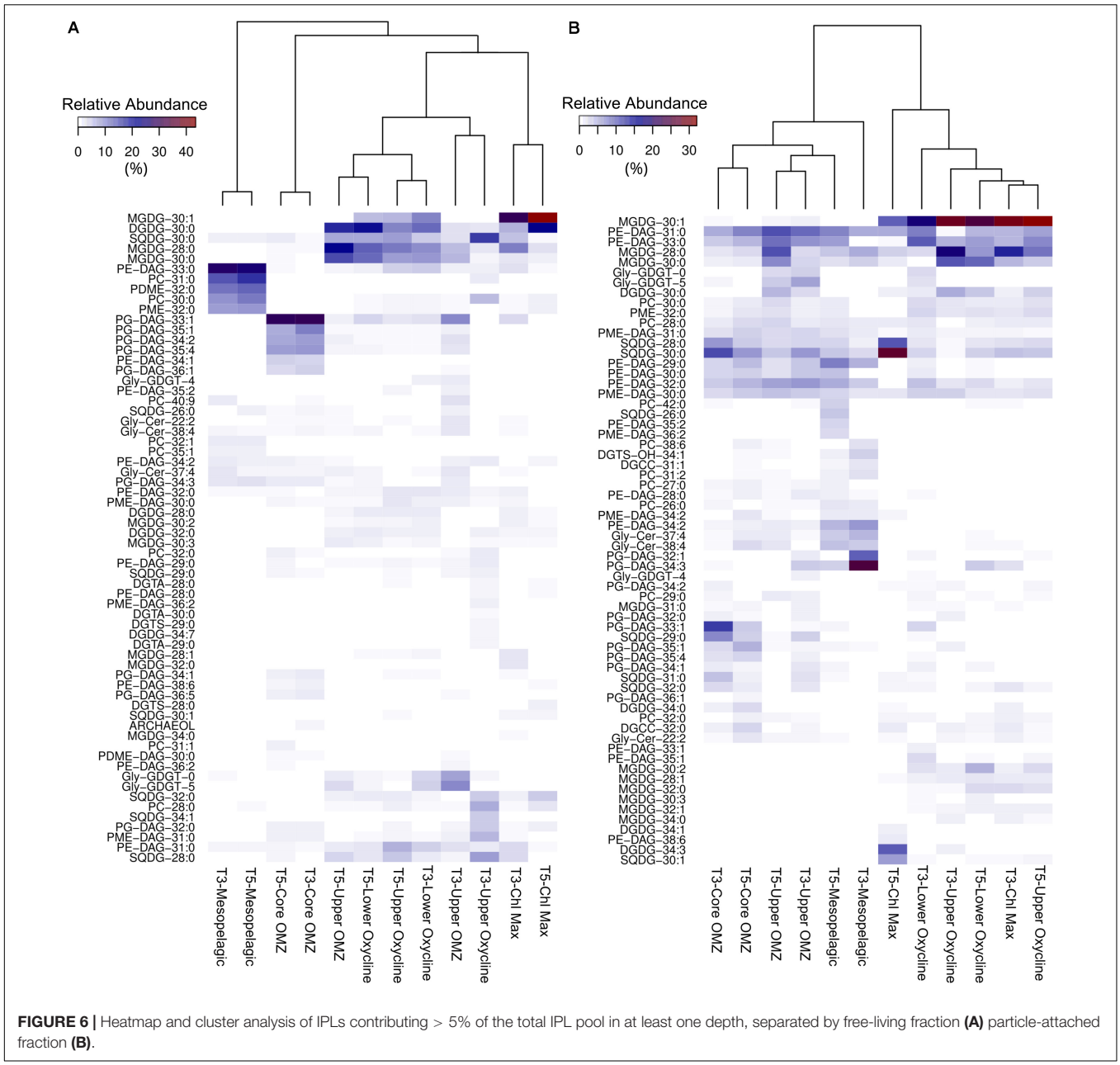

FIGURE 6 | Heatmap and cluster analysis of IPLs contributing > 5% of the total IPL pool in at least one depth, separated by free-living fraction **(A)** particle-attached fraction **(B)**.

in the ETSP, with 23, 42, and 20 unique compounds, respectively (**Supplementary Figures 6A–C**). Generally, BLs were associated with relatively high chlorophyll and O_2 concentrations (**Figure 5**) and were more abundant in the particle-attached fraction, except in the upper and core OMZ (see **Supplementary Figures 4, 5**).

Archaeal and Other Lipids

Archaeal lipids (AR) contributed less than 5–15% of the total IPL yield in the free-living fraction of the lower oxycline and upper OMZ (**Figure 3**). The most abundant intact gly-GDGTs (glycerol dialkyl glycerol tetraethers) were detected in nearly all depths amongst the free-living fraction (gly-GDGT-0 and gly-GDGT-5 – also known as gly-crenarchaeol), but only between the lower oxycline and upper OMZ in the particle-attached fraction (see **Supplementary Figure 3B**). Ornithine lipids and sphingosine lipids (grouped as "Other"), remained minor contributors to the total IPL pool at all depths (<5%; **Figure 3**).

DISCUSSION

Water Column Environment and IPL Abundances

The upper 25 m of the water column in both stations is characterized by high chlorophyll, POC and PON, but low nutrient concentrations (**Figure 2**), as commonly seen in the

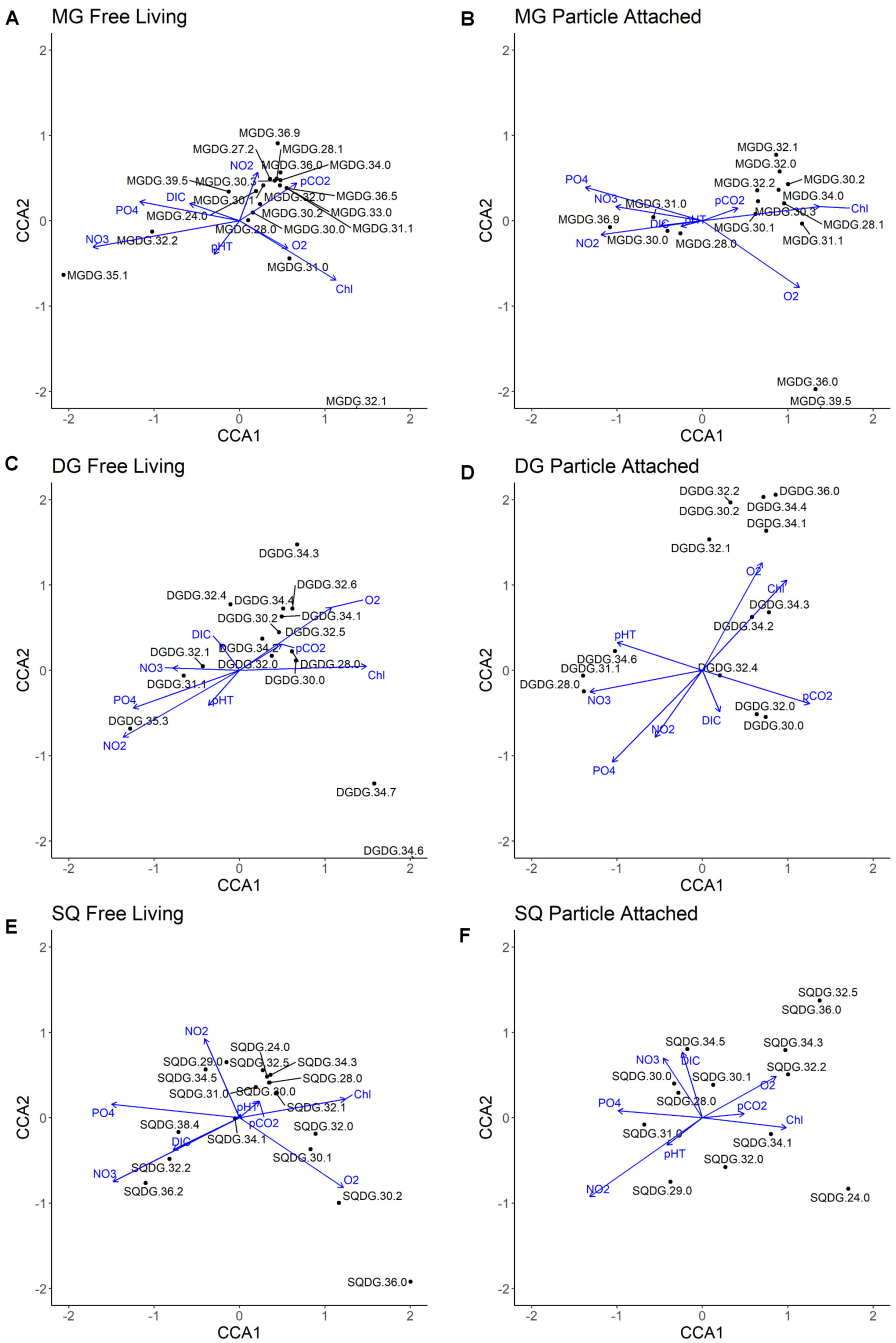

FIGURE 7 | Canonical correspondence analysis (CCA) of all molecular abundances within individual glycolipid classes and water column physiochemistry. Black dots indicate individual compounds, blue lines indicate physiochemical variables included in CCA. **(A)** MG Free Living fraction; **(B)** MG Particle Attached fraction; **(C)** DG Free Living fraction; **(D)** DG Particle Attached fraction; **(E)** SQ Free Living fraction; **(F)** SQ Particle Attached fraction.

highly productive surface waters of the ETSP (Molina et al., 2007; Galán et al., 2009; Molina and Farías, 2009; Ulloa et al., 2012). At these depths, total IPL yields are also at their highest, indicative of high phytoplanktonic biomass supplying the oxycline with organic substrates. Through the oxycline, PO_4^{3-} concentrations dramatically increase, reflecting high organic matter remineralization that quickly depletes the oxygen supply within 50–60 m from the surface. NO_3^- concentration increases in the oxycline as well, due to a high supply of remineralized NH_4^+ that fuels nitrification in the lower oxycline, particularly by archaea (Molina et al., 2010; Stewart et al., 2012), also coinciding with maximal archaeal IPL yields (**Figure 3**). The OMZ is characterized by a secondary minimum of NO_3^- as a result of denitrification; a sharp increase in NO_2^- is characteristic for the

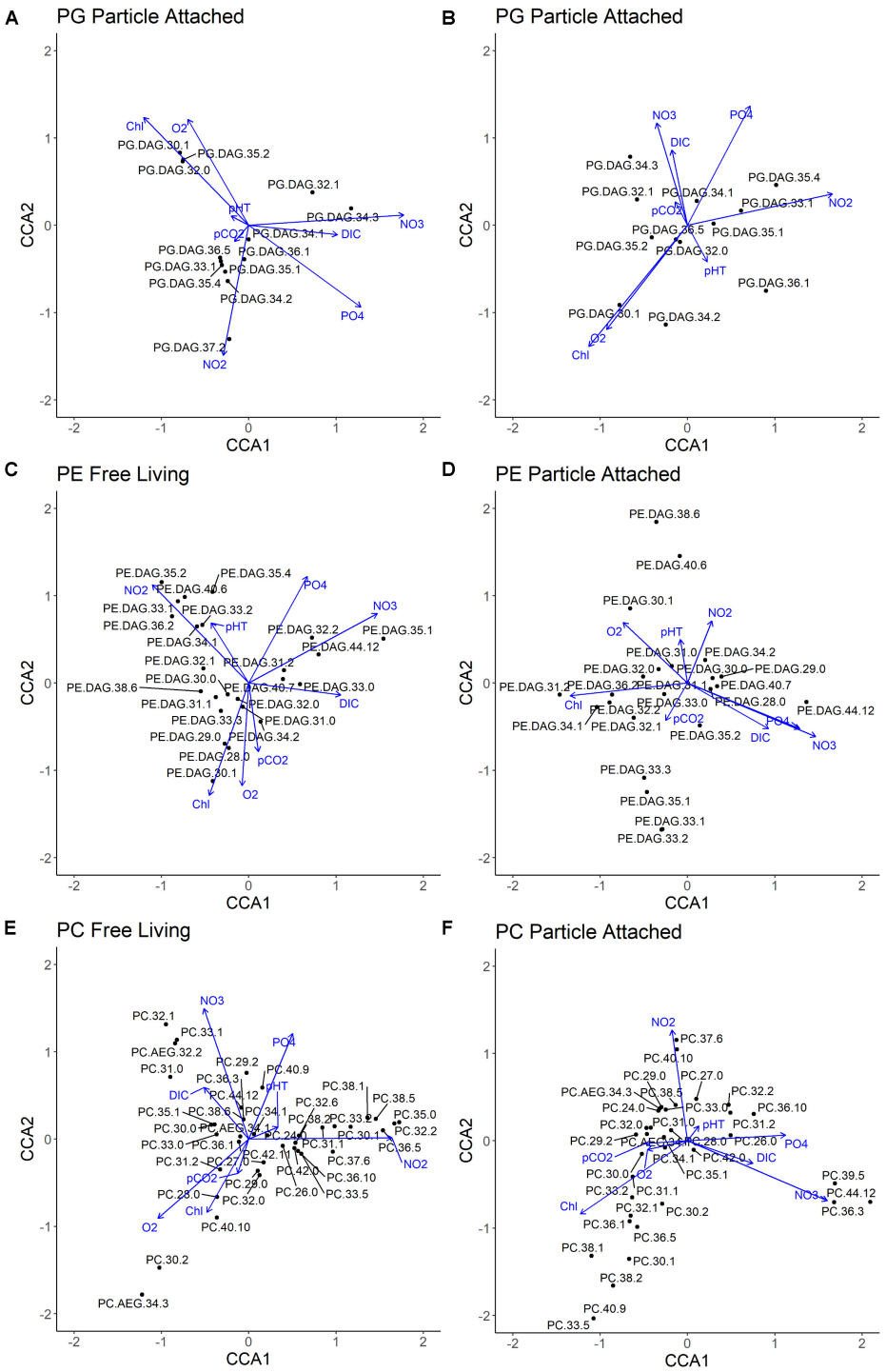

FIGURE 8 | Canonical correspondence analysis (CCA) of all molecular abundances within individual phospholipid class and water column physiochemistry. Black dots indicate individual compounds, blue lines indicate physiochemical variables included in CCA. **(A)** PG Free Living fraction; **(B)** PG Particle Attached fraction; **(C)** PE Free Living fraction; **(D)** PE Particle Attached fraction; **(E)** PC Free Living fraction; **(F)** PC Particle Attached fraction.

region resulting from nitrate reduction and as an intermediate of denitrification (Ulloa et al., 2012). Active expression of sulfur oxidizing/reducing bacteria have also been observed in the core OMZ (Walsh et al., 2009; Canfield et al., 2010; Ulloa et al., 2012). Anammox bacteria are also active in this region (Galán et al., 2009; Dalsgaard et al., 2012; Stewart et al., 2012) and may contribute significantly to total nitrogen loss (Kuypers et al., 2006; Thamdrup et al., 2006; Lam and Kuypers, 2011) in the form of N_2.

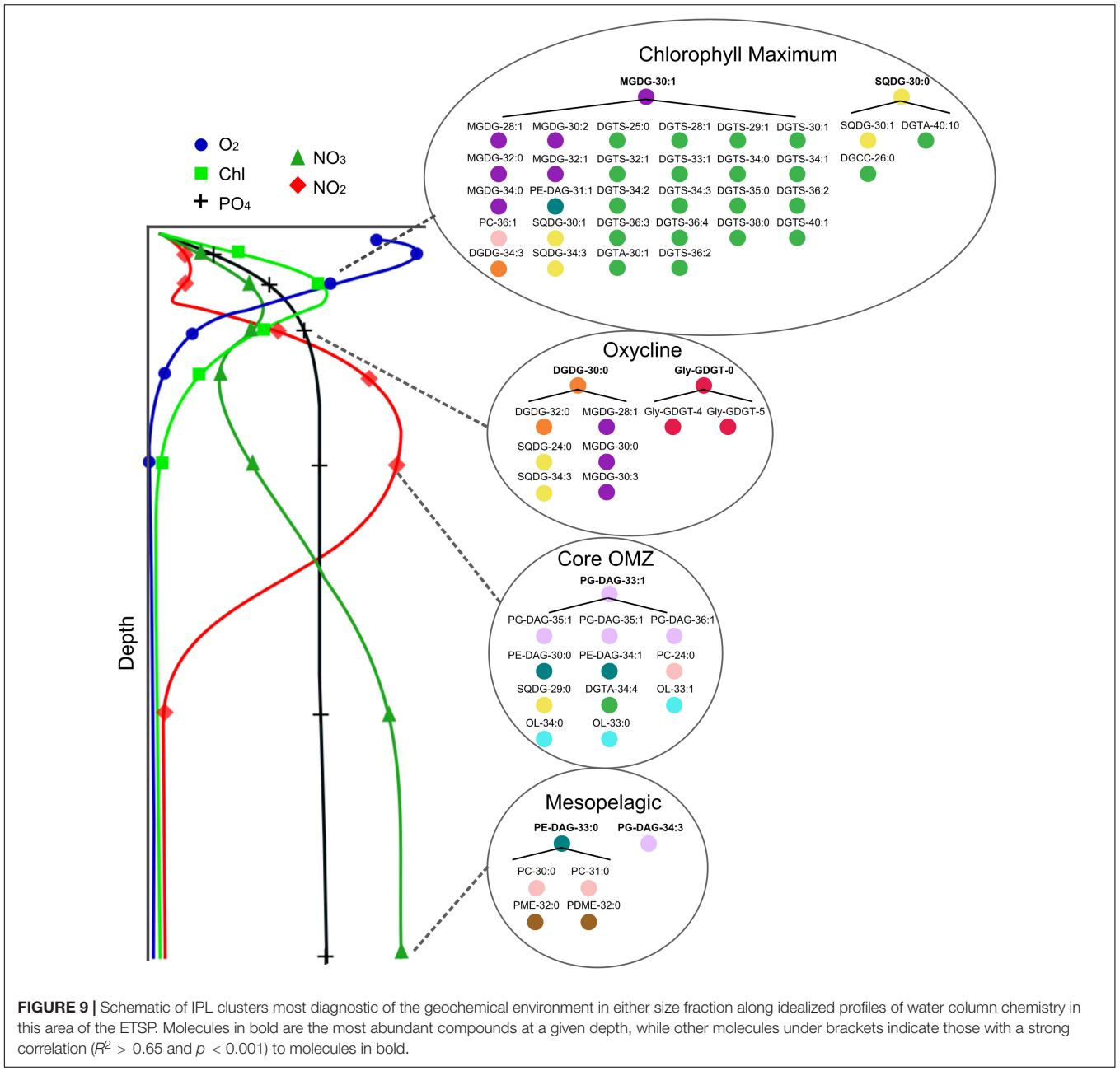

FIGURE 9 | Schematic of IPL clusters most diagnostic of the geochemical environment in either size fraction along idealized profiles of water column chemistry in this area of the ETSP. Molecules in bold are the most abundant compounds at a given depth, while other molecules under brackets indicate those with a strong correlation ($R^2 > 0.65$ and $p < 0.001$) to molecules in bold.

Thus, we expect IPLs along the chemocline to be reflective of a mixture of photoautotrophs, aerobic heterotrophs, and nitrifying microbes, while IPLs in the oxygen minimum zone are likely produced by nitrate reducers, denitrifiers, anaerobic ammonia oxidizers (anammox), and potentially sulfur oxidizing/reducing bacteria, among others.

Potential Sources of IPLs

MGDG (Monoglycosyldiacylglycerol)

MGDGs are the dominant constituents of chloroplast thylakoid membranes in both eukaryotic and bacterial photoautotrophs (Harwood, 1998; Wada and Murata, 1998). Indeed, in surface waters of other oxygen-depleted systems these lipids have been attributed to prochlorophytes as well as to algal sources (Van Mooy and Fredricks, 2010; Schubotz et al., 2018). Surface production in the ETSP is thought to be dominated principally by diatoms, although with a significant contribution of chlorophytes, and an increasing contribution of the cyanobacteria with depth (Franz et al., 2012).

High abundances of diatoms in this region (Franz et al., 2012) suggest that particle-attached MGDGs associated with high chlorophyll concentration (**Figure 7B**) are derived from predominantly algal sources. An especially high ratio of particle-attached to the free-living MGDGs

(see **Supplementary Figures 4C, 5C**) in the near-surface samples also supports their predominantly algal origins. Their molecular structure differs, however, from the typical polyunsaturated fatty acids observed in the IPLs of eukaryotic phytoplankton (Van Mooy and Fredricks, 2010; Schubotz et al., 2018). Instead, many are comprised of monounsaturated and saturated fatty acids (the most abundant being MGDG-30:1), which are typically more common in cyanobacteria (Harwood, 1998; Wada and Murata, 1998). The same highly abundant molecule (MGDG-30:1) in the free-living fraction clusters toward moderate pCO_2 and NO_2^- and provides evidence for a distinct bacterial source for the same molecule in the photic zone, possibly attributable to high cell counts of *Prochlorococcus* in subsurface waters (Lavin et al., 2010; Garcia-Robledo et al., 2017; Aldunate et al., 2020).

Contrary to the typical designation of MGDGs to photoautotrophic sources, Popendorf et al. (2011) demonstrated a substantial component of heterotrophic bacteria in the synthesis of MGDG membranes in regrowth incubations. Glycolipids are also known to be synthesized by aerobic/anaerobic gram-positive bacteria (Hölzl and Dörmann, 2007). In the ETSP, CCA clustering demonstrates that most MGDGs in the free-living fraction are associated with high NO_2^- and pCO_2 (**Figure 7A**), likely representing suboxic heterotrophic sources, as MGDGs are nearly absent in the core OMZ. Molecules that are weakly loaded on either CCA axis (e.g., MGDG-28:0), yet with increasing relative abundance at depth, may be indicative of more ubiquitous bacterial sources found across the oxycline.

DGDG (Diglycosyldiacylglycerol)

DGDGs are a significant IPL class amongst both eukaryotic and bacterial photoautotrophs (Wada and Murata, 1998; Kalisch et al., 2016). Molecules closely correlated to high chlorophyll and O_2 concentrations amongst free-living DGDGs (**Figures 7C,D**) suggest predominantly cyanobacterial origins. Most particle-attached DGDGs also demonstrate a similar correlation and are likely reflective of algal biomass. However, the most abundant DGDG (30:0) lacks correlation to chlorophyll and O_2, possibly as a result of vertical export from surface to subsurface waters, or due to a heterotrophic source relying on particle-attached organic substrates persisting through suboxic to anoxic (upper OMZ) waters.

Other DGDGs are unique to OMZ (i.e., 35:3 and 32:0) and mesopelagic (i.e., 32:4 and 31:1) waters (**Supplementary Figure 1B**), and potentially indicate previously unrecognized bacterial sources. A number of bacteria have demonstrated capability of producing DGDGs, such as lactic acid bacteria (Calvano et al., 2011), *Bacillus* and *Staphylococcus* gram positive bacteria (Shaw, 1974; Hölzl and Dörmann, 2007), and heterotrophic actinobacteria/proteobacteria (Yao et al., 2016). Relative abundances of 16s rRNA gene clone sequences indicate a prevalence of proteobacteria and the appearance of actinobacteria in the core OMZ of the ESTP (Stevens and Ulloa, 2008). Notably, the fractional abundance of free-living DGDGs is considerably higher at almost all depths (**Supplementary Figures 4C, 5C**) further supporting their potential synthesis from non-algal sources.

As observed in other glycolipids, the canonical photoautotrophic membrane IPLs detected in the ETSP are dominated by fatty acids most common to cyanobacteria (Volkman et al., 1989; Siegenthaler, 1998; Wada and Murata, 1998). Other water column environments have shown a greater proportion of polyunsaturated lipids in the photic zone such as in the eastern subtropical Pacific (Van Mooy and Fredricks, 2010), the eastern tropical north Pacific (Schubotz et al., 2018), the Black Sea (Schubotz et al., 2009), and the Cariaco Basin (Wakeham et al., 2012). However, Breteler et al. (2005) observed significant shifts toward saturated fatty acids in diatoms as the result of nutrient limitation (both N and P). The N:P ratios are low in the chlorophyll maximum and upper oxycline (<16; **Supplementary Table 2**), potentially indicating an impact of N-limitation/stress on the synthesis of glycolipid fatty acids (including both MGDGs and DGDGs).

SQDG (Sulfoquinovosyldiacylglycerol)

SQDGs, a common glycolipid class in the surface ocean, are found in thylakoid/chloroplast membranes (Siegenthaler, 1998; Wada and Murata, 1998) and are generally thought to reflect the presence of photoautotrophs in the water column (Van Mooy et al., 2006; Popendorf et al., 2011). These lipids constitute a significant proportion of cyanobacterial, diatom, brown and green algal chloroplast membranes (Harwood, 1998). However, in the ETSP, the relative contribution of SQDGs in the photic zone is larger in the free-living fraction than the particle-attached fraction (see **Supplementary Figures 4C, 5C**), suggesting a likely higher contribution of cyanobacteria than algae to this pool of IPLs.

CCA analyses in the free-living fraction are consistent with abundant SQDG molecules attributed to cyanobacteria (**Figure 7E**); however, many of these same molecules have a negative correlation to chlorophyll in the particle-attached fraction (**Figure 7F**). Furthermore, SQDG molecules in the core OMZ and mesopelagic region are largely dominated by the same molecules as the surface. Export of surface-derived photoautotrophic membranes may explain this distribution and a negative correlation to chlorophyll concentration. The negative correlation to chlorophyll may also be explained by the contribution of low-light adapted *Prochlorococcus* in the chemocline and upper OMZ of the ETSP where chlorophyll concentrations drop rapidly (Garcia-Robledo et al., 2017; Aldunate et al., 2020).

SQDGs associated with high NO_2^- or NO_3^- concentrations potentially suggest previously undescribed non-photoautotrophic sources in marine settings. Indeed, the genes involved in lipid biosynthesis discovered in *Rhodobacter* (*Rba.*) *sphaeroides* and other proteobacteria include the *sqd* gene for the synthesis of SQDGs (Tamot and Benning, 2009). The strong correlation of SQDG-29:0 for instance, with NO_2^- in both size fractions (**Figures 7E,F**) suggests no strong preference for a free-living or particle-associated life modes. In addition, some SQDGs are unique to the mesopelagic region, which indicates that their distribution is related to the distinct geochemical environment and not simply a result of particle export from waters above.

PG (Phosphatidylglycerol)

PGs are phospholipids with highly diverse biological origins, including nitrifying (Goldfine and Hagen, 1968), green sulfur (Barridge and Shively, 1968; Imhoff, 1995), *Pelagibacter ubique* type Proteobacteria (Van Mooy et al., 2009), sulfate reducing bacteria (Rütters et al., 2001), and methanotrophic bacteria (Makula, 1978; Fang et al., 2000). PGs are also an essential component of thylakoid membranes in both algal and bacterial photoautotrophs (Gombos et al., 2002; Sato et al., 2000). The CCA clustering in both size fractions suggest that few PGs are likely derived from photoautotrophs in the ETSP. These are limited to PG-30:1, 32:0, and 35:2 in the free-living fraction and PG-30:1, 34:2, and potentially 36:1 in the particle-attached. A predominantly non-algal source is also supported by a higher fractional abundance of PGs in the free-living fraction (see **Supplementary Figures 4C, 5C**).

PG relative abundances broadly increase with depth and have been mostly attributed to bacterial sources in similar environments influenced by the presence of an OMZ (Van Mooy and Fredricks, 2010; Schubotz et al., 2018). Most PGs are associated with higher NO_2^- and pCO_2 concentrations in the free-living fraction (**Figure 8A**), suggesting a core OMZ origin. However, the distribution of PG-34:2, 36:1, and 36:5 in the particle-attached fraction all cluster along distinct geochemical environments than in the free-living fraction (**Figures 8A,B**). This size partitioning may be related to a tendency for anaerobic heterotrophs to rely on organic substrates supplied via particle export (Karl et al., 1984; Arístegui et al., 2009), while autotrophic bacteria capable of fixing inorganic carbon may be more common in a free-living life mode. The 16S transcript abundances encoding enzymes for key denitrification steps have been measured to be 28-fold higher in particle-associated fractions, while anammox transcript abundances indicate a 15-fold enrichment in free-living fractions (Ganesh et al., 2015). While bacteriohopanepolyols (BHPs) associated with anammox bacteria in this OMZ system have been shown to be slightly more abundant in the particle-associated fraction, they are thought to be produced in the free-living fraction and accumulated in the larger fraction via the process of particle aggregation (Matys et al., 2017). Thus, non-ladderane phospholipids produced by anammox bacteria (Rattray et al., 2009) are a possible origin of free-living PGs in the OMZ. Indeed, the relative contribution of PGs are highest in the core OMZ (**Figure 3**), where expression of anammox transcripts are highest (Galán et al., 2009; Ulloa et al., 2012). PG-34:1 is also present at most depths and both size fractions (see **Supplementary Figure 2B**), and shows little correlation to any highly distinct geochemical environment (**Figures 8A,B**). This result suggests broadly ubiquitous origins, such as the ubiquitous heterotrophic *Pelagibacter ubique* (part of the SAR11 clade), shown to exclusively synthesize PG and PE membrane lipids (Van Mooy et al., 2009).

PE (Phosphatidylethanolamine)

PEs are commonly found in bacterial membranes from organisms with diverse metabolisms that include: nitrifying/denitrifying bacteria (Goldfine and Hagen, 1968), methanotrophic (Makula, 1978; Fang et al., 2000), sulfur oxidizing (Barridge and Shively, 1968; Imhoff, 1995), and SO_4 reducing bacteria (Rütters et al., 2001; Sturt et al., 2004). They have been largely attributed to heterotrophic bacteria in similar environments (Van Mooy and Fredricks, 2010; Schubotz et al., 2018). They can be a minor component of algal membranes as well (Dembitsky, 1996).

The most abundant PEs in both size fractions (e.g., PE-31:0, 33:0) lack strong correlations to chlorophyll and O_2 (**Figures 8C,D**), indicating minimal photoautotrophic sources in the photic zone. We interpret the occurrence of PEs in the chlorophyll maximum and oxycline as largely derived from ubiquitous aerobic heterotrophs. This is supported by their predominantly monounsaturated and saturated core structures more commonly found in bacterial fatty acids (Harwood, 1998; Wada and Murata, 1998), a lack of strong correlation to physiochemical environment, and their high abundance in *Pelagibacter ubique* (Van Mooy et al., 2009).

PE-32:2, PE-35:1, and PE-44:12 are associated with high NO_3^- concentrations in the free-living fraction (**Figure 8C**), while constrained to the lower oxycline and mesopelagic (**Supplementary Figure 2C**), suggesting nitrifying bacterial sources. This observation is supported by a prevalence of nitrifiers in free-living life modes in this area (Ganesh et al., 2014, 2015).

PEs that are positively correlated with NO_2^- concentrations (33:1, 33:2, 34:1, 35:4, 35:2, and 36:2; **Figure 8C**) have many potential sources in the highly diverse core OMZ including denitrifying, nitrate reducing, or sulfur cycling bacteria (Canfield et al., 2010; Ulloa et al., 2012). Non-ladderane PEs are also produced by anammox bacteria (Rattray et al., 2009), and may be contributing to these free-living IPLs unique to the core OMZ. These multiple biological sources are also reflected in the considerably diverse distribution of PEs found in the core OMZ (**Supplementary Figure 2C**).

Some clarity in the potential sources of these core OMZ PEs may be illuminated by differences in their physicochemical correlations in the two size fractions. For instance, several of the free-living PEs (33:1, 33:2, and 35:2) in high NO_2^- environments are negatively correlated to NO_2^- in the particle-attached fraction (**Figure 8D**). These differences could be an indication of largely heterotrophic bacteria relying on organic substrates in the particle-attached fraction, and a prevalence of autotrophic bacteria in the free-living fraction capable of fixing dissolved inorganic carbon. These observations demonstrate the importance of size-fractionated analyses to differentiate between microbial sources of different life modes.

PC (Phosphatidylcholine)

In marine settings, PCs are predominantly attributed to eukaryotic sources (Van Mooy et al., 2006; Van Mooy and Fredricks, 2010), or heterotrophic bacteria (Popendorf et al., 2011). Photoheterotrophic bacteria have also been shown to produce PCs (Van Mooy et al., 2006); however, since ornithine lipids, a common membrane lipid of photoheterotrophs (Benning, 1998), were hardly detected in our samples, such a source is rather unlikely.

The correlations of PC-30:0, the most abundant PC in the photic zone (**Supplementary Figure 2A**), with water column conditions (**Figures 8E,F**) likely indicate aerobic heterotrophic sources in the free-living fraction, and algal sources in the particle-attached. Clusters of PC molecules in the particle-attached fraction correlated to high chlorophyll vs. moderate concentrations of both chlorophyll and NO_2^-, may differentiate between photoautotrophs in near surface and intermediate waters.

PCs in the free-living fraction show a large diversity that correlates to core OMZ water column chemistry (**Figure 8E**), suggesting predominantly anaerobic sources of these molecules. Considering the increased diversity and unique distribution of these PC molecules in core OMZ waters, it is unlikely that they represent exported material from photoautotrophs in the surface. Rather, there seems to be a considerable contribution of *in situ* production in the core OMZ. For instance, the genes relevant to synthesis of PC have also been found in homologs of numerous chemoheterotrophic and chemoautotrophic bacteria (Sohlenkamp et al., 2003). Furthermore, in the mesopelagic region, a notable contribution of PC-31:0 correlating with NO_3^-, and to a lesser extent O_2 (**Figure 8E**), suggests possible deep-water nitrification.

While the observation of non-photoautotrophic sources of PCs in OMZ systems is novel, we can only speculate at this time as to which of the many organisms present in the core OMZ could be responsible for these lipids. A size-fractionated analysis that combines transcriptomic and lipidomic measurements may be necessary to determine more specific biological sources.

PME/PDME [Phosphatidyl(di)methylethanolamine]

PME/PDME have been loosely attributed to bacteria along chemoclines in marine environments (Schubotz et al., 2009; Wakeham et al., 2012), as their synthesis is predominantly found amongst Proteobacteria (Oliver and Colwell, 1973; Goldfine, 1984). The particle-attached fraction shows the majority of molecules (PME-32:0, PME-33:1, PDME-31:1, PDME-33:2, PDME-35:1, and PDME-36:2) clustering between PO_4^{3-} and pCO_2, and negatively correlated to O_2, which suggests predominantly heterotrophic sources (**Supplementary Figure 6B**). Several compounds (PME-30:0, PME-31:0, and PDME-29:4) also cluster between O_2 and pH, possibly indicating differentiation between aerobic and anaerobic heterotrophs. The free-living fraction shows a clustering of these molecules along pCO_2 and chlorophyll concentrations, possibly suggesting a cyanobacterial source (**Supplementary Figure 6A**). Furthermore, the greater diversity seen in core OMZ waters, in addition of their positive correlation with NO_2^-, are again suggestive of denitrifying or nitrate reducing bacteria. Possible candidates of nitrifying bacterial lipids include PME-35:4 and PDME-33:1.

Betaine Lipids

Most common forms of betaine lipids in surface marine environments (DGTS; *diacylglyceryl trimethylhomoserine*, DGTA; *diacylglyceryl hydroxymethyl-trimethyl-b-alanine*, and DGCC; diacylglyceryl carboxyhydroxymethylcholine; Schubotz et al., 2009, 2018; Van Mooy and Fredricks, 2010; Wakeham et al., 2012) were found in low relative abundance compared to glyco- and phospholipids (**Figure 3**). While betaine lipids are most common to eukaryotic phytoplankton (Kato et al., 1996), it has also been suggested that their origins may be considerably more diverse than previously assumed (Schubotz et al., 2018). In the photic zone, it remains likely that they are synthesized by photosynthetic eukaryotes, but their diversity and unique distributions (**Supplementary Figures 7A–C**), and increased presence in the free-living fraction in the upper and core OMZ (**Supplementary Figures 4C, 5C**) suggest additional, previously non-recognized microbial sources.

While lipid remodeling in response to phosphorus limitation (Benning et al., 1995) in oligotrophic regions has been well described (Van Mooy et al., 2009; Carini et al., 2015; Sebastián et al., 2016), only the restructuring of fatty acids in glycolipids has been observed under N-limitation (Breteler et al., 2005). The strikingly low abundance of betaine lipids in the photic zone of the ETSP suggests that further investigation in the potential lipid substitution of glyco- or phospolipids under N-depleted conditions is warranted.

Archaeal Lipids

Archaeal lipids have been shown to be abundant along the oxycline of similar marine environments (Schouten et al., 2012; Xie et al., 2014; Schubotz et al., 2018) where ammonia oxidizing crenarchaeota supply the water column with oxidized nitrogen species (Francis et al., 2007). Indeed, in the ETSP, ammonia oxidizing archaea are considerably more abundant than nitrifying bacteria (Bouskill et al., 2012). We succeeded in measuring 3 of the suspected intact glycosidic-GDGTs in greatest abundance along the oxycline and upper OMZ, demonstrating a present albeit underrepresented archaeal contribution to the total IPL pool (**Figure 3**). While the most common glycosidic-GDGTs (GDGT-0 and GDGT-5 or crenarchaeol; Pitcher et al., 2011) were detected (**Supplementary Figure 3B**), our analyses likely show limited representation of archaeal lipids, possibly a result of vastly different ionization efficiencies of this IPL class and relatively poor detection limits with the available volumes of seawater.

Utility of IPLs as Biomarkers for *in situ* Planktonic/Microbial Communities

The interpretation of IPL distributions in the environment is limited by factors that complicate the determination of the exact biological source(s) of a given molecule. The varying lability of individual lipids, in addition to varying residence times of IPLs driven by particle fluxes, influence the relative contribution of IPLs potentially exported to underlying depths. While IPLs are often considered to hydrolyze quickly after cell death (White et al., 1979; Petersen et al., 1991), it has been demonstrated that certain compounds can remain intact for weeks to months (Harvey et al., 1986; Brandsma, 2011; Logemann et al., 2011). Slower degradation rates were found to be most pronounced in SQDGs (Brandsma, 2011) suggesting a higher potential of this lipid class to survive export to the deep ocean. While a large percentage of SQDGs from the core OMZ and mesopelagic do not appear in the photic zone, molecules that are abundant throughout the water column (such as SQDG-30:0 and 28:0) may

contribute 10–20% of the particle-attached total IPL yield in the OMZ core and ∼10% in the mesopelagic, suggesting the potential for a significant contribution of exported material.

Statistical analyses such as CCAs that include IPLs concentrations and physiochemical conditions allow us to refine interpretations of biogeochemical trends beyond the relative abundances of IPL classes. A CCA of all detected IPL abundances under a range of geochemical conditions (**Figure 4**) indicates that each geochemical environment through the water column exhibits a statistically distinct total IPL distribution. There are several characteristic clusters of IPLs in surface waters, along the oxycline, and OMZ waters that correlate with the distribution of key nutrient species (i.e., NO_3^-, PO_4^{3-}, and NO_2^-), in addition to chlorophyll and O_2. This indicates that despite the overlap in some IPLs detected between geochemical environments, their overall distributions suggest that IPL export is limited and does not significantly hinder their utility as biomarkers of *in situ* planktonic/microbial biomass in the OMZ of the ETSP.

Our results indicate that the specificity of determining IPL sources can be improved upon by incorporating size-fractionated analyses. Despite some similarities between the free-living and particle-attached size fractions of POM, there is significant variability within size-fractionated IPL distributions as well, illuminating potential differences between microbial life modes. Our CCA analyses indicate that many phospholipids abundant in both size fractions correlate strongly with different physicochemical conditions, supporting the observation of distinct transcriptomic abundances between particle-attached and free-living life modes (Wright et al., 2012; Ganesh et al., 2014, 2015). Free-living microbes are exposed directly to biogeochemical variations, whereas particle-attached organisms may reflect redox-driven niche partitioning (Wright et al., 2012). Furthermore, particles sinking to the core OMZ taxonomically reflect those of particles in the oxic zone, potentially serving as a mechanism for the transport of bacteria to OMZ depths (Ganesh et al., 2014). Size-fractionated IPL analyses thus provide additional information in determining the biological origins of molecules common to multiple biological sources.

Total IPL assays are also constrained by limits in our knowledge of the full extent of IPL diversity in the marine environment and the exact biological origins of individual compounds. While we have shown that there are differences in IPL distributions due to differing life modes at a given depth, there are IPLs consistently dominant in specific geochemical environments (see **Figure 6**). To identify molecules that are particularly diagnostic of the geochemical environment we selected the most abundant molecules present in each environment and calculated clusters of highly correlated molecules ($R^2 > 0.65$ and $p < 0.001$; **Figure 9**). These clusters summarize much of the unique IPL distributions between water column conditions found in the ETSP. The oxygenated chlorophyll maximum is dominated by a number of glycolipids and a high diversity albeit lower concentration of betaine lipids, indicative of IPLs largely associated with photoautotrophs. The oxycline sees a shift to distinct glycolipid assemblages potentially due to an increased contribution in cyanobacterial and heterotrophic bacterial sources. In addition, the oxycline sees increased contribution of ammonia oxidizing archaeal GDGTs. The core OMZ is dominated by phospholipids reflecting both heterotrophic and chemoautotrophic bacteria. Finally, the oxygenated mesopelagic denotes a unique distribution of predominantly phospholipids associated with aerobic heterotrophs.

Contribution of Microbial Biomass to Suspended Organic Matter

Total IPL concentrations in the ETSP dramatically decrease with depth (**Figure 3**), as also seen in similar systems around the world (Van Mooy and Fredricks, 2010; Schubotz et al., 2018). However, the contribution of IPLs to total organic carbon stocks is larger in the chemocline than in the chlorophyll maximum, suggesting a potentially significant contribution of predominantly microbial biomass that characterizes these subsurface environments. Also, the fractional abundance of IPLs from the free-living fraction tends to increase with depth, indicating a greater contribution of free-living organisms and a reduced contribution of exported or particle-associated biomass.

The fractional abundances of IPL classes with depth indicates which classes are dominant amongst free-living or particle-attached communities. At most depths, DGs, PGs, and ARs are more abundant in the free-living fraction. Conversely, DGCCs, PEs, and PME/PDMEs are at most depths higher in the particle-attached fraction. The biological sources of these IPLs present at multiple depths in the water column may be disentangled by their associated life modes. Namely, the prevalence of denitrifying/nitrate reducing bacteria and the SAR324 cluster (with genomic potential for chemolithoautotrophy via sulfur or methane oxidation; Swan et al., 2011) in particle-attached niches, and nitrifying archaea/anammox bacteria in free-living niches (Wright et al., 2012; Ganesh et al., 2015).

If we assume that the total IPL concentrations at each respective depth are proportional to the concentration of living biomass, we can roughly compare the microbial carbon standing stocks of the OMZ to the photic zone. This simple exercise includes a depth-averaged IPL concentration for the photic zone (defined as the upper 55 and 60 m in the nearshore and offshore stations, respectively), and a depth averaged IPL concentration for the OMZ using the values from the upper and core OMZ (i.e., 55–500 m and 60–500 m in the nearshore and offshore stations, respectively). To account for the contribution of potentially more refractory IPLs exported in the particle-attached fraction, we assume that only 75% of the IPL pool is produced *in situ* (a conservative estimate based on the IPL distributions discussed above). We can then calculate the microbial biomass in any given water parcel of the photic zone and the OMZ. This exercise shows that the total IPLs stock (and thus microbial carbon standing stock) in OMZ waters is 10–20% greater than that in the photic zone, with a greater relative contribution of OMZ carbon stocks in the nearshore station. These first order calculations are subject to large uncertainties (e.g., vertical variability of biomass, relative lability of compounds, seasonality)

and are meant to be semi-quantitative at most. However, they suggest a potential for microbially derived biomass to account for a significant fraction of the total organic carbon in this OMZ system. This microbial contribution to organic carbon production may indicate a greater contribution of microbes to organic carbon export, as recently observed in Arabian Sea sediments (Lengger et al., 2020).

CONCLUSION

Size-fractionated IPL distributions in suspended organic matter from the ETSP off northern Chile indicate that particle-attached and free-living microbial biomass can differ significantly within the same geochemical environment, suggesting that size-fractionated IPL analysis provides improved utility in exploring the diversity of IPLs in the environment and determining their biological origins. Phospholipid distributions and CCA with physiochemical conditions across the oxycline and core OMZ provide evidence that autotrophic microbes may be more abundant in free-living modes, and heterotrophic biomass in particle-attached modes. In addition, these size-specific analyses may aid in identifying IPLs that may not reflect living biomass, but potentially export efficiency based on their relative lability, significant abundance at all depths and both size fractions, and the lack of significant correlation to a distinct geochemical environment. We expect potentially exported IPLs to be largely limited to few glycolipids in the particle-attached fraction and to not significantly convolute biomass interpretations in the OMZ of the ETSP.

The relative contribution of IPLs in the free-living fraction is larger than in the particle-associated fraction in OMZ and mesopelagic waters, suggesting a greater relative contribution of submicron organics to standing carbon stocks in the deep ocean. Furthermore, a first-order approximation on the total IPL standing stocks between the oxic part of the photic zone and OMZ waters indicates that microbial biomass in the latter may rival that of the former. This warrants further investigation into the common assumption that biomass production in the photic zone is the main source of organic carbon export to the deep ocean. Our results suggest that dark carbon fixation in OMZ waters could contribute to carbon export to the deep ocean.

The distribution of IPLs in the ETSP system of northern Chile exhibits some unique features compared to the eastern subtropical south Pacific and tropical North Pacific. Namely, the low abundance of betaine/aminolipids, a common IPL found in eukaryotic photoautotrophs, possibly suggests a physiological response to nitrogen limitation. Furthermore, the low abundance of polyunsaturated fatty acids in the photic zone, which are most abundant in algal IPLs, suggest that the commonly evoked dichotomy between bacterial and eukaryotic fatty acids may vary in distinct environments. Finally, the appearance of glycolipids and betaine lipids unique to the OMZ or mesopelagic suggest previously undescribed microbial sources contributing significantly to the total IPL pool.

DATA AVAILABILITY STATEMENT

The data have been published on PANGAEA pending a DOI but will be available here: https://doi.org/10.1594/PANGAEA.921190.

AUTHOR CONTRIBUTIONS

SC, JS, CV, and PD designed the study. CV, PD, and JS funded the research and the LowpHOx-2 cruise. SC carried out the sampling, sample preparation, developed the HPLC-MS analytical methods with assistance from ND and JS, performed the biomarker and elemental analysis, and processed the data. CH-C assisted with statistical analyses. SC and JS interpreted the results and wrote the manuscript with input from all co-authors. All authors contributed to the article and approved the submitted version.

FUNDING

This study was funded by CONICYT-Chile FONDECYT Grant 1170065 (CARbon Cycling and Physiological Traits in Phytoplankton Functional Groups under low pH/low OXygen conditions, CARpHOX) and by CONICYT-Chile National Competition for ship time (AUB 170002). Partial funding was provided by the Millennium Institute of Oceanography (IMO). SC and JS acknowledge financial support from the Department of Geological Sciences and INSTAAR at the University of Colorado Boulder (CU Boulder). The workshop was funded by the Deutsche Forschungsgemeinschaft (DFG, German Research Foundation) – project number: 422798570.

ACKNOWLEDGMENTS

We thank the captain and crew of the AGS-61 Cabo de Hornos, the chief scientist of the LowpHOx-2 cruise, Dr. Wolfgang Schneider (UdeC), in addition to personnel from the Millennium Institute of Oceanography (IMO) and the Laboratory of Aquatic Ecosystem Functioning at the University of Concepción for their assistance during the LowpHOx-2 cruise. We are particularly grateful to P. Contreras and Nicole Castillo (UdeC), K. Rempfert (CU Boulder), and B. Davidheiser-Kroll (CU Boulder) for their assistance with cruise logistics, IPL, and elemental analyses, respectively. JS thanks the Hanse-Wissenschaftskolleg Delmenhorst, Germany, for sponsoring the "Marine Organic Biogeochemistry" workshop in April 2019. We thank the associate editor and two reviewers for comments that improved the final version of the manuscript.

SUPPLEMENTARY MATERIAL

The Supplementary Material for this article can be found online at: https://www.frontiersin.org/articles/10.3389/fmars.2020.540643/full#supplementary-material

REFERENCES

Aldunate, M., Henríquez-Castillo, C., Ji, Q., Lueders-Dumont, J., Mulholland, M. R., Ward, B. B., et al. (2020). Nitrogen assimilation in picocyanobacteria inhabiting the oxygen-deficient waters of the eastern tropical North and South Pacific. *Limnol. Oceanogr.* 65, 437–453. doi: 10.1002/lno.11315

Arístegui, J., Gasol, J. M., Duarte, C. M., and Herndld, G. J. (2009). Microbial oceanography of the dark ocean's pelagic realm. *Limnol. and Oceanogr.* 54, 1501–1529. doi: 10.4319/lo.2009.54.5.1501

Arrigo, K. R. (2005). Marine microorganisms and global nutrient cycles. *Nature* 437, 349–355. doi: 10.1038/nature04159

Azam, F. (1998). Microbial control of oceanic carbon flux: the plot thickens. *Science* 280, 694–696. doi: 10.1126/science.280.5364.694

Azam, F., Fenchel, T., Field, J. G., Gray, J. S., Meyer-Reil, L. A., and Thingstad, F. (1983). The ecological role of water-column microbes in the sea. *Mar. Ecol. Prog. Ser.* 10, 257–263. doi: 10.3354/meps010257

Barridge, J. K., and Shively, J. M. (1968). Phospholipids of the Thiobacilli. *J. Bacteriol.* 95, 2182–2185. doi: 10.1128/jb.95.6.2182-2185.1968

Benning, C. (1998). "Membrane lipids in anoxygenic photosynthetic bacteria," in *Lipids in Photosynthesis: Structure, Function and Genetics*, eds P.-A. Siegenthaler and N. Murata (Dordrecht: Springer), 83–101. doi: 10.1007/0-306-48087-5_5

Benning, C., Huang, Z. H., and Gage, D. A. (1995). Accumulation of a novel glycolipid and a betaine lipid in cells of *Rhodobacter sphaeroides* grown under phosphate limitation. *Arch. Biochem. Biophys.* 317, 103–111. doi: 10.1006/abbi.1995.1141

Bligh, E. G., and Dyer, W. J. (1959). A rapid method of total lipid extraction and purification. *Cana. J. Biochem. Physiol.* 37, 911–917. doi: 10.1139/o59-099

Boumann, H. A., Hopmans, E. C., Van De Leemput, I., Op den Camp, H. J., Van De Vossenberg, J., Strous, M., et al. (2006). Ladderane phospholipids in anammox bacteria comprise phosphocholine and phosphoethanolamine headgroups. *FEMS Microbiol. Lett.* 258, 297–304. doi: 10.1111/j.1574-6968.2006.00233.x

Bouskill, N. J., Eveillard, D., Chien, D., Jayakumar, A., and Ward, B. B. (2012). Environmental factors determining ammonia-oxidizing organism distribution and diversity in marine environments. *Environ. Microbiol.* 14, 714–729. doi: 10.1111/j.1462-2920.2011.02623.x

Brandsma, J. (2011). *The Origin and Fate of Intact Polar Lipids in the Marine Environment*, Vol. 5. Utrecht: Utrecht university.

Brandsma, J., Hopmans, E. C., Brussaard, C. P., Witte, H. J., Schouten, S., and Sinninghe Damsté, J. S. (2012). Spatial distribution of intact polar lipids in North Sea surface waters: relationship with environmental conditions and microbial community composition. *Limnol. Oceanogr.* 57, 959–973. doi: 10.4319/lo.2012.57.4.0959

Breteler, W. K., Schogt, N., and Rampen, S. (2005). Effect of diatom nutrient limitation on copepod development: role of essential lipids. *Mar. Ecol. Prog. Ser.* 291, 125–133. doi: 10.3354/meps291125

Calvano, C. D., Zambonin, C. G., and Palmisano, F. (2011). Lipid fingerprinting of Gram-positive lactobacilli by intact cells–matrix-assisted laser desorption/ionization mass spectrometry using a proton sponge based matrix. *Rapid Commun. Mass Spectrom.* 25, 1757–1764. doi: 10.1002/rcm.5035

Canfield, D. E., Stewart, F. J., Thamdrup, B., De Brabandere, L., Dalsgaard, T., Delong, E. F., et al. (2010). A cryptic sulfur cycle in oxygen-minimum–zone waters off the Chilean coast. *Science* 330, 1375–1378. doi: 10.1126/science.1196889

Carini, P., Van Mooy, B. A., Thrash, J. C., White, A., Zhao, Y., Campbell, E. O., et al. (2015). SAR11 lipid renovation in response to phosphate starvation. *Proc. Natl. Acad. Sci. U.S.A.* 112, 7767–7772. doi: 10.1073/pnas.1505034112

Carpenter, J. H. (1965). The chesapeake bay institute technique for the winkler dissolved oxygen method. *Limnol. Oceanogr.* 10, 141–143. doi: 10.4319/lo.1965.10.1.0141

Chao, A., Chiu, C. H., and Hsieh, T. C. (2012). Proposing a resolution to debates on diversity partitioning. *Ecology* 93, 2037–2051. doi: 10.1890/11-1817.1

Close, H. G., Shah, S. R., Ingalls, A. E., Diefendorf, A. F., Brodie, E. L., Hansman, R. L., et al. (2013). Export of submicron particulate organic matter to mesopelagic depth in an oligotrophic gyre. *Proc. Natl. Acad. Sci. U.S.A.* 110, 12565–12570. doi: 10.1073/pnas.1217514110

Close, H. G., Wakeham, S. G., and Pearson, A. (2014). Lipid and 13C signatures of submicron and suspended particulate organic matter in the Eastern Tropical North Pacific: implications for the contribution of Bacteria. *Deep Sea Res. Part I Oceanogr. Res. Pap.* 85, 15–34. doi: 10.1016/j.dsr.2013.11.005

Czeschel, R., Stramma, L., Schwarzkopf, F. U., Giese, B. S., Funk, A., and Karstensen, J. (2011). Middepth circulation of the eastern tropical South Pacific and its link to the oxygen minimum zone. *J. Geophys. Res. Oceans* 116:C01015.

Dalsgaard, T., Thamdrup, B., Farías, L., and Revsbech, N. P. (2012). Anammox and denitrification in the oxygen minimum zone of the eastern South Pacific. *Limnol. Oceanogr.* 57, 1331–1346. doi: 10.4319/lo.2012.57.5.1331

Daneri, G., Dellarossa, V., Quiñones, R., Jacob, B., Montero, P., and Ulloa, O. (2000). Primary production and community respiration in the Humboldt Current System off Chile and associated oceanic areas. *Mar. Ecol. Prog. Ser.* 197, 41–49. doi: 10.3354/meps197041

De La Rocha, C. L., Nowald, N., and Passow, U. (2008). Interactions between diatom aggregates, minerals, particulate organic carbon, and dissolved organic matter: further implications for the ballast hypothesis. *Global Biogeochem. Cycles* 22:GB4005.

De Pol-Holz, R., Robinson, R. S., Hebbeln, D., Sigman, D. M., and Ulloa, O. (2009). Controls on sedimentary nitrogen isotopes along the Chile margin. *Deep Sea Res. Part II Top. Stud. Oceanogr.* 56, 1042–1054. doi: 10.1016/j.dsr2.2008.09.014

Dembitsky, V. M. (1996). Betaine ether-linked glycerolipids: chemistry and biology. *Prog. Lipid Res.* 35, 1–51. doi: 10.1016/0163-7827(95)00009-7

Dickson, A. G. (1990). Standard potential of the reaction: AgCl (s)+ 12H2 (g)= Ag (s)+ HCl (aq), and and the standard acidity constant of the ion HSO4- in synthetic sea water from 273.15 to 318.15 K. *J. Chem. Thermodyn.* 22, 113–127. doi: 10.1016/0021-9614(90)90074-z

Dickson, A. G., Afghan, J. D., and Anderson, G. C. (2003). Reference materials for oceanic CO2 analysis: a method for the certification of total alkalinity. *Mar. Chem.* 80, 185–197. doi: 10.1016/s0304-4203(02)00133-0

Dickson, A. G., and Millero, F. J. (1987). A comparison of the equilibrium constants for the dissociation of carbonic acid in seawater media. *Deep Sea Res. Part A Oceanogr. Res. Pap.* 34, 1733–1743. doi: 10.1016/0198-0149(87)90021-5

Ducklow, H. W. (2001). *Bacterioplankton, Encyclopedia of Ocean Sciences*. San Diego, CA: Academic Press, 217–224.

Duret, M. T., Pachiadaki, M. G., Stewart, F. J., Sarode, N., Christaki, U., Monchy, S., et al. (2015). Size-fractionated diversity of eukaryotic microbial communities in the Eastern Tropical North Pacific oxygen minimum zone. *FEMS Microbiol. Ecol.* 91:fiv037.

Dyhrman, S. T., Ammerman, J. W., and Van Mooy, B. A. (2007). Microbes and the marine phosphorus cycle. *Oceanography* 20, 110–116. doi: 10.5670/oceanog.2007.54

Elling, F. J., Könneke, M., Lipp, J. S., Becker, K. W., Gagen, E. J., and Hinrichs, K. U. (2014). Effects of growth phase on the membrane lipid composition of the thaumarchaeon Nitrosopumilus maritimus and their implications for archaeal lipid distributions in the marine environment. *Geochim. Cosmochim. Acta* 141, 579–597. doi: 10.1016/j.gca.2014.07.005

Falkowski, P. G., Fenchel, T., and Delong, E. F. (2008). The microbial engines that drive Earth's biogeochemical cycles. *Science* 320, 1034–1039. doi: 10.1126/science.1153213

Fang, J., Barcelona, M. J., and Semrau, J. D. (2000). Characterization of methanotrophic bacteria on the basis of intact phospholipid profiles. *FEMS Microbiol. Lett.* 189, 67–72. doi: 10.1111/j.1574-6968.2000.tb09207.x

Finkel, Z. V., Beardall, J., Flynn, K. J., Quigg, A., Rees, T. A. V., and Raven, J. A. (2010). Phytoplankton in a changing world: cell size and elemental stoichiometry. *J. Plankton Res.* 32, 119–137. doi: 10.1093/plankt/fbp098

Francis, C. A., Beman, J. M., and Kuypers, M. M. M. (2007). New processes and players in the nitrogen cycle: The microbial ecology of anaerobic and archaeal ammonia oxidation. *ISME J.* 1, 19–27. doi: 10.1038/ismej.2007.8

Franz, J., Krahmann, G., Lavik, G., Grasse, P., Dittmar, T., and Riebesell, U. (2012). Dynamics and stoichiometry of nutrients and phytoplankton in waters influenced by the oxygen minimum zone in the eastern tropical Pacific. *Deep Sea Res. Part I Oceanogr. Res. Pap.* 62, 20–31. doi: 10.1016/j.dsr.2011.12.004

Fuenzalida, R., Schneider, W., Garcés-Vargas, J., Bravo, L., and Lange, C. (2009). Vertical and horizontal extension of the oxygen minimum zone in the eastern South Pacific Ocean. *Deep Sea Res. Part II Top. Stud. Oceanogr.* 56, 992–1003. doi: 10.1016/j.dsr2.2008.11.001

Galán, A., Molina, V., Thamdrup, B., Woebken, D., Lavik, G., Kuypers, M. M., et al. (2009). Anammox bacteria and the anaerobic oxidation of ammonium in the oxygen minimum zone off northern Chile. *Deep Sea Res. Part II Top. Stud. Oceanogr.* 56, 1021–1031. doi: 10.1016/j.dsr2.2008.09.016

Ganesh, S., Bristow, L. A., Larsen, M., Sarode, N., Thamdrup, B., and Stewart, F. J. (2015). Size-fraction partitioning of community gene transcription and nitrogen metabolism in a marine oxygen minimum zone. *ISME J.* 9, 2682–2696. doi: 10.1038/ismej.2015.44

Ganesh, S., Parris, D. J., DeLong, E. F., and Stewart, F. J. (2014). Metagenomic analysis of size-fractionated picoplankton in a marine oxygen minimum zone. *ISME J.* 8, 187–211. doi: 10.1038/ismej.2013.144

Garcia-Robledo, E., Padilla, C. C., Aldunate, M., Stewart, F. J., Ulloa, O., Paulmier, A., et al. (2017). Cryptic oxygen cycling in anoxic marine zones. *Proc. Natl. Acad. Sci. U.S.A.* 114, 8319–8324. doi: 10.1073/pnas.1619844114

Goldfine, H. (1984). Bacterial membranes and lipid packing theory. *J. Lipid Res.* 25, 1501–1507.

Goldfine, H., and Hagen, P. O. (1968). N-Methyl groups in bacterial lipids III. phospholipids of hyphomicrobia. *J. Bacteriol.* 95, 367–375. doi: 10.1128/JB.95.2.367-375.1968

Gombos, Z., Várkonyi, Z., Hagio, M., Iwaki, M., Kovács, L., Masamoto, K., et al. (2002). Phosphatidylglycerol requirement for the function of electron acceptor plastoquinone QB in the photosystem II reaction center. *Biochemistry* 41, 3796–3802. doi: 10.1021/bi011884h

Grasshoff, K., Kremling, K., and Ehrhardt, M. (eds) (2009). *Methods of Seawater Analysis*. Hoboken, NJ: John Wiley & Sons.

Harvey, H. R., Fallon, R. D., and Patton, J. S. (1986). The effect of organic matter and oxygen on the degradation of bacterial membrane lipids in marine sediments. *Geochim. Cosmochim. Acta* 50, 795–804. doi: 10.1016/0016-7037(86)90355-8

Harwood, J. L. (1998). "Membrane lipids in algae," in *Lipids in Photosynthesis: Structure, Function and Genetics*, eds P.-A. Siegenthaler and N. Murata (Dordrecht: Springer), 53–64. doi: 10.1007/0-306-48087-5_3

Helly, J. J., and Levin, L. A. (2004). Global distribution of naturally occurring marine hypoxia on continental margins. *Deep Sea Res. Part I Oceanogr. Res. Pap.* 51, 1159–1168. doi: 10.1016/j.dsr.2004.03.009

Herbert, R. A. (1999). Nitrogen cycling in coastal marine ecosystems. *FEMS Microbiol. Rev.* 23, 563–590. doi: 10.1111/j.1574-6976.1999.tb00414.x

Hölzl, G., and Dörmann, P. (2007). Structure and function of glycoglycerolipids in plants and bacteria. *Prog. Lipid Res.* 46, 225–243. doi: 10.1016/j.plipres.2007.05.001

Imhoff, J. F. (1995). "Taxonomy and physiology of phototrophic purple bacteria and green sulfur bacteria," in *Anoxygenic Photosynthetic Bacteria*, eds R. E. Blankenship, M. T. Madigan, and C. E. Bauer (Dordrecht: Springer), 1–15. doi: 10.1007/0-306-47954-0_1

Jetten, M. S. (2008). The microbial nitrogen cycle. *Environ. Microbiol.* 10, 2903–2909. doi: 10.1111/j.1462-2920.2008.01786.x

Kalisch, B., Dörmann, P., and Hölzl, G. (2016). "DGDG and glycolipids in plants and algae," in *Lipids in plant and algae development* (Cham: Springer), 51–83.

Karl, D. M., Knauer, G. A., Martin, J. H., and Ward, B. B. (1984). Bacterial chemolithotrophy in the ocean is associated with sinking particles. *Nature* 309, 54–56. doi: 10.1038/309054a0

Karstensen, J., and Ulloa, O. (2019). *Peru–Chile Current System*. Amsterdam: Elsevier.

Kato, M., Sakai, M., Adachi, K., Ikemoto, H., and Sano, H. (1996). Distribution of betaine lipids in marine algae. *Phytochemistry* 42, 1341–1345. doi: 10.1016/0031-9422(96)00115-x

Kuypers, M. M., Lavik, G., and Thamdrup, B. (2006). "Anaerobic ammonium oxidation in the marine environment," in *Past and Present Water Column Anoxia*, ed. L. N. Neretin (Dordrecht: Springer), 311–335. doi: 10.1007/1-4020-4297-3_13

Lam, P., and Kuypers, M. M. (2011). Microbial nitrogen cycling processes in oxygen minimum zones. *Annu. Rev. Mar. Sci.* 3, 317–345. doi: 10.1146/annurev-marine-120709-142814

Lavin, P., González, B., Santibáñez, J. F., Scanlan, D. J., and Ulloa, O. (2010). Novel lineages of Prochlorococcus thrive within the oxygen minimum zone of the eastern tropical South Pacific. *Environ. Microbiol. Rep.* 2, 728–738. doi: 10.1111/j.1758-2229.2010.00167.x

Lengger, S., Rush, D., Mayser, J. P., Blewett, J., Schwartz-Narbonne, R., Talbot, H., et al. (2020). Dark carbon fixation contributes to sedimentary organic carbon in the Arabian Sea oxygen minimum zone. *Global Biogeochem. Cycles* 33, 1715–1732. doi: 10.1029/2019gb006282

Logemann, J., Graue, J., Köster, J., Engelen, B., Rullkötter, J., and Cypionka, H. (2011). A laboratory experiment of intact polar lipid degradation in sandy sediments. *Biogeosci. Discuss.* 8, 3289–3321. doi: 10.5194/bgd-8-3289-2011

Makula, R. A. (1978). Phospholipid composition of methane-utilizing bacteria. *J. Bacteriol.* 134, 771–777. doi: 10.1128/jb.134.3.771-777.1978

Matys, E. D., Sepúlveda, J., Pantoja, S., Lange, C. B., Caniupán, M., Lamy, F., et al. (2017). Bacteriohopanepolyols along redox gradients in the humboldt current system off northern Chile. *Geobiology* 15, 844–857. doi: 10.1111/gbi.12250

Mehrbach, C., Culberson, C. H., Hawley, J. E., and Pytkowicx, R. M. (1973). Measurement of the apparent dissociation constants of carbonic acid in seawater at atmospheric pressure 1. *Limnol. Oceanogr.* 18, 897–907. doi: 10.4319/lo.1973.18.6.0897

Molina, V., Belmar, L., and Ulloa, O. (2010). High diversity of ammonia-oxidizing archaea in permanent and seasonal oxygen-deficient waters of the eastern South Pacific. *Environ. microbiol.* 12, 2450–2465. doi: 10.1111/j.1462-2920.2010.02218.x

Molina, V., and Farías, L. (2009). Aerobic ammonium oxidation in the oxycline and oxygen minimum zone of the eastern tropical South Pacific off northern Chile (20° S). *Deep Sea Res. Part II Top. Stud. Oceanogr.* 56, 1032–1041. doi: 10.1016/j.dsr2.2008.09.006

Molina, V., Ulloa, O., Farías, L., Urrutia, H., Ramírez, S., Junier, P., et al. (2007). Ammonia-oxidizing β-*proteobacteria* from the oxygen minimum zone off northern Chile. *Appl. Environ. Microbiol.* 73, 3547–3555. doi: 10.1128/aem.02275-06

Moran, S. B., and Buesseler, K. O. (1992). Short residence time of colloids in the upper ocean estimated from 238 U–234 Th disequilibria. *Nature* 359, 221–223. doi: 10.1038/359221a0

Oliver, J. D., and Colwell, R. R. (1973). Extractable lipids of gram-negative marine bacteria: phospholipid composition. *J. Bacteriol.* 114, 897–908. doi: 10.1128/jb.114.3.897-908.1973

Pantoja, S., Sepúlveda, J., and González, H. E. (2004). Decomposition of sinking proteinaceous material during fall in the oxygen minimum zone off northern Chile. *Deep Sea Res. Part I Oceanogr. Res. Pap.* 51, 55–70. doi: 10.1016/j.dsr.2003.09.005

Parsons, T. R., Maita, Y., and Lalli, C. M. I. I. (1984). *A Manual of Chemical and Biological Methods for Seawater Analysis*, Vol. 1. Oxford: Pergamon Press, 73.

Passow, U., and De La Rocha, C. L. (2006). Accumulation of mineral ballast on organic aggregates. *Global Biogechem. Cycles* 20:GB1013.

Paulmier, A., and Ruiz-Pino, D. (2009). Oxygen minimum zones (OMZs) in the modern ocean. *Prog. Oceanogr.* 80, 113–128. doi: 10.1016/j.pocean.2008.08.001

Pearson, A., and Ingalls, A. E. (2013). Assessing the use of archaeal lipids as marine environmental proxies. *Annu. Rev. Earth Planet. Sci.* 41, 359–384. doi: 10.1146/annurev-earth-050212-123947

Petersen, S. O., Henriksen, K., Blackburn, T. H., and King, G. M. (1991). A comparison of phospholipid and chloroform fumigation analyses for biomass in soil: potentials and limitations. *FEMS Microbiol. Lett.* 85, 257–267. doi: 10.1111/j.1574-6968.1991.tb04732.x

Pierrot, D., Lewis, E., and Wallace, D. W. R. (2006). *MS Excel Program Developed for CO2 System Calculations. ORNL/CDIAC-105a.* . Oak Ridge, TN: Oak Ridge National Laboratory, 10.

Pitcher, A., Hopmans, E. C., Mosier, A. C., Park, S. J., Rhee, S. K., Francis, C. A., et al. (2011). Core and intact polar glycerol dibiphytanyl glycerol tetraether lipids of ammonia-oxidizing archaea enriched from marine and estuarine sediments. *Appl. Environ. Microbiol.* 77, 3468–3477. doi: 10.1128/aem.02758-10

Pomeroy, L. R. (1974). The ocean's food web, a changing paradigm. *Bioscience* 24, 499–504. doi: 10.2307/1296885

Pomeroy, L. R., Williams, P. J. I., Azam, F., and Hobbie, J. E. (2007). The microbial loop. *Oceanography* 20, 28–33.

Popendorf, K. J., Lomas, M. W., and Van Mooy, B. A. (2011). Microbial sources of intact polar diacylglycerolipids in the Western North Atlantic Ocean. *Organic Geochem.* 42, 803–811. doi: 10.1016/j.orggeochem.2011.05.003

Rattray, J. E., Geenevasen, J. A., Van Niftrik, L., Rijpstra, W. I. C., Hopmans, E. C., Strous, M., et al. (2009). Carbon isotope-labelling experiments indicate that ladderane lipids of anammox bacteria are synthesized by a previously undescribed, novel pathway. *FEMS Microbiol. Lett.* 292, 115–122. doi: 10.1111/j.1574-6968.2008.01483.x

Rush, D., Hopmans, E. C., Wakeham, S. G., Schouten, S., and Damste, J. S. (2012). Occurrence and distribution of ladderane oxidation products in different oceanic regimes. *Biogeosci. Discuss.* 9, 2407–2418. doi: 10.5194/bg-9-2407-2012

Rütters, H., Sass, H., Cypionka, H., and Rullkötter, J. (2001). Monoalkylether phospholipids in the sulfate-reducing bacteria *Desulfosarcina variabilis* and *Desulforhabdus amnigenus*. *Archiv. Microbiol.* 176, 435–442. doi: 10.1007/s002030100343

Sato, N., Hagio, M., Wada, H., and Tsuzuki, M. (2000). Requirement of phosphatidylglycerol for photosynthetic function in thylakoid membranes. *Proc. Natl. Acad. Sci. U.S.A.* 97, 10655–10660. doi: 10.1073/pnas.97.19.10655

Schouten, S., Middelburg, J. J., Hopmans, E. C., and Damsté, J. S. S. (2010). Fossilization and degradation of intact polar lipids in deep subsurface sediments: a theoretical approach. *Geochim. Cosmochim. Acta* 74, 3806–3814. doi: 10.1016/j.gca.2010.03.029

Schouten, S., Pitcher, A., Hopmans, E. C., Villanueva, L., van Bleijswijk, J., and Sinninghe Damsté, J. S. (2012). Intact polar and core glycerol dibiphytanyl glycerol tetraether lipids in the Arabian Sea oxygen minimum zone: I. Selective preservation and degradation in the water column and consequences for the TEX86. *Geochim. Cosmochim. Acta* 98, 228–243. doi: 10.1016/j.gca.2012.05.002

Schubotz, F., Wakeham, S. G., Lipp, J. S., Fredricks, H. F., and Hinrichs, K. U. (2009). Detection of microbial biomass by intact polar membrane lipid analysis in the water column and surface sediments of the Black Sea. *Environ. Microbiol.* 11, 2720–2734. doi: 10.1111/j.1462-2920.2009.01999.x

Schubotz, F., Xie, S., Lipp, J. S., Hinrichs, K. U., and Wakeham, S. G. (2018). Intact polar lipids in the water column of the eastern tropical North Pacific: abundance and structural variety of non-phosphorus lipids. *Biogeosciences* 15, 6481–6501. doi: 10.5194/bg-15-6481-2018

Sebastián, M., Smith, A. F., González, J. M., Fredricks, H. F., Van Mooy, B., Koblížek, M., et al. (2016). Lipid remodelling is a widespread strategy in marine heterotrophic bacteria upon phosphorus deficiency. *ISME J.* 10, 968–978. doi: 10.1038/ismej.2015.172

Shaw, N. (1974). Lipid composition as a guide to the classification of bacteria. *Adv. Appl. Microbiol.* 17, 63–108. doi: 10.1016/s0065-2164(08)70555-0

Siegenthaler, P. A. (1998). "Molecular organization of acyl lipids in photosynthetic membranes of higher plants," in *Lipids in Photosynthesis: Structure, Function and Genetics* (Dordrecht: Springer), 119–144.

Sievert, S. M., Kiene, R. P., and Schulz-Vogt, H. N. (2007). The sulfur cycle. *Oceanography* 20, 117–123.

Sinninghe Damsté, J. S., Rijpstra, W. I. C., Geenevasen, J. A. J., Strous, M., and Jetten, M. S. M. (2005). Structural identification of ladderane and other membrane lipids of planctomycetes capable of anaerobic ammonium oxidation (anammox). *FEBS J.* 272, 4270–4283. doi: 10.1111/j.1742-4658.2005.04842.x

Sohlenkamp, C., López-Lara, I. M., and Geiger, O. (2003). Biosynthesis of phosphatidylcholine in bacteria. *Prog. Lipid Res.* 42, 115–162. doi: 10.1016/s0163-7827(02)00050-4

Sollai, M., Hopmans, E. C., Schouten, S., Keil, R. G., and Sinninghe Damsté, J. S. (2015). Intact polar lipids of *Thaumarchaeota* and *Anammox bacteria* as indicators of N cycling in the eastern tropical North Pacific oxygen-deficient zone. *Biogeosciences* 12, 4725–4737. doi: 10.5194/bg-12-4725-2015

Stevens, H., and Ulloa, O. (2008). Bacterial diversity in the oxygen minimum zone of the eastern tropical South Pacific. *Environ. Microbiol.* 10, 1244–1259. doi: 10.1111/j.1462-2920.2007.01539.x

Stewart, F. J., Ulloa, O., and DeLong, E. F. (2012). Microbial metatranscriptomics in a permanent marine oxygen minimum zone. *Environ. Microbiol.* 14, 23–40. doi: 10.1111/j.1462-2920.2010.02400.x

Sturt, H. F., Summons, R. E., Smith, K., Elvert, M., and Hinrichs, K. U. (2004). Intact polar membrane lipids in prokaryotes and sediments deciphered by high-performance liquid chromatography/electrospray ionization multistage mass spectrometry - New biomarkers for biogeochemistry and microbial ecology. *Rapid Commun. Mass Spectrom.* 18, 617–628. doi: 10.1002/rcm.1378

Suzumura, M. (2005). Phospholipids in marine environments: a review. *Talanta* 66, 422–434. doi: 10.1016/j.talanta.2004.12.008

Swan, B. K., Martinez-Garcia, M., Preston, C. M., Sczyrba, A., Woyke, T., Lamy, D., et al. (2011). Potential for chemolithoautotrophy among ubiquitous bacteria lineages in the dark ocean. *Science* 333, 1296–1300. doi: 10.1126/science.1203690

Tamot, B., and Benning, C. (2009). "Membrane lipid biosynthesis in purple bacteria," in *The Purple Phototrophic Bacteria. Advances in Photosynthesis and Respiration*, Vol. 28, eds C. N. Hunter, F. Daldal, M. C. Thurnauer, and J. T. Beatty (Dordrecht: Springer), doi: 10.1007/978-1-4020-8815-5_7

Taylor, G. T., Iabichella, M., Ho, T. Y., Scranton, M. I., Thunell, R. C., Muller-Karger, F., et al. (2001). Chemoautotrophy in the redox transition zone of the Cariaco Basin: a significant midwater source of organic carbon production. *Limnol. Oceanogr.* 46, 148–163. doi: 10.4319/lo.2001.46.1.0148

Thamdrup, B. (2012). New pathways and processes in the global nitrogen cycle. *Annu. Rev. Ecol. Evol. Syst.* 43, 407–428. doi: 10.1146/annurev-ecolsys-102710-145048

Thamdrup, B., Dalsgaard, T., Jensen, M. M., Ulloa, O., Farías, L., and Escribano, R. (2006). Anaerobic ammonium oxidation in the oxygen-deficient waters off northern Chile. *Limnol. Oceanogr.* 51, 2145–2156. doi: 10.4319/lo.2006.51.5.2145

Thamdrup, B., Dalsgaard, T., and Revsbech, N. P. (2012). Widespread functional anoxia in the oxygen minimum zone of the Eastern South Pacific. *Deep Sea Res. Part I Oceanogr. Res. Pap.* 65, 36–45. doi: 10.1016/j.dsr.2012.03.001

Ulloa, O., Canfield, D. E., DeLong, E. F., Letelier, R. M., and Stewart, F. J. (2012). Microbial oceanography of anoxic oxygen minimum zones. *Proc. Natl. Acad. Sci. U.S.A.* 109, 15996–16003. doi: 10.1073/pnas.1205009109

Ulloa, O., and Pantoja, S. (2009). The oxygen minimum zone of the eastern South Pacific. *Deep Sea Res. Part II Top. Stud. Oceanogr.* 56, 987–991.

Valentine, D. L. (2007). Adaptations to energy stress dictate the ecology and evolution of the Archaea. *Nat. Rev. Microbiol.* 5, 316–323. doi: 10.1038/nrmicro1619

Van Mooy, B. A. S., and Fredricks, H. F. (2010). Bacterial and eukaryotic intact polar lipids in the eastern subtropical South Pacific: water-column distribution, planktonic sources, and fatty acid composition. *Geochim. Cosmochim. Acta* 74, 6499–6516. doi: 10.1016/j.gca.2010.08.026

Van Mooy, B. A. S., Fredricks, H. F., Pedler, B. E., Dyhrman, S. T., Karl, D. M., Koblížek, M., et al. (2009). Phytoplankton in the ocean use non-phosphorus lipids in response to phosphorus scarcity. *Nature* 458, 69–72. doi: 10.1038/nature07659

Van Mooy, B. A. S., Rocap, G., Fredricks, H. F., Evans, C. T., and Devol, A. H. (2006). Sulfolipids dramatically decrease phosphorus demand by picocyanobacteria in oligotrophic marine environments. *Proc. Natl. Acad. Sci. U.S.A.* 103, 8607–8612. doi: 10.1073/pnas.0600540103

Volkman, J. K., Jeffrey, S. W., Nichols, P. D., Rogers, G. I., and Garland, C. D. (1989). Fatty acid and lipid composition of 10 species of microalgae used in mariculture. *J. Exp. Mar. Bio. Ecol.* 128, 219–240. doi: 10.1016/0022-0981(89)90029-4

Wada, H., and Murata, N. (1998). *Membrane Lipids in Cyanobacteria. Lipids in Photosynthesis: Structure, Function and Genetics*. Dordrecht: Springer, 65–81.

Wakeham, S. G., Amann, R., Freeman, K. H., Hopmans, E. C., Jørgensen, B. B., Putnam, I. F., et al. (2007). Microbial ecology of the stratified water column of the Black Sea as revealed by a comprehensive biomarker study. *Org. Geochem.* 38, 2070–2097. doi: 10.1016/j.orggeochem.2007.08.003

Wakeham, S. G., Turich, C., Schubotz, F., Podlaska, A., Li, X. N., Varela, R., et al. (2012). Biomarkers, chemistry and microbiology show chemoautotrophy in a multilayer chemocline in the Cariaco Basin. *Deep. Res. Part I Oceanogr. Res. Pap.* 63, 133–156. doi: 10.1016/j.dsr.2012.01.005

Walsh, D. A., Zaikova, E., Howes, C. G., Song, Y. C., Wright, J. J., Tringe, S. G., et al. (2009). Metagenome of a versatile chemolithoautotroph from expanding oceanic dead zones. *Science* 326, 578–582. doi: 10.1126/science.1175309

Weijers, J. W. H., Schouten, S., Hopmans, E. C., Geenevasen, J. A. J., David, O. R. P., Coleman, J. M., et al. (2006). Membrane lipids of mesophilic anaerobic bacteria thriving in peats have typical archaeal traits. *Environ. Microbiol.* 8, 648–657. doi: 10.1111/j.1462-2920.2005.00941.x

White, D. C., Davis, W. M., Nickels, J. S., King, J. D., and Bobbie, R. J. (1979). Determination of the sedimentary microbial biomass by extractible lipid phosphate. *Oecologia* 40, 51–62. doi: 10.1007/BF00388810

Wilson, J. D., Barker, S., and Ridgwell, A. (2012). Assessment of the spatial variability in particulate organic matter and mineral sinking fluxes in the ocean interior: Implications for the ballast hypothesis. *Global Biogeochem. Cycles* 26, 1–15. doi: 10.1029/2012GB004398

Wörmer, L., Lipp, J. S., Schröder, J. M., and Hinrichs, K. U. (2013). Application of two new LC–ESI–MS methods for improved detection of intact polar lipids (IPLs) in environmental samples. *Organic Geochem.* 59, 10–21. doi: 10.1016/j.orggeochem.2013.03.004

Wright, J. J., Konwar, K. M., and Hallam, S. J. (2012). Microbial ecology of expanding oxygen minimum zones. *Nat. Rev. Microbiol.* 10, 381–394. doi: 10.1038/nrmicro2778

Xie, S., Liu, X. L., Schubotz, F., Wakeham, S. G., and Hinrichs, K. U. (2014). Distribution of glycerol ether lipids in the oxygen minimum zone of the Eastern Tropical North Pacific Ocean. *Org. Geochem.* 71, 60–71. doi: 10.1016/j.orggeochem.2014.04.006

Yao, M., Elling, F. J., Jones, C., Nomosatryo, S., Long, C. P., Crowe, S. A., et al. (2016). Heterotrophic bacteria from an extremely phosphate-poor lake have conditionally reduced phosphorus demand and utilize diverse sources of phosphorus. *Environ. Microbiol.* 18, 656–667. doi: 10.1111/1462-2920.13063

Conflict of Interest: The authors declare that the research was conducted in the absence of any commercial or financial relationships that could be construed as a potential conflict of interest.

frontiers in Marine Science

ORIGINAL RESEARCH
published: 24 September 2020
doi: 10.3389/fmars.2020.543124

Aggregate Feeding by the Copepods *Calanus* and *Pseudocalanus* Controls Carbon Flux Attenuation in the Arctic Shelf Sea During the Productive Period

*Helga van der Jagt[1,2], Ingrid Wiedmann[3], Nicole Hildebrandt[1], Barbara Niehoff[1] and Morten H. Iversen[1,2]**

[1] Alfred Wegener Institute Helmholtz Center for Polar and Marine Research, Bremerhaven, Germany, [2] MARUM and University of Bremen, Bremen, Germany, [3] UiT The Arctic University of Norway, Tromsø, Norway

OPEN ACCESS

Edited by:
Cindy Lee,
Stony Brook University, United States

Reviewed by:
Karen Stamieszkin,
College of William & Mary, United States
Slawomir Kwasniewski,
Polish Academy of Sciences, Poland
Jordan Toullec,
UMR 6539 Laboratoire des Sciences de L'Environnement Marin (LEMAR), France

***Correspondence:**
Morten H. Iversen
morten.iversen@awi.de;
morten.iversen@uni-bremen.de

Specialty section:
This article was submitted to Marine Biogeochemistry, a section of the journal Frontiers in Marine Science

Received: 15 March 2020
Accepted: 12 August 2020
Published: 24 September 2020

Citation:
van der Jagt H, Wiedmann I, Hildebrandt N, Niehoff B and Iversen MH (2020) Aggregate Feeding by the Copepods Calanus and Pseudocalanus Controls Carbon Flux Attenuation in the Arctic Shelf Sea During the Productive Period. Front. Mar. Sci. 7:543124. doi: 10.3389/fmars.2020.543124

Up to 95% of the oceanic primary production is recycled within the upper few hundred meters of the water column. Marine snow and zooplankton fecal pellets in the upper water column are often recycled at rates exceeding those measured for microbial degradation, suggesting that zooplankton might be important for flux attenuation of particulate organic carbon in the upper ocean. However, direct evidence for interactions between zooplankton and settling aggregates are still rare. We investigated the importance of zooplankton aggregate feeding for carbon flux attenuation in the upper ocean by determining aggregate ingestion rates and feeding behavior on settling aggregates by the dominant Arctic filter-feeding copepods *Calanus* spp. and *Pseudocalanus* spp. Both genera were observed to detect and feed on settling aggregates. Using *in situ* zooplankton and aggregate abundances in combination with the measured aggregate feeding rates, we calculated that 60–67% of the total carbon flux attenuation at three Arctic locations could be explained by *Calanus* spp. and *Pseudocalanus* spp. aggregate feeding alone. When including microbial degradation of the settling aggregates, we could explain up to 77% of the total carbon flux attenuation. Our results suggest that by directly ingesting and fragmenting settling marine snow, mesozooplankton are key organisms for flux attenuation in Arctic waters.

Keywords: marine snow, zooplankton aggregate feeding, *in situ* optics, sediment traps, zooplankton feeding behavior

INTRODUCTION

The export of particulate organic carbon (POC) from the euphotic zone to the deep ocean is an important process in the global carbon cycle, as it governs the oceanic sequestration of atmospheric carbon dioxide (Siegenthaler and Sarmiento, 1993). This export is driven by the formation and sinking of aggregates, and attenuated by bacterial- and zooplankton-mediated degradation (Buesseler and Boyd, 2009; Iversen et al., 2017). Downward POC flux often follows a power function with increasing depth, showing high flux attenuation in the upper water column

which gets progressively lower in the deeper parts of the water column, resulting in a nearly constant flux in the deep ocean (Martin et al., 1987; DeVries et al., 2012; Marsay et al., 2015; Weber et al., 2016). This low flux attenuation in the deep ocean has been attributed to limited microbial remineralization as a result of low temperature, low dissolved oxygen and high pressure in the deep ocean (Iversen and Ploug, 2013; Tamburini et al., 2013; Marsay et al., 2015). Flux attenuation in the upper few hundred meters of the water column often exceeds the measured microbial remineralization rates, indicating that zooplankton attenuate POC flux in the upper ocean by feeding on the sinking material (Stemmann et al., 2004; Iversen et al., 2010; Jackson and Checkley, 2011).

The importance of zooplankton for flux attenuation has proven difficult to quantify *in situ* (Steinberg et al., 2008; Giering et al., 2014). *In situ* observations and on-board studies have suggested that zooplankton are responsible for decreases in aggregate abundances and changes in particle sizes at the base of the mixed layer (Lampitt et al., 1993; Stemmann et al., 2004; Iversen et al., 2010). Zooplankton feeding activity has also been suggested to be the cause of diel variations in aggregate abundances (Stemmann et al., 2000; Jackson and Checkley, 2011), and *in situ* imaging has shown that thin layers of high aggregate concentrations are also associated with increased zooplankton abundance (Möller et al., 2012).

Observational measurements have suggested that zooplankton aggregate feeding and disaggregation are more important than microbial remineralization for flux attenuation in the upper water column (Iversen et al., 2010). In contrast, respiration measurements and modeling approaches have indicated that zooplankton can be responsible for only 8 to 50% of POC flux attenuation (Steinberg et al., 2008; Giering et al., 2014). As such, Giering et al. (2014) concluded that zooplankton were responsible for only a minor part of the POC flux attenuation via direct aggregate feeding. These authors suggested that fragmentation of settling aggregates enhanced the development of the aggregate-associated microbial communities by providing more time for conversion of detritus into essential biochemical compounds (proteins and lipids) that may be efficiently harvested by the zooplankton, i.e., microbial gardening (Giering et al., 2014; Mayor et al., 2014). These results contrast with observations from experimental studies, in which several copepod species have been observed to directly feed on sinking aggregates and fecal pellets (Koski et al., 2005, 2017; Iversen and Poulsen, 2007; Lombard et al., 2013). These experiments are however difficult to translate to *in situ* POC flux attenuation due to the use of laboratory aggregates formed from fresh phytoplankton material or freshly produced appendicularian houses, while *in situ* aggregates are typically composed of older detritus material and egested compounds with lower organic matter contents (Ploug et al., 2008a).

Specialized flux feeders, such as pteropods and polychaetes, feed on sinking aggregates which they capture below the euphotic zone with their mucous feeding nets (Jackson, 1993). Zooplankton without feeding nets, such as copepods of the genera *Microsetella* (Harpacticoida) and *Oncaea* (Cyclopoida), attach to sinking aggregates and may reside for minutes to hours on the aggregates while feeding on the aggregated material (Alldredge, 1972; Ohtsuka et al., 1993; Koski et al., 2005). The genera *Pseudocalanus* and *Temora* (Calanoida) have also been observed to reside on aggregates both *in situ* and during laboratory experiments, presumably feeding on available organic matter (Möller et al., 2012; Lombard et al., 2013; Koski et al., 2017).

Copepods may recognize the hydrodynamic signals created by settling aggregates (Visser, 2001) or find and follow chemical trails of organic solutes leaking from sinking aggregates (Kiørboe and Thygesen, 2001). Such abilities increase the chance of finding sinking aggregates in the three-dimensional ocean where food sources are patchy, but have so far only been shown in *Temora longicornis* (Lombard et al., 2013). Copepods can fragment fecal pellets and marine snow into smaller, slower-sinking aggregates on which they may feed. This has been observed for *Calanus* and *Pseudocalanus* (Iversen and Poulsen, 2007) as well as other zooplankton (Dilling and Alldredge, 2000; Dilling and Brzezinski, 2004; Goldthwait et al., 2004; Poulsen and Kiørboe, 2005). Fragmentation of sinking aggregates reduces their size-specific sinking velocities and increases their surface to volume ratios, allowing more time for microbial degradation in the upper ocean, thereby increasing POC flux attenuation in the surface ocean (Lampitt et al., 1990; Mayor et al., 2014). Aggregate fragmentation has recently been hypothesized to be the primary process controlling oceanic sequestration of settling carbon (Briggs et al., 2020).

Direct evidence for interactions between zooplankton and settling aggregates are still rare and therefore their role for flux attenuation in the ocean is unclear. This is especially true for polar environments where ice-conditions make access difficult. In this study we investigated the quantitative importance of the dominant mesozooplankton genera, i.e., the calanoid copepods *Calanus* and *Pseudocalanus* as well as balanid nauplii, for POC flux attenuation in three Arctic regions. The Arctic has high POC export out of the surface ocean but this export is strongly attenuated in the upper water column (Wassmann et al., 2003). We incubated freshly collected copepods and balanid nauplii with *in situ* collected aggregates to determine aggregate grazing rates, and used direct video observations to investigate copepod and balanid nauplii feeding behavior. We combined these measurements with vertical profiles of *in situ* zooplankton and aggregate abundances and species- and size-distributions to calculate the impact of zooplankton aggregate feeding on flux attenuation in the upper 50 m of the water column. The POC flux attenuation was directly measured from sediment trap deployments and derived from *in situ* profiles of aggregate abundance and size-distribution using an *in situ* camera system.

MATERIALS AND METHODS

Sampling and incubation experiments were performed on-board the *R/V Helmer Hanssen* during the ARCEx cruise from 17 to 29 May 2016 in Hornsund, Erik Eriksen Strait, and Storfjorden (**Figure 1** and **Table 1**).

FIGURE 1 | Overview of the research locations Hornsund, Storfjorden and Erik Eriksen Strait during the Helmer Hanssen ArcEx cruise around Svalbard.

TABLE 1 | Overview of the deployments of the marine snow catcher (MSC), WP-2-net, sediment trap, *in situ* camera (ISC), and MultiNet (MN).

Location	Device	Date	Depth	Notes
Hornsund	MSC	19.05.2016	20 m	*Pseudocalanus* experiments
	WP-2	19.05.2016	90 m	*Pseudocalanus* experiments
	WP-2	19.05.2016	113 m	
	Trap	19.05.2016	20, 30, 40, 60, 90 m	Anchored
	ISC	19.05.2016	122 m	
	ISC	20.05.2016	95 m	
	ISC	20.05.2016	93 m	
	ISC	20.05.2016	126 m	
	ISC	20.05.2016	112 m	
	ISC	20.05.2016	135 m	
Erik Eriksen St.	MSC	23.05.2016	22 m	*Calanus* experiments
	WP-2	23.05.2016	40 m	*Calanus* experiments
	Trap	23.05.2016	30, 40, 60, 90, 120, 150 m	Attached to ice floe
	MN	23.05.2016	25, 50, 100, 150, 250 m	
	ISC	23.05.2016	263 m	
	ISC	23.05.2016	262 m	
	ISC	23.05.2016	235 m	
	ISC	23.05.2016	251 m	
	ISC	23.05.2016	61 m	
Storfjorden	MSC	21.05.2016	25 m	Balanid nauplii experiments
	WP-2	21.05.2016	95 m	Balanid nauplii experiments
	WP-2	21.05.2016	95 m	
	ISC	21.05.2016	86 m	

Zooplankton Collection

We collected the most abundant zooplankton genera at each station for incubations and video recordings using a WP-2 net with a mesh size of 200 μm and equipped with a large, filtering cod-end to minimize damage to the zooplankton (**Table 2**). *Pseudocalanus*, *Calanus*, and balanid nauplii were collected in Hornsund, Erik Eriksen Strait, and Storfjorden, respectively. The content of the cod-end was directly transferred into several large containers filled with surface water and stored at *in situ* temperature (0°C) in darkness. Individual adult and copepodite stage copepods and balanid nauplii were sorted using a stereo microscope and a wide-bore pipette. Sorted zooplankton were incubated overnight in GF/F filtered seawater in 25 L food grade buckets to allow them to empty their guts. The next morning, we selected healthy and actively swimming copepods and balanid nauplii and transferred them to either roller tanks, to determine grazing on aggregates, or an aquarium to record aggregate feeding behavior. As the zooplankton organisms needed to be handled quickly, we did not identify *Calanus* species or developmental stages prior to incubation but picked specimens of similar sizes (prosome length: 2.9 ± 0.5 mm) for the experiments. After the incubations, the experimental individuals were preserved in 4% formaldehyde solution in seawater, and the species were identified after the cruise in the laboratory. Identification of species of the genus *Calanus* (*C. hyperboreus, C. glacialis*, and *C. finmarchicus*) was made on the basis of prosome length measurements for each developmental stage according to Arnkværn et al. (2005). The identification showed that the *Calanus* specimens in the incubations were a mixture of C5 stages of *C. hyperboreus* and C4, C5, and adult stages of *C. glacialis*. We therefore refer to these collectively as *Calanus* spp. hereafter (**Table 3**).

Collection of Aggregates

Intact aggregates were collected with a Marine Snow Catcher (MSC, Ocean Scientific International Ltd., United Kingdom) at each station where the zooplankton were collected. The MSC is a 100 L water sampler which does not destroy large aggregates during sampling (e.g., Belcher et al., 2016a; Busch et al., 2017; Flintrop et al., 2018). The MSC was lowered open to 10 m below the fluorescence maximum whereupon it was closed immediately using a releaser and a messenger before it was brought back on deck. We left the MSC on deck for approximately 3 h to allow the aggregates to settle to the bottom compartment. The height of the MSC was 2 m, which means that aggregates sinking faster than 18 m d^{-1} would able to sink from the top to the bottom of the MSC during 3 h. Hereafter, we gently drained and GF/F filtered the overlaying water and stored it for use during grazing incubations, video observations, and acclimation of the copepods. The bottom part of the MSC was brought to the

TABLE 2 | Zooplankton abundance in the upper 25 m of the water column at Hornsund, Erik Eriksen Strait, and Storfjorden.

Zooplankton type	Copepod stage	Hornsund – WP-2		Erik Eriksen Strait – MN		Storfjorden – WP-2	
		Abundance (ind m^{-3})	Biomass (mg DW)	Abundance (ind m^{-3})	Biomass (mg DW)	Abundance (ind m^{-3})	Biomass (mg DW)
C. finmarchicus	C1	0.00	0.00	0.00	0.00	0.00	0.00
C. finmarchicus	C2	0.00	0.00	0.00	0.00	6.65	0.31
C. finmarchicus	C3	3.32	0.15	0.00	0.00	9.97	0.46
C. finmarchicus	C4	6.65	0.85	37.33	4.78	3.32	0.43
C. finmarchicus	C5	8.31	2.28	93.33	25.57	46.55	12.75
C. finmarchicus	Adult female	4.99	1.63	10.67	3.49	40.00	13.05
C. finmarchicus	**Sum of all stages**	**23.27**	**4.91**	**141.33**	**33.84**	**106.39**	**26.99**
C. glacialis	C1	3.32	0.02	10.67	0.07	16.62	0.12
C. glacialis	C2	1.66	0.07	0.00	0.00	3.32	0.14
C. glacialis	C3	6.65	0.29	2.67	0.12	0.00	0.00
C. glacialis	C4	38.23	6.46	162.67	27.49	19.95	3.37
C. glacialis	C5	11.64	9.05	32	24.90	13.30	10.35
C. glacialis	Adult female	18.29	16.27	42.67	37.93	33.25	29.59
C. glacialis	**Sum of all stages**	**79.79**	**32.17**	**250.67**	**90.55**	**86.44**	**43.57**
C. hyperboreus	C1	14.96	0.11	53.33	0.37	83.12	0.58
C. hyperboreus	C2	0.00	0.00	0.00	0.00	6.65	0.29
C. hyperboreus	C3	0.00	0.00	0.00	0.00	0.00	0.00
C. hyperboreus	C4	0.00	0.00	0.00	0.00	0.00	0.00
C. hyperboreus	C5	1.66	1.70	53.33	54.45	6.65	6.79
C. hyperboreus	Adult female	0.00	0.00	0.00	0.00	0.00	0.00
C. hyperboreus	**Sum of all stages**	**16.62**	**1.80**	**106.67**	**54.83**	**96.42**	**7.66**
Pseudocalanus spp.	C1	0.00	0.00	0.00	0.00	0.00	0.00
Pseudocalanus spp.	C2	0.00	0.00	0.00	0.00	0.00	0.00
Pseudocalanus spp.	C3	1.66	0.04	0.00	0.00	0.00	0.00
Pseudocalanus spp.	C4	34.91	0.80	5.33	0.12	9.97	0.23
Pseudocalanus spp.	C5	118.03	2.72	5.33	0.12	49.87	1.15
Pseudocalanus spp.	Adult female	29.92	0.69	16.00	0.37	123.01	2.83
***Pseudocalanus* spp.**	**Sum of all stages**	**184.52**	**4.24**	**26.67**	**0.61**	**182.86**	**4.21**
Other copepods		92.68	2.45	186.67	4.93	132.99	3.51
Calanoid nauplii		8.83	0.01	3469.33	3.47	4511.58	4.51
Balanid nauplii		**160.72**	**0.32**	**0.00**	**0.00**	**2686.34**	**5.37**
Other zooplankton		4.05	0.15	10.67	0.40	43.22	1.61
Investigated zooplankton							
Calanus spp.	**Sum of all**	119.68	38.88	**498.67**	179.22	289.25	78.22
Pseudocalanus spp.	**Sum of all**	**184.52**	4.24	26.67	0.61	182.86	4.21
Balanid nauplii		160.72	0.32	0.00	0.00	**2686.34**	5.37

At Hornsund and at Storfjorden the zooplankton were collected by a WP-2 net with mesh-size of 200 μm. At Erik Eriksen Strait the zooplankton were collected by a MultiNet with a mesh-size of 200 μm. Bold fonts in the upper panel indicate the sum of all stages for Calanus finmarchicus, C. glacialis, C. hyperboreus, Pseudocalanus spp. and balanid nauplii. Bold fonts in the lower panel indicate the most abundant of the investigated zooplankton at each of the three regions.

laboratory and kept at 0°C in darkness until the aggregates were picked for experiments.

Grazing Incubations

Grazing rates on settling aggregates of balanid nauplii, adults and copepodites IV and V of *Calanus* spp., and egg-bearing females of *Pseudocalanus* spp. were determined in roller tanks (1.15 L, diameter: 14 cm, depth: 7.5 cm). Roller tanks are cylindrical aquariums that are rotated with three rounds per minute on a roller table. The rotation creates solid body rotation of the water within the roller tanks, which gently keeps aggregates and zooplankton suspended without introducing turbulence, much like settling through an infinite tube (see Shanks and Edmondson, 1989). We executed one incubation experiment for each of the three zooplankton organisms. For each experiment, five roller tanks were filled with GF/F filtered water from the MSC and 20 balanid nauplii, three or four *Calanus*, or ten *Pseudocalanus* females gently added to each roller tank (**Table 3**). We picked similar types, sizes and amounts of aggregates from the MSC collection into 10 Petri dishes for each experiment. We removed all copepod fecal pellets from the Petri dishes and photographed each dish to analyze the aggregate sizes in order to determine

TABLE 3 | Overview of the three grazing incubations; *Calanus* spp. experiment, *Pseudocalanus* spp. experiment, and balanid nauplii experiment.

Experiment/roller tank	Incubation time (days)	Zooplankton incubation species (stage)	Start POC_{AGG} (μg POC)	End POC_{AGG} (μg POC)	Ingestion rate (μgPOC ind^{-1} d^{-1})
Calanus* spp. *experiment					
Roller tank 1	1.15	*C. glacialis* (2xC4, 2xC5)	80	32.9	10.22
Roller tank 2	1.24	*C. glacialis* (1xm, 1xf, 1xC4)	109.5	37.0	19.47
Roller tank 3	1.26	*C. hyperboreus* (4xC5)	85.2	35.8	9.81
Roller tank 4	1.29	*C. hyperboreus* (2xC5) *C. glacialis* (2xC4)	100.7	15.6	16.48
Roller tank 5	1.33	*C. hyperboreus* (2xC5) *C. glacialis* (1xC4, 1xC5)	107.6	48.5	11.11
Average ± SD	1.25 ± 0.07		96.60 ± 13.32	33.96 ± 11.86	13.43 ± 4.33
Pseudocalanus* spp. *experiment					
Roller tank 1	1.54	10 x *Pseudocalanus* spp.	98.3	27.4	4.60
Roller tank 2	1.54	10 x *Pseudocalanus* spp.	129.2	43	5.60
Roller tank 3	1.63	10 x *Pseudocalanus* spp.	87.4	38.9	2.98
Roller tank 4	1.65	10 x *Pseudocalanus* spp.	164.1	43.5	7.31
Roller tank 5	1.69	10 x *Pseudocalanus* spp.	160.2	17.2	8.46
Average ± SD	1.61 ± 0.07		127.80 ± 34.90	34.00 ± 11.41	5.79 ± 2.17
Balanid nauplii experiment	**Incubation time (days)**	**Zooplankton incubation (ind roller $tank^{-1}$)**	**FP production (# ind^{-1} d^{-1})**	**FP production (μgPOC ind^{-1} d^{-1})**	**Ingestion rate (μgPOC ind^{-1} d^{-1})**
Roller tank 1	1.69	20 x balanid nauplii	1.54	0.05	0.14
Roller tank 2	1.79	20 x balanid nauplii	1.68	0.05	0.15
Roller tank 3	1.85	20 x balanid nauplii	1.81	0.06	0.16
Roller tank 4	2.35	20 x balanid nauplii	1.23	0.04	0.11
Roller tank 5	2.43	20 x balanid nauplii	1.24	0.04	0.11
Average ± SD	2.02 ± 0.34		1.5 ± 0.26	0.05 ± 0.01	0.13 ± 0.02

The table shows the incubation time and number, type, and stage of zooplankton incubated for each roller tank in each experiment. For the Calanus and Pseudocalanus experiments we were able to measure start and end concentrations of aggregates POC. This was not possible for the balanid nauplii experiments and we therefore used the fecal pellet production as an estimate for their grazing on aggregates (see section "Aggregate Feeding Rate" in the Results).

the amount of aggregated material which was added to each roller tank. To determine the initial POC concentrations of the added aggregates, the contents of five of the ten Petri dishes were filtered onto one pre-combusted GF/F filter and total POC concentration was measured on a GC elemental analyzer (see below). The photographs of the aggregates in the five Petri dishes that were filtered for POC were analyzed to calculate the total filtered aggregate volume. Hence, using the measured POC concentration and aggregate volumes, we determined the start POC to volume ratios of the incubated aggregates from which we calculated the start aggregate POC for each roller tank (**Table 3**). Note that the MSC collection did not contain enough *in situ* collected marine aggregates to measure the POC content of the aggregates added at the start of the incubation for balanid nauplii. We instead used the fecal pellet production to estimate their feeding rate on aggregates (see section "Aggregate Feeding Rate" in the Results). The roller tanks were incubated on a roller table that rotated with three rounds per min for >1 day in darkness at *in situ* temperature (0°C) (**Table 3**). The slow rotation speed of the roller table was adjusted to keep the aggregates in suspension and at the same time taking care not to disturb the zooplankton feeding behavior. At the end of the incubation we gently picked all copepods and balanid nauplii and ensured that they were alive before preservation in 4% formaldehyde solution for later genus and developmental stage identification. All visible aggregates from each roller tank were carefully transferred to a Petri dish using a wide-bore pipette. The remaining particles and fecal pellets were gently concentrated by gravity filtration through a 5 μm mesh. All fecal pellets were separated from the aggregates and particles. Both fecal pellets and aggregates were photographed to determine sizes and abundances. All collected aggregates from the five roller tanks for each incubation experiment were pooled and filtered onto one pre-combusted GF/F filter for later POC determinations. The POC to volume ratios were used to determine the amount of aggregate POC in each roller tank at the end of the incubation.

POC Determination

The filters with the pooled aggregates were dried at 40°C for 24 h, fumed with 37% HCL to remove inorganic carbon, and analyzed with a GC elemental analyzer (Elementar vario EL III, precision of ±0.7 μg C or ±0.3%) to obtain the total POC. We corrected for eventual contamination by measuring POC values of blank filters. Images of aggregates filtered at the start and end of the incubations were analyzed with the program ImageJ to determine the size of each individual aggregate. The images were converted into 8-bit, the background removed by duplicating the image and blurring the duplicate with a Gaussian Blur (200

pixel radius) before subtracting the duplicate from the original image. This created an even, dark background that was removed with a manual threshold of pixel-intensity 10, which identified all aggregates as objects that were having pixel-intensities brighter than 10. We calculated the equivalent spherical diameter (ESD) from the projected area of each aggregate. POC content per aggregate was calculated from their volumes using the measured POC to volume ratios determined at the start and at the end of the grazing incubations. Since marine snow aggregates have increasing porosities with increasing sizes, their size-specific POC content is best described by a power function $POC = a \times V^b$, where the POC content of an aggregate was in μg C, the aggregate volume V was in mm^3, b was fixed to 0.5, and a was a constant that was fitted to the volume of each aggregate so the sum of aggregate POC matched the measured POC for the pooled aggregates (after Alldredge, 1998, 2000; Alldredge et al., 1998; Ploug and Grossart, 2000). The volumetric POC relationship for the aggregates filtered at the start of the experiment was applied to aggregates added to the roller tanks to obtain the start aggregate POC concentration for each roller tank (POC_{start}). The volumetric POC relationship for the aggregates filtered at the end of the experiment was used to calculate the aggregate POC concentration at the end of the incubation (POC_{end}). Carbon ingestion from aggregate feeding was estimated by dividing the carbon loss per roller tank by the number of individual zooplankton in the roller tank and the incubation time.

Video Recordings

The video recordings were done in an aquarium (5 × 5 × 20 cm) with two Basler acA1300-30gc cameras (1 Mega-pixel, IR-filter removed) recording simultaneously from the front and left side of the aquarium. The aquarium was illuminated from the back and right side with two infrared-backlights (MBJ DBL plate, 880 nm, and custom-build plate with Vishay LEDs, 850 nm). This provided two camera views with back lighting from which we obtained 90° stereoscopic shadow images of the aggregates and copepods. One of the cameras was placed in a fixed position and used to determine the swimming speed of the copepods, and the size and sinking velocity of the settling aggregates. The other camera was attached to a stand that allowed movements in *x*-, *y*- and *z*- directions in order to keep individual aggregates in focus while they sank through the aquarium. Zoom and focus were kept constant for both cameras during the incubations to obtain a constant pixel-size of the recordings. All video recordings were done in darkness, with only infrared illumination, at *in situ* water temperature (0°C). The aquarium was filled with GF/F filtered seawater from the MSC. Copepods and balanid nauplii were allowed to acclimate in the aquarium for 1 h prior to filming. In order to ensure that enough individuals were in the middle of the aquarium (field of view of the camera), we added 30 balanid nauplii, 10 *Calanus* and 20 *Pseudocalanus* specimen, respectively. This was four-fold the concentration compared to the roller tank incubations (**Table 3**). However, we did not observe that the copepod or balanid nauplii abundances caused interactions and stress among the organisms during the incubations, and generally just a few of the individuals were in the middle of the aquarium simultaneously. Aggregates were first placed in a Petri dish containing seawater from the aquarium to ensure that the temperature and salinity of the pore water in the aggregates was similar to that in the aquarium. During a video sequence, one aggregate was gently transferred from the Petri dish to the aquarium with a wide bore-pipette. The aggregate was allowed to sink out of the pipette and into the aquarium. The aggregate was kept in focus during its descend through the aquarium. The aggregates ranged in size from 0.06 to 1.22 mm with settling velocities between 0.8 to 381 m d^{-1}. It typically took an aggregate 5 min to sink through the aquarium, whereafter the cameras and infrared lights were switched off for 5 min to minimize water heating and to dilute any chemical trails left in the wake of the previously recorded aggregate.

Video Analyses

In total 98, 73, and 65 individual aggregates were allowed to sink through the aquarium for feeding behavior investigations of *Calanus*, *Pseudocalanus*, and balanid nauplii, respectively. All video sequences were analyzed frame by frame to detect all zooplankton-aggregate interactions. We did not detect any encounters between balanid nauplii and aggregates during our video recordings (approximately a total of 5 h of video recordings). We identified four main responses upon encounters between copepods and sinking aggregates: attachment, avoidance, rejection and no reaction. Attachment was defined as a situation in which a copepod stayed attached to an aggregate for longer than 1 s. Rejection was defined when a copepod that attached to an aggregate for a period shorter than 1 s either detached from it or, for small aggregates, 'kicked' the aggregate away from its feeding appendages. Avoidance was defined when a copepod swam toward an aggregate but changed its swimming direction in the vicinity of the aggregate, seemingly to avoid encounter. No reaction was defined when a copepod was close to an aggregate without showing any visible reaction to the presence of the aggregate. This also included copepods that were swimming into an aggregate without altering swimming speed or direction and without attaching to the aggregate. For each response, the detection distance (distance at which a reaction was observed: <69 mm) and position of the copepod relative to the aggregate (above, below, beside) was recorded together with the impact of the encounter (e.g., whether the aggregate settling was altered or if the aggregate was fragmented). All events when aggregates were not within detection distance (>69 mm) of a copepod were defined as 'other.' Additionally, we recorded the duration of each attachment and any change in aggregate volume caused by the attachment. Aggregate sizes were determined by measuring the *x*- and *y*-axes of the aggregates in a video frame captured by the fixed camera. The shorter of the two axes was used as z-axis to calculate the volume of an aggregate assuming an ellipsoid form [Sun and Liu, 2003, Eq. (1)]. When possible, control measurements of the *z*-axes were done using the footage from the other camera, and a comparison of both methods showed good matches.

The aggregate volume (V, mm^3) was calculated using the *x*, *y*, and *z* lengths (mm), based on the following formula:

$$V = \frac{\pi}{6} xyz \quad (1)$$

The ESD was calculated from the aggregate volume as follows:

$$ESD = 2 \times \left(\frac{3}{4} V \times \frac{1}{\pi} \right)^{\frac{1}{3}} \quad (2)$$

Aggregate sinking velocity was determined using the fixed camera only, by analyzing the trajectory of the settling aggregate in ImageJ using the plugin MTrackJ. The length of the vertical trajectory was divided by the number of frames of the track and multiplied with the frame rate (frames s^{-1}) to obtain the sinking velocity. When possible, we determined aggregate volume and sinking velocity before the aggregates had encountered zooplankton.

Calculating *in situ* Zooplankton Aggregate Feeding

Zooplankton Abundance

We used a MultiNet (Midi, Hydro-Bios, Kiel) with nets of 200 μm mesh-size to determine the abundance of zooplankton in five depth-intervals in Erik Eriksen Strait (**Table 2**). Due to a malfunction of the MultiNet, a WP-2 net (200 μm mesh-size) without closing mechanism was used to determine zooplankton abundance in Hornsund and Storfjorden. Sampling was done in one vertical net haul, thus, the vertical distributions at these stations could not be determined. The flow-meter on the MultiNet showed that the filter-efficiency was 0.77 and we assumed that the WP-2 had a similar filter-efficiency. The MultiNet analyses showed that 72% of all *Calanus* and 69% of all *Pseudocalanus* resided in the upper 25 m. We therefore assumed that this was similar for the WP-2 nets from Hornsund and Storfjorden. All zooplankton samples were preserved in 4% formaldehyde solution buffered with Borax and analyzed in the home laboratory. Biomass was estimated using literature values for the dry weight of specific copepod developmental stages (Richter, 1994).

In situ Aggregate Size and Abundance

The vertical aggregate abundance and size-distribution was measured with an *in situ* camera system (ISC) in Hornsund, Storfjorden and Erik Eriksen Strait. The ISC is a camera system that is illuminated by an infrared backlight (Markussen et al., 2020). During our cruise, the ISC sampled a water volume of 20 ml every 15 cm during the down-cast. The pixel size was 24 μm, resulting in quantitative detection of particles that have ESDs > 100 μm. The ISC was connected to a SeaBird 19 CTD that was equipped with a fluorescence sensor. We processed the images with the Imaging Processing Toolbox in Matlab (The Mathworks) to characterize individual particles (see Markussen et al., 2020). The size of a particle was determined from its area and converted into ESD. Detected particles were sorted into logarithmically spaced size bins based on their ESDs. The concentration particle size spectra (n_C) were calculated for each size bin from the particle number concentration (ΔN_C) within a given size bin (Δd) for each water depth imaged:

$$n_c = \frac{\Delta N_C}{\Delta d} \quad [\#m^{-3}\ cm^{-1}] \quad (3)$$

We binned 10 images and obtained a vertical depth-resolution of ∼1.5 m.

POC Fluxes and Attenuation From Sediment Traps

We deployed drifting sediment traps in Hornsund and Erik Eriksen Strait. The sediment trap cylinders (KC Denmark A/S, Ø 7.2 cm, 45 cm long) were deployed at 20, 30, 40, 60, and 90 m in Hornsund and at 30, 40, 60, 90, 120, and 150 m depth in Erik Eriksen Strait. Each collection depth was equipped with four sediment trap cylinders. The deployment time was 20 h and 50 min in Hornsund and 23 h in Erik Eriksen Strait. We transferred the content from the four trap cylinders at each collection depth into a carboy immediately after recovery and stored the carboys at 0°C in darkness for a maximum of 6 h while filtrations for biogeochemical analyses were done. We subsampled the exported material from the carboys to determine POC fluxes from each collection depth. This was done by filtering the subsamples onto pre-combusted GF/F filters in triplicates within 6 h after the sediment trap array was retrieved. The filters were immediately frozen and stored at −20°C until arrival at the laboratory where the samples were dried for 48 h at 50°C, fumed with fuming HCl (37%) for 24 h to remove calcium carbonate, and analyzed with a GC elemental analyzer (Elementar vario EL III). We used the POC flux from 30 and 60 m (F_{30} and F_{60}, respectively) to calculate the fractional loss in carbon flux between the two depths. This was calculated by $1\text{-}F_{60}/F_{30}$. This approach assumes that the settling aggregates sank vertically through the water column and that the flux at 60 m was directly comparable to that at 30 m, i.e., vertical downward export.

Volumetric POC Relationships

We redeployed the traps at the same location immediately after each recovery of the first and long trap deployment in Hornsund and Erik Eriksen Strait. For the second trap deployment we only deployed two trap cylinders at each collection depth (20, 30, 40, 60, and 90 m). One trap cylinder at each depth was equipped with an insert cup that was filled with a viscous gel (TissueTek, OCT, cryogel from Sakura Finetek), which allowed preservation of size and three-dimensional structure of the aggregates collected in the gel trap (Wiedmann et al., 2014; Thiele et al., 2015; Flintrop et al., 2018). The second trap cylinder from each depth was used to collect biogeochemical fluxes, as described above. The second trap deployment lasted between 2 and 3 h to ensure that the settling aggregates did not overlap in the gel traps. After recovery, the content of the gel-free trap cylinder from each depth was transferred to one carboy and analyzed as described above. The gel traps were gently removed from the collection cylinder and frozen until imaging in the home laboratory. The images were analyzed as described in Wiedmann et al. (2014) to determine size, abundance, and

types of the collected particles and aggregates. We determined the size-specific POC content of the aggregates collected at each depth in the gel traps using a power function to relate the total POC content that was collected by the trap cylinder which was deployed simultaneously with the gel traps. The size-specific POC content was calculated by a power function $POC = a \times V^b$, where the POC content of an aggregate was in μg C, the aggregate volume V was in mm^3, b was fixed to 0.5, and a was a constant that was fitted to the volume of each aggregate collected in the gel traps. We adjusted a until the sum of aggregated POC from the gel traps matched the total measured POC collected by sediment trap cylinder. As there was no gel trap deployed in Storfjorden, we used the volumetric POC relationship of the MSC aggregates from the *Pseudocalanus* incubation, which was within the range of those determined for the gel traps.

POC Attenuation From ISC

We used the vertical particle size-distribution and abundance measured with the ISC to calculate POC concentration profiles for the size-range of aggregates that the ISC detected. This was calculated by applying the volumetric POC relationships, as determined from the gel trap deployments, to the different particle abundances for each size bin from the ISC, and summed the total POC concentrations from all size bins for each depth. To identify the depth interval in which the highest POC degradation took place, we plotted the POC concentration over depth and identified the depth range with the largest rate of change. This was identified from the POC peak (POC_{peak}, typically found between 5 and 20 m) and the depth where the rapid decline in POC concentrations ceased and the POC concentration became quasi constant with increasing depth (POC_{low}, typically 18 to 25 m below the depth of POC_{peak}). The fractional POC loss through this depth interval was calculated by 1-POC_{low}/POC_{peak}.

Encounter and Ingestion Rates

Encounter and ingestion rates for *Calanus* and *Pseudocalanus* were calculated as described in Koski et al. (2005) with slight adaptations, using parameters obtained from the incubations and video recordings (see units and values in **Table 4**). All ingestion rates were determined from the roller tank incubations while the copepod feeding behavior, encounter rate, detection distance, time a copepod spend on an aggregate, aggregate size-specific settling velocity, and copepod swimming speed were determined from the video recordings (**Table 4**). We did not observe any encounters between balanid nauplii and aggregates during the video recordings and, therefore, we only applied the following calculations to *Calanus* spp. and *Pseudocalanus* spp. The encounter kernel β describes the volume of water that a copepod can search per unit time for a given aggregate radius:

$$\beta(r) = v \times \pi \times \left(\frac{s}{2} \times l \times r\right)^2 \quad (4)$$

where v is the average swimming speed (including pause events), s is the total length of the copepod's first antenna, l is the detection distance at which the copepod can perceive a sinking aggregate, and r is the ESD radius of the sinking aggregate.

TABLE 4 | Parameters obtained from the experiments and *in situ* measurements used for calculating *in situ* aggregate feeding.

Parameter		Unit	*Calanus*	*Pseudocalanus*
Sinking velocity	sv	m d^{-1} (ESD:mm)	$48*ESD^{0.85}$	
Antenna length	h	mm	5.7	1.7
Detection distance	l	mm	0.69	0.69
Swimming velocity	v	mm s^{-1}	1.21	0.89
Fraction attachments	f		0.07	0.49
Time on aggregate	δ	s	35	12
Ingestion rate	i	μg C s^{-1} (r:mm)	$\frac{0.117}{1+e^{\frac{0.697-r}{0.161}}}$	$\frac{0.0322}{1+e^{\frac{0.379-r}{0.0966}}}$
POC content		μg C (vol:mm^3)		
Erik Eriksen St			$4.29*vol^{0.5}$	
Hornsund			$0.84*vol^{0.5}$	
Storfjorden			$3.19*vol^{0.5}$	

Sinking velocity was obtained from the video recordings of aggregates from Storfjorden, the length of the first antenna, detection distance, swimming velocity, the fraction of interactions that leads to an attachment, and the time spend on an aggregate were determined from the video recordings. The ingestion rates were fitted to the incubation experiments using the previous parameters. The POC content of an aggregate was determined from the sediment traps at Erik Eriksen St and Hornsund, and the MSC at Storfjorden.

Using β, the numbers of copepods that a sinking aggregate with radius r encounters during its descent through a water column of depth z is:

$$E(r) = \beta(r) \times C \times \frac{z}{u(r)} \quad (5)$$

where C is the average copepod concentration over depth z, and (ur) is the size-specific aggregate sinking velocity. The fractional degradation (κ) caused by copepod feeding of an aggregate that sinks to depth z is:

$$\kappa(r) = \frac{E(r) \times \alpha \times i \times \delta}{POC(r)} \quad (6)$$

where α is the fraction of encounters that lead to attachment, δ is the time a copepod spends on an aggregate, i is the carbon ingestion rate of a copepod when feeding on an aggregate and $POC(r)$ is the size-specific POC-content of the aggregate. All input parameters were directly obtained from the video recordings and the incubations. For δ we averaged the attachment times, as there was no relationship between aggregate size and time spend on the aggregate. We therefore assume that the ingestion (i) is a sigmoid function of aggregate size (since small aggregates contain little POC but can be ingested whole and ingestion per time on large aggregates reach a maximum independent on how much POC the aggregate contains):

$$i = \frac{a}{1 + e^{\frac{b-r}{c}}} \quad (7)$$

To fit the parameters a, b, and c for i, we first calculated i by assuming that κ was constant for different aggregate sizes and used the overall fractional degradation found from the roller tank incubations as a value for κ. We then fitted a sigmoid curve to the i values against aggregate sizes using the non-linear least-squares method in R (nls) and used the

resulting fit to determine the size-specific i for each of the investigated copepod species and aggregate types found at the three locations (Hornsund, Storfjorden, and Erik Eriksen Strait). In this way, Eq. (6) provided the total ingestion by copepods that a settling aggregate with a given radius would be exposed to as it sinks through a water depth with a known copepod concentration.

Calculating POC Attenuation by Zooplankton

Using the previously fitted parameters, the concentration of *Pseudocalanus* and *Calanus* in the upper 25 m, the depth interval z per ISC cast, and the POC_{peak} from the ISC casts, we calculated the *in situ* encounter kernel β, the number of encounters E, and the fraction degradation κ. The POC degradation per aggregate size-bin by each zooplankton (POC_{zoo}) is multiplied by the start POC (POC_{peak}) per size-bin. The fraction of POC that is degraded by zooplankton is:

$$\kappa_{tot} = 1 - \frac{\Sigma POC_{zoo}}{\Sigma POC_{peak}} \quad (8)$$

where both POC values are summed for all aggregate sizes (sum of all aggregate size-bins). We also estimated the microbial degradation, assuming the carbon-specific degradation is 0.03 d^{-1} (Morata and Seuthe, 2014; Belcher et al., 2016b):

$$\kappa_{micro}(r) = 1 - e^{-\frac{0.03}{u(r)} * z} \quad (9)$$

RESULTS

On-Board Experiments

Aggregate Feeding Rates

We performed aggregate feeding incubations with three dominant zooplankton representatives: copepods of the genera *Pseudocalanus* and *Calanus* and balanid nauplii at each of the three investigated regions: Hornsund, Erik Eriksen Strait, and Storfjorden, respectively (**Table 2**). The *Calanus* incubations were carried out with a mixture of different stages of *Calanus glacialis* and *Calanus hyperboreus* with an average prosome length of 3.08 ± 0.38 mm (SD, here and in the following text). *Pseudocalanus* incubations were carried out only using adult females with an average prosome length of 0.85 ± 0.08 mm (**Table 3**). Two species of the genus *Pseudocalanus* (*P. minutus* and *P. acuspes*) commonly occur in the regions studied, and their *in vivo* distinction is practically impossible. For this reason, it was assumed that the results of the incubation experiments should be treated as representative for genera and not specific species. When describing results we refer to *Calanus* or *Pseudocalanus*.

The average ingestion rate of *Calanus* was three times higher than that of *Pseudocalanus* (13.4 ± 4.34 and 5.79 ± 2.17 μg C ind^{-1} d^{-1}, respectively). We only had a limited number of collected aggregates for the balanid nauplii incubations, which were not enough to measure a start POC concentration (see section "Materials and Methods"). We therefore decided to estimate the ingestions from the fecal pellet numbers and sizes at the end of the experiments. However, the balanid nauplii only produced 1.5 fecal pellets ind^{-1} d^{-1} during the incubations and even when pooling all the pellets on one filter there was not enough material to be above the detection limit for the elemental analyzer. We measured the sizes of 27 of the produced pellets, which were on average 135 ± 31 μm long, with an average diameters of 71 ± 15 μm, resulting in an average volume of $3.9 \pm 1.9 \times 10^4$ mm^3, when using Eq. (1) to calculate the volume of an ellipsoid. We used POC to volume ratios of 80 μg C mm^{-3} for Arctic copepods provided by Reigstad et al. (2005) to estimate the POC content of the balanid fecal pellets. The average volume of a balanid fecal pellet was 0.0004 mm^3, which suggested that each pellet contained 0.03 μg C. A rough estimation of ingestion has traditionally assumed that one third is egested, one third used for growth and one third is respired (Kiørboe et al., 1985; Lenz et al., 1993; Båmstedt et al., 1999). Using those assumptions and the egestion rate of 1.5 fecal pellets ind^{-1} d^{-1} (0.05 ± 0.01 μgC ind^{-1} d^{-1}), we estimated that one balanid nauplii ingested 0.14 ± 0.02 μg C ind^{-1} d^{-1} during the aggregate grazing incubations (**Table 3**).

Aggregate Size, Sinking Velocity and Interactions

Aggregates used in the incubations with *Calanus* and *Pseudocalanus* were of similar size, with an average ESD of 0.35 ± 0.27 mm and 0.39 ± 0.28 mm, respectively (Wilcoxon rank sum test, $p = 0.37$). Aggregate sinking velocities measured during the experiment with *Calanus* were on average three-fold higher (92 ± 98 m d^{-1}, $n = 98$) than those measured during the experiments with *Pseudocalanus* (28 ± 25 m d^{-1}, $n = 73$), however, they were not significantly different (Spearman Rank Order Correlation, $p > 0.05$). The differences in the average sinking velocities was due to some large and fast-settling aggregates in the *Calanus* video incubations, which sank through the aquarium without being within detection distance of the copepods.

Copepod Feeding Behavior on Settling Aggregates

Pseudocalanus reacted to a higher fraction of the aggregates in its vicinity (within detection distance) than *Calanus*, and only 6% of the aggregates that were within 0.5 body-length from *Pseudocalanus* did not cause a behavioral response, compared to 48% for *Calanus* (**Supplementary Video 1**). We observed two clear ingestion events for *Calanus* (reaction to 7% of the aggregates in their vicinity) with one event involving a small slow-sinking aggregate (ESD 0.1 mm, SV 5.9 m d^{-1}) and one event involving a larger aggregate (ESD 0.3 mm, SV 58 m d^{-1}, **Supplementary Video 2**). During these two events *Calanus* attached to the aggregates for 2.3 s and 67.5 s, respectively. Four attachments resulted in rejections within 1 s after attaching. In these cases aggregate ESDs ranged between 0.15 and 0.22 mm and the aggregates sank with velocities between 3 and 17 m d^{-1} (**Supplementary Video 3**). Seven aggregates were actively avoided, of which four had sinking velocities higher than 100 m d^{-1}. In contrast, *Pseudocalanus* attached more frequently to aggregates, with 26 recorded attachments. Here aggregate ESDs ranged between 0.06 and 0.83 mm and sinking velocities were between 0.8 and 58 m d^{-1} (**Supplementary Video 4**). The average attachment time was 12 ± 14.5 s (range: 1 to 66 s). *Pseudocalanus* actively avoided 21 aggregates, with ESDs ranging

between 0.1 and 1.22 mm and sinking velocities between 2.7 and 96 m d^{-1} (**Supplementary Video 5**). Four aggregates were rejected directly upon attachment, with ESDs ranging between 0.04 and 0.55 mm and sinking velocities between 3 and 48 m d^{-1}.

Detection Distance

The two observed *Calanus* attachments were established by copepods that approached the aggregate from the side, and detected the aggregate at a distance of 0.69 ± 0.08 mm (**Supplementary Video 2**, **Figure 2**). The aggregates that were avoided (**Supplementary Video 3**, **Figure 2**) were in a similar proximity (0.67 ± 0.63 mm), although when the copepod was swimming above the sinking aggregate this distance was slightly larger (0.95 ± 0.69 mm). We observed *Calanus* to encounter aggregates during swimming events without capturing the aggregates, however, some of these encounters fragmented the aggregates. Most of the *Pseudocalanus* attachments occurred during filter feeding events while the aggregate sank into the feeding current from above, whereupon the filter feeding activity would be interrupted and the copepod would capture and attach to the aggregate by grapping it with the mandibles (**Supplementary Video 4**, **Figure 2**). The average detection distance for these events was 0.46 ± 0.40 mm, whereas the detection distance for copepods that approached aggregates from above or aside was 1.08 ± 0.85 mm and 0.78 ± 0.43 mm, respectively. Avoidance events occurred within similar reaction distances as those observed for the attachment events. One exception occurred when a copepod swam 13.4 mm above the aggregate and followed the track of the sinking aggregate (likely following the chemical trail at the wake of the aggregate) but avoided it from a distance of 0.96 mm (ESD 0.81, SV 84 m d^{-1}) (**Supplementary Video 5**, **Figure 2**). Additionally, four aggregates were rejected within 1 s upon attachment.

In situ Zooplankton Aggregate Feeding

Zooplankton Abundances

The total copepod abundance was the highest in Erik Eriksen Strait and the lowest in Hornsund (**Table 2**). Calanoid nauplii contributed 83% to the total zooplankton abundance in Erik Eriksen Strait, balanid nauplii contributed 28% to the total zooplankton abundance at Hornsund, and nauplii from copepods and balanid contributed 91% to the total zooplankton abundance in Storfjorden (**Table 2**). Combined *Calanus* spp. and *Pseudocalanus* spp. contributed to the total zooplankton abundance with 13%, 53%, and 6% in Erik Eriksen Strait, Hornsund, and Storfjorden, respectively (**Table 2**). *Calanus* abundances in the upper 25 m (NB: only Erik Eriksen Strait were sampled with MultiNet while the other two were sampled with WP-2 in the full water column – see "Materials and Methods") were 120, 498, and 289 ind. m^{-3}, *Pseudocalanus* abundances were 185, 27, and 183 ind. m^{-3}, and balanid nauplii abundances were 161, zero, and 2686 ind. m^{-3} in Hornsund, Erik

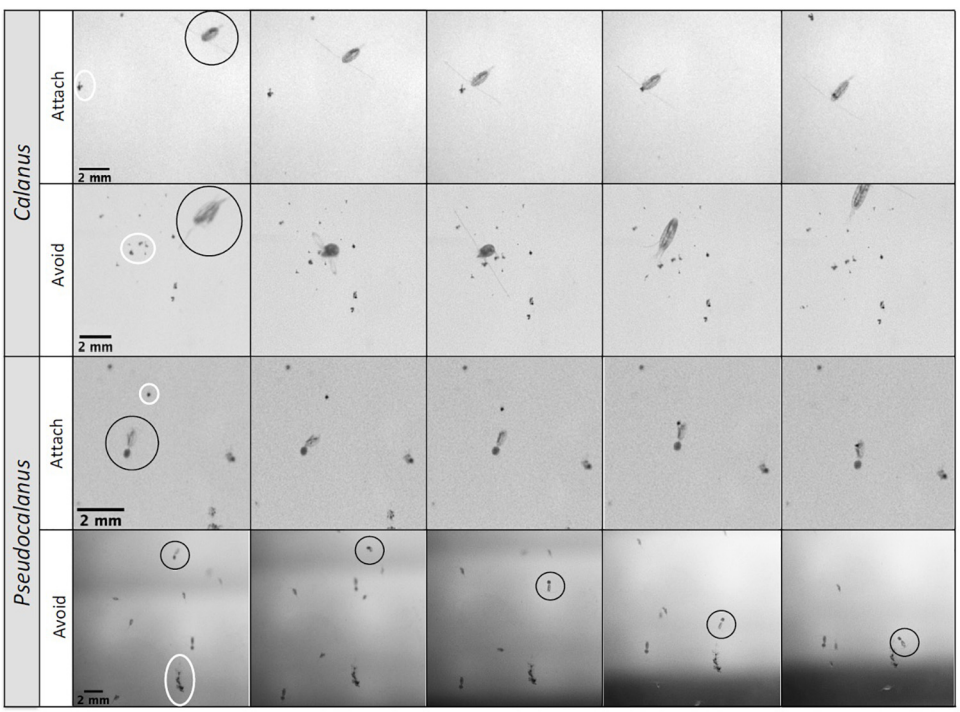

FIGURE 2 | Stills from videos with interactions between copepods (marked with black circles) and sinking aggregates (marked with white circles). ***Calanus* Attach:** *Calanus* spp. swims from the side toward an aggregate and attaches to it. ***Calanus* Avoid:** *Calanus* spp. swims, changes course, touches an aggregate with its swimming legs (3rd photo), and jumps away. ***Pseudocalanus* Attach:** *Pseudocalanus* spp. female is filter feeding, jumps, swims toward the sinking aggregate, attaches to the aggregate with its swimming legs, and sinks while feeding. ***Pseudocalanus* Avoid:** *Pseudocalanus* spp. (circle) swims back and forth 13 mm above a sinking aggregate, follows its trail down, but swims away from the aggregate when in the vicinity.

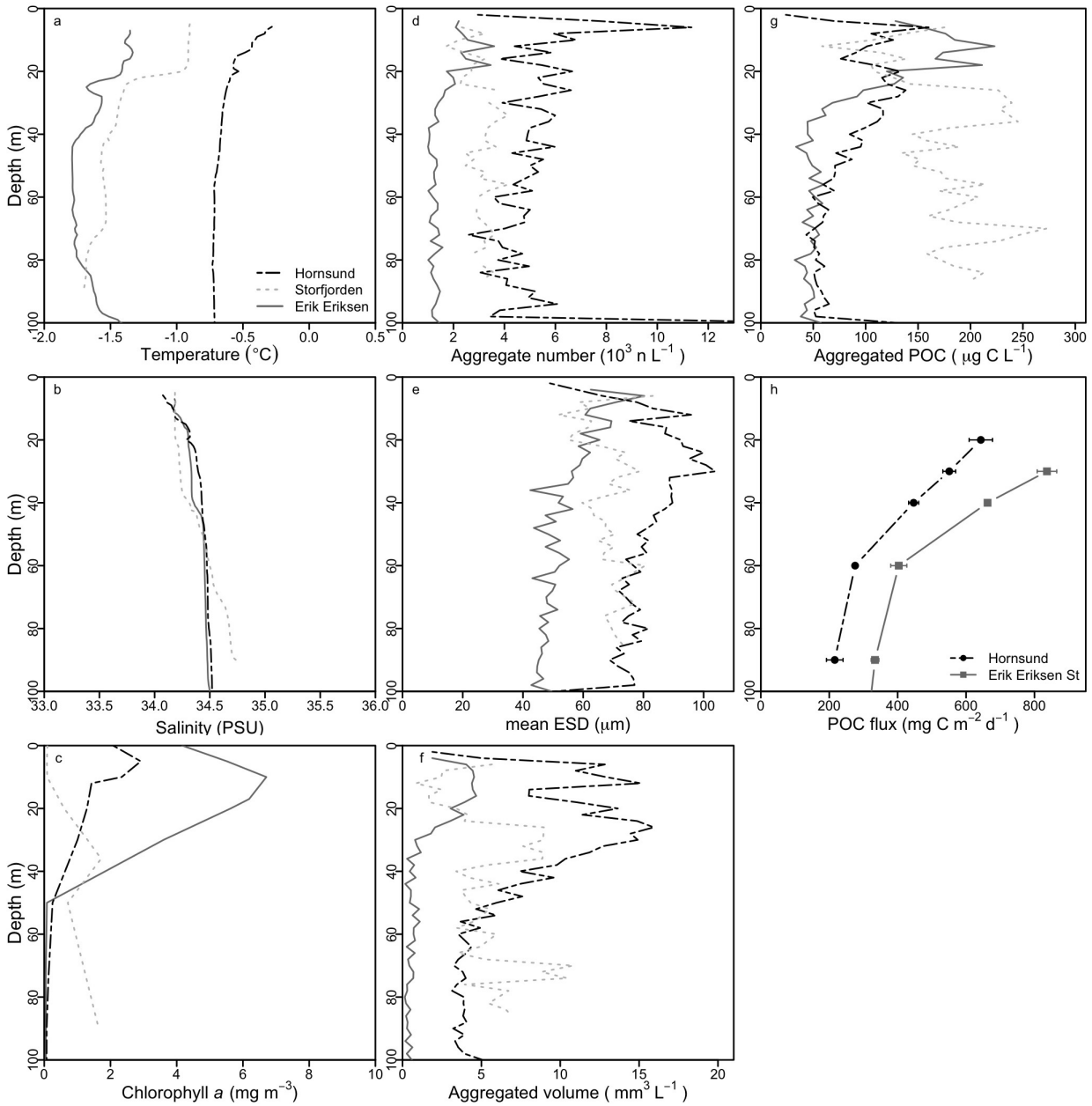

FIGURE 3 | Averaged depth profiles for investigated properties for measurements from stations in Erik Eriksen Strait (averaged values for five measurements), in Hornsund (averaged values for six measurements) and in Storfjorden (only one measurement), and POC fluxes from the sediment traps. **(a)** Temperature, **(b)** salinity, **(c)** chlorophyll *a*, **(d)** number of aggregates, **(e)** mean equivalent spherical diameter (ESD), **(f)** total aggregate volume, **(g)** total aggregated particulate organic carbon (POC), and **(h)** POC fluxes from sediment traps (average ± sd).

Eriksen Strait, and Storfjorden, respectively. In terms of biomass, however, *Pseudocalanus* and *Calanus* dominated the zooplankton community at all three stations with 94%, 95%, and 85% of the total zooplankton biomass in Hornsund, Erik Eriksen Strait, and Storfjorden, respectively.

Aggregate Abundances and Flux Attenuation

We determined *in situ* aggregate abundance and size-distribution from 12 vertical profiles with the ISC. The total number of aggregates, the mean aggregate size, and the total aggregated volume was the highest in Hornsund, followed by Storfjorden, and the lowest in Erik Eriksen Strait, however, the highest POC concentrations in the upper 25 m was found in Erik Eriksen Strait while Storfjorden had the highest POC concentrations at depths below 25 m (**Figure 3**). We used the volumetric POC ratios to convert the total aggregated volume into total aggregated POC concentrations. At all three stations this showed a decrease in the POC concentration from the peak concentration down to 50 m:

by 46 ± 16% (number of profiles $n = 6$) at Hornsund, by 39% at Storfjorden ($n = 1$), and by 55 ± 21% at Erik Eriksen Strait ($n = 5$). POC flux collected by the free-drifting sediment traps was higher at Erik Eriksen Strait compared to Hornsund (**Figure 3h**), and the flux attenuation between 30 and 60 m, calculated based on these measurements was 58 and 50%, respectively (**Figure 4**).

In situ Aggregate Feeding

Compared to the POC flux attenuation determined from the sediment trap measurements (see above), the attenuation estimated based *in situ* camera profiles was 55 ± 21%, 46 ± 16%, and 39% at Erik Eriksen Strait, Hornsund, and Storfjorden, respectively (**Figure 4**). We used Eqs (3–8) to test the potential contribution from aggregate feeding by *Calanus* and *Pseudocalanus* to the observed POC flux attenuation. Based on these calculations *Calanus* aggregate feeding alone could account for 38–62% of the total observed POC attenuation at all three stations while *Pseudocalanus* feeding could account for 1.5–29% of the total observed POC attenuation. Assuming that microbes have a carbon-specific degradation of 0.03 d^{-1} in the polar waters (Morata and Seuthe, 2014; Belcher et al., 2016b), Eq. (9) suggested that microbial degradation accounted for 12–16% of the total observed POC flux attenuation at the three stations. When combining *Calanus* and *Pseudocalanus* feeding on settling aggregates with microbial degradation, we could explain 76%, 77%, and 77% of the total POC flux attenuation at Hornsund, Erik Eriksen Strait, and Storfjorden, respectively. The observed POC attenuation between the sediment traps at 30 and 60 m was 276 and 436 mg C m^{-2} d^{-1} in Hornsund and Erik Eriksen Strait, respectively. *Calanus* aggregate feeding was found to reach 102 and 269 mg C m^{-2} d^{-1} in Hornsund and Erik Eriksen Strait, respectively, while *Pseudocalanus* had a carbon-equivalent aggregate feeding of 76 and 6.3 mg C m^{-2} d^{-1} in Hornsund and Erik Eriksen Strait, respectively. Potential aggregate feeding by the balanid nauplii only accounted for 0.24 to 0.58% of the total observed flux attenuation at the three investigated regions.

Size-Specific Aggregate-Loss in the Upper 50 m

Compared to the observed POC concentration at 50 m from the ISC profiles, our calculations showed a stronger decline in the abundance of small aggregates and only a limited decline in the abundance of large aggregates (**Figure 5**). Still, the calculations clearly suggested that primarily zooplankton grazing and to some extent microbial degradation of small slow-sinking aggregates (ESD < 0.2 mm) accounted for the majority of the observed POC flux attenuation.

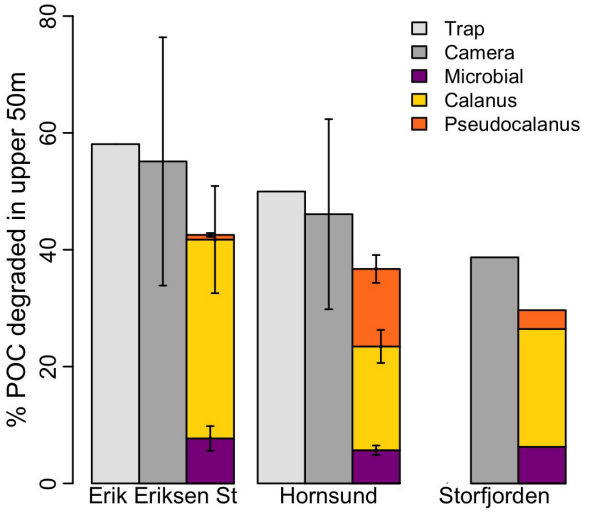

FIGURE 4 | POC degradation in the upper 50 m estimated based on measurements from drifting sediment traps (light gray), from camera profiles (dark gray), calculated microbial degradation based on a C-specific degradation of 0.03 d^{-1} (magenta), and calculated *Calanus* (yellow) and *Pseudocalanus* degradation (orange).

DISCUSSION

Our study showed that the majority of the POC flux attenuation in an Arctic shelf sea during the productive season took place in the upper 50 m of the water column. Attenuation processes are still under debate, e.g., the importance of microbial degradation versus zooplankton grazing and fragmentation, but evidence is increasingly showing that zooplankton play a major role in flux attenuation in the upper ocean (Iversen et al., 2010; Jackson and Checkley, 2011; Möller et al., 2012). *Calanus* spp. and *Pseudocalanus* spp. are important copepods and often dominate the zooplankton biomass in Arctic waters (Basedow et al., 2018; Carstensen et al., 2019), yet little is known about their contribution to POC flux attenuation. We observed that representatives of both *Calanus* and *Pseudocalanus* were able to detect, capture and feed on sinking aggregates. Both copepods were observed to attach to aggregates that were within a distance of half a body length, suggesting that they were detecting hydromechanical signals generated by the sinking aggregates (Visser, 2001). Additionally, it appeared that *Pseudocalanus* individuals were able to detect chemical trails from dissolved compounds leaking out of the sinking aggregates (**Supplementary Video 4**), a trait that has previously only been observed for the copepod *Temora longicornis* (Lombard et al., 2013). This detection did not, however, lead to aggregate capture. *Pseudocalanus* only captured aggregates that they detected via hydrodynamic signals. The results of this study suggest that the main mechanisms used to detect settling aggregates are based on hydromechanical signals in both *Calanus* and *Pseudocalanus*. While there were some instances where it seemed as though aggregates were detected via chemoreception, the recorded instances were too few to make any firm conclusion about the role of this mechanism for these two calanoid copepod genera.

Pseudocalanus attached more often to the encountered aggregates than *Calanus*. However, the larger size and higher swimming velocity resulted in a larger volume of water searched per time for an individual *Calanus* compared to an individual *Pseudocalanus*. Consequently, the probability of finding an aggregate was higher for individual *Calanus* compared to individual *Pseudocalanus*. Additionally, *Calanus* spent more

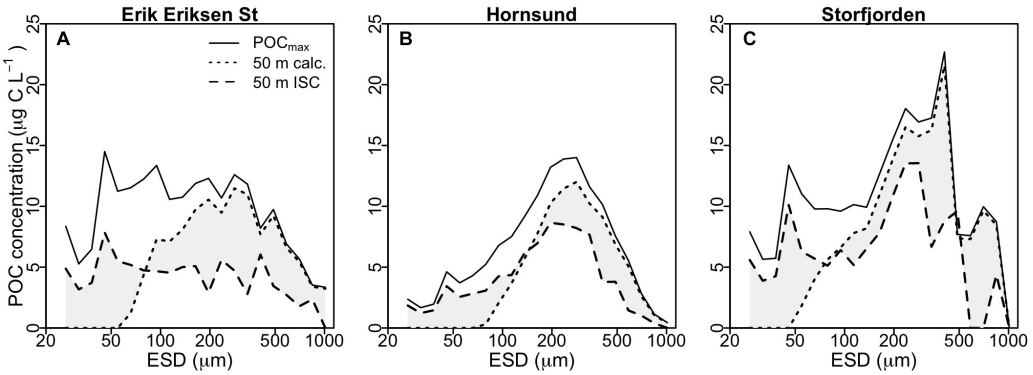

FIGURE 5 | Average POC distribution for different particle size classes at Erik Eriksen Strait **(A)**, Hornsund **(B)**, and Storfjorden **(C)**. Continuous lines show the POC_{max} values from the ISC profiles, used as input in the calculations, dotted black lines show the calculated values at 50 m, based on microbial degradation and *Calanus* and *Pseudocalanus* aggregate feeding, and black dashed lines show the measured values at 50 m from the ISC profiles. Gray shaded area indicates differences between observed and calculated POC concentration at 50 m.

time attached to an aggregate than *Pseudocalanus* and each *Calanus* ingested three-fold more aggregated POC than each *Pseudocalanus* (average aggregate ingestion was 13.4 ± 4.34 and 5.79 ± 2.17 µg C ind^{-1} d^{-1} for *Calanus* and *Pseudocalanus*, respectively). This is within previously reported grazing rates for these genera (Koski et al., 1998; Seuthe et al., 2007; Grote et al., 2015). Put in relation to the copepod carbon content (∼128 and ∼9 µg C ind^{-1} for *Calanus* and *Pseudocalanus*, respectively (Debes et al., 2008; Swalethorp et al., 2011), the carbon-specific ingestion rates for *Calanus* and *Pseudocalanus* were 0.12 ± 0.05 and 0.64 ± 0.24 d^{-1}, respectively. This is in the upper range of carbon-specific ingestion rates observed previously for those genera (Mayor et al., 2006; Arendt et al., 2010; Alcaraz et al., 2014) and it therefore seems possible that both species can sustain their carbon demand via aggregate feeding alone. While these calculations should be viewed as estimates, our direct video observations provide evidence that both *Calanus* and *Pseudocalanus* perceive settling aggregates as a food source.

The ecological impact of the two genera depends on their quantitative contribution to the zooplankton community in a given location. By combining aggregate ingestion rates of zooplankton with zooplankton abundance from net hauls and *in situ* abundance and size distribution of aggregates at the study location, we calculated that aggregate grazing by local populations of *Calanus* and *Pseudocalanus* could be responsible for 38 to 62% and 1.5 to 29%, respectively, of the total POC flux attenuation. Microbial respiration associated with the aggregates could account for a further 12–16% of the flux attenuation, when assuming an aggregate carbon-specific microbial degradation of 0.03 d^{-1}, as previously measured for aggregates from polar seas (Morata and Seuthe, 2014; Belcher et al., 2016b). Hence, combining aggregate feeding by *Calanus* and *Pseudocalanus* with microbial degradation explained as much as 77% of the total POC flux attenuation in the upper 50 m of the water column.

The remaining ∼23% of the flux attenuation can possibly be attributed to other zooplankton, nekton, and physical disturbances. The most abundant zooplankton groups at the three stations were balanid nauplii and calanoid nauplii, although they contributed little to the total zooplankton biomass due to their small sizes. Estimations from our incubations carried out with the balanid nauplii suggested that they only contributed of up to 0.58% of the total observed POC flux attenuation, despite their high abundance. Of the remaining observed zooplankton in the net hauls, only calanoid nauplii (Green et al., 1992), *Microsetella norvegica* (Koski et al., 2005, 2007), *Oncaea* spp. (Green and Dagg, 1997; Koski et al., 2017), and euphausiids (Dilling et al., 1998) have previously been observed to feed on sinking aggregates. Using published aggregate ingestion rates, euphausiids may have contributed 0.14–5.9% to the flux attenuation (Dilling et al., 1998), and small copepods, such as *Oncaea* spp. and *Oithona* spp., may have contributed <0.01–1.6%, assuming an aggregate ingestion rate of 1.08 µg C ind^{-1} d^{-1} (Kiørboe, 2000). Additionally, we observed dinoflagellates, which may also feed on settling aggregates (Poulsen and Iversen, 2008; Poulsen et al., 2011; Svensen et al., 2012). However, even combined, the contribution of zooplankton groups other than *Calanus* and *Pseudocalanus* is unlikely to alone explain the remaining 23%.

Another mechanism which may explain part of the remaining ∼23% of the POC flux attenuation is aggregate fragmentation, which has previously been suggested as a major process controlling the export of organic matter (Dilling and Alldredge, 2000; Goldthwait et al., 2004; Briggs et al., 2020). Fragmentation may increase the residence time of the settling aggregates in the upper water column by disaggregating them into smaller, slower-settling aggregates. This allows more time for microbial degradation (Iversen and Ploug, 2010; van der Jagt et al., 2018) and grazing by zooplankton (Iversen and Poulsen, 2007; Poulsen and Iversen, 2008; Giering et al., 2014; Mayor et al., 2014), thus decreasing the efficiency of the biological carbon pump. It has to be noted that encounters between zooplankton and settling aggregates may lead to aggregate fragmentation as well as aggregate feeding. This has been shown for *Calanus*, *Pseudocalanus*, and euphausiids (Dilling and Alldredge, 2000; Iversen and Poulsen, 2007). The major fragmentation mechanism, however, is likely aggregate break-up due to physical

forces in the upper water column (e.g., turbulence) (Jackson et al., 1995; Ruiz, 1997). We found that the modeled size-spectra (**Figure 5**) underestimated the *in situ* abundance of small aggregates and overestimated the abundance of large aggregates. This suggests that, while our calculations do include zooplankton activities, they are missing the physical aggregate fragmentation that converts large aggregates into small fragments. The main reason for this shortfall, is that our experimental setup (roller tanks), on which the model is based, did not allow for turbulence or other physical disturbances in the water. Hence, physical aggregate fragmentation may have been an important mechanism for *in situ* flux attenuation during our study and would explain the discrepancy between our calculated and observed POC size spectra at 50 m and potentially be the explanation for the additional ∼23% flux attenuation.

Polar marine environments are characterized by high primary production and high export flux out of the upper mixed layer, but strong POC flux attenuation at the base of the mixed layer (Berelson, 2001; Wassmann et al., 2003). Here we show that *Calanus* and *Pseudocalanus* were responsible for 60–67% of the flux attenuation. Both genera are ubiquitous in productive temperate and subtropical environments (Boxhall, 2001), which exhibit similar patterns of flux attenuation (e.g., Martin et al., 1983; Iversen et al., 2010; Belcher et al., 2016a). Currently, receding sea-ice cover and inflow of warm Atlantic water are leading to dramatic changes in the Arctic pelagic ecosystem. For example, environmental changes promote small flagellates (Li et al., 2009) and boreal zooplankton may be expatriated into the Arctic, replacing large Arctic species with smaller species of Atlantic origin (Hirche and Kosobokova, 2007). With the currently available data, it is difficult to predict how these changes at the base of the food web will impact the flux attenuation. Our study, however, confirms the suggestion by Jackson and Checkley (2011) that zooplankton may act as gatekeepers of the POC flux. In a future Arctic, where small copepods species with low impact on the attenuation prevail, carbon export may increase. It is, however, also possible that the shift from diatoms to flagellates will decrease the settling velocities of the formed aggregates (Ploug et al., 2008b) and thereby decrease carbon export and the efficiency of the biological carbon pump. This study shows that zooplankton feeding on aggregates can be an important attenuation mechanism in the Arctic. This highlights the necessity to understand the seasonal and regional role of zooplankton for both export and carbon flux attenuation and how future changes in Arctic trophic interactions and particle flux will alter ecosystem functions and services.

DATA AVAILABILITY STATEMENT

The original contributions presented in the study are included in the article/**Supplementary Material**, further inquiries can be directed to the corresponding author.

AUTHOR CONTRIBUTIONS

MI and HJ designed the experiments. HJ, IW, and MI did the measurements during the cruise. NH and BN counted and identified the zooplankton plankton samples. HJ, IW, NH, BN, and MI analyzed the data. HJ and MI wrote the manuscript with input from NH, IW, and BN. All authors contributed to the article and approved the submitted version.

FUNDING

The cruise and IW were funded by 'ARCEx' (Norwegian Research Council #228107 and industry partners). This study was supported by the Helmholtz Association, the Alfred Wegener Institute Helmholtz Centre for Polar and Marine Research and the DFG-Research Center/Cluster of Excellence "The Ocean in the Earth System" at MARUM. This publication was supported by the HGF Young Investigator Group SeaPump "Seasonal and regional food web interactions with the biological pump": VH-NG-1000.

ACKNOWLEDGMENTS

We thank Cindy Lee, Stuart Wakeham, Kai-Uwe Hinrichs, Carol Arnosti, Anne Pearson, and Thorsten Dittmar for organizing the Marine Organic Biogeochemistry workshop held at the Hanse-Wissenschaftskolleg, Delmenhorst, Germany, April 27 to 30th 2019. We thank Christiane Lorenzen for the POC measurements and the crew of the R/V Helmer Hanssen for assistance during the cruise. We thank the editor and three reviewers for valuable input.

SUPPLEMENTARY MATERIAL

The Supplementary Material for this article can be found online at: https://www.frontiersin.org/articles/10.3389/fmars.2020.543124/full#supplementary-material

REFERENCES

Alcaraz, M., Felipe, J., Grote, U., Arashkevich, E., and Nikishina, A. (2014). Paper II Life in a warming ocean: thermal thresholds and metabolic balance of Arctic zooplankton. *J. Plankton Res.* 36, 3–10. doi: 10.1093/plankt/fbt111

Alldredge, A. (1998). The carbon, nitrogen and mass content of marine snow as a function of aggregate size. *Deep. Res. I* 45, 529–541. doi: 10.1016/s0967-0637(97)00048-4

Alldredge, A. L. (1972). Abandoned larvacean houses: a unique food source in the pelagic environment. *Science* 177, 885–887. doi: 10.1126/science.177.4052.885

Alldredge, A. L. (2000). Interstitial dissolved organic carbon (DOC) concentrations within sinking marine aggregates and their potential contribution to carbon flux. *Limnol. Oceanogr.* 45, 1245–1253. doi: 10.4319/lo.2000.45.6.1245

Alldredge, A. L., Passow, U., and Haddock, S. H. D. (1998). The characteristics and transparent exopolymer particle (TEP) content of marine snow formed from thecate dinoflagellates. *J. Plankton Res.* 20, 393–406. doi: 10.1093/plankt/20.3.393

Arendt, K. E., Nielsen, T. G., Rysgaard, S., and Tönnesson, K. (2010). Differences in plankton community structure along the Godthåbsfjord, from the Greenland

Ice Sheet to offshore waters. *Mar. Ecol. Prog. Ser.* 401, 49–62. doi: 10.3354/meps08368

Arnkværn, G., Daase, M., and Eiane, K. (2005). Dynamics of coexisting *Calanus finmarchicus*, *Calanus glacialis* and *Calanus hyperboreus* populations in a high-Arctic fjord. *Polar Biol.* 28, 528–538. doi: 10.1007/s00300-005-0715-8

Båmstedt, U., Nejstgaard, J. C., Solberg, P. T., and Høisoeter, T. (1999). Utilisation of small-sized food algae by *Calanus finmarchicus* (Copepoda, Calanoida) and the significance of feeding history. *Sarsia* 84, 19–38. doi: 10.1080/00364827.1999.10420449

Basedow, S. L., Sundfjord, A., von Appen, W. J., Halvorsen, E., Kwasniewski, S., and Reigstad, M. (2018). Seasonal variation in transport of zooplankton into the arctic basin through the Atlantic Gateway, Fram Strait. *Front. Mar. Sci.* 5:194. doi: 10.3389/fmars.2018.00194

Belcher, A., Iversen, M., Giering, S., Riou, V., Henson, S. A., Berline, L., et al. (2016a). Depth-resolved particle-associated microbial respiration in the north-east Atlantic. *Biogeosciences* 13, 4927–4943. doi: 10.5194/bg-13-4927-2016

Belcher, A., Iversen, M., Manno, C., Henson, S. A., Tarling, G. A., and Sanders, R. (2016b). The role of particle associated microbes in remineralization of fecal pellets in the upper mesopelagic of the Scotia Sea, Antarctica. *Limnol. Oceanogr.* 61, 1049–1064. doi: 10.1002/lno.10269

Berelson, W. M. (2001). The flux of particulate organic carbon into the ocean interior: a comparison of four U S. JGOFS regional studies. *Oceanography* 14, 59–67. doi: 10.5670/oceanog.2001.07

Boxhall, G. (2001). "Copepoda (excl. harpacticoida)," in *European Register of Marine Species: A Check-List of the Marine Species in Europe and a Bibliography of Guides to Their Identification. Collection Patrimoines Naturels*, eds M. J. Costello, C. Emblow, and R. J. White (Paris: Meséum Naitonal d'Histoire Naturelle), 252–268.

Briggs, N., Dall'Olmo, G., and Claustre, H. (2020). Major role of particle fragmentation in regulating biological sequestration of CO2 by the oceans. *Science* 367, 791–793. doi: 10.1126/science.aay1790

Buesseler, K. O., and Boyd, P. (2009). Shedding light on processes that control particle export and flux attenuation in the twilight zone of the open ocean. *Limnol. Ocean.* 54, 1210–1232. doi: 10.4319/lo.2009.54.4.1210

Busch, K., Endres, S., Iversen, M. H., Michels, J., Nöthig, E.-M., and Engel, A. (2017). Bacterial colonization and vertical distribution of marine gel particles (TEP and CSP) in the Arctic Fram Strait. *Front. Mar. Sci.* 4:166. doi: 10.3389/fmars.2017.00166

Carstensen, J., Olszewska, A., and Kwasniewski, S. (2019). Summer mesozooplankton biomass distribution in the West Spitsbergen current (2001–2014). *Front. Mar. Sci.* 6:202. doi: 10.3389/fmars.2019.00202

Debes, H., Eliasen, K., and Gaard, E. (2008). Seasonal variability in copepod ingestion and egg production on the Faroe shelf. *Hydrobiologia* 600, 247–265. doi: 10.1007/s10750-007-9238-3

DeVries, T., Primeau, F., and Deutsch, C. (2012). The sequestration efficiency of the biological pump. *Geophys. Res. Lett.* 39:L13601. doi: 10.1029/2012GL051963

Dilling, L., and Alldredge, A. L. (2000). Fragmentation of marine snow by swimming macrozooplankton: a new process impacting carbon cycling in the sea. *Deep. Res. I* 47, 1227–1245. doi: 10.1016/s0967-0637(99)00105-3

Dilling, L., and Brzezinski, M. A. (2004). Quantifying marine snow as a food choice for zooplankton using stable silicon isotope tracers. *Plankton J. Res.* 26, 1105–1114. doi: 10.1093/plankt/fbh103

Dilling, L., Wilson, J., Steinberg, D., and Alldredge, A. (1998). Feeding by the euphausiid Euphausia pacifica and the copepod *Calanus pacificus* on marine snow. *Mar. Ecol. Prog. Ser.* 170, 189–201. doi: 10.3354/meps170189

Flintrop, C. M., Rogge, A., Miksch, S., Thiele, S., Waite, A. M., and Iversen, M. H. (2018). Embedding and slicing of intact *in situ* collected marine snow. *Limnol. Oceanogr. Methods* 16, 339–355. doi: 10.1002/lom3.10251

Giering, S. L. C., Sanders, R., Lampitt, R. S., Anderson, T. R., Tamburini, C., and Boutrif, M. (2014). Reconciliation of the carbon budget in the ocean's twilight zone. *Nature* 507, 480–483. doi: 10.1038/nature13123

Goldthwait, S., Yen, J., Brown, J., and Alldredge, A. (2004). Quantification of marine snow fragmentation by swimming euphausiids. *Limnol. Oceanogr.* 49, 940–952. doi: 10.4319/lo.2004.49.4.0940

Green, E. P., and Dagg, M. J. (1997). Mesozooplankton associations with medium to large marine snow aggregates in the northern Gulf of Mexico. *Plankton J. Res.* 19, 435–447. doi: 10.1093/plankt/19.4.435

Green, E. P., Harris, R. P., and Duncan, A. (1992). The production and ingestion of faecal pellets by nauplii of marine calanoid copepods. *J. Plankton Res.* 14, 1631–1643. doi: 10.1093/plankt/14.12.1631

Grote, U., Pasternak, A., Arashkevich, E., Halvorsen, E., and Nikishina, A. (2015). Thermal response of ingestion and egestion rates in the Arctic copepod *Calanus glacialis* and possible metabolic consequences in a warming ocean. *Polar Biol.* 38, 1025–1033. doi: 10.1007/s00300-015-1664-5

Hirche, H. J., and Kosobokova, K. (2007). Distribution of *Calanus finmarchicus* in the northern North Atlantic and arctic ocean-expatriation and potential colonization. *Deep Res. Part II Top. Stud. Oceanogr.* 54, 2729–2747. doi: 10.1016/j.dsr2.2007.08.006

Iversen, M. H., Nowald, N., Ploug, H., Jackson, G. A., and Fischer, G. (2010). High resolution profiles of vertical particulate organic matter export off Cape Blanc, Mauritania: degradation processes and ballasting effects. *Deep Res. Part I Oceanogr. Res. Pap.* 57, 771–784. doi: 10.1016/j.dsr.2010.03.007

Iversen, M. H., Pakhomov, E. A., Hunt, B. P. V., van der Jagt, H., Wolf-Gladrow, D., and Klaas, C. (2017). Sinkers or floaters? Contribution from salp pellets to the export flux during a large bloom event in the Southern Ocean. *Deep Sea Res. Part II Top. Stud. Oceanogr.* 138, 116–125. doi: 10.1016/j.dsr2.2016.12.004

Iversen, M. H., and Ploug, H. (2010). Ballast minerals and the sinking carbon flux in the ocean: carbon-specific respiration rates and sinking velocities of marine snow aggregates. *Biogeosciences* 7, 2613–2624. doi: 10.5194/bg-7-2613-10

Iversen, M. H., and Ploug, H. (2013). Temperature effects on carbon-specific respiration rate and sinking velocity of diatom aggregates - potential implications for deep ocean export processes. *Biogeosciences* 10, 4073–4085. doi: 10.5194/bg-10-4073-2013

Iversen, M. H., and Poulsen, L. K. (2007). Coprorhexy, coprophagy, and coprochaly in the copepods *Calanus helgolandicus*, *Pseudocalanus elongatus*, and *Oithona similis*. *Mar. Ecol. Prog. Ser.* 350, 79–89. doi: 10.3354/meps07095

Jackson, G. A. (1993). Flux feeding as a mechanism for zooplankton grazing and its implications for vertical particulate flux. *Limnol. Oceanogr.* 38, 1328–1331. doi: 10.4319/lo.1993.38.6.1328

Jackson, G. A., and Checkley, D. M. Jr. (2011). Particle size distributions in the upper 100 m water column and their implications for animal feeding in the plankton. *Deep Res. I* 58, 283–297. doi: 10.1016/j.dsr.2010.12.008

Jackson, G. A., Logan, B. E., Alldredge, A. L., and Dam, H. G. (1995). Combining particle size spectra from a mesocosm experiment measured using photographic and aperture impedance (Coulter and Elzone) techniques. *Deep Res. II* 42, 139–157. doi: 10.1016/0967-0645(95)00009-f

Kiørboe, T. (2000). Colonization of marine snow aggregates by invertebrate zooplankton: abundance, scaling, and possible role. *Limnol. Oceanogr.* 45, 479–484. doi: 10.4319/lo.2000.45.2.0479

Kiørboe, T., Moehlenberg, F., and Hamburger, K. (1985). Bioenergetics of the planktonic copepod *Acartia tonsa*: relation between feeding, egg production and respiration, and composition of specific dynamic action. *Mar. Ecol. Prog. Ser. Oldend.* 26, 85–97. doi: 10.3354/meps026085

Kiørboe, T., and Thygesen, U. H. (2001). Fluid motion and solute distribution around sinking aggregates. II. Implications for remote detection by colonizing zooplankters. *Mar. Ecol. Prog. Ser.* 211, 15–25. doi: 10.3354/meps211015

Koski, M., Boutorh, J., and De La Rocha, C. (2017). Feeding on dispersed vs. aggregated particles: the effect of zooplankton feeding behavior on vertical flux. *PLoS One* 12:e0177958. doi: 10.1371/journal.pone.0177958

Koski, M., Breteler, W. K., and Schogt, N. (1998). Effect of food quality on rate of growth and development of the pelagic copepod *Pseudocalanus elongatus* (Copepoda, Calanoida). *Mar. Ecol. Prog. Ser.* 170, 169–187. doi: 10.3354/meps170169

Koski, M., Kiørboe, T., and Takahashi, K. (2005). Benthic life in the pelagic: aggregate encounter and degradation rates by pelagic harpacticoid copepods. *Limnol. Oceanogr.* 50, 1254–1263. doi: 10.4319/lo.2005.50.4.1254

Koski, M., Moller, E. F., Maar, M., and Visser, A. (2007). The fate of discarded appendicularian houses: degradation by the copepod, Microsetella norvegica, and other agents. *J. Plankton Res.* 29, 641–654. doi: 10.1093/plankt/fbm046

Lampitt, R. S., Noji, T., and Bodungen, B. V. (1990). What happens to zooplankton fecal pellets? Implications for material flux. *Mar. Biol.* 104, 15–23. doi: 10.1007/bf01313152

Lampitt, R. S., Wishner, K. F., Turley, C. M., and Angel, M. V. (1993). Marine snow studies in the Northeast Atlantic ocean: distribution, composition and role as a food source for migrating plankton. *Mar. Biol.* 116, 689–702. doi: 10.1007/bf00355486

Lenz, J., Morales, A., and Gunkel, J. (1993). Mesozooplankton standing stock during the North Atlantic spring bloom study in 1989 and its potential grazing pressure on phytoplankton: a comparison between low, medium and high latitudes. *Deep. Res. Part II* 40, 559–572. doi: 10.1016/0967-0645(93)90032-I

Li, W. K. W., McLaughlin, F. A., Lovejoy, C., and Carmack, E. C. (2009). Smallest algae thrive as the arctic ocean freshens. *Science* 326:539. doi: 10.1126/science.1179798

Lombard, F., Koski, M., and Kiørboe, T. (2013). Copepods use chemical trails to find sinking marine snow aggregates. *Limnol. Ocean.* 58, 185–192. doi: 10.4319/lo.2013.58.1.0185

Markussen, T. N., Konrad, C., Waldmann, C., Becker, M., Fischer, G., and Iversen, M. H. (2020). Tracks in the snow – advantage of combining optical methods to characterize marine particles and aggregates. *Front. Mar. Sci.* 7:476. doi: 10.3389/fmars.2020.00476

Marsay, C. M., Sanders, R. J., Henson, S. A., Pabortsava, K., Achterberg, E. P., and Lampitt, R. S. (2015). Attenuation of sinking particulate organic carbon flux through the mesopelagic ocean. *Proc. Natl. Acad. Sci. U.S.A.* 112, 1089–1094. doi: 10.1073/pnas.1415311112

Martin, J. H., Knauer, G. A., Broenkow, W. W., Bruland, K. W., Karl, D. M., Small, L. F., et al. (1983). Vertical transport and exchange of materials in the upper waters of the ocean (VERTEX): introduction to the program, hydrographic conditions and major component fluxes during VERTEX I. *Moss Land. Mar. Lab. Tech. Publ.* 83, 1–40. doi: 10.1007/978-1-4612-0353-7_1

Martin, J. H., Knauer, G. A., Karl, D. M., and Broenkow, W. W. (1987). VERTEX: carbon cycling in the northeast Pacific. *Deep Res.* 34, 267–285. doi: 10.1016/0198-0149(87)90086-0

Mayor, D. J., Anderson, T. R., Irigoien, X., and Harris, R. (2006). Feeding and reproduction of Calanus finmarchicus during non-bloom conditions in the Irminger Sea. *J. Plankton Res.* 28, 1167–1179. doi: 10.1093/plankt/fbl047

Mayor, D. J., Sanders, R., Giering, S. L. C., and Anderson, T. R. (2014). Microbial gardening in the ocean's twilight zone: detritivorous metazoans benefit from fragmenting, rather than ingesting, sinking detritus: fragmentation of refractory detritus by zooplankton beneath the euphotic zone stimulates the harvestable production of labile and nutritious microbial biomass. *Bioessays* 36, 1132–1137. doi: 10.1002/bies.201400100

Möller, K. O., John, M. S., Temming, A., Floeter, J., Sell, A. F., and Herrmann, J. P. (2012). Marine snow, zooplankton and thin layers: indications of a trophic link from small-scale sampling with the video plankton recorder. *Mar. Ecol. Prog. Ser.* 468, 57–69. doi: 10.3354/meps09984

Morata, N., and Seuthe, L. (2014). Importance of bacteria and protozooplankton for faecal pellet degradation. *Oceanologia* 56, 565–581. doi: 10.5697/oc.56-3.565

Ohtsuka, S., Kubo, N., Okada, M., and Gushima, K. (1993). Attachment and feeding of pelagic copepods on larvacean houses. *J. Oceanogr.* 49, 115–120. doi: 10.1007/BF02234012

Ploug, H., and Grossart, H. P. (2000). Bacterial growth and grazing on diatom aggregates: respiratory carbon turnover as a function of aggregate size and sinking velocity. *Limnol. Oceanogr.* 45, 1467–1475. doi: 10.4319/lo.2000.45.7.1467

Ploug, H., Iversen, M. H., and Fischer, G. (2008a). Ballast, sinking velocity, and apparent diffusivity within marine snow and zooplankton fecal pellets: implications for substrate turnover by attached bacteria. *Limnol. Oceanogr.* 53, 1878–1886. doi: 10.4319/lo.2008.53.5.1878

Ploug, H., Iversen, M. H., Koski, M., and Buitenhuis, E. T. (2008b). Production, oxygen respiration rates, and sinking velocity of copepod fecal pellets: direct measurements of ballasting by opal and calcite. *Limnol. Oceanogr.* 53, 469–476. doi: 10.4319/lo.2008.53.2.0469

Poulsen, L. K., and Iversen, M. H. (2008). Degradation of copepod fecal pellets: key role of protozooplankton. *Mar. Ecol. Prog. Ser.* 367, 1–13. doi: 10.3354/meps07611

Poulsen, L. K., and Kiørboe, T. (2005). Coprophagy and coprorhexy in the copepods Acartia tonas and *Temora longicornis*: clearance rates and feeding behaviour. *Mar. Ecol. Prog. Ser.* 299, 217–227. doi: 10.3354/meps299217

Poulsen, L. K., Moldrup, M., Berge, T., and Hansen, P. J. (2011). Feeding on copepod fecal pellets: a new trophic role of dinoflagellates as detritivores. *Mar. Ecol. Prog. Ser.* 441, 65–78. doi: 10.3354/meps09357

Reigstad, M., Riser, C. W., and Svensen, C. (2005). Fate of copepod faecal pellets and the role of *Oithona* spp. *Mar. Ecol. Ser.* 304, 265–270. doi: 10.3354/meps304265

Richter, C. (1994). *Regional and Seasonal Variability in the Vertical Distribution of Mesozooplankton in the Greenland Sea*. San Diego, CA: The University of California.

Ruiz, J. (1997). What generates daily cycles of marine snow? *Deep Res. Part I Oceanog. Res. Pap.* 44, 1105–1126. doi: 10.1016/s0967-0637(97)00012-5

Seuthe, L., Darnis, G., Riser, C. W., Wassmann, P., and Fortier, L. (2007). Winter–spring feeding and metabolism of Arctic copepods: insights from faecal pellet production and respiration measurements in the southeastern Beaufort Sea. *Polar Biol.* 30, 427–436. doi: 10.1007/s00300-006-0199-1

Shanks, A. L., and Edmondson, E. W. (1989). Laboratory-made artificial marine snow: a biological model of the real thing. *Mar. Biol.* 101, 463–470. doi: 10.1007/bf00541648

Siegenthaler, U., and Sarmiento, J. L. (1993). Atmospheric carbon dioxide and the ocean. *Nature* 365, 119–125.

Steinberg, D. K., Van Mooy, B. A. S., Buesseler, K. O., Boyd, P. W., Kobari, T., and Karl, D. M. (2008). Bacterial vs. zooplankton control of sinking particle flux in the ocean's twilight zone. *Limnol. Oceanogr.* 53, 1327–1338. doi: 10.4319/lo.2008.53.4.1327

Stemmann, L., Jackson, G. A., and Gorsky, G. (2004). A vertical model of particle size distributions and fluxes in the midwater column that includes biological and physical processes; Part II, application to a three year survey in the NW Mediterranean Sea. *Deep Res. I* 51, 885–908. doi: 10.1016/j.dsr.2004.03.002

Stemmann, L., Picheral, M., and Gorsky, G. (2000). Diel variation in the vertical distribution of particulate matter (>0.*15* mm) in the NW Mediterranean Sea investigated with the underwater video profiler. *Deep Sea Res. Part I Oceanogr. Res. Pap.* 47, 505–531. doi: 10.1016/S0967-0637(99)00100-4

Sun, J., and Liu, D. (2003). Geometric models for calculating cell biovolume and surface area for phytoplankton. *J. Plankton Res.* 25, 1331–1346. doi: 10.1093/plankt/fbg096

Svensen, C., Wexel Riser, C., Reigstad, M., and Seuthe, L. (2012). Degradation of copepod faecal pellets in the upper layer: role of microbial community and *Calanus finmarchicus*. *Mar. Ecol. Prog. Ser.* 462, 39–49. doi: 10.3354/meps09808

Swalethorp, R., Kjellerup, S., Dünweber, M., Nielsen, T. G., Møller, E. F., Rysgaard, S., et al. (2011). Grazing, egg production, and biochemical evidence of differences in the life strategies of *Calanus finmarchicus*, *C. glacialis* and *C. hyperboreus* in Disko Bay, Western Greenland. *Mar. Ecol. Prog. Ser.* 429, 125–144. doi: 10.3354/meps09065

Tamburini, C., Boutrif, M., Garel, M., Colwell, R. R., and Deming, J. W. (2013). Prokaryotic responses to hydrostatic pressure in the ocean - a review. *Environ. Microbiol.* 15, 1262–1274. doi: 10.1111/1462-2920.12084

Thiele, S., Fuchs, B. M., Amann, R., and Iversen, M. H. (2015). Colonization in the photic zone and subsequent changes during sinking determine bacterial community composition in marine snow. *Appl. Environ. Microbiol.* 81, 1463–1471. doi: 10.1128/aem.02570-14

van der Jagt, H., Friese, C., Stuut, J.-B. W., Fischer, G., and Iversen, M. H. (2018). The ballasting effect of Saharan dust deposition on aggregate dynamics and carbon export: aggregation, settling, and scavenging potential of marine snow. *Limnol. Oceanogr.* 63, 1386–1394. doi: 10.1002/lno.10779

Visser, A. W. (2001). Hydromechanical signals in the plankton. *Mar. Ecol. Prog. Ser.* 222, 1–24. doi: 10.3354/meps222001

Wassmann, P., Olli, K., Wexel Riser, C., and Svensen, C. (2003). "Ecosystem function, biodiversity and vertical flux regulation in the twillight zone," in *Marine Science Frontiers for Europe*, eds G. Wefer, F. Lamy, and F. Mantoura (Berlin: Springer-Verlag), 279–287. doi: 10.1007/978-3-642-55862-7_19

Weber, T., Cram, J. A., Leung, S. W., DeVries, T., and Deutsch, C. (2016). Deep ocean nutrients imply large latitudinal variation in particle transfer efficiency. *Proc. Natl. Acad. Sci. U.S.A.* 113, 8606–8611. doi: 10.1073/pnas.1604414113

Wiedmann, I., Reigstad, M., Sundfjord, A., and Basedow, S. (2014). Potential drivers of sinking particle's size spectra and vertical flux of particulate organic carbon (POC): turbulence, phytoplankton, and zooplankton. *J. Geophys. Res. Ocean.* 119, 6900–6917. doi: 10.1002/2013JC009754

Conflict of Interest: The authors declare that the research was conducted in the absence of any commercial or financial relationships that could be construed as a potential conflict of interest.

The reviewer JT declared a past co-authorship with one of the authors MI to the handling editor.

Advantages of publishing in Frontiers

OPEN ACCESS
Articles are free to read for greatest visibility and readership

FAST PUBLICATION
Around 90 days from submission to decision

HIGH QUALITY PEER-REVIEW
Rigorous, collaborative, and constructive peer-review

TRANSPARENT PEER-REVIEW
Editors and reviewers acknowledged by name on published articles

Frontiers
Avenue du Tribunal-Fédéral 34
1005 Lausanne | Switzerland

Visit us: www.frontiersin.org
Contact us: frontiersin.org/about/contact

REPRODUCIBILITY OF RESEARCH
Support open data and methods to enhance research reproducibility

DIGITAL PUBLISHING
Articles designed for optimal readership across devices

FOLLOW US
@frontiersin

IMPACT METRICS
Advanced article metrics track visibility across digital media

EXTENSIVE PROMOTION
Marketing and promotion of impactful research

LOOP RESEARCH NETWORK
Our network increases your article's readership